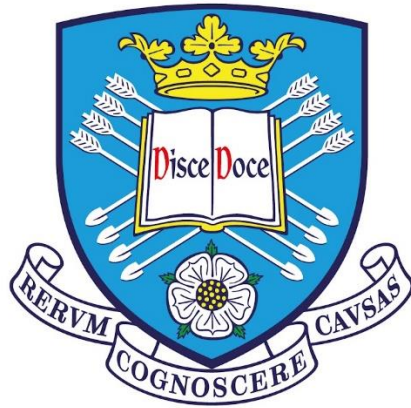


Understanding the Mechanisms Leading to Mitochondrial Abnormalities in Alzheimer's Disease



Katy Amanda Barnes

Thesis submitted for the degree of Doctor of Philosophy (PhD)

Sheffield Institute for Translational Neuroscience, Department of Neuroscience

The University of Sheffield

March 2022

Abstract

Alzheimer's disease (AD) is an incurable neurodegenerative disease, and the most common cause of dementia. Most cases are sporadic (sAD), with a complex aetiology and many interacting pathogenic mechanisms. Mitochondrial dysfunction is commonly seen, and previous work in the lab identified several deficits in sAD fibroblasts including reduced mitochondrial membrane potential (MMP), a more fused mitochondrial network, and reductions in total and mitochondria localised Drp1, a key mitochondrial fission protein. This project built on these findings, hypothesising that the mitochondrial phenotype seen in sAD cells is driven by abnormalities in fission and fusion processes, and that small molecules can be found which beneficially modulate the mitochondrial phenotype in AD. Mitochondrial quality control was investigated in sAD fibroblasts, including protein expression and localisation of Drp1 and its receptors, and interactions of Drp1 with its receptors. sAD fibroblasts showed reduced Drp1, Fis1, Mff, and MiD49, however no significant difference were seen in the localisation and interactions of these proteins compared to controls. The mitochondrial phenotype was investigated in patient derived iNeurons, and a decrease in MMP was seen, whereas morphology phenotypes were variable. Alterations in the fission process were seen in all lines, but there was no consistent pattern in the direction or severity. A library of 21,000 compounds was screened in sAD fibroblasts to identify compounds which have a beneficial effect on mitochondrial function and morphology. Some compounds rescued some of the deficits seen including increasing MMP, and positively altering mitochondrial morphology. However, this rescue effect was not consistent across all lines tested. Alterations in mitochondrial fission were common but variable in sAD fibroblasts and iNeurons. This variability is an important consideration, particularly in the search for new treatments for sAD, and highlights the benefits of better patient stratification, and a personalised medicine approach in improving patients' quality of life.

Acknowledgements

There are many people who have supported and guided me through the completion of my PhD.

Firstly, I would like to thank my primary supervisor, Professor Heather Mortiboys. Since I first started working with Heather as an MSc student five years ago, she has been a constant source of guidance and encouragement, both in the lab and out of it. Heather's support has shaped the scientist I am today, and I will always be grateful to her for providing her expertise, for being understanding when I have struggled, and for always believing in me. I would also like to thank my secondary supervisor, Dr Daniel Blackburn, for his support throughout my PhD.

I would like to thank the funders of this project, the faculty of Medicine, Dentistry, and Health Scholarship and the NIHR Sheffield Biomedical Research Centre. I would also like to thank the participants who donated skin biopsies, who made this research possible.

I would like to thank all past and present members of the Mortiboys lab group, for their help and support, and for being a great team to be a part of. I am grateful to Dr Simon Bell, for his contribution to the work on which this project was based, for taking the time to teach me at the start of my time in the lab, and for his continued support throughout my PhD. I would also like to thank Camilla Boschian, Aurelie Schwartzentruber, Dr Ruby Wallis, and Dr Chris Hastings, who were a huge source of support and friendship when I was first starting out. Completing a PhD during the COVID pandemic was challenging, and I would especially like to thank Toby Burgess, Tom Leah, Dr Lizzie Stephen, and Dr Fernanda Martins-Lopes for their help during the time when lab restrictions were the strictest. The biggest thank you to my lab other half, Rachel Hughes, who has been there through all the ups and downs of the PhD, for providing dog pictures, food, and for listening to me rant when I needed to.

I would also like to thank others at SITraN for their scientific guidance, in particular Dr Adrian Higginbottom for his expertise and assistance, especially with using the Echo 550, and for teaching me the molecular biology techniques.

I am grateful to Bridget Ashford, Martyna Matuszyk, and Sarah Harmon, for being the best people to share a desk with, for always being around for a cup of tea and a chat, and for reminding me to take a lunch break sometimes. Thanks also to John Harvey and Amelia Willcock, for continuing to provide laughs when I need them the most, and for always being around when I need a chat.

Finally, thank you to my family for their unconditional love and support. In particular, Christopher and Carys, for keeping me grounded, and for always being able to take my mind off work, and Mum and Dad, for always being on the other end of the phone, and for being my biggest supporters in everything I do.

Table of Contents

Abstract	2
Acknowledgements	3
List of Figures	9
List of Tables	14
List of Abbreviations	15
Chapter One: Introduction	18
1.1 Introduction to Alzheimer’s disease	18
1.1.1 Alzheimer’s disease	18
1.1.2 Alzheimer’s disease Neuropathology	19
1.1.3 Current Treatments and Therapeutic Strategies for Alzheimer’s disease	20
1.2 Introduction to Mitochondria	21
1.2.1 Mitochondrial Structure and Functions	22
1.2.2 Mitochondrial Morphology and Quality Control	22
1.2.3 Mitochondrial Contact with Other Organelles	27
1.2.4 Mitochondria in Disease	28
1.3 Mitochondria in Alzheimer’s disease	29
1.3.1 Mitochondrial Functional Abnormalities in Alzheimer’s disease	29
1.3.2 Mitochondrial Morphology Abnormalities in Alzheimer’s disease	30
1.3.3 Mitochondrial Quality Control Abnormalities in Alzheimer’s disease	31
1.3.4 Interactions of the Mitochondria with Amyloid and Tau	33
1.4 Local Cohort Used in this Study	35
1.5 Aims and Objectives	36
Chapter Two: Materials and Methods	38
2.1 Patient Information	38
2.2 Cell Culture	40
2.2.1 Human Fibroblast Cell Culture	40
2.2.2 Induced Neural Progenitor Cell Culture	41
2.2.3 Generic Neuron Differentiation	43
2.2.4 Fixing of Cells	45
2.3 Western Blotting	45
2.3.1 Cell Lysis	45
2.3.2 Bradford Assay	45
2.3.3 Gel Preparation	46
2.3.4 Sodium Dodecyl Sulphate – Polyacrylamide Gel Electrophoresis (SDS-PAGE)	47
2.3.5 Transfer	48
2.3.6 Blocking, Antibody Incubations and Imaging	49
2.3.7 Densitometry Analysis	51

2.4 Immunocytochemistry.....	51
2.4.1 Immunocytochemistry.....	51
2.4.2 Image Analysis.....	53
2.5 Proximity Ligation Assay.....	55
2.5.1 Proximity Ligation Assay.....	55
2.5.2 Image Analysis.....	56
2.6 Overexpression of Drp1 in Fibroblasts.....	57
2.6.1 Plasmid Information.....	57
2.6.2 Bacterial Culture.....	58
2.6.3 DNA Isolation.....	59
2.6.5 Transfection of Fibroblasts.....	60
2.6.6 Assessment of Transfection Efficiency.....	60
2.6.7 Assessment of Drp1 and Mitochondrial Morphology.....	60
2.7 Neurite Outgrowth Assay.....	61
2.7.1 Neurite Outgrowth Kit.....	61
2.7.2 Image Analysis.....	61
2.8 Mitochondrial Membrane Potential Assay in iNeurons.....	63
2.8.1 MMP Assay.....	63
2.8.2 Image Analysis.....	63
2.9 Live Neuron Assays under Stressed Conditions.....	65
2.10 Statistical Analysis.....	65
Chapter Three: Investigating Mitochondrial Dynamics in sAD Patient Fibroblasts.....	66
3.1 Introduction.....	66
3.1.1 Mitochondrial Phenotype in Patient Derived Fibroblasts.....	66
3.1.2 Previous Work.....	68
3.1.3 Aims and Objectives.....	68
3.2 Results.....	69
3.2.1 Drp1 Protein Expression in sAD Fibroblasts.....	69
3.2.2 Phosphorylated Drp1 in sAD Fibroblasts.....	71
3.2.2 OPA1 Protein Expression in sAD Fibroblasts.....	72
3.2.3 Drp1 Receptor Protein Expression in sAD Fibroblasts.....	75
3.2.4 Linear Regression Between Drp1 and Receptors in sAD Fibroblasts.....	80
3.2.5 Linear Regression Between Fission Proteins and Mitochondrial Function in sAD Fibroblasts.....	82
3.2.6 Linear Regression Between Fission Proteins and Mitochondrial Morphology in sAD Fibroblasts.....	84
3.2.7 Fis1 and Mff Localisation in sAD Fibroblasts.....	85
3.2.8 Fis1 and Mff Interactions with Drp1 in sAD Fibroblasts.....	91
3.2.9 Expression of Peroxisome Marker, Pex19, in sAD Fibroblasts.....	96
3.2.10 Fis1-BAP31 Mitochondria-ER Contact Sites in sAD Fibroblasts.....	98

3.2.11 Drp1 Overexpression in Control and sAD Fibroblasts.....	101
3.3 Discussion	106
3.3.1 Drp1	106
3.3.2 OPA1	108
3.3.3 Drp1 Receptors	109
3.3.4 Variability between Individual Cell Lines	115
3.3.5 Fis1 and Mff Localisation	116
3.3.6 Fis1 and Mff Interactions with Drp1	117
3.3.7 Peroxisomal Fission	119
3.3.8 Upstream Mechanisms of Mitochondrial Fission	120
3.3.9 Overexpression of Drp1 in Fibroblasts.....	121
3.3.10 The Use of Fibroblasts in AD Research	123
3.4 Conclusions and Future Work.....	124
Chapter Four: Investigating the Mitochondrial Phenotype in a Patient Derived Neuronal Model	127
4.1 Introduction	127
4.1.1 Induced Pluripotent Stem Cell Derived Models of Alzheimer’s disease	127
4.1.2 Induced Neural Progenitor Cells	129
4.1.3 Aims and Objectives	130
4.2 Results.....	131
4.2.1 Characterisation of the Generic Neuron Model	131
4.2.2 Neuronal Morphology and Viability in Control and sAD iNeurons Under Basal Conditions.....	153
4.2.3 Neuronal Morphology and Viability in Control and sAD iNeurons Under Stressed Conditions	158
4.2.4 Mitochondrial Function and Morphology in iNeurons Under Basal Conditions.....	160
4.2.5 Mitochondrial Function in iNeurons Under Stressed Conditions	166
4.2.6 Drp1 Expression in iNPCs and iNeurons	168
4.2.7 Drp1 Localisation in iNeurons.....	171
4.2.8 Drp1 Receptor Expression in iNPCs	174
4.2.9 Linear Regression Between Drp1 and Receptors in iNPCs.....	181
4.2.10 Drp1 Receptor Expression in iNeurons	183
4.2.11 Linear Regression Between Drp1 and Receptors in iNeurons	189
4.2.12 Linear Regression Between Fission Proteins and Mitochondrial Function in iNeurons	190
4.2.13 Linear Regression Between Fission Proteins and Mitochondrial Morphology in iNeurons.....	192
4.2.14 Drp1 and Receptor Expression in iNPCs and iNeurons Compared to Fibroblasts	195
4.2.15 Fis1 and Mff Localisation in iNeurons.....	197
4.2.16 Fis1 and Mff Interactions with Drp1 in iNeurons.....	202
4.2.17 Phosphorylation Status of Drp1 in iNPCs and iNeurons	207
4.3 Discussion	211
4.3.2 Characterisation of the Generic iNeuron Model	211

4.3.3 The Use of Generic iNeurons as a Model of Mitochondrial Dysfunction in AD	213
4.3.4 Neuronal Morphology and Viability in Control and sAD iNeurons	215
4.3.5 Mitochondrial Function in Control and sAD iNeurons	216
4.3.6 Neuronal Morphology and Viability, and Mitochondrial Function under Stressed Conditions.....	217
4.3.7 Mitochondrial Morphology in Control and sAD iNeurons	219
4.3.8 Drp1 Protein Expression in iNPCs and iNeurons.....	221
4.3.9 Drp1 Localisation in iNeurons.....	222
4.3.10 Drp1 Receptor Expression in iNPCs and iNeurons	223
4.3.11 Fis1 and Mff Localisation in iNeurons.....	224
4.3.12 Fis1 and Mff Interactions with Drp1 in iNeurons.....	225
4.3.13 Phosphorylation Status of Drp1 in iNPCs and iNeurons	226
4.3.14 Variability between iNeuron Lines.....	226
4.3.15 Differences in the Mitochondrial Phenotype in Fibroblasts and iNeurons	228
4.3 Conclusions and Future Work.....	229
Chapter Five: Screening for a Compound which Alters Mitochondrial Function and Morphology in Alzheimer’s Patient Fibroblasts.....	232
5.1 Introduction	232
5.1.1 Mitochondria Targeted Therapies for AD	232
5.1.2 Phenotypic vs Target Driven Approaches to Drug Screening	233
5.1.3 High Throughput Drug Screening using Patient Fibroblasts	235
5.1.4 Aims and Objectives	236
5.2 Drug Screening Methods	238
5.2.1 Compound Library	238
5.2.2 Primary Drug Screen	239
5.2.3 Primary Drug Screen Analysis	242
5.2.4 Screening compounds in one PSEN1 line	245
5.2.5 Dose Response Screen.....	245
5.2.6 Dose Response Analysis.....	247
5.2.7 Dose Response in a Locally Collected Cohort of Fibroblasts	247
5.2.8 Dose Response in a Locally Collected Cohort Analysis	248
5.3 Results.....	250
5.3.1 Primary Drug Screen in One sAD Fibroblast Line	250
5.3.2 Compounds Having an Effect in a sAD Line Do Not Have the Same Effect in a PSEN1 Line	255
5.3.3 Dose Response of Hit Compounds in One sAD Fibroblast Line	257
5.3.4 Dose Response of the Top 11 Compounds in Three Control and Three sAD Fibroblast Lines from a Locally Collected Cohort	261
5.3.5 Overall Performance of the Top 11 Compounds in all Stages of the Screen	269
5.4 Discussion	271

5.4.1 Primary Screen.....	271
5.4.2 Screening in a PSEN1 Fibroblast Line.....	272
5.4.3 Dose Response.....	273
5.4.4 Dose response in a Locally Collected Cohort.....	274
5.4.5 The Top 11 Compounds.....	275
5.4.6 Advantages and Limitations of this Screen.....	279
5.5 Conclusions and Future Work.....	280
Chapter Six: General Discussion.....	282
6.1 Models of Alzheimer’s disease.....	283
6.2 Mitochondrial Fission in sAD.....	284
6.3 Mitochondrial Involvement in Other sAD Mechanisms.....	287
6.4 Mitochondrial Quality Control as a Therapeutic Target in AD.....	288
6.5 Final Conclusions.....	290
Appendices.....	291
Appendix 1: Cortical Neuron Differentiation Optimisation.....	291
Appendix 1.2 Attempts to Optimise Cortical Neuron Differentiation from iNPCs Discussion.....	309
Appendix 2: Dose response analyses.....	312
Bibliography.....	315

List of Figures

Figure 1: Some of the key mechanisms implicated in AD..	21
Figure 2: The mitochondrial dynamic processes of fission and fusion..	26
Figure 3: Timeline of factors added during generic neuron differentiation.	43
Figure 4: Co-localisation analysis and segmentation of fibroblasts in Harmony analysis software.	54
Figure 5: PLA image analysis in Columbus software..	56
Figure 6: Map of pcDNA3YFP control plasmid.	57
Figure 7: Streaking pattern for growing individual bacterial colonies..	59
Figure 8: Segmentation and analysis of the neurite outgrowth assay in Harmony software..	62
Figure 9: Analysis of mitochondrial morphology in iNeurons from the MMP Assay, in Harmony analysis software..	65
Figure 10 : Total Drp1 protein levels are reduced in ten sAD patient fibroblast lines compared to ten controls (p < 0.0001).	70
Figure 11: Expression of pDrp1 (s637) and pDrp1 (s616) were very low in both control and sAD fibroblasts. This was unable to be quantified.	71
Figure 12: <i>There is no significant difference in total OPA1 protein levels between control and sAD patient fibroblasts.</i>	74
Figure 13: Total Fis1 protein levels are reduced in ten sAD patient fibroblast lines compared to ten controls (p < 0.0001).	76
Figure 14: Total Mff protein levels are reduced in ten sAD patient fibroblast lines compared to ten controls (p < 0.0001).	77
Figure 15: Total MiD49 protein levels are reduced in ten sAD patient fibroblast lines compared to ten controls (p = 0.0031).	78
Figure 16: Total MiD51 protein levels are not significantly different ten sAD patient fibroblast lines compared to ten controls (p = 0.5689).	79
Figure 17: Linear regression between protein levels of Drp1 and protein levels of Fis1, Mff, MiD49 and MiD51 in fibroblasts..	81
Figure 18: Linear regression between MMP and expression of fission proteins Drp1, Fis1, Mff, MiD49, and MiD51 in fibroblasts..	83
Figure 19: Linear regression between form factor, a measure of mitochondrial interconnectivity, and fission proteins Drp1, Fis1, Mff, MiD49, and MiD51 in fibroblasts.	85
Figure 20: Representative Images of Fis1-TOM20 co-localisation in control and sAD patient fibroblasts..	87
Figure 21: There is no significant difference in the amount of Fis1 co-localised to the mitochondria between control and sAD fibroblasts.	88
Figure 22: Representative Images of Mff-TOM20 co-localisation in control and sAD patient fibroblasts..	89
Figure 23: There is no significant difference in the amount of Mff co-localised to the mitochondria between control and sAD fibroblasts.	90
Figure 24: Representative image of Drp1 and Fis1, and Drp1 and Mff interactions in control and sAD fibroblasts. Scale bar = 50µM.	92
Figure 25: There is no difference in the number of Drp1 interactions with Fis1 between control and sAD patient fibroblasts..	93
Figure 26: There is no difference in the number of Drp1 interactions with Mff between control and sAD patient fibroblasts.	94
Figure 27: No significant difference in either control or sAD patient fibroblasts between the number of Drp1 interactions with Fis1 and Drp1 interactions with Mff.	95
Figure 28: No significant difference is seen in total pex19 protein levels between controls and sAD patient fibroblasts.	97
Figure 29: Representative Images of BAP31-Fis1 co-localisation in sAD and control fibroblasts.	99
Figure 30: No significant difference between BAP31-Fis1 mitochondria-ER contact sites between controls and sAD patient fibroblasts..	100

Figure 31: Mitochondrial morphology after transfection with control and Drp1 plasmids, in control 3 fibroblasts.....	102
Figure 32: Mitochondrial morphology after transfection with control and Drp1 plasmids, in sAD 5 fibroblasts.	103
Figure 33: Transfection efficiency and % Drp1 increase in control 3 and sAD 5 fibroblasts, after transfection with either pcDNA3YFP or pcDNA3Drp1YFP.	104
Figure 34: There is a large decrease in form factor, indicating an increase in fragmentation, in control and sAD fibroblasts after transfection with either pcDNA3YFP or pcDNA3Drp1YFP.	105
Figure 35: Representative images showing expression of neuronal markers in five control iNeurons lines. TUJ is shown in green, MAP2 shown in red, and Hoechst in blue. Scale bar = 50µM.	134
Figure 36: Representative images showing expression of neuronal markers in five sAD iNeurons lines. TUJ is shown in green, MAP2 shown in red, and Hoechst in blue. Scale bar = 50µM.....	136
Figure 37: Representative images showing expression of NeuN neuronal marker in five control iNeurons lines. NeuN is localised to the nucleus, and shown in red whilst Hoechst is shown in blue. Scale bar = 50µM.	137
Figure 38: Representative images showing expression of NeuN neuronal markers in five sAD iNeurons lines. NeuN is localised to the nucleus, and shown in red whilst Hoechst is shown in blue. Scale bar = 50µM.	138
Figure 39: All lines have above 87% TUJ positive cells, all with the exception of sAD 4 have above 60% MAP2 positive cells, and all with the exception of sAD 5 and sAD 6 have between 20% and 75% NeuN positive staining, n > 3.	139
Figure 40: There is no significant difference in TUJ protein levels between control and sAD iNeurons, at an individual or group level.	141
Figure 41: There is an increase in TUJ protein expression in iNeurons compared to iNPCs in each line.....	142
Figure 42: There is no significant difference in NeuN protein levels between control and sAD iNeurons, at an individual or group level.	143
Figure 43: There is an increase in NeuN protein expression in iNeurons compared to iNPCs in each line. ...	144
Figure 44: Representative images of ChAT, and vGlut1 staining in three control iNeuron lines.	146
Figure 45: Representative images of TBR1 staining in three control iNeuron lines.....	147
Figure 46: Representative images of Hb9 staining in three control iNeuron lines..	148
Figure 47: Representative images of ChAT and vGlut1 staining in three sAD iNeuron lines..	149
Figure 48: Representative images of TBR1 staining in three sAD iNeuron lines.....	150
Figure 49: Representative images of Hb9 staining in three sAD iNeuron lines..	151
Figure 50: There is variability in the expression of motor neuron marker Hb9, cholinergic neuron marker ChAT, glutamatergic neuron marker vGlut1, and early cortical neuron marker TBR1 in control and sAD iNeuron lines, n > 3.....	152
Figure 51: Representative images of the neurite outgrowth assay in control 10 and sAD 5, red staining shows the cell membrane stain, green stain shows the cell viability stain, scale bar = 100µM.	154
Figure 52: There is no difference in cell morphology between control and sAD neuron lines, n > 3..	155
Figure 53: Two sAD neuron lines have a significantly smaller cell area, and one sAD neuron line has a significantly increased area, n > 3..	156
Figure 54: sAD 8 has a significantly reduced viability compared to control 2, but there is no significant difference in any other pair, n > 3.....	157
Figure 55: There is no significant difference in neuronal morphology or viability with either low glucose, galactose containing media, or 30nM rotenone treatment. Bars represent the mean of repeats from different differentiations, and error bars show SD, n = 3.	159
Figure 56: Representative images of TMRM, shown in red, and MitoTracker Green staining in control 10 and sAD5 iNeurons. Hoechst staining of the nuclei is shown in blue, scale bar = 50µM.	161
Figure 57: There is a significant decrease in MMP in sAD 6 compared to control 5, but no significant difference in any other pairs, n > 3 with the exception of control 2 and sAD 8 where n = 1. For B-C, each dot represents the average of all biological repeats for one cell line. Errors bars represent SD..	162
Figure 58: There is no significant difference between control and sAD neurons in mitochondrial roundness, mitochondrial area, mitochondrial width, or mitochondrial length, n > 3, with the exception of sAD 8 where	

n = 1. For E-H, each dot represents the average of all biological repeats for one cell line. Errors bars represent SD.	163
Figure 59: There is no significant difference between control and sAD lines in mitochondrial count per cell, the percentage of mitochondria accumulated in the perinuclear region, and the form factor, a measure of mitochondrial interconnectivity, n > 3, with the exception of sAD 8 where n = 1. For D-F, each dot represents the average of all biological repeats for one cell line. Errors bars represent SD.	164
Figure 60: There is no significant difference in the percentage of the area taken up by long or short mitochondria. For C-D, each dot represents the average of all biological repeats for one cell line. Errors bars represent SD.	165
Figure 61: There is no significant difference in mitochondrial membrane potential between control and sAD lines with either low glucose, galactose containing media, or 30nM rotenone treatment.	167
Figure 62: There is a significant increase in Drp1 protein levels in sAD iNPC lines compared to controls.	169
Figure 63: There is a significant increase in Drp1 protein levels one sAD neuron line compared to a paired control.	170
Figure 64: Representative Images of Drp1-TOM20 co-localisation in control and sAD patient iNeurons.	172
Figure 65: There is no significant difference in the amount of Drp1 co-localised to the mitochondria in iNeurons, but a non-significant increase is seen, n = 3 except sAD 8 where n=1.	173
Figure 66: There is a significant increase in Fis1 protein levels in one sAD iNPC line, and a significant decrease in two sAD iNPC lines, compared to paired controls.	176
Figure 67: There is no significant difference in Mff protein levels in sAD iNPCs compared to controls.	177
Figure 68: There is no significant difference in MiD49 protein levels in sAD iNPCs compared to controls.	178
Figure 69: There is no significant difference in MiD51 protein levels in sAD iNPCs compared to controls.	179
Figure 70: Linear regression between protein levels of Drp1 and protein levels of Fis1, Mff, MiD49 and MiD51, in iNPCs.	182
Figure 71: There is a significant increase in Fis1 protein levels in one sAD neuron lines compared to a paired control.	184
Figure 72: There is no significant different in Mff protein levels in sAD neuron lines compared to controls.	185
Figure 73: There is a significant decrease in MiD49 protein levels in sAD neurons compared to controls.	186
Figure 74: There is a significant decrease in MiD51 levels in one sAD neuron line compared to a paired control.	187
Figure 75: Linear regression between protein levels of Drp1 and protein levels of Fis1, Mff, MiD49 and MiD51, in iNeurons.	189
Figure 76: Linear regression between MMP and expression of fission proteins Drp1, Fis1, Mff, MiD49, and MiD51 in iNeurons.	191
Figure 77: Linear regression between form factor and expression of fission proteins Drp1, Fis1, Mff, MiD49, and MiD51 in iNeurons.	193
Figure 78: Linear regression between mitochondrial count per cell normalised to cell area and expression of fission proteins Drp1, Fis1, Mff, MiD49, and MiD51 in iNeurons.	194
Figure 79: Representative Images of Fis1-TOM20 co-localisation in control and sAD patient iNeurons.	198
Figure 80: There is no significant difference in the amount of Fis1 co-localised to the mitochondria in iNeurons, n = 3.	199
Figure 81: Representative Images of Mff-TOM20 co-localisation in control and sAD patient iNeurons.	200
Figure 82: There is a significant increase in the amount of Mff co-localised to the mitochondria in iNeurons in one sAD line and a significant decrease in another line, n = 3.	201
Figure 83: Representative image of Drp1 and Fis1, and Drp1 and Mff interactions in control and sAD iNeurons. Scale bar = 50µM.	203
Figure 84: There is no significant difference in interactions between Drp1 and Fis1 in the whole cell or in the perinuclear region.	204
Figure 85: There is no significant difference in interactions between Drp1 and Mff in the whole cell or in the perinuclear region.	205

Figure 86: There is no significant difference in the number of interactions between Drp1 and Fis1, and the number of interactions between Drp1 and Mff, in the whole cell or the perinuclear region. Each dot represents the average of all biological repeats for one cell line. Errors bars represent SD.	206
Figure 87: There is a significant decrease in pDrp1(s616) protein levels in one sAD iNPC line, and a significant increase in another when compared to paired controls.....	208
Figure 88: There is no significant difference in pDrp1(s616) protein levels between control and sAD iNeurons, at an individual or a group level.....	209
Figure 89: There is a significant decrease in pDrp1(s637) protein levels in one sAD iNeuron line compared to a paired control.	210
Figure 90: A brief overview of the drug screen process carried out in this project.	238
Figure 91: Plate map used for 1536 well plates in the primary screen.	240
Figure 92: Plate map used for 384 well plates in the primary screen.	241
Figure 93: Analysis and segmentation of MMP assay in InCell Developer Toolbox in patient fibroblasts.....	244
Figure 94: Plate map used for dose response screen.....	246
Figure 95: Plate map used to assess dose response in a locally collected cohort of patient and control fibroblasts.....	249
Figure 96: Representative images of treated fibroblasts. The Hoechst stain is shown in blue, representing the nuclei. Green staining shows the mitochondria labelled by TMRM. All contrast settings are the same, set to the DMSO images.	253
Figure 97: Representative graphs showing results for one 1536 well plate.	255
Figure 98: Representative graphs showing compounds which have a positive effect in a sAD fibroblast line do not have the same effect in a PSEN1 fibroblast line. Each bar represents data from one well of a 1536 or 384 well plate.....	256
Figure 99: Representative graphs showing dose response in a range of compounds..	260
Figure 100 Dose response in MMP, Form Factor, and mitochondrial count per cell in two control and three sAD fibroblast lines, in compound E21.....	265
Figure 101: Dose response in MMP, Form Factor, and mitochondrial count per cell in two control and three sAD fibroblast lines, in compound K17.....	267
Figure 102: Dose response in combined controls and combined sAD lines, in MMP, FF, and mitochondrial count per cell, in compounds K17 and E21.....	269
Supplementary Figure 1: Representative images of cells plated at 20,000 per well throughout the first round of differentiation.	294
Supplementary Figure 2: Immunocytochemistry staining of cells on maintenance day 6 of the differentiation protocol, for neuronal marker TUJ and deep layer cortical neuron marker TBR1, scale bar = 50µm..	295
Supplementary Figure 3: Representative images of cells throughout the third round of differentiation.	296
Supplementary Figure 4: Immunocytochemistry staining for deep layer cortical neuron marker TBR1 at maintenance day 9, scale bar = 50µm.	297
Supplementary Figure 5: Representative images of GM04188 throughout the differentiation protocol.....	299
Supplementary Figure 6: Representative images of GM13335 throughout the differentiation protocol.	300
Supplementary Figure 7: Representative brightfield images of GM04188 at day 15 maintenance.	300
Supplementary Figure 8: Representative brightfield images of GM13335 at day 15 maintenance.....	301
Supplementary Figure 9: Representative immunocytochemistry staining for TBR1 and TUJ at maintenance day 15 in the BDNF and 10µM forskolin condition, scale bar = 100µm.....	301
Supplementary Figure 10: Representative images of cells throughout the fifth round of differentiation.....	302
Supplementary Figure 11: Representative brightfield images of GM04188 throughout the protocol at day 303	
Supplementary Figure 12: Immunocytochemistry staining for neuronal markers TUJ and MAP2 at day 23, scale bar = 100µm.....	304
Supplementary Figure 13: Immunocytochemistry staining for neuronal marker NeuN at day 23, scale bar = 100µm.	304
Supplementary Figure 14: Immunocytochemistry staining for upper layer cortical neuronal marker SATB2 at day 23, scale bar = 100µm.....	305

Supplementary Figure 15: Representative images of control 7 and sAD 9 throughout the differentiation protocol.....306
Supplementary Figure 16: Representative images of immunocytochemistry staining for neuronal markers TUJ and MAP2, and cortical neuron marker TBR1 in control 7, at day 13 after maintenance, scale bar = 50µm.307
Supplementary Figure 17: Representative images of control 7 during differentiation when seeded onto different coatings.308
Supplementary Figure 18: Representative images of control 7 with and without the ROCK inhibitor.....309

List of Tables

Table 1: Sex,age, and ApoE Status of cell lines used in this project, which were collected from a local population of patients.	39
Table 2: Sex,age, and ApoE status of cell lines used in this project, which were obtained from the NIGMS Human Genetic Cell Repository at the Coriell Institute for Medical Research.	40
Table 3: iNPC cell lines used, in age and sex matched pairs.	42
Table 4: Plating densities of iNPC lines for iNeuron differentiation.	42
Table 5: Different types of cell culture media used in this project.	44
Table 6: BSA standards used in Bradford Assay to produce a standard curve	46
Table 7: Reagents used to make up 4x sample buffer	46
Table 8: Reagents used to make up 12% resolving gel	47
Table 9: Reagents used to make up stacking gel	47
Table 10: Reagents used to make up SDS-PAGE running buffer	48
Table 11: Reagents used to make up transfer buffer	49
Table 12: Primary antibody used in western blotting.	50
Table 13: Secondary antibody used in western blotting	50
Table 14: Primary antibody used in immunocytochemistry.	52
Table 15: Secondary antibody used in immunocytochemistry	52
Table 16: Primary antibody used in the PLA	55
Table 17: Summary table of total protein levels of Drp1 and the four Drp1 receptors on the outer mitochondria membrane, Fis1, Mff, MiD49, and MiD51, in sAD patient fibroblasts.	80
Table 18: Age and sex matched pairs used in this chapter.	131
Table 19: Summary table of total protein levels of Drp1 and the four Drp1 receptors on the outer mitochondria membrane, Fis1, Mff, MiD49, and MiD51 in iNPCs.	180
Table 20: Summary table of total protein levels of Drp1 and the four Drp1 receptors on the outer mitochondria membrane, Fis1, Mff, MiD49, and MiD51 in iNeurons.	188
Table 21: A summary of total protein levels of Drp1 and the four Drp1 receptors on the outer mitochondria membrane, Fis1, Mff, MiD49, and MiD51 in fibroblasts, iNPCs, and iNeuron.	196
Table 22: The performance of the top 11 compounds across all stages of the screen, in MMP, form factor, and mitochondrial count per cell.	270
Table 23: The name and structure of the top 11 compounds identified in this screen.	278
Supplementary Table 1: Conditions used for cortical neuron differentiation optimisation.	291

List of Abbreviations

AD	Alzheimer's Disease
ADP	Adenosine Diphosphate
ALS	Amyotrophic Lateral Sclerosis
AMPK	AMP-Activated Protein Kinase
ApoE4	Apolipoprotein E epsilon 4
APP	Amyloid Precursor Protein
APS	Ammonium Persulphate
ATP	Adenosine Triphosphate
Aβ	Amyloid Beta
BAP31	B Cell Receptor-Associated Protein 31
BDNF	Brain Derived Neurotrophic Factor
BSA	Bovine Serum Albumin
CCCP	Carbonyl Cyanide M-Chlorophenyl Hydrazone
ChAT	Choline Acetyltransferase
CNS	Central Nervous System
CNTF	Ciliary Neurotrophic Factor
CTIP2	COUP TF1-interacting protein 2
CUX1	Cut-Like Homeobox 1
DAPT	N-[N-(3,5-difluorophenacetyl)-l-alanyl]-S-phenylglycine t-butyl ester
DMEM	Dulbecco's Modified Essential Media
DMSO	Dimethyl Sulfoxide
Dnm1	Dynamin 1
Dnm2	Dynamin 2
Dnm3	Dynamin 3
Drp1	Dynamin Related Protein 1
DTT	Dithiothreitol
EGF	Epidermal Growth Factor
EMEM	Eagle's Minimum Essential Media
ER	Endoplasmic Reticulum
fAD	Familial Alzheimer's Disease
FBS	Foetal Bovine Serum
FGFb	Fibroblast Growth Factor Basic
Fis1	Fission 1
GABA	Gamma-Aminobutyric Acid
Gal	Galactose Containing Media
Gal+Rot	Galactose Containing Media with 30mM Rotenone Treatment
GDAP1	Ganglioside-Induced Differentiation Associated Protein 1
Glu	Glucose Containing Media
GRP75	Glucose Regulated Protein 75
GTP	Guanosine Triphosphate
Hb9	Homeobox 9
IMM	Inner Mitochondrial Membrane
INF2	Inverted Formin 2

iNPCs	Induced Neural Progenitor Cells
IP3R	Inositol Triphosphate Receptor
iPSCs	Induced Pluripotent Stem Cells
LB	Luria-Bertani
LDV	Low Dead Volume
L-OPA1	Long Form Optic Atrophy 1
LRRK2	Leucine Rich Repeat Kinase 2
MAP2	Microtubule Associated Protein 2
MAVs	Mitochondrial Antiviral Signalling Protein
MDIVI1	Mitochondrial Division Inhibitor 1
MEM	Phenol Red Free Minimum Essential Media
Mff	Mitochondrial Fission Factor
Mfn1	Mitofusin 1
Mfn2	Mitofusin 2
MiD49	Mitochondrial Dynamic Protein of 49kDa
MiD51	Mitochondrial Dynamic Protein of 51kDa
MitoQ	Mitoquinone
MMP	Mitochondrial Membrane Potential
MPTP	1-methyl-4-phenyl-1,2,3,6-tetrahydropyridine
MRI	Magnetic Resonance Imaging
mtDNA	Mitochondrial DNA
NEAA	Non-Essential Amino Acids
NeuN	Neuronal Nuclei
NFTs	Neurofibrillary Tangles
NFkB	Nuclear Factor kB
NGN2	Neurogenin 2
NRF1	Nuclear Respiratory Factor 1
NRF2	Nuclear Factor-Erythroid Factor 2-Related Factor 2
OMM	Outer Mitochondrial Membrane
OPA1	Optic Atrophy 1
OXPHOS	Oxidative Phosphorylation
PAGE	Polyacrylamide Gel Electrophoresis
PAX6	Paired Box 6
PBS	Phosphate Buffered Saline
PBST	Phosphate Buffered Saline with Tween 20
PD	Parkinson's Disease
PEI	Polyethylenimine
PET	Positron Emission Topography
PEX19	Peroxisomal Biogenesis Factor 19
PFA	Paraformaldehyde
PGC1α	Proliferator Activated Receptor γ Coactivator 1 α
PIC	Protease Inhibitor Cocktail
PINK1	PTEN-Induced Kinase 1
PLA	Proximity Ligation Assay
pLo	Poly-Ornithine
PMP70	Peroxisomal Membrane Protein 70

PPARγ	Peroxisome Proliferator-Activated Receptor
PSD95	Post Synaptic Density Protein 95
PSEN1	Presenilin 1
PSEN2	Presenilin 2
PTPIP51	Protein Tyrosine Phosphatase Interacting Protein 51
PVDF	Polyvinylidene Fluoride Membrane
RA	Retinoic Acid
RIPA	Radioimmunoprecipitation Assay
RLRs	Retinoic Acid-Inducible Gene I-Like Receptors
ROCK	Rho Kinase
ROS	Reactive Oxygen Species
sAD	Sporadic Alzheimer's Disease
SAG	Smoothened Agonist
sAPPα	Soluble Amyloid Precursor Protein Alpha
sAPPβ	Soluble Amyloid Precursor Protein Beta
SATB2	Special AT-Rich Sequence Binding Protein 2
SD	Standard Deviation
SDS	Sodium Dodecyl Sulphate
SENPs	SUMO Specific Proteases
siRNA	Small Interfering RNA
SNO-Drp1	S-Nitrosylated Drp1
SOD1	Superoxide Dismutase 1
S-OPA1	Short Form Optic Atrophy 1
SOX2	SRY-Box Transcription Factor 2
SS	Szeto-Schiller
SUMO	Small Ubiquitin-Related Modifier Protein
TBC1D15	TBC1 Domain Family Member 15
TBC1D17	TBC1 Domain Family Member 17
TBK1	Tank Binding Kinase
TBR1	T Box, Brain 1
TBST	Tris Buffered Saline with Tween 20
TEMED	Tetramethylethyl Enediamine
TERF2	Telomeric Repeat Binding Factor
TFAM	Transcription Factor A
TGFβ	Transforming Growth Factor β
TMRM	Tetramethylrhodamine, methyl ester
TOM20	Translocase of Outer Mitochondrial Membrane 20
TPP	Triphenylphosphonium
TUDCA	Taurine Conjugated Ursodeoxycholic Acid
TUJ	Beta-III-Tubulin
UDCA	Ursodeoxycholic Acid
ULK1	Unc-51 Like Autophagy Activating Kinase
VAPB	Vesicle-Associated Membrane Protein-Associated Protein B
vGlut1	Vesicular Glutamate Transporter 1

Chapter One: Introduction

1.1 Introduction to Alzheimer's disease

1.1.1 Alzheimer's disease

Alzheimer's disease (AD) is a neurodegenerative disease, which is both progressive and incurable. It is the most common cause of dementia, a syndrome affecting memory and behaviour, which has a significant impact on patients, families, and caregivers. Early symptoms include changes in mood such as heightened anxiety or apathy, disruptions to sleep, and forgetfulness, before progressing to more advanced symptoms including major changes in behaviour, severe cognitive decline, disorientation, and confusion (Atri, 2019).

The most recent estimates suggest that there are almost 885,000 people living with dementia in the UK alone, and it is expected that this number will rise to approximately 1.6 million by 2040 (Wittenberg, Hu, and Barraza-Araiza, 2019). This is primarily driven by the ageing population. The biggest risk factor for dementia is age; as life expectancy increases, so too does the prevalence of dementia. With prevalence increasing, it is more important than ever to research the pathological mechanisms and potential therapeutics for AD.

Most cases of AD occur sporadically (sAD), but a small number are caused by genetic mutations (familial AD; fAD), in the amyloid precursor protein (APP), presenilin 1 (PSEN1) or presenilin 2 (PSEN2) genes, with PSEN1 mutations being the most common. Though they share many clinical symptoms, fAD usually has an earlier age of onset and more aggressive progression than sAD (Joshi *et al.*, 2012).

sAD is a complex and multifactorial disease, with many associated risk factors. As well as increasing age, there are genetic risk factors, with possession of the apolipoprotein E epsilon 4 (ApoE4) allele conferring the greatest risk. Genome wide association studies (GWAS) have identified many other genes associated with sAD, including triggering receptor expressed on myeloid cells 2 (TREM2), clusterin (CLU), bridging integrator 1 (BIN1), and complement receptor 1 (CR1) (Misra, Chakrabarti and Gambhir, 2018). A recent large GWAS identified 75 risk loci, with pathway enrichment analysis confirming the involvement of amyloid and tau pathways, and highlighting the involvement of innate immunity, inflammation, and microglia (Bellenguez *et al.*, 2022). Other risk factors for sAD include co-morbidities such as diabetes, vascular disease, hearing impairment, and traumatic brain injury, and environmental factors such as diet and air pollution (Livingston *et al.*, 2020). This complex aetiology has impacted understanding and treatment of sporadic disease.

1.1.2 Alzheimer's disease Neuropathology

AD was first reported by German psychiatrist Alois Alzheimer (1907), where he described the behavioural changes and memory impairment of a patient over the last five years of her life, and his post mortem findings of atrophy and unusual fibrils (Alzheimer, 1907; Stelzmann, Schnitzlein, & Murtagh, 1995). These days, AD pathology is defined as the presence of extracellular amyloid beta (A β) plaques and intracellular tau-containing neurofibrillary tangles (NFTs), and brain atrophy, particularly in the cortex (Balin and Hudson, 2014).

Many therapeutic approaches, and much research has focussed on the amyloid cascade hypothesis. Proposed by Hardy and Higgins (1992), this hypothesis states that it is the accumulation of A β plaques which directly leads to other pathology, such as NFTs, brain atrophy and cognitive decline. Evidence for the central role of A β in AD comes from the role of fAD associated genes in amyloid processing. APP is the precursor protein from which A β can be derived. In the non-amyloidogenic pathway, APP is cleaved by α secretase, resulting in the release of soluble APP α (sAPP α) (Chen *et al.*, 2017). In the amyloidogenic pathway, APP is instead cleaved by β secretase, resulting in the release of soluble APP β (sAPP β) which can be further processed by γ secretase to produce A β (Chen *et al.*, 2017). While the precise role of A β in a healthy system is not precisely understood, A β monomers have been proposed to be neuroprotective and neurotrophic, suggesting they play a key role (Chasseigneaux and Allinquant, 2012). A β monomers can go on to aggregate into various forms including large, insoluble fibrils, which can then go onto form plaques, and smaller, soluble oligomers (Chen *et al.*, 2017). PSEN1 and PSEN2 are key components of γ secretase, and mutations in these genes can lead to the abnormal processing of APP, including an increase in the production of A β 42 (Jankowsky *et al.*, 2004), the main component of amyloid plaques (Gu and Guo, 2013).

However, the amyloid cascade hypothesis has proved to be controversial. Amyloid plaque burden post mortem does not correlate well with disease progression (Savva *et al.*, 2009). As such, the hypothesis has been questioned and revised, and recently the A β oligomer hypothesis has become more widely accepted. This hypothesis implicates oligomers as the more toxic form of A β (Cline *et al.*, 2018).

Research has also turned to tau, the main component of neurofibrillary tangles. Tau is involved in many neurodegenerative diseases, called tauopathies, with many caused by autosomal dominant mutations in the gene encoding for tau, *MAPT*, including frontotemporal dementia with parkinsonism (Hutton *et al.*, 1998). Whilst tau has been implicated in microtubule assembly (Weingarten *et al.*, 1975), a neuron specific function has yet to be identified (Naseri *et al.*, 2019).

Post translational modification of tau has been shown to be important in AD pathology, in particular phosphorylation. Hyperphosphorylation of tau has been found to induce assembly into tangles (Alonso *et al.*, 2001), and indeed hyperphosphorylated tau is enriched in NFTs (Naseri *et al.*, 2019).

Unlike A β plaques, tau has been shown to correlate with the severity of AD symptoms (Arriagada *et al.*, 1992; Bierer *et al.*, 1995; Giannakopoulos *et al.*, 2003; Saint-Aubert *et al.*, 2016; Buckley *et al.*, 2017), though as with A β , it remains unclear whether the toxic form of tau is the fibrils themselves, or the soluble oligomers. Nevertheless, tau accumulation as measured by positron emission tomography (PET) imaging is emerging as a biomarker for AD (Naseri *et al.*, 2019).

1.1.3 Current Treatments and Therapeutic Strategies for Alzheimer's disease

Current treatments for AD are limited, only providing temporary symptomatic relief for some patients. Three of the licensed drugs for AD, donepezil, galantamine and rivastigmine, are targeted at the inhibition of acetylcholinesterase, an enzyme which breaks down the neurotransmitter acetylcholine. A meta-analysis found that on average, acetylcholinesterase inhibitors only delay cognitive decline by approximately 3 months (Knight *et al.*, 2018). Another licensed drug for AD is memantine, which blocks NMDA receptors in the glutamatergic system, and has a small effect on cognitive decline in patients with moderate to severe AD (Van Marum, 2009).

Many therapeutic strategies have focussed on the clearance of A β , though many proved to be unsuccessful in clinical trials (Doody *et al.*, 2013, 2014), despite promising preclinical results. However, aducanumab, a monoclonal antibody targeted at clearing A β and produced by Biogen, was recently approved for use in the treatment of AD by the US Food and Drug Administration. However, this approval was not without controversy, with other regulatory bodies including the European Medicines Agency refusing approval due to a lack of evidence of both safety and efficacy (Lythgoe, Jenei and Prasad, 2022). Whilst research into therapies targeting A β clearance is ongoing, it is clear that other therapeutic targets must also be studied.

These alternative therapeutic targets are varied; there are many underlying mechanisms implicated in AD pathology, some of which are outlined in figure 1. It is unlikely that any of these individual mechanisms act in isolation, instead interacting with each other, and this complexity is a significant factor in the difficulty in finding an effective, disease modifying treatment for AD.

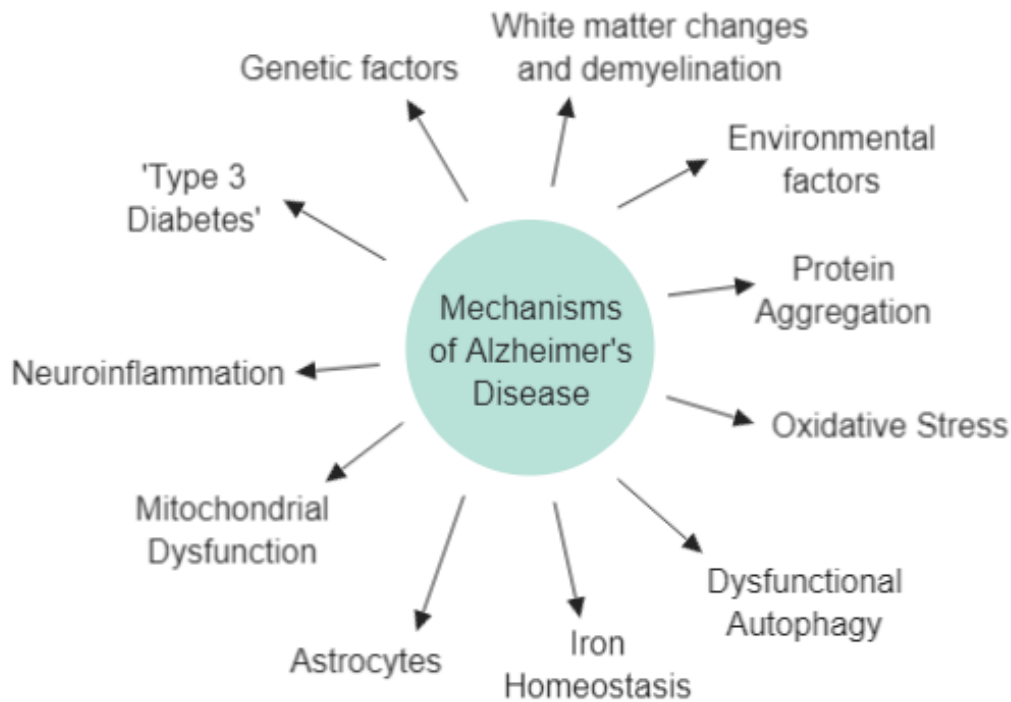


Figure 1: Some of the key mechanisms implicated in AD. Many cellular processes have been proposed to contribute to AD pathology, alongside protein aggregations. Genetic factors such as carrying the ApoE4 allele confer increased risk of developing AD, as well as environmental factors such as diet (Grant et al., 2002). AD has been linked to insulin resistance and has comorbidity with type 2 diabetes, leading to AD being described as 'type 3 diabetes' (Sharma et al., 2018). Key cellular processes such as autophagy, an essential degradation pathway which removes abnormal aggregations and damaged components from the cell, have been seen to be dysfunctional (Uddin et al., 2018). Iron homeostasis has also been proposed to contribute; increased iron deposition has been seen in AD patient brains which co-localises with amyloid plaques (Liu et al., 2018). Oxidative stress has also been implicated; neurons are more vulnerable to reactive oxygen species (ROS) due to their high oxygen consumption and a lack of antioxidant enzymes (Sharma et al., 2018). Glial cell dysfunction has also been proposed to contribute to neuronal loss; astrocytes have been seen to become reactive, undergoing molecular and morphological changes, which may affect their ability to support the neuron (Cassé et al., 2018). Microglia, which mediate the immune response in the brain, have been seen to induce an abnormal neuroinflammatory response which has also been proposed to contribute to AD pathology (Marttinen et al., 2018). There is also evidence of white matter alterations and demyelination, implicating oligodendrocytes (Nasrabad et al., 2018).

1.2 Introduction to Mitochondria

1.2.1 Mitochondrial Structure and Functions

Mitochondria are essential organelles, thought to have evolved from endo-symbiotic bacteria (Yang *et al.*, 1985; Roger, Muñoz-Gómez and Kamikawa, 2017). Mitochondria are double membrane bound, consisting of both an inner and an outer membrane. These membranes form several compartments within a mitochondrion; the mitochondrial matrix, the innermost compartment surrounded by the inner mitochondria membrane, the intermembrane space, between the two membranes, and the cristae, formed by the folding of the inner mitochondrial membrane (Kühlbrandt, 2015). Mitochondria also contain their own DNA (mtDNA), which encodes for many proteins critical to mitochondrial function. It forms closed circle, double stranded DNA, and is packed into nucleoids, which are distributed throughout the mitochondrial matrix (C. Yan *et al.*, 2019).

Mitochondria are important organelles, involved in several key cellular processes. One of their main functions is the generation of adenosine triphosphate (ATP) via oxidative phosphorylation (OXPHOS). This is carried out by the electron transport chain (ETC), which consists of five complexes, located on the inner mitochondrial membrane. During OXPHOS, hydrogen ions are pumped across the inner mitochondrial membrane into the intermembrane space by complexes I, III, and IV. This produces an electrochemical gradient across the membrane, which drives the synthesis of ATP by ATP synthase (complex V). Mitochondria also play an important role in several other key cellular processes including autophagy, intracellular signalling, and apoptosis (Golpich *et al.*, 2017).

A consequence of OXPHOS is the production of reactive oxygen species (ROS), mainly from complexes I and III. In a healthy system, ROS help to regulate growth, apoptosis, and other cellular signalling pathways, and play a key role in the immune system and inflammatory response. However, the balance of the production and clearance of ROS must be strictly maintained. This balance is maintained by antioxidants such as superoxide dismutases, thioredoxins, and glutathione peroxidases. An increase in ROS can cause oxidative stress, which can cause damage throughout the cell, including to the mitochondria themselves (Brieger *et al.*, 2012).

1.2.2 Mitochondrial Morphology and Quality Control

The bioenergetic needs of a cell continually fluctuate, and the mitochondria must be able to respond to these changes. As such, they form a highly complex and adaptable network within the cell, with constantly shifting morphology and distribution. This morphology is controlled by dynamic processes such as mitochondrial fusion and fission. A delicate balance between these two processes is essential to maintain a healthy population of mitochondria, and disruption to this balance can greatly impact mitochondrial function.

Mitochondrial fusion is the joining of two mitochondria, and is important for the exchange of contents, and cross-complementation of mtDNA to reduce accumulation of mutant mtDNA. Fusion is key under stress and starvation conditions as it can maximise the efficiency of mitochondrial metabolism via the sharing of metabolites (Tilokani *et al.*, 2018). During fusion, mitofusin 1 (Mfn1) and mitofusin 2 (Mfn2) form a tether between the two mitochondria and mediate the fusion of the outer mitochondrial membranes via guanosine triphosphate (GTP)ase activity. On the inner mitochondrial membrane, long form optic atrophy 1 (OPA1) interacts with cardiolipin on the opposite mitochondrion, then mediates inner membrane fusion, again via GTPase activity (Tadato *et al.*, 2010). This process is shown in figure 2.

The role of OPA1 has proven to be somewhat controversial. OPA1 is cleaved by metalloprotease OMA1 (Ehses *et al.*, 2009; Head *et al.*, 2009) to give long form OPA1 (L-OPA1) and short form OPA1 (S-OPA1). This often occurs in response to stress (Ehses *et al.*, 2009; Head *et al.*, 2009; Lee *et al.*, 2020; Gilkerson, De La Torre and St. Vallier, 2021). Whilst L-OPA1 is sufficient for mitochondrial fusion to take place (Anand *et al.*, 2014), the role of S-OPA1 is less clearly defined, though it has been linked to cell survival and maintenance of cristae (Lee, Smith and Yoon, 2017; Gilkerson, De La Torre and St. Vallier, 2021). It has also been suggested that it plays a role in fusion (Song *et al.*, 2007; Ge *et al.*, 2020), or in fission, as expression of S-OPA1 promoted mitochondrial fragmentation (Anand *et al.*, 2014).

Mitochondrial fission is the division of a mitochondrion into two daughter mitochondria. Fission is important for mitochondrial distribution, the removal of dysfunctional mitochondria, and mitochondrial biogenesis. It also occurs during apoptosis, and promotes the release of cytochrome c (Tilokani *et al.*, 2018). Fission is regulated by dynamin related protein 1 (Drp1). Alternative splicing of Drp1 can give up to 8 different isoforms, with cell type specific expression. Drp1 usually resides in the cytosol, but is recruited to the mitochondria during fission events by four receptors located on the outer mitochondrial membrane; fission 1 (Fis1), mitochondrial fission factor (Mff), and mitochondrial dynamic proteins of 49kDa and 51kDa (MiD49/MiD51). There is a partial redundancy in this recruitment system. All four Drp1 receptors are capable of recruiting Drp1 independently (Loson *et al.*, 2013), though the precise mechanism by which these four receptors interact is not well understood.

Fis1 was the first proposed receptor for Drp1 based on its discovery as an important outer mitochondrial membrane protein involved in the fission pathway in yeast, required for the localisation of dynamin 1 (Dnm1; yeast orthologue of Drp1) to the mitochondria (Mozdy, McCaffery and Shaw, 2000). It was identified as a component of mammalian fission machinery by James *et al.* (2003), as overexpression of Fis1 in HEK293, COS-7, and HeLa cells was seen to promote

mitochondrial fragmentation. Soon after, it was shown to interact with Drp1 (Yoon *et al.*, 2003), and be actively involved in the recruitment of Drp1 to the mitochondria from the cytosol (Yu *et al.*, 2005). However, there is some doubt about the necessity of Fis1 for fission to take place; deletion of Fis1 does not inhibit mitochondrial fission or lead to an increase in elongation (Otera *et al.*, 2010; Loson *et al.*, 2013).

Mff was the second discovered Drp1 receptor, initially identified in a small interfering RNA (siRNA) screen in *Drosophila* cells, and found to be a component of the mammalian fission machinery as transfection of Mff siRNA led to inhibition of mitochondrial fission and similar elongated morphology to cells transfected with Drp1 siRNA (Gandre-Babbe and van der Bliek, 2008). Overexpression of Mff in mammalian cells was found to increase recruitment of Drp1 to the mitochondria, and increase mitochondrial fission. Furthermore, knockdown of Mff led to an impairment of fission, in contrast to knockdown of Fis1 which had no significant effect, suggesting Mff is more important for fission to take place (Otera *et al.*, 2010; Loson *et al.*, 2013). It has been proposed the Mff selectively recruits active Drp1, which may explain why it is the more significant receptor in fission (Liu and Chan, 2015).

MiD49 and MiD51 are the most recently discovered, and most poorly understood, Drp1 receptors. MiD49 was first thought to be involved in Smith Magenis Syndrome, though this was later proven wrong (Slager *et al.*, 2003), whilst MiD51 was originally identified in a screen of uncharacterised human proteins, and found to affect mitochondrial distribution (Simpson *et al.*, 2000). It wasn't until several years later that Palmer *et al.* (2011) showed these proteins are localised to the mitochondria and are involved in the recruitment of Drp1. Both were found to be present at mitochondrial constriction sites, and knockdown was seen to lead to a more fused mitochondrial network, suggesting they play a role in mitochondrial fission. At a similar time, Zhao *et al.* (2011) also identified MiD51 (which they named mitochondrial elongation factor 1), and also found an interaction with Drp1. However, rather than an involvement with fission, they proposed that MiD51 promoted fusion and elongation of the mitochondria, as when it was overexpressed, they saw a more fused network. The same group later found many functional similarities with MiD49 (T. Liu *et al.*, 2013). In order to reconcile these differing findings, Palmer *et al.*, (2013) proposed that the fused network seen when MiD51 and MiD49 were overexpressed was due to inactivation of Drp1 at the mitochondrial membrane. This theory was further supported by Loson *et al.* (2013), who found that expression of either MiD49 or MiD51 in Fis1/Mff null mutants led to a partial rescue of Drp1 recruitment. They also saw a more fused network when MiD49 or MiD51 were overexpressed, but this was associated with an increase in Drp1 at the mitochondria, again supporting the hypothesis that MiD49 and MiD51 recruit inactive Drp1.

Once recruited to the mitochondria, Drp1 assembles into an oligomeric ring structure around the mitochondrion. GTP hydrolysis enables the constriction of this ring structure, leading to mitochondrial constriction. Another important consideration in the mitochondrial fission process is the post translational modifications of Drp1. In order to be active, it is thought that Drp1 must be phosphorylated at ser616 (Kashatus *et al.*, 2015) and dephosphorylated at ser637, as phosphorylation at this site has been seen to inhibit GTPase activity (Cribbs and Strack, 2007). Whilst it was originally thought that phosphorylation at ser637 prevented translocation to the mitochondria (Cereghetti *et al.*, 2008), more recently Drp1 phosphorylation status at ser637 has been seen to have no effect on recruitment to the mitochondria (Yu, Liu, *et al.*, 2019). This can be explained by the recruitment of inactive Drp1, and suggests that further triggers may be required at the mitochondrial membrane to initiate fission.

The final scission mechanism, physically separating the two mitochondria, remains somewhat unclear. It has been suggested that this process may involve dynamin 2 (Dnm2), another dynamin related protein. Dnm2 was seen to be present at mitochondria where Drp1 was also co-localised and knockdown of Dnm2 leads to a hyper-fused mitochondrial network (Lee *et al.*, 2016). However, it has since been shown that the absence of Dnm1, Dnm2, or dynamin 3 (Dnm3), had no effect on mitochondrial morphology or fission in mouse fibroblasts, whereas even a partial knockdown of Drp1 led to hyper-fusion of the network (Fonseca *et al.*, 2019). This suggests that only Drp1 is essential for fission to take place, and implies that Drp1 itself is sufficient for the final scission to take place. An overview of the mitochondrial fission process is outlined in figure 2.

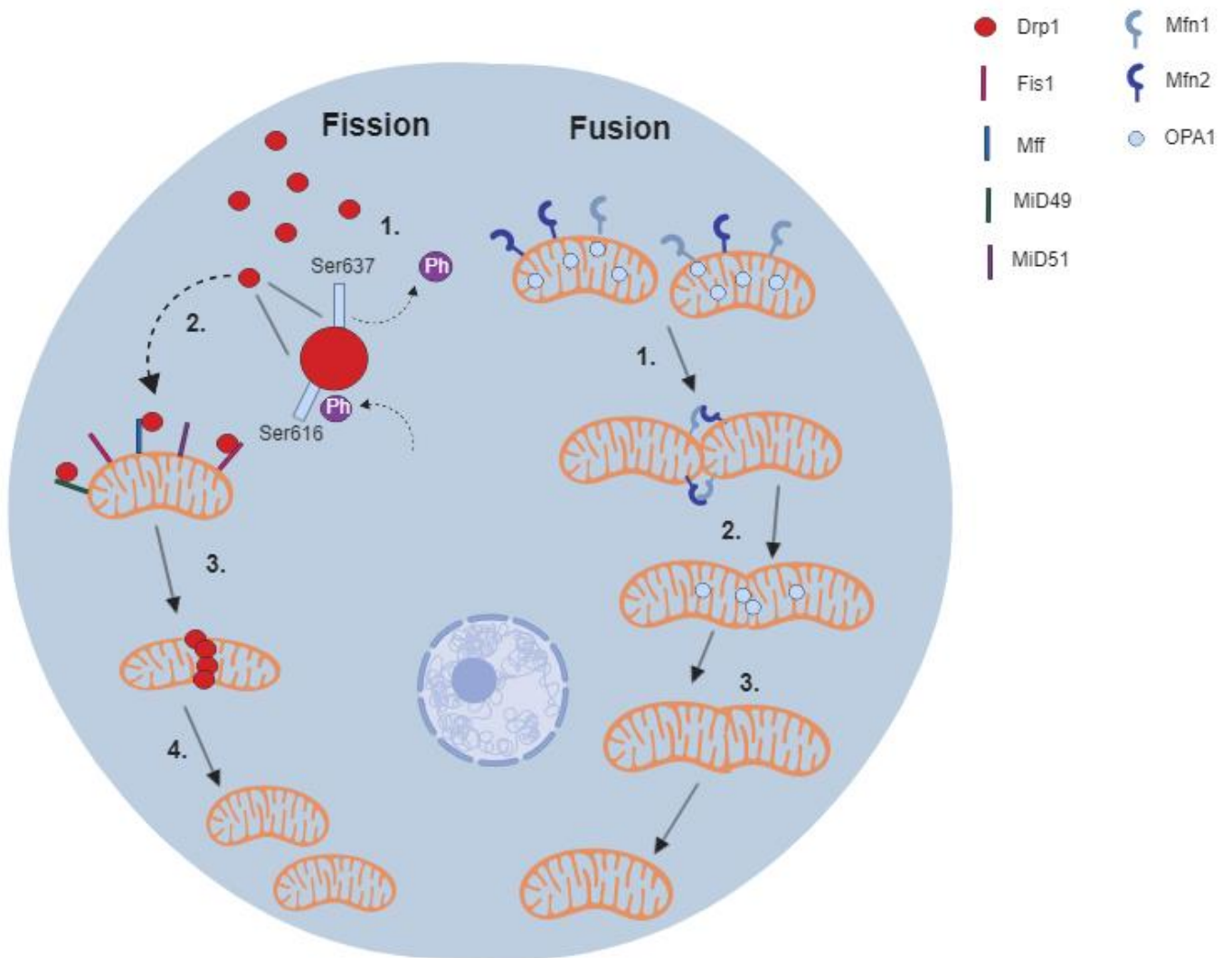


Figure 2: The mitochondrial dynamic processes of fission and fusion. The following steps occur during mitochondrial fission. 1. Drp1 is dephosphorylated at ser637, and phosphorylated at ser616, inducing a fission event. 2. Drp1 is recruited from the cytosol to the mitochondria by several receptors on the mitochondrial membrane; Fission1 (Fis1), Mitochondrial fission factor (Mff), Mitochondrial dynamic protein of 49kDa (MiD49) and Mitochondrial dynamic protein of 51kDa (MiD51). 3. Drp1 forms a ring structure around the mitochondrion. 4. The ring structure contracts, enabling the mitochondrion to divide into two mitochondria. The following steps occur during mitochondrial fusion. 1. Mfn1 and Mfn2 on the outer mitochondrial membrane (OMM) mediate fusion of the OMMs. 2. OPA1 mediates fusion of the inner mitochondrial membranes (IMM). 3. The contents of the mitochondria mix, forming one mitochondrion.

Following mitochondrial fission, damaged mitochondria are cleared from the cell via mitophagy. Mitophagy can occur via several pathways, but the most well studied is the PTEN-induced kinase 1 (PINK1)/Parkin pathway. PINK1 stabilises on the outer membrane of damaged mitochondria, where it phosphorylates ubiquitin, which then leads to the recruitment of the e3 ubiquitin ligase, parkin. This ultimately leads to the formation of the mitophagosome, which then fuses with the lysosome, leading to mitochondrial degradation. It has also been shown that mitophagy can occur in a parkin-independent manner (Fivenson *et al.*, 2017). Some of the proteins associated with mitochondrial fission have also been linked to mitophagy. For example, Fis1 is proposed to play a role (Shen *et al.*, 2014; Yamano *et al.*, 2014), and PINK1 has been implicated in the phosphorylation of Drp1 at ser616 (Han *et al.*, 2020).

1.2.3 Mitochondrial Contact with Other Organelles

The mitochondria do not act in isolation in the cell, instead forming contacts and working alongside several other organelles. Mitochondria have been shown to form direct contact with the nucleus (Desai *et al.*, 2020), lysosomes (Wong, Ysselstein and Krainc, 2018), and the plasma membrane (Montes de Oca Balderas, 2021). However, the most well defined contact sites are between the mitochondria and the endoplasmic reticulum (ER). Mitochondria-ER contact sites regulate several cellular processes including calcium homeostasis, lipid transfer, and autophagy (Xu, Wang and Tong, 2020). There are several types of contact site, with different tethering proteins involved including vesicle-associated membrane protein-associated protein B (VAPB)- protein tyrosine phosphatase interacting protein 51 (PTPIP51), B cell receptor-associated protein 31 (BAP31)-Fis1, voltage dependent anion channel (VDAC)- glucose regulated protein 75 (GRP75)- inositol triphosphate receptor (IP3R), and ER located Mfn2-mitochondrial Mfn1/2 (Xu, Wang and Tong, 2020), with some tethering proteins known to have specific functions such as VDAC-GRP75-IP3R, which is thought to be involved in calcium homeostasis (Wilson and Metzakopian, 2021).

Mitochondria-ER contact sites also play an important role in mitochondrial fission. A pre-constriction step is thought to take place before the recruitment of Drp1. The ring structure formed by Drp1 is much smaller than the diameter of the mitochondria, suggesting a prior, Drp1 independent mechanism (Friedman *et al.*, 2011). It is this pre-constriction step which involves the mitochondria-ER contact sites; a large proportion of fission events take place at contact sites, and both Drp1 and Mff localise to these sites (Friedman *et al.*, 2011; Korobova, Ramabhadran and Higgs, 2013). Several proteins have been implicated in this pre-constriction including ER localised inverted formin 2 (INF2), and mitochondrial Spire1c. These proteins work together to initiate the polymerisation of actin

(Korobova, Ramabhadran and Higgs, 2013; Chakrabarti *et al.*, 2018). Myosin II then enables the contraction of actin, which provides the mechanical force required for constriction of the mitochondria (Chakrabarti *et al.*, 2018).

1.2.4 Mitochondria in Disease

Given the essential role of the mitochondria in metabolism and cell survival, it is unsurprising that mitochondrial dysfunction is involved in a wide range of diseases. These include primary mitochondrial diseases, a group of genetic disorders arising from mutations in either mtDNA or nuclear genes encoding mitochondrial proteins. Symptoms can arise in either childhood or adulthood, with childhood disease often showing a more severe progression and a worse prognosis (Ng and Turnbull, 2016). The mutations associated with mitochondrial diseases usually affect proteins involved in oxidative phosphorylation, therefore impacting the ability of the mitochondria to produce enough energy, leading to a heterogeneous presentation of clinical symptoms, which can affect either one or many tissues, often those with the highest energy demand (Alston *et al.*, 2017). Mutations in genes involved in mitochondrial fusion and fission also cause diseases. Mutations in *Mfn2* cause Charcot-Marie-Tooth disease, a progressive neuropathy which causes muscle weakness (Morena, Gupta and Hoyle, 2019), whilst mutations in *OPA1* cause an optic neuropathy (Alward, 2003). Mitochondrial dysfunction has also been found to play a role in cancer pathology, in particular an overproduction of ROS, causing oxidative stress, thus increasing genomic instability, and modification of gene expression (Yang *et al.*, 2016).

Mitochondria are also involved in many neurodegenerative diseases. Neurons require a large amount of energy, around 4.7 billion molecules of ATP a second. They have a limited capacity for producing ATP via other pathways such as glycolysis, and so are heavily reliant on the efficient functioning of mitochondria (Hu *et al.*, 2017). Other neural cell types such as astrocytes and microglia rely mainly on glycolysis for ATP production, though mitochondria still play an important role in glial cell function (Rose *et al.*, 2017). Mitochondrial dysfunction is seen in amyotrophic lateral sclerosis (ALS; reviewed by Smith, Shaw and De Vos, 2019), a neurodegenerative disease characterised by the loss of upper and lower motor neurons and muscle atrophy. Complexes I, II, III, and IV of the ETC have been seen to be reduced in post mortem spinal cord (Wiedemann *et al.*, 2002), and ATP is reduced in lymphocytes from sporadic ALS patients (Ghiasi *et al.*, 2012). An imbalance in fission and fusion has also been seen, with the balance shifting towards an increase in fission (W. Liu *et al.*, 2013). Furthermore, some of the genes causing genetic forms of ALS are associated with the mitochondria, for example superoxide dismutase 1 (SOD1), an antioxidant.

A mitochondrial phenotype is also clearly seen in Parkinson's disease (PD; reviewed by Macdonald *et al.*, 2018), a motor disorder characterised by the loss of dopaminergic neurons in the substantia nigra leading to bradykinesia, a resting tremor, and muscle rigidity. This was first identified when drug users who had taken 1-methyl-4-phenyl-1,2,3,6-tetrahydropyridine (MPTP), which metabolises to complex I inhibitor MPP⁺, developed Parkinson's like symptoms (Ballard, Tetrud and Langston, 1985). Complex I deficiency in PD was soon confirmed in sporadic PD patient post mortem tissue (Schapira *et al.*, 1989, 1990). Several genetic causes of PD also have links to mitochondrial function, including mutations in leucine rich repeat kinase 2 (LRRK2), PINK1, and Parkin. LRRK2 has been shown to impact several mitochondrial processes including fission and fusion, mitophagy, and calcium homeostasis (Singh, Zhi and Zhang, 2019), while PINK1 and Parkin play significant roles in mitophagy (Fivenson *et al.*, 2017).

1.3 Mitochondria in Alzheimer's disease

1.3.1 Mitochondrial Functional Abnormalities in Alzheimer's disease

The association between mitochondrial dysfunction and AD is long standing. The earliest studies linking mitochondria and AD found abnormal mitochondria with increased matrix density in cortical dendrites from the frontal cortex of AD patients (Saraiva *et al.*, 1985), and impaired glucose metabolism in patient fibroblasts (Peterson and Goldman, 1986). One of the earliest discovered, and most consistently seen, pathogenic mechanisms is an impairment in complex IV of the electron transport chain. Reductions in complex IV have been consistently seen across multiple brain areas including the hippocampus and frontal, temporal and parietal cortices (Kish *et al.*, 1992; Mutisya, Bowling and Beal, 1994; Maurer, Zierz and Möller, 2000). Other patient derived models such as fibroblasts (Curti *et al.*, 1997), blood platelets (Parker, Filley and Parks, 1990; Parker, 1991; Parker *et al.*, 1994; Bosetti *et al.*, 2002), and plasma extracellular vesicles (Yao *et al.*, 2021) have also shown a decrease in complex IV activity, as have animal models including both transgenic (Hauptmann *et al.*, 2009; Calkins *et al.*, 2011; Rönnbäck *et al.*, 2016; Djordjevic *et al.*, 2020) and streptozotocin induced mouse models (Correia *et al.*, 2013). Findings in other OXPHOS complexes are less consistent; some see no changes (Maurer, Zierz and Möller, 2000; Bosetti *et al.*, 2002), some see an increase (Birnbaum *et al.*, 2018), whilst others see reductions in activity and expression (Mutisya, Bowling and Beal, 1994; Armand-Ugon *et al.*, 2017; Lunnon *et al.*, 2017; Djordjevic *et al.*, 2020; Yao *et al.*, 2021). More recently, deficiencies in complex I have been noted in living patients using brain imaging techniques such as PET imaging, and magnetic resonance imaging (MRI) (Terada *et al.*, 2021, 2022).

Deficits in OXPHOS can lead to a reduction in mitochondrial membrane potential (MMP), a finding which is also commonly seen in AD (Ye *et al.*, 2015; Rönnbäck *et al.*, 2016; Dixit, Fessel and Harrison, 2017; Amit U. Joshi *et al.*, 2018; Bell *et al.*, 2018). Patient derived fibroblasts, from both familial and sporadic patients, have also been shown to have a reduced basal and maximal oxygen consumption, as well as reduced spare respiratory capacity (Gray and Quinn, 2015; Amit U. Joshi *et al.*, 2018; Bell *et al.*, 2018), a finding which has also been seen in a triple transgenic mouse model (Djordjevic *et al.*, 2020). ATP levels are also seen to be reduced across multiple models of AD, including mouse models (Hauptmann *et al.*, 2009; Calkins *et al.*, 2011; Correia *et al.*, 2013; Zhang, Rissman and Feng, 2015; Dixit, Fessel and Harrison, 2017; Kandimalla *et al.*, 2018a), overexpression cell models (X. Wang *et al.*, 2008; X. C. Li *et al.*, 2016; Amit U. Joshi *et al.*, 2018), and patient fibroblasts (Gray and Quinn, 2015; Pérez *et al.*, 2017).

Oxidative stress is also widely reported in AD (Cioffi, Adam and Broersen, 2019). sAD fibroblasts have shown increased levels of ROS (Pérez *et al.*, 2017; 2018), as well as an accumulation of 8-oxo-guanine, an indicator of oxidative DNA damage (Ramamoorthy *et al.*, 2012). sAD fibroblasts have also been shown to be more susceptible to ROS, with glutamate uptake impaired in sAD fibroblasts in response to oxidative stress to a greater extent than control fibroblasts (Begni *et al.*, 2004).

Oxidative stress is also commonly seen in various mouse models of AD (Hamel *et al.*, 2008; Zhang *et al.*, 2018; Butterfield and Mattson, 2020; Klann *et al.*, 2020). Increased ROS has also been seen in induced pluripotent stem cell (iPSC) derived patient neurons, though this was only seen in three of five patients involved in the study (Birnbaum *et al.*, 2018).

1.3.2 Mitochondrial Morphology Abnormalities in Alzheimer's disease

Mitochondrial function is impacted by mitochondrial morphology, and this is also seen to be altered in AD. Many findings have indicated a more fragmented mitochondrial network, for example in M17, a human neuroblastoma cell line, expressing mutant APP (X. Wang *et al.*, 2008). This has also been seen in animal models, including primary neurons from an APP mouse model, where an increased number of fragmented mitochondria was seen in the cell body (Calkins *et al.*, 2011). This was replicated in an APP/PSEN1 transgenic mouse model (Xu *et al.*, 2017), and also in a *Drosophila* model (Wang and Davis, 2021). Furthermore, in these animal models alterations in mitochondrial morphology appear before the onset of cognitive symptoms (Xu *et al.*, 2017; Wang and Davis, 2021), as well as the formation of amyloid plaques (Trushina *et al.*, 2012). In contrast, in patient fibroblasts less fragmentation has been seen, with both less and smaller mitochondria found to be separated from the network (Drabik, Piecyk, *et al.*, 2021). Changes in mitochondrial length have also been seen in AD patient fibroblasts, though findings are inconsistent with some seeing a decrease in length

(Pérez *et al.*, 2017; Amit U. Joshi *et al.*, 2018) while others see an increase (Xinglong Wang *et al.*, 2008; Bell *et al.*, 2018).

Changes in the distribution of mitochondria throughout the cell have also been seen. Mitochondria are usually transported to the region around the nucleus, the perinuclear region, to be degraded. In AD, an increase in the number of mitochondria in the perinuclear region has been seen in patient derived fibroblasts (Xinglong Wang *et al.*, 2008; Martín-Maestro, Gargini, A. Sproul, *et al.*, 2017; Bell *et al.*, 2018), as well as in an APP/PSEN1 mouse model (Xu *et al.*, 2017). This may indicate an increase in the number of dysfunctional mitochondria, or an impairment in either the transport or degradation of damaged mitochondria. Drabik *et al.* (2021) investigated the age of mitochondria in the perinuclear region and the distal regions of the cell in control and sAD patient fibroblasts. They found that in controls, mitochondria in the perinuclear region were older than those in the distal regions, but this was not seen in sAD fibroblasts, where instead there was no significant difference in mitochondrial age between different regions of the cell. This suggests an impairment in mitochondrial transport as well as in the clearance of old and dysfunctional mitochondria.

1.3.3 Mitochondrial Quality Control Abnormalities in Alzheimer's disease

As mentioned above, mitochondrial morphology is strictly regulated by the dynamic processes of fission and fusion. The balance of these two processes is key in the efficient functioning of the mitochondria. The proteins controlling these processes have been widely studied in AD, though results have been inconsistent. Mfn1 and Mfn2 were seen to be reduced in a Tg2576 mouse model (Calkins *et al.*, 2011), while Mfn2 was also decreased in a triple transgenic mouse model (Djordjevic *et al.*, 2020), a tau mouse model (Kandimalla *et al.*, 2018a) and sAD patient fibroblasts (Drabik, Piecyk, *et al.*, 2021). On the other hand, increased Mfn2 levels were seen in an APP/PSEN1 mouse by 12 months (Xu *et al.*, 2017), and both Mfn1 and Mfn2 were increased in HEK293 cells, an embryonic kidney line, when human tau was overexpressed (X. C. Li *et al.*, 2016), whilst others have seen no change at all (Trushina *et al.*, 2012; Bell *et al.*, 2018).

Results with regard to OPA1 levels are equally contrasting. OPA1 was found to be increased in an APP/PSEN1 mouse by 12 months (Xu *et al.*, 2017), and in HEK293 cells overexpressing human tau (X. C. Li *et al.*, 2016). However, reduced OPA1 was seen in the M17 neuroblastoma line overexpressing wild type APP (X. Wang *et al.*, 2008), in a tau mouse model (Kandimalla *et al.*, 2018a), and in patient derived fibroblasts (Pérez *et al.*, 2017). Others saw no difference in OPA1 levels (Wang *et al.*, 2008; Bell *et al.*, 2018; Drabik, Piecyk, *et al.*, 2021), but Drabik, Piecyk, *et al.* (2021) did see a decrease in the ratio of L-OPA1 to S-OPA1, even though no difference in total OPA1 was observed.

Fission proteins have also been studied in various models of AD, with most of the focus on Drp1. Increased Drp1 has been seen in post mortem tissue (Manczak, Calkins and Reddy, 2011), and in several mouse models, including both transgenic (Trushina *et al.*, 2012; Xu *et al.*, 2017; Kandimalla *et al.*, 2018a) and streptozotocin induced (Paidi *et al.*, 2015). In fact, a partial reduction of Drp1 in tau mice was found to improve performance on the Morris Water Maze and rotarod tests, suggesting an improvement in cognition (Kandimalla *et al.*, 2021). Interestingly, in triple transgenic mice, Drp1 was seen to be increased in females, but decreased in males (Djordjevic *et al.*, 2020). Decreased Drp1 levels have also been noted in the M17 neuroblastoma line overexpressing APP (X. Wang *et al.*, 2008), and post mortem tissue (Wang *et al.*, 2009). A reduction in Drp1 has also been widely reported in both sAD and fAD patient fibroblasts (Xinglong Wang *et al.*, 2008; Martín-Maestro *et al.*, 2017; Bell *et al.*, 2018; Drabik, Piecyk, *et al.*, 2021), though again this is not consistent (Amit U. Joshi *et al.*, 2018). An important consideration when studying Drp1 is the localisation within the cell; Drp1 is recruited to the mitochondria during fission events. The amount of Drp1 localised to the mitochondria has been seen to be reduced in sAD and fAD patient fibroblasts (Martín-Maestro, Gargini, García, *et al.*, 2017; Bell *et al.*, 2018), and Drabik, Piecyk, *et al.* (2021) found that a higher proportion of total Drp1 was localised to the mitochondria, but a lower proportion of mitochondria were localised with Drp1. This may be due to the reduced overall levels of Drp1, or may suggest an impairment in the recruitment of Drp1 to the mitochondria.

The four receptors involved in the recruitment of Drp1 to the mitochondria are less well studied in AD. Fis1 is the best studied, with an increase noted in various transgenic mouse models (Jia *et al.*, 2015; Kandimalla *et al.*, 2018a; Manczak *et al.*, 2018; Reddy, Manczak, *et al.*, 2018), post mortem tissue (Manczak, Calkins and Reddy, 2011), and patient fibroblasts (Xinglong Wang *et al.*, 2008). Mff was reported to be decreased in sAD patient fibroblasts (Drabik, Piecyk, *et al.*, 2021), but increased in post mortem tissue (Wang *et al.*, 2019), transgenic mice (Q. W. Yan *et al.*, 2019), and A β treated cell lines (Ahmed *et al.*, 2019; Wang *et al.*, 2019). MiD49 and MiD51 have not, to our knowledge, been studied before in AD.

The topic of mitochondrial fission and fusion proteins in AD is controversial, with no real consensus in the literature. It is plausible that different mechanisms are occurring at different stages in the disease, or that different mechanisms occur in different cell types. More than ever, this highlights the need for better, more relevant models of AD, to truly elucidate the impact of these processes in human disease. To date, very few studies have investigated these proteins in a patient derived, disease relevant cell type, though Birnbaum *et al.* (2018) used iPSC derived neurons from five patients and two controls, and saw no change in Mfn1, Mfn2 or Drp1.

As well as alterations to fission and fusion, mitophagy is also altered in AD. An accumulation of damaged mitochondria is commonly seen in AD (Ye *et al.*, 2015; Martín-Maestro *et al.*, 2016; Martín-Maestro, Gargini, A. Sproul, *et al.*, 2017), suggesting that there may be a deficit in the mitophagy process. In one of the earliest studies investigating mitophagy in an AD model, neurons from an APP transgenic mouse showed an increase in Parkin translocation to the mitochondria, a finding which was confirmed in post mortem AD tissue. Furthermore, cytosolic Parkin progressively decreased in post mortem patient tissue as disease severity increased, again implying an increase in Parkin localised to the mitochondria. This suggested that mitophagy was enhanced in AD; however, an abnormal accumulation of mitophagosomes and an increased number of damaged mitochondria were also seen. This suggests that while the induction of mitophagy was increased, there was an impairment downstream in the mitophagy process, for example in lysosomal degradation (Ye *et al.*, 2015). In models where tau is overexpressed, a reduction in Parkin translocation has been noted (Hu *et al.*, 2016; Cummins *et al.*, 2019), a finding also seen in sAD patient fibroblasts (Martín-Maestro *et al.*, 2016). PINK1 levels have also been found to be altered; they were decreased in mutant APP mouse models (Manczak *et al.*, 2018; Reddy, Yin, *et al.*, 2018), but showed an accumulation at the mitochondria in both sAD patient fibroblasts (Martín-Maestro *et al.*, 2016) and fibroblasts overexpressing tau and APP (Martín-Maestro, Gargini, A. Sproul, *et al.*, 2017). In recent years, several studies have shown that inducing mitophagy improves several pathogenic features of AD including reducing A β and tau accumulation (Fang *et al.*, 2019; Xiong *et al.*, 2020; Xie *et al.*, 2022), improving ATP levels (Xiong *et al.*, 2020) and cell survival (Xie *et al.*, 2022), and improving cognition in animal models (Fang *et al.*, 2019; Xie *et al.*, 2022).

1.3.4 Interactions of the Mitochondria with Amyloid and Tau

The importance of amyloid and tau in the pathogenesis of AD is a central question within the field, with many aiming to answer the question of whether they are a cause or consequence of another disease causing mechanism. Nevertheless, they are a key hallmark of AD and their interactions with other pathogenic mechanisms is a widely researched area. Whether mitochondrial impairment is induced by amyloid or tau pathology or whether it occurs independently remains unknown. There is much evidence to suggest that impairment of the mitochondria precedes protein pathology (Yao *et al.*, 2009; Hartl *et al.*, 2012). Moreover, mice with a genetic complex I defect, or transgenic mice treated with a complex I inhibitor have shown an increase in A β levels. This was shown to be due to mitochondria derived ROS, as treatment with an antioxidant reduced A β accumulation (Leuner *et al.*, 2012). Recently, it has been discovered that changes in mitochondrial membrane potential influence

A β secretion, where reduced MMP led to a decrease in A β secretion in SH-SY5Y cells, suggesting that A β levels may serve as a biomarker for mitochondrial function (Wilkins *et al.*, 2022). This has led to the proposal of the mitochondrial cascade hypothesis, which places mitochondria at the centre of AD pathology (Swerdlow and Khan, 2004; Swerdlow, Burns and Khan, 2010, 2014).

There is also much evidence to suggest that both amyloid and tau directly interact with the mitochondria, impacting their function. Synthetic A β monomers have been seen to enhance glucose uptake in neurons, and increase glycolysis in response to stress. Increased glycolysis in response to OXPHOS inhibition was prevented by blocking endogenous A β ; this was re-established by treatment with synthetic A β monomers (Santangelo *et al.*, 2021). It is possible that in AD, A β monomers aggregate to form oligomers or plaques, thus preventing this response to mitochondrial stress. Deficiency in complex IV has been found to be dependent on A β (Rhein *et al.*, 2009), and treatment with A β oligomers in wild type and triple transgenic mice was seen to decrease MMP and ATP, as well as increase mitophagy protein Parkin (Kam *et al.*, 2020). A β 40 treatment of platelets also led to decreased MMP, as well as reduced maximal respiration and increased ROS, though no change was seen in mitophagy protein PINK1, or fusion protein OPA1 (Donner *et al.*, 2021).

Tau pathology has been linked with the dysregulation of complex I. In triple transgenic mice, deregulation of complex I was seen to be dependent on tau (Rhein *et al.*, 2009), while in PET imaging studies carried out on people living with AD, tau burden was seen to correlate with the function of complex I (Terada *et al.*, 2021). It is important to note that in this imaging study, there is no way to know whether there is a causative relationship between tau and complex I deficiency. Tau has also been shown to accumulate at dendritic mitochondria, and this was only seen in mice which also had amyloid pathology, suggesting that amyloid is necessary for this pathology to occur (Cuadrado-Tejedor *et al.*, 2021). Loss of synaptic mitochondria is commonly seen in tauopathies, and recently this has been attributed to a broad activation of the Parkin mitophagy pathway (Jeong *et al.*, 2022). Not all studies have found an interaction between tau and the mitochondria. Alavi (2021) investigated the link between tau phosphorylation and OPA1 processing, and found that the two occurred independently of each other. This suggests that there is another pathway impacting both tau pathology and the mitochondria; it may be that this is related to amyloid, or it could be an entirely separate pathway.

It is clear that whichever occurs first in AD, mitochondrial dysfunction and tau and amyloid pathology interact with each other. It is likely that a cycle occurs in which they continually exacerbate each other, and it may be a combination of the two, plus other mechanisms, which drive AD progression. This highlights the necessity of looking at multiple mechanisms as therapeutic

targets, and the mitochondria in particular. Should mitochondrial dysfunction prove to be an upstream event in AD pathology, it provides an attractive target for modulating the disease.

1.4 Local Cohort Used in this Study

The locally collected cell lines used in this project were collected as part of a multicentre project funded by the EU, the Virtual Physiological Human – Dementia REsearch Enabled by IT (VPH-DARE@IT; <http://www.vph-dare.eu/>) initiative. Patients were clinically diagnosed with sAD using the McKhann et al. (2011) criteria, after assessment by both a consultant neurologist and professor of neuropsychology. No amyloid or tau biomarkers were used in the diagnosis. Each patient underwent brain MRI and cognitive profiling. Patients were excluded if they had a medical diagnosis of clinical concern which could justify the presence of cognitive difficulties, MRI images showing abnormalities other than the effects of aging and/or neurodegeneration, medical or radiological evidence of acute or chronic cerebrovascular disease, history of transient ischemic attacks, cardiovascular disease, uncontrolled seizures, peptic ulcer, sick sinus syndrome, neuropathy with conduction defects, abnormal levels of folate, vitamin B12, or thyroid stimulating hormone, treatments with medications for research purposes or with significant toxic effects on internal organs, or evidence of a psychiatric or psychological cause of cognitive impairment.

1.5 Aims and Objectives

Previous work in the lab has shown that both functional and morphological abnormalities are present in sporadic and PSEN1 Alzheimer's fibroblasts compared to age and sex matched controls. These abnormalities include a reduced mitochondrial membrane potential, as well as fewer mitochondria per cell, an increased percentage of long mitochondria, and an increased percentage of mitochondria accumulated in the perinuclear region. Furthermore, reduced total levels of Drp1, a key mitochondrial fission protein, as well as reduced levels at the mitochondria have been seen (Bell et al., 2018). The aim of this project is to build upon these findings, investigating the hypothesis that the mitochondrial phenotype seen in Alzheimer's patient cells is driven by abnormalities in fission and fusion processes, and that small molecules can be found which beneficially modulate the mitochondrial phenotype in AD.

Aim 1: To investigate mechanisms leading to and resulting from reduced levels of Drp1 in an expanded cohort of Alzheimer's disease patient and control fibroblasts

Objectives:

1. To measure total protein expression of Drp1 in an expanded cohort
2. To measure total protein expression of the four Drp1 receptors, Fis1, Mff, MiD49, and MiD51
3. To measure interactions between Drp1 and the receptors
4. To investigate post translational modifications of Drp1, primarily phosphorylation at ser637 and ser616
5. To investigate mechanisms upstream of Drp1 recruitment
6. To determine whether Drp1 overexpression can rescue the deficits seen in sAD patient fibroblasts

Aim 2: To investigate the mitochondrial phenotype seen in sAD patient fibroblasts in a patient derived neuronal model

Objectives:

1. To develop a differentiation protocol from induced neuronal progenitor cells
2. To characterise a patient derived neuronal model
3. To determine the mitochondrial phenotype of a patient derived neuronal model

Aim 3: To determine whether the same mechanisms are present leading to mitochondrial morphological changes in AD derived neurons as fibroblasts

Objectives:

1. To measure protein expression of Drp1 in patient derived neurons
2. To measure protein expression of the four Drp1 receptors, Fis1, Mff, MiD49, and MiD51, in patient derived neurons
3. To measure interactions between Drp1 and the receptors
4. To investigate post translational modifications of Drp1, primarily phosphorylation at ser637 and ser616

Aim 4: To screen a compound library for compounds which have a beneficial effect on mitochondrial function and morphology in sAD patient fibroblasts

Objectives:

1. To screen a 21,000 compounds library in one sAD fibroblast line and identify those which have a significant effect on MMP, percentage of mitochondria in the perinuclear region, percentage of the cell taken up by long mitochondria, and mitochondrial count per cell
2. To assess the dose response of compounds identified as hits from objective 1 in one sAD line, and identify a final hit list of top performing compounds
3. To investigate whether these compounds have a similar effect in fibroblasts taken from a patient with a PSEN1 mutation
4. To assess the top performing compounds in further control and sAD lines taken from a different patient cohort, to validate their positive effect on mitochondrial parameters

Chapter Two: Materials and Methods

Unless otherwise stated, materials were obtained from Merck.

2.1 Patient Information

Two patient cohorts were used in this study; most studies were carried out in a cohort of local patients involved in the MODEL-AD study (Control: 64.2 years \pm 10.9, Sporadic: 68.4 years \pm 14.9; table 1) (Research and Ethics Committee number: 16/YH/0155), while a cohort obtained from the NIGMS Human Genetic Cell Repository at the Coriell Institute for Medical Research (Control: 63 years \pm 12.2, Sporadic: 58 \pm 11.9; table 2) was used for limited studies. Local patients were diagnosed with Alzheimer's Disease using the McKhann *et al.*, (2011) criteria.

Table 1: Sex, age, and ApoE Status of cell lines used in this project, which were collected from a local population of patients.

Cell Line	Disease State	Sex	Age	ApoE Status
Control 1	Control	Male	53	3/3
Control 2	Control	Male	54	3/4
Control 3	Control	Female	61	2/3
Control 4	Control	Male	66	3/3
Control 5	Control	Female	100	3/4
Control 6	Control	Female	54	3/4
Control 7	Control	Male	56	2/3
Control 8	Control	Female	73	3/3
Control 9	Control	Male	75	2/3
Control 10	Control	Female	75	3/3
sAD 1	Sporadic	Male	53	2/3
sAD 2	Sporadic	Male	60	3/3
sAD 3	Sporadic	Male	57	3/3
sAD 4	Sporadic	Male	63	4/4
sAD 5	Sporadic	Female	59	2/3
sAD 6	Sporadic	Female	63	Unknown
sAD 7	Sporadic	Male	60	4/4
sAD 8	Sporadic	Male	60	3/3
sAD 9	Sporadic	Female	79	3/4
sAD 10	Sporadic	Female	61	3/3

Table 2: Sex, age, and ApoE status of cell lines used in this project, which were obtained from the NIGMS Human Genetic Cell Repository at the Coriell Institute for Medical Research.

Cell Line	Disease State	Sex	Age	ApoE Status
ND29510	Control	Female	55	Unknown
GM04188	Control	Female	77	Unknown
GM13335	Control	Male	57	Unknown
AG08597	Sporadic	Male	50	4/4
AG07872	Sporadic	Male	53	4/4
AG08243	Sporadic	Male	72	4/4
ND34733	Presenilin 1 (P264L mutation)	Male	60	Unknown

2.2 Cell Culture

2.2.1 Human Fibroblast Cell Culture

Skin biopsies were obtained from healthy controls and Alzheimer’s disease patients using a skin punch, and fibroblasts were set up as described in Bell et al. (2018). This work was carried out by Dr Simon Bell. Fibroblasts were cultured in complete Eagle’s minimum essential media (EMEM), supplemented as described in table 5. Cells were maintained in T75 flasks (Corning) at 37°C and 5% CO₂, with media changed every 2-3 days.

When cells reached confluency, they were split into new flasks. All media was removed, and cells were washed twice with phosphate buffered saline (PBS). 5ml of 1 x Trypsin EDTA (Sigma) was used to detach the cells, which were incubated for five minutes at 37°C. Trypsin EDTA was quenched using complete EMEM media. Cells were spun at 550g for four minutes, and the pellets were then re-suspended in complete EMEM media and added to new flasks or into plates to be fixed or assayed. All cells used in experiments from the locally collected cohort were between passage 8 and 16, and control and sAD lines were matched to within 3 passages. Cells from the Coriell institute are bought commercially and so come in at a higher passage than those which are sourced locally. For experiments with these lines, all cells were below passage 20.

Cells were stored at -80°C, or in liquid nitrogen. When freezing, all media was removed, and cells washed twice with PBS. Cells were detached from flasks using 1 x Trypsin EDTA (Sigma), and incubated for five minutes at 37°C. Trypsin EDTA was quenched using complete EMEM media, and cells spun at 550g for four minutes. Pellets were re-suspended in 2ml complete EMEM media with 10% Dimethyl Sulphoxide (DMSO; Sigma) and 10% Foetal Bovine Serum (FBS; Biosera), and transferred into two cryovials (ThermoFisher) per flask. Cryovials were placed into a CoolCell freezing container (Biocision) to ensure a controlled rate of freezing of -1°C per minute, and kept at -80°C. After one hour, cells were transferred to long term storage at either -80°C or in liquid nitrogen.

2.2.2 Induced Neural Progenitor Cell Culture

Fibroblasts were reprogrammed to induced neural progenitor cells (iNPCs), as described by Meyer et al. (2014). Reprogramming of fibroblasts to iNPCs was carried out by Dr Simon Bell, and Professor Laura Ferraiuolo. iNPC identity was confirmed by positive paired box 6 (Pax6) and Nestin staining, in work carried out by Dr Simon Bell, and as previously described in Meyer et al. (2014). Cell lines used are shown in age and sex matched pairs in table 3.

iNPCs were cultured continuously in 10cm dishes (ThermoFisher), in complete NPC media: Dulbecco's modified essential media/Ham's F12 nutrient mixture (DMEM/F12) (Gibco; 10565018) with supplements as described in table 5. Cells were maintained at 37°C and 5% CO₂. When splitting, cells were detached using 1ml Accutase (Sigma) and incubated for five minutes at 37°C. Accutase was then quenched with PBS. Cells were spun at 200g for four minutes, and pellets then re-suspended in complete NPC media and added to new dishes, pre-coated with 5ng/ml fibronectin (Millipore) for ten minutes. All cells used for experiments and for differentiation were below passage 20, and control and sAD lines were matched to within three passages.

Cells were stored at -80°C, or in liquid nitrogen. When freezing, cells were detached using 1ml Accutase (Sigma), and incubated for five minutes at 37°C. Accutase was quenched with PBS, then cells were spun at 200g for four minutes. Pellets were re-suspended in complete NPC media with 10% DMSO, and transferred into cryovials. Cryovials were placed into a CoolCell freezing container (Biocision) to ensure a controlled rate of freezing of -1°C per minute, and kept at -80°C. After one hour, cryovials were transferred into long term storage either at -80°C or in liquid nitrogen.

For neuron differentiation, iNPCs were plated into 6 well plates, pre-coated with 5ng/ml fibronectin for ten minutes. Plating density was optimised for each line, and is given in table 4. Differentiation was started when cells reached approximately 90% confluency.

Table 3: iNPC cell lines used, in age and sex matched pairs.

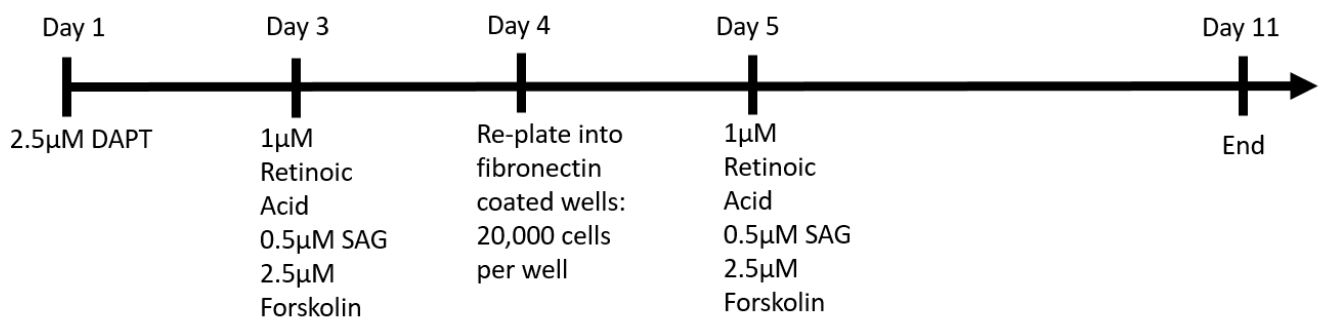
Control	Age	Sex	sAD	Age	Sex
Control 3	61	Female	sAD 5	59	Female
Control 7	56	Male	sAD 4	63	Male
Control 10	75	Female	sAD 9	79	Female
Control 5	100	Female	sAD 6	63	Female
Control 2	54	Male	sAD 8	60	Male

Table 4: Plating densities of iNPC lines for iNeuron differentiation.

Cell Line	Plating Density
Control 2	80,000
Control 3	80,000
Control 5	60,000
Control 7	100,000
Control 10	100,000
sAD 4	100,000
sAD 5	80,000
sAD 6	80,000
sAD 8	50,000
sAD 9	60,000

2.2.3 Generic Neuron Differentiation

Generic neuron differentiation was carried out according to the protocol described in Webster *et al.*, (2016). Media used for differentiation was complete neuron media, Dulbecco's modified essential media/Ham's F12 nutrient mixture (DMEM/F12; Gibco) supplemented as described in table 5. Cells were maintained at 37°C and 5% CO₂, with media changed every other day. A timeline of differentiation is shown in figure 3. Briefly, on day one, cells were treated with 2.5µM N-[N-(3,5-difluorophenacetyl)-l-alanyl]-S-phenylglycine t-butyl ester (DAPT; Sigma). On day three, factors were introduced to the cell media as follows; 1µM retinoic acid (RA; Sigma), 0.5µM smoothed agonist (SAG; Peprotech) and 2.5µM forskolin (Cayman Chemical Company). On day four, cells were re-plated into 96 well plates (Greiner). All media was removed from the wells, and 500µl Accutase (Sigma) added. Cells were incubated at 37°C for five minutes, before Accutase was quenched with



PBS and cells spun at 200g for four minutes. Pellets were re-suspended in complete neuron media with factors added as described above, and plated into 96 well plates pre-coated with 5ng/ml fibronectin for ten minutes, at a density of 20,000 cells per well. Cells were given complete neuron media with factors as described for a further seven days.

Figure 3: Timeline of factors added during generic neuron differentiation.

Table 5: Different types of cell culture media used in this project.

Media Type	Base Media	Supplements	Cell Type
Complete EMEM media	EMEM (1000mg/L glucose) (Corning; MT10009CV)	10% FBS (Biosera) 50µg/ml Uridine (Alfa Aesar) 1mM Sodium pyruvate (Sigma) 100µM Non-essential amino acids (NEAA) (Lonza) 0.1x MEM Vitamins (Lonza) 100UI/ml Penicillin 100µg/ml Streptomycin (Lonza)	Fibroblasts
Complete NPC media	DMEM/F12 (Gibco; 10565018)	1% B27 (Gibco) 1% N2 (Gibco) 40ng/ml FGFb (PeproTech) 100UI/ml Penicillin 100µg/ml Streptomycin (Lonza)	iNPCs
Complete Neuron media	DMEM/F12 (Gibco; 10565018)	2% B27 (Gibco) 1% N2 (Gibco) 100UI/ml Penicillin 100µg/ml Streptomycin (Lonza)	Generic neurons

2.2.4 Fixing of Cells

For fibroblasts, all media was removed and cells were fixed in 4% paraformaldehyde (PFA; Fisher Scientific) in PBS for ten minutes at room temperature, then washed twice in PBS. For neurons, 4% PFA was added dropwise to wells without removing any media in order to best preserve neuronal processes, and incubated at 37°C for 30 minutes. All media and PFA was then removed, and cells were fixed in 4% PFA for a further ten minutes, then washed twice with PBS. Plates were stored at 4°C in 0.1% sodium azide.

2.3 Western Blotting

2.3.1 Cell Lysis

Frozen cell pellets were re-suspended in 50µl radioimmunoprecipitation assay (RIPA) buffer (Sigma-Aldrich: R0278), 5µl protease inhibitor cocktail (PIC; Sigma-Aldrich: P8340), and 5µl phosphatase inhibitor cocktail (Merck: P0044). The resuspension was then placed on ice for 30 minutes, then centrifuged at 13,000g. The supernatant was placed into a clean Eppendorf and the pellet was discarded.

2.3.2 Bradford Assay

A Bradford Assay was carried out to quantify the amount of protein in the sample. 5µl of bovine serum albumin (BSA; ThermoScientific) concentrations (see table 6) and dH₂O, as a negative control, were pipetted in triplicate into a clear 96 well plate (Corning), as well as 2µl of cell sample diluted 1:4 in dH₂O. 250µl coomassie blue (ThermoScientific) was added to each well, and protein absorbance was measured using the PHERAstar plate reader (BMG Labtech). Linear regression analysis was applied using GraphPad Prism, and Microsoft Excel used to calculate protein concentrations in cell samples. 4 x sample buffer (see table 7) was added to the cell samples, which were then boiled at 95°C for five minutes. Samples were stored in 20µg aliquots at -80°C.

Table 6: BSA standards used in Bradford Assay to produce a standard curve

BSA (μl from 2mg/ml stock)	dH₂O (μl)	BSA Concentration ($\mu\text{g}/\text{ml}$)
50	950	100
62.5	937.5	125
125	875	250
125	375	500
187.5	312.5	750
250	250	1000
300	200	1200

Table 7: Reagents used to make up 4x sample buffer

Reagent	Amount	Supplier
Tris-HCl pH8.0	0.62g	Tris, Sigma-Aldrich; HCl, Fisher
Glycerol	8ml	Sigma-Aldrich
Sodium dodecyl sulphate (SDS)	1.8g	Thermo-Fisher Scientific
Bromophenol Blue	0.008g	Sigma-Aldrich
Dithiothreitol (DTT)	0.8g	Sigma-Aldrich
2-mercaptoethanol	10ml	Sigma-Aldrich

2.3.3 Gel Preparation

For later western blots, 12% precast gels were used (Biorad) due to time constraints. When gels were hand-poured, 1.0cm glass plates were placed in the Mini-PROTEAN gel casting apparatus (BioRad). 12% resolving gel was made up according to table 8 and pipetted into the glass plates. Isopropanol was pipetted over the resolving gel to remove any bubbles, and the gel was left for approximately 15 minutes to set. Once set, the isopropanol layer was poured off, and stacking gel was made up according to table 9. Stacking gel was pipetted into the glass plates, and a 1.0cm comb inserted to form ten wells in the gel. The stacking gel was left for approximately 15 minutes to set.

Table 8: Reagents used to make up 12% resolving gel

Reagent	Amount	Supplier
30% Bis/Acrylamide	4ml	National Diagnostics
1.5M Tris-HCl pH8.8	2.5ml	Tris, Sigma-Aldrich; HCl, Fisher
dH ₂ O	3.3ml	Nanopure
10% SDS	100µl	Thermo-Fisher Scientific
10% Ammonium Persulphate (APS)	100µl	Sigma-Aldrich
Tetramethylethyl enediamine (TEMED)	4µl	Melford

Table 9: Reagents used to make up stacking gel

Reagent	Amount	Supplier
30% Bis/Acrylamide	500µl	National Diagnostics
1.5M Tris-HCl pH8.8	380µl	Tris, Sigma-Aldrich; HCl, Fisher
dH ₂ O	2.1ml	Nanopure
10% Ammonium Persulphate (APS)	30µl	Sigma-Aldrich
Tetramethylethyl enediamine (TEMED)	3µl	Melford

2.3.4 Sodium Dodecyl Sulphate – Polyacrylamide Gel Electrophoresis (SDS-PAGE)

Plates containing either hand-poured or precast gels were placed in a Mini-PROTEAN Tetra Electrode assembly (BioRad), which was placed in a Mini-PROTEAN Tetra Cell tank (BioRad) filled with SDS-PAGE running buffer (see table 10). The comb was removed and 10µg of cell samples was added to the wells, along with 5µl of molecular weight ladder (Precision Plus Protein™ Dual Colour Standards; BioRad). The tank was attached to a PowerPac Basic Power Supply (BioRad), and run at a constant

voltage of 50V for 30 minutes to allow samples to run through the stacking gel, then voltage was increased to 120V for approximately 90 minutes to allow separation through the resolving gel. Once samples had separated through the resolving gel, the plates were opened and the stacking gel was removed.

Table 10: Reagents used to make up SDS-PAGE running buffer

Reagent	Amount	Supplier
Tris	30g	Sigma-Aldrich
Glycine	144g	Melford
SDS	10g	Fisher Chemical
dH ₂ O	Up to 10L	Nanopure

2.3.5 Transfer

The transfer assembly was arranged in a transfer cassette (BioRad), whilst soaked in transfer buffer (as described in table 11), as follows: sponge, filter paper, resolving gel, polyvinylidene fluoride membrane (PVDF; Millipore) pre-soaked in methanol, filter paper, sponge. Any air was removed from the transfer assembly, and the cassette was closed and placed in a Mini Trans-Blot Cell (BioRad). This was then placed in the Mini-PROTEAN Tetra Cell tank, which was filled with transfer buffer, with an ice pack to prevent overheating. Tank was attached to the PowerPac, and run at constant 250mAmps for one hour.

Table 11: Reagents used to make up transfer buffer

5x Transfer Buffer		
Reagent	Amount	Supplier
Tris	150g	Sigma-Aldrich
Glycine	720g	Melford
dH ₂ O	Up to 10L	Nanopure
1x Transfer Buffer		
Reagent	Amount	Supplier
5 x Transfer Buffer	200ml	--
Methanol	100ml	Merck
dH ₂ O	700ml	Nanopure

2.3.6 Blocking, Antibody Incubations and Imaging

PVDF membrane was removed from the transfer assembly and blocked in 5% Non-Fat Dry Milk in Tris Buffered Saline with Tween-20 (TBST) for at least one hour. Phosphorylated proteins were blocked in 5% BSA. Membranes were then incubated in primary antibody in TBST (or 5% BSA for phosphorylated proteins) at 4°C overnight. A list of primary antibodies used is described below in table 12. Membranes were then washed three times with TBST, then incubated for one hour in secondary antibody in TBST. A list of secondary antibodies used is described in table 13 below. Membranes were washed a further three times in TBST.

For imaging, the membrane was incubated with 2ml ECL solution (EZ-ECL HRP kit; Biological Industries), for approximately one minute, then imaged using the G-Box intelli-chemi system (GENEsys; SynGene).

The antibody incubations and imaging process were repeated for loading control proteins (highlighted in table 12), which were included on each membrane to account for loading error.

Table 12: Primary antibody used in western blotting.

Primary Antibody	Dilution	Supplier
Drp1	1:1000	Abcam (ab56788)
OPA1	1:1000	BD Biosciences (612606)
Fis1	1:1000	Proteintech (10956-1-AP)
Mff	1:1000	Proteintech (17090-1-AP)
MiD49	1:500	Proteintech (16413-1-AP)
MiD51	1:1000	Proteintech (16413-1-AP)
pDrp1 (ser616)	1:1000	Cell Signalling Technology (3455)
pDrp1 (ser637)	1:1000	Cell Signalling Technology (4867)
Pex19	1:1000	Proteintech (14713-1-AP)
INF2	1:1000	Proteintech (20466-1-AP)
Beta-III-Tubulin	1:1000	Merck (AB9354)
NeuN	1:1000	Abcam (ab9354)
Loading Controls Primary Antibody	Dilution	Supplier
β -Actin	1:1000	St John's Laboratory (stj97089)
GAPDH	1:2000	Proteintech (60004-1-Ig)
α -Tubulin	1:1000	Invitrogen (62204)

Table 13: Secondary antibody used in western blotting

Secondary Antibody	Dilution	Supplier
Anti-rabbit HRP	1:5000	Dako (P044801-2)
Anti-mouse HRP	1:10,000	Abcam (ab97040)

2.3.7 Densitometry Analysis

Densitometry was analysed using GeneTools software (SynGene), using a rolling disk background correction. Raw data for the protein of interest was normalised to the loading control. Data was then normalised to the average of all controls on the membrane. To determine statistically significant differences between sAD lines and controls at a group level, a Student's t test was performed. To determine statistically significant differences between individual sAD lines and controls, a one-way ANOVA with Dunnett's multiple comparisons test was performed. To determine statistically significant associations between different protein levels, as well as between protein levels and mitochondrial morphological measures, a simple linear regression was performed. All statistical tests were performed using GraphPad Prism 7.

2.4 Immunocytochemistry

2.4.1 Immunocytochemistry

Cells were permeabilised with 0.1% triton (Alfa Aesar) in PBS with 10% Tween-20 (PBST) for ten minutes, then washed twice with PBST. Cells were blocked in 5% horse serum (Sigma) for one hour at room temperature, then incubated in primary antibody in blocking solution, at 4°C overnight. Antibodies used are described in table 14 below. On day 2, cells were washed three times with PBST, then incubated in secondary antibody in PBST for one hour. Secondary antibodies used are described in table 15. Cells were then washed in PBST three times, incubated with 10µM Hoechst (Sigma) for two minutes, then washed a final three times with PBST.

Cells were imaged on the Opera Phenix (Perkin Elmer), using the 40x water objective, using the appropriate AlexaFluor channels (AlexaFluor 488 excitation 488/emission 525, AlexaFluor 568 excitation 561/emission 603, AlexaFluor 647 excitation 640/emission 665), and the DAPI channel (excitation 405/emission 461). For fibroblasts, 20 fields of view were imaged with 3 Z planes imaged per field. For neurons, 20 fields of view were imaged with 5-6 Z planes imaged per plane. Exposure time and exact Z plane positioning were optimised per plate.

Table 14: Primary antibody used in immunocytochemistry.

Primary Antibody	Dilution	Supplier
TOM20 (Mouse)	1:1000	BD Biosciences (612278)
TOM20 (Rabbit)	1:1000	Santa Cruz Biotech (FL145)
Fis1	1:1000	Proteintech (10956-1-AP)
Mff	1:1000	Proteintech (17090-1-AP)
Drp1	1:1000	BD Biosciences (611113)
TUJ	1:1000	Merck (AB9354)
NeuN	1:1000	Abcam (ab9354)
MAP2	1:1000	Abcam (ab32454)
TBR1	1:1000	Abcam (ab31940)
SATB2	1:100	Abcam (ab51502)
Hb9	1:1000	Abcam (ab221884)
vGlut1	1:1000	Abcam (ab242204)
ChAT	1:1000	Millipore (AB144P)

Table 15: Secondary antibody used in immunocytochemistry

Secondary Antibody	Dilution	Supplier
AlexaFluor 488 anti-chicken	1:1000	Invitrogen (A32931)
AlexaFluor 488 anti-rabbit	1:1000	Invitrogen (A32790)
AlexaFluor 488 anti-mouse	1:1000	Invitrogen (A32766)
AlexaFluor 488 anti-rat	1:1000	Invitrogen (A48262)
AlexaFluor 568 anti-mouse	1:1000	Invitrogen (A-11004)
AlexaFluor 568 anti-rabbit	1:1000	Invitrogen (A-11036)
AlexaFluor 647 anti-rabbit	1:1000	Invitrogen (A32733)

2.4.2 Image Analysis

2.4.2.1 *Analysis of positive expression of neuronal markers*

Analysis of positive expression was carried out using Columbus software (Perkin Elmer). Firstly, Z stacks were combined to give the maximum projection, and a basic flatfield correction was applied. Next, the nuclei were segmented, followed by the cytoplasm of the cell. The intensity of the staining inside the cytoplasm was then assessed and cells with a mean intensity over a certain threshold, determined by the background staining as measured using secondary only control wells, were selected as being positive for that marker. For markers which are located in the nucleus, such as neuronal nuclei (NeuN), intensity of staining was assessed in the nuclear region.

2.4.2.2 *Analysis of co-localisation to mitochondria*

Co-localisation analysis was carried out using Harmony analysis software (Perkin Elmer). As described above, Z stacks were combined to give the maximum projection and a basic flatfield correction was applied. The nuclei were then segmented, followed by the cytoplasm of the cell. In some cases, the cytoplasm could not be accurately segmented, and so the whole image region was used instead. The mitochondria were then segmented based on staining of the mitochondrial marker, translocase of outer mitochondria membrane 20 (TOM20). Then spots of the protein of interest were segmented, and selected based on size and intensity to eliminate any background staining. Then selected protein of interest spots were identified within the mitochondrial region as defined by TOM20 segmentation. Percentage of the protein of interest localised to the mitochondria was calculated as follows: $\text{Number of protein spots within the mitochondrial region} / \text{Total number of protein spots} \times 100$. Example images of this segmentation analysis are shown in figure 4.

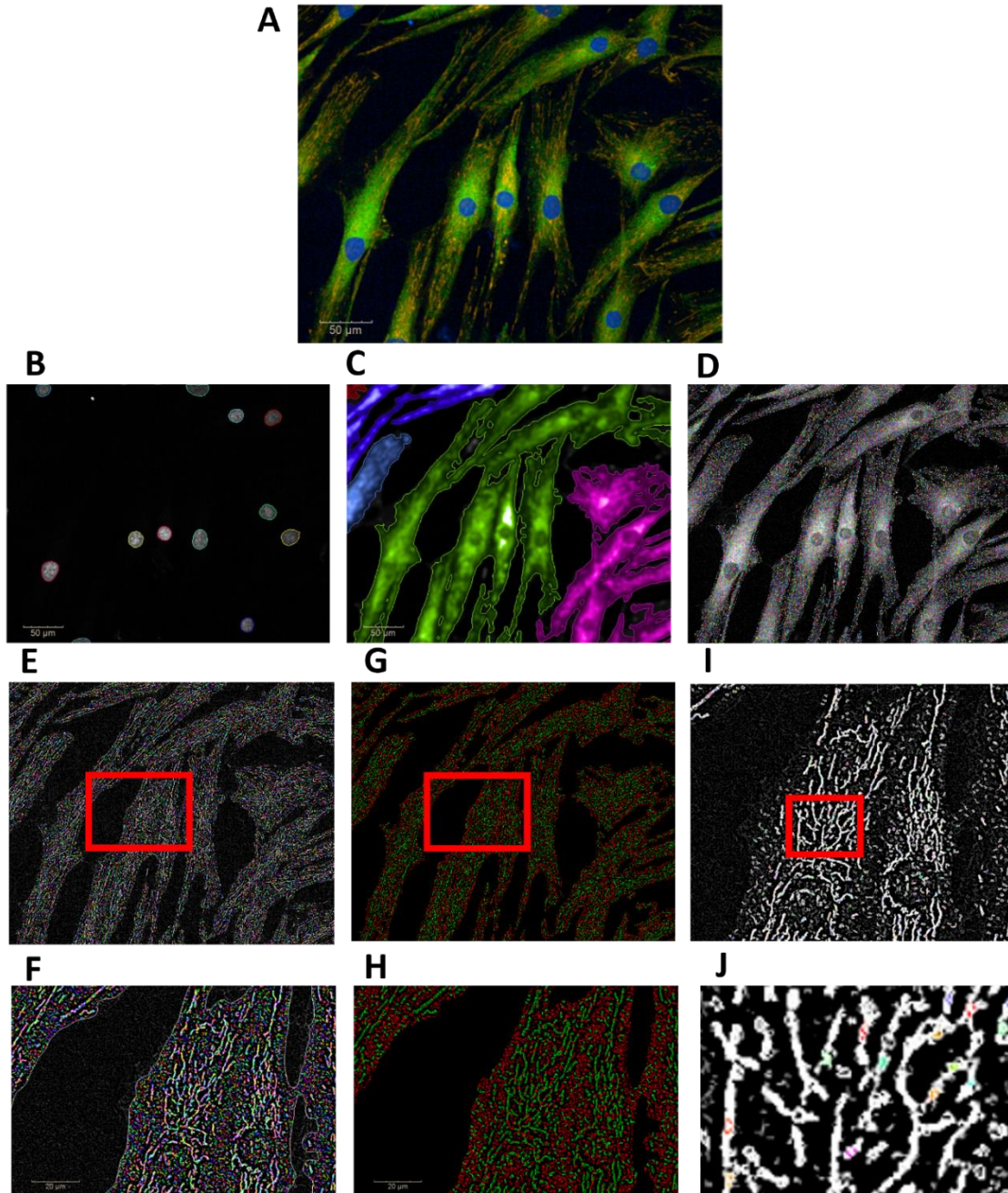


Figure 4: Co-localisation analysis and segmentation of fibroblasts in Harmony analysis software. A) Original input image, where mitochondrial marker TOM20 is shown in red, and protein of interest in green, and nuclei are shown in blue. B) Segmentation of the nuclei. C) Segmentation of the image region. D) Segmentation of the protein of interest. E) Segmentation of all mitochondria. F) Zoomed in image of the area in the red box in E, showing all mitochondria. G) Segmentation of selected mitochondria; mitochondria in red have been excluded based on small size and low intensity, mitochondria in green have been selected as true mitochondria. H) Zoomed in image of the area in the red box in G, showing selected mitochondria. I) Protein of interest present in the selected mitochondria, coloured dots indicate where co-localisation occurs. J) Zoomed in image of the area in the red in I, where coloured dots show areas of co-localisation between mitochondria and protein of interest.

2.5 Proximity Ligation Assay

2.5.1 Proximity Ligation Assay

The proximity ligation assay (PLA) was used to detect endogenous protein interactions, using Duolink PLA technology (Merck). PLA was carried out mostly as described by the manufacturer's instructions, with some changes to account for practical differences in using 96 well plates instead of slides. Cells were fixed as previously described, then permeabilised with 0.1% triton (Alfa Aesar) for ten minutes, then washed three times with PBST. Cells were then blocked with 5% horse serum for an hour, before primary antibodies were added diluted in 5% horse serum (see table 16 for a list of antibodies used in this assay). Cells were incubated at 4°C overnight.

On day two, primary antibody was removed from the wells, and cells were washed twice with Wash Buffer A at room temperature. PLUS and MINUS assay probes were diluted 1:5 in antibody diluent, and 100µl added per well. Cells were incubated for one hour at 37°C. Cells were again washed twice with Wash Buffer A. 100µl 1:40 ligase in 1 x ligation buffer was added, and cells were incubated at 37°C for 30 minutes. Cells were washed twice with Wash Buffer A, before 100µl 1:80 polymerase in 1 x amplification buffer was added, and cells were incubated for 100 minutes at 37°C. Cells were washed with 1 x Wash Buffer B twice, before a final wash with 0.01 x Wash Buffer B. To visualise the nuclei, Hoechst diluted in PBST was added for two minutes, before cells were finally washed three times with PBST. Cells were imaged using the Opera Phenix using the AlexaFluor 568 (excitation 561/emission 603) and the DAPI channel (excitation 405/emission 461), with a total of 20 fields per well analysed, and 3 Z planes for fibroblasts, and 5 Z planes for neurons. Exposure time was optimised per each plate.

Table 16: Primary antibody used in the PLA

Primary Antibody	Dilution	Supplier
Drp1	1:1000	BD Biosciences (611113)
Fis1	1:1000	Proteintech (10956-1-AP)
Mff	1:1000	Proteintech (17090-1-AP)

2.5.2 Image Analysis

PLA images were analysed using Columbus software (Perkin Elmer). Nuclei were segmented, as were the spots indicating protein-protein interactions, as shown in figure 5. To get an approximate number of spots per cell, the total number of spots was divided by the total number of nuclei. The perinuclear region was identified by finding the 'surrounding region' of the nucleus as defined by Columbus software, and the number of spots within this region was also identified.

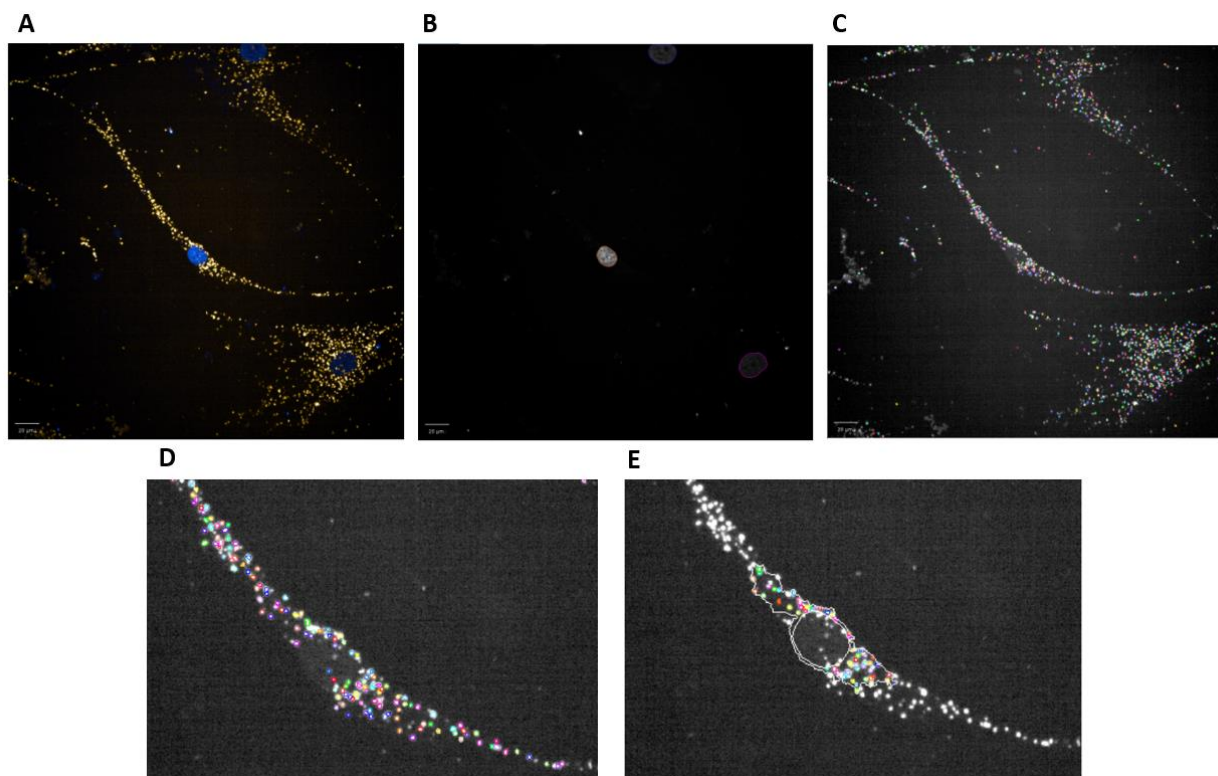


Figure 5: PLA image analysis in Columbus software. A) The original image, where each dot indicates a protein-protein interaction and nuclei are shown in blue. B) Segmentation of the nuclei. C) Segmentation of spots indicating individual interactions. D) Zoomed in segmentation of individual spots. E) Segmentation of spots in the perinuclear region.

2.6 Overexpression of Drp1 in Fibroblasts

2.6.1 Plasmid Information

pcDNA3YFP plasmid was obtained from Dr Chun Guo. Glycerol stocks of pcDNA3Drp1YFP were obtained from Professor Kurt de Vos. A map of the control pcDNA1YFP plasmid is shown in figure 6. Drp1 was inserted at the BsrG1 restriction site.

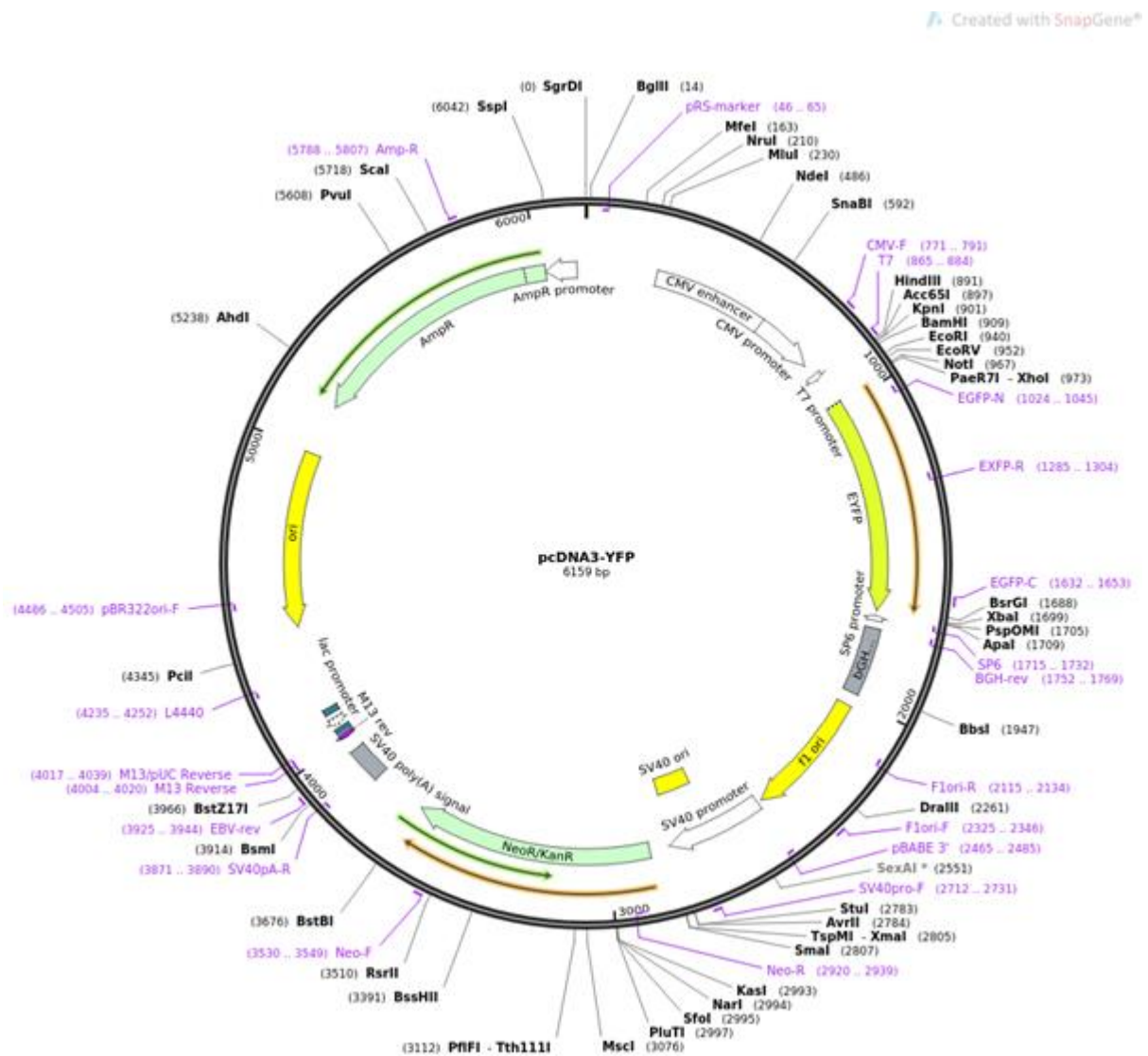


Figure 6: Map of pcDNA3YFP control plasmid.

2.6.2 Bacterial Culture

Luria-Bertani (LB) agar plates were produced by dissolving 40g LB agar (Fisher Scientific) in 400ml dH₂O and autoclaving. This was then cooled to approximately 50°C, and 400µl 50mg/ml carbenicillin (Sigma) in 1:1 ethanol and water was added under aseptic conditions. This was then poured into 10cm dishes and left to set.

Luria-Bertani (LB) broth was made up by dissolving 25g LB broth (Fisher Scientific) in 1L dH₂O. This was divided into conical flasks for larger cultures, and smaller bottles for smaller cultures, leaving space to aerate, and autoclaved. 1:1000 50mg/ml carbenicillin was added where appropriate.

2.6.2.1 Bacterial Transformation

10µl chemically competent cells (Sigma) were added to a pre-cooled Eppendorf. 1µg DNA was added and cells and DNA were allowed to mix for ten minutes on ice. The mixture was then heated at 42°C for one minute, before being cooled on ice.

Under aseptic conditions, LB broth was added without antibiotic, and mixture was heated at 37°C whilst shaking for one hour. Culture was then pipetted onto a pre-warmed LB agar plate and raked across the plate. Plate was incubated at 37°C overnight.

2.6.2.2 Streaking to grow individual colonies from glycerol stocks

Under aseptic conditions, a small amount of frozen glycerol stock was scraped off using a sterile platinum loop and left to melt onto the plate. This was then streaked across the plate using a sterile platinum loop following the pattern shown in figure 7, to isolate individual colonies.

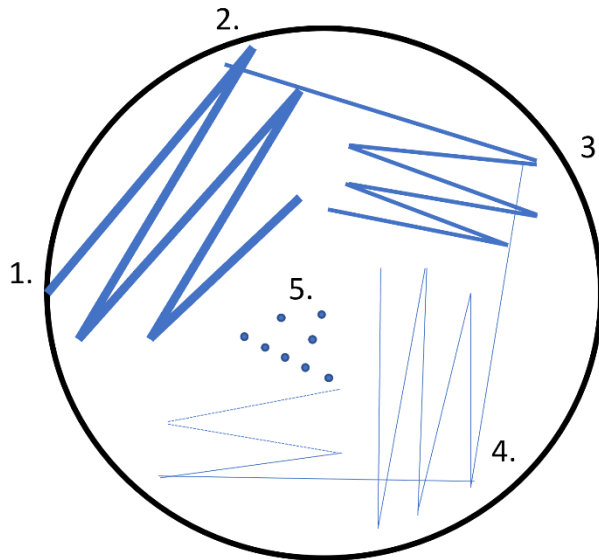


Figure 7: Streaking pattern for growing individual bacterial colonies. 1. A small amount of frozen glycerol stock is melted onto the LB agar plate, and then swiped across the plate in a zig-zag pattern using a sterile platinum loop, leading to heavy growth of bacteria. 2. The platinum loop is then dragged through the original streak, and down in a zig-zag pattern, leading to less heavy growth. 3+4. The process is repeated twice more, each time leading to less bacterial growth until 5. Individual colonies grow.

2.6.2.3 Culture of Individual Colonies

Individual colonies were picked using a sterile platinum loop under aseptic conditions and put into a universal tube in 5-10ml LB broth with carbenicillin. Universal tubes were incubated overnight at 37°C whilst shaking. For larger cultures, 5-10ml of this overnight culture was added to a conical flask containing 100ml LB broth with carbenicillin, and left to incubate overnight at 37°C whilst shaking. For long term storage, culture was stored in 15% glycerol, snap frozen, and kept at -80°C.

2.6.3 DNA Isolation

Bacterial cultures grown from individual colonies were harvested by centrifuging in a 50ml falcon tube for 20 minutes at 3800g. Supernatant was discarded. Plasmid DNA was isolated from the pellet by either the Isolate II Plasmid Mini Kit (Bioline) for smaller cultures, or the NucleoBond PC100 Midi Kit (Machery-Nagel) for larger cultures, according to the manufacturer's instructions. Briefly, the pellet was re-suspended using resuspension buffer 1 containing RNAses, then lysed with buffer 2 containing detergent and NaOH to break down fats and melt DNA into single strands. Tubes were inverted several times, and left for five minutes. Buffer 3, potassium acetate, was then added and the solution was mixed so a white precipitate formed. This was then clarified by centrifuging at

11,000g until supernatant was completely clear. For the mini kit, clear supernatant was added to a spin column in a collection tube and centrifuged at 11,000g for one minute. For the midi kit, clear supernatant was added to a large collection column and left until it had completely run through. The membrane in the column was then washed twice with the provided wash buffers. DNA was then eluted by adding elution buffer and collecting the flowthrough in an Eppendorf. Purity and amount of DNA was then assessed using the Nanodrop spectrophotometer (ThermoFisher).

2.6.5 Transfection of Fibroblasts

Fibroblasts were plated into 96 well plates and grown to approximately 70% confluency. For each well, 83ng of DNA was mixed with 0.29 μ g polyethylenimine (PEI) and added to 8 μ l OptiMEM media (PEI and OptiMEM were obtained from Dr Guillaume Hautbergue), and vortexed 15 times. The mixture was incubated for 10 minutes to allow DNA-liposome complexes to form. 8 μ l of this mixture was added to each well and cells were incubated for approximately 8 hours. Media was then removed and replaced with complete EMEM media.

2.6.6 Assessment of Transfection Efficiency

After 24 hours, cells were treated with 10 μ M Hoechst and incubated for one hour. Cells were then imaged on the Opera Phenix, using the 40x water objective and the AlexaFluor 488 (excitation 488/emission 525), and the DAPI channel (excitation 405/emission 450-455). Transfection efficiency was calculated using Harmony analysis software. Nuclei were segmented followed by the image region. The intensity of fluorescence in the image region was then assessed and cells with a maximum intensity over 250 were identified as being YFP positive and thus, successfully transfected. This threshold was determined based on the level of background staining.

2.6.7 Assessment of Drp1 and Mitochondrial Morphology

Immunocytochemistry was carried out as described above, using mitochondrial marker TOM20 (Santa Cruz Biotech; FL145) and Drp1 (BD Biosciences; 611113). Mitochondria and Drp1 spots were segmented and analysed in Harmony software as previously described.

2.7 Neurite Outgrowth Assay

2.7.1 Neurite Outgrowth Kit

The neurite outgrowth assay was carried out using a kit available from Thermofisher (A15001). At the endpoint of generic neuron differentiation, 100 μ l working buffer was added to the wells, consisting of 1:500 membrane marker, 1:500 cell viability marker and 10 μ M Hoechst in phenol red free minimum essential media (MEM; Gibco). Cells were incubated for 30 minutes at 37°C, then media was removed and 100 μ l 1:100 background buffer was added in MEM. Plates were then imaged on the Opera Phenix (Perkin Elmer) using the 20x air objective, and the AlexaFluor 488 (excitation 488/emission 525), AlexaFluor 568 (excitation 561/emission 603), and the DAPI channel (excitation 405/emission 461). Approximately 12 fields were imaged per well, with approximately 5 Z planes imaged per field. Exposure time and exact Z plane positioning was optimised per plate.

2.7.2 Image Analysis

Analysis of the neurite outgrowth assay was completed using Harmony analysis software (Perkin Elmer). As previously described, Z stacks were combined to give the maximum projection and a basic flatfield correction was applied. The nuclei were then segmented, followed by the cytoplasm of the cell. Cell morphology was assessed based on the membrane marker. Viability of cells was assessed by measuring the intensity of the viability marker inside the cytoplasm. Harmony software was also trained to recognise cells as 'neuronal' or 'non-neuronal' based on morphology, and well was given a neuron score, based on the ratio of cells with typical neuronal morphology to non-neuronal morphology. This is shown in figure 8.

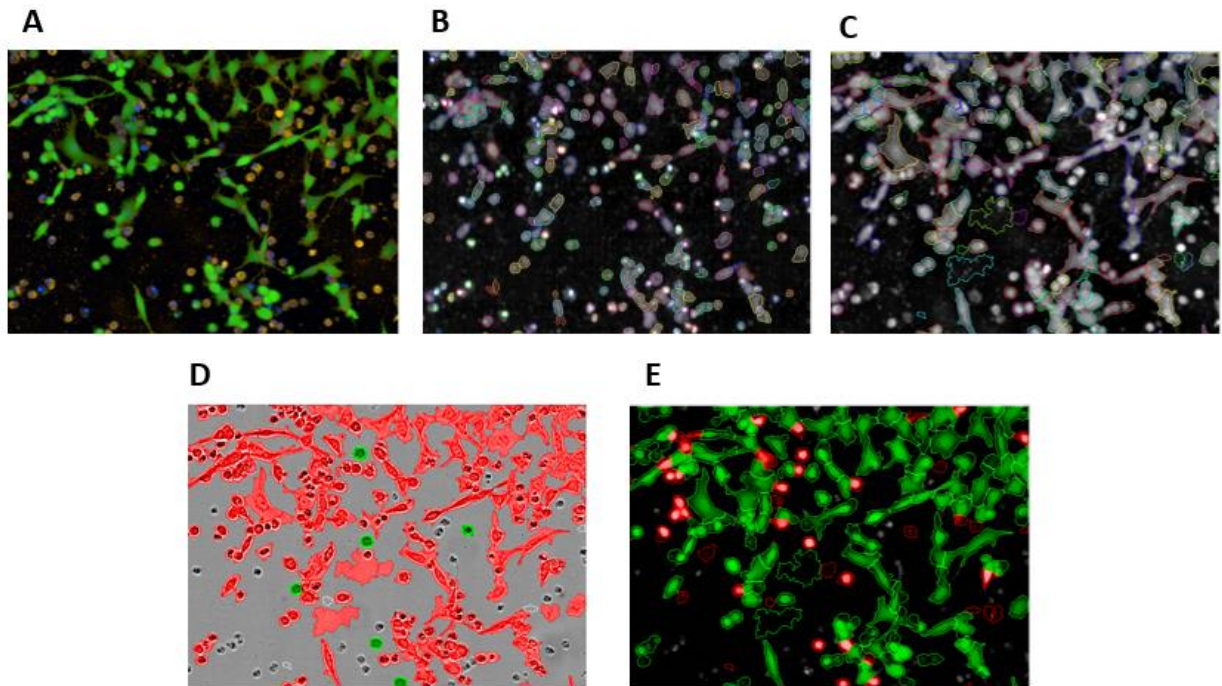


Figure 8: Segmentation and analysis of the neurite outgrowth assay in Harmony software. A) Original input image showing the membrane stain in red and viability stain in green. B) Segmentation of the nuclei. C) Segmentation of the cytoplasm. D) Harmony software is trained to differentiate between cells with typical neuronal morphology, shown in red and cells lacking typical neuronal morphology, shown in green. E) Viable cells are selected based on intensity of the viability stain, viable cells shown in green.

2.8 Mitochondrial Membrane Potential Assay in iNeurons

2.8.1 MMP Assay

At the endpoint of differentiation, cells were incubated for one hour with a working solution of 80nM tetramethylrhodamine, methyl ester (TMRM; Invitrogen), 10nM MitoTracker green (Invitrogen) and 10 μ M Hoechst (Sigma) in MEM. TMRM is cationic, staining the most negative part of the cell, and so can be used as a measure of mitochondrial membrane potential. However, TMRM can be used in two modes; to determine that staining is in the correct mode, in previous work a validation assay was carried out using carbonyl cyanide m-chlorophenyl hydrazone (CCCP; Sigma), a mitochondrial uncoupler which dissipates the membrane potential. A reduction in fluorescent intensity was noted, indicating TMRM was being used correctly. Immediately before imaging, wells were washed with 100 μ l MEM. Neurons were imaged using the Opera Phenix, using the 40x water objective. Approximately 20 fields of view and 5 Z planes were imaged per well using the AlexaFluor 488 (excitation 488/emission 525), AlexaFluor 568 (excitation 561/emission 603), and the DAPI channel (excitation 405/emission 461). Exposure time and exact Z plane positioning was optimised for each plate.

2.8.2 Image Analysis

Images were analysed using Harmony analysis software (Perkin Elmer). Z stacks were combined to give the maximum projection and a basic flatfield correction was applied. The nuclei and cell cytoplasm were segmented. The intensity of TMRM staining was assessed, while mitochondria were segmented and morphology analysed using the MitoTracker green stain. Mitochondria in the perinuclear region were assessed by selecting an area around the nucleus with an outer border of 25%. Form factor was assessed using the following equation: $(pm^2)/(4\pi am)$ where pm is the length of the mitochondrial perimeter and am is the area of the mitochondrion. Long and short mitochondria were separated into two separate populations with long mitochondria defined as mitochondria with a form factor over 1.4, and short mitochondria defined as those with a form factor below 1.4. This was set based on the control form factor values, to give approximately 55% long mitochondria. Images of this analysis are shown in figure 9.

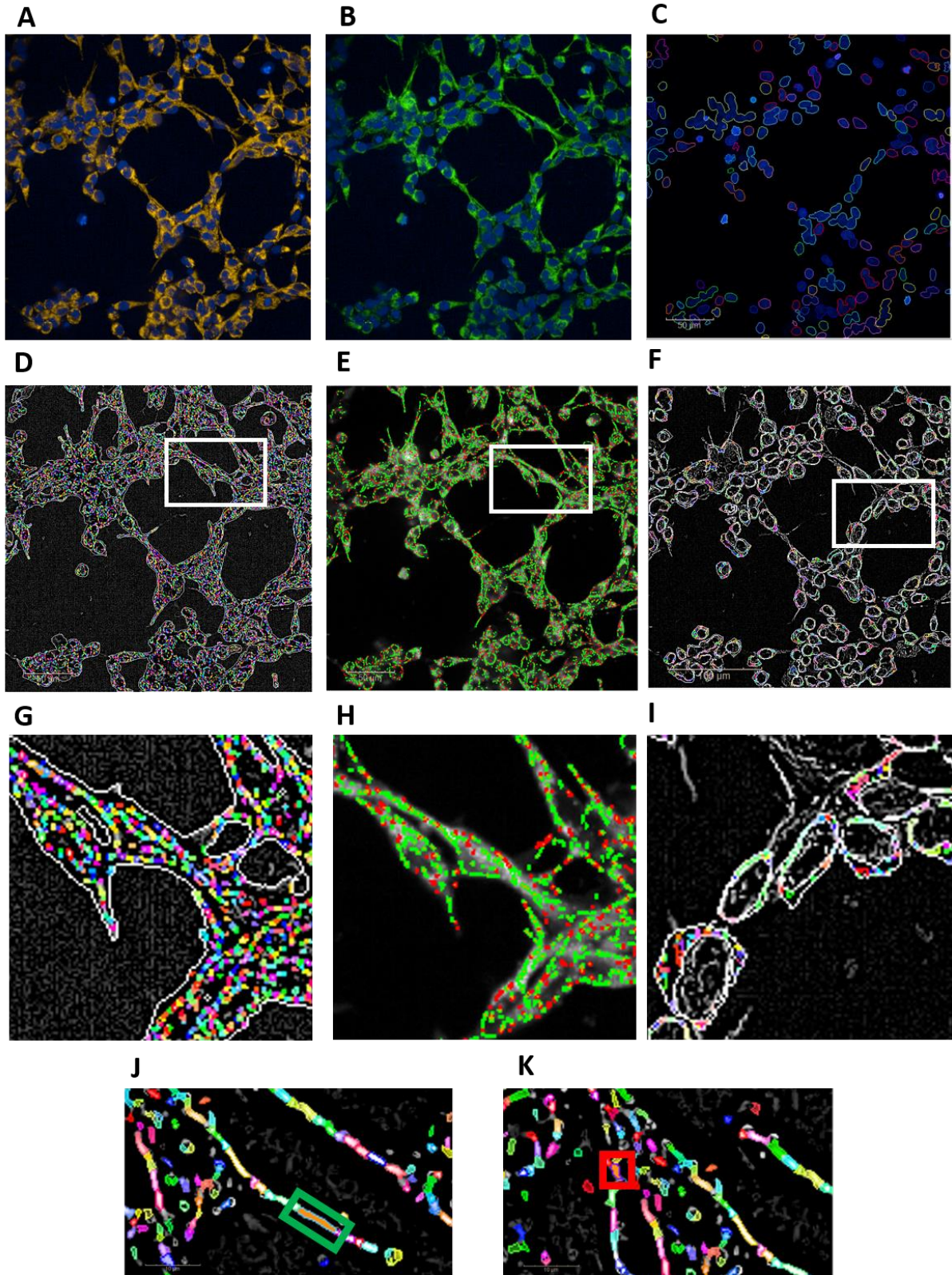


Figure 9: Analysis of mitochondrial morphology in iNeurons from the MMP Assay, in Harmony analysis software. A) Input image showing TMRM staining. B) Input image showing MitoTracker Green staining. C) Segmentation of the nuclei. D) Segmentation of the mitochondria, from the MitoTracker Green stain. E) Segmentation of long mitochondria, shown in green, and short mitochondria, shown in red. F) Segmentation of the perinuclear region, and mitochondria within the perinuclear region. G) Zoomed in image of the area in the white box in D. H) Zoomed in image of the area in the white box in E. I) Zoomed in image of the area in the white box in F. J) A long mitochondrion with a higher form factor of 1.6, highlighted in the green box. K) A short mitochondrion with a lower form factor of 1.0, highlighted in the red box.

2.9 Live Neuron Assays under Stressed Conditions

Neurons were differentiated as described above. On day 5, neurons were re-plated into low glucose (5mM) media, with added galactose (20mM). This consisted of a 1:1 mixture of Ham's F12 media (11765-054) with DMEM no glucose media (11966-025), with supplements and factors added as used in complete neuron media. They were grown in this media until the end of the protocol. On day 9, 30nM rotenone (Sigma) was added in galactose media, and cells were treated with this until the end of the protocol. At the endpoint of differentiation, the neurite outgrowth assay and MMP assay were carried out and analysed as described above.

2.10 Statistical Analysis

All statistical analysis was carried out in GraphPad Prism 7. For controls vs sAD group analyses, an unpaired t test was used. For analysis of individual lines, a One Way ANOVA with either Dunnett's or Sidak's multiple comparisons was used. For assessment of associations between parameters, a linear regression analysis was used.

Chapter Three: Investigating Mitochondrial Dynamics in sAD Patient Fibroblasts

3.1 Introduction

3.1.1 Mitochondrial Phenotype in Patient Derived Fibroblasts

This project will investigate mitochondrial abnormalities utilising patient-derived cell models of sAD. The first model to be assessed is fibroblasts sourced locally as part of the MODEL-AD study, from both sAD patients and healthy controls, age and sex matched as closely as possible. Fibroblasts are dermal cells, present in connective tissue. They are cultured from a skin punch biopsy, a relatively simple procedure with very few complications (Auburger *et al.*, 2012). They are robust in culture and storage, and have been used to investigate neurodegenerative disorders, including AD, for many years.

Whilst fibroblasts are not directly implicated in AD pathology, their relevance as a disease model is based on the proposed systemic nature of AD. This is a long-standing theory (Blass and Zemcov, 1984; Baker, Ko and Blass, 1988), and states that many of the cellular changes present in neural cells are also present in peripheral cells, and it is the vulnerability of neurons and other neural cell types which cause the brain to be so severely affected (reviewed by Trushina, 2019). Fibroblasts also maintain the genetic background of the patient, and aged characteristics of the cell. sAD in particular is difficult to model due to the complex aetiology, and patient cells are a key model which is able to do this. Fibroblasts recapitulate many pathological features of AD including the accumulation of A β (Joachim, Mori and Selkoe, 1989; Soininen *et al.*, 1992; Citron *et al.*, 1994; Johnston *et al.*, 1994; Gray and Quinn, 2015; Bhattacharya *et al.*, 2020) and expression of tau (Matsuyama and Bondareff, 1994) which is phosphorylated in Alzheimer's patient fibroblasts (Jong *et al.*, 2003; Ploia *et al.*, 2011).

Importantly for this project, fibroblasts from AD patients also have altered mitochondrial function, including decreased complex IV activity (Curti *et al.*, 1997), decreased ATP levels (Gray and Quinn, 2015; Pérez *et al.*, 2017), and decreased mitochondrial membrane potential (Amit U. Joshi *et al.*, 2018; Bell *et al.*, 2018, 2020). Reduced basal and maximal oxygen consumption and spare respiratory capacity (Gray and Quinn, 2015; Amit U. Joshi *et al.*, 2018; Bell *et al.*, 2018, 2020) have also been noted, in both sAD and fAD fibroblasts. Recently, our lab has discovered a correlation between mitochondrial function and neuropsychological tests, specifically mitochondrial spare capacity and

delayed episodic recall (Bell *et al.*, 2020), highlighting the benefit of studying these pathological mechanisms in peripheral cells.

Alterations in mitochondrial morphology have also been seen, though findings are not consistent. Mitochondria have been seen to accumulate around the perinuclear region (Xinglong Wang *et al.*, 2008; Martín-Maestro, Gargini, García, *et al.*, 2017; Bell *et al.*, 2018), suggesting a collapse in the mitochondrial network. Since work on this project began, Drabik *et al.* (2021) have identified a decrease in fragmentation of the mitochondrial network, noting a reduction in both the number and area of mitochondria which were separated from the network. They also saw an increase in branch length, while Wang *et al.* (2008) found an increase in mitochondrial length, and we found an increase in the percentage of the cell taken up by long mitochondria (Bell *et al.*, 2018). In contrast, Pérez *et al.* (2017) and Joshi *et al.* (2018) both saw a reduction in mitochondrial length, indicating a more fragmented network. Taken as a whole, the literature is clear that there are alterations in mitochondrial morphology in AD patient fibroblasts, but there is no consensus as to whether the network is more or less fragmented.

Mitochondrial morphology is controlled by several dynamic processes, including fission and fusion. These processes, and the proteins involved in them, have also been investigated. Drabik *et al.* (2021) found reduced rates of both fission and fusion, as well as reduced levels of fusion protein Mfn2. Others have seen reductions in several OPA1 isoforms (Pérez *et al.*, 2017), though some have seen no change (Xinglong Wang *et al.*, 2008). Several studies have noted a decrease in mitochondrial fission protein Drp1 (Xinglong Wang *et al.*, 2008; Martín-Maestro, Gargini, García, *et al.*, 2017; Bell *et al.*, 2018; Drabik, Piecyk, *et al.*, 2021), though this is also inconsistent (Amit U. Joshi *et al.*, 2018). Drp1 is usually located in the cytosol and is recruited to mitochondria during fission events; Drp1 localised to the mitochondria has been seen to be both reduced (Martín-Maestro, Gargini, García, *et al.*, 2017; Bell *et al.*, 2018), and increased (Amit U. Joshi *et al.*, 2018). Interestingly, the proportion of total Drp1 localised to the mitochondria has been seen to be increased, while the proportion of total mitochondria with Drp1 was decreased (Drabik, Piecyk, *et al.*, 2021). This does not indicate whether there are higher or lower levels of Drp1 localised to the mitochondria, but does suggest that despite more of the cell's total Drp1 being used at the mitochondria, the cell is still unable to recruit Drp1 to as many mitochondria as in healthy cells, which may lead to a reduction in fission. Alterations in Drp1 localisation may be due to alterations in total levels of Drp1, or may suggest an impairment in the recruitment of Drp1 to the mitochondria. Drp1 is recruited by four proteins on the outer mitochondrial membrane: Fis1, Mff, MiD49, and MiD51. These proteins are less well studied in AD fibroblasts, though Wang *et al.* (2008) noted an increase in Fis1, whilst Drabik *et al.* (2021) saw no change in Fis1 but did see a decrease in Mff.

Considering the differing findings with regard to mitochondrial morphology in AD fibroblasts, it is not surprising that investigations into the processes controlling this morphology also yield differing results. This chapter will investigate these mechanisms on a deeper level, in an attempt to better understand these processes and how they contribute to mitochondrial dysfunction in AD patient fibroblasts.

3.1.2 Previous Work

Previous work in our lab, carried out by the author as part of a previous MSc project and others, has looked into mitochondrial function and morphology in both locally collected control and sAD fibroblast lines, and commercially available lines from controls, sAD, and patients with a PSEN1 mutation. Mitochondrial membrane potential, as well as spare capacity, were reduced in both sporadic and PSEN1 cohorts; these deficits were improved by treatment with ursodeoxycholic acid (UDCA), a known modulator of mitochondrial function (Bell *et al.*, 2018, 2020). Mitochondrial morphology was also altered, with an increase in the percentage of the cell taken up by long mitochondria and more mitochondria accumulated around the perinuclear region. Total Drp1 levels, as well as Drp1 localised to the mitochondria, were reduced in a smaller subset of the locally collected cohort, as well as in the commercially available cohort.

3.1.3 Aims and Objectives

The aim of this chapter is to investigate further the mechanisms leading to and resulting from reduced levels of Drp1 in an expanded, locally collected cohort of sAD patient fibroblasts and healthy controls. The objectives are:

1. To measure total protein expression of Drp1 in an expanded cohort
2. To measure total protein expression of the four Drp1 receptors, Fis1, Mff, MiD49, and MiD51
3. To measure interactions between Drp1 and the receptors
4. To investigate post translational modifications of Drp1, primarily phosphorylation at ser637 and ser616
5. To investigate mechanisms upstream of Drp1 recruitment
6. To determine whether overexpression of Drp1 can rescue deficits seen

3.2 Results

3.2.1 Drp1 Protein Expression in sAD Fibroblasts

Previous work found a reduction in total levels of Drp1 in four sAD patient fibroblast lines from the MODEL-AD study (sAD4, sAD5, sAD6, sAD7), as well as three sAD patients and three PSEN1 patients from the Coriell cell repository, compared to four MODEL-AD and three Coriell control lines.

Total cellular protein levels of Drp1 were assessed via western blotting in a further six controls and six sAD patients (sAD1, sAD2, sAD3, sAD8, sAD9, sAD10) from the MODEL-AD study, expanding the cohort from work carried out previously. Drp1 undergoes alternative splicing to give different isoforms, with cell type specific expression (Rosdah *et al.*, 2020). The splice variants shown here have been seen in fibroblasts in previously published work (Xinglong Wang *et al.*, 2008; Drabik, Piecyk, *et al.*, 2021).

It was found that in the ten sAD patients and ten controls included in the MODEL-AD study, Drp1 was reduced by 35% (controls 1.02 ± 0.01 ; sAD 0.67 ± 0.33) in sAD patient fibroblasts compared to controls (figure 10c; $p < 0.0001$). At an individual level, a significant decrease was seen in seven sAD lines compared to controls; sAD 1 was decreased by 45.7% ($p = 0.0009$; figure 10b), sAD 2 was decreased by 46.7% ($p = 0.0002$; figure 10b), sAD 4 was decreased by 54% ($P < 0.0001$; figure 10b), sAD 5 was decreased by 78% ($p < 0.0001$; figure 10b), sAD 6 was decreased by 48.1% ($p = 0.0005$; figure 10b), sAD 7 was decreased by 25.7% ($p = 0.0376$; figure 10b), and sAD 8 was decreased by 50.2% ($p = 0.0003$; figure 10b). sAD 10 was the only line which showed a significant increase in Drp1 levels, of 41.6% ($p = 0.0026$; figure 10b).

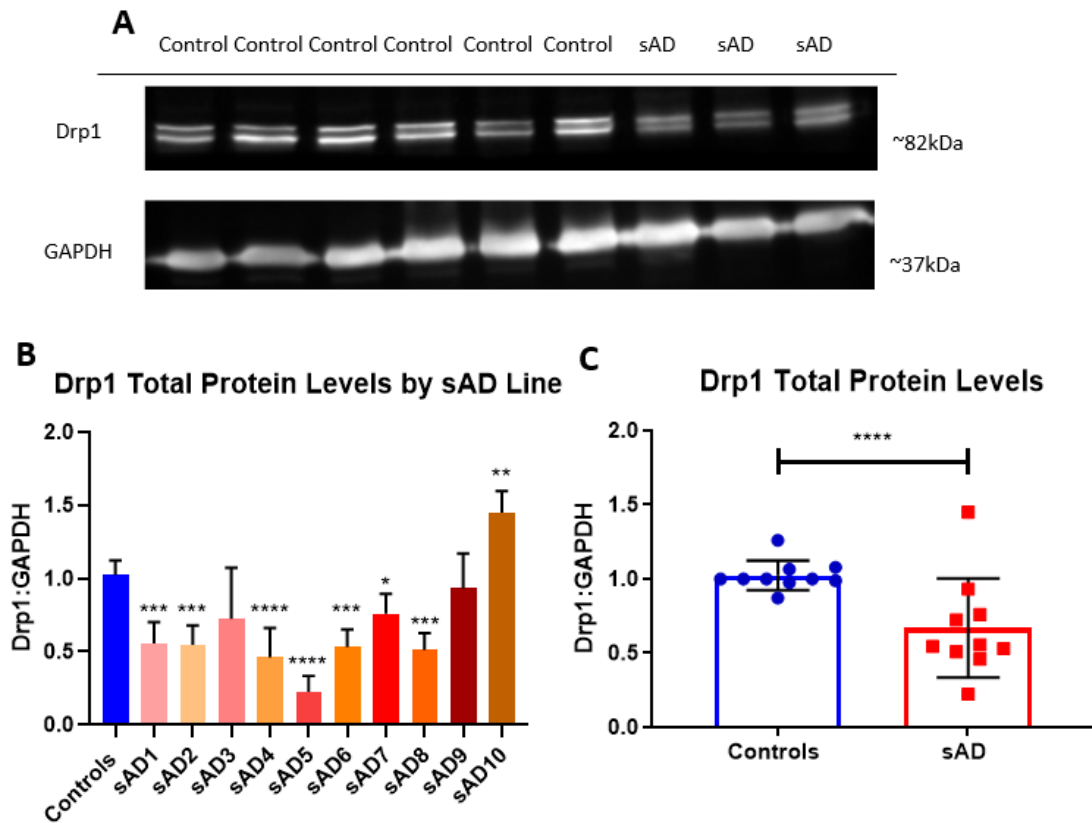


Figure 10 : Total Drp1 protein levels are reduced in ten sAD patient fibroblast lines compared to ten controls ($p < 0.0001$). A) A representative blot of Drp1 and GAPDH loading control in 6 control and 3 sAD patient fibroblast lines, with 10 μ g protein loaded per lane. The double band is expected as Drp1 exists as two isoforms in fibroblasts, and both bands have been quantified together here. B) Quantification of Drp1 in ten controls and ten sAD patients, where controls are shown as a group and sAD lines shown individually. Each line was measured from samples of 3 separate passages. A significant decrease in Drp1 protein levels is seen in seven of ten sAD patient fibroblast lines, and a significant increase in one line (* $p < 0.05$, ** $p < 0.01$, *** $p < 0.001$, **** $p < 0.0001$; One way ANOVA with Dunnett's multiple comparisons). Four controls plus sAD4, sAD5, sAD6 and sAD7 were assessed by the author as part of previous work carried out by the lab. Bars represent mean, and error bars represent SD. C) Drp1 protein levels are significantly decreased by 35% when the sAD group are compared to the control group (**** $p < 0.0001$; t test). Each dot represents the mean of three replicates per line, bars represent overall mean and error bars represent standard deviation (SD).

3.2.2 Phosphorylated Drp1 in sAD Fibroblasts

Post translational modifications of Drp1 are key in its fission activity; Drp1 must be dephosphorylated at serine 637 and phosphorylated at serine 616. To determine whether this is affected in sAD, levels of phosphorylated Drp1 were assessed via western blotting. Unfortunately, very low levels of phosphorylated Drp1 were seen in both control and sAD fibroblasts, and this could not be quantified (figure 11).

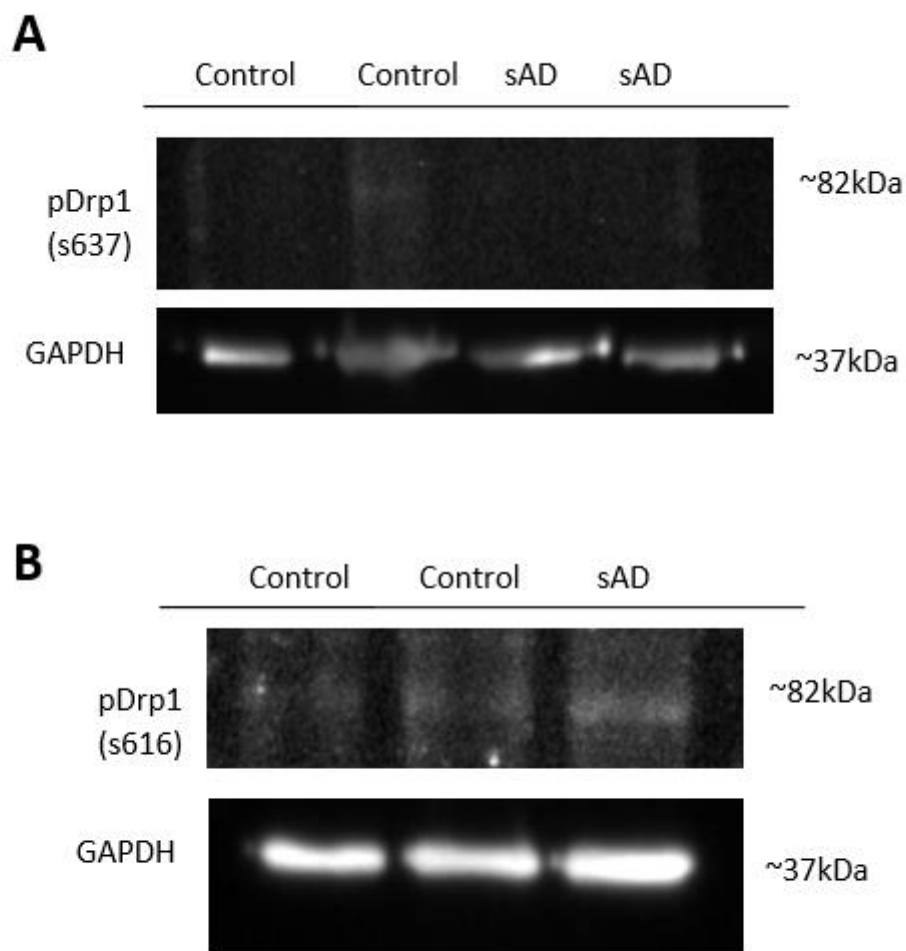
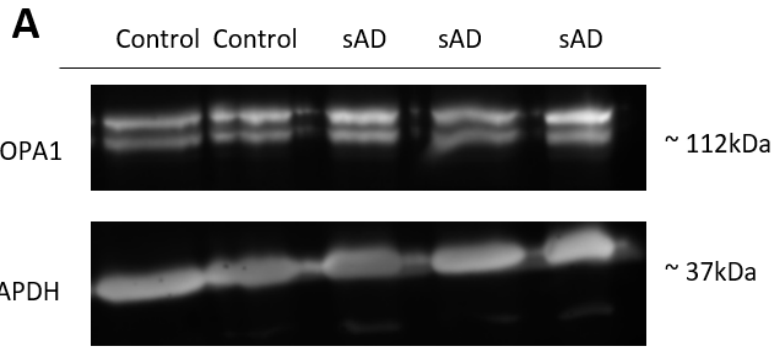


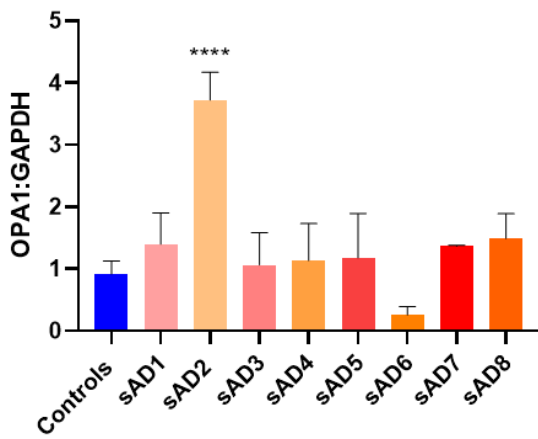
Figure 11: Expression of pDrp1 (s637) and pDrp1 (s616) were very low in both control and sAD fibroblasts. This was unable to be quantified.

3.2.2 OPA1 Protein Expression in sAD Fibroblasts

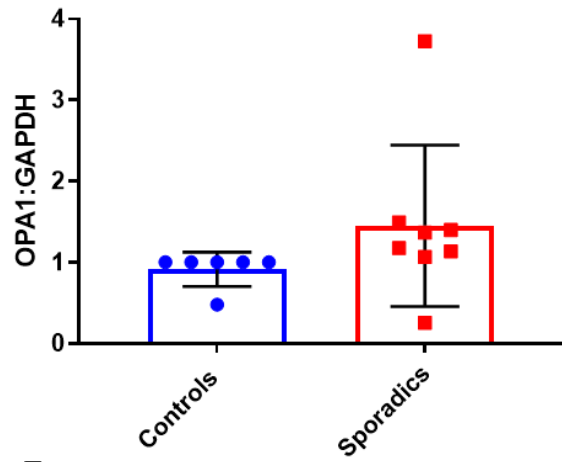
Increased levels of short form OPA1 have been proposed to play a role in fission, while the longer form is involved in fusion (Anand *et al.*, 2014). Total cellular protein levels of OPA1 were investigated via western blotting in six control and eight sAD patient fibroblast lines, as well as the ratio of short form OPA1 to long form OPA1. A change in this ratio would indicate that there is a change in the processing of OPA1, potentially due to a shift in the fission fusion balance. One line, sAD 2, showed a significant increase in total OPA1 expression levels of 407% ($p < 0.0001$; figure 12b) however when group-wise comparisons were undertaken, no significant difference was seen (controls 0.91 ± 0.21 ; sAD 1.45 ± 1.0 ; $p = 0.2214$; figure 12c). There was some variability seen in sAD lines, with many showing an increase, and sAD6 in particular showing a decrease of 72% ($p = 0.3589$; figure 12b). There was no significant difference seen in the ratio of the short OPA1 isoform to the long OPA1 isoform (controls 0.36 ± 0.08 ; sAD 0.37 ± 0.09 ; $p = 0.7990$; Figure 12d-e), suggesting that there is no difference in OPA1 processing between control and sAD fibroblasts.



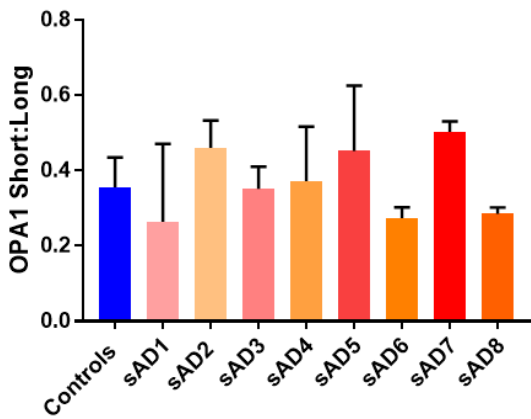
B
OPA1 Total Protein Levels by sAD Line



C
Total OPA1 Protein Levels



D
OPA1 Short:Long Ratio



E
OPA1 Short:Long Ratio

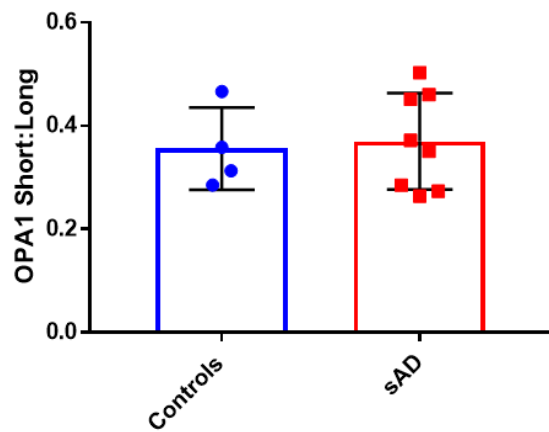


Figure 12: There is no significant difference in total OPA1 protein levels between control and sAD patient fibroblasts. A) A representative blot of OPA1 and GAPDH loading control in two control and three sAD patient fibroblast lines, with 10 μ g protein loaded per lane. B) Quantification of total OPA1 in six controls and eight sAD patients at a minimum of two passages per line, with a significant increase seen in one line (**** $p < 0.0001$; One way ANOVA with Dunnett's multiple comparisons). Bars show the mean, and error bars represent SD. C) There is no significant difference in OPA1 total protein levels when individual lines are combined ($p = 0.2214$; t test). Each dot shows the mean of the replicates for each line, bars represent the overall mean, and error bars represent SD. D) Quantification of the ratio of short OPA1 isoform to long OPA1 isoform in four controls and eight sAD patients, at a minimum of 2 passages per line. Bars show the mean, and error bars represent SD. E) There is no significant difference in the ratio of short OPA1 to long OPA1 when individual lines are combined ($p = 0.7990$; t test). Each dot shows the mean of the replicates for each line, bars represent the overall mean, and error bars represent SD.

3.2.3 Drp1 Receptor Protein Expression in sAD Fibroblasts

In order to determine whether other proteins involved in fission are also reduced in sAD patient fibroblasts, total cellular protein levels of the four Drp1 receptors present on the outer mitochondrial membrane, Fis1, Mff, MiD49, and MiD51, were assessed via western blotting, in ten sAD patients and ten controls from the MODEL-AD study. Fis1 was found to be reduced in eight individual lines; sAD 1 was decreased by 67.1% ($p < 0.001$; figure 13b), sAD 2 was decreased by 44.2% ($p = 0.003$; figure 13b), sAD 4 was decreased by 72.7% ($p < 0.0001$; figure 13b), sAD 5 was decreased by 54.2% ($p = 0.001$; figure 13b), sAD 6 was decreased by 41.0% ($p = 0.0169$; figure 13b), sAD 8 was decreased by 38% ($p = 0.0294$; figure 13b), sAD 9 was decreased by 65.5% ($p < 0.0001$; figure 13b), and sAD 10 was decreased by 52.8% ($p = 0.0014$; figure 13b). At a group level, there was an overall reduction of 48% (controls 1.05 ± 0.23 ; sAD 0.54 ± 0.19) in sAD patient fibroblasts compared to controls (figure 13c; $p < 0.0001$).

Mff levels were seen to be reduced in six individual sAD fibroblasts lines; sAD 1 was decreased by 58.9% ($p = 0.0013$; figure 14b), sAD 2 was decreased by 64.7% ($p = 0.0004$; figure 14b), sAD 3 was decreased by 50.3% ($p = 0.0073$; figure 14b), sAD 5 was decreased by 56.1% ($p = 0.0007$; figure 14b), sAD 8 was decreased by 51.2% ($p = 0.0061$; figure 14b), and sAD 9 was decreased by 40.3% ($p < 0.0001$; figure 14b). At a group level, a decrease of 42% (Controls 1.09 ± 0.19 ; sAD 0.63 ± 0.31) was seen in sAD fibroblast lines compared to controls (figure 14c; $p < 0.0001$).

MiD49 was reduced in three individual sAD lines; sAD 1 was decreased by 57.0% ($p = 0.0252$; figure 15b), sAD 2 was decreased by 57.9% ($p = 0.0225$; figure 15b), and sAD 6 was decreased by 66.9% ($p = 0.0063$; figure 15b). At a group level, there was an overall reduction of 36% (Controls 1.03 ± 0.28 ; sAD 0.66 ± 0.26) in sAD fibroblasts compared to controls (figure 15c; $p = 0.0031$).

There was no significant difference in MiD51 protein levels between controls and patients, at an individual or group level (Controls 1.08 ± 0.35 ; sAD 1.06 ± 0.20 ; $p = 0.5689$; figure 16).

Overall, when considering all the protein assessed thus far, sAD1 and sAD2 showed deficits in the most proteins, with four of five proteins investigated reduced compared to controls. sAD3, sAD7, and sAD10 showed deficits in the least number of proteins, with only one of five proteins reduced compared to controls (table 17).

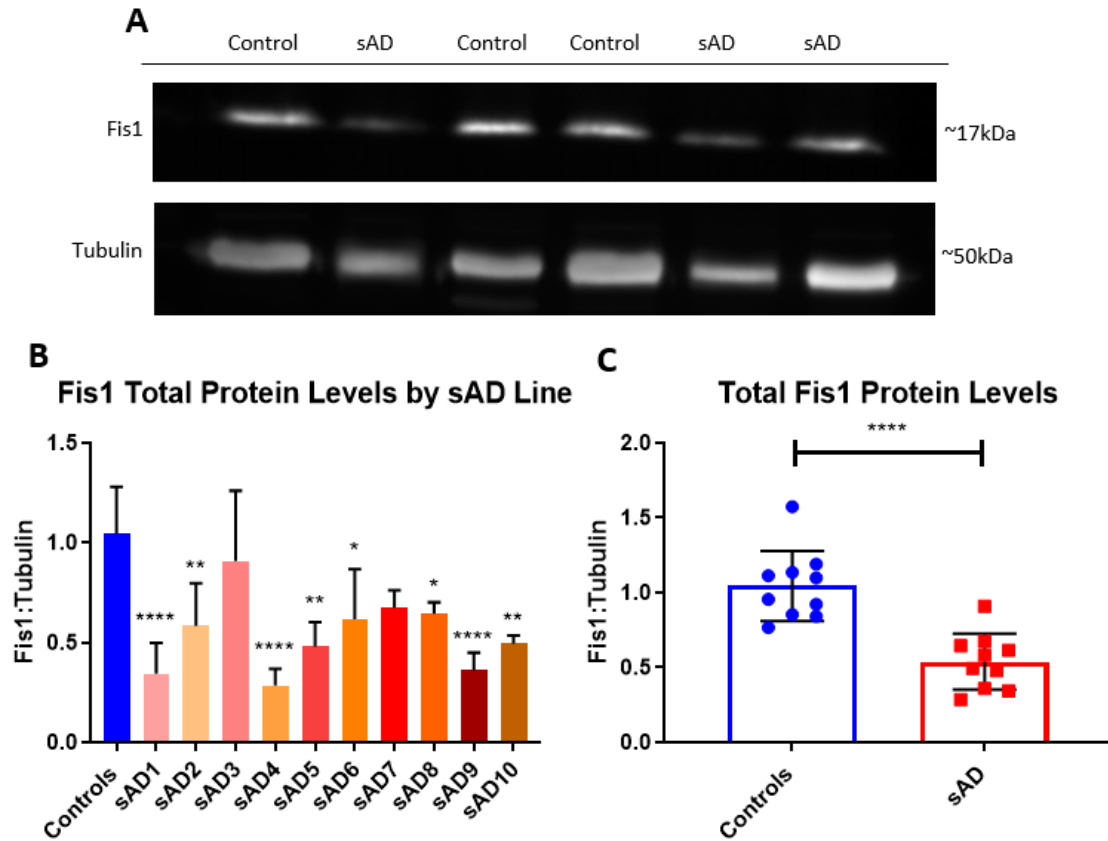


Figure 13: Total Fis1 protein levels are reduced in ten sAD patient fibroblast lines compared to ten controls ($p < 0.0001$). A) A representative blot of Fis1 and tubulin loading control in three controls and three sAD patient fibroblast lines, with 10 μ g protein loaded per lane. B) Quantification of Fis1 in ten controls and ten sAD patients at 3 passages per line, with a significant decrease in Fis1 protein levels seen in eight of ten sAD patient fibroblast lines (* $p < 0.05$ ** $p < 0.01$, *** $p < 0.001$, **** $p < 0.0001$; One way ANOVA with Dunnett's multiple comparisons). Bars represent the mean and error bars represent SD. C) Fis1 protein levels are significantly decreased by 48% when individual lines are combined (**** $p < 0.0001$; t test). Each dot represents the mean of replicates for each line, bars represent the overall mean, and error bars represent SD.

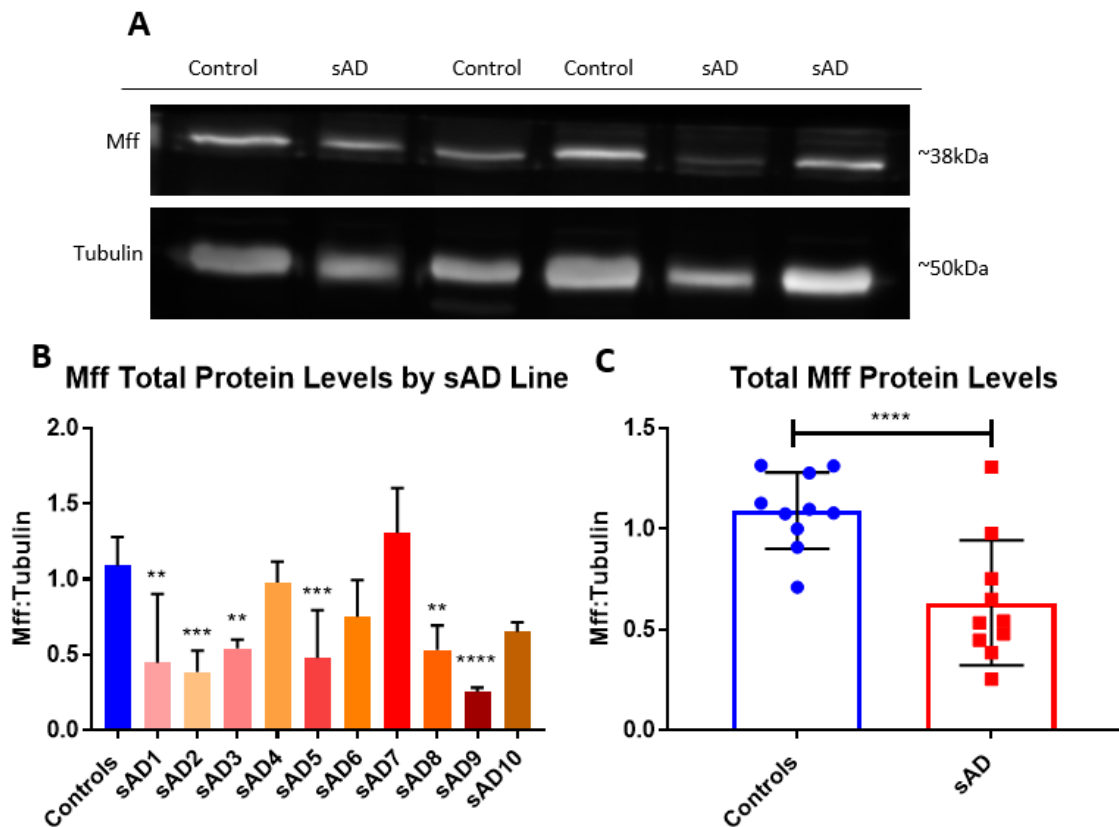


Figure 14: Total Mff protein levels are reduced in ten sAD patient fibroblast lines compared to ten controls ($p < 0.0001$). A) A representative blot of Mff and tubulin loading control in three controls and three sAD patient fibroblast lines, with 10 μ g protein loaded per lane. B) Quantification of Mff in ten controls and ten sAD patients at 3 passages per line, with a significant decrease in Mff protein levels seen in six of ten sAD patient fibroblast lines (* $p < 0.05$ ** $p < 0.01$, *** $p < 0.001$, **** $p < 0.0001$; one way ANOVA with Dunnett's multiple comparisons). Bars represent the mean and error bars represent SD. C) Mff protein levels are significantly decreased by 42% when individual lines are combined (**** $p < 0.0001$; t test). Each dot represents the mean of replicates for each line, bars represent the overall mean, and error bars represent SD.

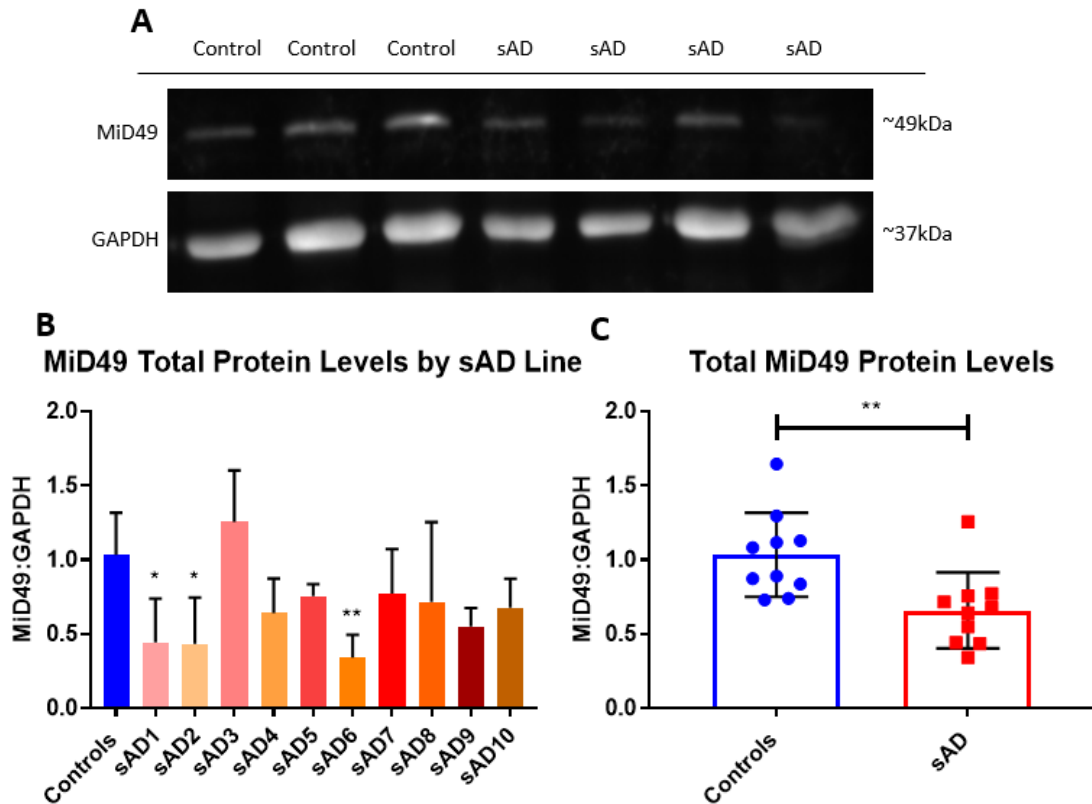


Figure 15: Total MiD49 protein levels are reduced in ten sAD patient fibroblast lines compared to ten controls ($p = 0.0031$). A) A representative blot of MiD49 and GAPDH loading control in three controls and four sAD patient fibroblast lines, with 10 μ g protein loaded per lane. B) Quantification of MiD49 in ten controls and ten sAD patients at 3 passages per line, with a significant decrease in MiD49 protein levels seen in three of ten sAD patient fibroblast lines (* $p < 0.05$ ** $p < 0.01$; one way ANOVA with Dunnett's multiple comparisons). Bars represent the mean and error bars represent SD. C) MiD49 protein levels are significantly decreased by 36% when individual lines are combined ($p = 0.0031$; t test). Each dot represents the mean of replicates for each line, bars represent the overall mean, and error bars represent SD.**

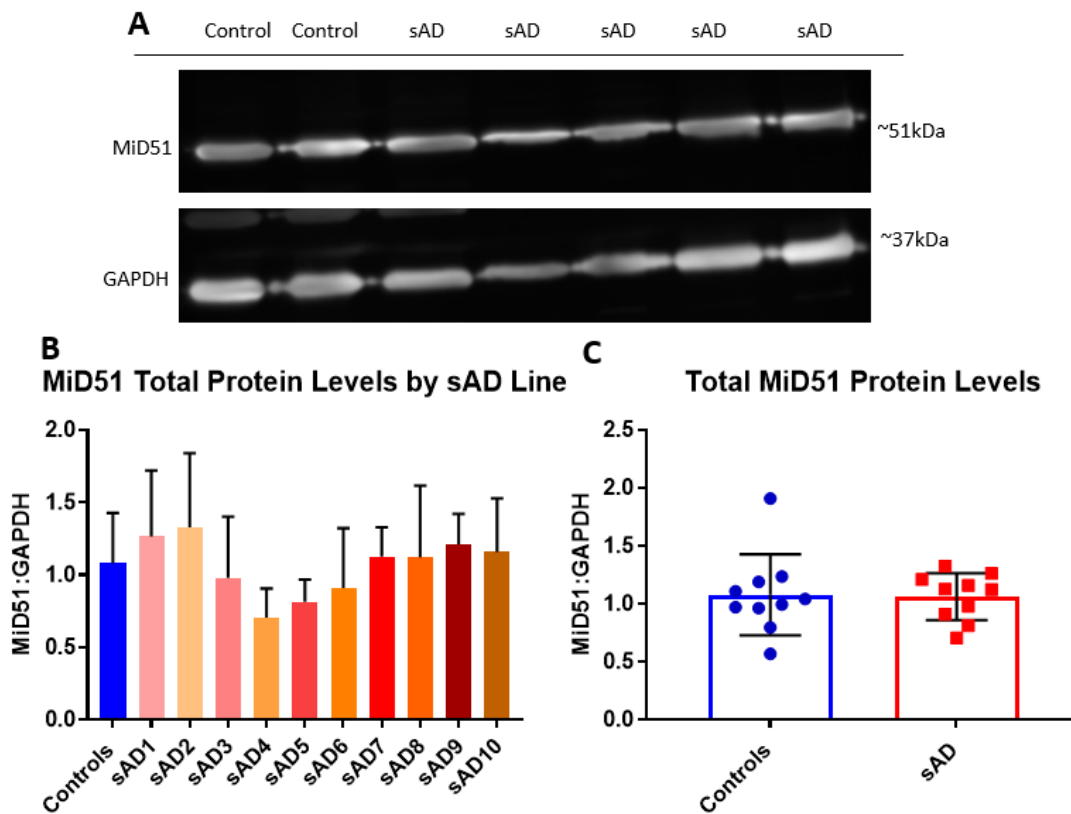


Figure 16: Total MiD51 protein levels are not significantly different ten sAD patient fibroblast lines compared to ten controls ($p = 0.5689$). A) A representative blot of MiD51 and GAPDH loading control in two controls and five sAD patient fibroblast lines, with 10 μ g protein loaded per lane. B) Quantification of MiD51 in ten controls and ten sAD patient fibroblast lines at three passages per line, with no significant difference in any patient (one way ANOVA with Dunnett's multiple comparisons). Bars represent the mean and error bars represent SD. C) MiD51 protein levels are not significantly different when individual lines are combined ($p = 0.5689$; t test). Each dot represents the mean of replicates for each line, bars represent the overall mean, and error bars represent SD.

Table 17: Summary table of total protein levels of Drp1 and the four Drp1 receptors on the outer mitochondria membrane, Fis1, Mff, MiD49, and MiD51, in sAD patient fibroblasts. A green arrow represents a significant increase, a red arrow represents a significant decrease and a yellow bar represents no significant difference (** $p < 0.0001$, *** $p < 0.001$, ** $p < 0.01$, * $p < 0.05$). sAD1 and sAD2 show the most deficits, in four out of five proteins, while sAD3, sAD7, and sAD10 show the least, in only one of four proteins.**

	sAD1	sAD2	sAD3	sAD4	sAD5	sAD6	sAD7	sAD8	sAD9	sAD10
Drp1 Total Protein	*** ↓	*** ↓	—	**** ↓	**** ↓	*** ↓	* ↓	*** ↓	—	** ↑
Fis1 Total Protein	**** ↓	** ↓	—	**** ↓	** ↓	* ↓	—	* ↓	**** ↓	** ↓
Mff Total Protein	** ↓	*** ↓	** ↓	—	*** ↓	—	—	** ↓	**** ↓	—
MiD49 Total Protein	* ↓	* ↓	—	—	—	** ↓	—	—	—	—
MiD51 Total Protein	—	—	—	—	—	—	—	—	—	—

3.2.4 Linear Regression Between Drp1 and Receptors in sAD Fibroblasts

To help to determine the importance of each receptor in the recruitment of Drp1, and whether this changes in sAD, linear regression between Drp1 protein levels and protein levels of each receptor was investigated. There is a significant linear regression between Drp1 and Fis1 ($r^2 = 0.2437$; $p = 0.0269$; figure 17a), and Drp1 and Mff ($r^2 = 0.24$; $p = 0.0283$; figure 17b). In Mff, a significant linear regression was seen in the controls as an individual group ($r^2 = 0.5924$; $p = 0.009$; figure 17b), but not in sAD fibroblasts. There is no significant linear regression between MiD49 and Drp1, or MiD51 and Drp1 (figure 17c-d).

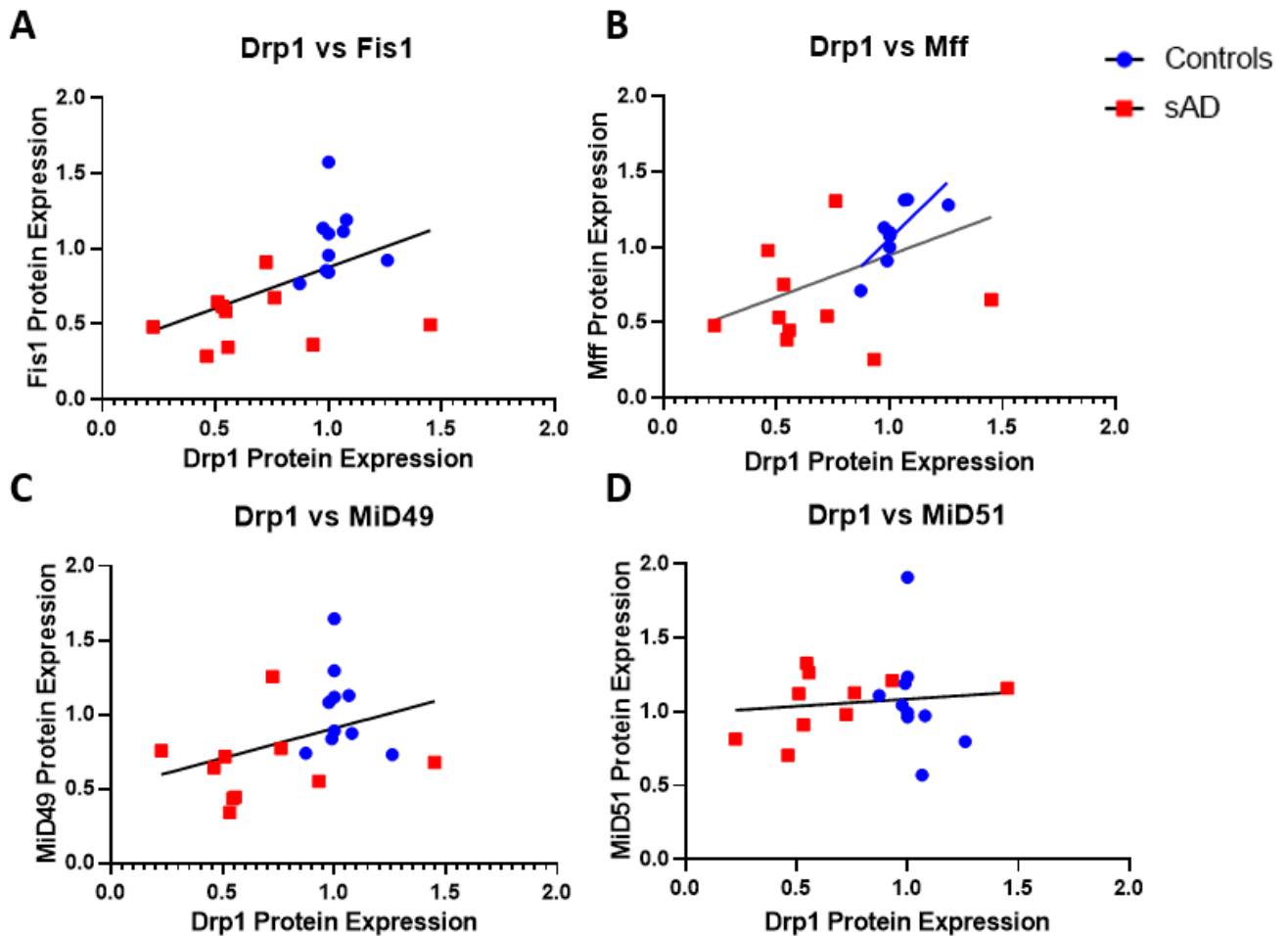


Figure 17: Linear regression between protein levels of Drp1 and protein levels of Fis1, Mff, MiD49 and MiD51 in fibroblasts. A) There is a significant linear regression between Drp1 and Fis1 levels ($r^2 = 0.2437$; $p = 0.0269$), but this is not present in either control or sAD fibroblasts as individual groups. B) There is a significant linear regression between Drp1 and Mff overall (black line; $r^2 = 0.24$; $p = 0.0283$). This is seen in control fibroblasts (blue line; $r^2 = 0.5924$; $p = 0.009$), but not in sAD patient fibroblasts. C) There is no significant linear regression between Drp1 and MiD49 protein levels overall, or in either control or sAD fibroblasts. D) There is no significant linear regression between Drp1 and MiD51 overall, or in either control or sAD fibroblasts.

3.2.5 Linear Regression Between Fission Proteins and Mitochondrial Function in sAD Fibroblasts

In order to understand the relationship between the expression of fission proteins and mitochondrial function, linear regression between the fission protein expression and mitochondrial membrane potential was investigated. Mitochondrial membrane potential in this cohort of sAD fibroblast was assessed in previous work carried out in part by the author as part of a previous MSc project, and in part by Dr Simon Bell. A significant linear regression was seen between MMP and Drp1 ($r^2 = 0.3633$; $p = 0.0049$; figure 18a), and MMP and Fis1, ($r^2 = 0.2797$; $p = 0.0187$; figure 18b). No significant regression was seen between MMP and Mff, MMP and MiD51, and MMP and MiD49, though MiD49 was approaching significance ($r^2 = 0.1825$; $p = 0.0603$; figure 18c-e).

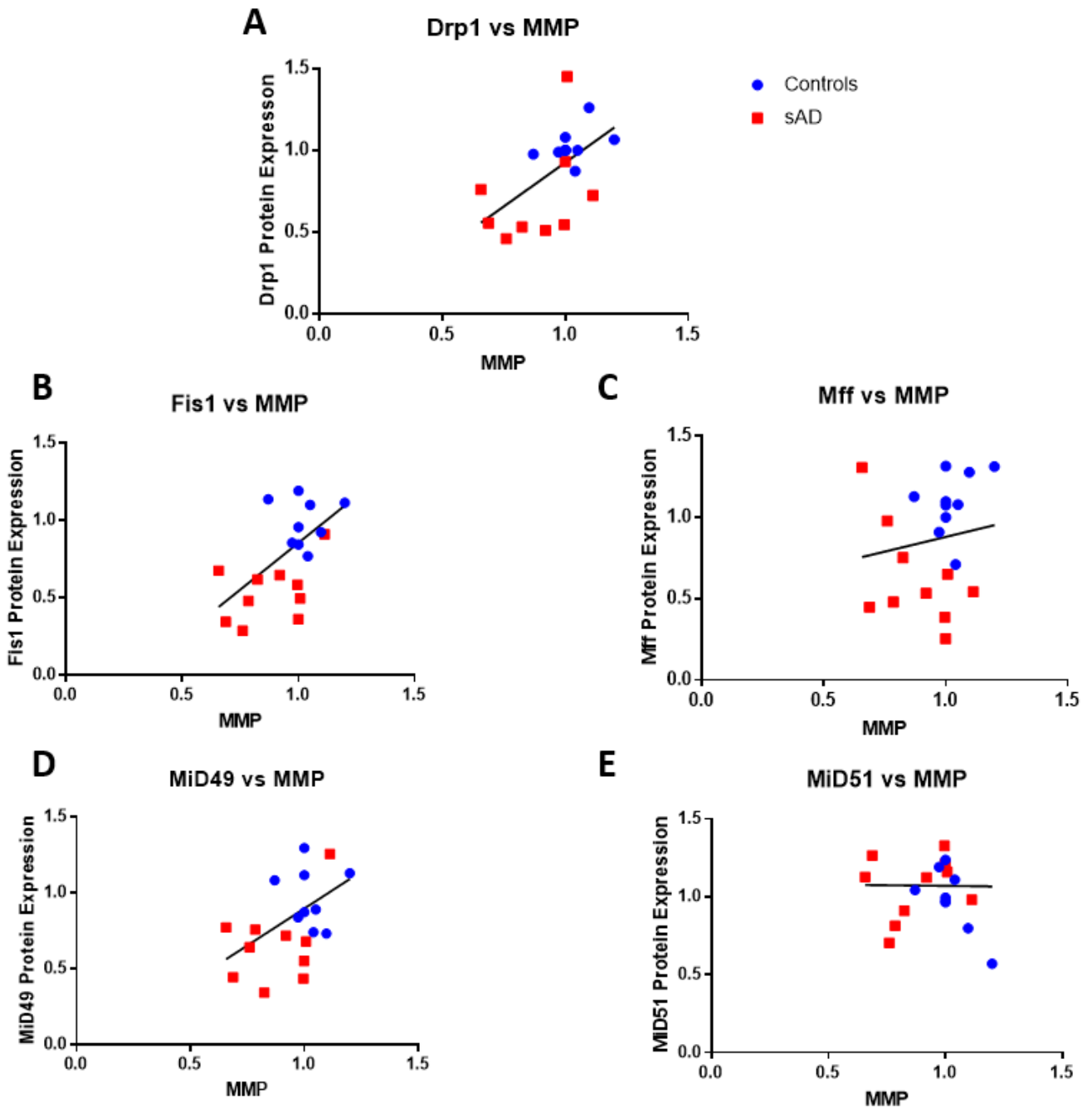


Figure 18: Linear regression between MMP and expression of fission proteins Drp1, Fis1, Mff, MiD49, and MiD51 in fibroblasts. A) There is a significant linear regression between MMP and Drp1 ($r^2 = 0.3633$; $p = 0.0049$). B) There is a significant linear regression between MMP and Fis1 ($r^2 = 0.2797$; $p = 0.0187$). C) There is no significant linear regression between MMP and Mff. D) There is no significant linear regression between MMP and MiD49, though this is approaching significance ($r^2 = 0.1825$; $p = 0.0603$). E) There is no significant linear regression between MMP and MiD51.

3.2.6 Linear Regression Between Fission Proteins and Mitochondrial Morphology in sAD Fibroblasts

In order to understand the relationship between mitochondrial fission proteins and mitochondrial morphology, the linear regression between the expression of these proteins and form factor, a measure of mitochondrial interconnectivity, calculated using the following equation: $(pm^2)/(4\pi am)$ where pm is the length of the mitochondrial perimeter and am is the area of the mitochondrion, was assessed. An increase in form factor indicates a more fused mitochondrial network. Mitochondrial form factor was assessed in this cohort of fibroblasts by Dr Simon Bell (Bell et al., 2018; Dr Simon Bell's PhD Thesis). A significant linear regression was seen between Drp1 protein expression and mitochondrial form factor ($r^2 = 0.3135$; $p = 0.0127$; figure 19a), and Fis1 expression and mitochondrial form factor ($r^2 = 0.2605$; $p = 0.0256$; figure 19b). Linear regression between Mff expression and mitochondrial form factor was very close to being significant ($r^2 = 0.3079$; $p = 0.0509$; figure 19c). There was no significant linear regression seen between form factor and MiD49, or form factor and MiD51 (figure 19d-e).

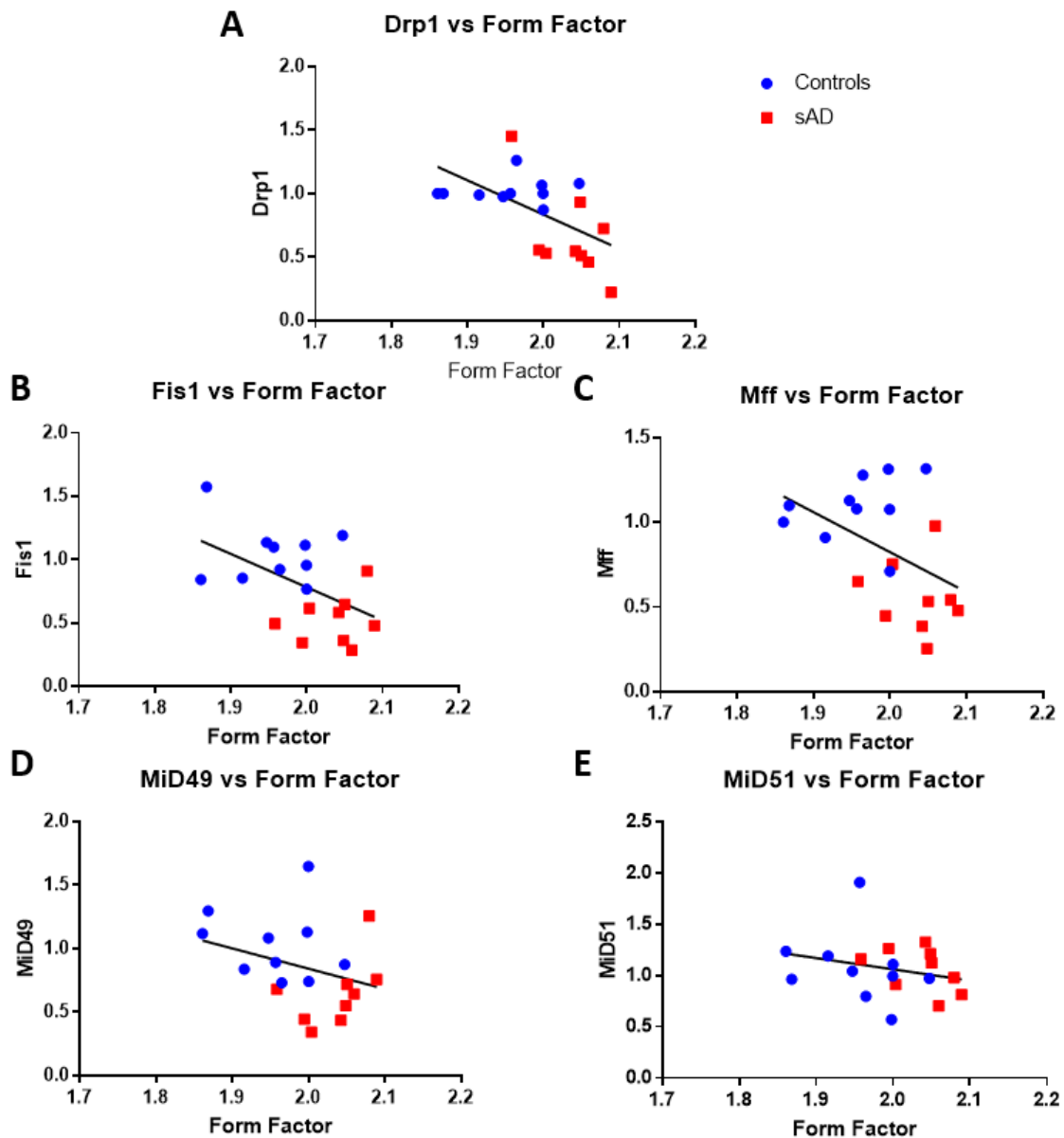


Figure 19: Linear regression between form factor, a measure of mitochondrial interconnectivity, and fission proteins Drp1, Fis1, Mff, MiD49, and MiD51 in fibroblasts. A) There is a significant linear regression between form factor and Drp1 ($r^2 = 0.3135$; $p = 0.0127$). B) There is a significant linear regression between Fis1 and form factor ($r^2 = 0.2605$; $p = 0.0256$). C) Linear regression between Mff and form factor is very close to significance ($r^2 = 0.3079$; $p = 0.0509$). D) There is no significant linear regression between MiD49 and form factor. E) There is no significant linear regression between MiD51 and form factor.

3.2.7 Fis1 and Mff Localisation in sAD Fibroblasts

To investigate whether reduced total levels of Drp1 receptors leads to a reduced amount of receptors localised to the mitochondria, fibroblasts were co-stained for receptors alongside TOM20,

a commonly used mitochondrial marker. Representative images are shown in figure 20 and figure 22. Due to limitations in available antibodies, only Fis1 and Mff were investigated. Due to time constraints owing to reduced access to laboratories during the Covid-19 pandemic including a full laboratory closure, only 1-2 repeats per line could be obtained and as such, statistical analysis was not carried out. Some sAD lines showed a decrease in the amount of Fis1 localised to the mitochondria, sAD 6 and sAD 9 especially, with a smaller decrease seen in sAD 8 and sAD 10 (figure 21a). These lines all showed a deficit in total Fis1 protein expression when assessed by western blot (figure 13), and hence were included for this analysis. Interestingly, deficits in Fis1 protein expression were seen in sAD 1 and sAD 5, both of which show an increase in Fis1 localised to the mitochondria (figure 21a). When data for individual lines was combined, there was no difference seen between control and sAD lines in the amount of Fis1 localised to the mitochondria (figure 21b). As well as a decrease in the amount of Fis1 localised to the mitochondria, sAD 8 and sAD 9 showed an increase in the percentage of total Fis1 localised to the mitochondria (figure 21c). This suggests that despite using a greater proportion of the total Fis1, the cells are still unable to bring Fis1 co-localised with the mitochondria back to control levels. sAD 1 and sAD 5 also showed an increase in the percentage of total Fis1 co-localised to the mitochondria, but these lines were able to sufficiently increase the amount of Fis1 at the mitochondria to reach, or surpass, control levels (figure 21c). sAD 6 and sAD 10 both showed a decrease in the percentage of total Fis1 localised to the mitochondria (figure 21c), which may contribute to the decrease seen in these lines in the amount of Fis1 localised to the mitochondria. When individual lines were combined, there was no overall difference seen between sAD and control fibroblasts in the percentage of total Fis1 localised to the mitochondria (figure 21d).

Some sAD lines showed a decrease in the amount of Mff localised to the mitochondria, specifically sAD 3, sAD 6, and sAD 9 (figure 23a). sAD 3 and sAD 9 also showed a deficit in the total protein expression of Mff, though sAD 6 showed no statistical difference (figure 14). sAD 1 and sAD 5 also showed a decrease in Mff total protein expression when assessed by western blot (figure 14), but here show an increase in the levels of Mff co-localised to the mitochondria (figure 23a). When individual lines were combined, there was no difference in the amount of Mff localised to the mitochondria between control and sAD lines (figure 23b). All sAD lines tested show no difference in the percentage of total Mff localised to the mitochondria, with the exception of sAD 9 which showed an increase (figure 23c). When individual lines were combined, there was no difference in the percentage of total Mff which was localised to the mitochondria between control and sAD patient fibroblasts (figure 23d).

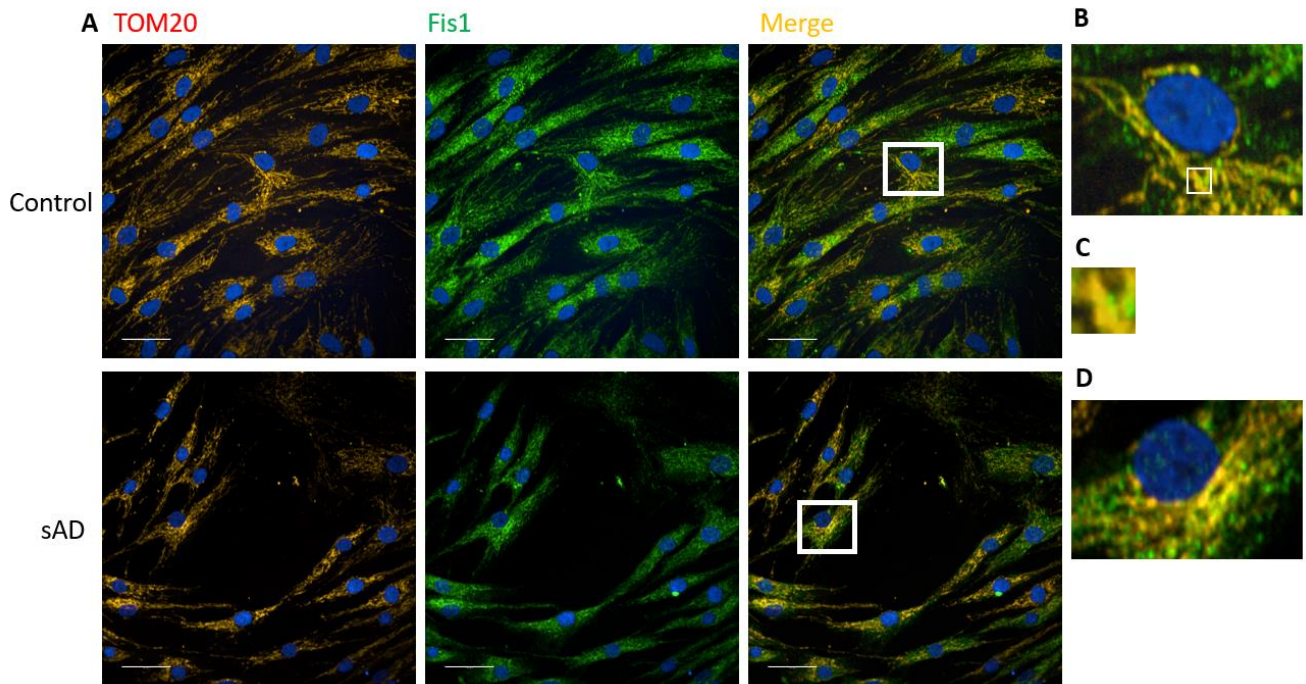


Figure 20: Representative Images of Fis1-TOM20 co-localisation in control and sAD patient fibroblasts. A) Representative images of Fis1 and TOM20 co-localisation staining. TOM20 is shown in red, Fis1 in green, and nuclei in blue. Scale = 50 μ m. B) Zoomed in image of Fis1-TOM20 co-localisation in control fibroblasts, showing the area in the white box. C) Further zoomed in image of the white box shown in B, to demonstrate co-localisation of Fis1 and TOM20. D) Zoomed in image of Fis1-TOM20 co-localisation in sAD fibroblasts, showing the area in the white box.

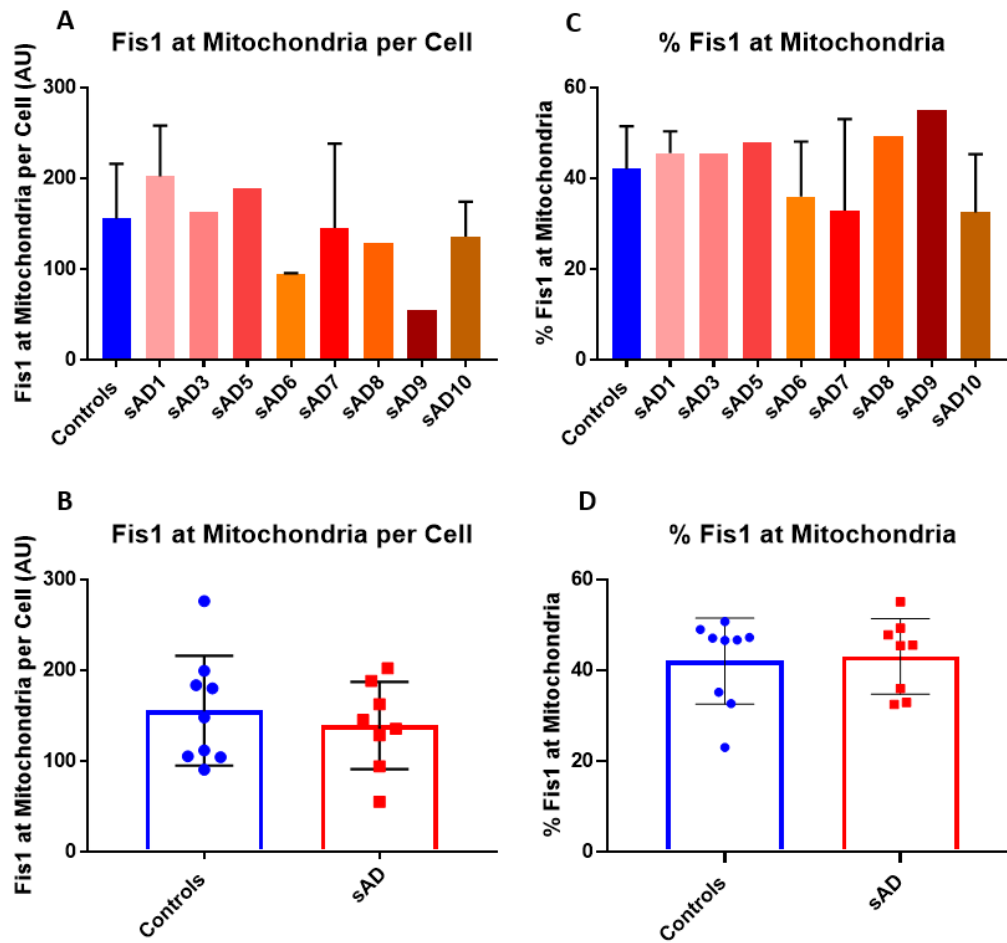


Figure 21: There is no significant difference in the amount of Fis1 co-localised to the mitochondria between control and sAD fibroblasts. A) Quantification of Fis1 co-localisation with mitochondrial marker TOM20, n=1-2. Statistical analysis was not performed due to a low number of repeats. B) There is no difference in the amount of Fis1 localised to the mitochondria between sAD and control fibroblasts when individual lines are combined C) Quantification of the percentage of total Fis1 which is localised to the mitochondria, n=1-2. Statistical analysis was not performed due to a low number of repeats. D) There is no difference in the percentage of total Fis1 localised to the mitochondria when individual lines are combined.

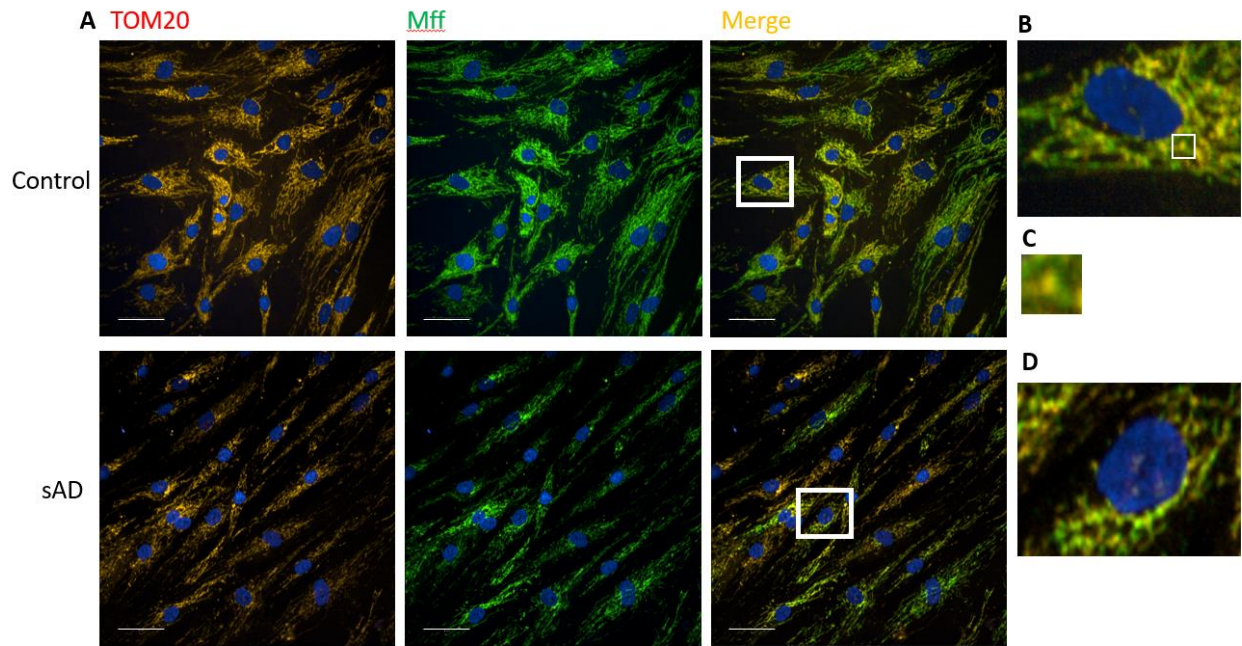


Figure 22: Representative Images of Mff-TOM20 co-localisation in control and sAD patient fibroblasts. A) Representative images of Mff and TOM20 co-localisation staining. TOM20 is shown in red, Mff in green, and nuclei in blue. Scale = 50 μ m. B) Zoomed in image of Mff-TOM20 co-localisation in control fibroblasts, showing the area in the white box. C) Further zoomed in image of the white box shown in B, to demonstrate co-localisation of Mff and TOM20. D) Zoomed in image of Mff-TOM20 co-localisation in sAD fibroblasts, showing the area in the white box.

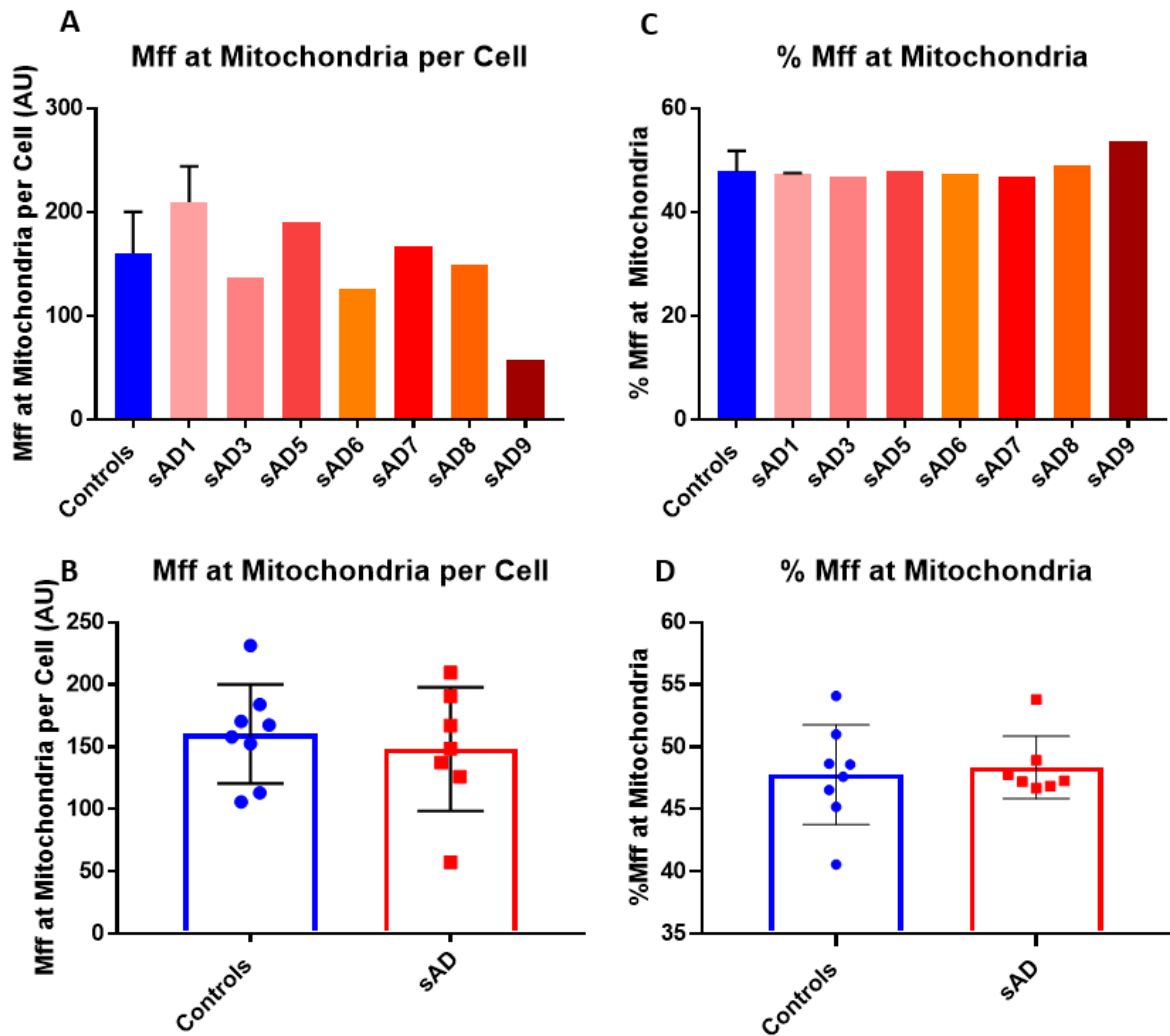


Figure 23: There is no significant difference in the amount of Mff co-localised to the mitochondria between control and sAD fibroblasts. A) Quantification of Mff co-localisation with mitochondrial marker TOM20, n=1-2. Statistical analysis was not performed due to a low number of repeats. B) There is no difference in the amount of Mff localised to the mitochondria when individual lines are combined. C) Quantification of the percentage of total Mff which is localised to the mitochondria, n=1-2. Statistical analysis was not performed due to a low number of repeats. D) There is no difference in the percentage of total Mff localised to the mitochondria.

3.2.8 Fis1 and Mff Interactions with Drp1 in sAD Fibroblasts

To investigate whether reduced protein levels of Drp1, Fis1, and Mff leads to a decrease in interactions between these proteins, the proximity ligation assay was used to measure interactions between Drp1 and Fis1, and Drp1 and Mff. Unfortunately, MiD49 and MiD51 interactions with Drp1 could not be investigated due to antibody issues. During the PLA, two primary antibodies for the proteins of interest are added to the cells. The PLA probes are then added; these are oligonucleotide labelled secondary antibodies which bind to the primary antibodies. These oligonucleotides can then be joined into closed, circular DNA by connector oligonucleotides and ligase if they are in close enough proximity, within 40nm. DNA polymerase then amplifies this signal and fluorescent probes are used to visualise the signal. Each interaction is represented as an individual spot, as shown in figure 24.

sAD cell lines for these experiments were chosen as they were those with the largest deficits in total protein expression. When interactions across the whole cell were assessed, no significant difference was seen between control and sAD patient fibroblasts in Drp1 interactions with either Fis1 (controls 43.3 ± 5.2 ; sAD 40.7 ± 4.0 ; figure 25a, c) or Mff (controls 43.9 ± 9.2 ; sAD 36.1 ± 15.9 ; figure 26a, c). There was also no significant difference between control and sAD fibroblasts of the interactions specifically in the perinuclear region for Fis1 (controls 17.4 ± 1.9 ; sAD 21.4 ± 3.4 ; figure 25b, d) or Mff (controls 18.0 ± 5.4 ; sAD 17.8 ± 4.4 ; figure 26 b, d). There is more variability seen between cell lines in Drp1 interactions with Mff, particularly in the sAD fibroblasts. When comparing the number of Drp1 interactions with Fis1 to Drp1 interactions with Mff, there is no difference seen in either control or patient fibroblasts (figure 27).

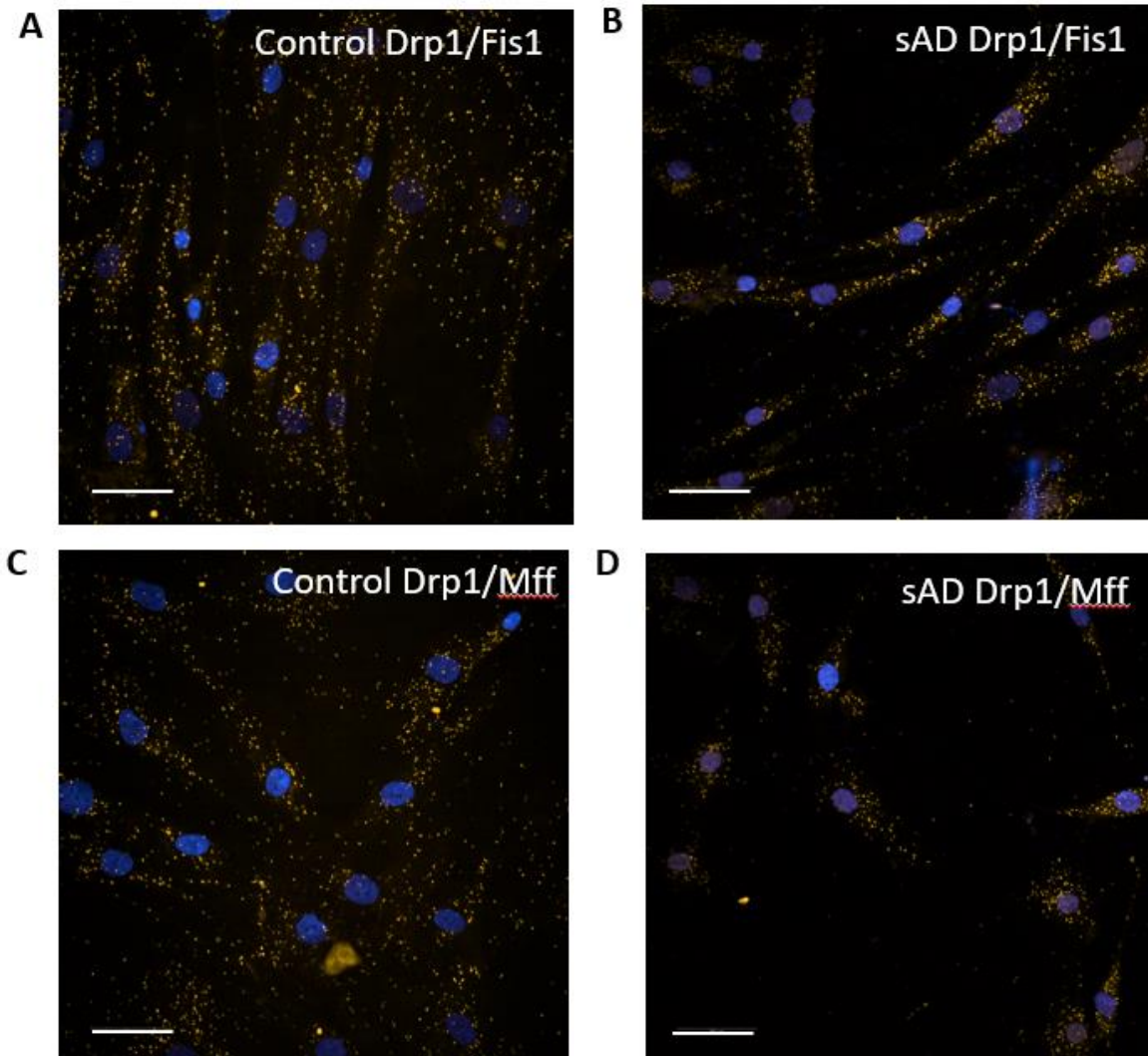


Figure 24: Representative image of Drp1 and Fis1, and Drp1 and Mff interactions in control and sAD fibroblasts. Scale bar = 50 μ M. A) Representative image of Drp1 and Fis1 interactions in control fibroblasts - each orange dot represents a single interaction. B) Representative image of Drp1 and Fis1 interactions in sAD fibroblasts. C) Representative image of Drp1 and Mff interactions in control fibroblasts. D) Representative image of Drp1 and Mff interactions in sAD fibroblasts.

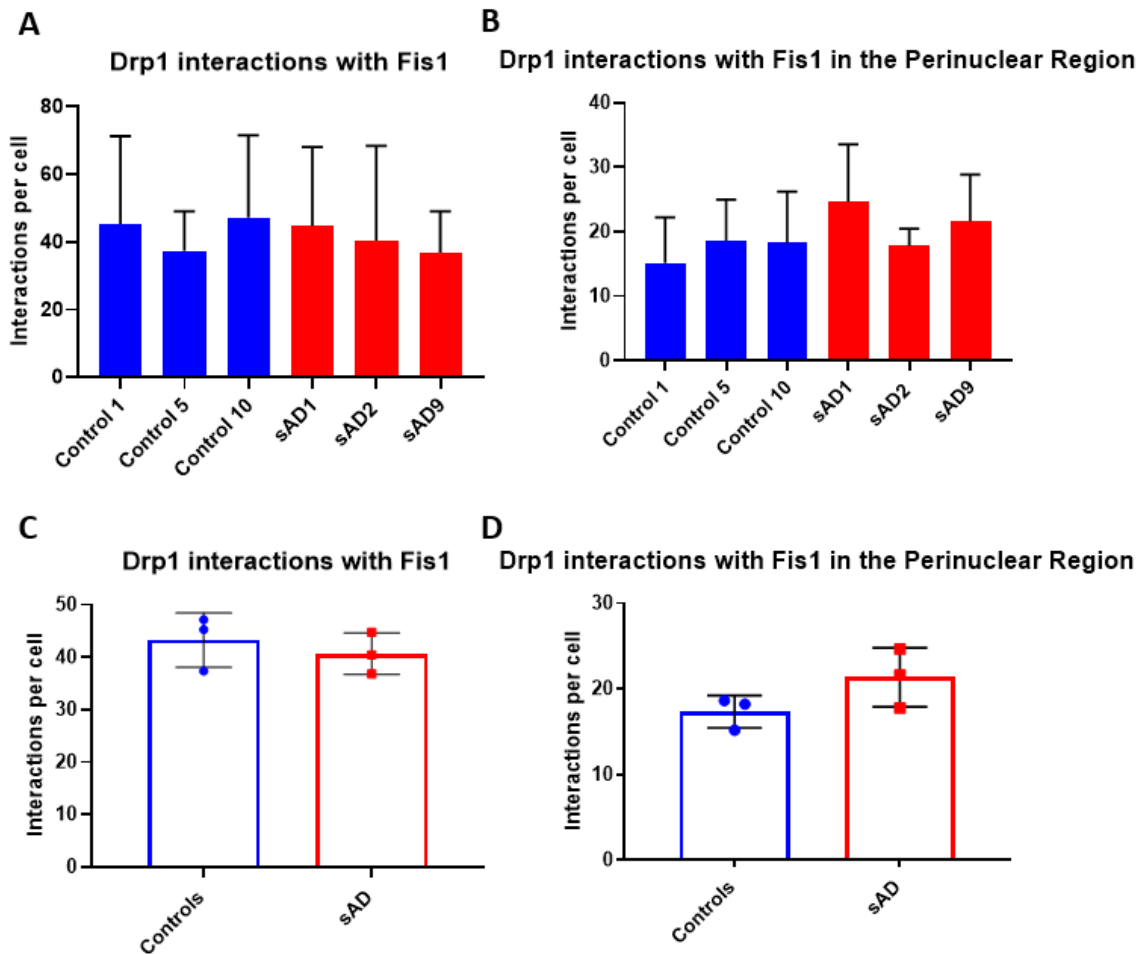


Figure 25: There is no difference in the number of Drp1 interactions with Fis1 between control and sAD patient fibroblasts. A) Quantification of Drp1 interactions with Fis1 in three controls and three sAD patient fibroblast lines in the whole cell, measured at three different passages. Bars represent the mean and error bars represent SD. B) Quantification of Drp1 interactions with Fis1 in three controls and three sAD patients in the perinuclear region, measured at three different passages. Bars represent the mean and error bars represent SD. C) No significant difference in Drp1 interactions with Fis1 in the whole cell between control and sAD fibroblasts when individual lines are combined ($p = 0.9843$). Each dot represent the mean of the replicates per line, bars represent the mean, and error bars represent SD. D) No significant difference in Drp1 interactions with Fis1 in the perinuclear region between controls and sAD patient fibroblasts when individual lines are combined ($p = 0.5083$; one way ANOVA). Each dot represent the mean of the replicates per line, bars represent the mean, and error bars represent SD.

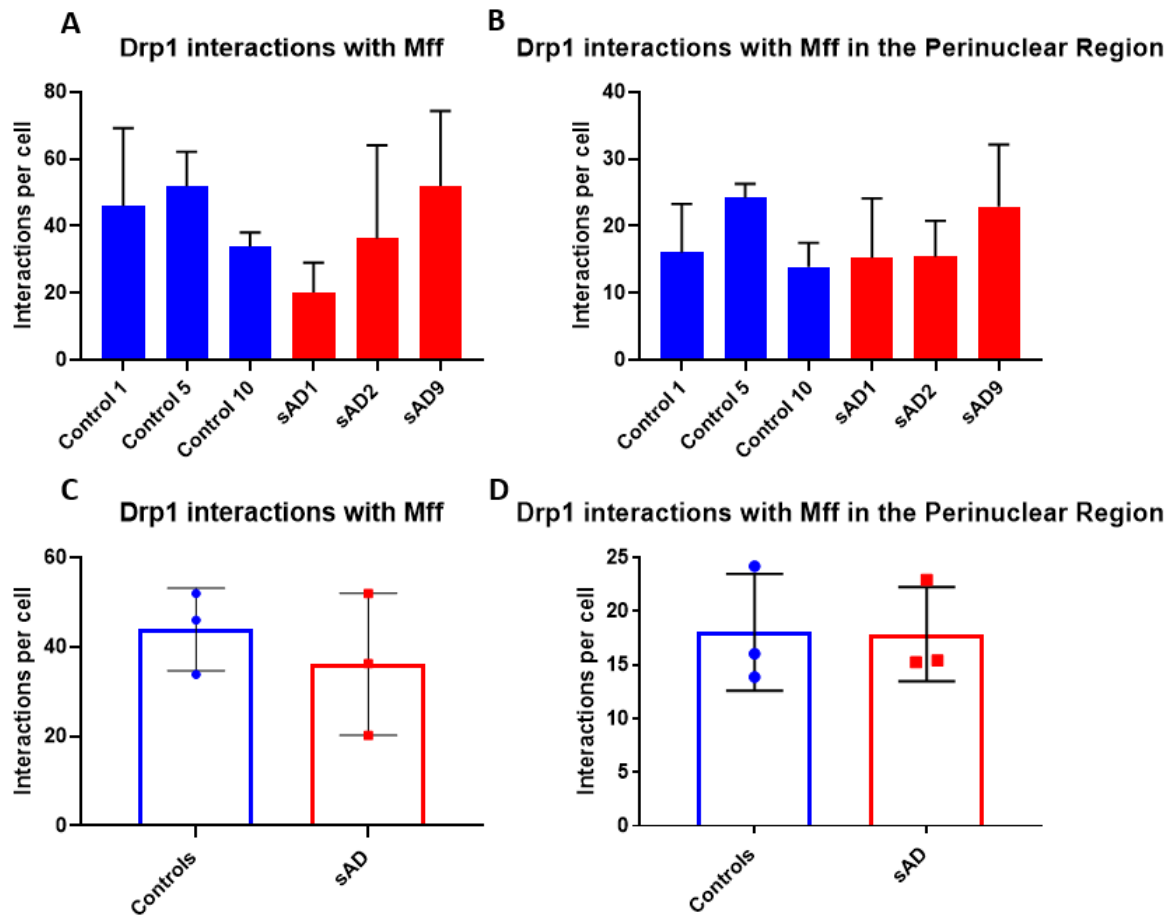


Figure 26: There is no difference in the number of Drp1 interactions with Mff between control and sAD patient fibroblasts. A) Quantification of Drp1 interactions with Mff in three controls and three sAD patient fibroblast lines in the whole cell, measured at three different passages. Bars represent the mean and error bars represent SD. B) Quantification of Drp1 interactions with Mff in three controls and three sAD patients in the perinuclear region, measured at three different passages. Bars represent the mean and error bars represent SD. C) No significant difference in Drp1 interactions with Mff in the whole cell between control and sAD fibroblasts when individual lines are combined ($p = 0.3668$). Each dot represent the mean of the replicates per line, bars represent the mean, and error bars represent SD. D) No significant difference in Drp1 interactions with Mff in the perinuclear region between controls and sAD patient fibroblasts when individual lines are combined ($p = 0.3105$; one way ANOVA). Each dot represent the mean of the replicates per line, bars represent the mean, and error bars represent SD.

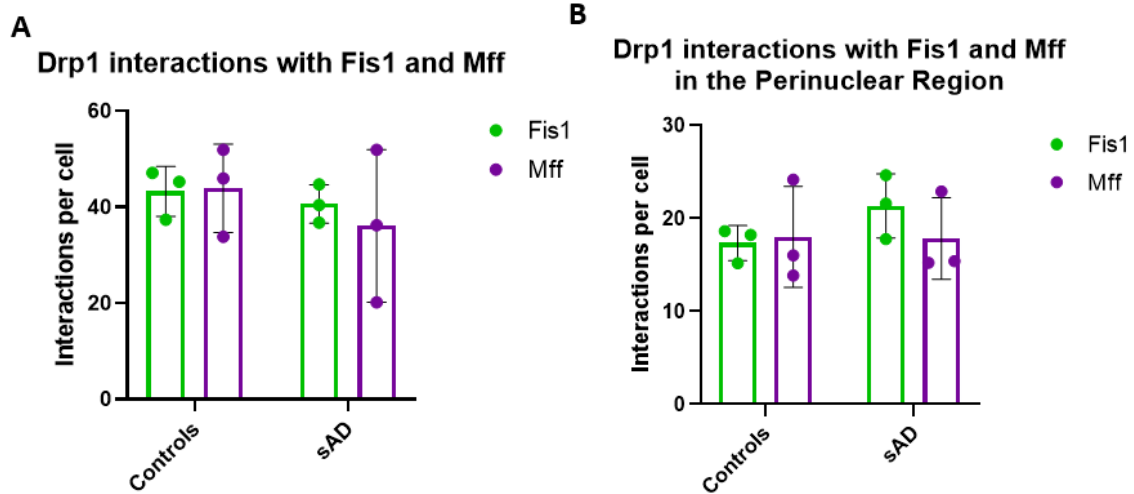


Figure 27: No significant difference in either control or sAD patient fibroblasts between the number of Drp1 interactions with Fis1 and Drp1 interactions with Mff. A) No significant difference between Drp1 interactions with Fis1 and Drp1 interactions with Mff in either control or sAD patient fibroblasts in the whole cell. There is increased variability in Mff interactions, especially in sAD lines. Each dot represent the mean of the replicates per line, bars represent the mean, and error bars represent SD. B) No significant difference between Drp1 interactions with Fis1 and Drp1 interactions with Mff in either control or sAD patient fibroblasts in the perinuclear region. Each dot represent the mean of the replicates per line, bars represent the mean, and error bars represent SD.

3.2.9 Expression of Peroxisome Marker, Pex19, in sAD Fibroblasts

Drp1, Fis1, and Mff are also involved in peroxisomal fission; the decreased levels of these proteins may impact peroxisomal morphology. Many sAD lines are able to maintain the level of Fis1 and Mff localised to the mitochondria at control, or close to control, levels. It may be that the decreased total levels of these proteins are having a greater impact on the peroxisome. To investigate this possibility, total cellular protein levels of peroxisome marker, peroxisomal biogenesis factor 19 (Pex19), were assessed via western blotting in four controls and four sAD patients, as a general marker of peroxisomal mass. No significant difference was observed (Controls 1.001 ± 0.169 ; sAD 0.891 ± 0.130) between controls and sAD patient fibroblasts ($p = 0.5084$; figure 28).

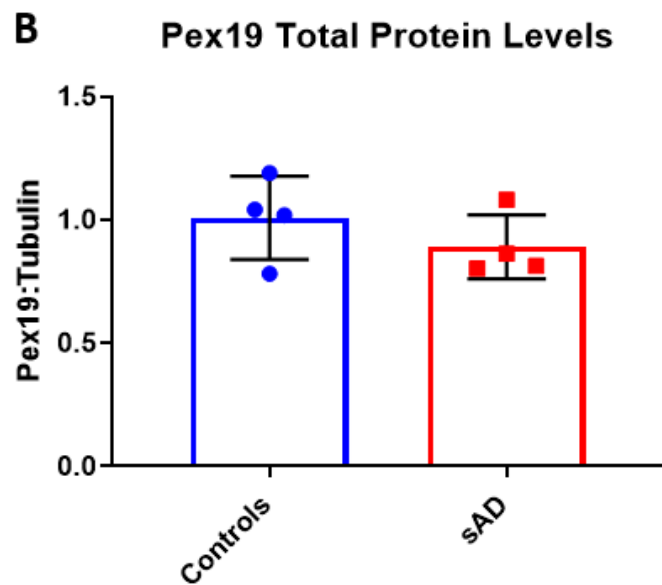
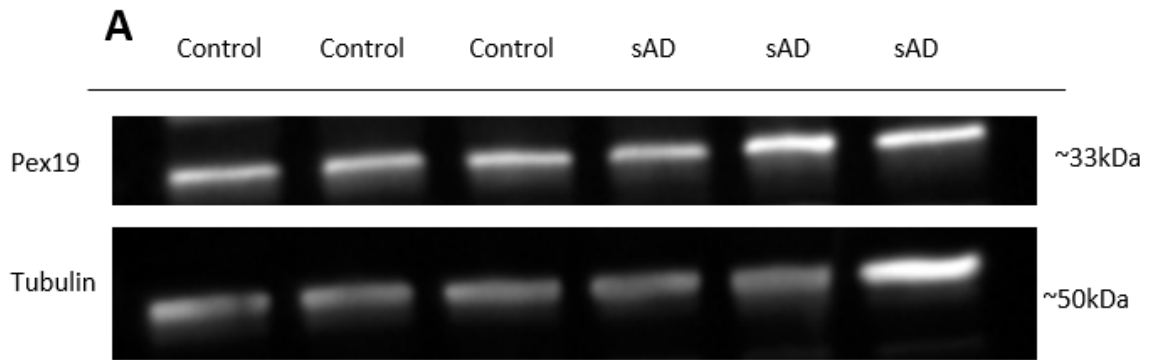


Figure 28: No significant difference is seen in total pex19 protein levels between controls and sAD patient fibroblasts. A) Representative blot of pex19 and tubulin loading control in three controls and three sAD patients, with 10µg protein loaded per lane. B) Quantification of pex19 protein levels in four controls and four sAD patient fibroblast line, at three passages per line, with no significant difference seen ($p = 0.5084$; one way ANOVA). Each dot represent the mean of the replicates per line, bars represent the mean, and error bars represent SD.

3.2.10 Fis1-BAP31 Mitochondria-ER Contact Sites in sAD Fibroblasts

To explore the possibility that changes in Drp1 are being affected by changes upstream in the fission process, the mitochondria-ER contact sites were studied using co-localisation immunocytochemistry. Representative images are shown in figure 29. Fis1-BAP31 contact sites were chosen based on the role of Fis1 in mitochondrial fission, as well as previous findings showing reduced Fis1 in eight of ten sAD patient lines. Unfortunately, due to limitations in both time (due to COVID-19 related lab closures and restricted access) and antibody availability, no further contact sites were investigated. It was found that there was no significant difference between the number of Fis1-BAP31 co-localisation sites, normalised to cell area (controls 0.029 ± 0.011 ; sAD 0.042 ± 0.007 ; figure 30a-b). There was also no significant difference in the percentage of total BAP31 which was co-localised with Fis1 (controls 15.3 ± 6.9 ; sAD 19.5 ± 1.5 ; figure 30c-d), or the percentage of total Fis1 which was co-localised with BAP31 (controls 33.4 ± 14.2 ; sAD 23.4 ± 1.5 ; figure 30e-f) between controls and sAD patient lines. However, control 10 did have significantly increased percentage of BAP31 co-localised with Fis1, and a significantly reduce percentage of Fis1 co-localised with BAP31 compared to other controls (figure 30c, e).

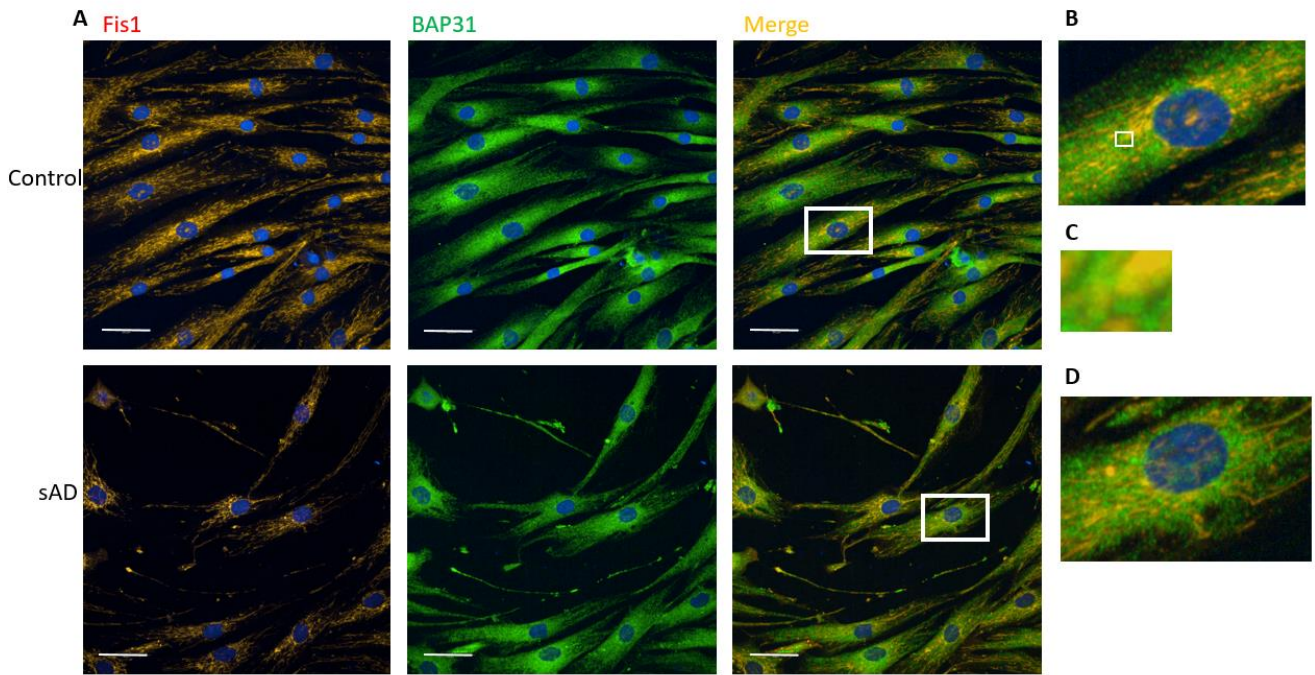


Figure 29: Representative Images of BAP31-Fis1 co-localisation in sAD and control fibroblasts. A)

Representative images of BAP31-Fis1 co-localisation immunocytochemistry in control and sAD fibroblasts. Red stain shows Fis1, green shows BAP31, and blue shows the nuclei. Scale bar = 50 μ m. B) Zoomed in image of BAP31-Fis1 co-localisation in control fibroblasts, showing the area in the white box. C) Further zoomed in image of the white box shown in B, to demonstrate co-localisation of Fis1 and BAP31. D) Zoomed in image of BAP31-Fis1 co-localisation in sAD fibroblasts, showing the area in the white box.

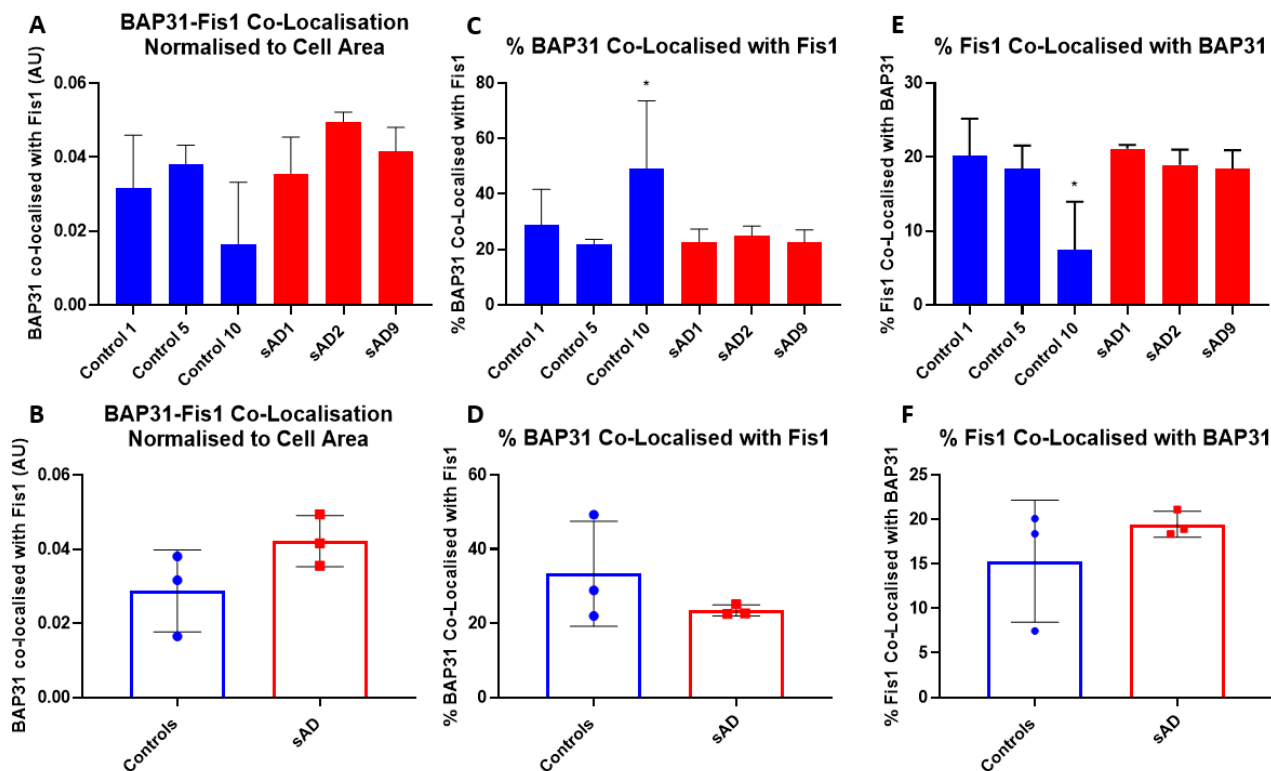


Figure 30: No significant difference between BAP31-Fis1 mitochondria-ER contact sites between controls and sAD patient fibroblasts. A) Quantification of BAP31-Fis1 co-localisation normalised to cell area, $n=4$. Each bar represent mean and the error bars represent SD. B) There is no significant difference in BAP31-Fis1 co-localisation between control and sAD patient lines when individual lines are combined ($p = 0.1492$, unpaired t test). Each dot represents the mean of replicates for each line, bars represent the overall mean, and error bars represent SD. C) Quantification of the percentage of total BAP31 which is co-localised with Fis1, $n=4$. Control 10 is significantly higher than control 5 and sAD lines 1 and 9 ($p < 0.05$, one way ANOVA). Each bar represent mean and the error bars represent SD. D) No significant difference in the percentage of BAP31 co-localised with Fis1 when individual lines are combined ($p = 0.2942$, t test). Each dot represents the mean of replicates for each line, bars represent the overall mean, and error bars represent SD. E) Quantification of the percentage of total Fis1 co-localised with BAP31, $n=4$. Control 10 is significantly lower than all other control and sAD lines ($p < 0.05$, one way ANOVA). Each bar represent mean and the error bars represent SD. F) No significant difference in the percentage of Fis1 co-localised with BAP31 when individual lines are combined ($p = 0.3634$, t test). Each dot represents the mean of replicates for each line, bars represent the overall mean, and error bars represent SD.

3.2.11 Drp1 Overexpression in Control and sAD Fibroblasts

Reductions in total Drp1 levels were seen across multiple sAD fibroblast lines, and previously, less Drp1 was seen to co-localise to the mitochondria. To determine whether this is a key factor driving the mitochondrial phenotype seen in sAD fibroblasts, Drp1 was transiently overexpressed in control and sAD fibroblasts, to determine if increasing Drp1 levels could rescue the alterations seen in mitochondrial morphology. Due to time constraints, this was conducted in triplicate in one control line, control 3, and one sAD line, sAD 5, only. Cells were transfected with either a control plasmid (pcDNA3YFP) or a Drp1 plasmid (pcDNA3Drp1YFP), both conjugated to YFP so transfection efficiency could be assessed by fluorescence. A transfection efficiency of between 18% and 25% was achieved (control 3 pcDNA3YFP 18.8% \pm 8.3, control 3 pcDNA3Drp1YFP 24.5% \pm 16.0, sAD 5 pcDNA3YFP 20.0% \pm 10.5, sAD 5 pcDNA3Drp1YFP 22.7% \pm 6.8; figure 31a, 32a, 33a).

The levels of Drp1 were calculated in both transfected and non-transfected cells in the same well, and the percentage increase in the transfected cells over the non-transfected cells was assessed. Drp1 levels were increased in all transfection conditions, both control and Drp1 plasmids, though this was somewhat variable between the three repeats carried out (control 3 pcDNA3YFP 127% \pm 90, control 3 pcDNA3Drp1YFP 150% \pm 37, sAD 5 pcDNA3YFP 90% \pm 27, sAD 5 pcDNA3Drp1YFP 258% \pm 107; figure 33b). This is potentially due to a stress response in the cells as a result of the transfection. In sAD fibroblasts, a much bigger increase was seen in the pcDNA3Drp1YFP condition than the control plasmid condition, as would be expected. However, this was not the case in control fibroblasts. This may be due to compensatory mechanisms in the cell; mitochondrial fission is carefully regulated, and it may be that the cell has mechanisms to prevent Drp1 levels increasing too much as this would be detrimental. In sAD fibroblasts, the starting Drp1 levels are lower, and so a greater increase is possible.

Mitochondrial morphology was assessed by measuring the form factor, to measure interconnectivity of the mitochondrial network. sAD fibroblasts show a more fused network, and so a decrease in form factor would be expected here as a rescue effect of Drp1 overexpression. However, it was found that the increased Drp1 in all conditions caused a large increase in fragmentation in the mitochondrial network compared to YFP negative cells, as shown in figure 31 and figure 32, and quantified in figure 34. This stress response masked any meaningful data in regard to a rescue of the mitochondrial morphology phenotype in the sAD fibroblasts.

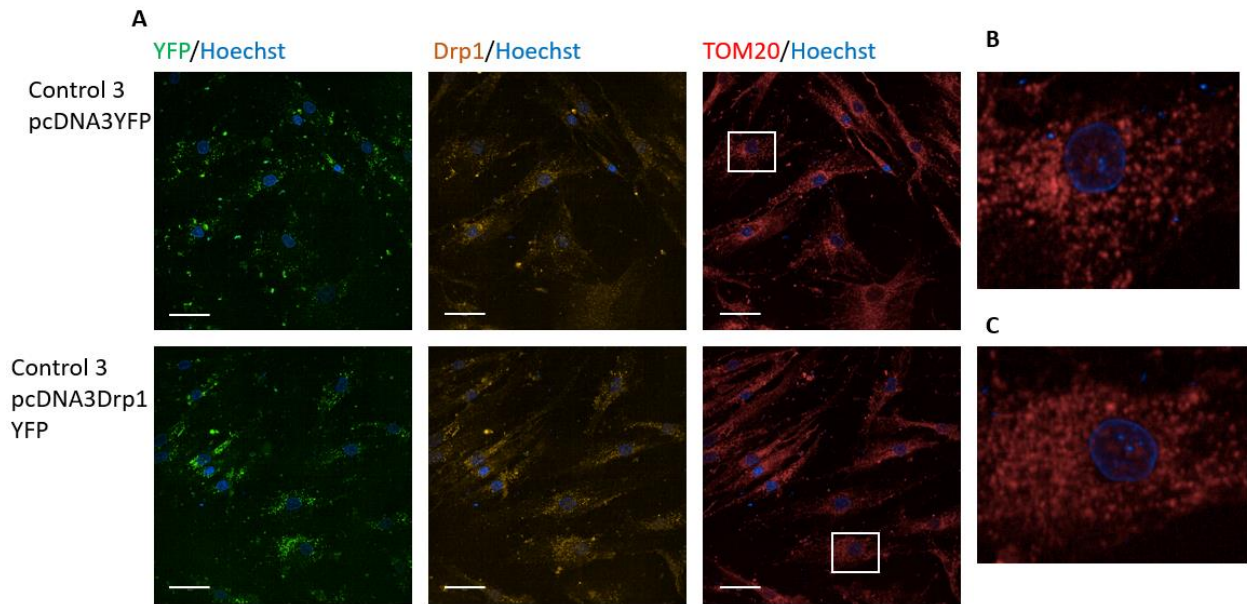


Figure 31: Mitochondrial morphology after transfection with control and Drp1 plasmids, in control 3 fibroblasts. A) Representative images of mitochondrial morphology in control fibroblasts after transfection with either pcDNA3YFP or pcDNA3Drp1YFP. YFP representing successful transfection is shown in green, Drp1 is shown in orange, and mitochondrial marker TOM20 is shown in red. Scale bar = 50 μ M. B) Zoomed in image of the area in the white box, showing mitochondrial morphology in control fibroblasts after transfection with pcDNA3YFP. Mitochondrial network is highly fragmented. C) Zoomed in image of the area in the white box, showing mitochondrial morphology in control fibroblasts after transfection with pcDNA3Drp1YFP. Mitochondrial network is highly fragmented.

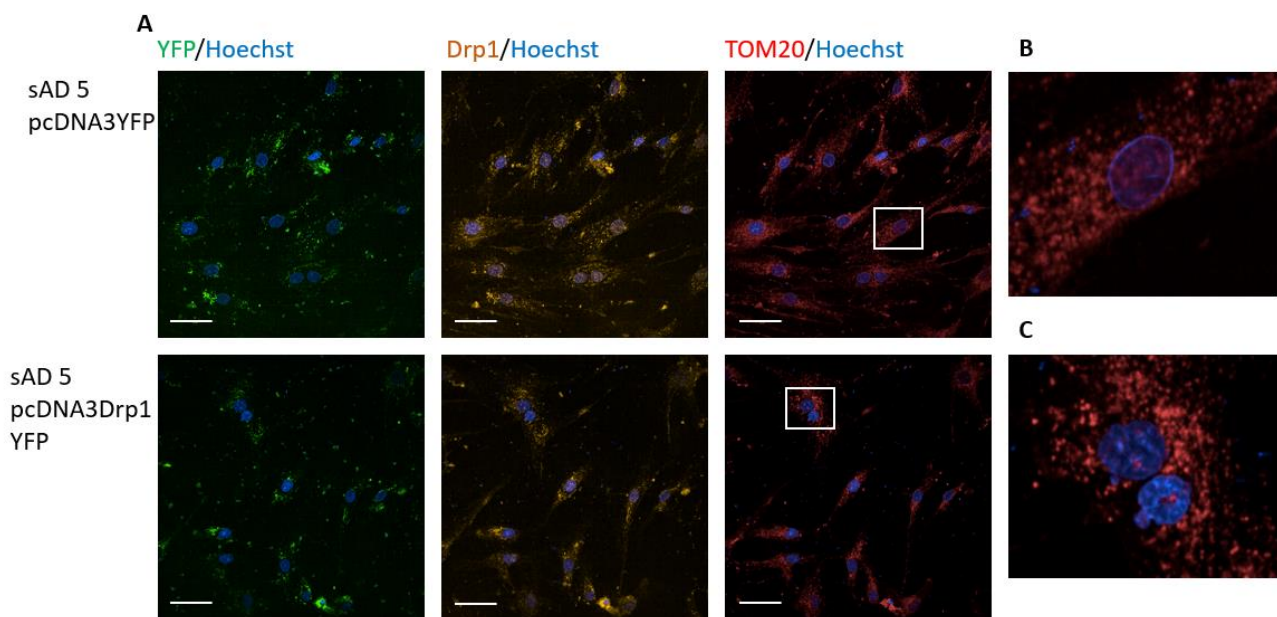


Figure 32: Mitochondrial morphology after transfection with control and Drp1 plasmids, in sAD 5 fibroblasts.

A) Representative images of mitochondrial morphology in sAD fibroblasts after transfection with either pcDNA3YFP or pcDNA3Drp1YFP. YFP representing successful transfection is shown in green, Drp1 is shown in orange, and mitochondrial marker TOM20 is shown in red. Scale bar = 50 μ M. B) Zoomed in image of the area in the white box, showing mitochondrial morphology in sAD fibroblasts after transfection with pcDNA3YFP. Mitochondrial network is highly fragmented. C) Zoomed in image of the area in the white box, showing mitochondrial morphology in sAD fibroblasts after transfection with pcDNA3Drp1YFP. Mitochondrial network is highly fragmented.

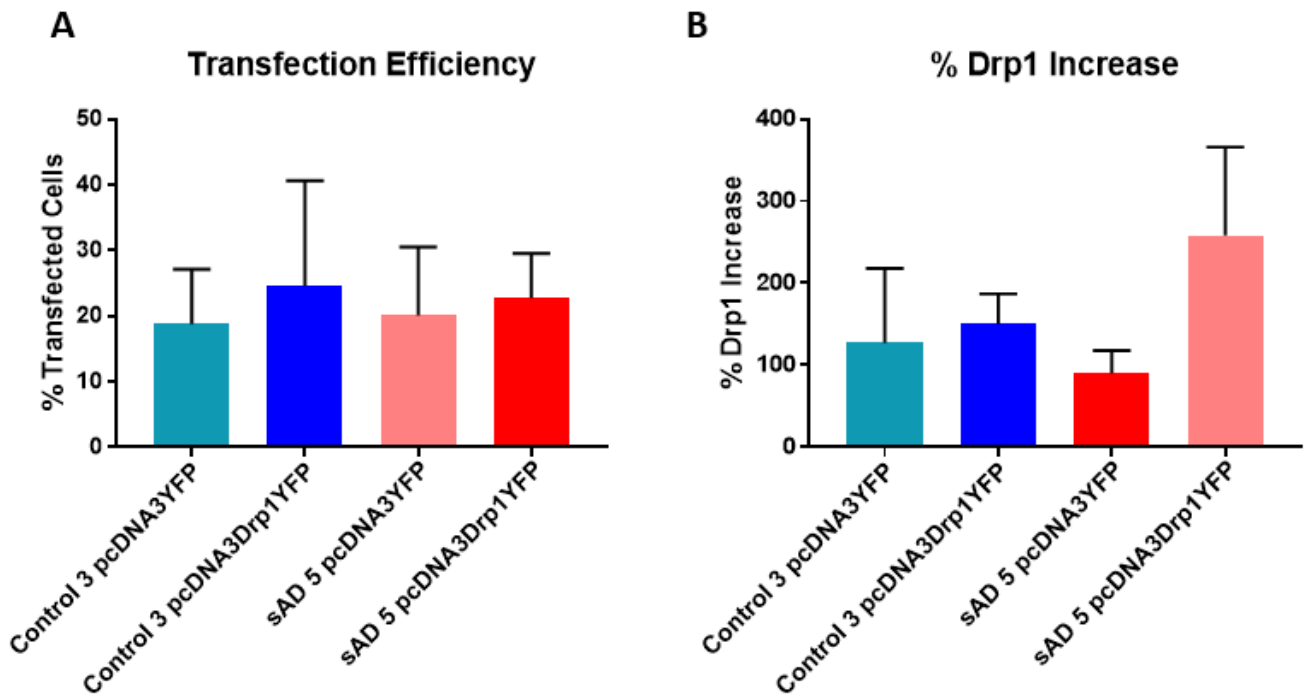


Figure 33: Transfection efficiency and % Drp1 increase in control 3 and sAD 5 fibroblasts, after transfection with either pcDNA3YFP or pcDNA3Drp1YFP. A) Transfection efficiency in control 3 and sAD 5 fibroblasts of pcDNA3YFP and pcDNA3Drp1YFP. B) Percentage increase in Drp1 levels in control 3 and sAD 5 fibroblasts after transfection of either pcDNA3YFP or pcDNA3Drp1YFP. Control 3 pcDNA3YFP shows a 127% \pm 90 increase, while control 3 pcDNA3Drp1YFP shows a 150% \pm 37 increase. sAD 5 pcDNA3YFP shows a 90% \pm 27 increase, and the greatest increase seen in sAD5 pcDNA3Drp1YFP, which shows a 258% \pm 107 increase.

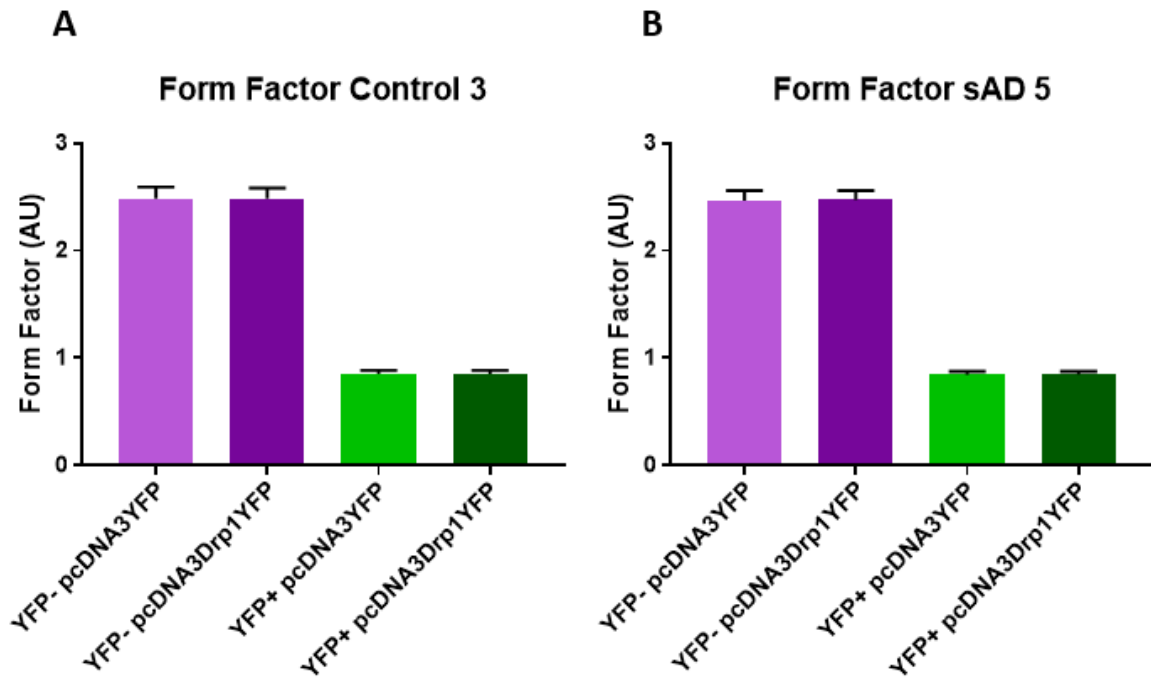


Figure 34: *There is a large decrease in form factor, indicating an increase in fragmentation, in control and sAD fibroblasts after transfection with either pcDNA3YFP or pcDNA3Drp1YFP. A) In control 3 fibroblasts, there is a large decrease in form factor in YFP+ cells compared to YFP- cells, after transfection with either pcDNA3YFP or pcDNA3Drp1YFP. B) In sAD 5 fibroblasts, there is a large decrease in form factor in YFP+ cells compared to YFP- cells, after transfection with either pcDNA3YFP or pcDNA3Drp1YFP.*

3.3 Discussion

This chapter focussed on mitochondrial dysfunction, in particular alterations in mitochondrial quality control, in control and sAD patient fibroblasts. A locally sourced cohort of ten sAD patients and ten healthy, age and sex matched controls were used, with some experiments carried out on lower sample numbers due to time constraints and COVID-19 related lab restrictions. Overall, findings showed a decrease in several key mitochondrial fission proteins, but no significant changes in the localisation or interactions of these proteins. There was also no change seen in BAP31-Fis1 mitochondria-ER contact sites, or mitochondrial fusion protein, OPA1.

3.3.1 Drp1

Drp1 is the key protein involved in mitochondrial fission. During fission events, Drp1 is recruited to the mitochondria, where it forms an oligomeric ring structure, which constricts allowing the mitochondria to divide. Previous work in the lab found that total protein levels of Drp1 were significantly reduced in a small cohort of both sAD and fAD patient fibroblasts (Bell *et al.*, 2018), work which I contributed to as part of my MSc. The first aim of this chapter was to assess total Drp1 protein levels in an expanded, locally sourced cohort. It was found that of the ten sAD lines (including those previously assessed and those assessed as part of this project), seven showed a significant decrease in Drp1 total protein levels, with one showing a significant increase, and two showing no significant difference. Overall, this gave a significant decrease of approximately 35% when the lines were combined.

This finding agrees with several previously published studies which also noted a decrease in Drp1 protein levels in both sAD and fAD patient fibroblasts (Xinglong Wang *et al.*, 2008; Martín-Maestro, Gargini, García, *et al.*, 2017; Drabik, Piecyk, *et al.*, 2021), though others have found an increase, also in sAD and fAD fibroblasts (Amit U. Joshi *et al.*, 2018). It is worth noting that studies using other models of AD also disagree with this finding, with many finding increased Drp1 (Manczak, Calkins and Reddy, 2011; Trushina *et al.*, 2012; Li *et al.*, 2015; Xu *et al.*, 2017; Kandimalla *et al.*, 2018a; Manczak *et al.*, 2018; Reddy, Yin, *et al.*, 2018; Ahmed *et al.*, 2019). In fact, Reddy and colleagues have proposed reducing Drp1 as a therapeutic mechanism, with lower levels seen to protect against A β and tau induced mitochondrial dysfunction, and synaptic damage, as well improve cognitive performance in a tau mouse model (Kandimalla *et al.*, 2016, 2021; Manczak *et al.*, 2016). It may be that these inconsistencies are model, or cell type, specific; many studies which report increased Drp1 do so in models which consist of neural cells, such as animal models or post mortem tissue. These models have their own issues, but it may be that in this case, differences in the periphery do

not reflect the exact changes in the brain. Neural cells have very different energy requirements to fibroblasts, and so it is possible that the mitochondrial morphology requirements are also very different. Abnormalities in Drp1 are clearly seen in multiple models of varying cell types, and it may be that the difference in the direction of these abnormalities reflects the differing relationship between mitochondrial morphology and function in each specific cell type. This will be investigated further in the second chapter of this thesis.

Inconsistencies between models could also be explained by differences between sAD and fAD; many animal models are based on genetic forms of AD and it could be that different pathological mechanisms occur in this type of AD. In many previous studies, animal models show increased Drp1 (Trushina *et al.*, 2012; Xu *et al.*, 2017; Kandimalla *et al.*, 2018a; Manczak *et al.*, 2018; Reddy, Yin, *et al.*, 2018) suggesting that this may be a fAD specific mechanism. However, both sAD (Xinglong Wang *et al.*, 2008; Drabik, Piecyk, *et al.*, 2021) and fAD (Martín-Maestro, Gargini, García, *et al.*, 2017; Bell *et al.*, 2018) fibroblasts have been shown to have decreased Drp1, indicating that changes are more likely to be due to cell type rather than differences in the type of AD. It would have been interesting to investigate fAD fibroblasts as part of this project, however, time constraints meant that this was not possible.

Drp1 protein levels between individuals vary, both in the patient and control fibroblasts. This heterogeneity is expected when working with human-derived cells – no two individuals are the same, with genetics and environmental factors playing a role in these differences. Variability between different individuals was also seen by Manczak, Calkins and Reddy (2011), who studied post mortem frontal cortex tissue. Whilst they saw an increase in Drp1 levels on a group level, two of 20 patient samples studied showed a decrease. sAD has no single known cause, and many known risk factors. It is therefore possible that different mechanisms occur to different extents in different people, as seen in this cohort. Some sAD patients may have a more mitochondrial driven disease, whilst in others, mitochondrial abnormalities may occur as a result of other pathogenic mechanisms. Despite this variability, Drp1 may prove to be an interesting target in the search for mitochondria-targeted AD treatments. Wang *et al.* (2008) found that overexpression of Drp1 rescued the collapsed mitochondrial network, whilst previous work in our lab has found that UDCA, a modulator of mitochondrial function, works in a Drp1 dependent manner in AD patient fibroblasts (Bell *et al.*, 2018). UDCA was seen to increase MMP to control levels, but this rescue effect was abolished when Drp1 was knocked down using siRNA (Bell *et al.*, 2018).

Changes in Drp1 expression do not necessarily correlate with changes in fission – overexpression of Drp1 does not always lead to increased mitochondrial fission (Otera, Ishihara and Mihara, 2013).

This suggests that a change in Drp1 levels may not be necessary to alter fission, and as such, the results seen here do not necessarily prove that sAD fibroblasts have a reduced level of mitochondrial fission. This could be tested in future studies by using time lapse imaging and mitochondrial markers in live cells, to assess mitochondrial fission events.

Another key factor is the post-translational modification of Drp1. Translocation of Drp1 is reliant on the phosphorylation state, Drp1 must be dephosphorylated at ser637 and phosphorylated at ser616 (van der Blik, Shen and Kawajiri, 2013). Phosphorylation of Drp1 at ser579 has also been associated with translocation to the mitochondria, particularly under oxidative stress conditions (Qi *et al.*, 2011), and blockage of this has been seen to protect primary cortical mouse neurons against A β induced dysfunction (XU *et al.*, 2021). Attempts were made to assess Drp1 phosphorylation status in this cohort of sAD patient fibroblasts, but this proved to be technically challenging, as expression appeared to be so low that it could not be quantified using the available antibodies. Other post-translational modifications of Drp1 are also thought to be important; small ubiquitin-related modifier protein (SUMO)ylation is thought to play a key role in the stabilisation of Drp1 on the mitochondrial membrane (Otera, Ishihara and Mihara, 2013), and increased s-nitrosylation has been seen in response to A β , leading to loss of synapses and neuronal damage (Cho *et al.*, 2009) though others have questioned the effect of s-nitrosylation on Drp1 activity (Bossy *et al.*, 2010). These modifications could be investigated further in these sAD fibroblasts to better understand the impact of reduced Drp1 expression on the mitochondrial fission process.

3.3.2 OPA1

The main role of OPA1 is to mediate mitochondrial fusion of the inner mitochondrial membrane, though the short form of OPA1 has been proposed to have a role in mitochondrial fission (Anand *et al.*, 2014). This project investigated total OPA1 protein expression in six control and eight sAD fibroblast lines, and found no significant differences at a group level despite seeing a significant increase in sAD 2. The ratio between the long and short forms of OPA1 was also calculated; the two isoforms are proposed to have differing roles, and as such the ratio between them can give an indication of the balance between mitochondrial fusion and fission, and whether alterations in OPA1 processing could contribute to the changes seen in mitochondrial morphology. No differences in long to short ratio were seen at either a group or individual level in four controls and eight sAD lines, demonstrating that any changes in total expression are due to changes in both isoforms, not just one.

The lack of overall significant difference between patient and control lines in L-OPA1 expression in this cohort of fibroblasts suggests that there are no clear alterations in fusion machinery; this is also

backed up by previous work in the lab which found no significant difference in OPA1 or Mfn1/2 levels at either a protein or RNA level in a small cohort of patient lines (Bell *et al.* 2018), though live time lapse imaging to assess fusion could be utilised to confirm that the fusion process in unaffected as total expression level of proteins does not tell us about the functionality of those proteins.

Previous work in the literature has found OPA1 to be both increased (X. C. Li *et al.*, 2016; Xu *et al.*, 2017) and decreased (X. Wang *et al.*, 2008; Pérez *et al.*, 2017; Kandimalla *et al.*, 2018a). As with Drp1 expression, variation in previous findings, as well as variations between cell lines used in this project, could be explained by the complex aetiology of sAD, or by model and cell type specific differences.

There is also no group change in the levels of S-OPA1. L-OPA1 is thought to be cleaved into S-OPA1 by OMA1 in response to stress conditions such as a loss of MMP (Lee *et al.*, 2020; Gilkerson, De La Torre and St. Vallier, 2021). The role of S-OPA1 within the mitochondria remains unclear, though the fact that healthy cells under normal conditions contain a mixture of both L-OPA1 and S-OPA1 indicates that it does have a functional purpose (Lee, Smith and Yoon, 2017). This is not necessarily directly involved in mitochondrial fusion; it has been linked to cell survival and maintenance of cristae (Lee, Smith and Yoon, 2017; Gilkerson, De La Torre and St. Vallier, 2021).

Nevertheless, it has been suggested that S-OPA1 is required for fusion of the inner mitochondrial membrane alongside L-OPA1 (Song *et al.*, 2007; Ge *et al.*, 2020). If this is the case, then these results contribute to previous results suggesting that there is no change in the fusion machinery in AD fibroblasts. On the other hand, there has also been suggestions that S-OPA1 is involved in the fission process, as expression of S-OPA1 promoted fragmentation, and it was also found to be partially localised with the fission machinery and mitochondria-ER contact sites, where mitochondrial fission occurs (Anand *et al.*, 2014). However, it must also be considered that S-OPA1 may be inactive and this increase in fragmentation is in fact due to a reduced amount of L-OPA1 leading to unopposed fission, rather than direct involvement of S-OPA1 (Gilkerson, De La Torre and St. Vallier, 2021). Whether S-OPA1 is directly involved in mitochondrial fission or not, there is no difference seen in S-OPA1 in these sAD fibroblasts, suggesting that the changes in morphology seen are not due to S-OPA1.

3.3.3 Drp1 Receptors

Previous work in the lab found that there was less Drp1 co-localised to the mitochondria in both sAD and PSEN1 patient fibroblasts (Bell *et al.*, 2018). Whilst it is possible that this is simply due to the reduced cellular levels of Drp1, it could also suggest that there is an impairment in the recruitment of Drp1 to the mitochondria. Drp1 is recruited to the mitochondria by four receptors on the outer mitochondrial membrane: Fis1, Mff, MiD49, and MiD51. Total cellular protein levels of these

receptors were assessed via western blot, and it was found that three of the four, Fis1, Mff, and MiD49 were decreased on a group level, though there was variation seen between individual lines.

3.3.3.1 Fis1

Fis1 was seen to be reduced in eight of the ten sAD lines, with an average decrease of 48%. Fis1 is the most well studied receptor in AD overall, with Drabik *et al.* (2021) seeing no change, and Wang *et al.* (2008) noting an increase in Fis1 in sAD fibroblasts, and several studies also noting an increase in various other models including transgenic animal models (Manczak *et al.*, 2010; 2018; Jia *et al.*, 2015; Kandimalla *et al.*, 2018; Reddy *et al.*, 2018), post mortem tissue (Manczak, Calkins and Reddy, 2011) and SHSY5Y cells treated with A β (Ahmed *et al.*, 2019). This is in contrast to the results seen in this project. These inconsistencies could be explained by the model differences described above in relation to Drp1, only a few studies have looked at Fis1 levels in fibroblasts with most being carried out in neural cell types; again, this will be investigated further in the second chapter of this thesis. It is also worth noting that many of these studies were carried out by the same group.

Though it was the first proposed receptor for Drp1 (Mozdy, McCaffery and Shaw, 2000), its role in fission has been questioned as deletion of Fis1 does not inhibit fission or lead to an increase in mitochondrial elongation (Otera *et al.*, 2010; Loson *et al.*, 2013). It has been suggested that Fis1 actually plays a bigger role in mitophagy, with Fis1 null *C. elegans* as well as Fis1 null HCT116 mammalian cells showing an accumulation of LC3 (Shen *et al.*, 2014), and Fis1 being shown to be key in binding TBC1 domain family member 15 (TBC1D15) and TBC1 domain family member 17 (TBC1D17), which play a role in the formation of the autophagosome and recruitment of lysosomes to damaged mitochondria. Recently, Kleele *et al.* (2021) discovered two distinct mechanisms of mitochondrial fission. Peripheral fission occurs at the periphery of the mitochondria, and is associated with the removal of damaged mitochondria. A decrease in MMP, increase in ROS, and increase in mitochondrial Ca²⁺ were seen prior to peripheral fission, and 92% of peripheral fission events were at lysosome-mitochondria contact sites. Kleele *et al.* (2021) also found that Fis1 was associated with peripheral fission; knockout of Fis1 reduced the number of peripheral fission events and increased levels of Fis1 were seen on the smaller daughter mitochondria, consistent with the proposed role of Fis1 in mitophagy. In this project, cellular levels of Fis1 were seen to be associated with changes in MMP via linear regression calculations, with a decrease in Fis1 being associated with a decrease in MMP. This fits with the theory that Fis1 is involved in removing dysfunctional mitochondria from the network; when there is less Fis1 present, less dysfunctional mitochondria are able to be removed. This association was also seen with Drp1 levels, but not any of the other receptors, suggesting that Fis1 is the key protein in this fission mechanism specifically relating to

mitophagy induction. Reduced levels of Fis1 seen suggests that there may be an impairment with fission of dysfunctional mitochondria and their subsequent degradation.

To investigate this theory further, it would be interesting to study mitophagy in these cells to determine if the decrease in Fis1 has an effect on the downstream processes of mitochondria recycling. This could be done by investigating the expression and localisation of proteins involved in mitophagy, for example parkin and PINK1, both of which have been previously seen to be altered in AD (Ye *et al.*, 2015; Hu *et al.*, 2016; Martín-Maestro *et al.*, 2016; Martín-Maestro, Gargini, A. Sproul, *et al.*, 2017; Manczak *et al.*, 2018; Reddy, Yin, *et al.*, 2018; Cummins *et al.*, 2019). Live mitophagy could also be measured, by assessing the co-localisation of mitochondrial and lysosomal stains in live fibroblasts. Previous work in the lab found that there is an increased percentage of mitochondria accumulated around the perinuclear region in sAD fibroblasts (Bell *et al.*, 2018); mitochondria are usually transported to the perinuclear region for degradation, and any deficits in mitophagy present in these fibroblasts may help to explain this accumulation.

In this project, Fis1 was seen to be associated with form factor, whereby a decrease in form factor (suggesting an increase in mitochondrial fragmentation) was associated with higher levels of Fis1. It has been suggested that Fis1-dependent fragmentation of the mitochondrial network is in fact due to Fis1 interactions with the fusion machinery; Fis1 mediated fragmentation occurs even in the absence of Drp1, and it can bind to Mfn1, Mfn2, and OPA1, inhibiting their GTPase activity (Yu, Jin, *et al.*, 2019). Reduced Fis1 present in sAD fibroblasts may lead to a reduction in Fis1 inhibition of fusion, leading to a more fused network. In contrast, it could be that reduced Fis1 leads to reduced recruitment of Drp1, leading to a reduction in fission, which results in a more fused network. Further work in this chapter focused on Fis1 interactions with Drp1, and will be discussed in detail later on potentially offering some insight into which of these mechanisms is correct.

3.3.3.2 Mff

Mff was decreased in six sAD lines, with an average reduction of 42%. As with Fis1, Mff is not well studied in a sAD fibroblast model though Drabik *et al.* (2021) did note a decrease, while an increase was seen in various other models including post mortem tissue (Wang *et al.*, 2019), transgenic mice (Q. W. Yan *et al.*, 2019), and A β treated cell lines (Ahmed *et al.*, 2019; Wang *et al.*, 2019).

While the role of Fis1 in fission has been questioned, the role of Mff is reasonably well established. Inhibition or knockdown of Mff leads to an inhibition of fission (Gandre-Babbe and van der Blik, 2008; Otera *et al.*, 2010; Loson *et al.*, 2013), and overexpression of Mff has been seen to increase recruitment of Drp1 to the mitochondria and increase fission (Otera *et al.*, 2010; Loson *et al.*, 2013). It has been suggested that Mff selectively recruits the more active form of Drp1, dephosphorylated

at ser637 (Liu and Chan, 2015; Atkins *et al.*, 2016), suggesting that Mff is the more important receptor for mitochondrial fission. In the results presented in this project, Mff protein levels were significantly associated with Drp1 levels, a relationship which was not seen between MiD49 or MiD51 and Drp1, supporting the theory that Mff is the more important protein in Drp1 recruitment and mitochondrial fission. This association was present in control cells but not sAD cells, suggesting that in sAD, the activity of Mff may be affected. Post translational modifications of Mff are important in its function; Mff has been shown to be phosphorylated at ser155 and ser172 by AMP-activated protein kinase (AMPK), a modification which is key in the recruitment of Drp1 to the mitochondria following AMPK activation (Toyama *et al.*, 2016). The phosphorylation status of Mff would be an interesting area for future work in these fibroblasts; if there is a reduction in phosphorylated Mff in sAD fibroblasts, this would impair the ability of Mff to recruit Drp1, and would perhaps explain the reduction in Drp1 localised to the mitochondria seen in the sAD fibroblasts.

As previously mentioned, Kleele *et al.* (2021) recently discovered two distinct mechanisms of mitochondrial fission. The second of these is mid-zone fission, where fission takes place in the middle of the mitochondrion, and is associated with Mff. This was shown by the increased amounts of Mff at the mid-zone compared to the periphery, and by knocking down Mff, which led to a reduction in mid-zone fission events. Mid-zone fission was found to be linked to mitochondrial biogenesis and proliferation; daughter mitochondria contained an elevated number of twinkle positive nucleoids, a protein involved in the production of mtDNA, and when cardiomyocytes were treated with micro-RNA-199 mimic to induce cell proliferation, mid-zone fission was increased but not peripheral fission. Furthermore, no mitochondrial dysfunction was seen prior to fission, a finding which fits with the lack of association between Mff and MMP seen in this project in the fibroblast model. Reductions in Mff seen in this project would suggest an issue with mid-zone fission in sAD fibroblasts as well as peripheral fission, though perhaps not to as great an extent. If mid-zone fission is affected in sAD, this would indicate a potential problem with mitochondrial biogenesis and proliferation, and it would be expected that a decrease in this type of fission would lead to a decrease in the number of mitochondria, something which has been noted in these fibroblasts (Bell *et al.*, 2018), though this was not seen to be significantly associated with Mff protein expression. Mitochondrial biogenesis could be further investigated in these fibroblasts through investigating the expression of proteins involved in this process, in particular peroxisome proliferator activated receptor γ coactivator 1 α (PGC1 α), the master regulator of mitochondrial biogenesis, which has previously been seen to be reduced in AD (Qin *et al.*, 2009; Gong *et al.*, 2010; Katsouri *et al.*, 2011; Wang *et al.*, 2021).

Reductions were seen in both Fis1 and Mff, indicating that both types of fission are affected in sAD fibroblasts. However, reductions in Fis1 are seen in a greater number of sAD fibroblast lines, plus there is a slightly greater average decrease per line, suggesting that peripheral fission is more affected. To confirm this, peripheral and mid-zone fission events could be studied in the fibroblast model, using similar high resolution imaging techniques to Kleele et al. (2021). However, the results shown here suggest that in this model, there may be a bigger deficit in fission leading to mitophagy than in fission leading to mitochondrial biogenesis. This is an important consideration when considering a treatment targeting this process; it may not be beneficial to increase fission indiscriminately if one type is more affected than the other. Generally, the findings here suggest that the cells are unable to degrade dysfunctional mitochondria efficiently, but are also less able to replace mitochondria via mitochondrial biogenesis, though further work is needed to confirm this. This combination would lead to an increase in the percentage of mitochondria which are damaged, and would have a major impact on the ability of the mitochondria to function efficiently.

3.3.3.3 MiD49 and MiD51

MiD49 was seen to be reduced in three of ten sAD patients, leading to an overall decrease of 36%, while MiD51 was not seen to be decreased in any individual sAD line, or when lines were combined. To our knowledge, MiD49 and MiD51 protein expression has not been studied before in any model of AD, though a rare mutation in MiD51 was identified as being associated with AD in a meta-analysis of extended family data sets (Cukier *et al.*, 2017).

Previous research has shown that MiD49 and MiD51 interact with Drp1 (Palmer *et al.*, 2011; Zhao *et al.*, 2011), and they have been found to partially rescue recruitment of Drp1 in Fis1/Mff null mutants, suggesting that they can function independently (Loson *et al.*, 2013). However, their role in fission has proven to be controversial, with some proposing that they are actually more involved in the fusion process, as an overexpression of either led to a hyper-fused network (Zhao *et al.*, 2011; T. Liu *et al.*, 2013). However, later research suggested that this fused network was actually due to inactivation of Drp1 at the mitochondrial membrane, as it was also associated with increased Drp1 at the mitochondria and an increase in phosphorylation of Drp1 at ser637 (which inhibits fission) (Loson *et al.*, 2013; Palmer *et al.*, 2013). These findings led to the proposal that MiD49 and MiD51 recruit inactive Drp1, phosphorylated at ser637, to the mitochondria, which is then dephosphorylated in response to further triggers (Atkins *et al.*, 2016). It remains unclear as to what these triggers may be, though it has been seen that the binding of adenosine diphosphate (ADP) to MiD51 was required for the activation of Drp1; in the absence of ADP, MiD51 inhibited Drp1 assembly and GTPase activity (Losón *et al.*, 2014). MiD51 protein expression was not seen to be

affected in this cohort of sAD fibroblasts. It may be that a higher proportion of the Drp1 which is localised to the mitochondria was recruited by MiD51, to compensate for deficits seen in the other receptors. This Drp1 may be inactive, and so unable to initiate fission, leading to increased fusion of the mitochondrial network. As mentioned above, the phosphorylation status of Drp1 is a key area for further study, and would help to elucidate whether the increased fusion seen in the mitochondrial network is simply due to the lack of Drp1 present at the mitochondria, or if the inability of Drp1 to initiate fission is also involved. It would also be interesting to investigate whether the binding of MiD51 to ADP is affected, as this would also give some indication as to the activation status of Drp1.

Kleele et al. (2021) found that knockout of MiD49 and MiD51 did not completely inhibit either peripheral or mid-zone fission events, but did cause around a 35% reduction in both. This suggests that while neither is necessary for any fission mechanism to occur, both are involved in both mechanisms in some way. However, Kleele et al. (2021) did not knock out MiD49 and MiD51 separately; it is possible that they are involved in different processes and this is being masked by using a double knockout rather than knocking them out individually. Regardless, in this case the reduction in MiD49 seen here would not necessarily have a big impact on either peripheral or mid-zone fission. Recently, Yu *et al.* (2021) investigated the possibility that MiD49 and MiD51 have a role to play in both fission and fusion. It was found that they interacted with components of both the fission and fusion machinery, and overexpression of either was able to rescue mitochondrial fragmentation seen in Mfn1, Mfn2, and OPA1 deficient cells. They have also been shown to decrease interactions between Fis1 and Mfn1 and Mfn2, preventing the Fis1 mediated inhibition of mitochondrial fission. They concluded that MiD49 and MiD51 may regulate both fission and fusion machinery, and play an important role in balancing these opposing mechanisms. A reduction in MiD49 may lead to an imbalance between these two processes, though it is possible this is retained by the unaffected levels of MiD51.

Despite sharing 45% sequence identity (Simpson *et al.*, 2000), it seems that MiD49 and MiD51 may be functionally different. MiD49 has been shown to form complexes with Drp1, perhaps to constrict the Drp1 assembly to enable fission to occur (Koirala *et al.*, 2013), while no evidence has been seen of this mechanism in MiD51 (Atkins *et al.*, 2016). MiD51 has been associated with mitophagy, with decreased levels seen to enhance PINK1-Parkin mitophagy, while overexpression led to a resistance to mitophagy (Xian and Liou, 2019). In this project, MiD49 levels were seen to be close to a significant association with MMP but MiD51 levels were not, supporting the idea that the two have different roles to play. Only MiD49 was seen to be reduced in sAD fibroblasts, again indicating that they may have different roles.

MiD51 is the only Drp1 receptor not affected in any of the sAD patient fibroblast lines; it is interesting to consider why this is. This project found that MiD51 was not associated with Drp1 levels, MMP, or form factor. It may be that MiD51 has a role outside of mitochondrial dynamics which is unaffected by sAD. It may also be that the deficits seen in other receptors are caused by deficits seen in mitochondrial function and morphology, or reduced levels of Drp1. The lack of association between these parameters and MiD51 may mean that MiD51 levels are less affected.

3.3.4 Variability between Individual Cell Lines

Whilst three of four receptors show a decrease in protein expression on a group level, this is not consistent in all ten sAD lines tested, with much variation seen between the patient lines. This is not unexpected, as mentioned previously, a level of heterogeneity is expected when working with human-derived cells in both control and patient lines. Despite variability seen between lines, all ten sAD lines did have a deficit in at least one fission protein. This suggests that while precise deficits and the extent of alterations can change, issues in the fission machinery appear to be a common mechanism in sAD fibroblasts. It is unknown whether mitochondrial dysfunction are a causal mechanism in AD, with several differing theories proposed (Hardy and Higgins, 1992; Swerdlow and Khan, 2004; Swerdlow, Burns and Khan, 2014). If mitochondrial dysfunction does occur as a result of something else, whether that is A β and tau accumulation, or a separate mechanism entirely, it could be that different patient's cells are more or less able to cope with this pathology, and so a variety of deficits are seen dependant on the resilience of the cell. On the other hand, mitochondrial dysfunction may play a more key role in the aetiology of sAD. sAD is complex, and it is unlikely that there is one unifying pathological mechanism across all cases. This suggests the need for precision medicine and better stratification of patients; if it can be identified which patients have a mitochondrial element to their sAD, these patients could be given treatments specifically targeted to improving mitochondrial function. Whether dysfunctional mitochondria are a cause or consequence, improving the function of the mitochondria, perhaps through correcting changes seen in mitochondrial morphology, may prove to be a worthwhile target for future drug screening. This will be investigated in the fifth chapter of this thesis.

Drp1 protein levels were also seen to be variable between different patient lines. A significant relationship was noted between Drp1 and Fis1, and Drp1 and Mff. It therefore is expected that as Drp1 levels vary, so too will the levels of the receptors. This could be explained several ways. Firstly, it could be that changes in Drp1 directly affect the levels of the receptors or vice versa. Alternatively, it may be that there is a separate mechanism which is having an effect on both Drp1 and receptor levels. A way to determine which of these is more likely would be to assess the levels of the

receptors in cells where Drp1 was overexpressed; an increase in the receptors when Drp1 was overexpressed would suggest that the levels of Drp1 have a direct effect on the levels of the receptors. The receptors could also be overexpressed, and Drp1 levels examined; an increase in Drp1 after receptor overexpression would indicate that the receptor levels are having a direct effect on Drp1 expression. It would also be interesting to see which receptor had the biggest effect on Drp1 levels, based on the associations seen in this project, it is likely that Fis1 and Mff would have a greater effect on Drp1 levels than MiD49 or MiD51. Work was planned within this project to investigate the receptor levels in fibroblasts where Drp1 has been overexpressed, but unfortunately this was not possible due to time constraints, and restricted lab access due to COVID-19.

3.3.5 Fis1 and Mff Localisation

In order to better understand the effect that reduced levels of Drp1 and its receptors have on the fission process, the localisation of Fis1 and Mff was studied. Unfortunately, this was not possible for MiD49 and MiD51 due to the available antibodies not being suitable for ICC. It was found that there was no significant difference in the amount or the percentage of total Fis1 or Mff localised to the mitochondria at a group level. Due to only one or two repeats being obtained for each line, statistical analysis was not carried out. However, variations were seen in individual lines, with some showing an increase and some showing a decrease.

Several lines showed control, or close to control, levels of Fis1 localised to the mitochondria despite having decreased cellular levels of Fis1. In some of these cases (sAD 1, sAD 5, sAD 8), there was also an increase in the percentage of total Fis1 present at the mitochondria. It would seem that these lines are able to compensate for the lower levels of total Fis1 by using a higher proportion of that Fis1 at the mitochondria. This was less successful in other cell lines (sAD 8, sAD 9), which were not able to rescue Fis1 levels at the mitochondria despite using an increased percentage of the available Fis1. Some lines (sAD 6, sAD 10) had a lower percentage of total Fis1 localised to the mitochondria, which perhaps led to the lower amounts of Fis1 present at the mitochondria.

Localisation of Mff also showed variation, with some lines showing a decrease in the amount of Mff localised to the mitochondria (sAD 3, sAD 6, sAD 9) while others showed an increase (sAD 1, sAD 5). Interestingly, there was no differences seen between control and sAD fibroblasts in the percentage of available Mff localised to the mitochondria, with the exception of sAD 9 which was increased.

On the whole, there are no consistent differences seen between the amount of Fis1 and Mff localised to the mitochondria. Though it is difficult to draw conclusions from only one or two

repeats, and further repeats must be carried out to confirm these results, it would seem that many lines are able to retain levels of Fis1 at the mitochondria by increasing the percentage of the total Fis1 available which is used at the mitochondria, though not all cells are able to do this. It is possible that a similar mechanism occurs with Mff which is not being picked up in this small sample.

3.3.6 Fis1 and Mff Interactions with Drp1

Previous work published by the lab has found that there are reduced levels of Drp1 present at the mitochondria (Bell *et al.*, 2018), but work on a small number of repeats in this project seems to show that there is no difference in the amount of Fis1 or Mff localised to the mitochondria despite reduced cellular levels seen at a group level. It may be that while the amount of Fis1 and Mff localised to the mitochondria is unchanged, the ability of these receptors to interact with Drp1 is. As previously mentioned, interaction of Drp1 with Mff is dependent on post translational modifications of Mff (Toyama *et al.*, 2016), as well as the activation of Drp1 by dephosphorylation at ser637 (Zhang *et al.*, 2016).

The number of interactions between Drp1 and Fis1, and Drp1 and Mff, was investigated using the proximity ligation assay. As with the localisation assays, MiD49 and MiD51 were unable to be assessed due to antibody issues. Due to time limits, this was only carried out in a small subset of the fibroblast lines, and these were chosen as they demonstrated the most deficits compared to the other sAD lines. No significant difference was seen in the number of interactions between Drp1 and Fis1, or Drp1 and Mff, between patient and control fibroblasts. Interactions were also investigated specifically in the perinuclear region; mitochondria are often transported to the perinuclear region for degradation, and an accumulation of mitochondria here is indicative of a collapse of the mitochondrial network (Xinglong Wang *et al.*, 2008). An increase in the percentage of mitochondria in the perinuclear region has been seen by the group previously in sAD fibroblasts (Bell *et al.*, 2018). It would be expected that if there are more dysfunctional mitochondria in the perinuclear region, there would also be an increase in the number of Drp1 interactions with Fis1 and Mff here, perhaps Fis1 more so based on the peripheral fission theory of Kleele *et al.* (2021) and the association seen between reduced MMP and Fis1 seen in this project. However, no significant difference was seen in the number of interactions in the perinuclear region of Drp1 with either Fis1 or Mff.

These findings suggest that despite reduced cellular levels of Drp1, Fis1, and Mff, and reduced levels of Drp1 at the mitochondria, cells are able to maintain the level of Drp1 interactions with Mff and Fis1. It is possible that this reduced level of Drp1 at the mitochondria is a result of lower cellular levels of MiD49, the localisation of which was unable to be assessed. However, generally evidence points to MiD49 and MiD51 being the least important receptors for Drp1 recruitment to take place

(Atkins *et al.*, 2016; Kleele *et al.*, 2021; Yu *et al.*, 2021), and this project has found that there is no significant relationship between total cellular Drp1 levels and either MiD49 or MiD51.

To assess whether Drp1 preferentially interacts with one receptor over the other, the number of interactions between Fis1 and Drp1, and the number of interactions between Mff and Drp1, were also compared. It was found that there is no significant difference in either control or sAD patient fibroblasts. This suggests that Drp1 interacts with both Fis1 and Mff equally both in the whole cell, and specifically in the perinuclear region. It would be interesting to compare this to the number of Drp1 interactions with MiD49 and MiD51, since these are proposed to be less important in Drp1 recruitment.

It is possible that the changes in mitochondrial morphology observed may be caused by mechanisms other than a deficit in Drp1 recruitment. It has been suggested that Fis1 may not be a Drp1 receptor at all (Osellame *et al.*, 2016) and is instead implicated in mitochondrial fission because of its role in lysosomal recruitment to the mitochondria (Kleele *et al.*, 2021), or its interactions with the fusion machinery which inhibits their activity (Yu, Jin, *et al.*, 2019). The data presented in this chapter does not agree with these suggestions; Fis1 cellular protein levels were seen to correlate with cellular Drp1 levels, and an interaction between Drp1 and Fis1 is clearly seen here. However, it would be of interest to also study the potential interactions of Fis1 with the fusion machinery; since no differences in the interactions with Drp1 were observed here, it may be that there is a reduction in the interactions between Fis1 and the fusion machinery which is reducing the inhibitory effect of Fis1 on fusion, leading to the more fused network previously observed in these fibroblasts (Bell *et al.*, 2018).

Interactions between Fis1 and Drp1 have been studied in both AD and other neurodegenerative diseases. These studies utilise P110, an specific inhibitor of Fis1/Drp1 interactions, which has no effect on the other Drp1 receptors (Qi *et al.*, 2013). In a range of AD models, inhibiting Drp1/Fis1 interactions with P110 was seen to prevent alterations to mitochondrial morphology and improve mitochondrial function (Joshi *et al.*, 2018a). Similar protective effects were seen with P110 treatment in septic cardiomyopathy (Haileselassie *et al.*, 2019), amyotrophic lateral sclerosis (Joshi *et al.*, 2018b), and Huntington's disease (Joshi *et al.*, 2019). It is important to note that these protective effects are seen in AD models where Fis1 is seen to be increased. In a model where Fis1 is already decreased, inhibiting Drp1 and Fis1 interactions would likely not be protective. In the fibroblasts used here, it would be interesting to use P110 to inhibit Drp1 and Fis1 interactions in the control cells, and observe the downstream effects of this on mitochondrial morphology, mitophagy, and mitochondrial function. This would give an indication as to how important these interactions are in maintaining the mitochondrial network, and shed some light on the effects of reductions in these

interactions. Though no difference was seen in the interactions between Drp1 and Fis1 in the sAD fibroblasts, using P110 to discover the role of Fis1 in downstream mechanisms of fission would give an indication as to the relevance of reduced Fis1 seen in the sAD fibroblasts.

3.3.7 Peroxisomal Fission

Several of the key mitochondrial fission proteins are not just important in fission of the mitochondria. Drp1, Fis1, and Mff have all been shown to be involved in fission of peroxisomes (Koch *et al.*, 2005; 2016; Fransen, Lismont and Walton, 2017). Peroxisomes are involved in several metabolic pathways including fatty acid β oxidation, and metabolism of ROS, as well as other cellular pathways including cellular signalling, and the immune response (Islinger *et al.*, 2018). There is evidence for the involvement of peroxisomal dysfunction in AD (Zarrouk *et al.*, 2018), including the presence of very long chain fatty acids in the brains (Kou *et al.*, 2011), plasma, and red blood cells (Zarrouk *et al.*, 2015) of AD patients.

Since many sAD lines are able to maintain levels of Fis1 and Mff present at the mitochondria at control, or close to control, levels, it may be that these reduced levels are having more of an effect on the peroxisome. In order to determine whether the reduced levels of Drp1, Fis1, and Mff have an effect on the peroxisome, Pex19 protein expression levels were assessed as a general marker of peroxisomal mass. Previous work has shown that peroxisomal markers peroxisomal membrane protein 70 (PMP70) and Pex5p are increased in a Tg2576 mouse brain (Cimini *et al.*, 2009), though more recently PMP70 and Pex14 were seen to be decreased in the hippocampus of rats treated with A β 42 (Aslan Karakelle, Dinçer and Yar Sağlam, 2021). No significant difference was seen in Pex19 protein expression between control and sAD patient fibroblasts. This indicates that there is no change in peroxisomal mass, though this would need to be confirmed by using immunocytochemistry, or live imaging, to better visualise peroxisomal morphology. It may be that whilst a similar mass is maintained, there are changes to the structure, size, and number of peroxisomes in AD. Furthermore, to assess whether there is a change in the amount of Drp1, Fis1, and Mff localised to the peroxisome, immunocytochemistry could be used to assess the co-localisation of these proteins with pex19, or another peroxisomal marker. This could also be assessed by isolating mitochondria and peroxisomes via cellular fractionation, and carrying out western blotting for fission proteins in the specific mitochondria and peroxisome fractions.

3.3.8 Upstream Mechanisms of Mitochondrial Fission

Mitochondria-ER contact sites have been shown to play a role in fission; a large proportion of fission events have been seen to take place at these contact sites (Friedman *et al.*, 2011; Korobova, Ramabhadran and Higgs, 2013). It has been proposed that INF2 on the ER and Spire1c on the mitochondria initiate actin polymerisation (Korobova, Ramabhadran and Higgs, 2013; Chakrabarti *et al.*, 2018), and myosin II enables actin contraction, providing the mechanical force to drive constriction of the mitochondria (Chakrabarti *et al.*, 2018). There are several different types of mitochondria-ER contact sites, composed of a wide range of tethering proteins. Some of the most common are VAPB-PTPIP5, ER located Mfn2-mitochondrial Mfn1/2, BAP31-Fis1, and VDAC-GRP75-IP3R (Xu, Wang and Tong, 2020). Specific tethering proteins are known to have different functions, for example VDAC-GRP75-IP3R are thought to be involved in calcium homeostasis (Wilson and Metzakopian, 2021), and VAPB-PTPIP51 may be involved in lipid transfer (Xu, Wang and Tong, 2020). It remains unclear which tethering proteins are the most involved in mitochondrial fission. BAP31-Fis1 was chosen as the first type of mitochondria-ER contact site to be investigated based on the role of Fis1 in fission, as well as the reduced levels of Fis1 seen in this project. Furthermore, BAP31-Fis1 contact sites have been proposed to be involved in apoptosis (Chandra *et al.*, 2004; Simmen *et al.*, 2005), a process in which mitochondrial fragmentation and Drp1 also play a role (Frank *et al.*, 2001; Pascucci *et al.*, 2021). Due to time and antibody constraints, no further types were investigated.

It was found that there was no significant difference in the number of BAP31-Fis1 contact sites between control and sAD fibroblasts, in the subset of lines tested here, as well as no significant differences in the percentage of total BAP31 co-localised with Fis1, or the percentage of total Fis1 co-localised with BAP31. This suggests that the reduced levels of Fis1 seen in these sAD fibroblasts had no effect on BAP31-Fis1 contact sites. Interestingly, one control line, control 10, showed a significantly higher percentage of BAP31 co-localised with Fis1, and a significantly lower percentage of Fis1 co-localised with BAP31. There was no significant difference in the number of BAP31-Fis1 co-localisations between control 10 and the other controls, but there was a non-significant decrease.

Co-localisation staining is not the most accurate way to assess mitochondria-ER contact sites, and may be insufficient to pick up interactions between tethering proteins. A PLA could be used as a more sensitive measure of interactions between these proteins, though the gold standard for measuring mitochondria-ER contact sites is electron microscopy, and this may highlight differences not seen here. Furthermore, it is possible that there are differences in other mitochondria-ER contact sites not tested here. Mfn2-Mfn1/2 contact sites are thought to play a role in mitochondrial fusion (Wilson and Metzakopian, 2021); it could be that alterations at these sites lead to an increase

in fusion, which could contribute to the fused network seen in sAD fibroblasts. Other contact sites, such as VAPB-PTPIP5 and VDAC-GRP75-IP3R, may also play a role in mitochondrial dynamics and so levels of these would also be interesting to assess.

It is also possible that while the number of contact sites is unaffected, other aspects of the pre-constriction process are. As part of this project, INF2 levels were investigated via western blot but this proved to be difficult in the fibroblast system, and so no reliable data was obtained. It would be also be valuable to look at actin polymerisation; this could be done using tagged actin or an actin probe such as LifeAct (Melak, Plessner and Grosse, 2017).

When researching mid-zone and peripheral fission, Kleele *et al.* (2021) suggested that mitochondria-ER contact sites are only involved in mid-zone fissions, leading to mitochondrial biogenesis. They found that while mid-zone fission sites were in contact with the ER prior to fission, most peripheral sites were not. Furthermore, actin was seen to polymerise at the mid-zone, but not the periphery. In this case, a lack of alterations seen in mitochondria-ER contact sites may suggest that there is more of an effect on peripheral fission than mid-zone fission, suggesting that sAD fibroblasts have a bigger deficit in removing damaged mitochondria than generating new mitochondria. This is in agreement with deficits in mitophagy previously seen in AD (Ye *et al.*, 2015; Hu *et al.*, 2016; Cummins *et al.*, 2019), including in sAD patient fibroblasts (Martín-Maestro *et al.*, 2016), and again, this would be an interesting area for further study in the fibroblasts investigated here.

Mitochondria-ER contact sites have long been thought to play a role in AD. PSEN1 and PSEN2 are enriched at mitochondria-ER contact sites (Area-Gomez *et al.*, 2009), and APP has been seen to be processed here (Del Prete *et al.*, 2017). Furthermore, in AD fibroblasts, an increase in contact has been seen plus an increase in various functions which occur at these sites (Area-Gomez *et al.*, 2012). It is still unknown how these changes affect mitochondrial fission in AD, but given the varied and complicated role of mitochondria-ER contact sites, it is likely only one part of their impact on AD pathology.

3.3.9 Overexpression of Drp1 in Fibroblasts

To investigate whether overexpression of Drp1 could rescue the mitochondrial morphology phenotype seen in sAD patient fibroblasts, Drp1 was transiently overexpressed via plasmid transfection. Fibroblasts are difficult to transfect, in many cases yielding a low transfection efficiency (Koster and Waterham, 2017; Kucharski, Mrowiec and Oćłoń, 2021). Generally, fibroblasts become less metabolically active as they reach higher passages, and so a low passage is ideal, usually lower than passage 5. Unfortunately, due to the cells available in the lab, the lowest passage used was 7 and the highest was 9. That said, the transfection efficiency achieved of 18-25% is relatively high

with many transfection protocols in fibroblasts yielding less than 10% successful transfection (Kucharski, Mrowiec and Ochoń, 2021).

However, the transfection itself led to stress in the cells, and this response obscured any meaningful data with regard to Drp1 in sAD. Increased cellular stress and cytotoxicity has previously been seen in response to transfection, for example, transfection has been seen to induce the innate immune response (Chen *et al.*, 2003), in which mitochondrial dynamics play a role (Castanier *et al.*, 2010; Zemirli *et al.*, 2014), which may explain the increased fragmentation seen. There are several potential optimisation steps which could be taken to reduce this response. Firstly, the amount of transfection reagent and plasmid DNA used were taken from a protocol obtained from Dr Lydia Castelli and Dr Guillaume Hautbergue, which was optimised for immortalised cell lines. Further optimisations of these amounts for the fibroblast model may have given a better result. Different transfection reagents may also reduce the stress response. The transfection reagent used, PEI, is a cationic polymer; it has a high density of positive charges, which interact with negative charges in the phosphate backbone of the DNA and condense into particles which bind to the cell surface and are taken up by endocytosis (Ming Hsu and Uluda Ğ, 2012). Though it has previously been successful in transfection of primary human fibroblasts (Ming Hsu and Uluda Ğ, 2012; Becerra Colorado *et al.*, 2018), it has also been seen to be cytotoxic (Khansarizadeh *et al.*, 2016). There are also several alternative chemical transfection reagents which could be tested, including FuGENE (Promega), which was found to cause the least side effects when tested in HeLa cells compared to six other commercially available transfection reagents (Antczak *et al.*, 2014).

Alternative methods of overexpression could also be carried out including transduction using a viral vector. One option is transient overexpression using an adenovirus vector. In fibroblasts, adenoviral gene delivery has been seen to give a transfection efficiency of 70%, and only showed cytotoxic effects after ten days (Hirsch *et al.*, 2006). Another possible transfection strategy is a physical transfection method such as electroporation. Nucleic acids enter the cell through temporary pores in the plasma membrane, caused by brief electrical charges (Kumar, Nagarajan and Uchil, 2019). A specialised version of electroporation, nucleofection, allows nucleic acids to directly enter the nucleus using a Nucleofector device (Lonza; developed by Amaxa), and this has been found to have both increased transfection efficiency and cell viability in human fibroblasts, though it is high cost compared to many of the other methods discussed here (Kucharski, Mrowiec and Ochoń, 2021).

A successful overexpression transfection would give an indication as to whether Drp1 is directly involved in the morphological phenotype seen in sAD fibroblasts. For example, if sAD cells overexpressing Drp1 showed a rescued morphology, more similar to that of control cells, this would suggest that the reduction seen in Drp1 levels in sAD fibroblasts plays an important role in this

pathology. If overexpression of Drp1 did not lead to a rescue in the morphology parameters assessed, this would suggest that there is another mechanism occurring within the cell which is leading to the morphology phenotype seen. For example, it may be that reductions in the receptors involved in Drp1 recruitment are more crucial in the sAD phenotype, and this could be assessed by overexpression of these proteins should Drp1 overexpression fail to impact the sAD morphology phenotype.

3.3.10 The Use of Fibroblasts in AD Research

Fibroblasts have been used as a model of AD for many years, as many of the changes seen in neural cells are also seen in peripheral cells such as fibroblasts (Trushina, 2019). There are many advantages to using fibroblasts to model AD; they maintain the genetic background of the patient, as well as changes which have accumulated in the cell with age. This is particularly important in AD as age is the biggest risk factor. Another advantage of fibroblasts is their ability to model sporadic disease; this is difficult as the aetiology of sporadic AD is complex and poorly understood. Many models, such as transgenic animal models, are based on genetic mutations which cause fAD. However, fAD only accounts for a small percentage of AD and it may be that mechanisms which occur in fAD are different in sAD.

However, there are also several disadvantages. Fibroblasts are not neural cells, and are not directly implicated in AD, reducing disease relevance. They are also cultured as a 2D culture, which does not represent the physiological complexity of the brain. Several of the alterations seen in this chapter, and previous results seen in fibroblasts, differ from results previously seen in other, neural based cell models including tumour based neural models, post mortem tissue, and animal models. It may be that different mechanisms are occurring in the periphery which would reduce the relevance of the fibroblast model. However, as mentioned above, fibroblasts are metabolically very different to neural cell types, particularly neurons. Mitochondrial morphology is intrinsically linked to mitochondrial function, and differing functional requirements likely lead to differing morphology requirements which may explain the differences seen in sAD phenotype. It is still valuable to assess these differences to determine whether the process in general is impaired, whichever direction this may be in. To investigate this further, a patient derived neural cell model will be used in the second chapter of this thesis.

There are also practical considerations which must be considered when culturing fibroblasts. Insufficient nutrition from culture media can have a significant effect on cells, especially the mitochondria; nutrient starvation has been seen to lead to changes in mitochondrial morphology, as they become more elongated and interconnected, mediated by the downregulation of Drp1

(Rambold *et al.*, 2011). This may introduce uncertainty as to whether the results seen are disease specific or due to the culturing of the cells. Fibroblasts used in this project have been cultured in EMEM supplemented with FBS, NEAA, Sodium pyruvate, uridine and vitamins. Sodium pyruvate and uridine are required for survival in cells where mitochondrial deficits are present. Pyruvate is an intermediate in the glycolysis pathway, and so improves the cell's ability to metabolise glucose. Dysfunction in the ETC can also affect de novo pyrimidine synthesis, so uridine is also added (Olgun and Akman, 2007).

Despite not being a directly involved cell type, fibroblasts can be useful in other ways, for example, in the search for a biomarker. There are multiple types of biomarker, including diagnostic biomarkers, prognostic markers which relate to the stage of AD, or biomarkers which can predict a faster or slower progression. The potential use of the proteins studied in this chapter as biomarkers has been investigated in peripheral blood lymphocytes. Wang *et al.* (2012) found that differences in Fis1, Drp1, and s-nitrosylated Drp1 (SNO-Drp1) were specific and sensitive enough to differentiate AD patients from controls, implying that these proteins may have potential as biomarkers. While this may not be feasible as a diagnostic biomarker, it has potential as a biomarker of disease progression; significant changes were also seen in patients with mild cognitive impairment. Although this work was carried out in lymphocytes rather than fibroblasts, it does indicate that peripheral cells in general may be useful when looking for disease biomarkers.

3.4 Conclusions and Future Work

This chapter aimed to investigate the mechanisms surrounding the reduced levels of Drp1 protein seen in sAD patient fibroblasts. Firstly, the protein expression of the four Drp1 receptors on the outer mitochondrial membrane were investigated to see if this could be contributing to the reduced levels of Drp1 seen localised to the mitochondria. Whilst a deficit was seen in Fis1, Mff, and MiD49, there were no differences seen in the localisation of Fis1 and Mff, or the number of interactions between these proteins and Drp1. These findings suggest that reduced Drp1 at the mitochondria is not due to reductions in Fis1 or Mff, as the level of interaction is maintained. Interactions between Drp1 and Fis1 and Mff were only investigated in a small subset of the total cohort, and differences have been seen between patient lines suggesting that a reduction in interactions may be seen in other lines should they be investigated. However, since the lines chosen demonstrated the biggest deficits, this does not seem likely.

If the reduction in Drp1 at the mitochondria is not due to alterations in Fis1 or Mff, it may be that it is due to reductions seen in MiD49. Whilst MiD49 levels were not seen to correlate with Drp1 levels, and several studies have found MiD49 to be less crucial for Drp1 recruitment, it still has a role to

play and may prove to be important in sAD. Future studies should investigate the interactions between MiD49 and Drp1, as well as MiD51 and Drp1 to confirm this. Unlike Fis1 and Mff, MiD49 and MiD51 are only found at the mitochondria and are not involved in the fission of other organelles. The lack of change seen at the peroxisome (though this requires further investigation), may suggest that it is actually the relationship between Drp1 and MiD49 and MiD51 which is altered in sAD fibroblasts. Further study should be done to determine how MiD49 and MiD51 are affected in other models of sAD, as well as in fAD. To date, this is an area which remains understudied in the field.

Previous work in our lab has clearly shown changes to mitochondrial morphology in sAD patient fibroblasts, indicating a more fused network. This may not simply be due to less Drp1 being available in the cell. Post translational modifications of Drp1 are key in its fission activity, in particular phosphorylation, and this is an important area for further study. It may be that the Drp1 recruited to the mitochondria is inactive and unable to initiate fission, and that this is leading to the changes in morphology seen.

Changes seen in mitochondrial morphology may be the result of alterations to only one type of fission, as defined by Kleele et al. (2021), either peripheral or mid-zone. Reductions in both Fis1 and Mff would suggest both, but greater deficits were seen in Fis1. To investigate this further, both mitophagy and mitochondrial biogenesis could be studied to assess whether one is more impacted than the other. This is important in terms of treatments for AD; if only one type of fission is affected, it would not be beneficial to globally inhibit or stimulate all fission (Kleele *et al.*, 2021).

Changes in morphology may also be due to mechanisms occurring upstream of Drp1, such as pre-constriction of the mitochondria. Whilst a single type of mitochondria-ER contact site, BAP31-Fis1, showed no differences in a subset of the lines studied in this chapter, it could be that other types are affected. Other aspects of the pre-constriction such as expression of INF2 and Spire1c, and the polymerisation of actin should also be investigated.

Finally, changes in morphology may also be explained by changes in mitochondrial fusion. While no significant differences were seen in the expression of OPA1, and previous work in the lab has found no changes in Mfn1 or Mfn2 either, there are further mechanisms which must be considered. For example, the ability of Mfn1 and Mfn2 to interact with each other on opposing mitochondria, or the ability of OPA1 to interact with cardiolipin on the opposing inner membrane, both of which are key for fusion to take place (Tilokani *et al.*, 2018). Fis1 has also been shown to interact with fusion proteins, inhibiting their activity (Yu, Jin, *et al.*, 2019). The reduced levels of Fis1 seen in this chapter may actually be having more of an impact on the fusion machinery, leading to increased levels of

fusion as opposed to reduced levels of fission, and thus leading to a more fused mitochondrial network.

To conclude, from the evidence presented here, it seems unlikely that changes in recruitment of Drp1 by Fis1 and Mff are significantly contributing to changes in mitochondrial morphology. Future work should focus on the relationship between Drp1 and Mid49 and Mid51, post translational modifications of Drp1, upstream mechanisms of fission such as pre-constriction of the mitochondria and downstream mechanisms such as mitophagy and biogenesis, and mitochondrial fusion to better understand the precise mechanisms which lead to the changes seen in mitochondrial morphology in sAD patient fibroblasts. Future work should also focus on validating findings in patient fibroblasts in further models of AD to confirm whether these changes also occur in the central nervous system, and are not just present in the periphery.

Chapter Four: Investigating the Mitochondrial Phenotype in a Patient Derived Neuronal Model

4.1 Introduction

4.1.1 Induced Pluripotent Stem Cell Derived Models of Alzheimer's disease

There are many advantages to fibroblasts as a patient derived model of Alzheimer's disease, but a key disadvantage is that they are not a disease relevant cell type. Takahashi and Yamanaka (2006) first demonstrated that somatic cells could be reprogrammed into induced pluripotent stem cells (iPSCs) using four key transcription factors, Oct3/4, Sox2, c-Myc, and Klf4. iPSCs have the potential to be differentiated into any cell type, thus retaining the genetic background of the patient while also providing a more disease relevant cell model, for example, neurons, astrocytes, oligodendrocytes, and microglia.

In AD, amyloid and tau neuropathology begins in the entorhinal cortex, before spreading through the hippocampus, limbic system, and neocortex (Braak and Braak, 1991, 1995; Cho *et al.*, 2016). Mitochondrial pathology has also been found to begin in the entorhinal cortex (Armand-Ugon *et al.* 2017). In contrast, cells in the brain stem, cerebellum, and basal ganglia, controlling motor and autonomic functions, are able to function effectively (Wang *et al.*, 2020). As such, when modelling AD, a cortical neuron model is the most relevant cell type to investigate and so was initially chosen for this project.

In general, differentiation of cortical neurons from iPSCs requires three steps: neural induction, patterning to a dorsal or ventral fate, and terminal differentiation. These steps are achieved by mimicking neurodevelopment, and the application of various signalling molecules involved in the determination of neural fate (McCaughey-Chapman and Connor, 2018). Many studies use cortical neuron differentiation protocols based on a protocol developed by Shi, Kirwan and Livesey (2012). Neural induction is achieved using dual inhibition of SMAD, a family of proteins involved in the transforming growth factor β (TGF β) signalling pathway, via dorsomorphin and SB431542. Following this, cells are cultured in a basic differentiation media, containing N2 and B27, to give glutamatergic cortical neurons. After 20 days, early cortical neurons positive for T box brain 1 (TBR1) and COUP TF1-interacting protein 2 (CTIP2) begin to form, becoming a larger population around day 30. After 70 days differentiation, upper layer cortical neurons begin to form, positive for BRN2, special AT-rich sequence binding protein (SATB2), and cut-like homeobox 1 (CUX1), as well as vesicular glutamate transporter 1 (vGlut1). Physical synapses are seen from day 28 of the protocol, and begin to become

functional at day 30, with many functional synapses seen by day 50. This protocol has been adapted by others in several ways, for example alterations to the patterning stage (Boissart *et al.*, 2013), addition of extra factors such as sonic hedgehog inhibitor, cyclopamine (Cao *et al.*, 2017), and overexpression of neurogenin 2 (NGN2) to bypass the neural induction and patterning stages, speeding up the differentiation process (Zhang *et al.*, 2013). The time required for this process has also been reduced by the addition of DAPT to promote neurogenesis, and shorten the initial induction step (Tay *et al.*, 2021).

iPSC derived cortical neurons have been used in many studies to investigate various AD phenotypes, with several different protocols used. Bergström *et al.* (2016), following the Shi, Kirwan, and Livesey (2012) protocol, showed neurite outgrowth between days 49 and 59, TBR1 positive staining from day 45, and increased TUJ staining from day 60. By day 90, high levels of vGlut1 staining throughout the neurite network, and whole cell patch clamping demonstrated functionality of glutamatergic and gamma-aminobutyric acid (GABA)ergic synapses. APP processing was seen to change throughout differentiation, with A β 1-42 detected from day 75, and in fAD iPSC derived cortical neurons, the A β 40:42 ratio was seen to be increased (Arber *et al.*, 2019). Also following the Shi, Kirwan, and Livesey (2012) protocol, Fang *et al.* (2019) differentiated iPSCs derived from AD patients, and saw positive expression of microtubule associated protein 2 (MAP2), TUJ, and upper cortical neuron marker BRN2. They also saw evidence of synapse formation via the expression of synaptophysin and postsynaptic density protein 95 (PSD95). iPSC derived AD neurons were also seen to show many of the cellular features seen in AD brain tissue, including increased DNA damage. AD iPSC cortical neurons have also been generated via alternative protocols. For example, Birnbaum *et al.* (2018) cultured sAD iPSC derived neurons following the protocol by Zhang *et al.* (2013), with cells showing neuronal morphology, MAP2 expression, and presynaptic marker synapsin.

While iPSC derived cells are still a relatively new model, they have been used to investigate a range of mitochondrial phenotypes in AD. For example, alterations in mitophagy have been noted in iPSC derived neurons from patients with a PSEN1 mutation, which were seen to have increased total parkin levels and increased parkin present at the mitochondria, as well as increased mitochondrial surface area (Martín-Maestro, Gargini, A. Sproul, *et al.*, 2017). Reduced levels of PINK1 have also been seen in iPSC neurons derived from an sAD patient, and a patient with an APP mutation, as well as reduced phosphorylation of other mitophagy related proteins, tank binding kinase 1 (TBK1) and unc-51 like autophagy activating kinase (ULK1) (Fang *et al.*, 2019). This study also found impaired mitochondrial function, shown by a reduction in ATP, as well as alterations in the post translational modifications of fission proteins, including increased phosphorylated Drp1 (ser616) and increased phosphorylated Mff. A further study using iPSC neurons derived from sAD patients found increased

ROS, and increased expression of subunits of complexes I, III, IV and V. The study also investigated fission and fusion proteins, but saw no difference in Mfn1, Mfn2, or Drp1. While this study presents some interesting findings, phenotypes were not consistently seen in all five of the lines assessed (Birnbaum *et al.*, 2018). The mitochondrial phenotype in other cell types has also been investigated; iPSC derived astrocytes from patients with a PSEN1 mutation have been found to have increased ROS, and decreased glycolysis suggesting that AD astrocytes are more oxidative (Oksanen *et al.*, 2017).

4.1.2 Induced Neural Progenitor Cells

One of the limitations of iPSC derived cells is that they do not maintain the characteristics of the cell which occur as a result of patient age, a factor especially relevant to AD as age is the biggest risk factor. Reprogramming of iPSCs induces an embryonic state, and thus resets many of the phenotypes associated with aging such as telomere size and gene expression profiles (Lapasset *et al.*, 2011).

There are several alternatives to iPSC derived cells, which retain aged characteristics of the original patient cells, as well as maintaining the advantages of being a patient derived, disease relevant model. One alternative is the transdifferentiation of somatic cells directly into neural cells including neurons (Vierbuchen *et al.*, 2010), astrocytes (Caiazzo *et al.*, 2015; Tian *et al.*, 2016), microglia (Ohgidani *et al.*, 2014) and oligodendrocyte precursors (Yang *et al.*, 2013). This has been done via the forced expression of pro-neural transcription factors (Vierbuchen *et al.*, 2010; Ladewig *et al.*, 2012; Liu *et al.*, 2013) or a chemical cocktail of small molecules (Hu *et al.*, 2015). Transdifferentiated neurons have been shown to maintain age specific phenotypes, including genetic profiles, and decreased levels of RanBP17, a nuclear transport receptor (Mertens *et al.*, 2015, 2021). However, the proliferative capacity of these cells in culture is limited, reducing the practicality of this model for in vitro modelling of AD.

The conversion of somatic cells to induced neural progenitor cells (iNPCs) is another option. Kim *et al.* (2011) were among the first to convert mouse fibroblasts directly to iNPCs, with others confirming these findings and also applying them to human fibroblasts (Ambasudhan *et al.*, 2011; Son *et al.*, 2011; Ring *et al.*, 2012; Cheng *et al.*, 2014). Meyer *et al.* (2014) were the first to apply this technique to neurodegenerative disease, successfully reprogramming fibroblasts from ALS patients to iNPCs, and these iNPCs to a range of neural cells including astrocytes, oligodendrocytes and neurons.

There are several advantages to iNPCs. They are proliferative, so can be expanded in vitro enabling a sufficient number of cells to be generated, whilst also being less time and labour intensive.

Furthermore, whilst iPSC cell populations are often generated from a single clone, iNPC derived cells are taken from across a cell population, reducing potential bias. iNPC derived astrocytes have also been shown to retain age-related phenotypes including reductions in mRNA levels of RanBP17, telomeric repeat binding factor 2 (TERF2), and laminin subunit alpha 3 (LAMA3), and changes to nuclear morphology including nuclear folding and blebbing. Changes in aged phenotypes relating to the mitochondria have also been seen including increased ROS levels, and reduced levels of antioxidants nuclear factor-erythroid factor 2-related factor 2 (NRF2) and SOD1 (Gatto *et al.*, 2021).

4.1.3 Aims and Objectives

In the previous chapter and previously published work, alterations have been seen in mitochondrial quality control mechanisms in sAD fibroblasts compared to controls (Bell *et al.*, 2018). This chapter will determine whether these alterations are also present in patient derived neurons generated from iNPCs. iNPCs reprogrammed from some of the fibroblast lines used in chapter 3 were readily available in the lab. Reprogramming was carried out by Dr Simon Bell, and Professor Laura Ferraiuolo, and iNPCs were confirmed to express pax6 and nestin (Dr Simon Bell's PhD Thesis).

The first aim of this chapter is to investigate the mitochondrial phenotype seen in sAD patient fibroblasts in a patient derived neuronal model. The objectives are:

1. To develop a differentiation protocol to produce patient derived neurons from induced neuronal progenitor cells
2. To characterise a patient derived neuronal model
3. To determine the mitochondrial phenotype of a patient derived neuronal model

The second aim of this chapter is to determine whether the same mechanisms are present leading to mitochondrial morphological changes in AD derived neurons as fibroblasts. The objectives are:

1. To measure protein expression of Drp1 in patient derived neurons
2. To measure protein expression of the four Drp1 receptors, Fis1, Mff, MiD49, and MiD51, in patient derived neurons
3. To measure interactions between Drp1 and the receptors
4. To investigate post translational modifications of Drp1, primarily phosphorylation at ser637 and ser616

4.2 Results

In this chapter, control and sAD lines have been analysed as age and sex matched pairs due to an increase in the variability between control and sAD lines (shown in table 18), as well as at a whole group level.

Table 18: Age and sex matched pairs used in this chapter.

Control	Age	Sex	sAD	Age	Sex
Control 3	61	Female	sAD 5	59	Female
Control 7	56	Male	sAD 4	63	Male
Control 10	75	Female	sAD 9	79	Female
Control 5	100	Female	sAD 6	63	Female
Control 2	54	Male	sAD 8	60	Male

Due to time restraints, and difficulties encountered in growing some lines, control 2 and sAD 6 were not included in all data sets. Where these lines have not been used, control 5 and sAD 8 have been analysed as a pair.

4.2.1 Characterisation of the Generic Neuron Model

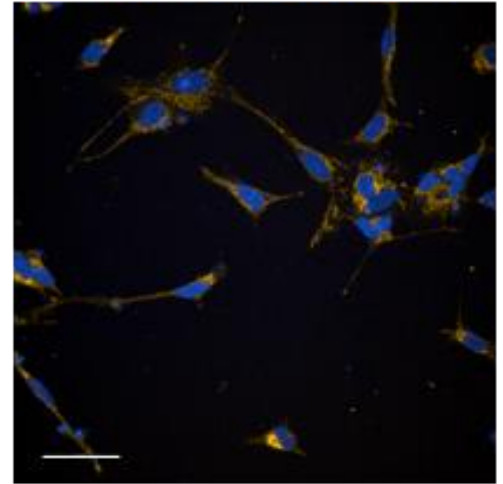
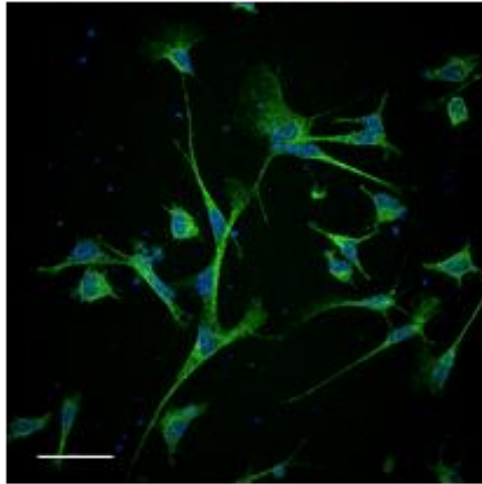
Initially, attempts were made to optimise differentiation of cortical neurons from iNPCs (Appendix 1). This proved to be unsuccessful in the time frame available, and so a protocol to differentiate a more general neuronal population was chosen to move forward, as described in Webster *et al.* (2016). This population was characterised by assessing expression of neuronal markers. Primary and secondary only controls were included to ensure that staining seen was not due to non-specific background staining. Each line showed expression of TUJ, and representative images can be seen in figure 35 and figure 36. The percentage of cells expressing TUJ was assessed for each line, with all lines showing above 87% TUJ positive cells (control 9 92.1% \pm 6.9; control 7 99.3% \pm 1.0; control 10 99.1% \pm 0.95; control 5 87.1% \pm 15.5; control 2 99.0% \pm 11.9; sAD 5 97.3% \pm 4.0; sAD 4 96.7% \pm 4.2; sAD 9 97.0% \pm 5.5; sAD 6 92.2% \pm 12.5; sAD 8 92.6% \pm 11.9). There was no significant difference in the percentage of TUJ positive cells between control and sAD lines (figure 39a), at either an individual or group level (controls 95.4% \pm 5.4, sAD 95.2% \pm 2.5; $p = 0.945$; figure 39d). Cells were also assessed for expression of MAP2. All lines showed some expression of MAP2, as shown in figure 35 and figure 36. The majority lines showed over 60% MAP2 positive cells (control 9 93.8% \pm 4.3;

control 7 74.4% ± 33.3; control 10 81.5% ± 15.7; control 5 90.1% ± 14.3; control 2 71.9% ± 28.9; sAD 5 98.6% ± 1.5; sAD 9 89.3% ± 12.5; sAD 6 77.1% ± 13.7; sAD 8 60.0% ± 30), with sAD 4 being the only exception, showing only 29.3% ± 1.1 MAP2 positive cells. There was only a significant difference in MAP2 positive cells in sAD 4 ($p = 0.014$; figure 39b) at an individual level, and no significant difference at a group level (control 82.3% ± 9.6; sAD 70.8% ± 27.4; $p = 0.401$; figure 39e). NeuN expression localised to the nucleus was also assessed, and representative images are shown in figure 37 and figure 38. In general, there was a low percentage of NeuN positive cells, and more variation between the different lines. This is to be expected, as NeuN is a marker of later stage neurons, and the shorter protocol used gives less time for these neurons to mature. There were very little NeuN positive cells in sAD 5 and sAD 6 (sAD 5 3.4% ± 4.4, $p = 0.01$; sAD 6 2.2% ± 2.9, $p = 0.02$; figure 39c), but the rest of the lines showed between 20% and 75% NeuN positive cells (control 9 53.8% ± 22.6; control 7 33.7% ± 27.1; control 10 73.5% ± 16.2; control 5 48.4% ± 25.4; control 2 22.1% ± 10.9; sAD 4 57.2% ± 21.0; sAD 9 35.5% ± 29.0; sAD 8 48.4% ± 25.3). There was no significant difference between NeuN positive cells in controls and sAD lines at a group level (controls 46.1% ± 19.6, sAD 26.8% ± 23.6; $p = 0.193$; figure 39f).

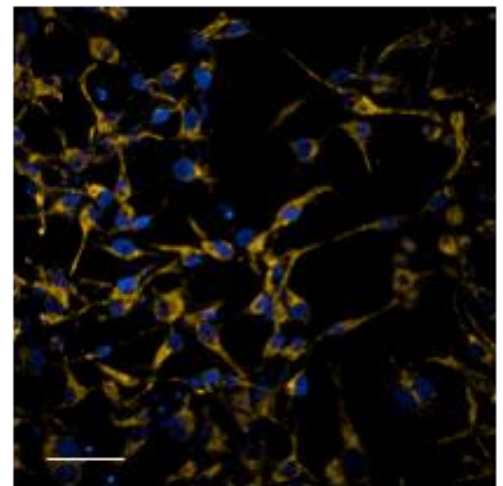
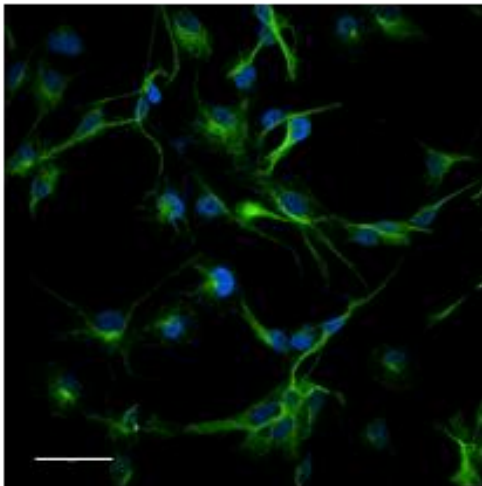
TUJ/Hoechst

MAP2/Hoechst

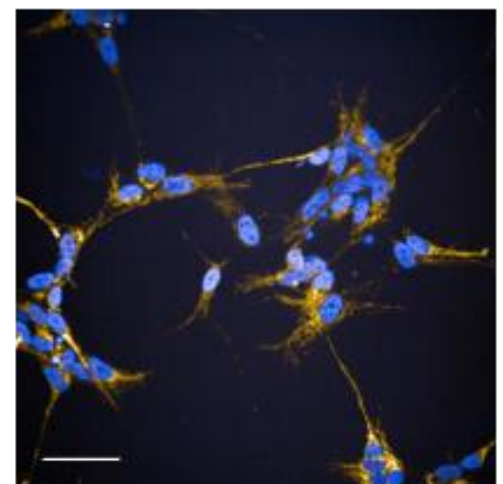
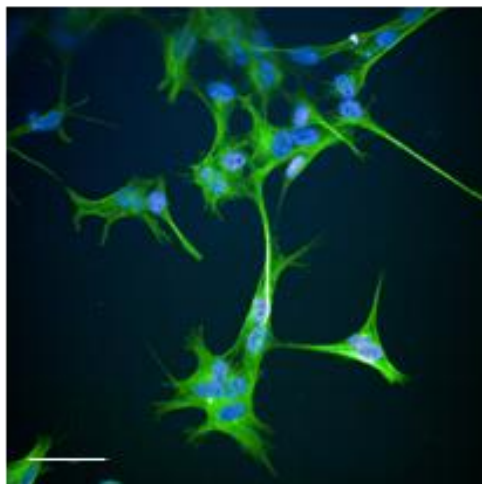
Control 3



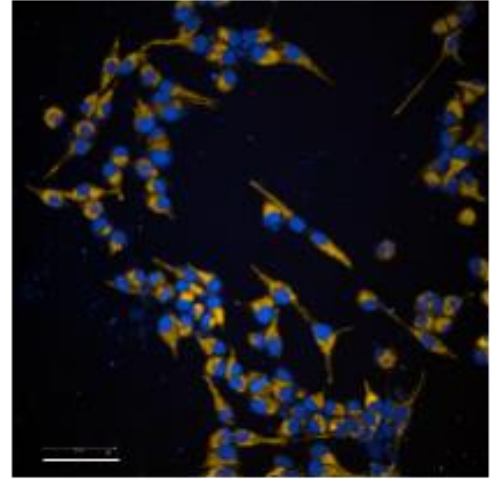
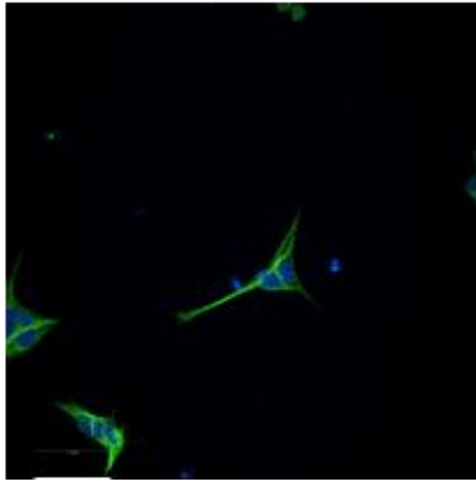
Control 7



Control 10



Control 5



Control 2

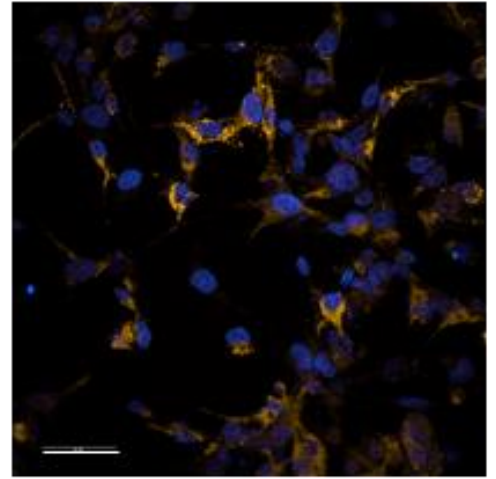
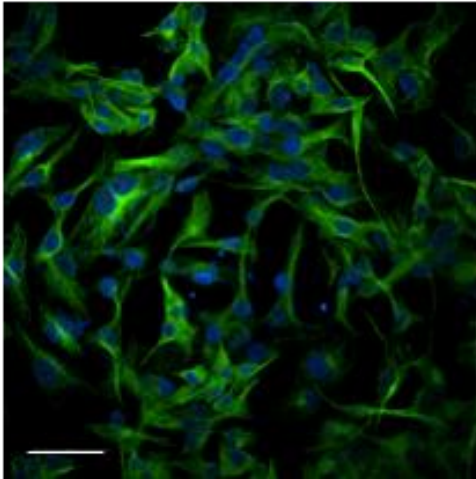
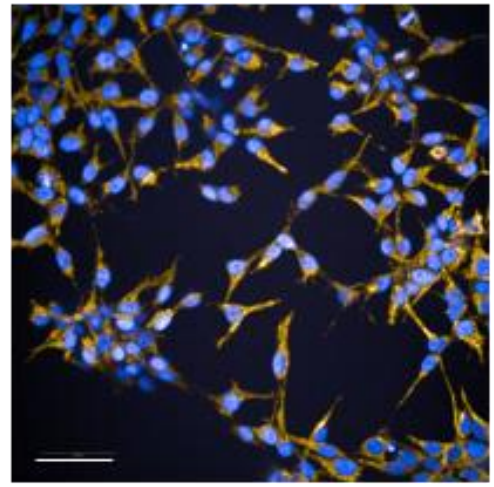
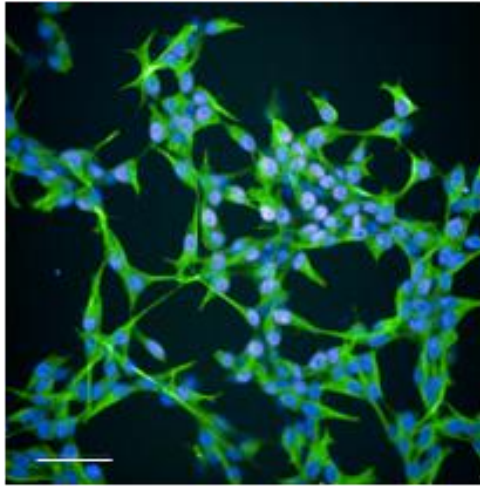


Figure 35: Representative images showing expression of neuronal markers in five control iNeurons lines. TUJ is shown in green, MAP2 shown in red, and Hoechst in blue. Scale bar = 50 μ M.

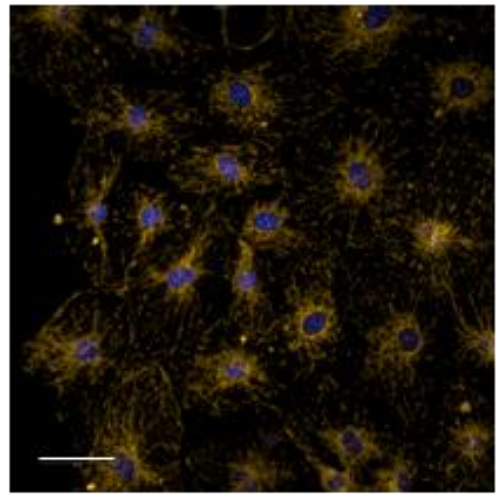
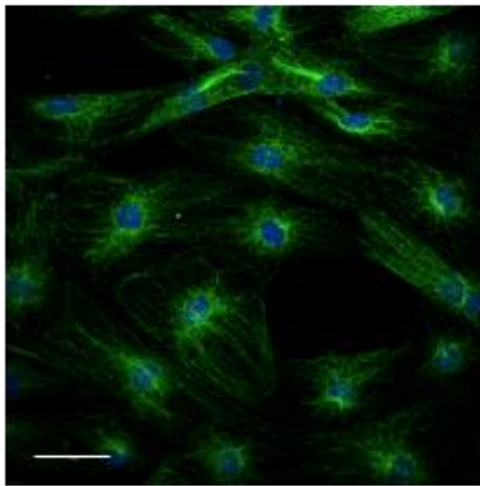
TUJ/Hoechst

MAP2/Hoechst

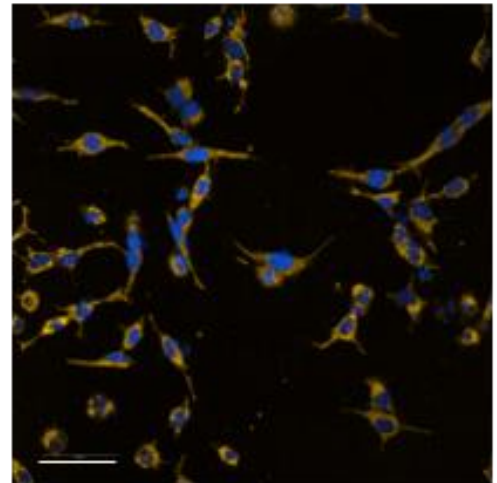
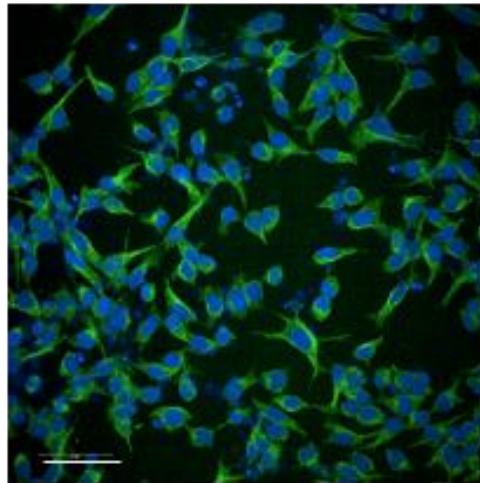
sAD 5



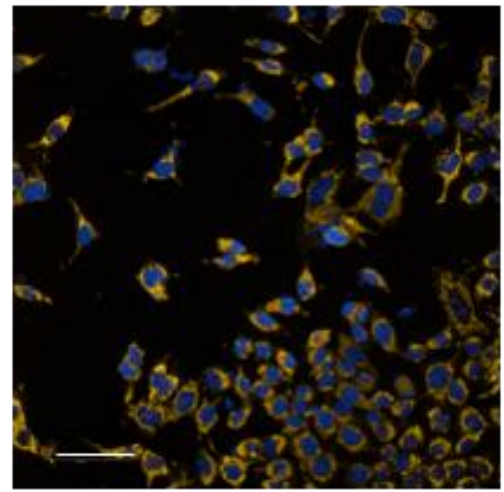
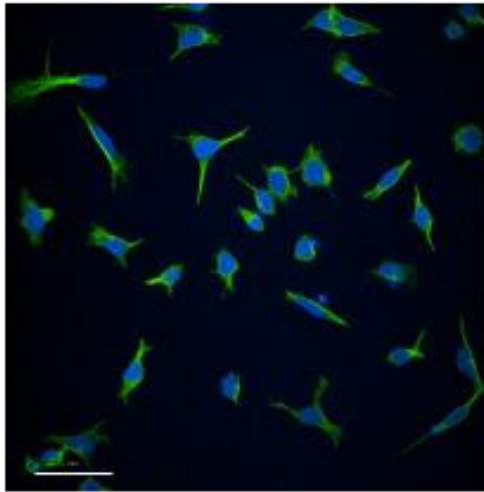
sAD 4



sAD 9



sAD 6



sAD 8

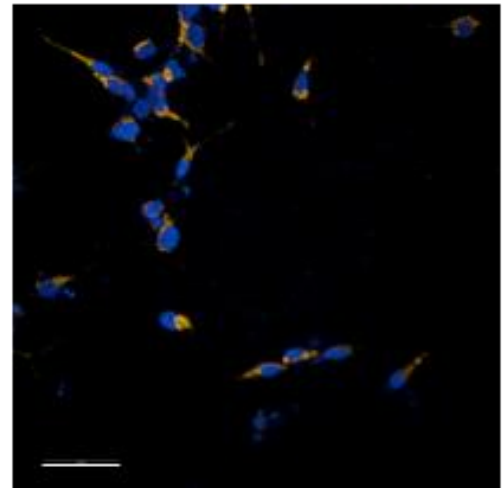
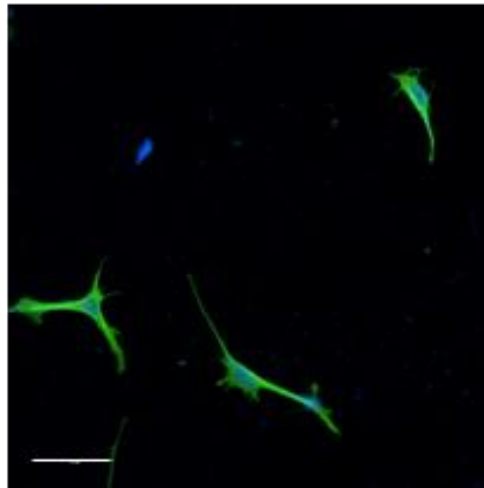


Figure 36: Representative images showing expression of neuronal markers in five sAD iNeurons lines. TUJ is shown in green, MAP2 shown in red, and Hoechst in blue. Scale bar = 50 μ M.

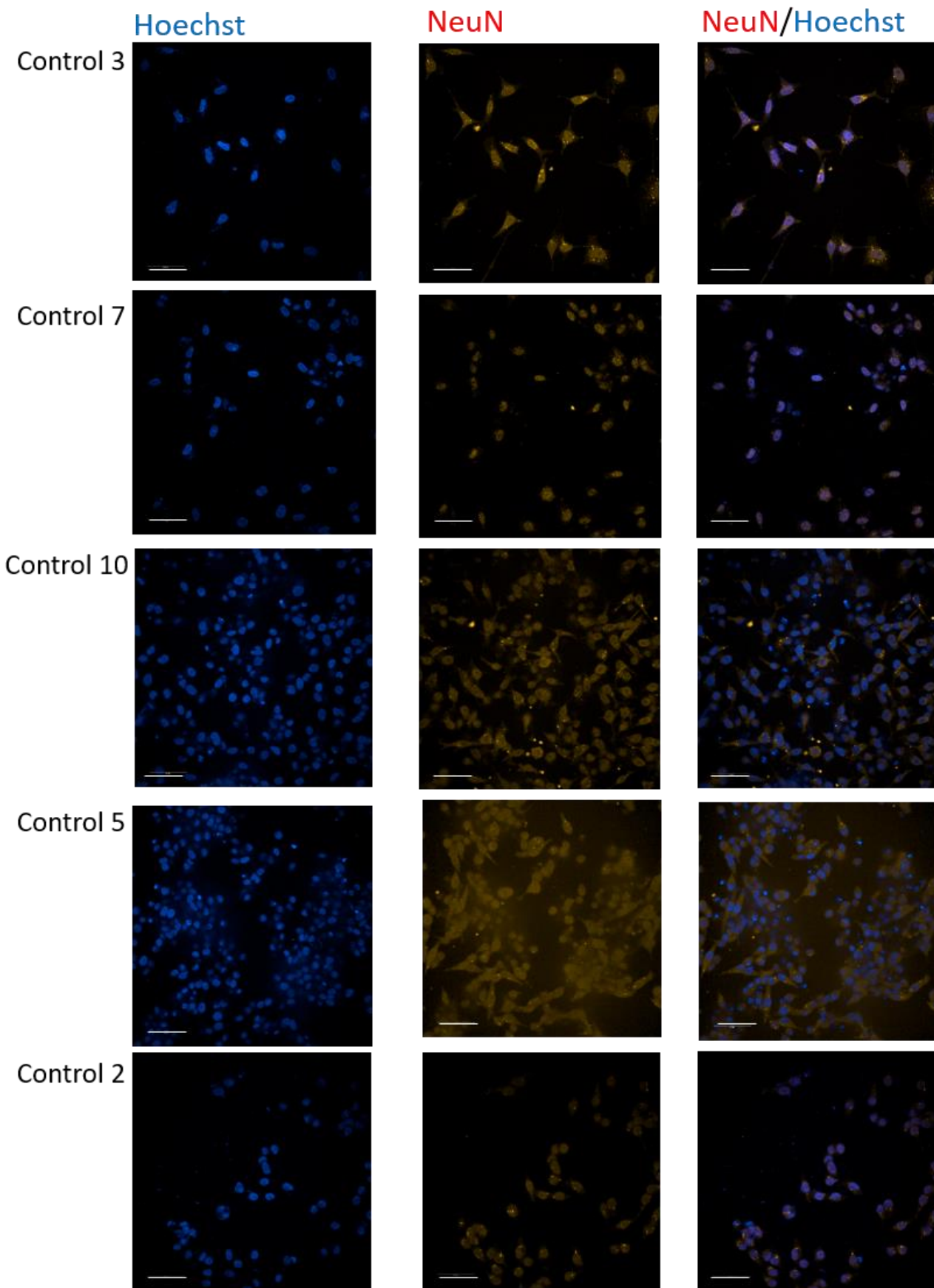


Figure 37: Representative images showing expression of NeuN neuronal marker in five control iNeurons lines. NeuN is localised to the nucleus, and shown in red whilst Hoechst is shown in blue. Scale bar = 50µM.

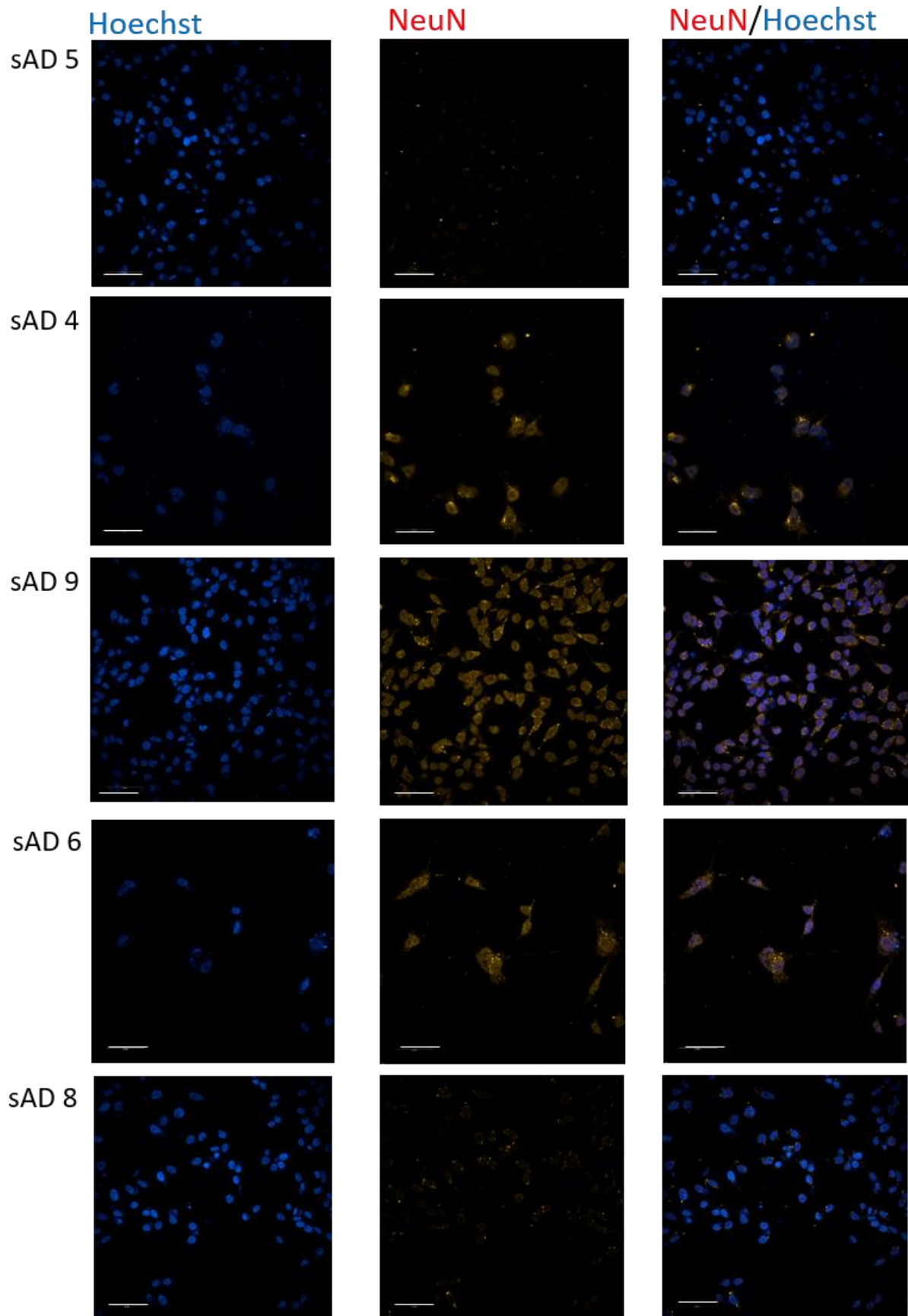


Figure 38: Representative images showing expression of NeuN neuronal markers in five sAD iNeurons lines. NeuN is localised to the nucleus, and shown in red whilst Hoechst is shown in blue. Scale bar = 50 μ M.

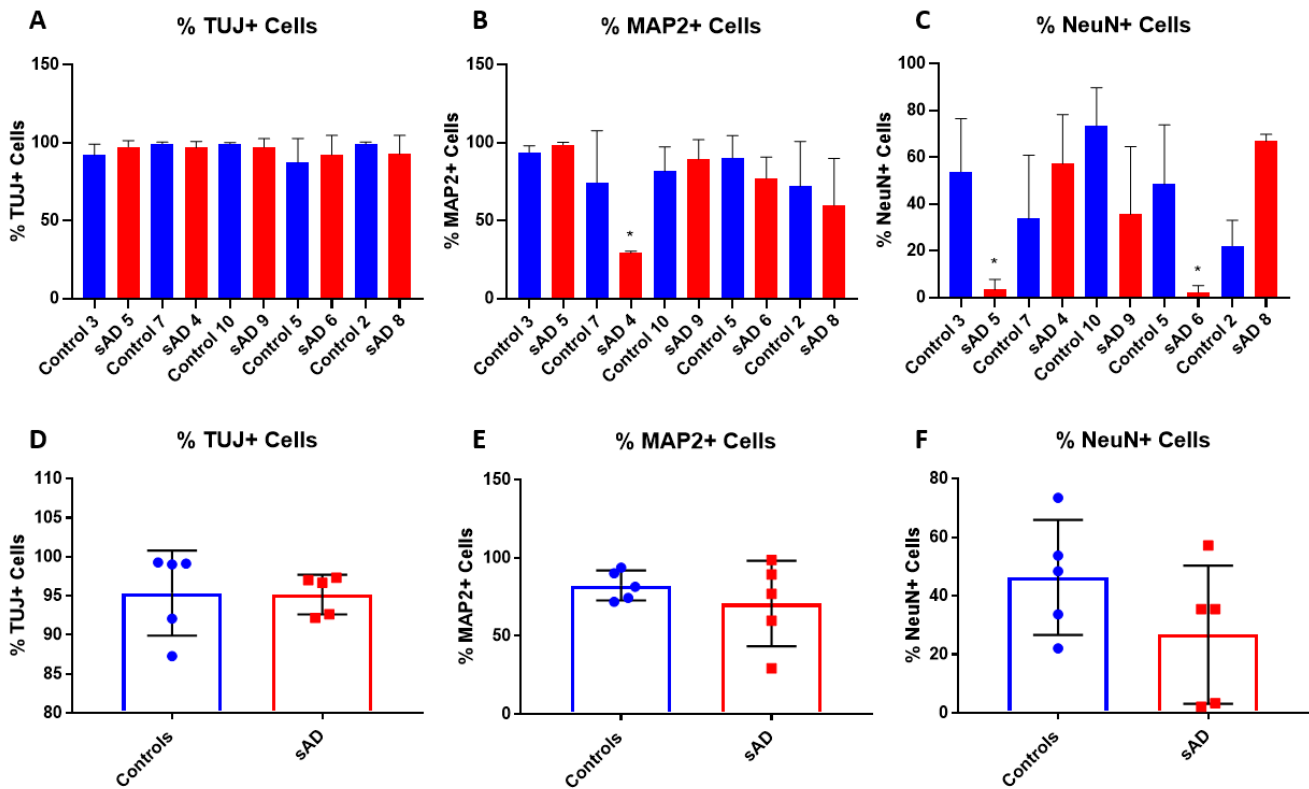


Figure 39: All lines have above 87% TUJ positive cells, all with the exception of sAD 4 have above 60% MAP2 positive cells, and all with the exception of sAD 5 and sAD 6 have between 20% and 75% NeuN positive staining, $n > 3$. There are no significant differences between control and sAD lines at a group level. Each bar represents the mean, each dot represents the mean of all repeats in each line, error bars show SD. A) All lines show above 87% TUJ positive cells. B) Most lines show above 60% MAP2 positive cells, except for sAD 4 which shows 29.3% (* $p < 0.05$; One way ANOVA with Sidak's multiple comparisons). C) Most lines show between 20% and 75% NeuN positive cells, except for sAD 5 which shows 3.4%, and sAD 6 which shows 2.2% (* $p < 0.05$; One way ANOVA with Sidak's multiple comparisons). D) There is no significant difference in the percentage of TUJ positive cells between control and sAD lines at a group level ($p = 0.945$; t test). E) There is no significant difference in the percentage of MAP2 positive cells between control and sAD lines at a group level ($p = 0.401$; t test). F) There is no significant difference in the percentage of NeuN positive cells between control and sAD lines at a group level ($p = 0.193$; t test).

Expression of TUJ and NeuN was also confirmed by western blot. This was carried out in four controls, control 3, control 7, control 10, and control 5, and four sAD lines, sAD 5, sAD 4, sAD 9, and sAD 8. All lines showed expression of TUJ, and again, no difference was seen between control and sAD lines (controls 1.03 ± 0.18 , sAD 0.87 ± 0.25 ; $p = 0.425$; figure 40). TUJ expression in iNeurons was also compared to expression in iNPCs in a subset of the lines. An increase was seen in all four iNeuron lines compared to the same iNPC line, however, a smaller increase was seen in the sAD lines compared to controls (control 7 iNPC 1 iNeuron 3.2 ± 2.3 ; control 10 iNPC 1 iNeuron 2.9 ± 2.5 ; sAD 5 iNPC 1 iNeuron 1.5 ± 0.6 ; sAD 9 iNPC 1 iNeuron 1.3 ± 0.7 ; figure 41).

NeuN expression was also seen in all lines, though there was lower expression in sAD 5 (0.42 ± 0.27 ; figure 42b), and control 5 (0.27 ± 0.17 ; figure 42b). Whilst lower expression in sAD 5 is to be expected, due to the reduced percentage of NeuN positive cells, control 5 showed 48.4% of NeuN positive cells. It may be that in control 5, even though there is a higher percentage of NeuN positive cells, the amount of NeuN per cell is lower. sAD 8 shows an increased expression (2.96; figure 42b) of NeuN, though this is only from one repeat. It is important to note that NeuN positive cells were only counted if the NeuN was correctly localised to the nucleus, whereas the western blot takes into account expression in the whole cell. There was no significant difference seen in NeuN expression between control and sAD cells at a group level (controls 1.02 ± 0.5 , sAD 1.4 ± 1.1 ; $p = 0.574$; figure 42c). NeuN expression in iNeurons was also compared to expression in iNPCs in a subset of lines. Though this was only carried out in one repeat, there is an increase seen in all iNeuron lines compared to the same iNPC lines (control 7 iNPC 1 iNeuron 1.6; control 10 iNPC 1 iNeuron 1.4; sAD 5 iNPC 1 iNeuron 1.4; sAD 9 iNPC 1 iNeuron 1.3; figure 43).

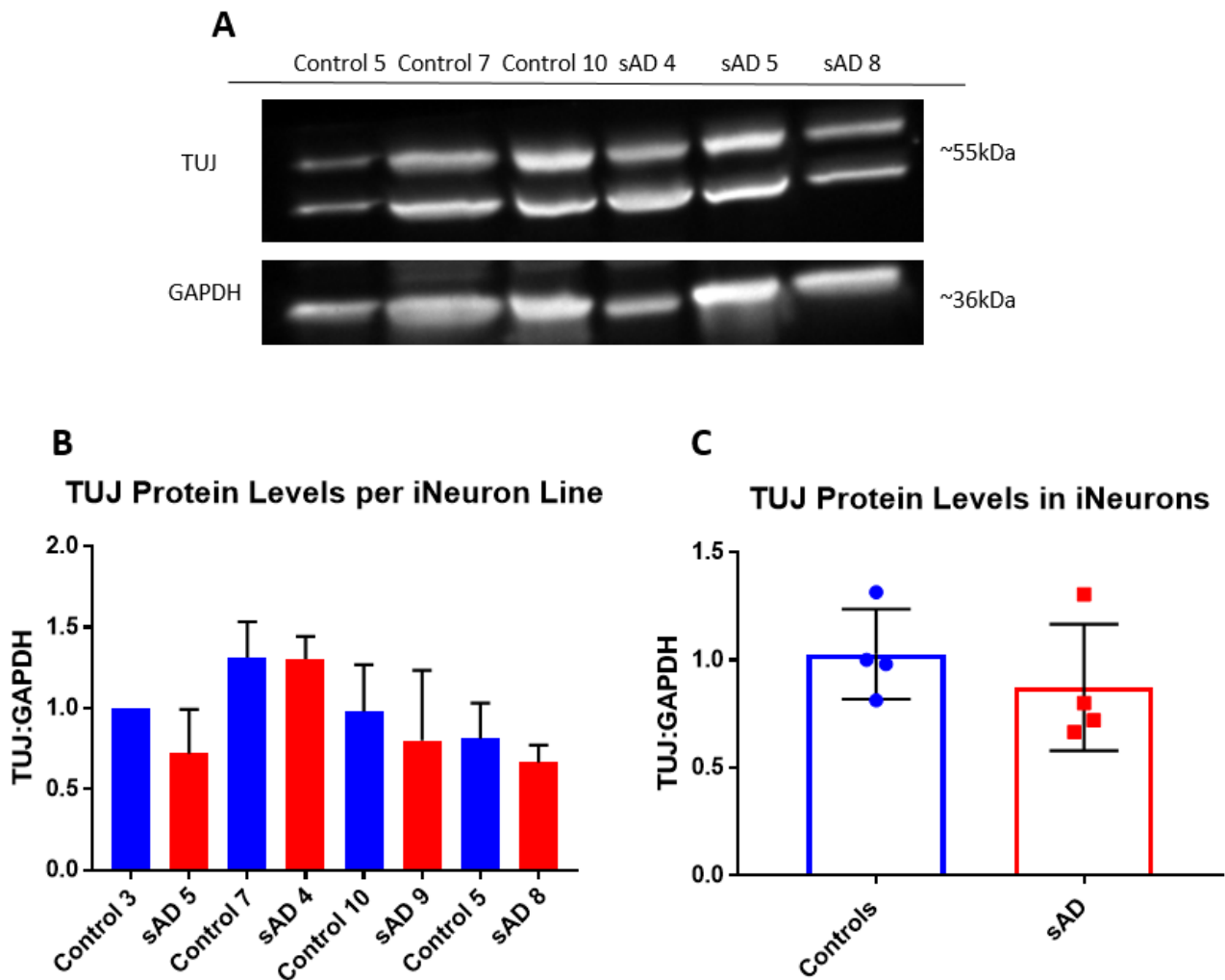


Figure 40: There is no significant difference in TUJ protein levels between control and sAD iNeurons, at an individual or group level. A) Representative blot of TUJ and GAPDH loading control in controls 5, 7, and 10, and sAD 4, 5, and 8. TUJ is double banded, as seen in (Shi et al., 2021), and ran at the expected molecular weight of approximately 55kDa. 10 μ g protein was loaded per lane. B) Quantification of TUJ protein levels in four control and sAD lines. Each line was assessed from samples from three separate differentiations. No significant difference is seen in any line. Bars shown represent the mean and error bars represent SD. C) There is no significant difference when the sAD group is compared to the control group ($p = 0.424$; t test). Each dot represents the mean of three replicates per line, the bar represents the group mean, and the error bars show SD.

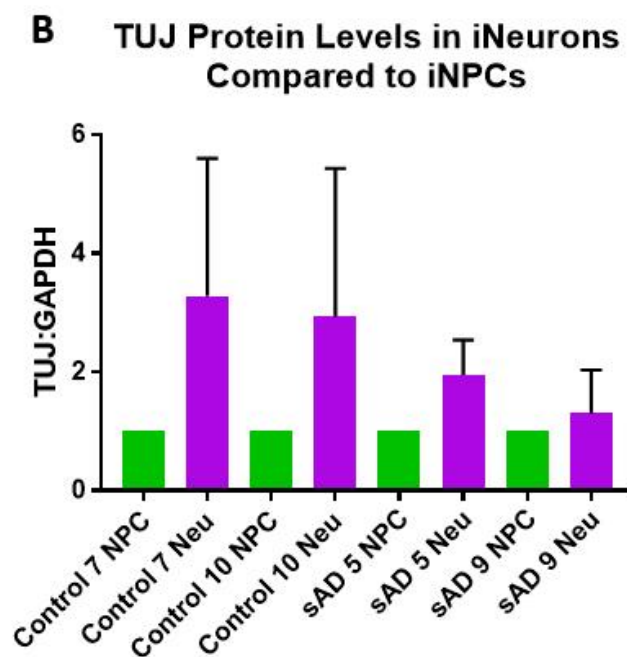
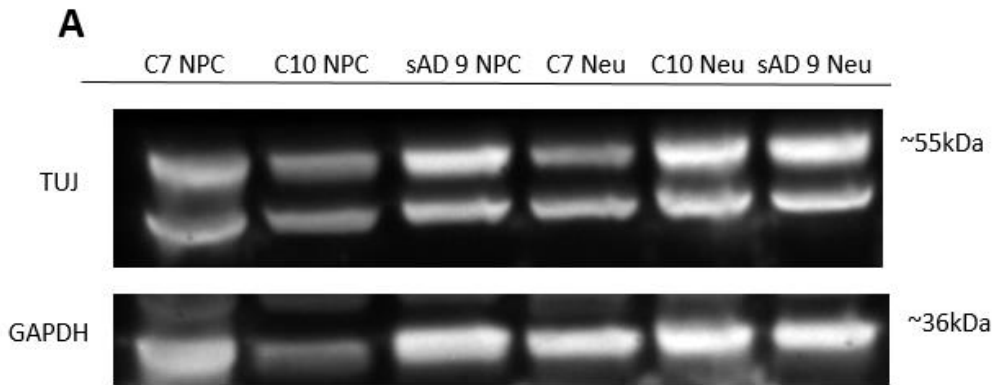


Figure 41: There is an increase in TUJ protein expression in iNeurons compared to iNPCs in each line. A) Representative blot of TUJ and GAPDH loading control in control 7, 10, and sAD 9 iNPCs and iNeurons. TUJ is expected to be double banded and ran at the expected molecular weight of 55kDa. 10 μ g protein was loaded per lane. **B)** Quantification of TUJ protein expression in four control and four sAD iNPC and iNeuron lines. There is an increase in iNeurons in every line, with a greater increase in controls than sAD lines. Each bar represents the mean of two samples from two separate differentiations. iNeuron repeats were normalised to iNPC repeats per line.

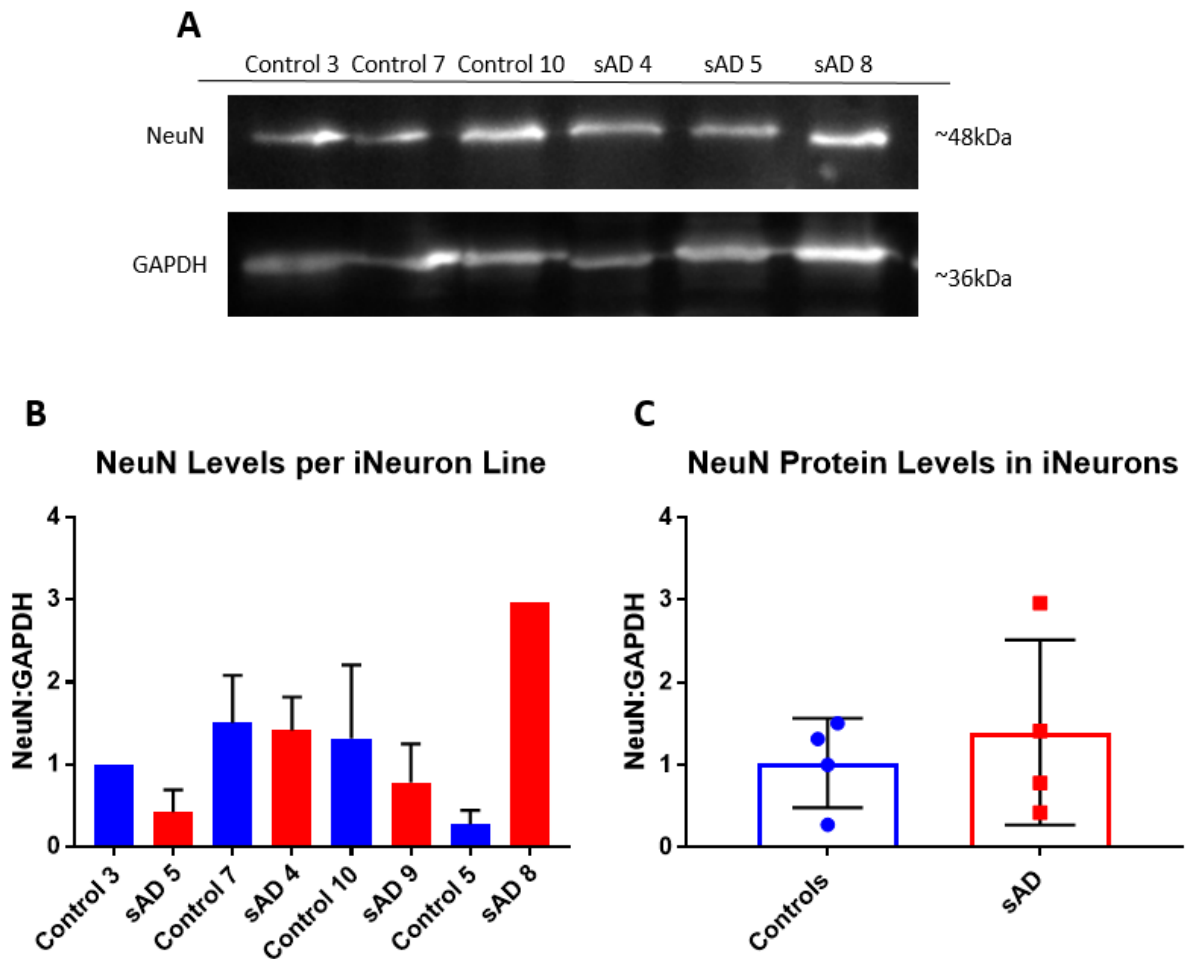


Figure 42: There is no significant difference in NeuN protein levels between control and sAD iNeurons, at an individual or group level. A) Representative blot of NeuN and GAPDH loading control in control 3, 7, 10, and sAD 4, 5, and 8. NeuN ran at the expected molecular weight of 48kDa. 10 μ g protein was loaded per lane. B) Quantification of NeuN protein levels in four control and four sAD lines, with each line assessed from three separate differentiations apart from control 3 and sAD 8 which were assessed from one sample only. No significant difference is seen in any line. Bars represent the mean and error bars represent SD. C) There is no significant difference in NeuN expression at a group level ($p = 0.574$; t test). Each dot represents the mean of the replicates per line, the bar represents the group mean, and the error bars show SD.

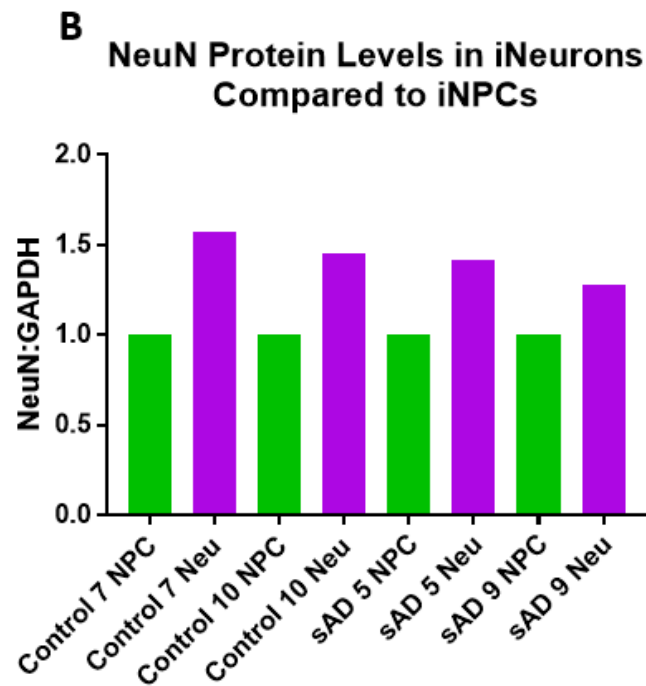
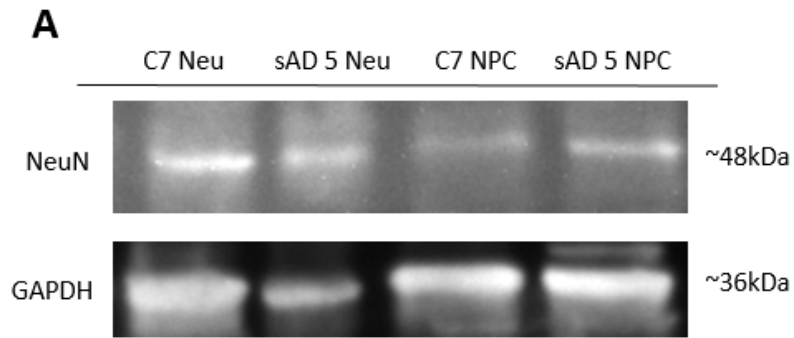


Figure 43: There is an increase in NeuN protein expression in iNeurons compared to iNPCs in each line. A) Representative blot of NeuN and GAPDH loading control in control 7 and sAD 5 iNPCs and iNeurons. 10 μ g protein was loaded per line. B) Quantification of NeuN protein expression in four control and four sAD iNPC and iNeuron lines. There is an increase in every iNeuron line. Each bar represents a single repeat, iNeuron data was normalised to iNPC data for each line.

To better characterise the general iNeuron population, three control and three sAD iNeuron lines were also assessed for neuronal markers for more specific populations across three separate differentiations. These included homeobox 9 (Hb9), a nuclear marker of motor neurons, choline acetyltransferase (ChAT), a marker of cholinergic neurons found throughout the cell body and processes, vGlut1, a marker of glutamatergic neurons found in the cell bodies and processes, and TBR1, a nuclear marker of early cortical neurons. Primary and secondary only controls were included to ensure that staining seen was not due to non-specific background staining. Representative images of specific neuronal marker expression are shown in figures 62-67. There was a clear difference in expression of these markers seen between different rounds of differentiation (figure 50), and representative images are taken from some differentiations with positive marker expression, and some which had no positive marker expression. When the potential reasons for this heterogeneity were explored, no obvious link was seen with iNPC passage or batch, cell number, or cell viability.

Hb9 expression varied between 0% and 26.4% in controls (control 3 0 – 19.2%, control 7 0 – 1.7%, control 10 0 – 26.4%; figure 50a), and between 0% and 11.7% in sAD lines, though in the majority of differentiation rounds, less than 1% of sAD cells expressed Hb9 (sAD 5 0 – 0.15%, sAD 4 0 – 0.9%, sAD 9 0 – 11.2%; figure 50a). ChAT expression was below 3% in all control (control 3 0%, control 7 0 – 0.4%, control 10 0 – 2.4%; figure 50b) and sAD (sAD 5 0 – 0.15%, sAD 4 0 – 0.12%, sAD 9 0 – 0.2%; figure 50b) lines. vGlut1 expression showed some of the highest levels of expression, but was also still very variable between different differentiations. Expression in the control lines ranged between 0% and 41.5% (control 3 0 – 33.7%, control 7 0 – 41.5%, control 10 0 – 26.4%; figure 50c), and sAD lines between 0 and 35.5% (sAD 5 0.2 – 0.6%, sAD 4 0 – 35.5%, sAD 9 0 – 11.7%; figure 50c). TBR1 expression in the nucleus varied between 0% and 50% in controls (control 3 0 – 50%, control 7 0 – 21.6%, control 10 0 – 25%; figure 50d), but was below 4% in all sAD lines (sAD 5 0.2 – 3.5%, sAD 4 0 – 0.5%, sAD 9 0 – 3.2%; figure 50d).

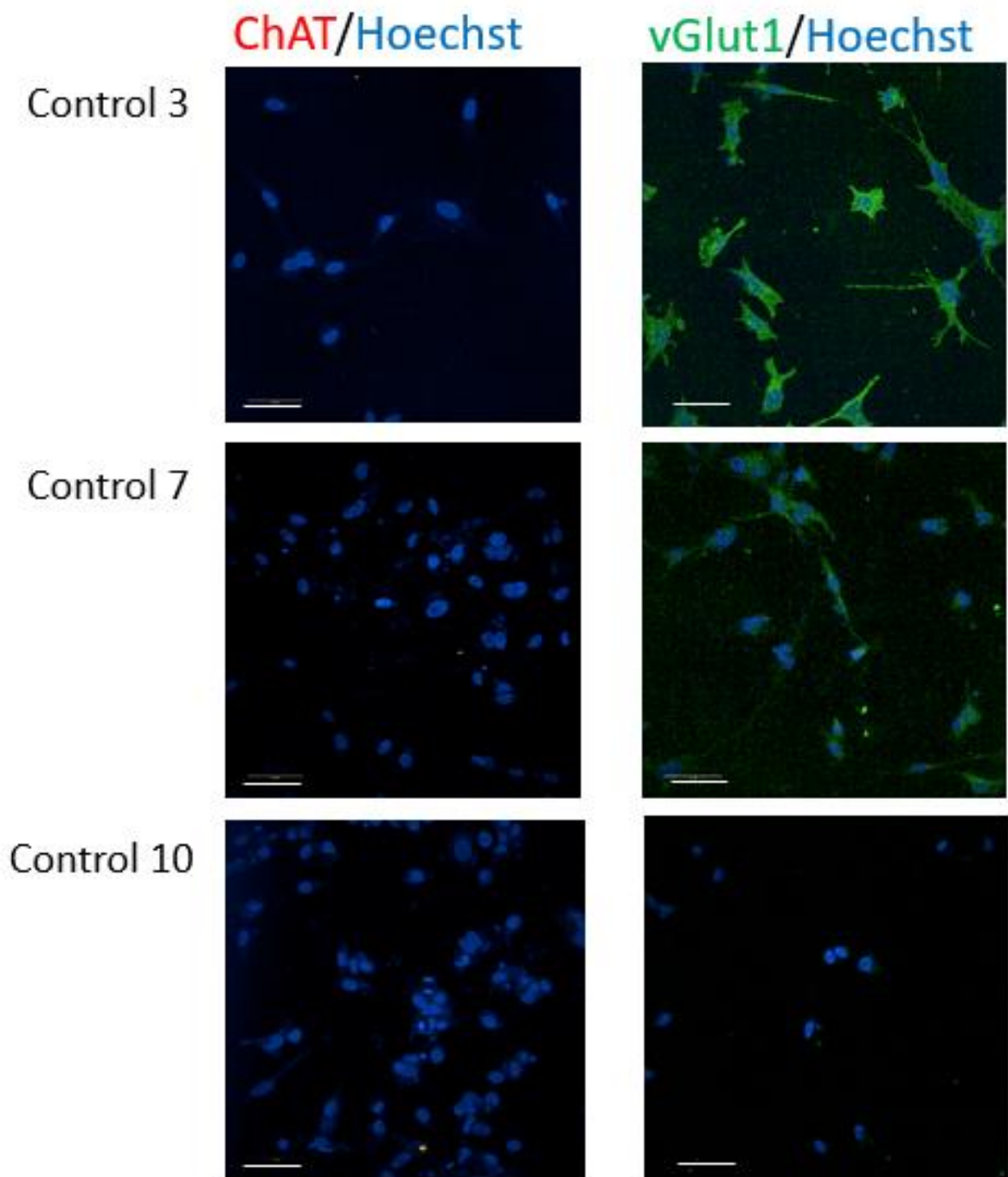


Figure 44: Representative images of ChAT, and vGlut1 staining in three control iNeuron lines. vGlut1 is shown in green, and positive staining is seen in control 3 and control 7, and no positive staining is seen in control 10. ChAT is shown in red, and no positive staining is seen in any control line. Hoechst staining for the nuclei is shown in blue. Scale bar = 50 μ M.

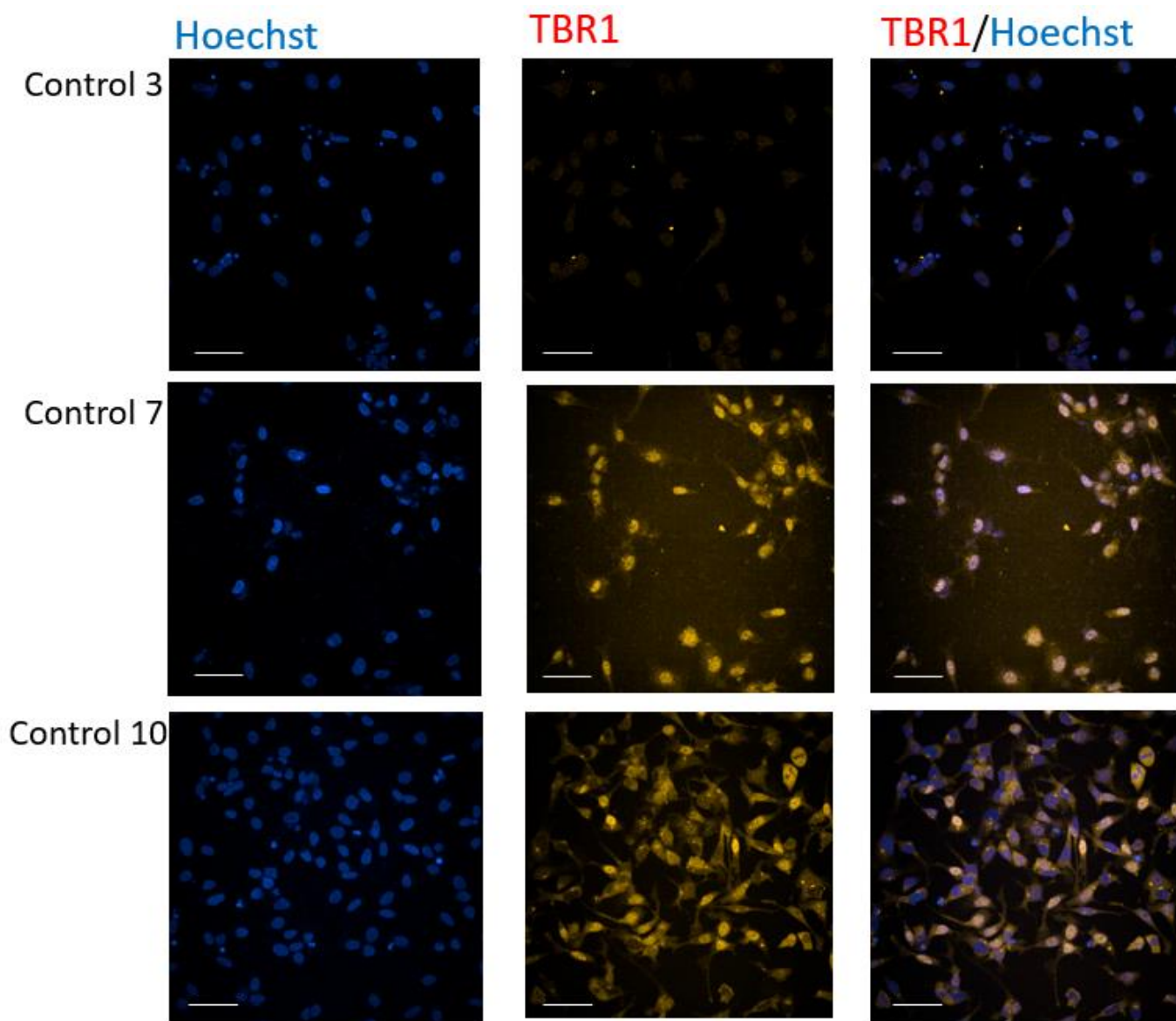


Figure 45: Representative images of TBR1 staining in three control iNeuron lines. TBR1 is shown in red, and positive staining in the nucleus is seen in control 7 and control 10. No positive staining is seen in control 3. Hoechst staining for the nuclei is shown in blue. Scale bar = 50 μ M.

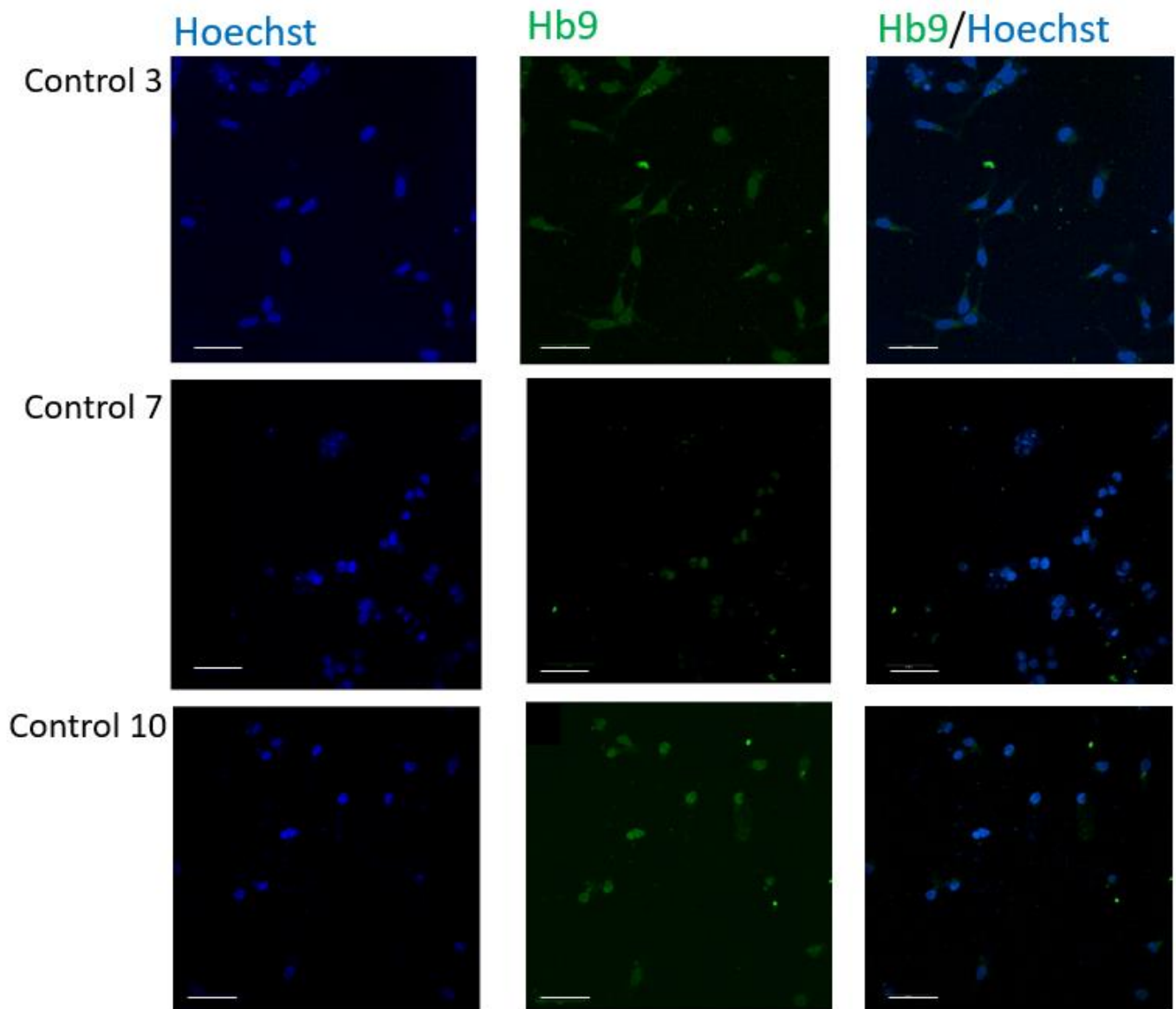


Figure 46: Representative images of Hb9 staining in three control iNeuron lines. Hb9 is shown in green, and positive nuclear staining is seen in control 3 and control 10. No staining which meets the positive threshold is seen in control 7. Hoechst staining for the nuclei is shown in blue. Scale bar = 50 μ M.

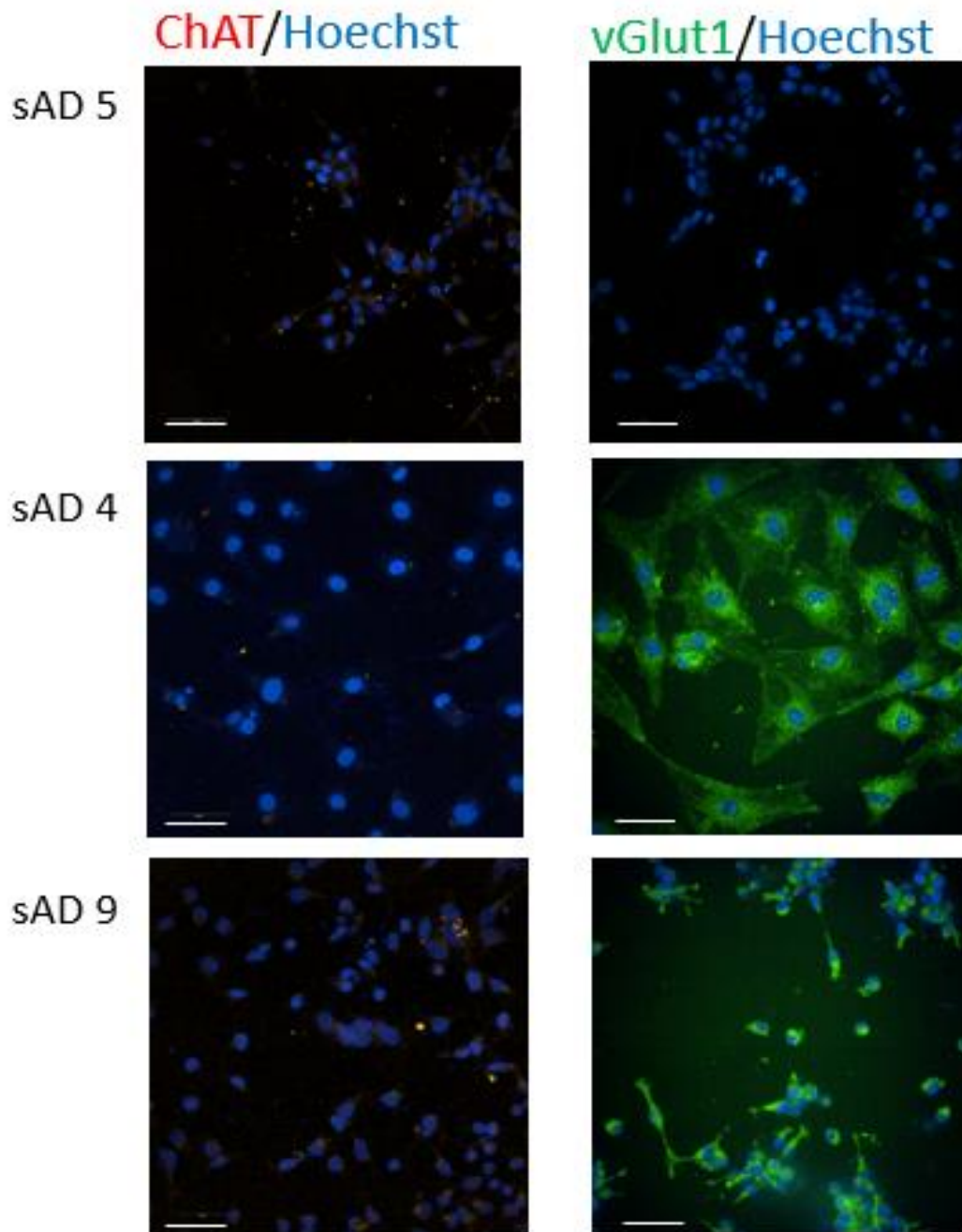


Figure47: Representative images of ChAT and vGlut1 staining in three sAD iNeuron lines. vGlut1 is shown in green, positive staining is seen in sAD 4 and sAD 9, but not in sAD 5. ChAT is shown in red, and no staining which meets the positive threshold is seen in any line. Hoechst staining for the nuclei is shown in blue. Scale bar = 50 μ M.

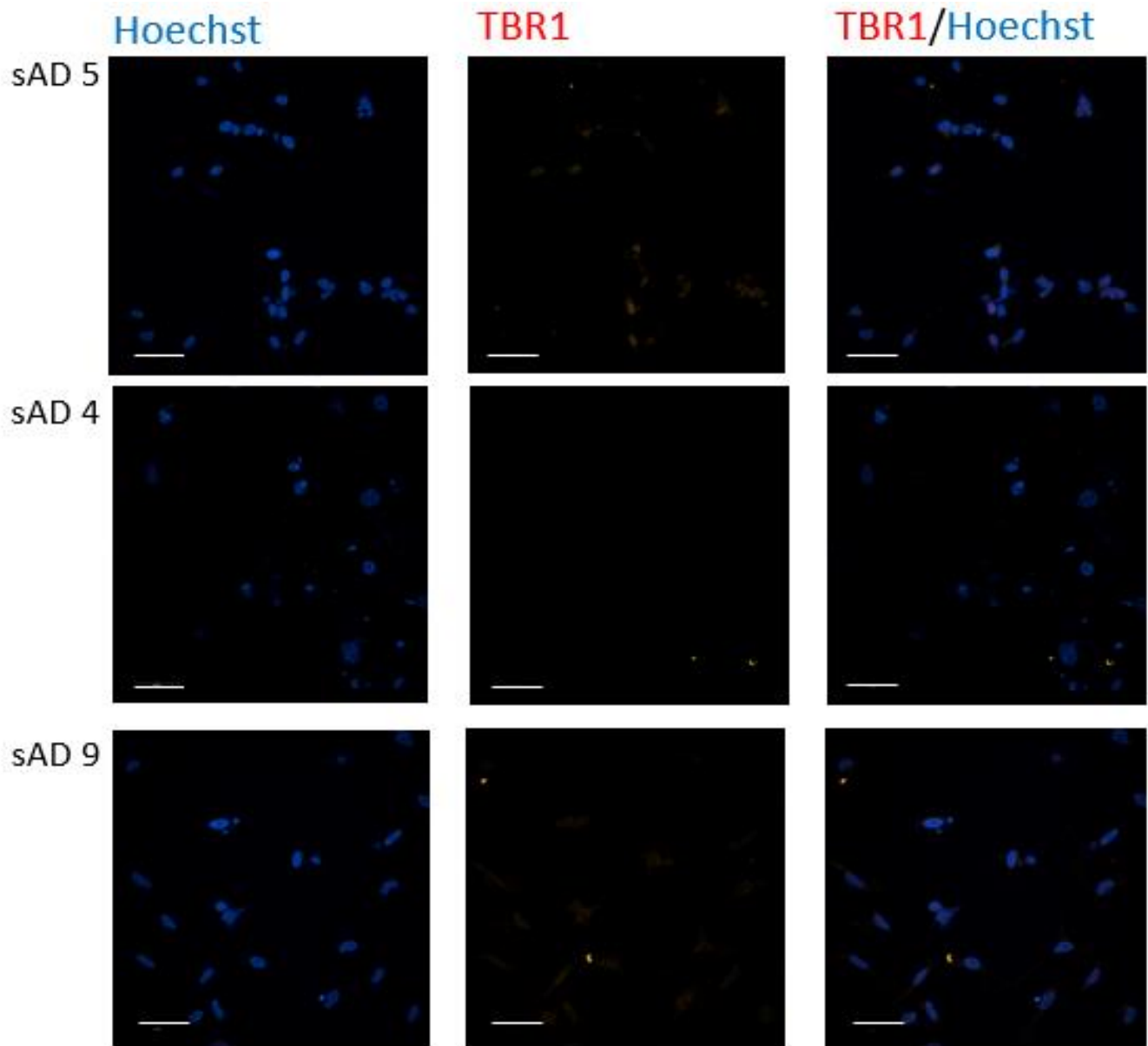


Figure48: Representative images of TBR1 staining in three sAD iNeuron lines. TBR1 is shown in red, and no line shows staining which meets the threshold for positive expression. Hoechst staining for the nuclei is shown in blue. Scale bar = 50 μ M.

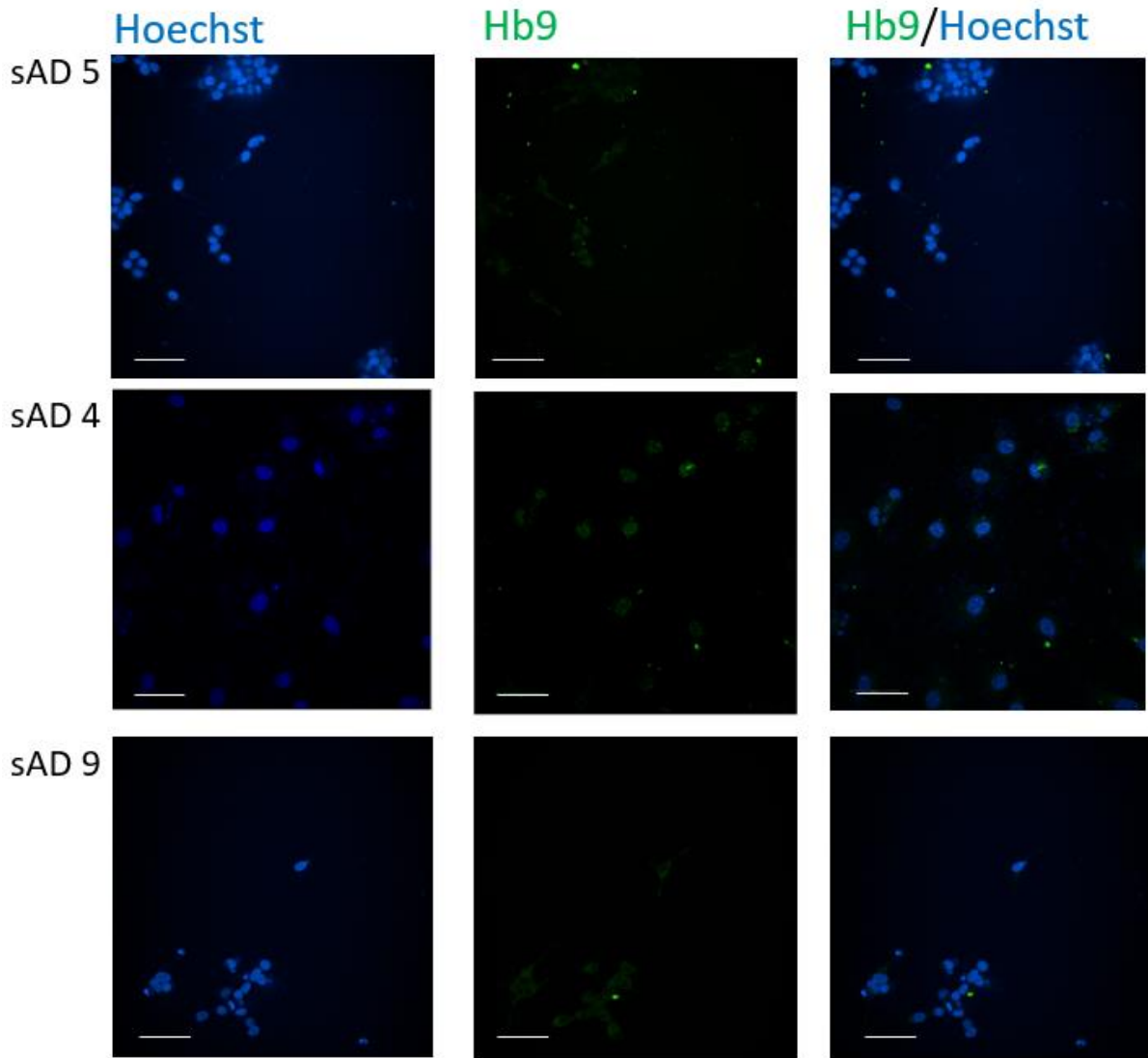


Figure49: Representative images of Hb9 staining in three sAD iNeuron lines. Hb9 is shown in green, and no staining in any line meets the positive threshold. Hoechst staining for the nuclei is shown in blue, scale bar = 50 μ M.

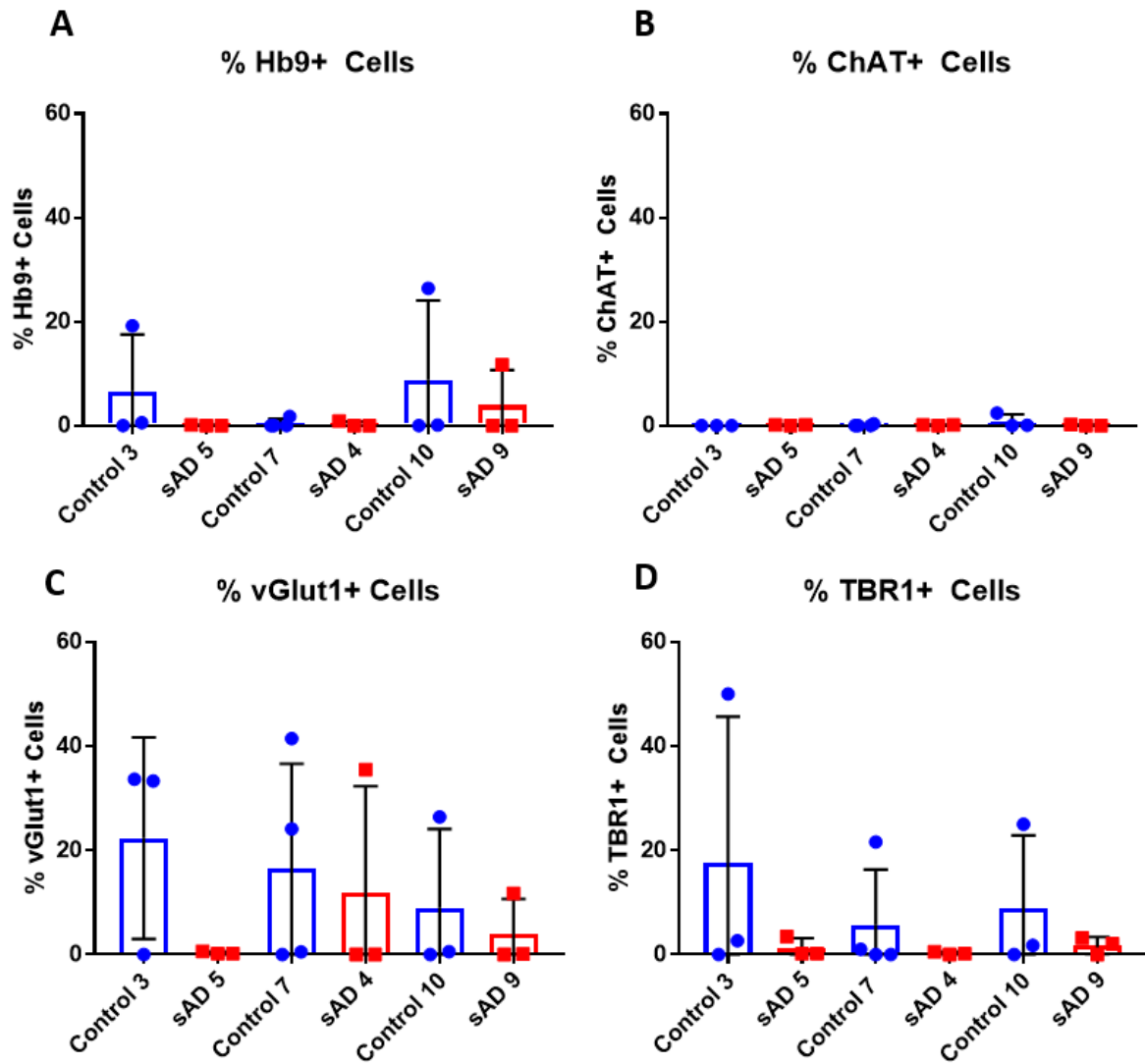


Figure50: There is variability in the expression of motor neuron marker Hb9, cholinergic neuron marker ChAT, glutamatergic neuron marker vGlut1, and early cortical neuron marker TBR1 in control and sAD *iNeuron* lines, $n > 3$. Each dot represents expression in a separate differentiation, the bar represents the mean, and error bars represent SD. A) Hb9 expression varied between 0% and 26.4% in control lines, and 0% and 11.7% in sAD lines. B) ChAT expression was below 3% in all control and sAD lines. C) vGlut1 expression varied between 0% and 41.5% in controls and 0% and 35.5% in sAD lines. D) TBR1 expression varied between 0% and 50% in control lines, but was below 4% in all sAD lines.

4.2.2 Neuronal Morphology and Viability in Control and sAD iNeurons Under Basal Conditions

Neuronal morphology and viability was assessed under basal conditions using the neurite outgrowth assay kit; representative images of control 10 and sAD 5 are shown in figure 51, where the red stain shows the membrane stain and the green shows the viability stain. There was no difference seen between paired control and sAD neuron lines in several morphology parameters assessed including cell roundness (figure 52a), cell width to length ratio (figure 52b), and neuron score, a ratio of cells showing neuronal morphology compared to those which do not (figure 52c). The neuron score in particular showed a large amount of variability between different technical repeats, though an increase was seen in sAD 5 compared to control 3 ($p = 0.453$), and a decrease seen in sAD 8 compared to control 2 (figure 52c). There was also no difference seen overall when control and sAD lines were combined, in cell roundness ($p = 0.4807$; figure 52d), cell width to length ratio ($p = 0.4819$; figure 52e), and neuron score ($p = 0.6838$; figure 52f).

However, there was a significant difference seen in three of four paired lines in the cell area. sAD 5 was significantly reduced compared to control 3 (control 3 0.925 ± 0.148 , sAD 5 0.446 ± 0.104 ; $p = 0.0023$; figure 53a), and sAD 6 was also significantly reduced compared to control 5 (control 5 1.09 ± 0.186 , sAD 6 0.664 ± 0.116 ; $p = 0.0076$; figure 53a), whilst a decrease was seen between control 10 and sAD 9 (control 10 1 ± 0 , sAD 9 0.711 ± 0.181 ; $p = 0.132$; figure 53a) and between control 2 and sAD 8 (control 2 1 ± 0 , sAD 8 0.740 ± 0.228 ; $p = 0.315$; figure 53a). In contrast, sAD 4 was significantly increased compared to control 7 (control 7 0.92 ± 0.35 , sAD 4 1.39 ± 0.196 ; $p = 0.011$; figure 53a). When control and sAD lines were combined, there was no significant difference in cell area overall (controls 0.987 ± 0.069 , sAD 0.790 ± 0.354 ; $p = 0.258$; figure 53b). However, when sAD 4 was excluded as an obvious outlier, a significant difference was seen (controls 0.987 ± 0.069 , sAD 0.64 ± 0.133 ; $p = 0.0014$; figure 53c). This difference in cell area can also be seen in the representative images shown in figure 51. In general, there is no difference in the morphology of the cells, with both patient and control cells showing the same elongation and processes, but the patient cells, with the exception of sAD 4, are smaller than the control cells.

As part of the assay, cell viability was also assessed. No significant difference was seen in the majority of neuron pairs, but there was a significant decrease in viability in sAD 8 compared to control 2 (control 2 $64.2\% \pm 26.0\%$, sAD 8 $17.2\% \pm 7.19\%$; $p = 0.01$; figure 54a). For this reason, it was difficult to get full datasets for sAD 8, as there was often not enough cells to complete assays. There was also a decrease in sAD 6 compared to control 5 (control 5 $59.98\% \pm 19.11\%$, sAD 5 $39.37\% \pm 7.9\%$; $p = 0.405$; figure 54a). When all control and sAD lines were combined, there was no significant

difference in cell viability overall (controls $70.39\% \pm 7.44\%$, sAD $58.36\% \pm 25.73\%$; $p = 0.396$; figure 55b).

Control 10

sAD 5

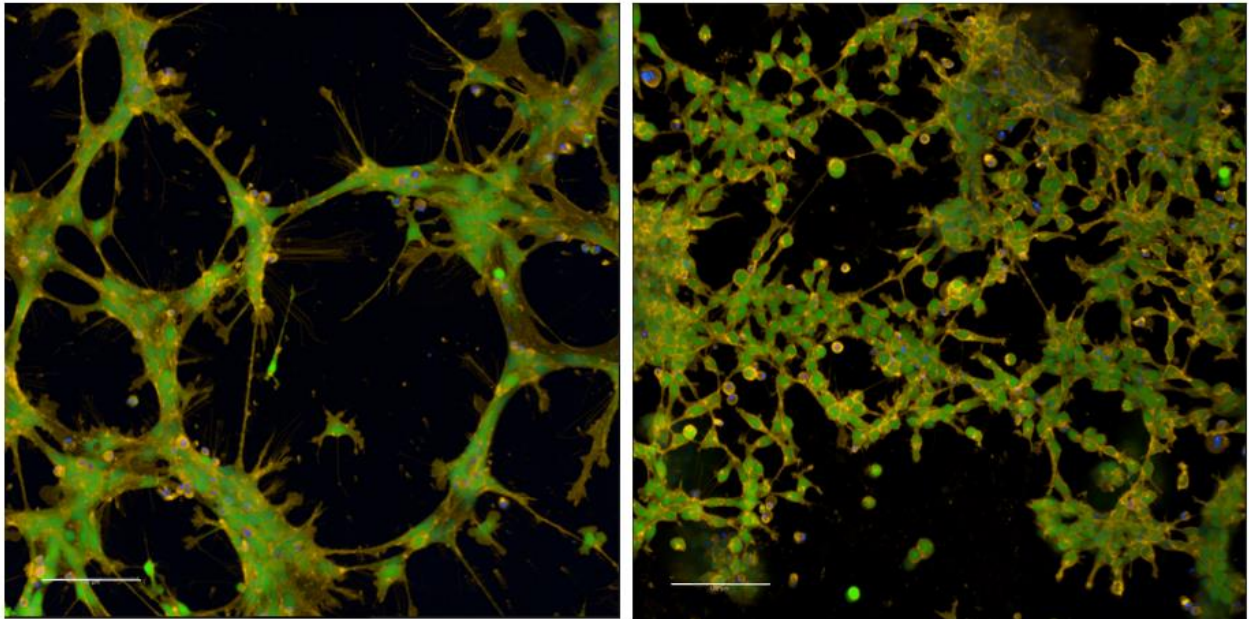


Figure51: Representative images of the neurite outgrowth assay in control 10 and sAD 5, red staining shows the cell membrane stain, green stain shows the cell viability stain, scale bar = 100 μ M. There is a clear difference in the size of the cells, with sAD 5 being much smaller than control 10. There is no difference in any other morphology, with both showing collecting of the cell bodies, and elongated processes.

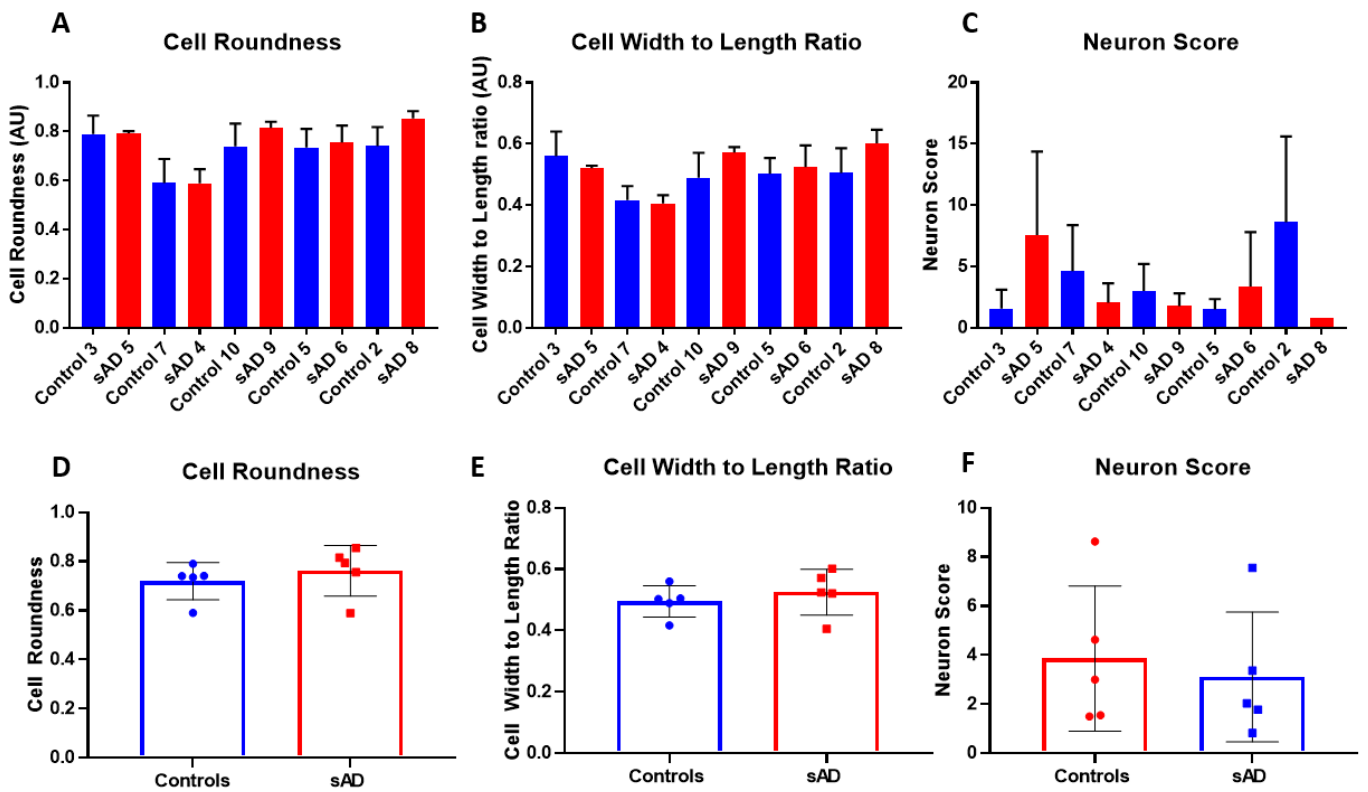


Figure 52: *There is no difference in cell morphology between control and sAD neuron lines, $n > 3$. For D-F, each dot represents the mean of all biological repeats for one cell line. Errors bars represent SD. A) There is no difference in cell roundness between paired control and sAD lines. B) There is no difference in cell width to length ratio between paired control and sAD lines. C) There is no difference in neuron score, a ratio of cells showing neuronal morphology compared to those which do not, between paired control and sAD lines. However, a lot of variation is seen between technical repeats for individual lines. D) There is no significant difference in cell roundness when control and sAD lines are combined ($p = 0.4807$; t test). E) There is no difference in cell width to length ratio when control and sAD lines are combined ($p = 0.4819$; t test). F) There is no difference in neuron score when control and sAD lines are combined ($p = 0.6838$; t test).*

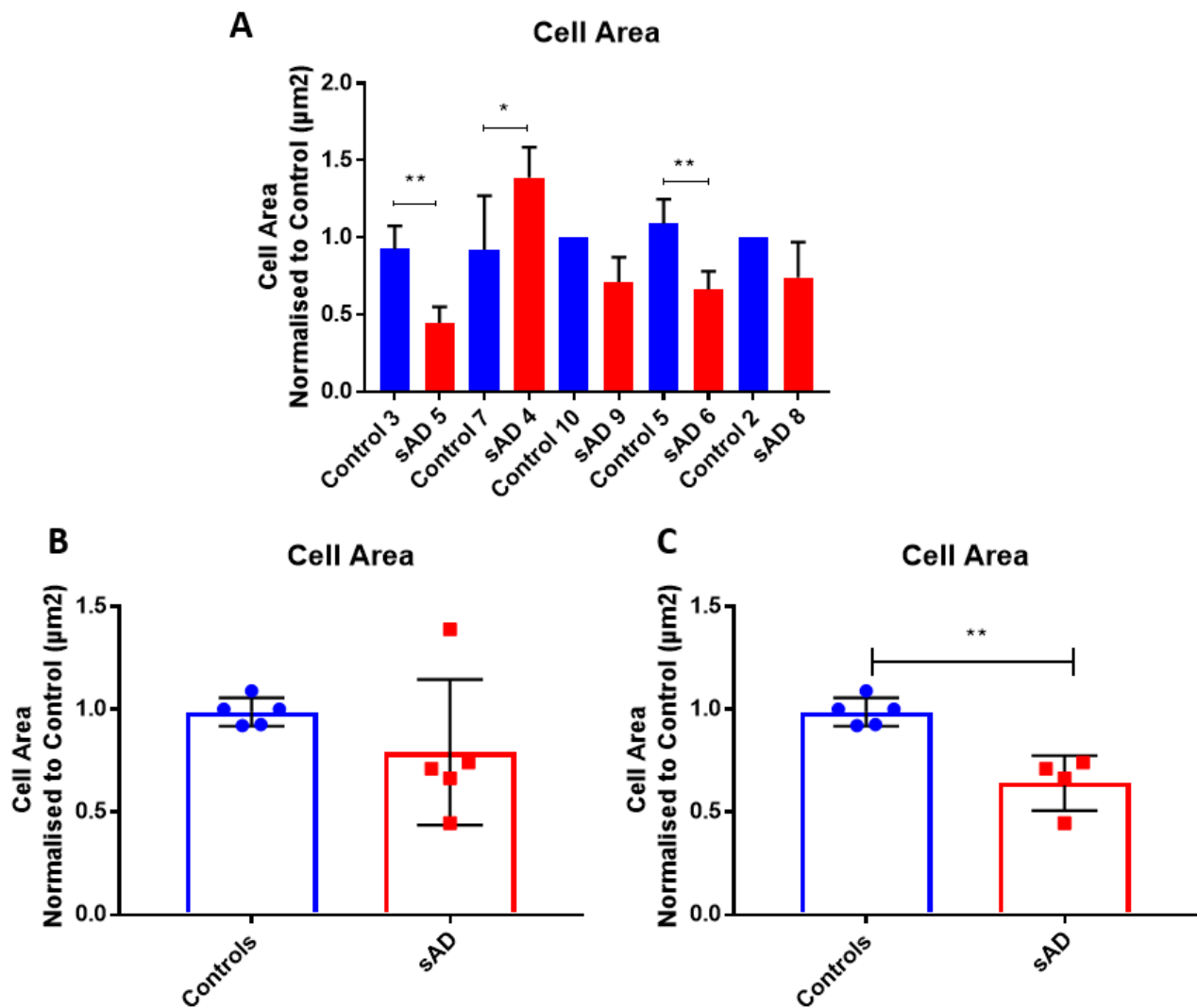


Figure 53: Two sAD neuron lines have a significantly smaller cell area, and one sAD neuron line has a significantly increased area, $n > 3$. For B-C, each dot represents the mean of all biological repeats for one cell line. Errors bars represent SD. A) There is a significant decrease in cell area between control 3 and sAD 5, and control 5 and sAD 6. There is a significant increase in sAD 4 compared to control 7 (* $p < 0.05$, ** $p < 0.01$, *** $p < 0.001$, **** $p < 0.0001$; One way ANOVA with Sidak's multiple comparisons). B) There is no significant difference between controls and sAD when all lines are combined. C) There is a significant decrease in cell area when control and sAD neuron lines are combined, with sAD 4 excluded due to being an outlier (** $p < 0.01$, t test).

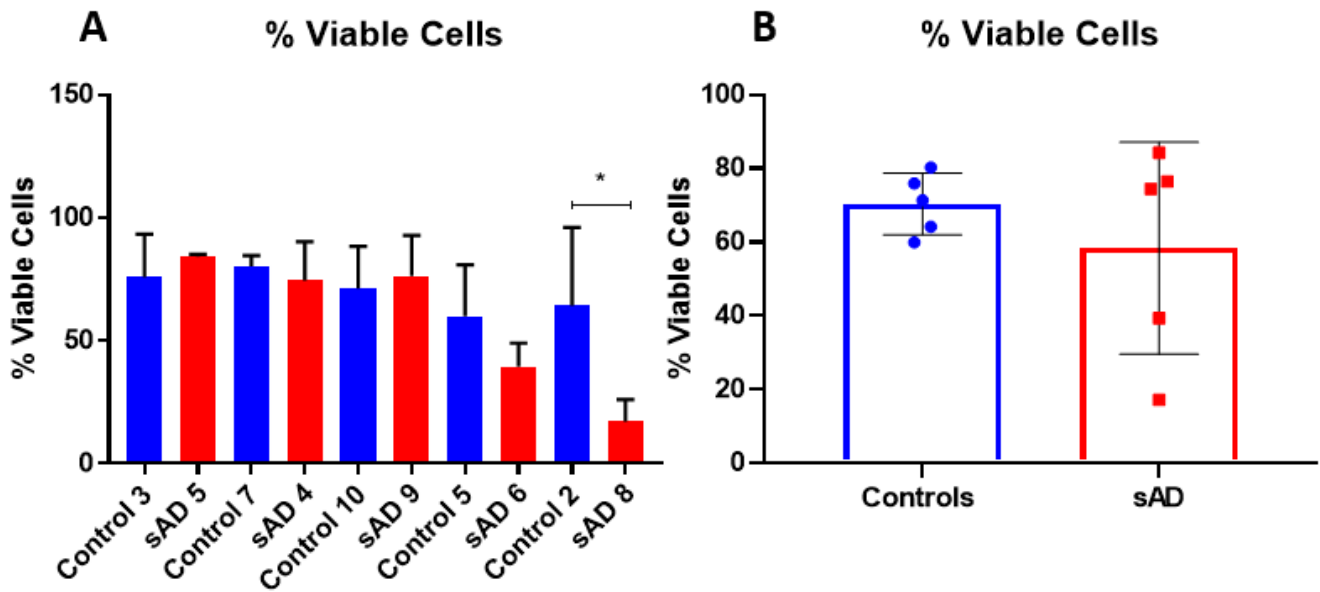


Figure 54: sAD 8 has a significantly reduced viability compared to control 2, but there is no significant difference in any other pair, $n > 3$. Errors bars represent SD. A) There is a significant decrease in cell viability in sAD 8 compared to control 2, but no significant difference in any other pair ($* p < 0.05$; One way ANOVA with Sidak's multiple comparisons). B) There is no difference in cell viability when control and sAD lines are combined. Each dot represents the mean of all biological repeats for one cell line.

4.2.3 Neuronal Morphology and Viability in Control and sAD iNeurons Under Stressed Conditions

Neuronal morphology was also assessed under stressed conditions, in two control (7, 10) and two sAD (5, 9) iNeuron lines. Cells were investigated in normal glucose containing media (Glu), low glucose (5mM) media with added galactose (20mM; Gal), and galactose media with 30nM rotenone treatment (Gal+Rot). Galactose media drives the cells into generating ATP via OXPHOS, while rotenone is a complex I inhibitor. No significant difference was seen in cell roundness or cell width to length ratio between different media conditions or between control and sAD iNeurons (figure 55 a-b). Neuron score was again variable, and the previously seen increase in neuron score in sAD 5 was not seen here. However, there was a decrease in neuron score under stressed conditions in both control 10 (Glu 2.2 ± 0.4 , Gal 1.7 ± 0.4 , Gal+Rot 1.9 ± 0.6 ; figure 55c) and sAD 9 (Glu 2.6 ± 0.6 , Gal 1.9 ± 0.4 , Gal+Rot 2.0 ± 0.55 ; figure 55c), though no differences were seen between the control and patient lines in any condition.

A reduction in cell viability was also seen in the stressed conditions in control 10 (Glu $81\% \pm 1.4\%$, Gal $69\% \pm 2.25$, Gal+Rot $73\% \pm 0.6\%$; figure 55d) and sAD 9 (Glu $65\% \pm 6.7\%$, Gal $54\% \pm 9.2\%$, Gal+Rot $54\% \pm 9.1\%$; figure 55d), as well as a previously unseen decrease in sAD 9 compared to sAD 10 in all conditions. A reduction in cell viability in sAD 5 in all media conditions was also noted (Glu $45\% \pm 6\%$, Gal $43\% \pm 9\%$, Gal+Rot $46\% \pm 5\%$; figure 55d), as well as in control 7 (Glu $53\% \pm 12\%$, Gal $48\% \pm 14\%$, Gal+Rot $53\% \pm 10\%$; figure 55d) compared to previous basal results. These inconsistencies may be explained by an iNPC related issue; all iNeurons used in this set of experiments were differentiated from the same starting batch of iNPCs (at different passages). There may have been an issue in this iNPC batch which affected the differentiation and viability of the cells.

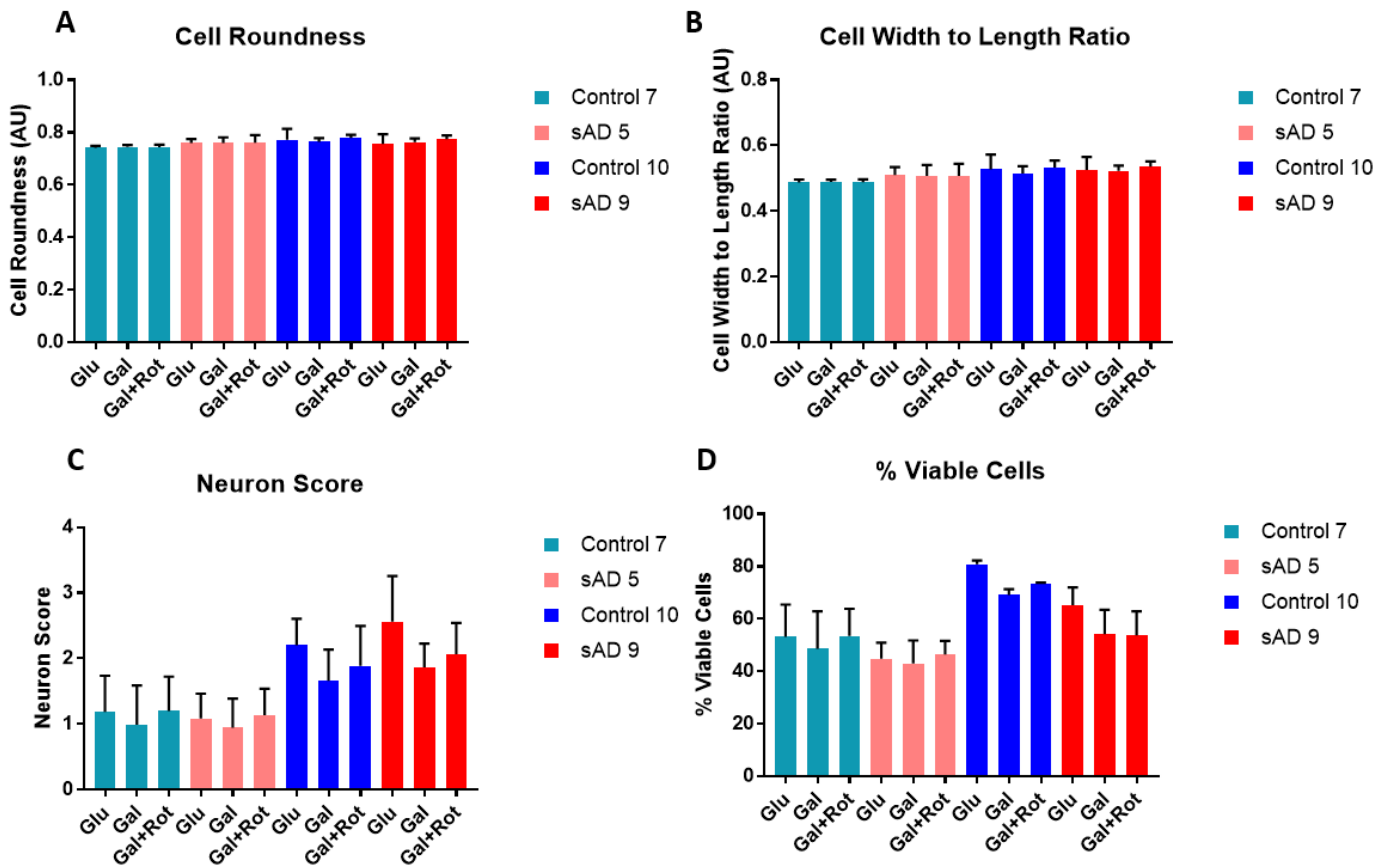


Figure 55: There is no significant difference in neuronal morphology or viability with either low glucose, galactose containing media, or 30nM rotenone treatment. Bars represent the mean of repeats from different differentiations, and error bars show SD, $n = 3$. A) There is no significant difference in cell roundness between media conditions or control and sAD iNeurons. B) There is no significant difference in cell width to length ratio between different media conditions or control and sAD iNeurons. C) There is no significant difference in neuron score between different media conditions or control and sAD iNeurons. D) There is no significant difference in cell viability between different media conditions or control and sAD iNeurons.

4.2.4 Mitochondrial Function and Morphology in iNeurons Under Basal Conditions

Mitochondrial function and morphology were assessed under basal conditions using the MMP assay. Representative images are shown in figure 56. Mitochondrial membrane potential was assessed and normalised to the control on the day of the experiment, to reduce the noise seen from variability between different days. MMP was significantly reduced in sAD 6 compared to control 5 (control 5 1.17 ± 0.34 , sAD 6 0.363 ± 0.06 ; $p = 0.022$, figure 57a). There was also a decrease seen in sAD 5 compared to control 3 (control 3 0.938 ± 0.108 , sAD 5 0.476 ± 0.265 ; $p = 0.497$; figure 57a), in sAD 4 compared to control 7 (control 7 0.97 ± 0.4 , sAD 4 0.76 ± 0.4 , $p = 0.7480$; figure 57a), as well as in sAD 8 compared to control 2, though this was only in one technical repeat due to issues with the survival of sAD 8 to the end of the protocol (control 2 1, sAD 8 0.612; figure 57a). Interestingly, an increase was seen in sAD 9 compared to control 10, though this was variable (control 10 0.887 ± 0.196 , sAD 9 1.235 ± 0.454 ; $p = 0.636$; figure 57a). When all control and sAD lines were combined, there was no significant difference seen in MMP (controls 0.992 ± 0.108 , sAD 0.689 ± 0.34 ; $p = 0.0925$; figure 57b). However, a significant difference was seen when sAD 9 was excluded as an outlier (controls 0.992 ± 0.108 , sAD 0.552 ± 0.17 ; $p = 0.0021$; figure 57c).

In terms of morphology, no differences were seen under basal conditions between control and sAD neuron lines in mitochondrial roundness (figure 58a,e), mitochondrial width (figure 58c, g), or mitochondrial length (figure 58d, h) in either individual pairs, or when all lines were combined. There was a significant increase in mitochondrial area in sAD 5 compared to control 3, although this is affected by control 3 being lower than the other controls (control 3 0.79 ± 0.42 , sAD 5 1.37 ± 0.325 ; $p = 0.036$; figure 58b); control 9 was also lower in both width and length. There was no significant difference in mitochondrial area when all control and sAD lines were combined (figure 58f).

Other morphology parameters were assessed including mitochondrial count per cell, percentage of mitochondria accumulated in the perinuclear region, and mitochondrial form factor, a measure of interconnectivity in the mitochondrial network. There were few significant differences seen in these parameters at an individual pair (figure 59a-c), and no significant differences seen at a group level (figure 59d-f), however, there was more variability. The mitochondria count per cell was normalised to cell area, and a significant decrease was seen in sAD 5 compared to control 3 (control 3 0.19 ± 0.08 , sAD 5 0.05 ± 0.04 ; $p = 0.024$; figure 59a). There was also a decrease in sAD 9 compared to control 10 (control 10 0.16 ± 0.05 , sAD 9 0.09 ± 0.06 ; $p = 0.586$; figure 59a), and sAD 6 compared to control 5 (control 5 0.27 ± 0.1 , sAD 6 0.13 ± 0.02 ; $p = 0.078$; figure 59a). An increase was seen in sAD 4 compared to control 7 (control 7 0.13 ± 0.04 , sAD 4 0.17 ± 0.06 ; $p = 0.842$; figure 59a), and in sAD 8 compared to control 2 (control 2 0.15 ± 0.01 , sAD 8 0.25; figure 59a). The number of mitochondria

accumulated in the perinuclear region showed an increase in sAD 5 compared to control 3 (control 3 $15.24\% \pm 6.76\%$, sAD 5 $30.03\% \pm 11.81\%$; $p = 0.412$; figure 59b), as did sAD 8 compared to control 2 (control 2 $29.29\% \pm 2.0\%$, sAD 8 59.5% ; figure 59b), though this was only in one technical repeat and sAD 8 was much higher than any other line, suggesting this may not be an accurate result. Form factor was more consistent between the lines, but there was a slight increase in sAD 8, though again this was only in one repeat (figure 59b). The percentage of the area taken up by long/short mitochondria was also assessed, and no significant differences were seen under basal conditions, in either individual pairs or at a group level (figure 60a-d).

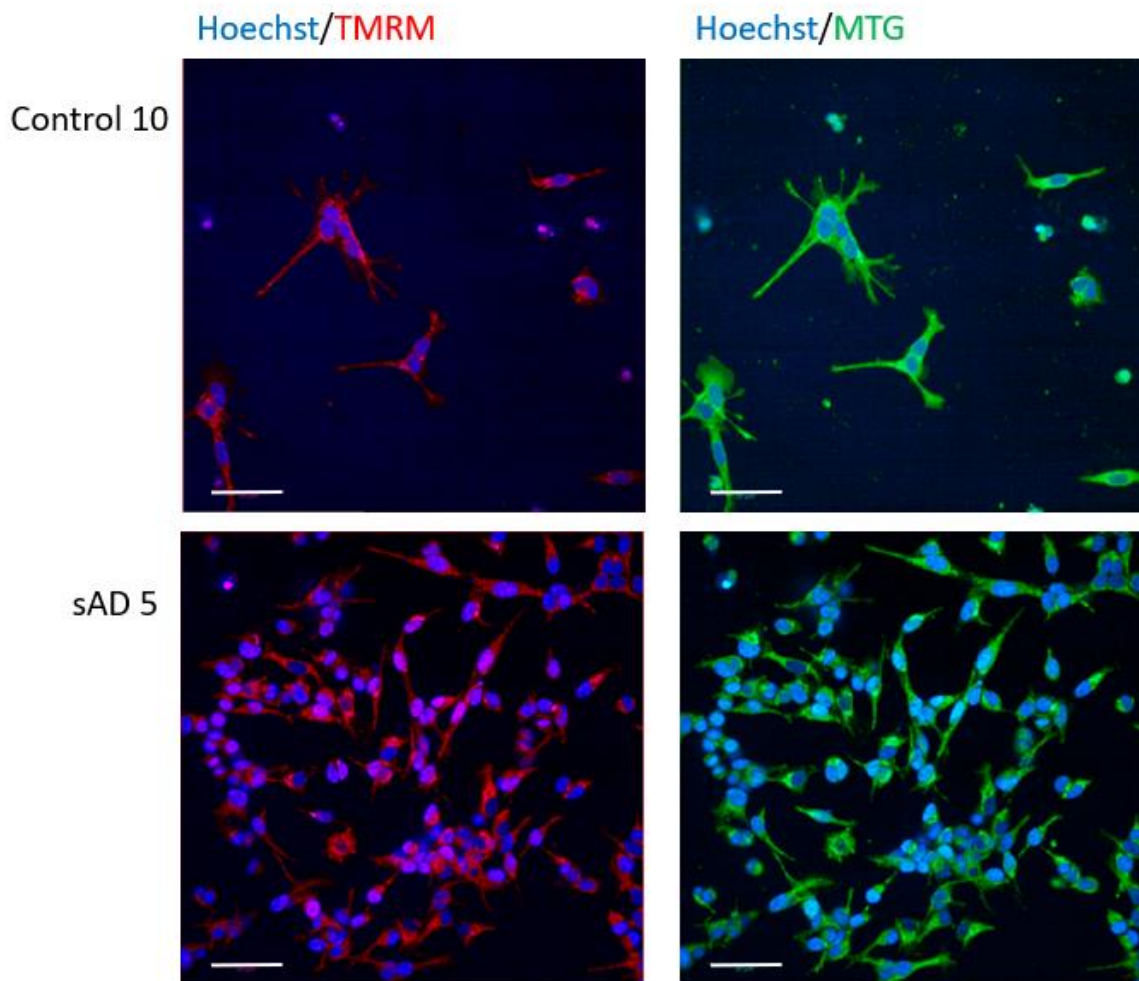


Figure 56: Representative images of TMRM, shown in red, and MitoTracker Green staining in control 10 and sAD5 iNeurons. Hoechst staining of the nuclei is shown in blue, scale bar = 50 μ M.

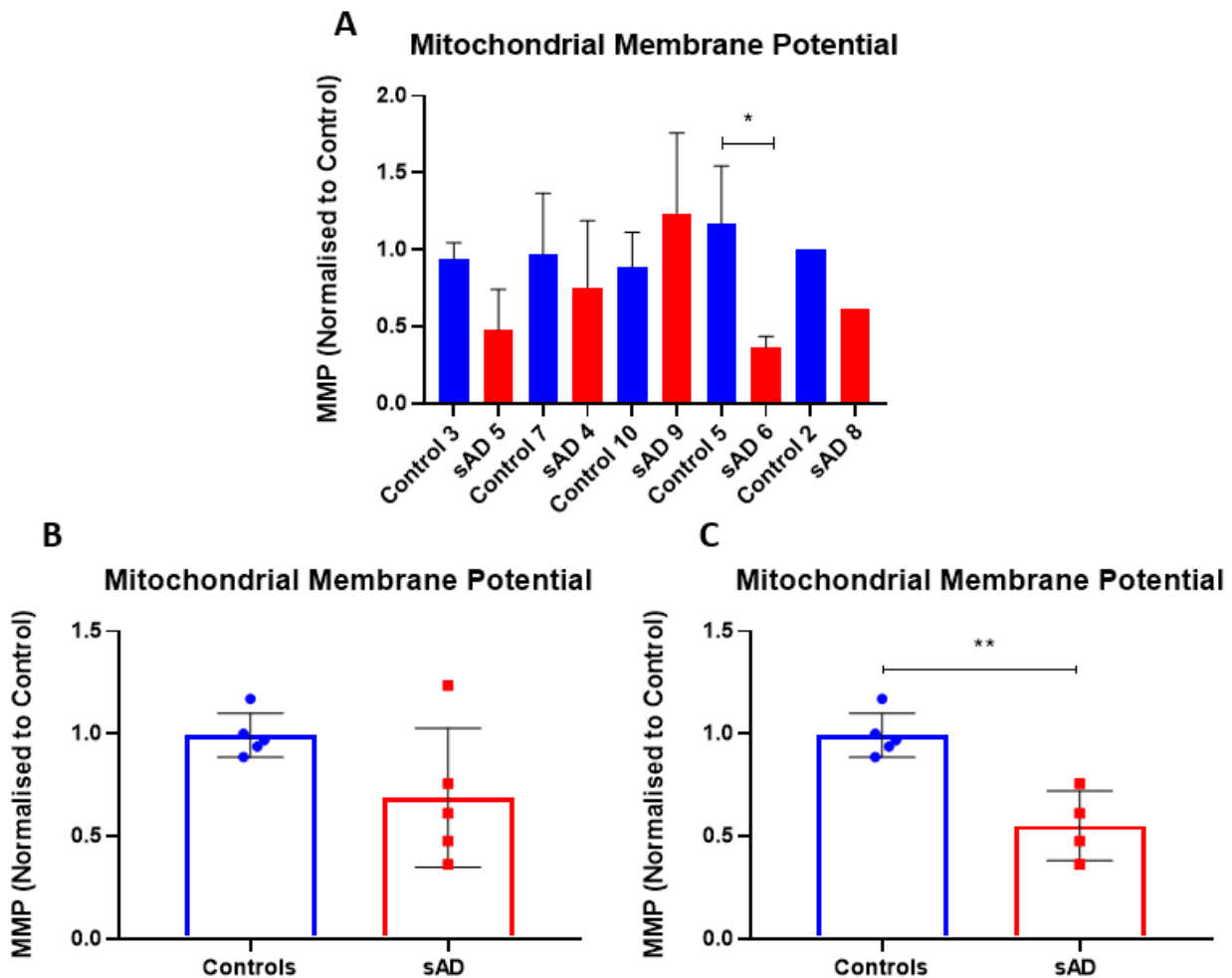


Figure 57: There is a significant decrease in MMP in sAD 6 compared to control 5, but no significant difference in any other pairs, $n > 3$ with the exception of control 2 and sAD 8 where $n = 1$. For B-C, each dot represents the average of all biological repeats for one cell line. Errors bars represent SD. A) There is a significant decrease in MMP in sAD 6 compared to control 5 ($* p < 0.05$; One way ANOVA with Sidak's multiple comparisons). There is a decrease in sAD 5 compared to control 3, as well as sAD 8 compared to control 2. B) There is no significant difference in MMP between controls and sAD when all lines are combined. C) There is a significant decrease in MMP in sAD neurons compared to controls when sAD 4 is excluded ($** p < 0.01$, t test).

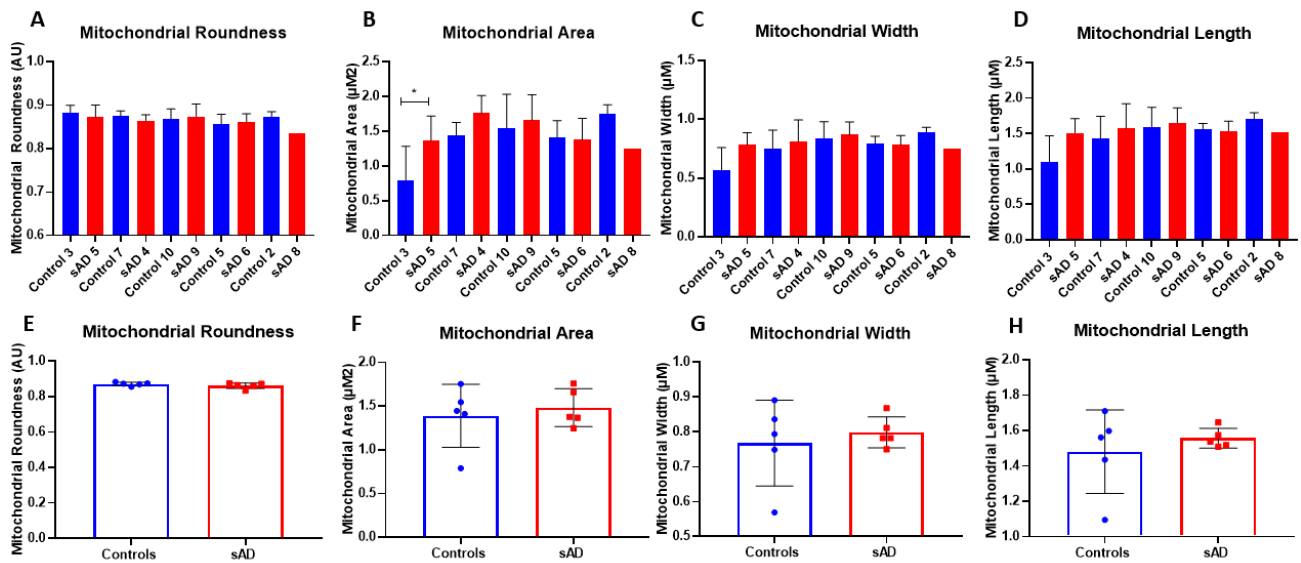


Figure 58: *There is no significant difference between control and sAD neurons in mitochondrial roundness, mitochondrial area, mitochondrial width, or mitochondrial length, $n > 3$, with the exception of sAD 8 where $n = 1$. For E-H, each dot represents the average of all biological repeats for one cell line. Errors bars represent SD. A) There is no significant difference in paired control and sAD neuron lines in mitochondrial roundness. B) There is a significant increase in mitochondrial area in sAD 5 compared to control 3 ($*p < 0.05$; One way ANOVA with Sidak's multiple comparisons), but not in any other pair. C) There is no significant difference in mitochondrial width in any neuron pair. D) There is no significant difference in any control and sAD pair in mitochondrial length. E) There is no significant difference in mitochondrial roundness when control and sAD lines are combined. F) There is no significant difference in mitochondrial area when control and sAD lines are combined. G) There is no significant difference between control and sAD lines in mitochondrial width when lines are combined. H) There is no significant difference in mitochondrial length when sAD and control lines are combined.*

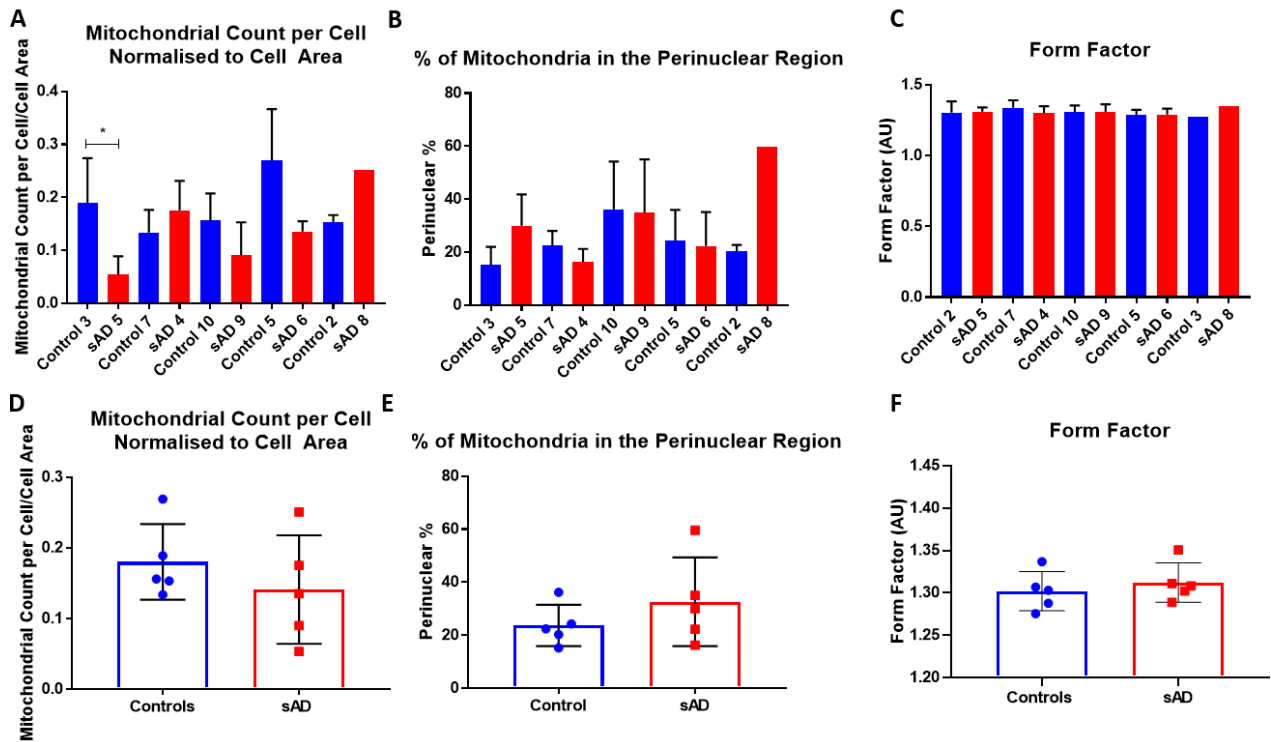


Figure 59: There is no significant difference between control and sAD lines in mitochondrial count per cell, the percentage of mitochondria accumulated in the perinuclear region, and the form factor, a measure of mitochondrial interconnectivity, $n > 3$, with the exception of sAD 8 where $n = 1$. For D-F, each dot represents the average of all biological repeats for one cell line. Errors bars represent SD. A) There is a significant decrease in mitochondrial count per cell normalised to cell area in sAD 5 compared to control 7 (* $p < 0.05$; One way ANOVA with Sidak's multiple comparisons), but no significant difference in any other pair. B) There is no significant difference in the percentage of mitochondria accumulated in the perinuclear region in any pair, though there is an increase in sAD 5 compared to control 3, as well as in sAD 8 compared to control 2. C) There is no significant difference in form factor in any control and sAD neuron pair. D) There is no significant difference in the mitochondrial count per cell normalised to cell area. E) There is no significant difference in the percentage of mitochondria accumulated in the perinuclear region when control and sAD lines are combined. F) There is no difference in form factor when control and sAD lines are combined.

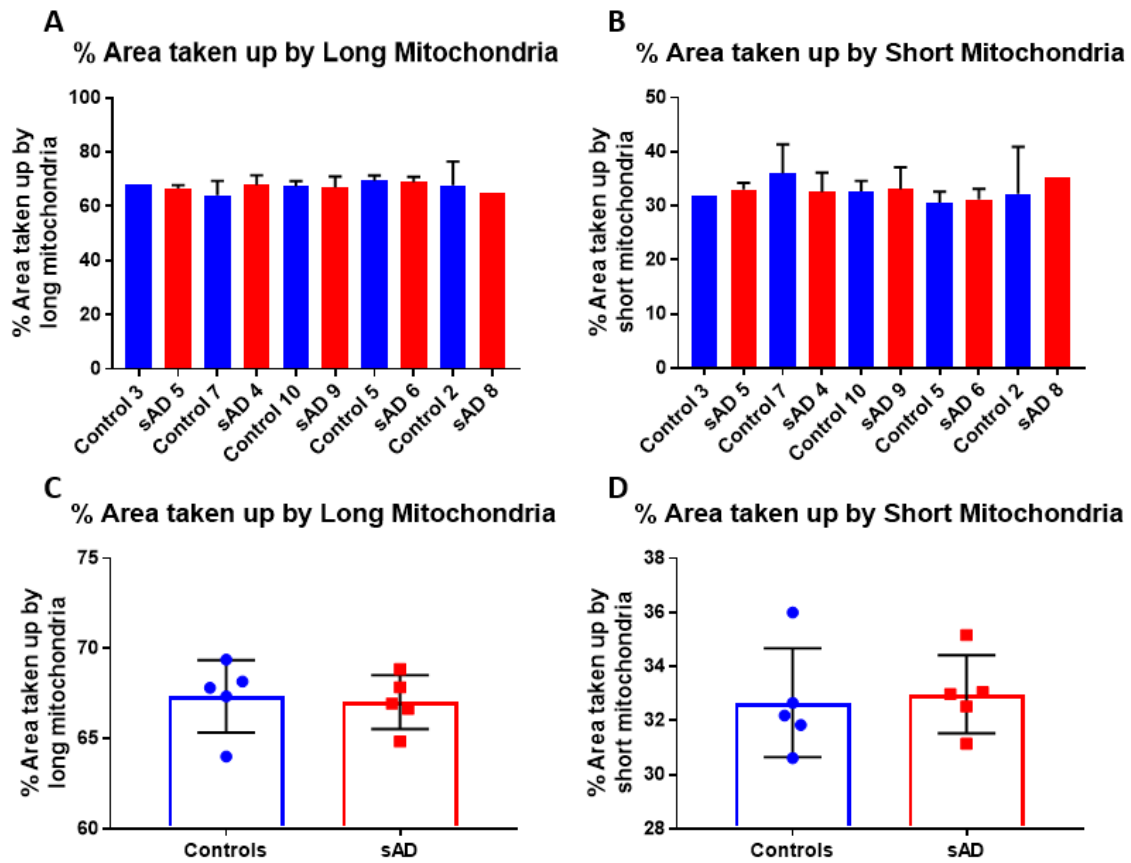


Figure 60: There is no significant difference in the percentage of the area taken up by long or short mitochondria. For C-D, each dot represents the average of all biological repeats for one cell line. Errors bars represent SD. A) There is no significant difference in the percentage of the area taken up by long mitochondria between any sAD and control neuron pair. B) There is no significant difference in the percentage of the area taken up by short mitochondria between any sAD and control neuron pair. C) There is no difference in the percentage of the area taken up by long mitochondria when control and sAD lines are combined. D) There is no significant difference in the area taken up by short mitochondria when control and sAD lines are combined.

4.2.5 Mitochondrial Function in iNeurons Under Stressed Conditions

Mitochondrial function was also assessed under stressed conditions, in two control (7, 10) and two sAD (5, 9) iNeuron lines. Conditions used were the same as described previously (section 4.2.4); glucose containing media, low glucose media (5mM) with added galactose (20mM), and galactose media with 30nM rotenone. No significant difference was seen in MMP between different media conditions or between control and sAD lines. A decrease was seen in sAD 5 in the glucose (control 7 1; sAD 5 0.77 ± 0.09 ; figure 61) and galactose (control 7 0.87 ± 0.09 ; sAD 5 0.7; figure 61) conditions, but this was not seen in the galactose with rotenone condition (control 7 0.92 ± 0.08 ; sAD 5 0.87 ± 0.15 ; figure 61). A decrease in sAD 5 was seen previously under basal conditions. In all lines, there was a reduced MMP in galactose media (control 7 Glu 1, Gal 0.87 ± 0.09 ; sAD 5 Glu 0.77 ± 0.09 , Gal 0.7; control 10 Glu 1, Gal 0.9 ± 0.09 ; sAD 9 Glu 1.06 ± 0.04 , Gal 0.93 ± 0.08 ; figure 61). This was not seen in the galactose with rotenone condition.

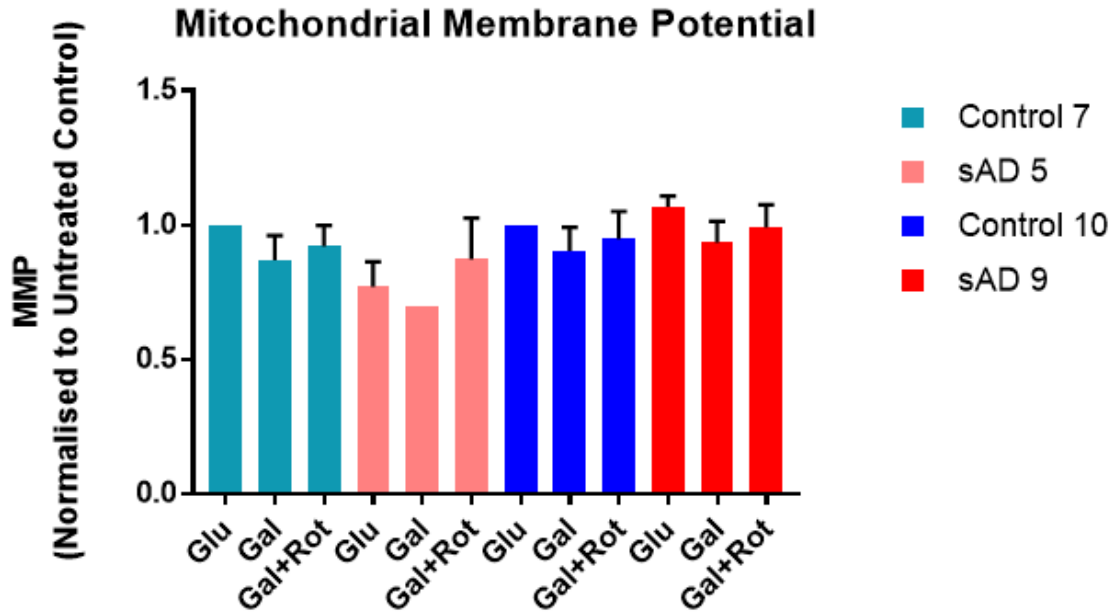


Figure 61: There is no significant difference in mitochondrial membrane potential between control and sAD lines with either low glucose, galactose containing media, or 30nM rotenone treatment. Bars represent the mean of repeats from different differentiations, and error bars show SD, $n = 3$ with the exception of control 7 gal where $n = 2$, and sAD 5 gal where $n = 1$.

4.2.6 Drp1 Expression in iNPCs and iNeurons

In order to determine whether the reduction seen in Drp1 and its receptors observed in sAD patient fibroblasts is also present in other cell types, total cellular levels were assessed via western blotting in four control and four sAD iNPC and iNeuron lines.

In the iNPC lines assessed, it was found that three of four showed a significant increase in protein expression of Drp1. sAD 5 showed a significant increase of 285% compared to control 7 (control 7 1.21 ± 0.19 , sAD 5 4.18 ± 0.83 ; $p < 0.0001$; figure 62b). sAD 4 also showed a significant increase of 124% compared to control 7 (control 7 1.17 ± 0.23 , sAD 4 2.63 ± 0.25 ; $p = 0.0002$; figure 62b). sAD 9 was also significantly increased, by 118% compared to control 10 (control 10 0.73 ± 0.2 , sAD 9 1.6 ± 0.39 ; $p = 0.36$; figure 62b). An increase was also seen in sAD 8 compared to control 5, though this was not found to be significant (control 5 0.93 ± 0.15 , sAD 8 1.43 ± 0.54 ; $p = 0.297$; figure 62b). When control and sAD iNPC lines were combined, an overall significant increase of 117% was seen (controls 1.0 ± 0.22 , sAD 2.18 ± 0.69 ; $p = 0.0178$; figure 62c).

Protein expression levels of Drp1 was also assessed via western blotting in iNeurons differentiated from the iNPC lines assessed previously. There was a significant increase of 315% in Drp1 protein levels in sAD 5 in comparison to control 3 (control 3 0.78 ± 0.32 , sAD 5 3.24 ± 1.07 ; $p < 0.0001$; figure 63b). No significant difference was seen in any other pair (figure 63b), though a decrease of 24% was seen in sAD 4 compared to control 7 (control 7 1.46 ± 0.3 , sAD 4 1.1 ± 0.6 ; $p = 0.8166$; figure 63b) and a decrease of 39% in sAD 9 compared to control 10 (control 10 1.3 ± 0.28 , sAD 9 0.79 ± 0.39 ; $p = 0.5783$; figure 63b). There an increase of 77% in sAD 8 compared to control 5 (control 5 0.6 ± 0.2 , sAD 8 1.07 ; figure 63b). When controls were compared to sAD lines at a group level, no significant difference was seen (controls 1.04 ± 0.41 , sAD 1.55 ± 1.14 ; $p = 0.427$; figure 63c).

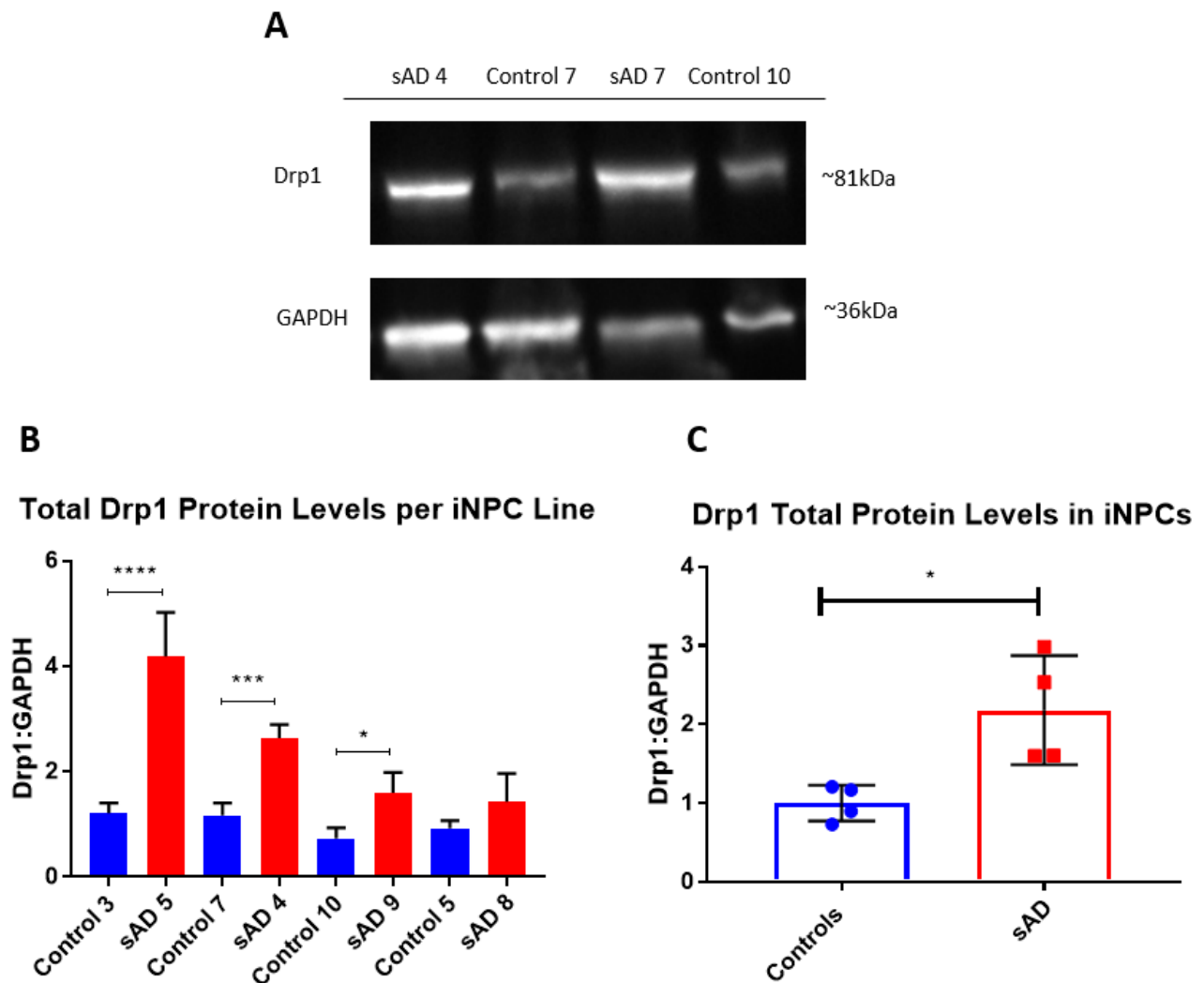


Figure 62: There is a significant increase in Drp1 protein levels in sAD iNPC lines compared to controls. A) Representative blot. **B)** Quantification of Drp1 protein levels in four control and sAD pairs. Each line was assessed from samples from three separate passages. A significant increase is seen in three of the four sAD lines compared to their paired control (* $p < 0.05$, *** $p < 0.001$, **** $p < 0.0001$; One way ANOVA with Sidak's multiple comparisons). Bars shown represent the mean and error bars represent SD. **C)** There is a significant increase of 117% when the sAD group is compared to the control group (* $p < 0.05$; t test). Each dot represents the mean of the three replicates per line, bars represent the group mean and error bars show SD.

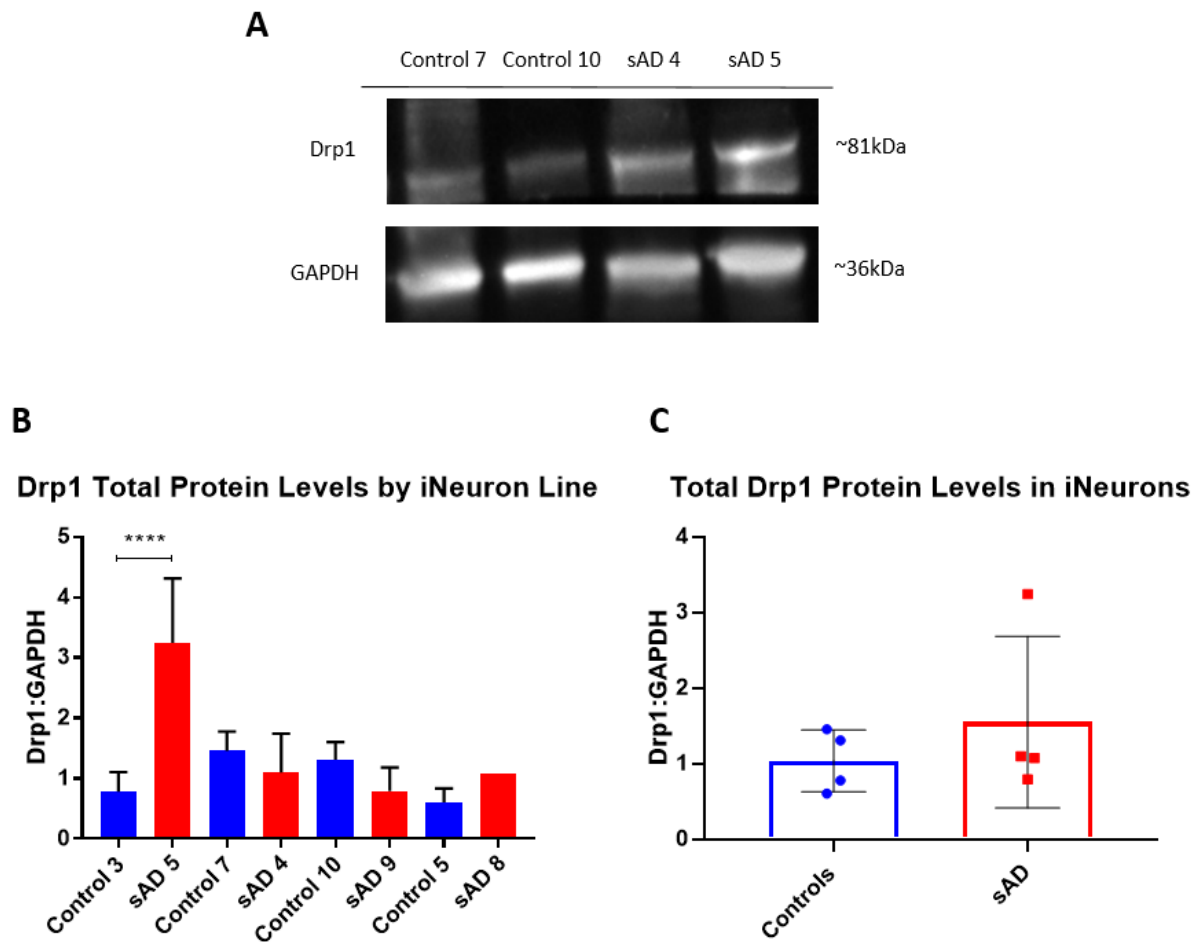


Figure 63: There is a significant increase in Drp1 protein levels one sAD neuron line compared to a paired control. A) Representative blot of Drp1 and GAPDH loading control, with 10 μ g protein loaded per lane. B) Quantification of Drp1 protein levels in four control and sAD pairs. Each line was assessed from samples from three separate differentiations. A significant increase was seen in sAD5 compared to control 3 (**** $p < 0.0001$; One way ANOVA with Sidak's multiple comparisons). Bars shown represent the mean and error bars represent SD. C) There is no significant difference when the sAD group is compared to the control group. Each dot represents the mean of the three replicates per line, bars represent the group mean and error bars show SD.

4.2.7 Drp1 Localisation in iNeurons

To investigate whether the changes seen in total protein levels affected the amount of Drp1 localised to the mitochondria, iNeurons were stained for mitochondrial marker TOM20, alongside Drp1. Representative images are shown in figure 64. There was no significant differences seen in individual pairs in Drp1 localised to the mitochondria, though all sAD lines showed an increase (figure 65a). When all lines were combined, no significant difference was seen in the amount of Drp1 localised to the mitochondria in the sAD group compared to the controls, though an increase was seen which was approaching significance (controls 0.011 ± 0.008 , sAD 0.031 ± 0.015 ; $p = 0.067$; figure 65c). However, there was no difference seen in the percentage of total Drp1 which was localised to the mitochondria at a group level (controls $28.7\% \pm 7.2$, sAD $28.3\% \pm 8.7$; $p = 0.9447$; figure 65d). On an individual level, there was an increase in sAD 4 compared to control 7 (control 7 $26.0\% \pm 14.3$, sAD 4 $40.7\% \pm 22.9$; $p = 0.5955$), but no difference in any other pair (figure 65b). sAD 5 was the only line which showed a significant increase in total Drp1 protein levels, but sAD 8 also showed an increase; this suggests that the increase in Drp1 present at the mitochondria in these lines is due to the increase in overall levels. sAD 4 showed a small decrease in total Drp1 levels, but an increase in the percentage of total Drp1 present at the mitochondria. It is likely that sAD 4 is able to compensate for this slight reduction in Drp1 by increasing the percentage of Drp1 localised to the mitochondria to bring the amount of Drp1 at the mitochondria to above control levels. sAD 9 also shows a decrease in Drp1 total levels, but showed an increase in the amount of Drp1 localised to the mitochondria despite no difference seen in the percentage of total Drp1 at the mitochondria. The paired control for sAD 9, control 10, shows lower levels of Drp1 present at the mitochondria than other controls, and this may impact the apparent increase in Drp1 at the mitochondria in sAD 9.

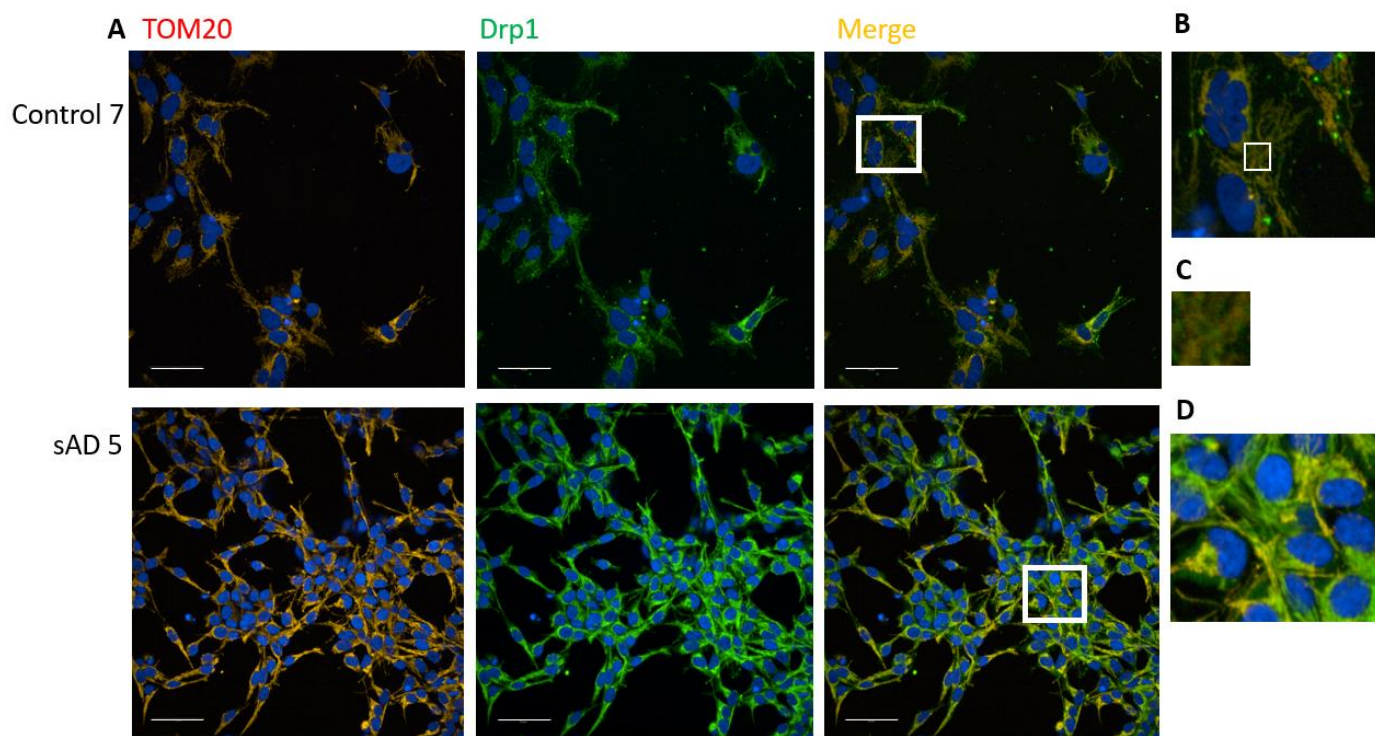


Figure 64: Representative Images of Drp1-TOM20 co-localisation in control and sAD patient iNeurons. A) Representative images of Drp1 and TOM20 co-localisation staining. TOM20 is shown in red, Drp1 in green, and nuclei in blue. Scale = 50 μ m. B) Zoomed in image of Drp1-TOM20 co-localisation in control iNeurons, showing the area in the white box. C) Further zoomed in image of the white box shown in B, to demonstrate co-localisation of Drp1 and TOM20. D) Zoomed in image of Drp1-TOM20 co-localisation in sAD iNeurons, showing the area in the white box.

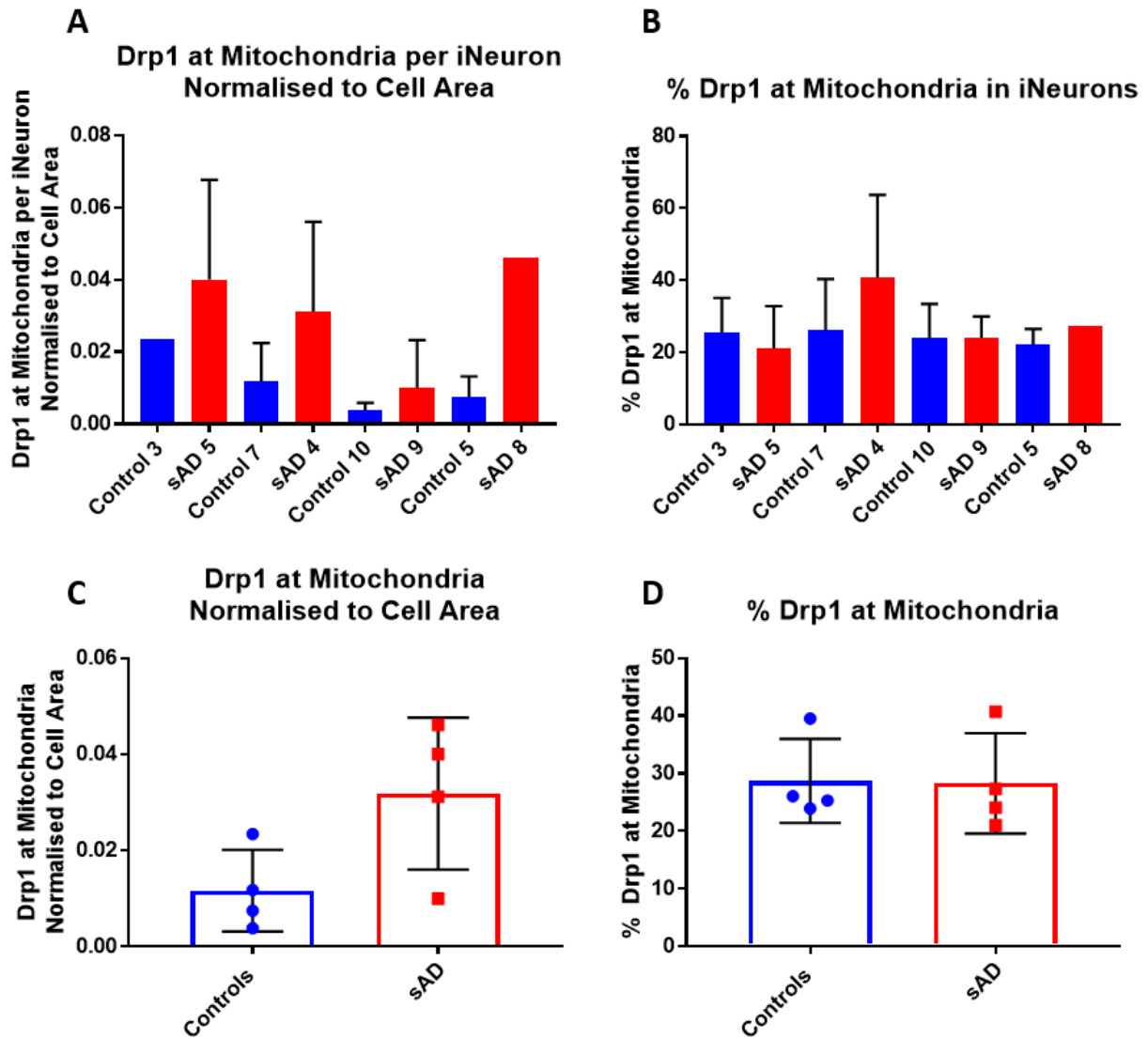


Figure 65: There is no significant difference in the amount of Drp1 co-localised to the mitochondria in iNeurons, but a non-significant increase is seen, $n = 3$ except sAD 8 where $n=1$. A) Quantification of Drp1 co-localisation with mitochondrial marker TOM20. There is no significant difference between any sAD and control pair. B) Quantification of the percentage of total Drp1 which is localised to the mitochondria. There is no significant difference between any control and sAD pair. C) There is a non-significant increase in Drp1 localised to the mitochondria between sAD and control iNeurons when individual lines are combined. D) There is no significant difference in the percentage of total Drp1 localised to the mitochondria when individual lines are combined.

4.2.8 Drp1 Receptor Expression in iNPCs

Protein levels of the Drp1 receptors on the outer mitochondrial membrane, Fis1, Mff, MiD49, and MiD51 were assessed in four control and four sAD iNPC lines. Fis1 levels were significantly increased in one sAD line; sAD 4 was significantly increased by 94% compared to control 7 (control 7 0.87 ± 0.23 , sAD 4 1.69 ± 0.07 ; $p = 0.0006$; figure 66b). However, in two lines Fis1 protein levels were significantly decreased compared to their paired controls; sAD 5 was significantly decreased by 83% compared to control 3 (control 3 0.97 ± 0.14 , sAD 5 0.15 ± 0.05 ; $p = 0.0014$; figure 66b), and sAD 8 was significantly decreased by 59% compared to control 5 (control 5 1.15 ± 0.24 , sAD 8 0.47 ± 0.04 ; $p = 0.0078$; figure 66b). sAD 9 also showed a decrease when compared to control 10, but this was not significant (control 10 1.18 ± 0.33 , sAD 9 0.79 ± 0.07 ; $p = 0.20$; figure 66b). When all control and sAD lines were combined, there was no significant difference seen (controls 1.04 ± 0.15 , sAD 0.78 ± 0.66 ; $p = 0.462$; figure 66c).

For Mff protein expression, there was no significant difference between any control and sAD pair, but three of the four pairs did show an increase. sAD 5 was increased by 33% compared to control 3 (control 3 1.12 ± 0.11 , sAD 5 1.5 ± 0.4 ; $p = 0.7$, figure 67b), sAD 4 was increased by 61% compared to control 7 (control 7 1.0 ± 0.08 , sAD 4 1.6 ± 0.2 ; $p = 0.206$; figure 67b), and sAD 9 was increased by 33% compared to control 10 (control 10 0.97 ± 0.17 , sAD 9 1.3 ± 0.49 ; $p = 0.894$; figure 67b). When control and sAD lines were combined, there was no significant difference, although again there was a non-significant increase (controls 1.02 ± 0.07 , sAD 1.33 ± 0.30 ; $p = 0.091$; figure 67c).

For MiD49 protein levels, there was again no significant difference between any of the paired lines, but three out of four lines showed a decrease. sAD 5 was decreased by 74% compared to control 3 (control 3 0.41 ± 0.18 , sAD 5 0.10 ± 0.07 ; $p = 0.857$; figure 68b), sAD 4 was decreased by 68% compared to control 7 (control 7 1.19 ± 0.34 , sAD 4 0.38 ± 0.22 ; $p = 0.137$; figure 68b), and sAD 8 was decreased by 28% compared to control 5 (control 5 2.0 ± 0.42 , sAD 8 1.45 ± 0.54 ; $p = 0.429$; figure 68b). In contrast, sAD 9 showed an increase of 93% compared to control 10, but this was also not significant (control 10 0.80 ± 0.34 , sAD 9 1.56 ± 0.62 ; $p = 0.182$; figure 68b). When all lines were combined, there was no significant difference between control and sAD lines (controls 1.07 ± 0.71 , sAD 0.71 ± 0.60 ; $p = 0.467$; figure 68c).

MiD51 protein expression showed no significant differences in the majority of the lines tested, however, there was a significant increase of 246% seen in sAD 4 compared to control 7 (control 7 1.0 ± 0.08 , sAD 4 3.47 ± 0.84 ; $p < 0.0001$; figure 69b). When all lines were combined, there was no

significant difference seen between control and sAD iNPCs (controls 1.0 ± 0.10 , sAD 1.70 ± 1.19 ; $p = 0.285$; figure 69c).

Overall, at least one alteration in a fission protein was seen in all iNPC lines. sAD 4 showed differences in the most proteins with an increase seen in three of the five proteins assessed, but these differences were sometimes in contrast with the other sAD lines. For example, while sAD 5 and 8 showed a decrease in Fis1, sAD 4 showed an increase. It is also the only line to show a significant difference in Mid51 levels (table 19).

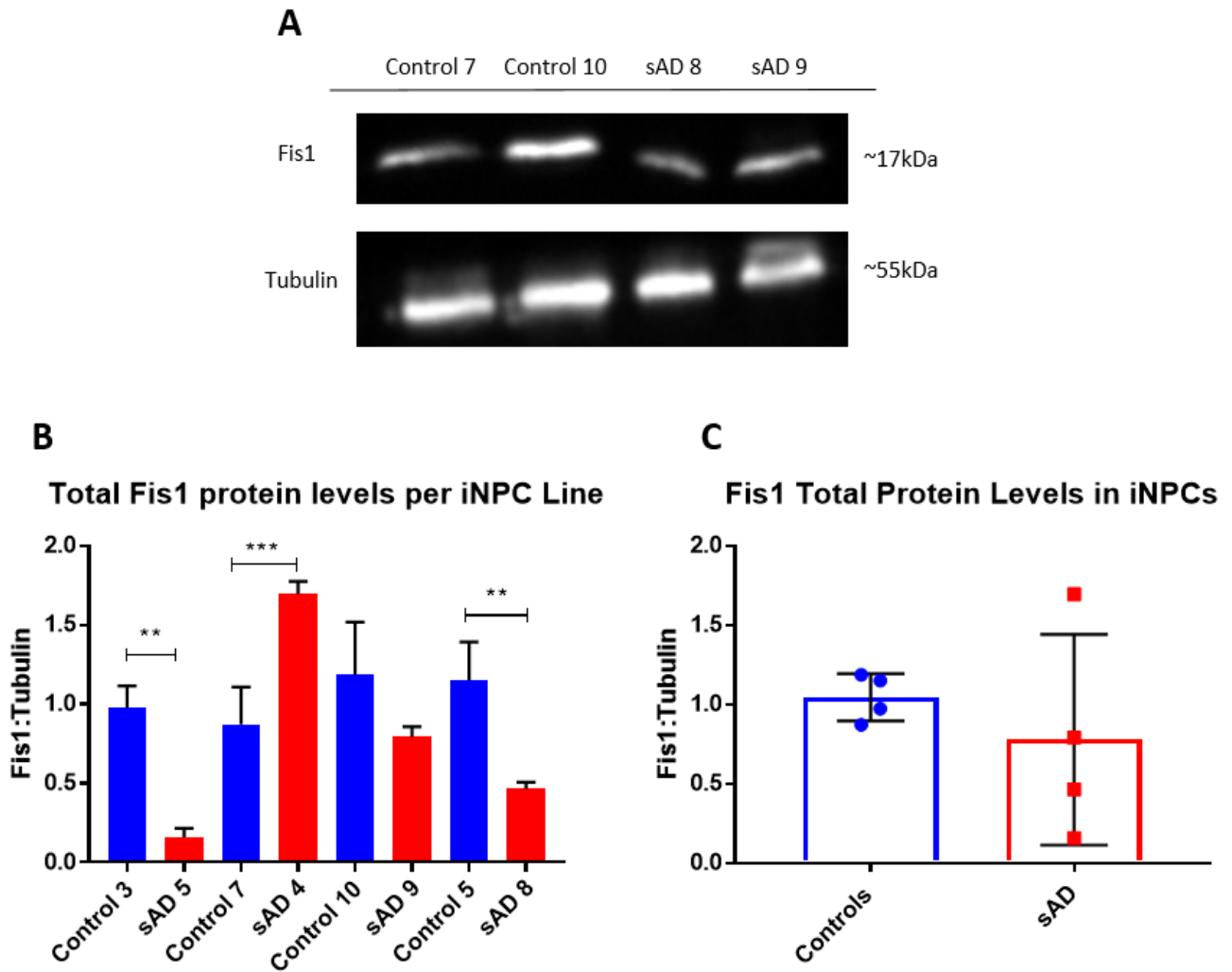


Figure 66: There is a significant increase in *Fis1* protein levels in one sAD iNPC line, and a significant decrease in two sAD iNPC lines, compared to paired controls. A) Representative blot of *Fis1* and tubulin loading control in controls 7 and 10, and sAD 8 and 9, with 10 μ g protein loaded per lane. B) Quantification of *Fis1* protein levels in four control and sAD pairs. Each line was assessed from samples from three separate passages. A significant increase is seen in one of the four sAD lines compared to their paired control, while a significant decrease is seen in two of four sAD lines compared to paired controls (** $p < 0.01$, *** $p < 0.001$; One way ANOVA with Sidak's multiple comparisons). Bars shown represent the mean and error bars represent SD. C) There is no significant difference when the sAD group is compared to the control group. Each dot represents the mean of the three replicates per line, bars represent the group mean and error bars show SD.

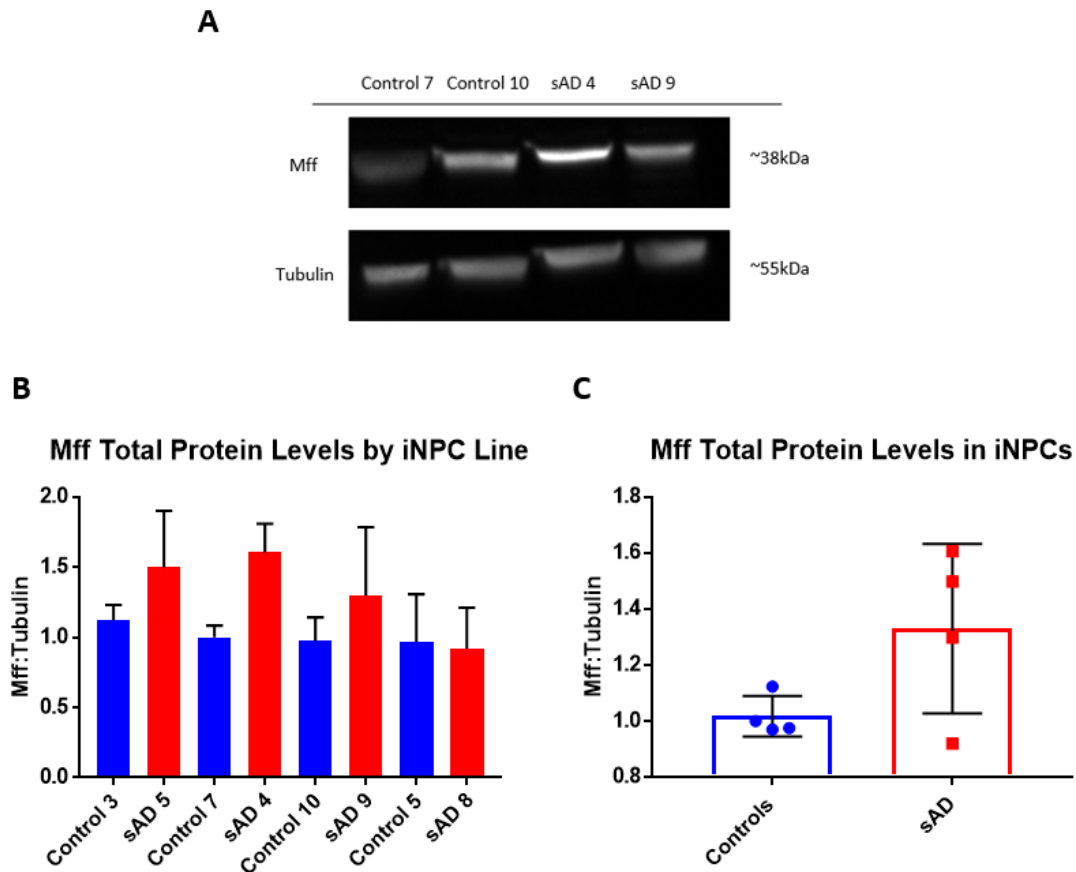


Figure 67: There is no significant difference in Mff protein levels in sAD iNPCs compared to controls. A) Representative blot of Mff and tubulin loading control in controls 7 and 10, and sAD4 9, with 10 μ g protein loaded per lane. B) Quantification of Mff protein levels in four control and sAD pairs. Each line was assessed from samples from three separate passages. No significant difference was seen in any pair, though three of four lines show an increase. Bars shown represent the mean and error bars represent SD. C) There is no significant difference when the sAD group is compared to the control group, though there is a non-significant increase. Each dot represents the mean of the three replicates per line, bars represent the group mean and error bars show SD.

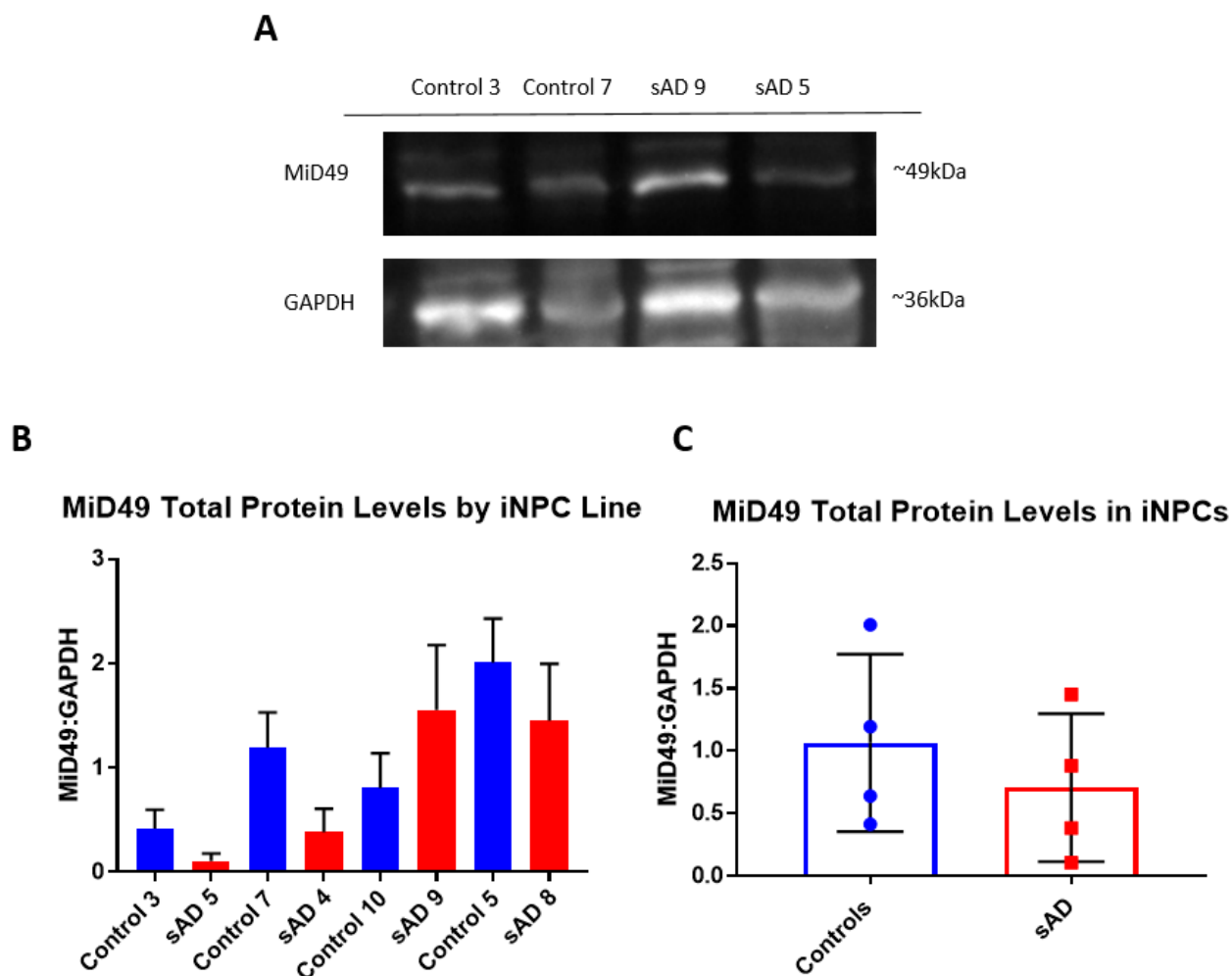


Figure 68: There is no significant difference in MiD49 protein levels in sAD iNPCs compared to controls. A) Representative blot of MiD49 and GAPDH loading control, with 10 μ g protein loaded per lane. **B)** Quantification of MiD49 protein levels in four control and sAD pairs. Each line was assessed from samples from two or three separate passages. No significant difference was seen in any pair, though three of four lines show a decrease, whilst sAD 9 showed an increase. Bars shown represent the mean and error bars represent SD. **C)** There is no significant difference when the sAD group is compared to the control group. Each dot represents the mean of the three replicates per line, bars represent the group mean and error bars show SD.

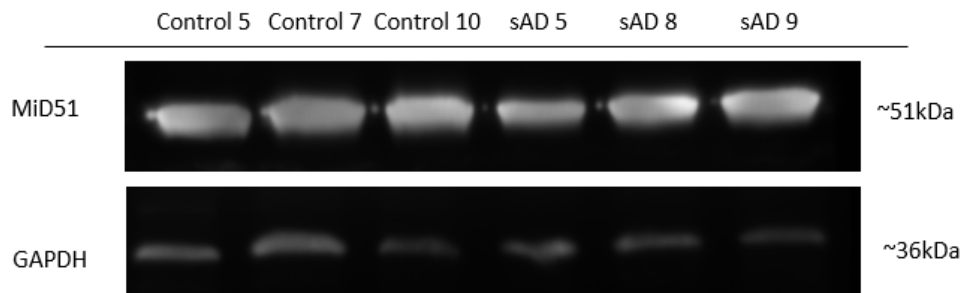
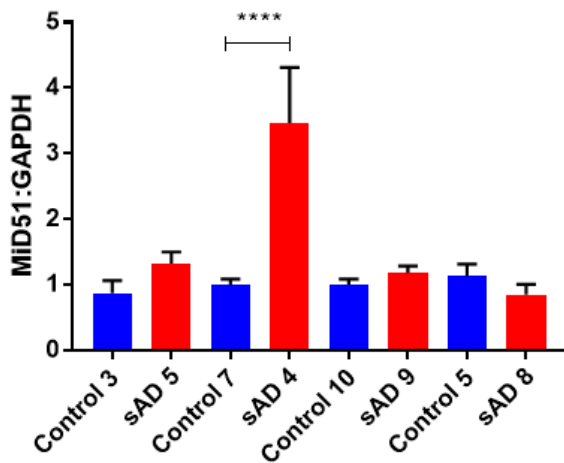
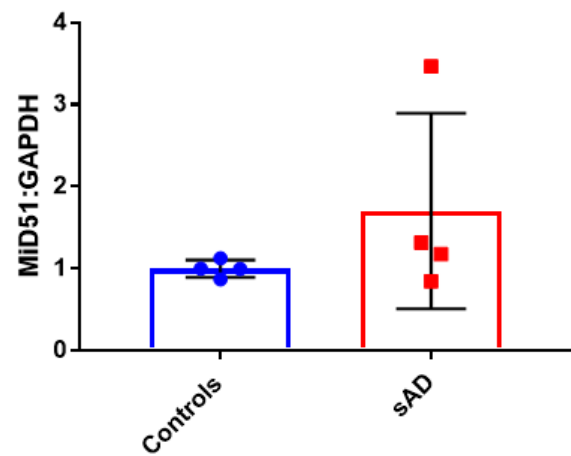




















A**B****MiD51 Total Protein Levels by iNPC Line****C****MiD51 Total Protein Levels in iNPCs**

Figure 69: There is no significant difference in MiD51 protein levels in sAD iNPCs compared to controls. A) Representative blot of MiD51 and GAPDH loading control, in control 5, 7, and 10, and sAD 5, 8, and 9, with 10 μ g protein loaded per lane. B) Quantification of MiD51 protein levels in four control and sAD pairs. Each line was assessed from samples from three separate passages. A significant increase was seen in sAD 4 compared to control 7 (**** $p < 0.0001$; One way ANOVA with Sidak's multiple comparisons). Bars shown represent the mean and error bars represent SD. C) There is no significant difference when the sAD group is compared to the control group. Each dot represents the mean of the three replicates per line, bars represent the group mean and error bars show SD.

Table 19: Summary table of total protein levels of Drp1 and the four Drp1 receptors on the outer mitochondria membrane, Fis1, Mff, MiD49, and MiD51 in iNPCs. A green arrow represents a significant increase, a red arrow represents a significant decrease and a yellow bar represents no significant difference (** $p < 0.0001$, *** $p < 0.001$, ** $p < 0.01$, * $p < 0.05$). sAD 4 shows alterations in the most proteins, but this is sometimes in contrast to the other lines tested, for example, Fis1 protein levels are increased in sAD 4 but decreased in both sAD 9 and sAD 8.**

	sAD 5	sAD 4	sAD 9	sAD 8
Drp1 Total Protein	**** 	*** 	* 	
Fis1 Total Protein	** 	*** 		** 
Mff Total Protein				
MiD49 Total Protein				
MiD51 Total Protein		**** 		

4.2.9 Linear Regression Between Drp1 and Receptors in iNPCs

The linear regression between Drp1 and its receptors was investigated in iNPC lines. There is a significant linear regression between Drp1 and Mff ($r^2 = 0.8028$; $p = 0.0026$; figure 70b) at a group level, as was seen in fibroblasts. Linear regression between Drp1 and MiD49 was approaching significance at a group level ($r^2 = 0.4389$; $p = 0.0734$; figure 70c). No significant linear regression was seen between Drp1 and Fis1, or Drp1 and MiD51 (figure 70a, d).

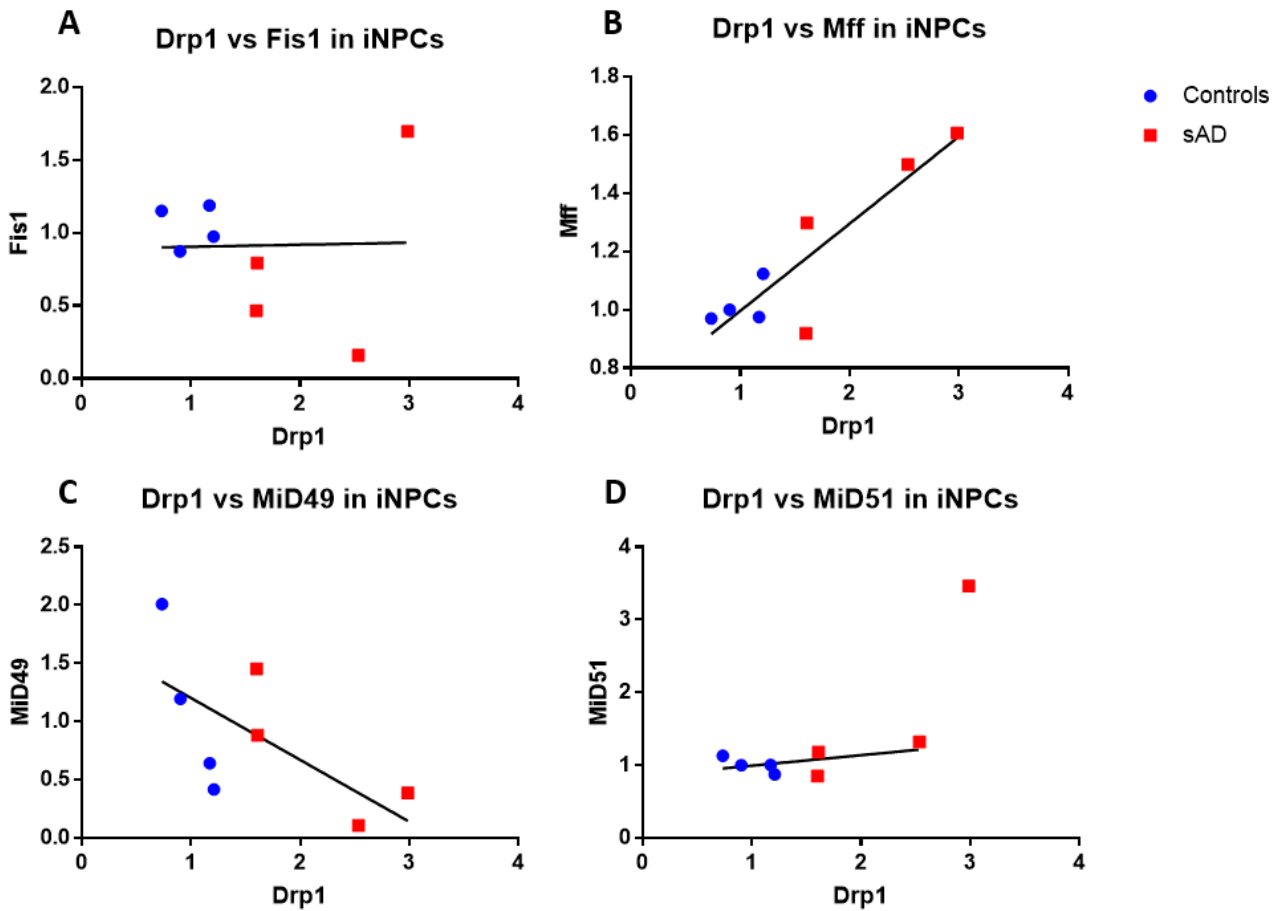


Figure 70: Linear regression between protein levels of Drp1 and protein levels of Fis1, Mff, MiD49 and MiD51, in iNPCs. A) There is no significant linear regression between Drp1 and Fis1 levels. B) There is a significant linear regression between Drp1 and Mff (black line; $r^2 = 0.8028$; $p = 0.0026$). C) No significant linear regression was seen between Drp1 and MiD49. D) There is no significant linear regression between Drp1 and MiD51.

4.2.10 Drp1 Receptor Expression in iNeurons

In iNeurons, Fis1 levels were seen to be significantly increased, by 78%, in sAD 5 compared to control 3 (control 3 0.82 ± 0.31 , sAD 5 1.47 ± 0.21 ; $p = 0.048$; figure 71b). There was no significant differences seen in any other pair, though there was an increase in sAD 4 compared to control 7 (control 7 0.98 ± 0.19 , sAD 4 1.22 ± 0.33 ; $p = 0.898$; figure 71b), and a decrease in sAD 9 compared to control 10 (control 10 1.7 ± 0.1 , sAD 9 1.5 ± 0.2 ; $p = 0.947$; figure 71b), and in sAD 8 compared to control 5 (control 5 1.4 ± 0.2 , sAD 8 0.8 ± 0.3 ; $p = 0.08$; figure 71b). There was no significant difference seen at a group level (controls 1.24 ± 0.4 , sAD 1.25 ± 0.31 ; $p = 0.974$; figure 71c).

Mff protein expression showed no significant difference in any pair, but three out of four lines showed a decrease. sAD 4 was decreased by 50% compared to control 7 (control 7 0.95 ± 0.18 , sAD 4 0.45 ± 0.16 , $p = 0.434$; figure 72b), sAD 9 was decreased by 30% compared to control 10 (control 10 1.08 ± 0.18 , sAD 9 0.75 ± 0.3 ; $p = 0.784$; figure 72b), and sAD 8 was decreased by 50% compared to control 5 (control 5 1.4 ± 0.4 , sAD 8 0.68 ± 0.2 ; $p = 0.157$; figure 72b). A decrease was also seen at a group level, where sAD lines were decreased by 30% compared to controls (controls 0.95 ± 0.38 , sAD 0.66 ± 0.14 ; $p = 0.205$; figure 72c).

Cellular MiD49 protein levels were significantly decreased by 80% in sAD 8 compared to control 5 (control 5 1.77 ± 0.25 , sAD 8 0.66 ± 0.15 ; $p = 0.008$; figure 73b). There was also a decrease in all other pairs; sAD 5 was decreased by 38% in comparison to control 3 (control 3 1.01 ± 0.68 , sAD 5 0.63 ± 0.05 ; $p = 0.919$; figure 73b), sAD 4 was decreased by 68% compared to control 7 (control 7 1.1 ± 0.11 , sAD 4 0.35 ± 0.07 ; $p = 0.346$; figure 73b), and sAD 9 was decreased by 27% compared to control 10 (control 10 1.07 ± 0.44 , sAD 9 0.78 ± 0.22 ; $p = 0.943$; figure 73b). At a group level, a significant decrease of 57% was seen (controls 1.24 ± 0.36 , sAD 0.53 ± 0.21 ; $p = 0.014$; figure 73c).

MiD51 levels were significantly decreased by 84% in sAD 4 compared to control 7 (control 7 1.2 ± 0.18 , sAD 4 0.19 ± 0.1 ; $p < 0.0001$; figure 74b). There was no significant difference seen in any other neuron pair. There was also no significant difference seen at a group level when controls and sAD lines were combined (controls 0.97 ± 0.19 , sAD 0.63 ± 0.3 ; $p = 0.097$; figure 74c).

Overall, at least one significant difference was seen in three of the four sAD lines assessed. No significant differences were seen in sAD 9. sAD 5 showed the most alterations, with a significant increase seen in Drp1 and Fis1 (table 20).

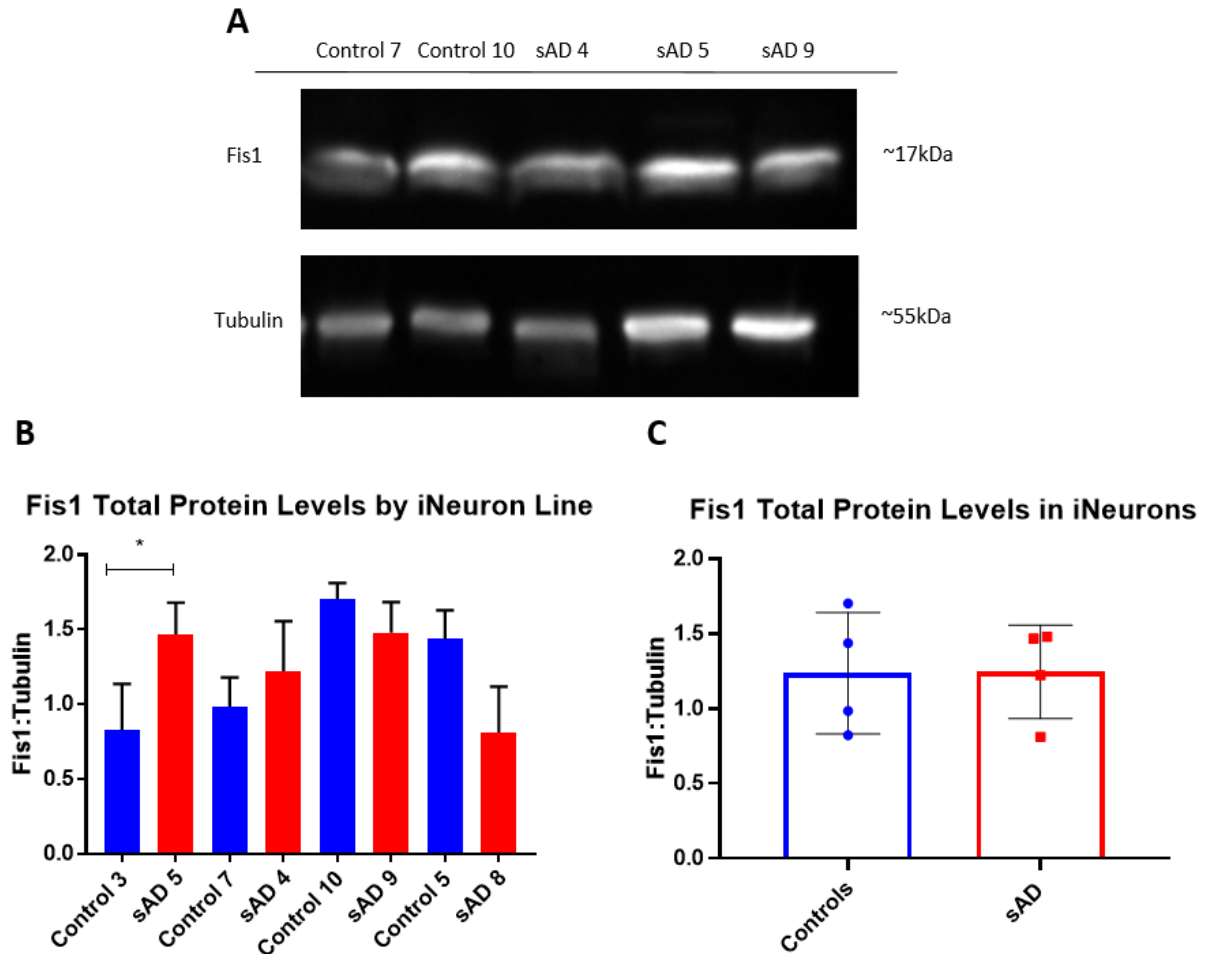


Figure 71: There is a significant increase in Fis1 protein levels in one sAD neuron lines compared to a paired control. A) Representative blot of Fis1 and Tubulin loading control, in control 7 and 10, and sAD 4, 5, and 9, with 10 μ g protein loaded per lane. B) Quantification of Fis1 protein levels in four control and sAD pairs. Each line was assessed from samples from three separate differentiations. A significant increase was seen in sAD5 compared to control 3 (* $p < 0.05$; One way ANOVA with Sidak's multiple comparisons). Bars shown represent the mean and error bars represent SD. C) There is no significant difference when the sAD group is compared to the control group. Each dot represents the mean of the three replicates per line, bars represent the group mean and error bars show SD.

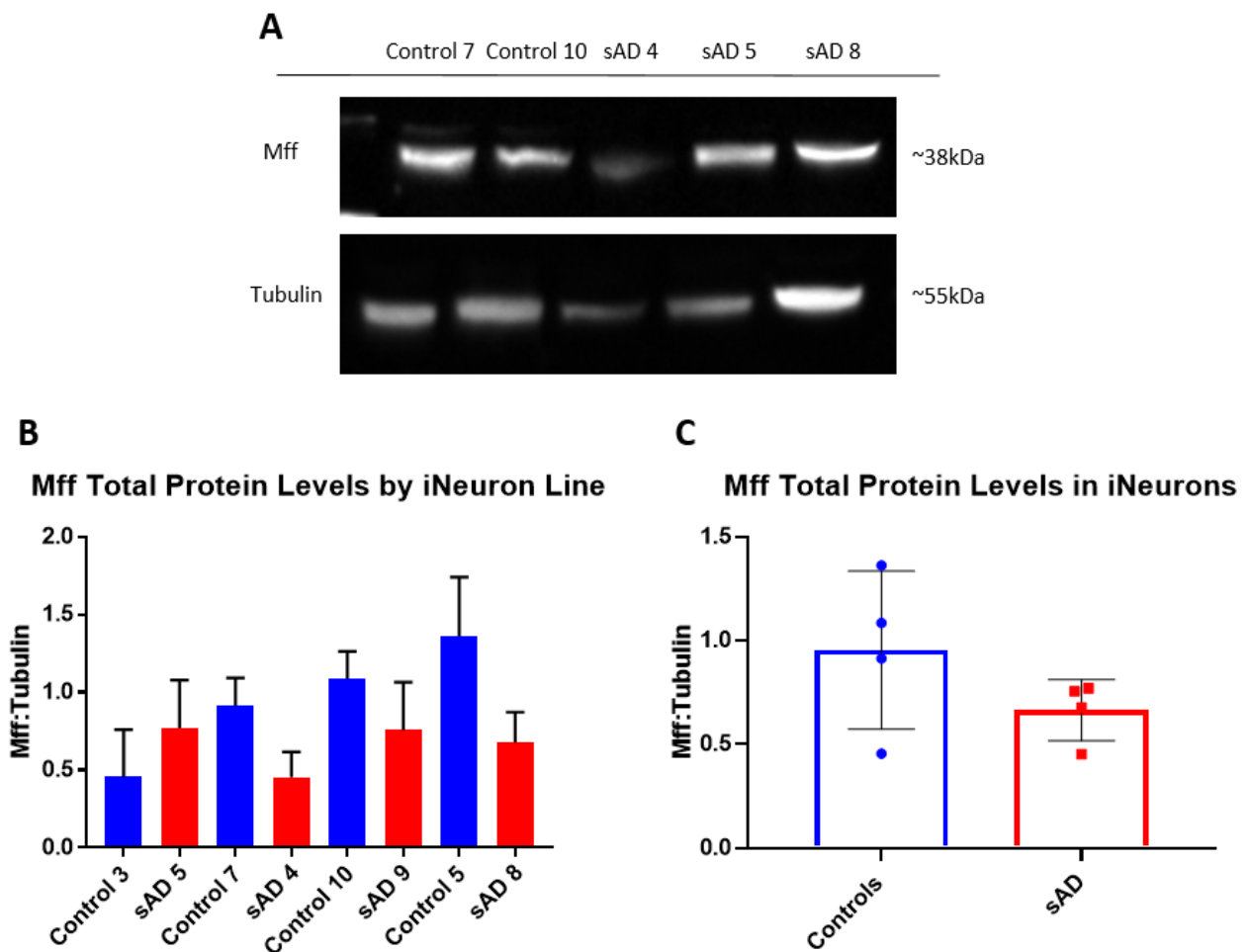
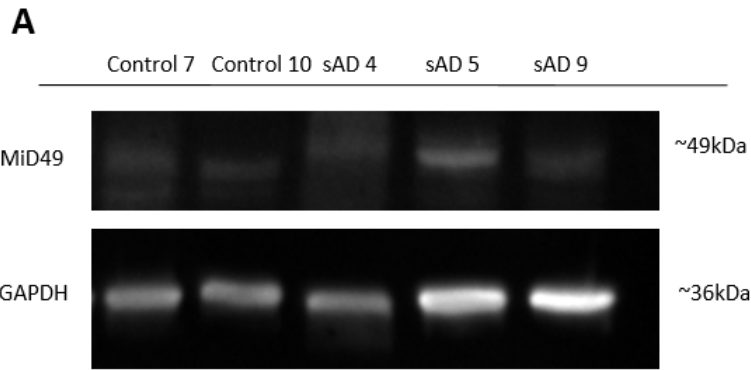
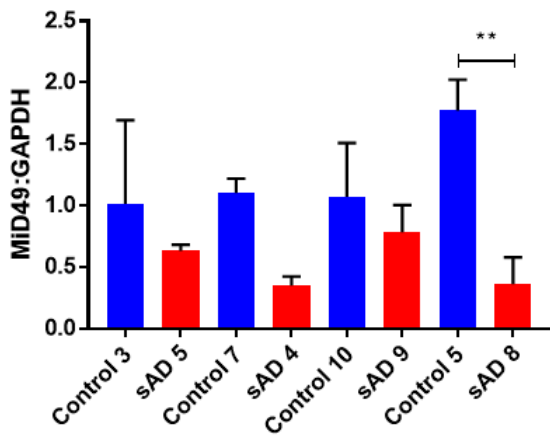


Figure 72: There is no significant different in Mff protein levels in sAD neuron lines compared to controls. A) Representative blot of Mff and Tubulin loading control, in control 7 and 10, and sAD 4, 5, and 8, with 10 μ g protein loaded per lane. B) Quantification of Mff protein levels in four control and sAD pairs. Each line was assessed from samples from two or three separate differentiations. No significant difference was seen in any pair. Bars shown represent the mean and error bars represent SD. C) There is no significant difference when the sAD group is compared to the control group. Each dot represents the mean of the three replicates per line, bars represent the group mean and error bars show SD.



B

MiD49 Total Protein Levels by iNeuron Line



C

MiD49 Total Protein Levels in iNeurons

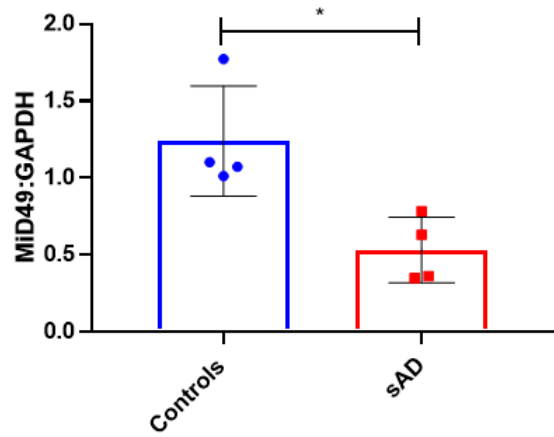


Figure 73: There is a significant decrease in MiD49 protein levels in sAD neurons compared to controls. A) Representative blot of MiD49 and GAPDH loading control, in control 7 and 10, and sAD 4, 5, and 9, with 10 μ g protein loaded per lane. B) Quantification of MiD49 protein levels in four control and sAD pairs. Each line was assessed from samples from two or three separate differentiations. A significant decrease was seen in sAD 8 compared with control 5 (** $p < 0.01$; One way ANOVA with Sidak's multiple comparisons). Bars shown represent the mean and error bars represent SD. C) A significant decrease is seen in grouped sAD lines compared to grouped controls (* $p < 0.05$; t test). Each dot represents the mean of the three replicates per line, bars represent the group mean and error bars show SD.

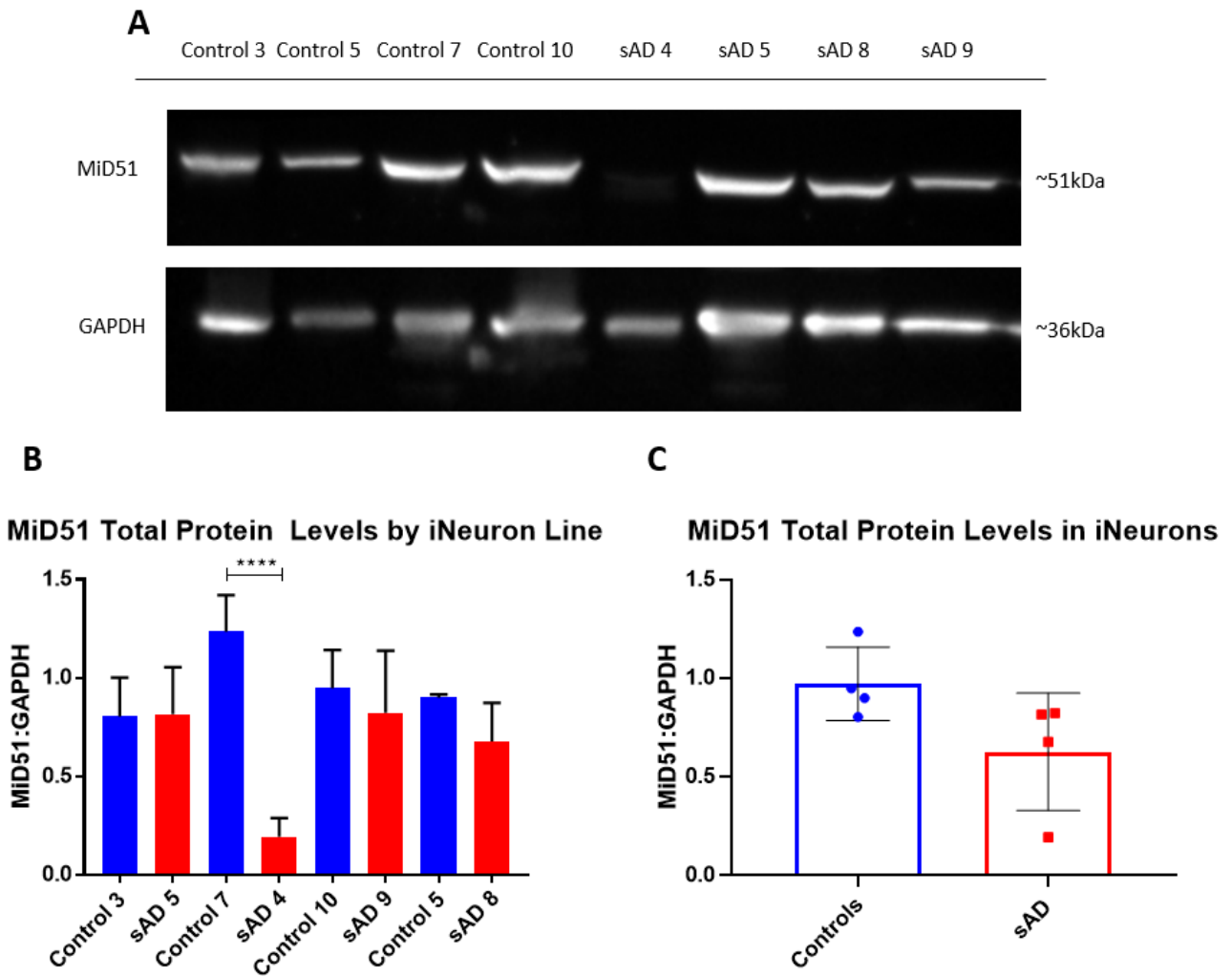


Figure 74: There is a significant decrease in MiD51 levels in one sAD neuron line compared to a paired control. A) Representative blot of MiD51 and GAPDH loading control, in control 3, 5, 7, and 10, and sAD 4, 5, 8, and 9, with 10 μ g protein loaded per lane. B) Quantification of MiD51 protein levels in four control and sAD pairs. Each line was assessed from samples from three separate differentiations. A significant decrease was seen in sAD 4 compared with control 7 (**** $p < 0.0001$; One way ANOVA with Sidak's multiple comparisons). Bars shown represent the mean and error bars represent SD. C) No significant difference is seen at a group level. Each dot represents the mean of the three replicates per line, bars represent the group mean and error bars show SD.

Table 20: Summary table of total protein levels of Drp1 and the four Drp1 receptors on the outer mitochondria membrane, Fis1, Mff, MiD49, and MiD51 in iNeurons. A green arrow represents a significant increase, a red arrow represents a significant decrease and a yellow bar represents no significant difference (** $p < 0.0001$, *** $p < 0.001$, ** $p < 0.01$, * $p < 0.05$). sAD 5 shows alterations in the most proteins, while sAD 9 shows no alterations in any of the proteins assessed.**

	sAD 5	sAD 4	sAD 9	sAD 8
Drp1 Total Protein	**** ↑	▬	▬	▬
Fis1 Total Protein	* ↑	▬	▬	▬
Mff Total Protein	▬	▬	▬	▬
MiD49 Total Protein	▬	▬	▬	** ↓
MiD51 Total Protein	▬	**** ↓	▬	▬

4.2.11 Linear Regression Between Drp1 and Receptors in iNeurons

The linear regression between Drp1 and its receptors was investigated in iNeuron lines. There was no linear regression seen between Drp1 and Fis1 (figure 75a), Drp1 and Mff (figure 75b), Drp1 and MiD49 (figure 75c), or Drp1 and MiD51 (figure 75d).

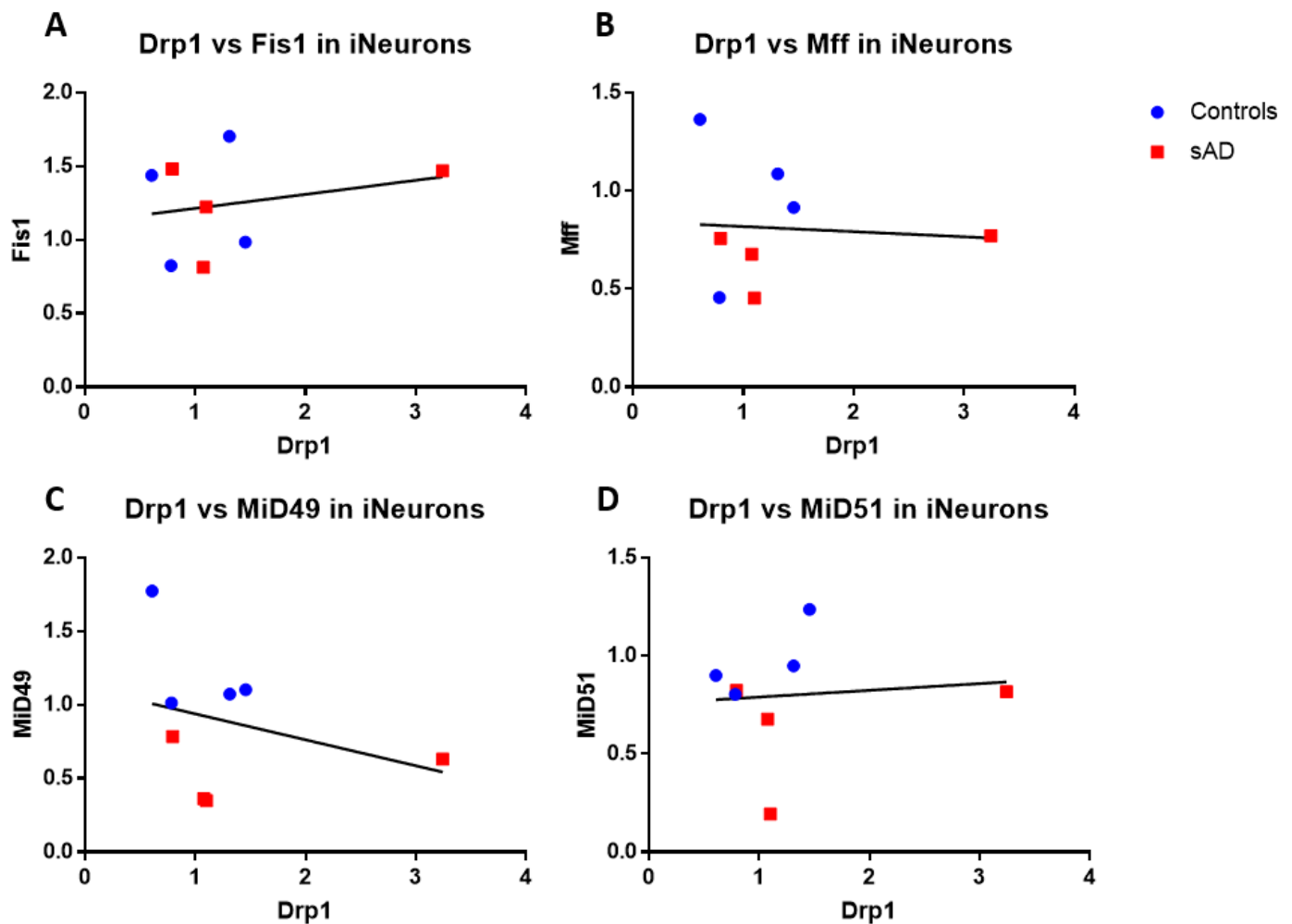


Figure 75: Linear regression between protein levels of Drp1 and protein levels of Fis1, Mff, MiD49 and MiD51, in iNeurons. A) There is no significant linear regression between Drp1 and Fis1 levels. B) There is no significant linear regression between Drp1 and Mff. C) There is no significant linear regression between Drp1 and MiD49. D) There is no significant linear regression between Drp1 and MiD51.

4.2.12 Linear Regression Between Fission Proteins and Mitochondrial Function in iNeurons

To better understand the relationship between mitochondrial fission and function in iNeurons, the linear regression between fission protein expression and MMP was assessed. There was a significant linear regression between Drp1 and MMP ($r^2 = 0.5205$; $p = 0.0434$; figure 76a), whereby higher levels of Drp1 were associated with a lower MMP. This was the opposite of what was seen in the fibroblasts, where a higher level of Drp1 was associated with a higher MMP (Chapter 3, figure 18a). There was no significant linear regression between Fis1 and MMP, Mff and MMP, MiD49 and MMP, or MiD51 and MMP (figure 76b, c, d, e).

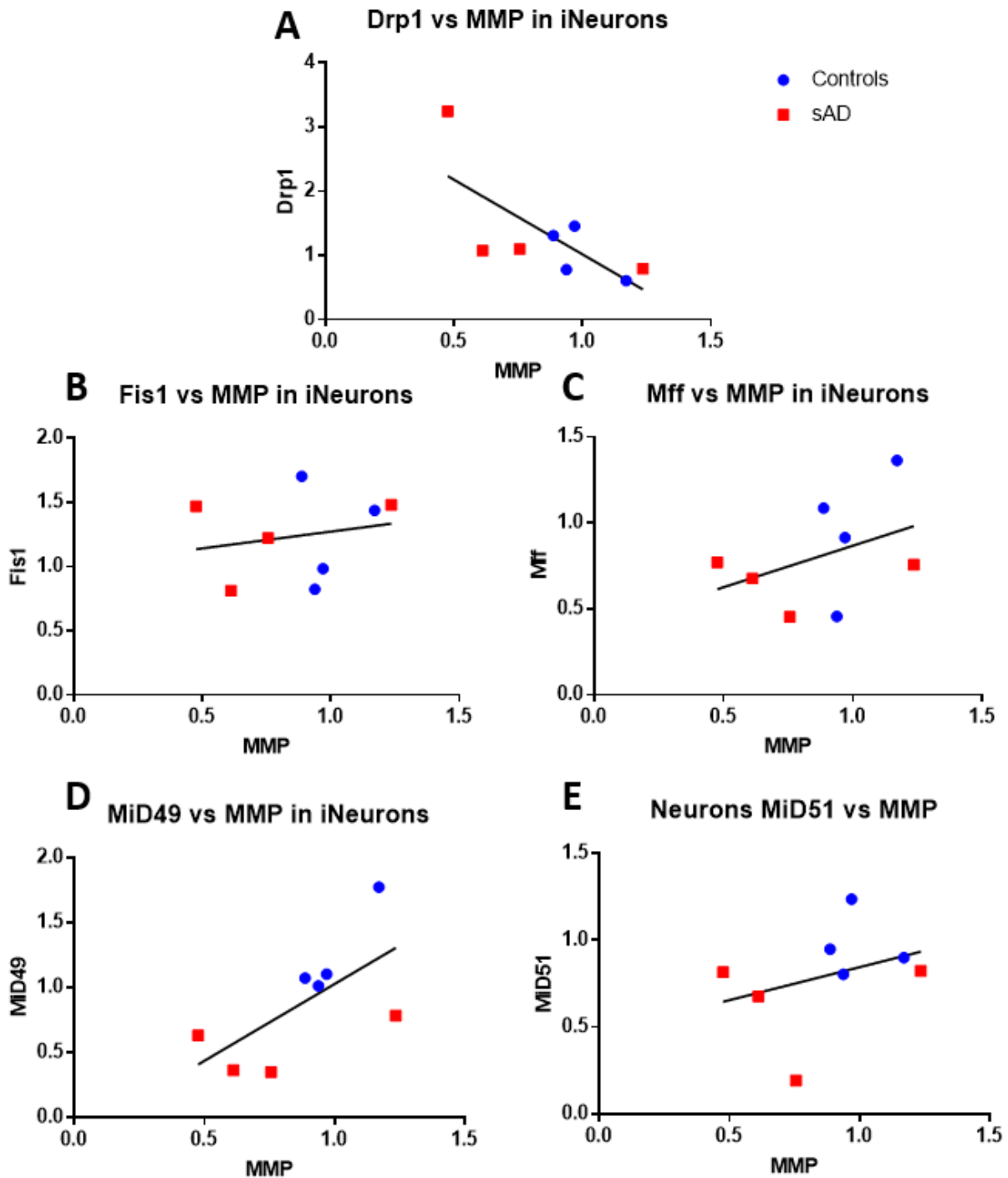


Figure 76: Linear regression between MMP and expression of fission proteins Drp1, Fis1, Mff, MiD49, and MiD51 in iNeurons. A) There is a significant linear regression between MMP and Drp1 ($r^2 = 0.5205$; $p = 0.0434$). B) There is no significant linear regression between MMP and Fis1. C) There is no significant linear regression between MMP and Mff. D) There is no significant linear regression between MiD49 and MMP. E) There is no significant linear regression between MMP and MiD51.

4.2.13 Linear Regression Between Fission Proteins and Mitochondrial Morphology in iNeurons

To further investigate the relationship between fission proteins and mitochondrial morphology, linear regression between Drp1 and the receptors and form factor, a measure of mitochondrial interconnectivity, as well as mitochondrial count per cell normalised to cell area was assessed. There was no significant linear regression seen between Drp1 and form factor, though this was approaching significance ($r^2 = 0.8409$; $p = 0.0830$; figure 77a). There was also no significant linear regression between Drp1 and mitochondrial count, though again this was approaching significance ($r^2 = 0.4502$; $p = 0.0685$; figure 78a). There was no significant linear regression between Fis1 and form factor (figure 77b), or mitochondrial count (figure 78b). There was no significant linear regression between Mff and either form factor or mitochondrial count (figure 77c, 96c). There was a significant linear regression between MiD49 and form factor ($r^2 = 0.6807$; $p = 0.0223$; figure 77d). There was no significant linear regression seen between MiD49 levels and mitochondrial count (figure 78d). There was no significant linear regression between MiD51 and either form factor or mitochondrial count (figure 77e, 96e).

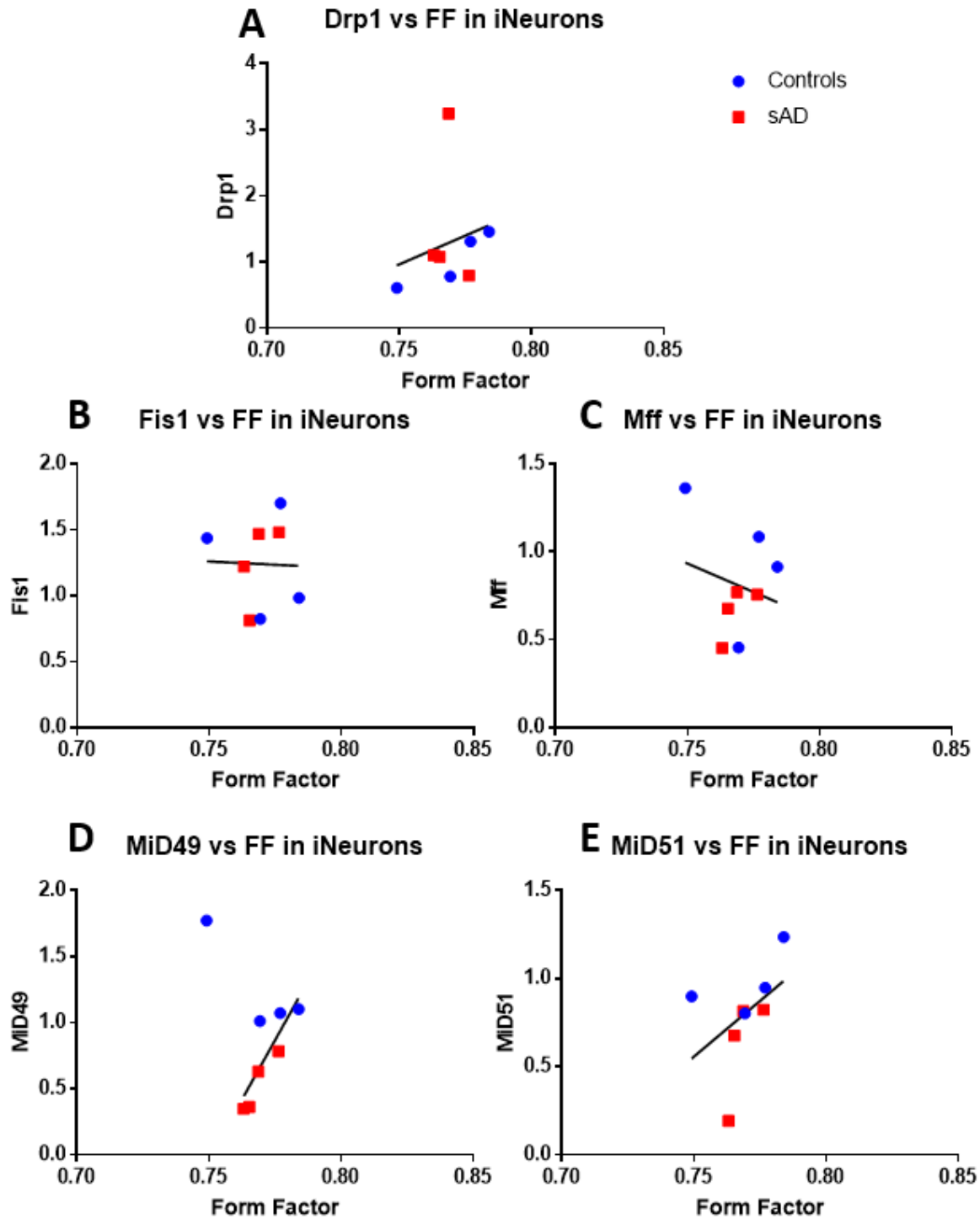


Figure 77: Linear regression between form factor and expression of fission proteins Drp1, Fis1, Mff, MiD49, and MiD51 in iNeurons. A) There is no significant linear regression between form factor and Drp1, though this is approaching significance ($r^2 = 0.8409$; $p = 0.0830$). B) There is no significant linear regression between form factor and Fis1. C) There is no significant linear regression between form factor and Mff. D) There is a significant linear regression between MiD49 and form factor ($r^2 = 0.6807$; $p = 0.0223$). E) There is no significant linear regression between form factor and MiD51.

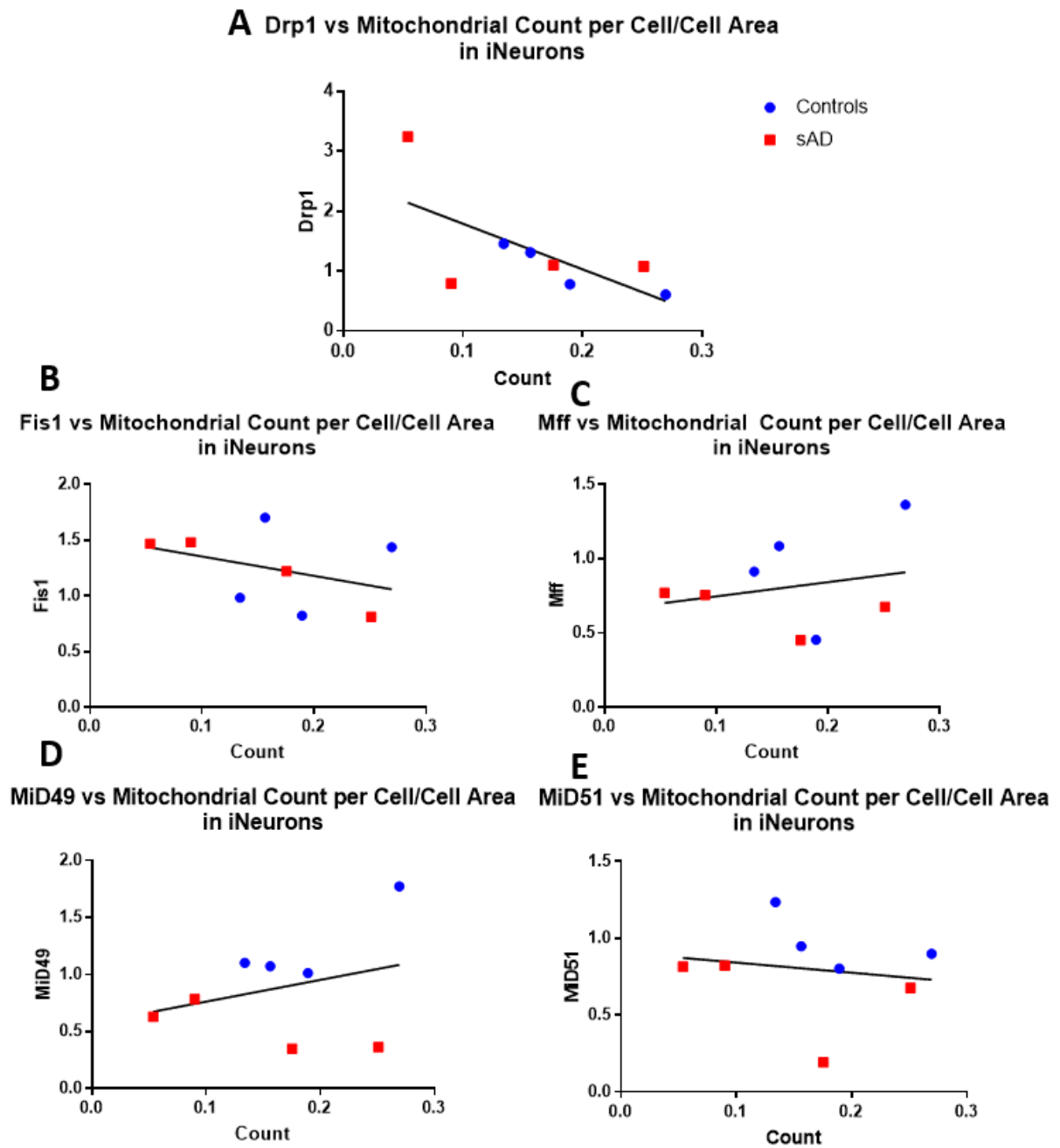


Figure 78: Linear regression between mitochondrial count per cell normalised to cell area and expression of fission proteins Drp1, Fis1, Mff, MiD49, and MiD51 in iNeurons. A) There is no significant linear regression between mitochondrial count and Drp1, though this is approaching significance ($r^2 = 0.4502$; $p = 0.0685$). B) There is no significant linear regression between mitochondrial count and Fis1. C) There is no significant linear regression between mitochondrial count and Mff. D) There is no significant linear regression between MiD49 and mitochondrial count. E) There is no significant linear regression between mitochondrial count and MiD51.

4.2.14 Drp1 and Receptor Expression in iNPCs and iNeurons Compared to Fibroblasts

The alterations in Drp1 and its four receptors Fis1, Mff, MiD49, and MiD51 in iNPCs and iNeurons, were compared to alterations in these proteins seen in the same control and sAD patient fibroblast lines, as assessed in Chapter 2. Table 21 summarises the differences seen in the four sAD lines assessed in all three cell types. Across the three cell types, the most alterations were seen in Drp1 and Fis1, with less cell lines showing differences between sAD and control cells in Mff, MiD49, or MiD51. In general, a greater number of significant differences were seen in fibroblasts, and the least number of significant differences were seen in iNeurons. It is worth noting that the two sAD fibroblast lines which showed the most significant differences compared to controls were unable to be assessed in iNeurons as these lines had not been reprogrammed and so were unavailable as iNPCs.

The direction of the changes was also different between the different cell types. In general, where significant differences were seen in fibroblasts, sAD lines showed reduced expression compared to controls. In contrast, in the neural cell types, iNPCs and iNeurons, there was a mixture of both increased and decreased expression in the five proteins assessed.

Table 21: A summary of total protein levels of Drp1 and the four Drp1 receptors on the outer mitochondria membrane, Fis1, Mff, MiD49, and MiD51 in fibroblasts, iNPCs, and iNeuron. A green arrow represents a significant increase, a red arrow represents a significant decrease and a yellow bar represents no significant difference (** $p < 0.0001$, *** $p < 0.001$, ** $p < 0.01$, * $p < 0.05$). Across the three cell types, the greatest number of alterations were seen in Drp1 and Fis1. In general, a greater number of significant changes were seen in fibroblasts. While sAD fibroblast lines were generally decreased compared to controls when differences were seen, a mixture of increased and decreased expression was seen in iNPCs and iNeurons.**

	Drp1 Total Protein			Fis1 Total Protein			Mff Total Protein			MiD49 Total Protein			MiD51 Total Protein		
	Fibro	iNPC	iNeu	Fibro	iNPC	iNeu	Fibro	iNPC	iNeu	Fibro	iNPC	iNeu	Fibro	iNPC	iNeu
sAD 5	**** ↓	**** ↑	**** ↑	** ↓	** ↓	* ↑	*** ↓	█	█	█	█	█	█	█	█
sAD 4	**** ↓	*** ↑	█	**** ↓	*** ↑	█	█	█	█	█	█	█	█	**** ↑	**** ↓
sAD 9	█	* ↑	█	**** ↓	█	█	**** ↓	█	█	█	█	█	█	█	█
sAD 8	*** ↓	█	█	* ↓	** ↓	█	** ↓	█	█	█	█	** ↓	█	█	█

4.2.15 Fis1 and Mff Localisation in iNeurons

To identify whether changes in total cellular Fis1 and Mff had an impact on their levels at the mitochondria, iNeurons were stained for Fis1 and Mff with mitochondrial marker TOM20. MiD49 and MiD51 were unable to be assessed due to antibody availability. Representative images are shown in figure 79 and figure 81. There were no significant differences seen in the amount of Fis1 localised to the mitochondria at an individual pair level (figure 80a), or a group level (controls 0.01 ± 0.008 , sAD 0.01 ± 0.01 ; $p = 0.7671$; figure 80c). There was also no significant difference in the percentage of total Fis1 localised to the mitochondria at an individual (figure 80a) or group level (controls $32.2\% \pm 7.5$, sAD $30.4\% \pm 8.8$; $p = 0.7634$; figure 80d). sAD 4 showed a decrease in the amount of Fis1 localised to the mitochondria despite showing an increase in total Fis1 protein levels. This is likely due to the reduced percentage of total Fis1 present at the mitochondria. sAD 9 also showed a decrease in Fis1 present at the mitochondria, likely caused by the decrease also seen in total Fis1 levels. sAD 8 showed decreased total Fis1 levels, but was able to compensate for this by increasing the percentage of Fis1 at the mitochondria, and increasing levels to above control levels. sAD 5 showed a significant increase in Fis1 total protein levels, but despite this was not able to bring the amount of Fis1 localised to the mitochondria up to control levels.

A significant decrease in the amount of Mff localised to the mitochondria was seen in sAD 5 compared to control 3 (control 3 0.068 ± 0.02 , sAD 5 0.008 ± 0.008 ; $p = 0.0001$; figure 82a) despite sAD 5 showing an increase in total protein levels. The percentage of total Mff localised to the mitochondria is decreased (figure 82b) which may explain the reduction seen in the amount of Mff at the mitochondria. sAD 4 and sAD 9 both showed a decrease in Mff at the mitochondria (figure 82a), which is likely a result of the reduced total levels seen. sAD 8 also showed a decrease in total Mff protein levels, but was able to compensate for this by increasing the percentage of total Mff at the mitochondria (figure 82b). There is no significant difference in the amount of Mff localised to the mitochondria (controls 0.020 ± 0.02 , sAD 0.016 ± 0.01 ; $p = 0.7724$; figure 82c) or the percentage of total Mff at the mitochondria at a group level (controls $28\% \pm 10.3$, sAD $22.1\% \pm 6.3$; $p = 0.3622$; figure 82d).

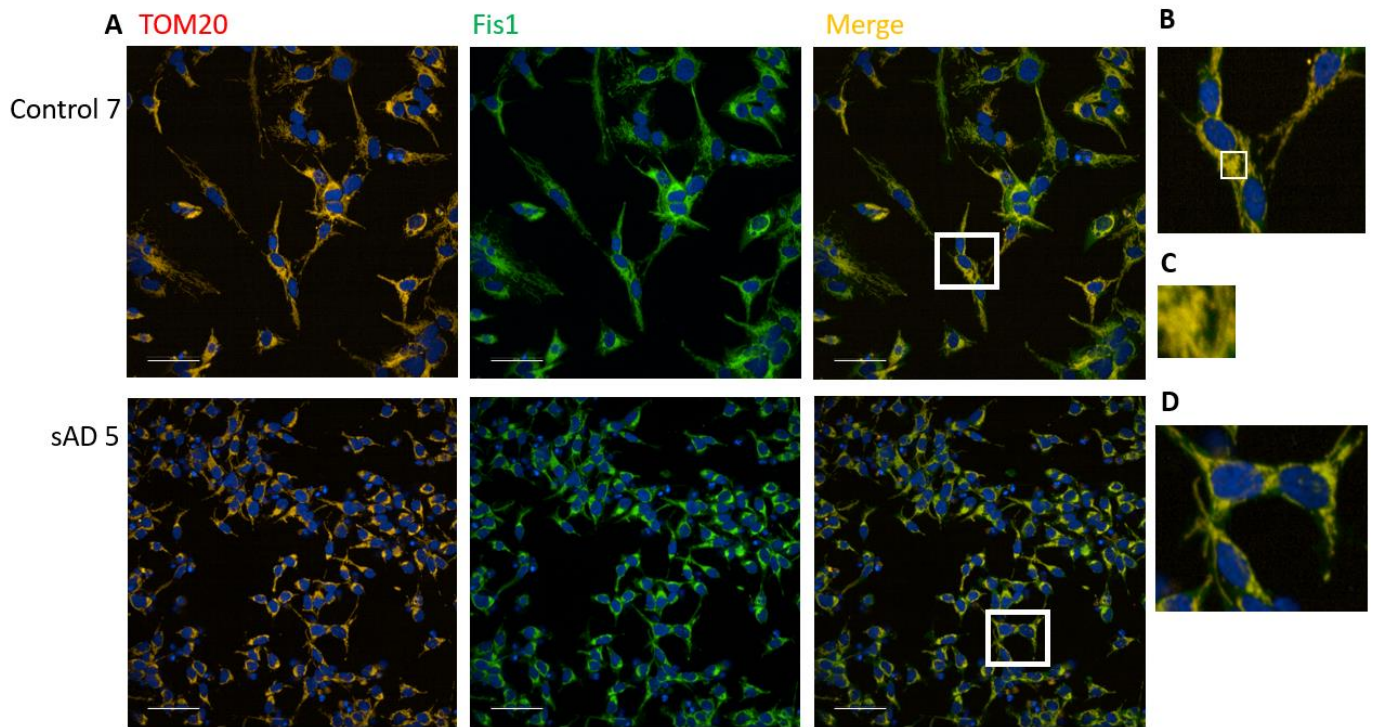


Figure 79: Representative Images of Fis1-TOM20 co-localisation in control and sAD patient iNeurons. A) Representative images of Fis1 and TOM20 co-localisation staining. TOM20 is shown in red, Fis1 in green, and nuclei in blue. Scale = 50 μ m. B) Zoomed in image of Fis1-TOM20 co-localisation in control iNeurons, showing the area in the white box. C) Further zoomed in image of the white box shown in B, to demonstrate co-localisation of Fis1 and TOM20. D) Zoomed in image of Fis1-TOM20 co-localisation in sAD iNeurons, showing the area in the white box.

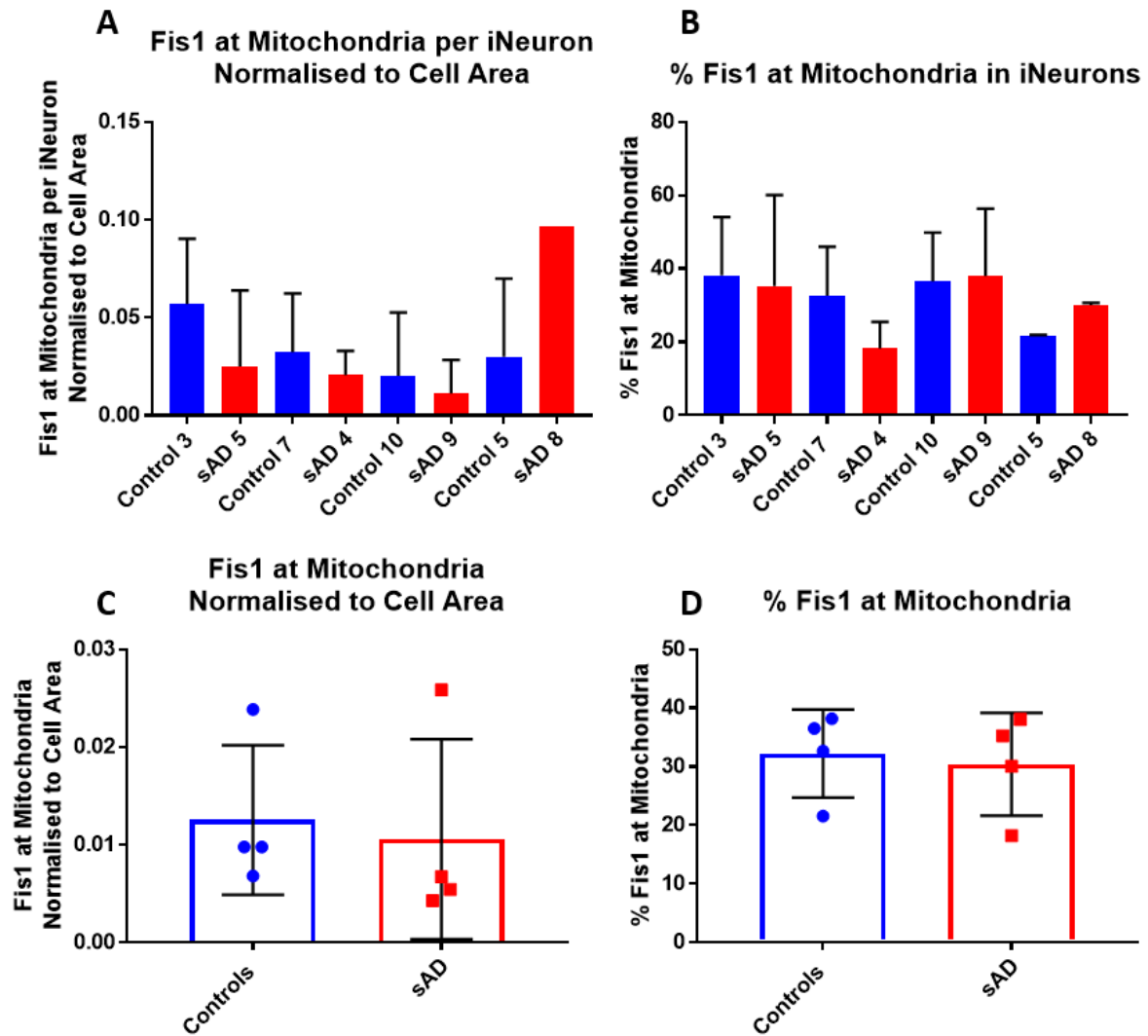


Figure 80: There is no significant difference in the amount of Fis1 co-localised to the mitochondria in *iNeurons*, $n = 3$. A) Quantification of Fis1 co-localisation with mitochondrial marker TOM20. There is no significant difference between any sAD and control pair. B) Quantification of the percentage of total Fis1 which is localised to the mitochondria. There is no significant difference between any control and sAD pair. C) There is no significant difference in Fis1 localised to the mitochondria between sAD and control *iNeurons* when individual lines are combined D) There is no significant difference in the percentage of total Fis1 localised to the mitochondria when individual lines are combined.

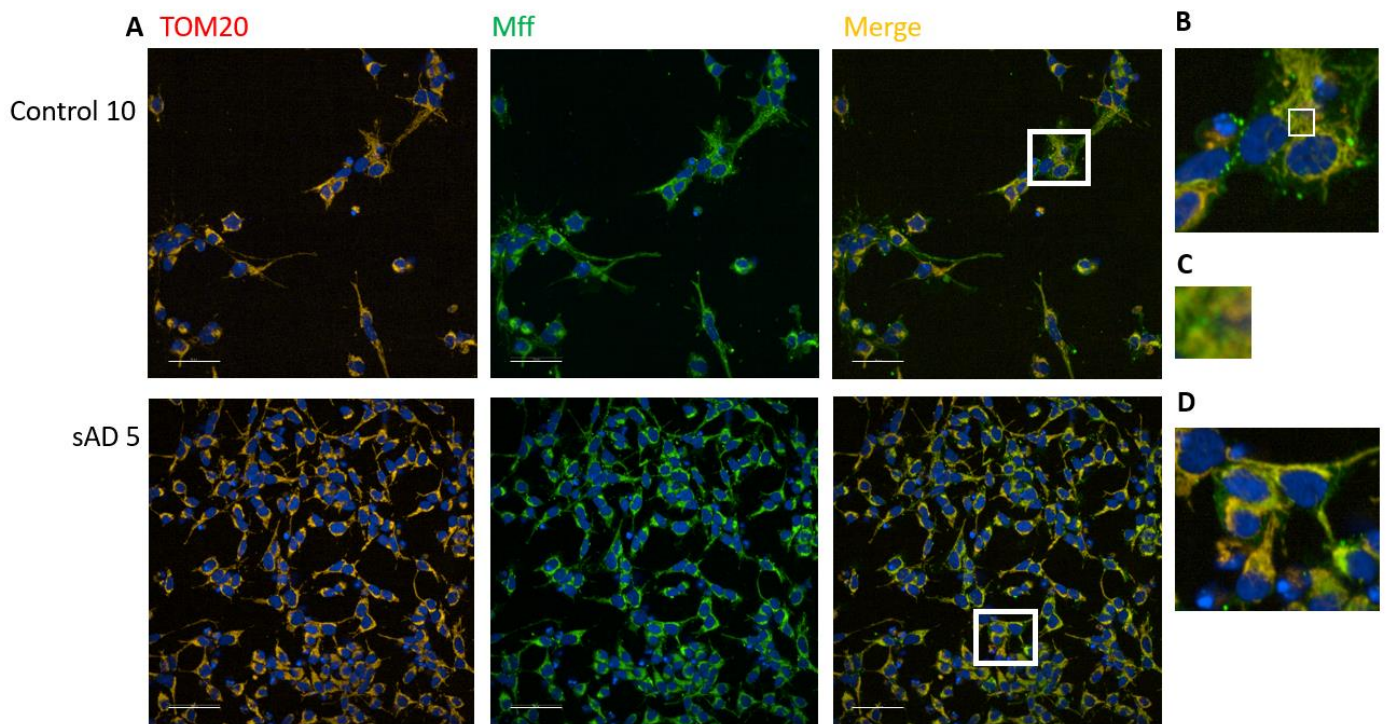


Figure 81: Representative Images of Mff-TOM20 co-localisation in control and sAD patient iNeurons. A) Representative images of Mff and TOM20 co-localisation staining. TOM20 is shown in red, Mff in green, and nuclei in blue. Scale = 50 μ m. B) Zoomed in image of Mff-TOM20 co-localisation in control iNeurons, showing the area in the white box. C) Further zoomed in image of the white box shown in B, to demonstrate co-localisation of Mff and TOM20. D) Zoomed in image of Mff-TOM20 co-localisation in sAD iNeurons, showing the area in the white box.

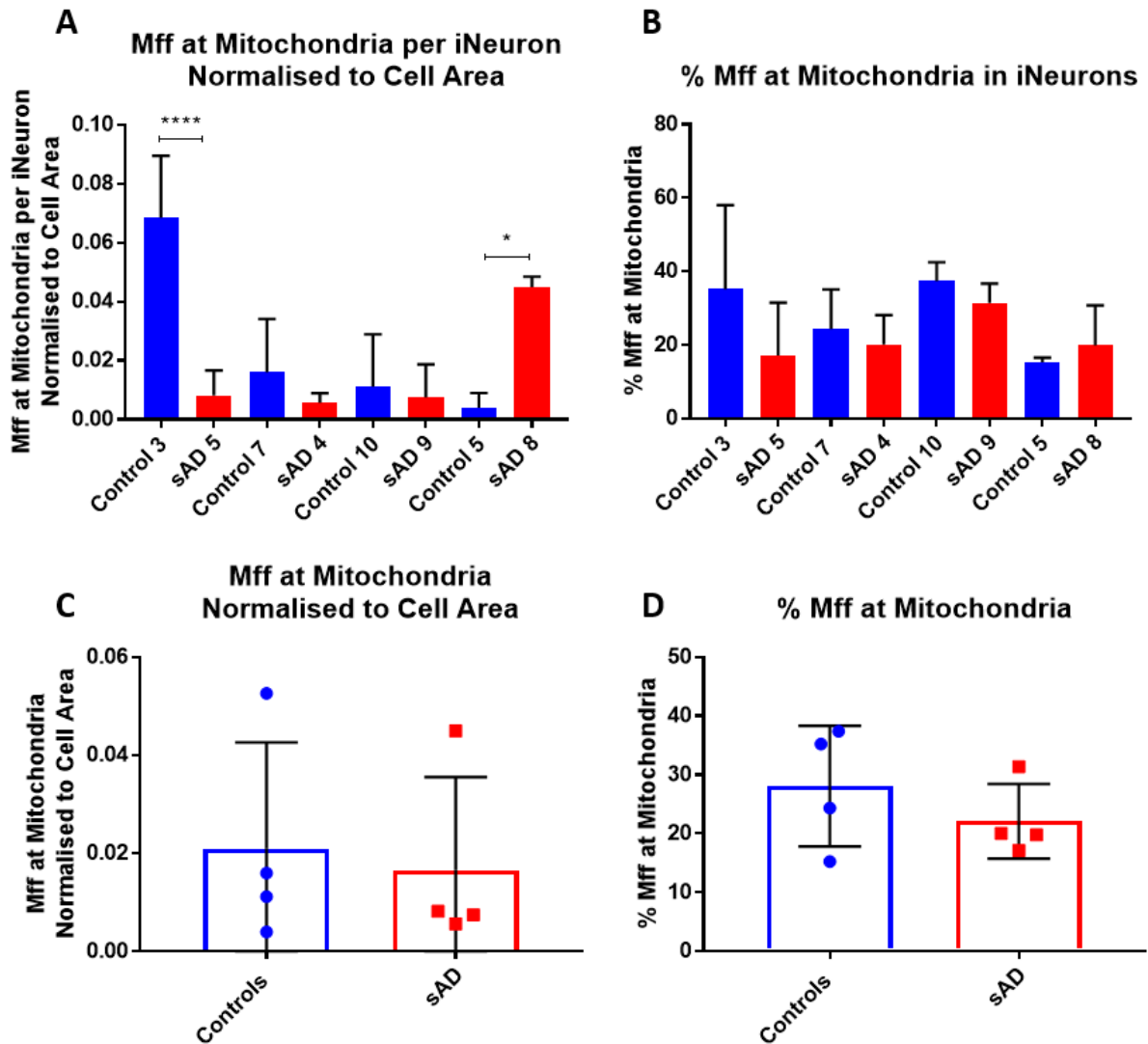


Figure 82: There is a significant increase in the amount of Mff co-localised to the mitochondria in iNeurons in one sAD line and a significant decrease in another line, $n = 3$. A) Quantification of Mff co-localisation with mitochondrial marker TOM20. There is a significant decrease in sAD 5 compared to control 3, and a significant increase in sAD 8 compared to control 5 (**** $p < 0.0001$, * $p < 0.05$; One way ANOVA with Sidak's multiple comparisons). B) Quantification of the percentage of total Mff which is localised to the mitochondria. There is no significant difference between any control and sAD pair. B) There is no significant difference in Mff localised to the mitochondria between sAD and control iNeurons when individual lines are combined. D) There is no significant difference in the percentage of total Mff localised to the mitochondria when individual lines are combined.

4.2.16 Fis1 and Mff Interactions with Drp1 in iNeurons

To investigate whether the number of interactions between Drp1 and Fis1, and Drp1 and Mff were changed, the proximity ligation assay was used as previously described. Representative images are shown in figure 83. There were no significant differences in Drp1 interactions with Fis1 in any of the neuron pairs, though there was a lot of variability. There is a decrease in sAD 5 compared to control 3 (control 3 9.6 ± 1.3 , sAD 5 4.7 ± 3.5 ; figure 84a), as well as in sAD 9 compared to control 10 (control 10 3.6 ± 1.01 , sAD 9 1.81 ± 1.1 ; $p = 0.103$; figure 84a) and sAD 8 compared to control 5 (control 5 3.9 ± 1.9 , sAD 8 2.8 ± 1.8 ; figure 84a). In contrast, there is an increase in sAD 4 compared to control 7 (control 7 4.8 ± 3.6 , sAD 4 3.4 ± 1.9 ; $p = 0.991$; figure 84a). When all lines are combined, there is no significant difference between control and sAD lines (controls 4.88 ± 3.2 , sAD 3.2 ± 1.2 ; $p = 0.367$; figure 84c). Specifically in the perinuclear region, there was a significant decrease in the number of interactions between Drp1 and Fis1 between control 3 and sAD 5 (control 3 4.4 ± 1.7 , sAD 5 0.50 ± 0.19 ; $p = 0.0008$; figure 84b), however, this is likely due to the increased number of interactions seen in control 3 compared to other controls. There is no significant difference in any other pair, though there is an increase in sAD 4 compared to control 7 (control 7 0.92 ± 0.60 , sAD 4 1.76 ± 0.80 ; $p = 0.979$; figure 84b), and sAD 8 compared to control 5 (control 5 0.87 ± 0.58 , sAD 8 1.23 ± 0.77 ; $p = 0.825$; figure 84b). When all lines were combined, there was no significant difference seen between control and sAD lines (figure 84c-d).

There was a significant decrease in Drp1 interactions with Mff in sAD 5, when compared to control 3 (control 3 11.06 ± 3.73 ; $p = 0.005$; figure 85a). There was also a decrease in sAD 9 compared to control 10 (control 10 5.24 ± 2.7 , sAD 9 1.48 ± 0.71 ; $p = 0.730$; figure 85a). When all lines were combined, there was no significant difference between control and sAD lines, though there was a decrease (controls 5.71 ± 3.74 , sAD 3.01 ± 1.09 ; $p = 0.214$; figure 85c). In the perinuclear region, there was a significant decrease in sAD 5 compared to control 3 (control 3 3.7 ± 1.43 , sAD 5 0.48 ± 0.12 ; $p = 0.0001$; figure 85b), as well as in sAD 9 compared to control 10 (control 10 3.44 ± 0.36 , sAD 9 0.63 ± 0.3 ; $p = 0.004$; figure 85b). This is likely due to the decreased interactions in the cell as a whole. When all lines were combined, there was no significant difference between control and sAD lines in the perinuclear region (controls 2.47 ± 1.39 , sAD 1.31 ± 0.88 ; $p = 0.211$; figure 85d). When comparing the number of Drp1 interactions with Fis1 to the number of Drp1 interactions with Mff, there was no significant difference in either the whole cell or the perinuclear region (figure 86a-b).

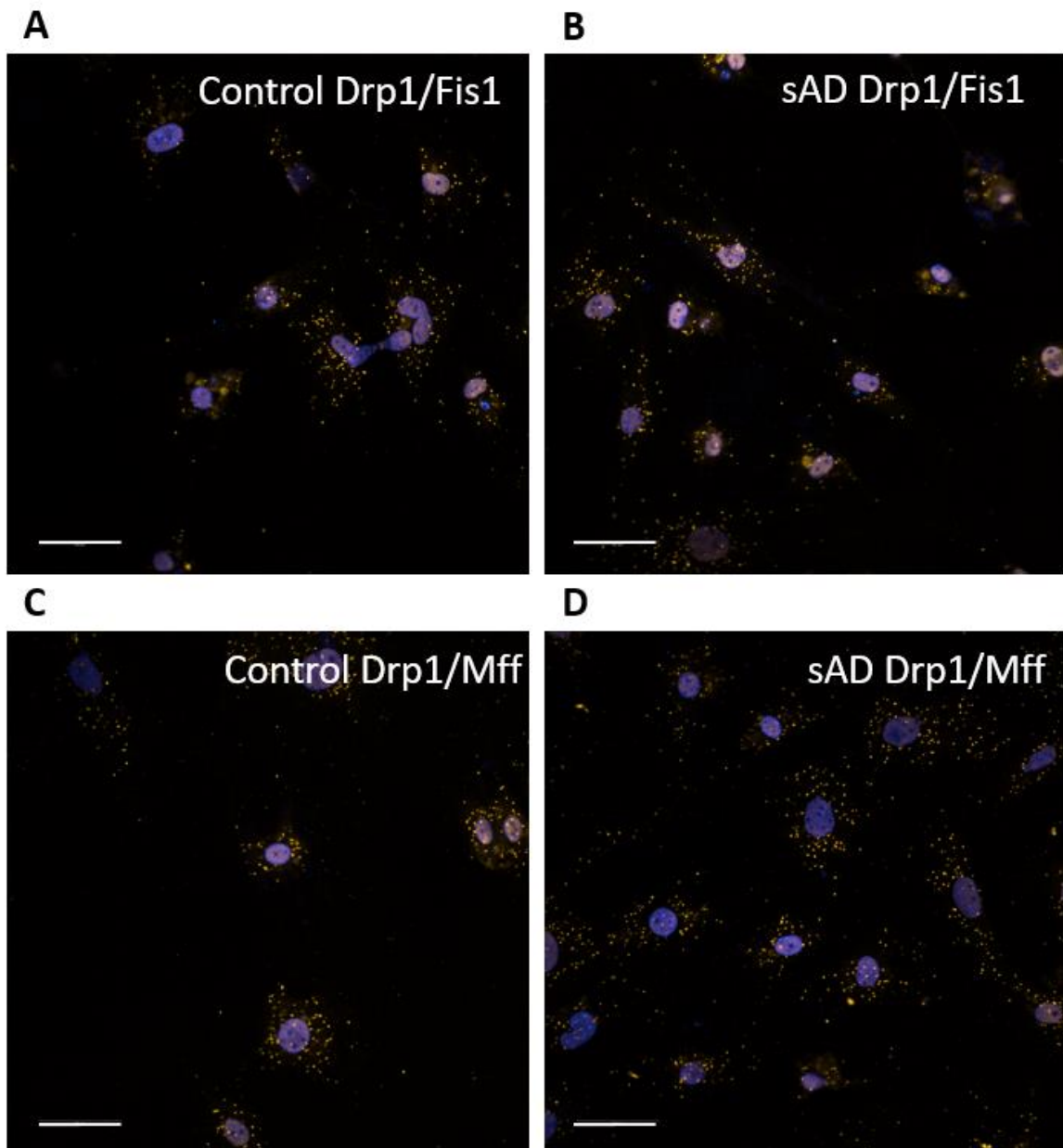


Figure 83: Representative image of Drp1 and Fis1, and Drp1 and Mff interactions in control and sAD iNeurons. Scale bar = 50 μ M. A) Representative image of Drp1 and Fis1 interactions in control iNeurons - each orange dot represents a single interaction. B) Representative image of Drp1 and Fis1 interactions in sAD iNeurons. C) Representative image of Drp1 and Mff interactions in control iNeurons. D) Representative image of Drp1 and Mff interactions in sAD iNeurons.

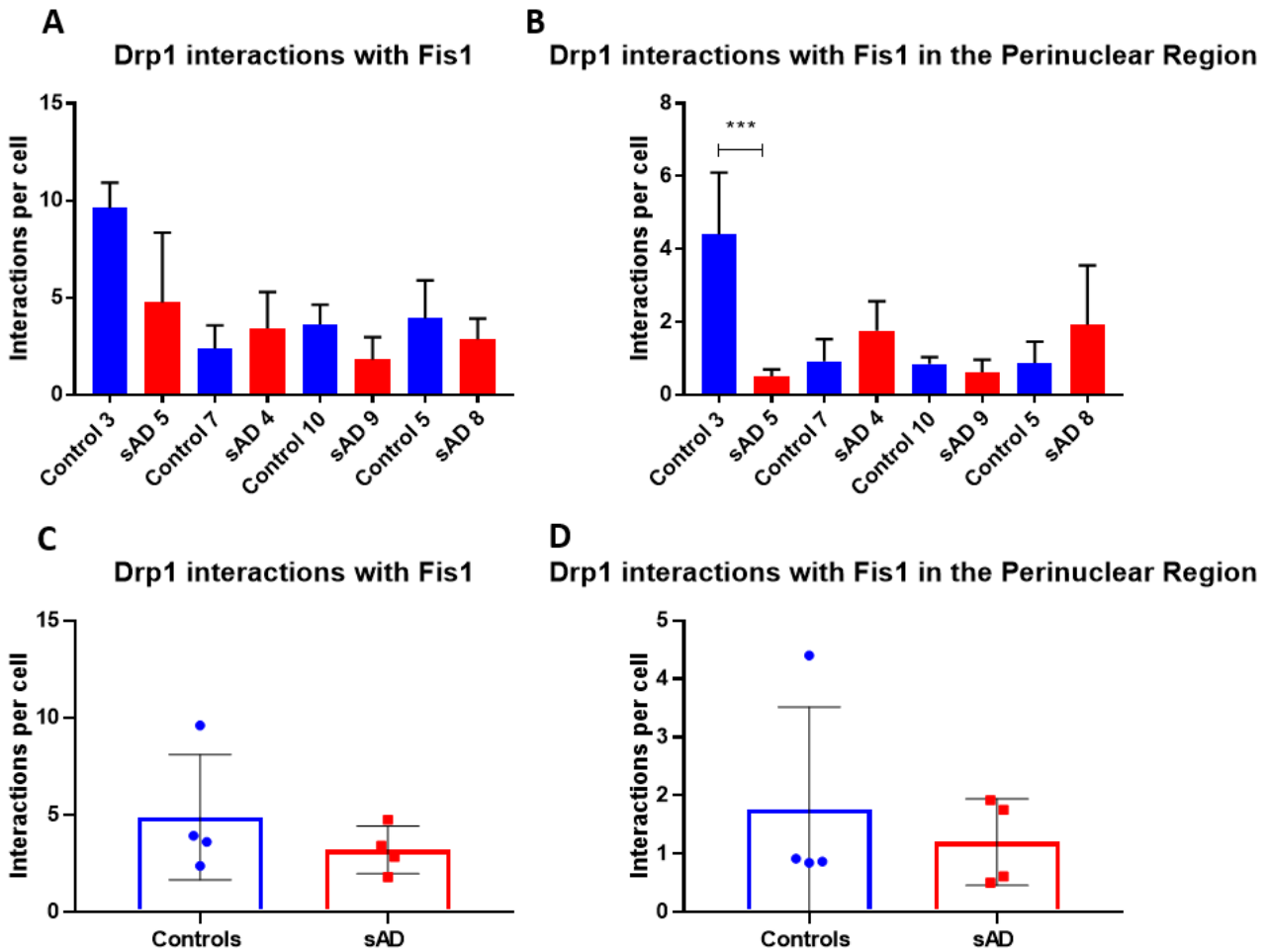


Figure 84: There is no significant difference in interactions between Drp1 and Fis1 in the whole cell or in the perinuclear region. For C-D, each dot represents the average of all biological repeats for one cell line. Error bars represent SD. A) There is no significant difference in individual paired lines in the number of interactions between Drp1 and Fis1. B) There is a significant decrease in the number of interactions between Drp1 and Fis1 in the perinuclear region in sAD 5 compared to control 3 ($*p > 0.001$; One way ANOVA with Sidak's multiple comparisons). There is no significant difference in any other pair. C) There is no significant difference in Drp1 interactions with Fis1 when all control and sAD lines are combined. D) There is no significant difference in Drp1 interactions with Fis1 in the perinuclear region when all control and sAD lines are combined.

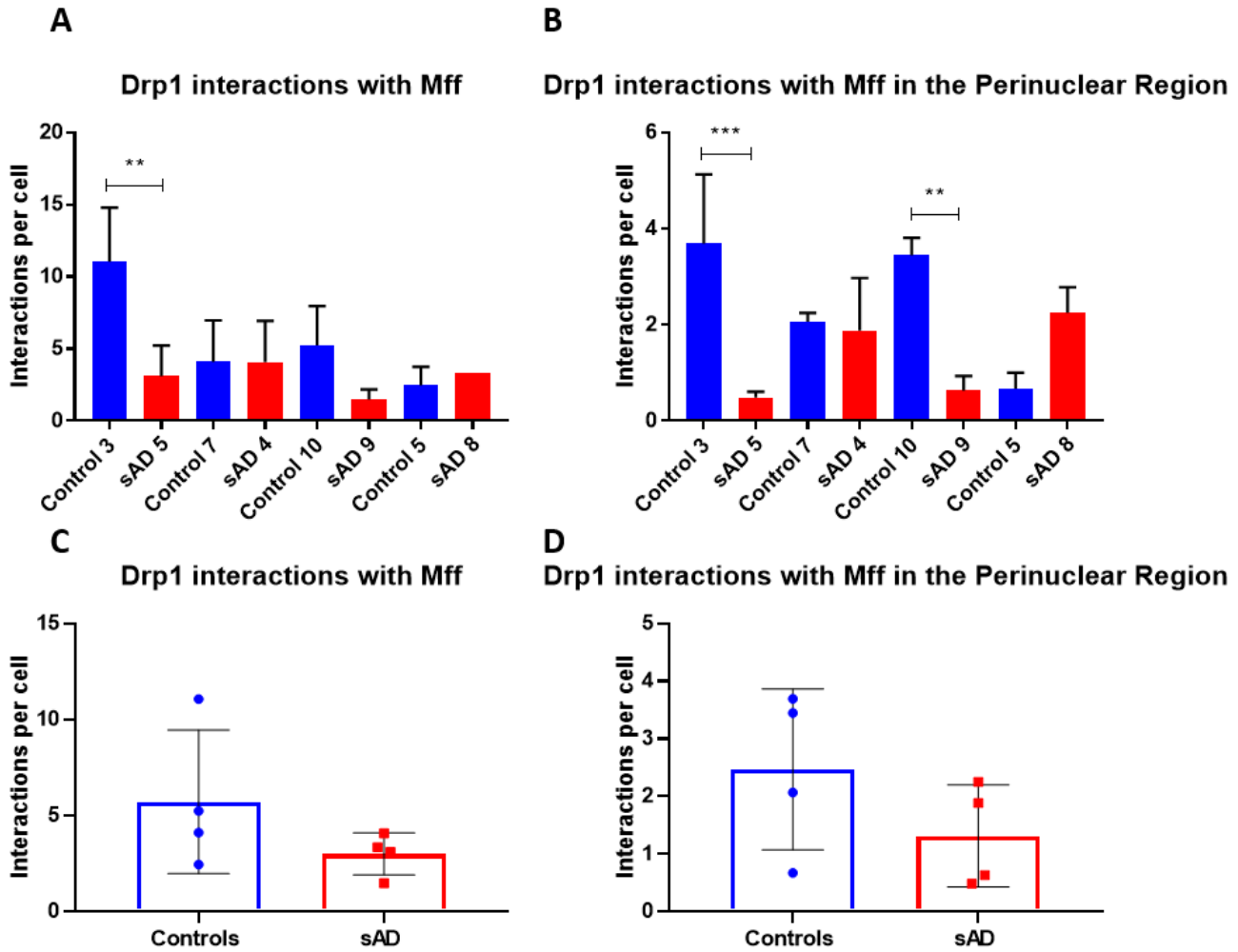


Figure 85: There is no significant difference in interactions between Drp1 and Mff in the whole cell or in the perinuclear region. For C-D, each dot represents the average of all biological repeats for one cell line. Errors bars represent SD. A) There is a significant difference in the number of interactions between Drp1 and Mff between control 3 and sAD 5 (** $p < 0.01$; One way ANOVA with Sidak's multiple comparisons), but no difference in other pairs. B) There is a significant decrease in the number of interactions between Drp1 and Mff in the perinuclear region in sAD 5 compared to control 3, and in sAD 9 compared to control 10 (** $p < 0.01$ *** $p > 0.001$; One way ANOVA with Sidak's multiple comparisons). There is no significant difference in any other pair. C) There is no significant difference in Drp1 interactions with Mff when all control and sAD lines are combined. D) There is no significant difference in Drp1 interactions with Mff in the perinuclear region when all control and sAD lines are combined.

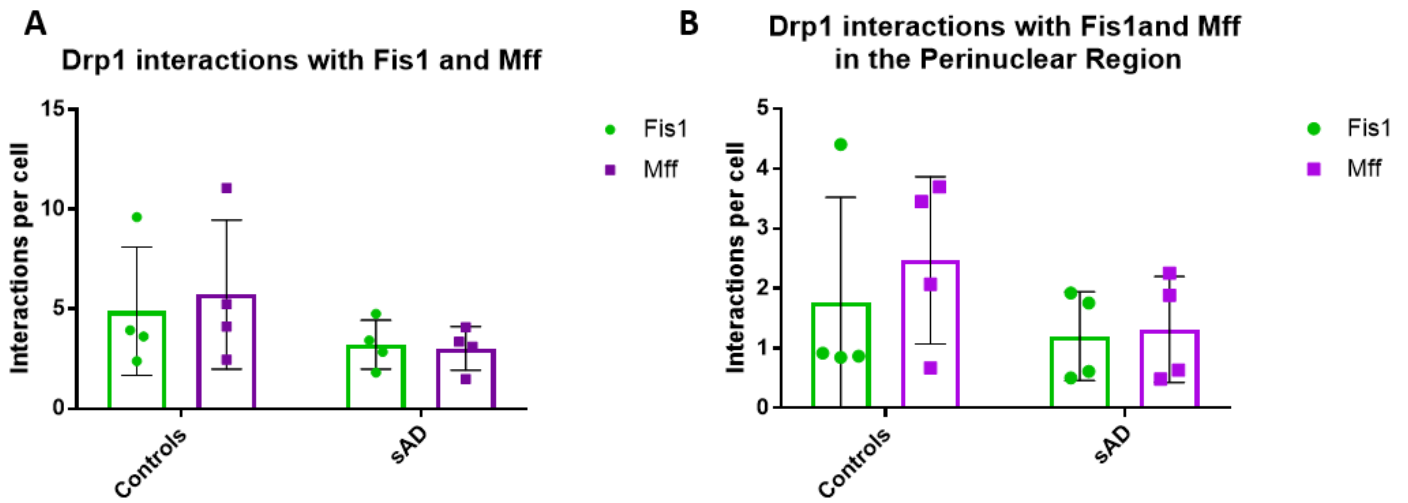


Figure 86: *There is no significant difference in the number of interactions between Drp1 and Fis1, and the number of interactions between Drp1 and Mff, in the whole cell or the perinuclear region. Each dot represents the average of all biological repeats for one cell line. Errors bars represent SD. A) There is no significant difference in the number of interactions between Drp1 and Fis1, and Drp1 and Mff in the whole cell. B) There is no significant difference in the number of interactions between Drp1 and Fis1, and Drp1 and Mff in the perinuclear region.*

4.2.17 Phosphorylation Status of Drp1 in iNPCs and iNeurons

The phosphorylation status of Drp1 is a key factor in the fission process. Unfortunately, it proved difficult to assess this in the fibroblast system, but it was possible in the iNeuron model. The expression of Drp1 phosphorylated at serine 616, which is required to initiate fission, and Drp1 phosphorylated at serine 637 which inhibits fission were assessed in iNeurons. The expression of Drp1 phosphorylated at serine 616 was also assessed in iNPCs. In iNPCs, there was a significant decrease of 80.6% in the expression of phosphorylated Drp1 (ser616) in sAD 9 compared to control 10 (control 10 1.4 ± 0.4 ; $p = 0.014$; figure 87b). In contrast, there was a significant increase of 134% in sAD 8 compared to control 5 (control 5 0.01 ± 0.3 , sAD 8 2.4 ± 0.14 ; $p = 0.003$; figure 87b). There was also an increase of 82.1% in sAD 4 compared to control 7, though only one repeat of sAD 4 could be obtained (control 7 0.8 ± 0.3 , sAD 4 1.5 ; figure 87b). When control and sAD lines were grouped, there was no significant difference seen (controls 1.0 ± 0.3 , sAD 1.17 ± 0.96 ; $p = 0.751$; figure 87c).

In iNeurons, there were no significant differences in levels of phosphorylated Drp1 (ser616) seen between any individual pair. However, there was a decrease of 57.4% in sAD 5 compared to control 3 (control 3 2.3 , sAD 5 0.98 ± 0.7 ; figure 88b), though only one repeat of control 3 could be obtained. There was also a decrease of 29.5% in sAD 4 compared to control 7 (control 7 1.4 ± 0.6 , sAD 4 1.0 ± 0.5 ; $p = 0.743$; figure 88b). There was an increase in sAD 9 compared to control 10 (control 10 0.76 ± 0.6 , sAD 9 1.02 ± 0.6 ; $p = 0.957$; figure 88b). At a group level, there was no significant difference seen in phosphorylated Drp1 (ser616) protein levels between control and sAD iNeurons (controls 1.2 ± 0.9 , sAD 0.87 ± 0.3 ; $p = 0.489$; figure 88c).

Phosphorylated Drp1 (ser637) protein levels were assessed in only three control (7, 10, and 5) and three sAD (4, 9, and 5) lines. In this case, control 5 and sAD 5 were paired. There was a significant decrease of 73.7% seen in phosphorylated Drp1 (ser637) in sAD 4 compared to control 7 (control 7 1.4 ± 0.5 , sAD 4 0.36 ± 0.2 ; $p = 0.014$; figure 89b). No other differences were seen. At a group level, no significant difference was seen between sAD and control lines (controls 0.95 ± 0.5 , sAD 0.56 ± 0.3 ; $p = 0.281$; figure 89c).

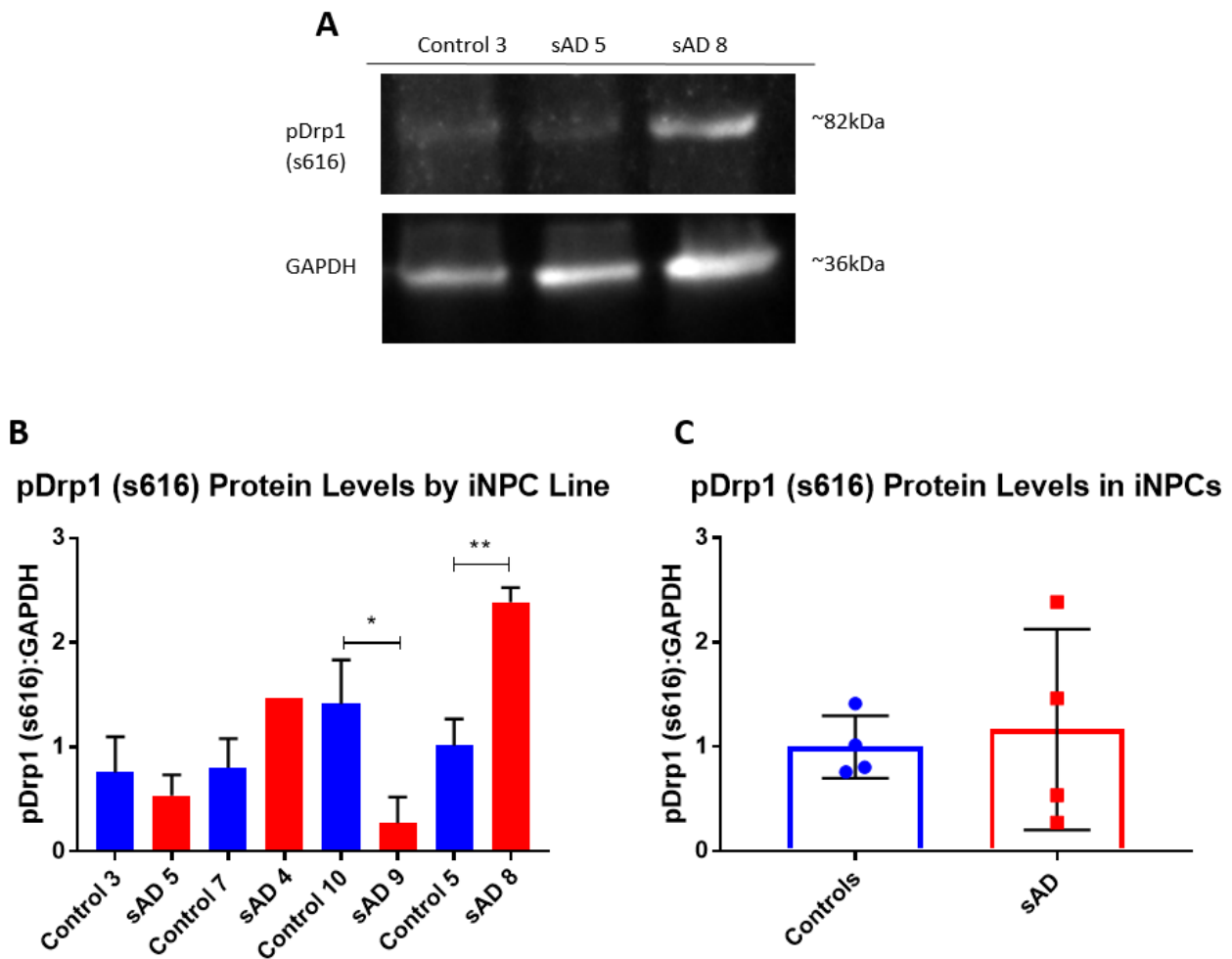


Figure 87: There is a significant decrease in pDrp1(s616) protein levels in one sAD iNPC line, and a significant increase in another when compared to paired controls. A) Representative blot of pDrp1(s616) and GAPDH loading control, in control 3, sAD 5 and sAD 8, with 10 μ g protein loaded per lane. B) Quantification of pDrp1(s616) levels in four control and four sAD pairs. There is a significant decrease seen in sAD 9 compared to control 10, and a significant increase in sAD 8 compared to control 5 (** $p < 0.01$, * $p < 0.05$; One way ANOVA with Sidak's multiple comparisons). Each line was assessed at two difference passages. C) No significant difference was seen at a group level. Each dot represents the mean of the two replicates per line, bars represent the group mean and error bars show SD ($p = 0.751$; t test).

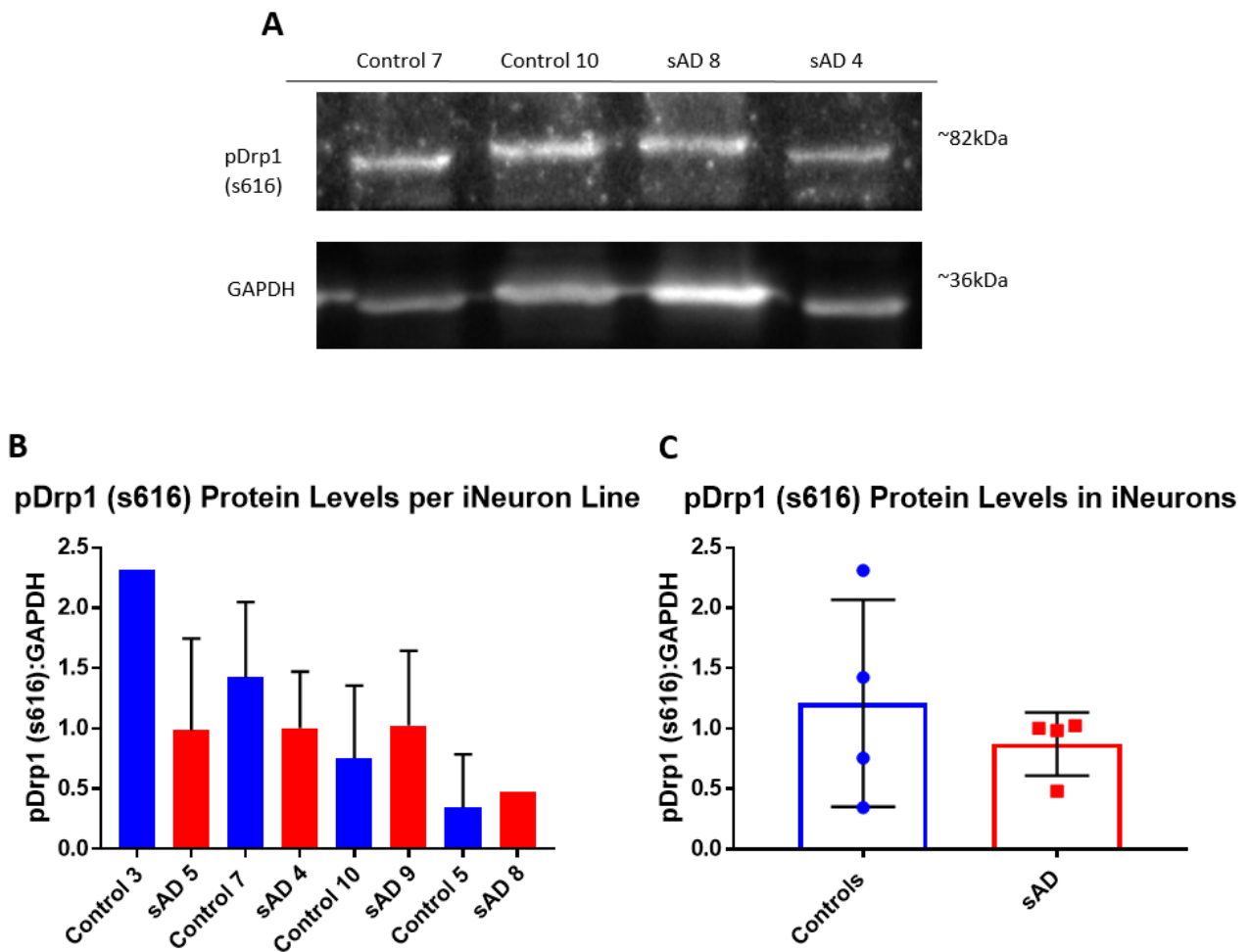


Figure 88: There is no significant difference in pDrp1(s616) protein levels between control and sAD iNeurons, at an individual or a group level. A) Representative blot of pDrp1(s616) and GAPDH loading control, in control 7, control 10, sAD 8 and sAD 4, with 10 μ g protein loaded per lane. B) Quantification of pDrp1(s616) levels in four control and four sAD pairs. There is no significant difference in any pair. Each line was assessed at three difference passages, except for control 3 and sAD 8 which were assessed at a single passage. C) No significant difference was seen at a group level. Each dot represents the mean of the two replicates per line, bars represent the group mean and error bars show SD ($p = 0.489$; t test).

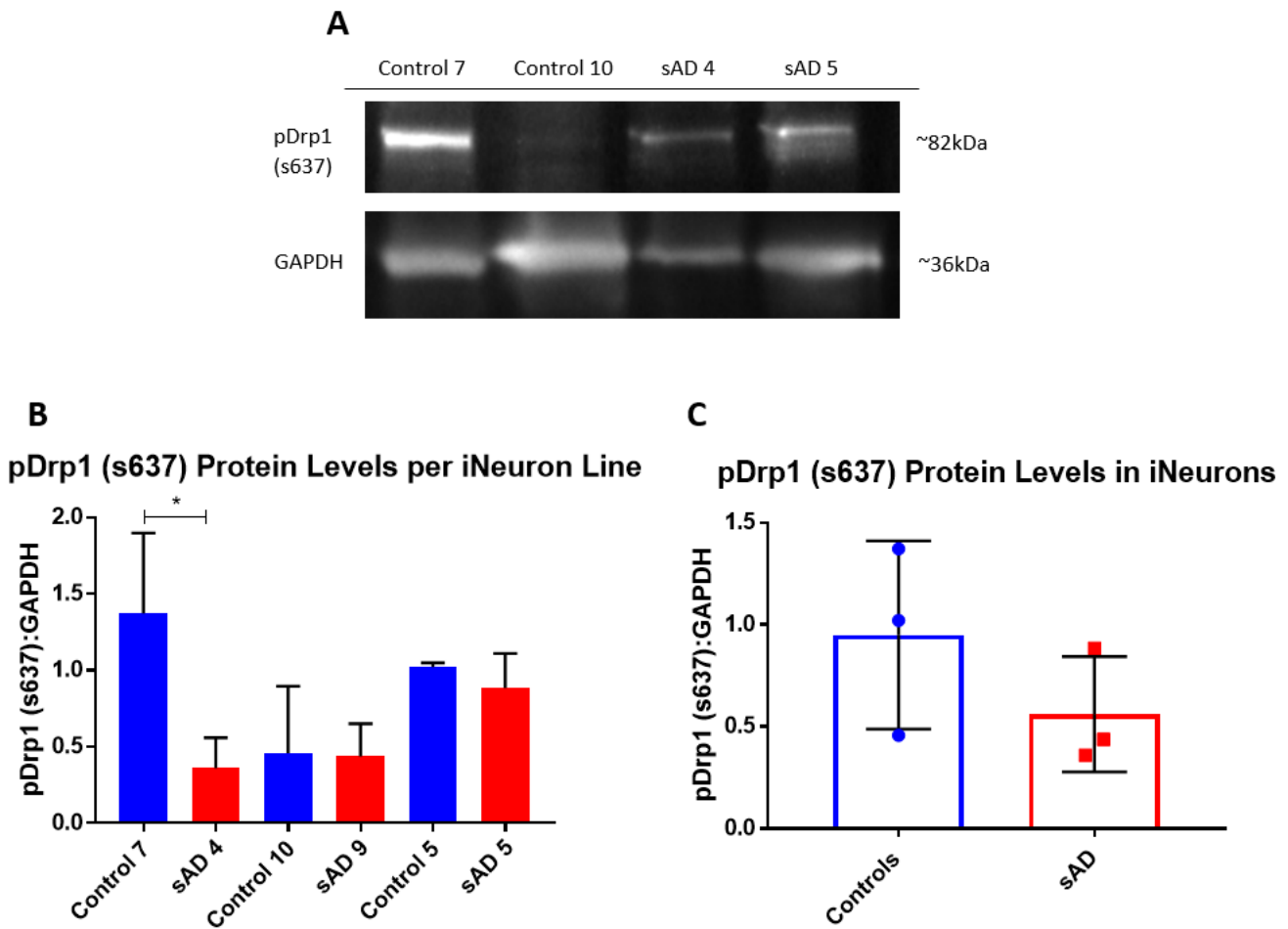


Figure 89: There is a significant decrease in pDrp1(s637) protein levels in one sAD iNeuron line compared to a paired control. A) Representative blot of pDrp1(s637) and GAPDH loading control, in control 7, control 10, sAD 8 and sAD 4, with 10µg protein loaded per lane. B) Quantification of pDrp1(s616) levels in four control and four sAD pairs. There is a significant decrease in sAD 4 compared to control 7 (* $p < 0.05$; One way ANOVA with Sidak's multiple comparisons). Each line was assessed at three difference passages. C) No significant difference was seen at a group level. Each dot represents the mean of the two replicates per line, bars represent the group mean and error bars show SD ($p = 0.289$; t test).

4.3 Discussion

This chapter focussed on establishing a patient derived iNeuron model from iNPCs, the characterisation of this model, and an investigation of the mitochondrial phenotype present in this model. A cortical neuron model could not be established within the time frame and restrictions due to COVID-19 and so a previously established protocol to produce a general population of neurons was taken forward instead. This population expressed neuronal markers TUJ, MAP2, and NeuN. iNeurons were also assessed for specific neuronal markers, and expression of these was seen to differ between different differentiations. sAD iNeurons were smaller in size than control neurons but showed no other morphological differences, though some lines did show a reduced viability. sAD neurons in general showed reduced membrane potential, and variable alterations in fission protein expression, localisation, interactions, and post translational modifications.

4.3.2 Characterisation of the Generic iNeuron Model

As an alternative to iNPC derived cortical neurons, a previously established protocol (Webster *et al.*, 2016) was used to generate a general population of iNeurons. This protocol uses RA, SAG, and forskolin to induce differentiation, with previous work producing 70% TUJ positive cells (Webster *et al.*, 2016). RA is commonly used to promote differentiation of neuronal cells, through the upregulation of neural genes SRY-box transcription factor 2 (SOX2), PAX6 and NeuroD1, and regulation of WNT signalling (Tonge and Andrews, 2010). SAG activates the sonic hedgehog signalling pathway, improving cell survival (Bragina *et al.*, 2010), and has more recently been shown to trigger BDNF secretion and regulate intracellular Ca²⁺ signalling (Delmotte *et al.*, 2020), while forskolin increases the activation of cyclic AMP, which promotes neuronal maturation and survival (Lepski *et al.*, 2013).

The iNeurons generated in this project were characterised by assessing the expression of several neuronal markers. As general neuronal markers, TUJ, MAP2, and NeuN were used. There was some variability between the expression of these markers in different lines, but all showed at least 87% TUJ positive cells, most showed at least 60% MAP2 positive cells, and whilst two sAD lines showed very little NeuN positive cells, the rest of the lines showed 20-75% NeuN positive cells. MAP2 and NeuN in particular are markers of mature neurons, and it is expected that expression of these markers would be lower than TUJ, which stains more immature neurons as well as mature neurons. This is in line with previously published work using this protocol (Webster *et al.*, 2016), and similar to iPSC derived cortical neurons (Boissart *et al.*, 2013; Zhang *et al.*, 2013). Expression of neuronal

markers TUJ and NeuN was confirmed via western blotting, and no significant differences were seen between control and sAD iNeurons overall. Expression of TUJ and NeuN in iNeurons was compared to iNPCs in a subset of lines, and an increase was seen in iNeurons compared to iNPCs in all lines.

To better determine the type of neurons present in the population, iNeurons were also stained for specific neuronal markers including Hb9, a marker of motor neurons, ChAT, a marker of cholinergic neurons, vGlut1, a marker of glutamatergic neurons, and TBR1, a marker of early cortical neurons. Expression of these markers varied both between individual lines, and between different differentiations. This shows that the protocol used did not give a consistent neuronal population every differentiation, with no obvious link to iNPC passage or batch, or cell number and viability. This variability may have had an impact on the mitochondrial data collected, though all experiments were repeated across multiple differentiations to reduce this bias as much as possible. Further optimisation of this protocol may have increased the consistency between different differentiations, giving a more homogeneous population, and thus removing any neuron type bias from the mitochondrial data.

In general, the ideal neuronal population for investigating sAD would be a cortical neuron population. When TBR1 was assessed as an early cortical neuron marker, very little expression was seen in sAD iNeurons, but up to 50% TBR1 positive iNeurons were seen in controls. This difference may be due to metabolic alterations seen in the sAD fibroblasts and/or iNPCs which are affecting the differentiation process. No markers of later stage cortical neurons, such as SATB2, were assessed, so it is possible that there are also late stage cortical neurons present in either control or sAD iNeurons. It has previously been shown that iPSC derived AD neurons, both with a PSEN1 mutation (Arber *et al.*, 2021), and with an ApoE4 allele (Lin *et al.*, 2018), mature prematurely; it is possible that no expression of TBR1 was seen in sAD lines as the cells had already been through this stage. Alternatively, it may be that a longer protocol was required for more consistent expression of TBR1. Optimising a longer or shorter protocol may have given more consistent TBR1 expression.

Cortical neurons are often glutamatergic, and expression of glutamatergic marker vGlut1 was also assessed. vGlut1 showed the highest expression across all lines, with at least one differentiation showing some expression in all lines except for sAD 5. This suggests that a proportion of the iNeuron population is likely to be glutamatergic. Cortical neurons can also be cholinergic; these neurons are some of the earliest affected in AD, and current treatments are focussed on improving the function of cholinergic neurons. Expression of ChAT was assessed, however, there were less than 3% of cells which were ChAT positive across all differentiations in all lines, suggesting that this differentiation protocol does not yield cholinergic neurons. Finally, Hb9 was assessed as a marker of motor neurons. Since motor neurons are not affected in AD, this would be the least relevant population for this

project. Whilst between 10% and 30% expression was seen in one differentiation of two controls and one sAD line, most lines and most differentiations showed very little Hb9 positive cells, suggesting that there is either no, or a very small proportion, of motor neurons in the iNeuron population. One major type of neuron which was not assessed were GABAergic neurons, the presence of which could be assessed with markers such as GABA transporter 1, or GABA receptors 1 and 2. This would help to further characterise the neuron population, and give further understanding of the characteristics of the general iNeuron population.

There are several further characterisation steps which could be undertaken in this neuronal population. The presence of synapses could be confirmed by staining of presynaptic markers such as synapsin and synaptophysin, and post synaptic markers such as homer and PSD95. A reduction and dysfunction in synapses is a key pathology in AD (reviewed by Padmanabhan, Kneynsberg and Götz, 2021; Wu *et al.*, 2021; Pelucchi *et al.*, 2022), and so this characterisation would be especially interesting. Neuronal activity could also be measured via assessing the electrophysiological activity, via patch clamp techniques, or by investigating calcium signalling either by genetically encoded (Dana *et al.*, 2019), or chemical (Paredes *et al.*, 2008) indicators. These steps would confirm that the iNeurons generated using this protocol are functional neurons. In general, iPSC derived neurons require many days of differentiation to demonstrate functionality. For example, Shi, Kirwan and Livesey (2012) saw functional synapses at 50 days, while Bergström *et al.* (2016) following the same protocol saw functional glutamatergic and GABAergic neurons at 90 days and Cao *et al.* (2017) noted increased glutamate release at 180 days. It may be that a longer differentiation would be required to see functional neurons in this population.

4.3.3 The Use of Generic iNeurons as a Model of Mitochondrial Dysfunction in AD

In general, a population of generic iNeurons is less relevant as a model of sAD than a cortical neuron model. It is known that different populations of neurons are differentially affected in AD, with cortical neurons affected more than other types of neuron, such as motor neurons. A cortical neuron model would provide a model more focussed on the affected cell type, and may show pathology which is not recapitulated in the general neuron population. There are alternative, well established ways to generate cortical neurons including iPSC derived cortical neurons (Shi, Kirwan and Livesey, 2012) and direct conversion of fibroblasts to cortical neurons (Miskinyte *et al.*, 2017). However, differentiation of iNPCs has several advantages, including practical considerations such as time and cost, the availability of the relevant iNPCs lines in the lab, as well as the ability of the iNPCs to proliferate in culture. Furthermore, iNPCs maintain characteristics of the cell which occur with patient age, including several phenotypes which are associated with the mitochondria, including

increased ROS and reduced levels of antioxidants (Gatto *et al.*, 2021). With more time, a comparison of models would have been beneficial, however in the available time and taking everything into account, generic iNeurons derived from iNPCs were chosen, as they remain a more relevant cell type than the patient fibroblasts, whilst still maintaining the advantages of iNPC derived differentiation. The protocol used did not give a consistent neuronal population between lines or between different differentiations of the same line. While multiple differentiations were used for each experiment to reduce bias from this heterogeneity, it must still be considered that this could affect the phenotypes measured.

Several considerations must be taken into account when using iNeurons to model mitochondrial phenotypes in sAD. The mitochondria play an important role in the reprogramming of somatic cells, and the differentiation of iNeurons. Throughout these processes, cells go through significant changes in metabolic activity, which may be important in driving the transformations forward. For example, during differentiation, cells will switch from relying more on glycolysis to OXPHOS (Zheng *et al.*, 2016; Schwartzentruber *et al.*, 2020). Drp1 is also known to play an important role in reprogramming somatic cells to iPSCs, with mitochondrial division inhibitor 1 (MDIV1), a Drp1 inhibitor, reducing the efficiency of reprogramming mouse fibroblasts to iPSCs (Vazquez-Martin *et al.*, 2012). Furthermore, inducing Drp1 dependent fission early in reprogramming has been seen to impair the generation of iPSC colonies, with Mff and MiD51 also proposed to play an important role (Prieto *et al.*, 2016). Drp1 is also important in the differentiation of neurons, with both overexpression and silencing of Drp1 shown to increase cell death during differentiation (Vantaggiato *et al.*, 2019). The precise role of Drp1 in the reprogramming of fibroblasts to iNPCs, and their subsequent differentiation into iNeurons, is unknown but it is important to consider how the mitochondrial defects seen in sAD fibroblasts will affect the ability of these cells to be reprogrammed.

Another important consideration which is particularly relevant to AD is the use of DAPT in differentiation. DAPT is used to rapidly induce cells to differentiate down a neuronal lineage. DAPT acts via the inhibition of γ secretase, blocking NOTCH signalling and leading to a rapid exit from the cell cycle (Borghese *et al.*, 2010; Qi *et al.*, 2017). γ secretase is important in the pathology of AD, involved in the cleavage of APP into A β and PSEN1 and PSEN2, genes associated with familial AD, encode key components of γ secretase. Though DAPT is only on the cells for a short amount of time, it must still be considered that this could affect the AD pathology in these cells, which could in turn impact the results seen. As an alternative to rapidly inducing differentiation with DAPT, other small molecules could be used. Qi *et al.* (2017) developed an accelerated differentiation protocol for neurons which used both DAPT and SU5402, an inhibitor of FGF signalling. Using these small

molecules, they were able to generate 75% post-mitotic neurons after 11 days of differentiation. Though this study used both molecules together, it may be that SU5402 alone would be a suitable alternative to DAPT. Another option would be to overexpress NGN2, which was found by Zhang et al. (2013) to speed up the differentiation process. The cells could also be left without any factor designed to speed up the induction of differentiation, though this would have the negative effect of increasing the time of the protocol.

4.3.4 Neuronal Morphology and Viability in Control and sAD iNeurons

iNeurons were assessed for neuronal morphology and viability using the neurite outgrowth assay. This is a commercially available kit (ThermoFisher) which uses a cell membrane marker to visualise differences in the length and number of projections from the cell body, and a dye which fluoresces green in the presence of intra cellular esterase activity as a measure of cell viability (Hancock *et al.*, 2015).

No significant differences were seen in the neuronal morphology between controls and sAD iNeurons. Both showed similar levels of cell roundness, and width to length ratio, and a similar ratio of cells showing neuronal morphology. However, there was a reduction seen in cell area in three of the four sAD iNeuron lines. This would have an effect on some of the mitochondrial parameters measured, and so to account for this going forward, parameters were normalised to cell area where relevant and possible. Previous work has reported alterations in the branching and density of dendritic spines in 5xfAD mice (Maiti *et al.*, 2021), and in post mortem patient tissue (Merino-Serrais *et al.*, 2013), though this morphology is not seen in this model, and so could not be assessed.

A significant decrease in cell viability was seen in sAD 8, as well as a decrease in sAD 6. As mentioned above (section 4.3.3), mitochondrial function and morphology play a key role in differentiation, and it is possible that mitochondrial deficits in these lines impacted the survival of the cells.

Furthermore, it has been shown that both PSEN1 neurons (Arber *et al.*, 2021) and neurons with an ApoE4 allele (Lin *et al.*, 2018) mature earlier than controls. This accelerated differentiation may occur in these sAD lines, leading to earlier cell death. This drop in viability has several impacts on work going forward. Firstly, a reduction in cell viability made it difficult to obtain a high enough yield of iNeurons to complete full data sets in these lines, and so many experiments are presented with a reduced number of repeats, reducing the reliability of this data. Secondly, it is possible that the cells which have died during the protocol are those which had the most severe deficits and alterations in their mitochondria. This would have an effect on the results seen, as the surviving cells may have fewer deficits, and show a less severe phenotype.

4.3.5 Mitochondrial Function in Control and sAD iNeurons

Mitochondrial function was investigated via the assessment of mitochondrial membrane potential, as measured by TMRM intensity. TMRM is a rhodamine based dye which is cationic, and therefore loads to the most negatively charged part of the cell. It can be used in either quenching or non-quenching mode. In quenching mode, TMRM is added at higher concentrations (usually 1-20 μ M), and forms aggregates within the mitochondria. Loss of membrane potential releases the dye, and so the fluorescent signal is increased. This paradigm is most applicable to measuring dynamic or immediate changes in MMP during the time the cells are being imaged. For measuring differences in MMP between two populations, non-quenching mode is more appropriate, and so was used here. A lower concentration of 80nM was added; this meant that TMRM did not aggregate, and so a reduction in TMRM intensity indicates a reduction in MMP (Perry *et al.*, 2011). TMRM is not the only cationic dye available for the assessment of MMP, others include TMRE, Rhod123, and JC1. TMRE, Rhod123, and JC1 have been shown to exhibit a greater level of mitochondrial binding and inhibition of the ETC than TMRM, though in low, non-quenching concentrations this level of inhibition is negligible. JC1, unlike the others, is a dual colour probe, shifting from green (non-aggregated) to red (aggregated) as more accumulates in the mitochondria, and mitochondrial polarisation can be assessed based on the ratio of the two colours. JC1 is slower to permeate the cell than TMRM, and so is sensitive to differences in surface to volume ratio either between cells or where cell morphology differs across a single cell (for example, the cell body and neurites in a neuron). Therefore, JC1 may give false differences in MMP, when changes in intensity are simply due to the difference in cell permeation (Perry *et al.*, 2011). This is especially relevant here given the heterogeneity in cell area between different cell lines.

A significant decrease in MMP was seen in only one line, sAD 6 compared to its paired control. However, a decrease was also seen in sAD 4, sAD 5, and sAD 8. Unlike the other lines, an increase was seen in sAD 9. In the fibroblasts from which these iNeurons were generated, MMP has been previously assessed (Bell *et al.*, 2018, 2020), and sAD 4, 5, 6, and 8 showed a decrease in MMP while sAD 9 showed no change. This shows that alterations in mitochondrial function are conserved across the two cell types. To our knowledge, MMP specifically has not been assessed previously in patient derived iNeurons, but it has been found to be decreased in a range of other AD models including transgenic mouse models (Rönnbäck *et al.*, 2016; Dixit, Fessel and Harrison, 2017) and patient fibroblasts (Amit U Joshi *et al.*, 2018).

Mitochondrial function was not the main focus of this project, and so no further indicators of function were assessed. However, there are many other measures of mitochondrial function which

could be investigated in these iNeurons. For example, cellular ATP levels, which have been shown to be decreased in both fAD and sAD iPSC derived neurons (Fang *et al.*, 2019), could be assessed using the ATPlite kit (PerkinElmer), a luminescence based assay. The complexes of the ETC themselves could be studied; a complex IV deficit is commonly seen in AD (Parker, Filley and Parks, 1990; Kish *et al.*, 1992; Mutisya, Bowling and Beal, 1994; Parker *et al.*, 1994; Curti *et al.*, 1997; Maurer, Zierz and Möller, 2000; Bosetti *et al.*, 2002; Hauptmann *et al.*, 2009; Calkins *et al.*, 2011; Correia *et al.*, 2013; Rönnbäck *et al.*, 2016; Djordjevic *et al.*, 2020; Yao *et al.*, 2021), and it would be interesting to see if this finding translates to patient derived iNeurons. Birnbaum *et al.* (2018) did see increased expression of complex IV subunits, alongside increase in expression of subunits of complex I, III, and V, in iPSC derived neurons from sAD patients, though this was not consistently seen in all lines. It would be interesting to measure the activity of the ETC complexes, as well as expression, to give a better indication of functional deficits seen in AD. Different aspects of mitochondrial respiration could also be assessed using the Seahorse XF Analyser (Agilent). This assay measures oxygen consumption rate and extracellular acidification rate, before and after the addition of various mitochondrial inhibitors, such as oligomycin (complex V inhibitor), antimycin (complex III inhibitor), rotenone (complex I inhibitor), and CCCP (mitochondrial uncoupler). This can then be used to assess parameters such as ATP-linked respiration, maximal respiratory capacity, and spare respiratory capacity. Previous work in the lab found spare respiratory capacity to be decreased in the sAD fibroblasts from which these iNeurons were generated, and this was found to correlate with neuropsychological changes (Bell *et al.*, 2020), and so this would be a particularly interesting measure to investigate in these iNeuron lines. To our knowledge, this technology has not yet been utilised in AD iPSC derived neurons, though it has been applied to iPSC derived dopaminergic neurons (Roy-Choudhury and Daadi, 2019), iPSC derived GABAergic interneurons from people with Down Syndrome (Xu *et al.*, 2022), and in iPSC derived glutamatergic cortical neurons in both healthy people (Aldana *et al.*, 2017), and those with frontotemporal dementia (Zhang *et al.*, 2017; Aldana *et al.*, 2020).

4.3.6 Neuronal Morphology and Viability, and Mitochondrial Function under Stressed Conditions

In order to investigate the response of the iNeurons to stress conditions, neuronal morphology and viability, and mitochondrial function were investigated in a subset of lines which were grown in low glucose, galactose containing media, and after treatment with 30nM rotenone. No significant differences were seen in any parameter measured between control and sAD lines or between the different media conditions, however, there was a reduction in neuron score and cell viability in

control 10 and sAD 9 in the stressed conditions, and decreased MMP in all lines grown in the galactose media.

Galactose media pushes the cells into generating ATP via OXPHOS over other metabolic pathways such as glycolysis. Two molecules of ATP are generated by the glycolytic metabolism of glucose, whereas the metabolism of galactose generates zero ATP molecules (Aguer *et al.*, 2011). This forces the cells to be more reliant on OXPHOS for the generation of ATP, and makes any mitochondrial deficits more apparent. It must be noted that not all glucose was removed from the media, and this small amount may have affected the results seen. Decreased MMP was seen in all lines when grown in galactose media. However, there was no difference seen between control and sAD lines. During differentiation, cells undergo a metabolic switch, from relying more on glycolysis to heavily depending on OXPHOS when fully differentiated into mature neurons (Zheng *et al.*, 2016; Schwartzenruber *et al.*, 2020). The differences seen in MMP here may indicate that these iNeurons are not entirely reliant on OXPHOS; if they were already heavily dependent on OXPHOS, we would not necessarily expect to see changes when they are pushed towards to OXPHOS by the addition of galactose media. This could be assessed by measuring ATP levels in the presence of a glycolysis inhibitor such as 2-deoxy-d-glucose, a glucose derivative which is unable to undergo glycolysis, or an OXPHOS inhibitor, such as oligomycin, an ATP synthase inhibitor, as described by Schwartzenruber *et al.* (2020). This would give an indication as to which of these metabolic pathways the iNeurons are more reliant on. Reduced neuron score and reduced cell viability was also seen in control 10 and sAD 9 in the galactose conditions. This is likely due to the cells being unable to produce as much ATP under these conditions, and so they cannot generate the energy needed to survive and maintain neuronal morphology.

Neuronal morphology and viability, and mitochondrial function, were also assessed after treatment with 30nM rotenone for three days. Rotenone is a complex I inhibitor, and is a well-established mitochondrial stressor. In general, it would be expected to see a reduction in MMP after rotenone treatment, though this was not seen in any line assessed. This may indicate that the treatment conditions require further optimisation. The concentration and length of treatment were decided based on previously used conditions in the lab, but it may be that in this particular system, a greater concentration of rotenone is required to observe the expected effects. Previously published work which has used rotenone as a mitochondrial stressor have used a more acute treatment, a higher concentration for a shorter period of time. For example, 0.5 μ M for 48 hours (LaRocca *et al.*, 2014), or 1 μ M for 12 hours (Jalewa, Sharma and Hölscher, 2016), or as short a time as 30 minutes (Baxter, Uittenbogaard and Chiaramello, 2012). Alternatively, a longer term treatment could be tested, though cell viability would be an important consideration.

4.3.7 Mitochondrial Morphology in Control and sAD iNeurons

Mitochondrial morphology was previously found to be altered in the fibroblasts from which these iNeurons were generated. While individual mitochondria didn't show much difference in average area per mitochondrion, there was a significant increase in the area of the cell taken up by long mitochondria in sAD fibroblasts (Bell *et al.*, 2018). An increase was also noted in the number of mitochondria per cell, the mitochondrial network was seen to be more interconnected, and there was a higher percentage of mitochondria accumulated in the perinuclear region (Bell *et al.*, 2018). These parameters were also assessed in the iNeurons via MitoTracker green, a dye which stains the mitochondria but is not dependent on membrane potential.

As was seen in the fibroblasts, there was no significant changes in the morphology of individual mitochondria, as measured by area, length, width, and roundness, between control and sAD iNeurons, with the exception of an increase in mitochondrial area in sAD 5. This data is based on an average value for all the mitochondria in a well. It is possible that if this was broken down further to look at each mitochondrion separately, more subtle differences would become apparent. Increased mitochondrial surface area, measured by TOM20 expression, has been seen in iPSC derived PSEN1 neurons (Martín-Maestro, Gargini, A. Sproul, *et al.*, 2017), while changes at an individual mitochondrion level have been variable in patient fibroblasts with a decrease in length seen by some (Pérez *et al.*, 2017; Amit U Joshi *et al.*, 2018) and an increase seen by others (Xinglong Wang *et al.*, 2008).

While looking at individual mitochondria offers some interesting insights, mitochondria do not act alone, instead forming a complex and dynamic network throughout the cell. It is therefore perhaps more interesting to look at the morphology of the mitochondrial network as a whole. Form factor, a measure of interconnectivity within the mitochondrial network was assessed but no change was seen between control and sAD iNeurons, with the exception of a small increase in sAD 8 indicating a more fused network. This is in contrast to patient fibroblasts, where a more consistently interconnected network was observed (Bell *et al.*, 2018), and evidence from animal models where in general, more fragmentation is seen (Calkins *et al.*, 2011; Xu *et al.*, 2017; Wang and Davis, 2021).

Mitochondrial count was found to be variable between lines, even when cell area was controlled for. Only one line showed a significant decrease, sAD 5, with sAD 9 and sAD 6 also showing a decrease. On the other hand, sAD 8 and sAD 4 showed an increase. In the corresponding patient fibroblasts, sAD 4, 5, 6, and 9, all had fewer mitochondria per cell compared to controls, while sAD 8 showed no difference (Bell *et al.*, 2018, 2020), again showing conservation of phenotype across the two cell types, with the exception of sAD 4.

The mitochondrial population was split into two separate populations, long and short mitochondria, to see if any differences were present between these two populations which may be missed when looking at the population as a whole. More short mitochondria would indicate a more fragmented network, while more long mitochondria would indicate a more interconnected network. When these parameters were assessed by the lab in patient fibroblasts, the area of the cell taken up by long mitochondria was increased (Bell *et al.*, 2018). Based on this finding, this parameter was also assessed in the iNeurons but no change was seen either at a group or individual level. The same was seen for the percentage of the cell taken up by short mitochondria.

Taken as a whole, mitochondrial network morphology parameters do not suggest either a more fragmented or more interconnected network in iNeurons. However, if the sAD lines are looked at individually, more differences become apparent. sAD 5 shows an increased individual mitochondrial area, and a decreased mitochondrial count per cell, both indicating a more interconnected mitochondrial network. On the other hand sAD 8 shows an increased number of mitochondria per cell, indicating a more fragmented network. This suggests that there is an imbalance in mitochondrial morphology in sAD iNeurons, though this imbalance is not always in the same direction.

Another important factor is the distribution of mitochondria throughout the cell. Neurons have a unique and complex morphology, and maintaining an appropriate distribution of mitochondria throughout the cell is key. Neurons generally consist of a population of mitochondria which remain in the soma, and a second population which are transported through the axons and dendrites (Plucińska and Misgeld, 2016). An increase in the percentage of mitochondria in the perinuclear region was previously seen in the sAD fibroblasts which correspond to these iNeurons (Bell *et al.*, 2018), a finding also seen in other patient fibroblasts (Xinglong Wang *et al.*, 2008; Martín-Maestro, Gargini, García, *et al.*, 2017) and animal models (Xu *et al.*, 2017). This was also assessed in the iNeurons. No significant differences were seen, though there was an increase in sAD 5 and sAD 8. In many cell types, mitochondria are transported to the perinuclear region to be degraded via mitophagy, though the practicalities of this in neurons, where the mitochondria in the processes may be great distances from the soma, has been questioned (Misgeld and Schwarz, 2017). It has been seen that mitochondria travelling retrograde, back towards the soma, have a lower MMP than those moving anterograde (Miller and Sheetz, 2004; Lin *et al.*, 2017), though others have failed to replicate this finding (Verburg and Hollenbeck, 2008). There is some evidence of mitophagy taking place in the processes themselves, including the recruitment of parkin to damaged mitochondria in axons (Ashrafi *et al.*, 2014), and also evidence in mice (Davis *et al.*, 2014) and *C. Elegans* (Melentijevic *et al.*, 2017) that mitochondria can be shed from neurons and degraded by glial cells.

This suggests that while a portion of damaged mitochondria are transported back to the soma for degradation, in certain circumstances, mitochondrial degradation can also take place in other regions of the cell. This may explain why fibroblasts show a greater increase of mitochondria in the perinuclear region than iNeurons, despite both showing an increase in mitochondrial dysfunction.

4.3.8 Drp1 Protein Expression in iNPCs and iNeurons

Chapter 3 showed that there are significant deficits in Drp1 and its four outer mitochondrial membrane receptors in sAD patient fibroblasts compared to controls. To determine whether these differences are also present in other cell types, western blotting was carried out in four sAD and four control iNPC lines, and iNeurons differentiated from those iNPCs.

In iNPCs, a significant increase in Drp1 expression was seen in three of the four sAD lines, leading to a significant increase overall, whilst in iNeurons only one of the four sAD lines showed a significant increase in total Drp1 protein. Drp1 levels have not been widely researched in AD patient derived neurons, though Birnbaum *et al.* (2018) saw no change when they investigated in five sAD iPSC derived neuron lines. However, in other models, neural cell types have been shown to have increased levels of Drp1, including neurons taken from transgenic animal models (Trushina *et al.*, 2012; Xu *et al.*, 2017; Kandimalla *et al.*, 2018b; Reddy, Manczak, *et al.*, 2018), and post mortem patient tissue (Manczak, Calkins and Reddy, 2011). Many of the implications of alterations in levels of Drp1, and further areas for investigation, have been discussed previously (see Chapter 3, Section 3.3.1), and so will not be discussed again here.

Drp1 is known to be important during neuronal differentiation. Knockdown of Drp1 has been seen to reduce the ability of embryonic stem cells to differentiate, especially in the neural lineage. This coincided with a delayed reduction in Oct4 and Nanog, which are involved in pluripotency (Wang *et al.*, 2014). Furthermore, Drp1 has been proposed to affect the response to retinoic acid induced differentiation; an increase in cell death during differentiation was seen both when Drp1 was overexpressed and when it was blocked or silenced (Vantaggiato *et al.*, 2019). The increase in Drp1 seen in the iNPCs here may have had an effect on the differentiation of these cell lines.

The complex morphology of neurons means that they are particularly sensitive to changes in the mitochondrial network, and as such, mitochondrial fission and Drp1. Hippocampal neurons transfected with dominant negative Drp1 had a reduction in the mitochondria present in the dendrites, while overexpression of wild type Drp1 gave the opposite effect. Drp1 was also seen to have an effect on excitatory synapse number; neurons transfected with the negative mutant showed a reduction in synapses while overexpression increased synapses (Li *et al.*, 2004, 2008). Drp1 is essential for embryonic development and synapse formation in mice, and a complete knockout of

Drp1 is embryonic lethal (Ishihara *et al.*, 2009; Wakabayashi *et al.*, 2009). A case study of a baby born with a de novo mutation in Drp1 reported that the patient showed abnormal brain development, among other symptoms, before passing away at 37 days old (Waterham *et al.*, 2009). This was proposed to be due to impaired assembly of Drp1 at the mitochondria, leading to decreased fission and altered mitochondrial distribution (Chang *et al.*, 2010). In the data presented here, fewer sAD iNeuron lines show differences in Drp1 expression than the corresponding iNPCs or fibroblasts. It is clear that alterations in Drp1 would have more of an impact on a neuron than other cell types; it may be that these cells are better able to compensate for disease mechanisms which in other cells may lead to alterations in Drp1. It is also possible that the cells with the greatest alterations in Drp1 are dying throughout differentiation, and so by the time cells are assayed, the cells which remain are those which are the least affected.

Drp1 levels in iNeurons were found to show a significant linear regression with functional measure MMP; when Drp1 is increased, MMP is decreased. A linear regression which was approaching significance was also seen between Drp1 and morphology parameters including form factor, and mitochondrial count per cell. However, this was not in the direction which would be expected, as an increase in Drp1 appears to be associated with a less fragmented network. There are several potential reasons why this may be. As stated previously (Chapter 3, Section 3.3.1), changes in Drp1 levels do not necessarily correlate directly with changes in mitochondrial fission. Western blotting measures total cellular Drp1; Drp1 is not just involved in mitochondrial fission. It is possible that the changes seen in total Drp1 levels is having more of an effect in other organelles than the mitochondria. Furthermore, post translational modifications of Drp1 are key in its activity. It may be that the Drp1 present is inactive, or that Drp1 is unable to be stabilised on the mitochondrial membrane, and so unable to initiate fission. To assess this further, the localisation and phosphorylation status of Drp1 was assessed, and will be discussed later in the chapter.

4.3.9 Drp1 Localisation in iNeurons

To determine whether altered levels of Drp1 in iNeurons affected the amount of Drp1 present at the mitochondria, the amount of Drp1 co-localised with mitochondrial marker TOM20 was assessed. While there was no significant differences seen, either in individual pairs or at a group level, a non-significant increase in Drp1 at the mitochondria was seen in all sAD lines. This may be simply due to the increased total levels of Drp1 seen in some lines, such as sAD 5 and sAD 8, as there is no difference seen in the percentage of total Drp1 which is localised to the mitochondria. Other lines showed a decrease in cellular Drp1 levels but an increase in Drp1 at the mitochondria. This may be

due to a change in the recruitment of Drp1 to the mitochondria by the receptors on the outer mitochondrial membrane.

4.3.10 Drp1 Receptor Expression in iNPCs and iNeurons

The protein levels of the four Drp1 receptors on the outer mitochondrial membrane were also assessed in both iNPCs and iNeurons. These receptors and their involvement in Drp1 recruitment was discussed previously (Chapter 3, Section 3.3.3).

In iNPCs, the most significant changes seen were in Fis1 levels, where two sAD lines showed a significant decrease and one showed a significant increase compared to paired controls. A significant increase was also seen in MiD51 in sAD 4 compared to control 7, but no other changes were seen. In iNeurons, an increase was seen in Fis1 levels in one line, while sAD 4 showed a significant decrease in MiD51 levels. At a group level, a significant reduction was seen in MiD49 levels. To our knowledge, the levels of Drp1 receptors have not previously been studied in patient derived neurons, though Fis1 has been reported to be increased in neurons from transgenic mouse models (Kandimalla *et al.*, 2018b; Manczak *et al.*, 2018; Reddy, Manczak, *et al.*, 2018), and post mortem patient tissue (Manczak, Calkins and Reddy, 2011), and Mff has also been seen to be increased in post mortem tissue (Wang *et al.*, 2019), as well as in neurons from transgenic mice (Q. W. Yan *et al.*, 2019).

Differences seen in iNPCs did not necessarily translate to differences seen in iNeurons, with some sAD iNeurons showing no change where differences were seen in iNPCs. As discussed in section 4.3.7 in regard to Drp1, neurons are much more sensitive to changes in the mitochondrial network, and it may be that cells with the most significant changes were unable to survive differentiation, or that iNeurons as a cell type are more resistant to pathological mechanisms which may lead to alterations in these proteins. However, in some sAD lines, the differences seen in iNeurons are in the opposite direction to changes seen in the iNPCs. This suggests that changes occur in these proteins over the course of differentiation. Mitochondrial fission is known to play a key role in differentiation (Wang *et al.*, 2014; Vantaggiato *et al.*, 2019), and mechanisms which occur over the course of differentiation may impact the levels of these proteins.

In iNPCs, Mff was the only receptor seen to have a significant linear regression with Drp1 levels. As discussed previously (Chapter 3, Section 3.3.4.2), Mff is thought to be the most important receptor in the recruitment of active Drp1 for fission, and this adds further evidence for this. However, there is no significant linear regression between Drp1 and any receptor in iNeurons. It is possible that there are other proteins involved in Drp1-mediated mitochondrial fission in neurons, for example ganglioside-induced differentiation associated protein 1 (GDAP1). GDAP1 is a protein on the outer mitochondrial membrane which is preferentially expressed in neurons, mutations of which are

associated with Charcot-Marie-Tooth disease (Pedrola *et al.*, 2005, 2008). Overexpression of GDAP1 has been seen to increase Drp1-dependent mitochondrial fission (Niemann *et al.*, 2005), and it has also been shown to interact with Mfn2 (Pijuan *et al.*, 2022). It may be that there are alterations in GDAP1 which are having an effect on mitochondrial morphology and quality control in sAD iNeurons; this could be investigated further by measuring GDAP1 levels via western blotting or immunocytochemistry in control and sAD iNeurons.

There is clear variability in both the severity and direction of alterations in the expression of Drp1 receptors, both in iNPCs and iNeurons. This was also seen in assessments of mitochondrial morphology in iNeurons, and provides further evidence that there is an imbalance of mitochondrial morphology and quality control in sAD iNeurons, but the direction of this imbalance is not always the same. The only group difference noted was a decrease in MiD49 levels in iNeurons. MiD49 is one of the less well understood Drp1 receptors, but has been proposed to be involved in both mitochondrial fission and fusion, playing an important role in regulating the balance between the two mechanisms (Yu *et al.*, 2021). This reduction of MiD49 may impact the balance between fission and fusion, and this could lead to the alterations in morphology and other fission proteins noted in sAD iNeurons. Mitochondrial fusion was not investigated in either the iNPCs or the iNeurons; it is possible that differences seen in morphology are also affected by changes in the mitochondrial fusion process, not just fission.

4.3.11 Fis1 and Mff Localisation in iNeurons

Since Fis1 and Mff are also involved in the fission of other organelles, the amount localised to the mitochondria was assessed. No significant differences were seen in the amount of Fis1 localised to the mitochondria but there was variation seen between the sAD lines, with some showing an increase and some showing a decrease. sAD 4 showed a decrease in the percentage of total Fis1 localised to the mitochondria, and a decrease in the total amount which was co-localised. sAD 9 also showed less Fis1 at the mitochondria, likely due to the reduced levels seen overall. sAD 8 showed increased levels co-localised, as well as an increased percentage of total Fis1 which was present at the mitochondria, while sAD 5 showed a decrease in the amount of Fis1 at the mitochondria despite a significant increase in the levels overall.

No significant differences were seen at a group level in the amount of Mff localised to the mitochondria, but a significant decrease was seen in sAD 5, even though total levels were increased. sAD 4, sAD 8, and sAD 9 all showed a decrease in total Mff levels. While sAD 4 and sAD 9 also

showed less Mff at the mitochondria, sAD 8 was able to increase Mff at the mitochondria to above control levels.

In general, it is not surprising that there are differences in the alterations in the amount of Fis1 and Mff localised to the mitochondria, given that there are differences in the total cellular levels. It seems, as in the fibroblasts, that some lines are able to compensate for changes in total receptor levels by boosting or decreasing the percentage which is localised to the mitochondria. However, not every sAD line seems able to do this. In fact, some seem to go too far; they will reduce the percentage of total receptor which is present at the mitochondria, but end up with levels below control level. This difference in response is likely linked to individual differences, and the heterogeneity seen in sporadic disease.

4.3.12 Fis1 and Mff Interactions with Drp1 in iNeurons

Different levels of alterations are seen in Drp1, Fis1, and Mff total levels and levels at the mitochondria, between the different sAD iNeuron lines. To better understand the effect that this has on the activity of Drp1, the interactions of Drp1 with both Fis1 and Mff were assessed. There was variability between the cell lines when interactions in the whole cell were measured, though no significant difference was seen between any sAD and control pair, or at a group level. There was a decrease seen in the majority of sAD lines, though sAD 4 showed an increase. Interactions in the perinuclear region were also assessed, and a significant decrease was seen in the number of interactions between Fis1 and Drp1 in sAD 5, though it must be noted that there was an increased number of interactions in control 3 which impacted the result in this pair. Other lines were increased; more Drp1 interactions with Fis1 in the perinuclear region may be due to an increase in dysfunctional mitochondria being separated from the network for degradation.

Drp1 interactions with Mff were significantly decreased in sAD 5, while a decrease was also seen in sAD 9, though no significant decrease was seen overall. Kleele *et al.* (2021) found that Mff is the receptor which is more involved in fission for mitochondrial biogenesis, and so a decrease in Mff interactions with Drp1 may indicate a deficit in this process. When interactions were assessed in the perinuclear region, a significant decrease was seen in sAD 5 and sAD 9. This is likely a result of the decreases seen across the whole cell.

The number of interactions of Drp1 with Fis1, and Drp1 with Mff were compared to identify whether Drp1 preferentially interacts with one receptor over another. No significant differences were seen in either the control group or the sAD group, suggesting that Drp1 interacts with both receptors equally in iNeurons.

4.3.13 Phosphorylation Status of Drp1 in iNPCs and iNeurons

Post translational modifications of Drp1 are highly important in its fission activity, with phosphorylation being particularly important in activating Drp1. Drp1 must be phosphorylated at ser616, and dephosphorylated at ser637, in order to initiate fission. The increase in Drp1 noted at the mitochondria may not ultimately increase the level of fission if this Drp1 is inactive.

In iNPCs, a significant decrease in Drp1 phosphorylated at ser616 was seen in sAD 9, while a significant increase was seen in sAD 8. In contrast, there were no significant differences seen in iNeurons, though an increase was seen in sAD 9, while no difference was seen in sAD 8. There was also a decrease in sAD 5 and sAD 4. Drp1 phosphorylated at ser637 was also investigated in three sAD iNeuron lines, and while a significant decrease was seen in sAD 4, there were no differences seen in the other two sAD lines assessed.

There may also be alterations in other post translational modifications of Drp1. The SUMOylation of Drp1 is important in its fission activity. There are three isoforms of SUMO, SUMO1, SUMO2, and SUMO3, which conjugate to lysine residues (Henley, Carmichael and Wilkinson, 2018).

SUMO1ylation is proposed to stabilise Drp1 (Harder, Zunino and McBride, 2004), while SUMO2/3ylation reduces recruitment of Drp1 to the mitochondria, potentially by reducing the binding of Drp1 to Mff (Guo *et al.*, 2013; Fu *et al.*, 2014). SUMOylation of Drp1 is regulated by SUMO-specific proteases (SENPs); for example, SENP2 knockout leads to increased SUMO1ylation of Drp1, as well as mitochondrial defects and neurodegeneration (Fu *et al.*, 2014), and deSUMOylation of Drp1 by SENP3 has been seen to enhance the interaction of Drp1 and Mff, and Drp1 interactions with apoptotic protein Bcl-xL (C. Guo *et al.*, 2021). It is possible that the SUMOylation is altered in the sAD iNeurons, which may lead to issues in Drp1 stabilisation, or binding to Mff and other receptors.

4.3.14 Variability between iNeuron Lines

It is clear that there is a lot of variation, both between sAD and control lines, and also between different differentiations of the same line. There are several factors which can impact differentiations, including the batch and passage of the starting iNPCs. To account for this, wherever possible all experiments were carried out on differentiations from multiple passages and multiple starting batches of iNPCs. While this has created more variability between repeats, it has removed the confounding variables and increases the likelihood that changes seen are due to disease state and not the effect of passage or iNPC batch. Control and sAD lines were also passage matched

wherever possible to within three passages of each other, again to eliminate any passage effects from the results.

Variability is also seen between each cell line, in both the controls and sAD lines. It is not uncommon to see variation in patient derived neurons; for example, Birnbaum et al. (2018) saw much variation in mitochondrial phenotypes between the five iPSC derived sAD lines assessed. The expected variability in sAD patient derived fibroblasts has already been discussed (Chapter 3, Section 3.3.5), and many of the same principles apply here. However, when compared to cells such as fibroblasts, neurons are far more complex, and more metabolically active. As such, it is expected that there will be more variation in mitochondrial phenotypes between the lines, even in controls.

The data presented here suggests that while there are alterations in mitochondrial fission seen in all of the lines, there is no unifying mechanism which can be applied to all. No consistent changes in morphology are seen, and the changes seen in fission differ in severity, direction, and the point in the process at which they occur. This may be because mitochondrial fission is not a driving mechanism in sAD pathology. If dysfunction in the fission process occurs as a result of another pathogenic mechanism, it is likely that different patient cells will respond in different ways. This is dependent on a number of factors including the resilience of the cell, co-morbidities, genetic factors, and age and sex of the patient. Though no explicit age and sex differences were noted here, the sample size is small and so these cannot be ruled out. Interestingly, sAD 4 often showed differing pathology to the other lines. For example, sAD 4 has an increased cell area compared to controls while all other sAD lines showed a smaller cell area. There were also dramatic differences seen in MiD51 levels in sAD 4, in both iNPCs and iNeurons. This was not seen in any other line. sAD 4 is the only sAD line tested to have two copies of the ApoE4 allele, and this may contribute to the differences seen in this line compared to the others; it has been shown that ApoE4 neurons mature earlier than those with other ApoE genotypes (Lin *et al.*, 2018), and it may impact the mitochondrial phenotype via this and other mechanisms. This observation needs further investigation in a much larger sample before any conclusions can be made, but it is an interesting direction for further study.

On the other hand, it may be that pathology in some lines is more driven by the fission process. sAD 5 shows more significant differences in the fission process than any other line. It may be that in this line, these changes are more of a driving factor in disease pathology. Again, this observation requires further investigation, but it does lend further support to the idea of personalised medicine and patient stratification. It is clear that sporadic disease has multiple interacting factors, and these do not occur in the same way in every patient. It is important to take this into account when looking for a treatment; a mitochondrial targeted treatment may be of huge benefit to a subset of patients, but not necessarily all.

4.3.15 Differences in the Mitochondrial Phenotype in Fibroblasts and iNeurons

There were several key differences seen between the mitochondrial phenotype seen in patient fibroblasts and iNeurons generated from those fibroblasts. Metabolically, fibroblasts and neurons are very different. Fibroblasts are more glycolytic, generating a greater proportion of their ATP from glycolysis, whereas neurons are far more reliant on OXPHOS. Furthermore, neurons have a much higher energy demand, and a unique morphology which means that the morphology of the mitochondrial network is of even more importance than in a fibroblast. In the fibroblasts assessed in chapter 3, it was found that a higher amount of cellular Drp1 was associated with a higher MMP, as well as increased mitochondrial interconnectivity. Drp1 levels were also seen to show a significant linear regression with Fis1 and Mff levels. Fis1 was also associated with MMP and form factor, whereas the other receptors were not.

These associations were not seen in iNeurons. In fact, in the case of MMP, the opposite association was seen; an increase in Drp1 is associated with a decrease in MMP. This suggests that the link between mitochondrial morphology and function differs in different cell types. In iNeurons, no linear regression was seen between Drp1 receptors and MMP. This suggests that Fis1 in particular is not as important in maintaining mitochondrial function in iNeurons as it is in fibroblasts. In terms of mitochondrial morphology, a close to significant association was seen between Drp1 and interconnectivity, and between Drp1 and mitochondrial count per cell. However, these associations were not in the direction which would be expected, with an increase in fission proteins being associated with more fused morphology. This may indicate that the Drp1 in iNeurons is not necessarily active Drp1 which is capable of initiating fission. No significant linear regression was seen between Drp1 levels and any of the receptors in iNeurons, though an association was seen between Mff and Drp1 levels in the iNPCs. This could be due to the fact that there are other neuron specific factors involved in mitochondrial fission, such as GDAP1.

Kleele et al. (2021) found that different receptors were involved in different types of fission; Fis1 was key in peripheral fission which led to mitophagy, while Mff was more involved in midzone fission, which led to mitochondrial biogenesis. Associations found in the fibroblasts seemed to fit in with this hypothesis, however, this was not seen in the iNeuron model. This may be due to differences in cell types. Kleele et al. (2021) completed their research in Cos7 cells and mouse cardiomyocytes. It may be that these processes are controlled differently in iNeurons. Further research should be undertaken as to whether these associations can be applied to more complex cell types such as iNeurons. However, it must also be noted that the sample size used in this study for iNeurons was

much smaller than that used in fibroblasts; it may simply be that a higher sample size would bring out these associations more clearly.

When looking at the sAD mitochondrial phenotype in the two different cell types, the functional deficits seem to be conserved across fibroblasts and iNeurons, with both showing a decrease in MMP, though this does vary between cell lines. Though mitochondrial function was not the main focus of this project, it would be interesting to investigate whether other functional deficits, as discussed above (section 4.3.5) seen in fibroblasts also translate to deficits in iNeurons. In contrast, the morphology differences seen differed between the cell types. Firstly, the differences in iNeurons were more varied than the differences seen in fibroblasts. Again, the sample size must be considered; a higher sample size may have shown more consistent results. In general, whilst fibroblasts showed a more fused morphology, several of the neuron lines showed a more fragmented mitochondrial network. This is also seen in other neuron-based models of AD including animal models (Calkins *et al.*, 2011; Xu *et al.*, 2017; Wang and Davis, 2021), and neuroblastoma cell lines treated with A β (X. Wang *et al.*, 2008). This may be due to the differing relationship seen between function and fission proteins in different cell types. The processes controlling mitochondrial morphology are highly regulated, and a disruption in either direction is equally detrimental to mitochondrial function. Even though the differences seen are not necessarily the same, dysfunction in mitochondrial control is seen in both fibroblasts and iNeurons, and any treatment targeted at this pathology should aim to rebalance these highly important processes.

One sAD phenotype which is the same across both fibroblasts and iNeurons is a decrease in MiD49 levels. Unfortunately, MiD49 could not be investigated beyond total cellular levels. The conserved decrease in MiD49 across differing cell types suggests that this could be a key pathology in sAD, contributing to the changes seen in both fibroblasts and iNeurons. Further work in these cell lines should focus on the localisation of MiD49, as well as the interactions between Drp1 and MiD49 to better understand the impact of this decrease. Little is known about the precise function of MiD49, and it is not well researched in AD. Further research should focus on the precise involvement of MiD49 in mitochondrial fission, in particular the differences between MiD49 and MiD51. MiD51 was not seen to be altered in any sAD fibroblast, and only in sAD 4 iNPCs and iNeurons. Much research focusses on the two together, but results shown here suggest that there are key differences between the two and this should be investigated further, both in a healthy and in an AD context.

4.3 Conclusions and Future Work

This chapter aimed to investigate the mitochondrial phenotype in a sAD patient derived neuronal model. Initially, attempts were made to optimise a protocol to produce cortical neurons from iNPCs.

An efficient protocol, with positive neuronal marker expression was optimised, but this did not translate well into different cell lines, with the biggest issue being with cell survival. Further optimisations were not carried out due to the COVID-19 pandemic related time constraints, but future work could focus on completing this optimisation using factors such as ascorbic acid, or neurotrophin 3 to enhance cell survival. Instead, a protocol was chosen which produced a general population of iNeurons from iNPCs. This yielded over 87% TUJ positive neurons, over 60% MAP2 positive neurons, and in most lines, 20-75% NeuN positive neurons. Heterogeneity was seen in neuronal types between different differentiations, with inconsistent TBR1, vGlut1, and Hb9 positive staining seen. No differences were seen between control and sAD iNeurons in terms of general neuronal markers or neuronal morphology, but sAD iNeurons were in general smaller than controls. Furthermore, some sAD lines showed a reduced viability at the end stage of the differentiation protocol, suggesting that alterations present in these lines may impact their ability to survive differentiation.

The mitochondrial phenotype was assessed in the sAD iNeurons, and reduced MMP was seen in the majority of the sAD lines, recapitulating the fibroblast phenotype. This was also assessed under stress conditions. While no further differences were seen between patients and controls, reduced MMP was seen in all lines when grown in galactose media. This suggests that the iNeurons may not be fully reliant on OXPHOS, as mature neurons usually are. Future work could investigate this further by assessing ATP production when glycolysis or OXPHOS are inhibited, which would give a better indication of the metabolic activity in these cells.

The morphology phenotype seen was variable between the different sAD lines assessed, with some lines showing a more fragmented network, while others were more fused. This is different to the fibroblasts, where less variation was seen and a consistently more fragmented mitochondrial phenotype was seen. When the mitochondrial quality control mechanisms were investigated, variation was again seen, with no consistent trend seen in protein expression, localisation, or interactions. Again, this is in contrast to the fibroblasts where though not every line showed alterations in the same proteins, all showed decreased levels of at least one fission protein. These differences may be explained by differences in the metabolism of these cell types, or differences in the relationship between function and morphology. The one alteration which was conserved from the fibroblasts in the iNeurons is a decrease in MiD49. Future work should focus on MiD49 in both health and sAD to determine the importance of this deficit in the mitochondrial phenotype. Drp1 phosphorylation status was assessed in the iNeurons, which was not able to be assessed in the fibroblasts. Again, this data was variable, but a general downregulation of Drp1 phosphorylation was seen. This, along with other post translational modifications of Drp1 such as SUMOylation, should be

investigated further in iNeurons to determine whether this has a significant effect on the mitochondrial fission process.

To conclude, a general neuronal population showing positive expression of general neuronal markers was generated from iNPCs, maintaining aged characteristics of the cell and the patient's genetic background. While mitochondrial function was generally reduced, as previously seen in the fibroblasts from which these iNeurons originated, mitochondrial morphology phenotypes were much more variable and did not necessarily match what was seen in the fibroblasts. This variation is particularly important when attempting to find treatments for sAD.

Chapter Five: Screening for a Compound which Alters Mitochondrial Function and Morphology in Alzheimer's Patient Fibroblasts

5.1 Introduction

5.1.1 Mitochondria Targeted Therapies for AD

Mitochondrial dysfunction is a commonly seen mechanism in AD, including deficits in OXPHOS, changes in morphology, and increased oxidative stress (Macdonald *et al.*, 2018), and as such several treatment strategies have been implemented targeting these deficits. One of the most commonly targeted pathologies is oxidative stress; several mitochondria targeted antioxidant therapies are being studied. One of these is mitoquinone (MitoQ), a derivative of ubiquinone specifically targeted to the mitochondria via conjugation to triphenylphosphonium (TPP), a lipophilic cation. MitoQ is known to protect mitochondria from oxidative damage and prevent lipid peroxidation (Kelso *et al.*, 2001), and in models of AD has been seen to improve MMP and ATP levels (Manczak *et al.*, 2010) as well as reducing A β accumulation, synaptic loss, and caspase activation, and improving cognitive decline in a triple transgenic mouse model (Meagan J McManus, Murphy and Franklin, 2011; Young and Franklin, 2019). MitoQ is currently in clinical trials for mild cognitive impairment (NCT03514875; Effects of Mitochondrial-targeted Antioxidant on Mild Cognitive Impairment (MCI) Patients). Other mitochondria targeted antioxidants include Szeto-Schiller (SS) peptides, antioxidant tetrapeptides which target the mitochondria via lipophilic chains and a positive charge. SS-31 has been seen to reduce A β levels, as well as reduce fission proteins, and rescue learning and memory deficits (Jia *et al.*, 2015; Reddy, Manczak and Kandimalla, 2017). However, many of these studies use a treatment paradigm in which the compound of interest is administered prior to the toxin inducing pathology. Whilst this can act as proof that the compound is affecting the intended target, it is less relevant for human disease, as treatments would not be administered until after pathology is present.

Mitochondrial dynamics is another target for AD treatment, particularly inhibition of Drp1. MDIVI1 has been proposed as an inhibitor of Drp1 GTPase activity, and has been seen to increase fusion, reduce fission protein levels, and improve mitochondrial function in A β treated N2a cells (Reddy, Manczak and Yin, 2017). MDIVI1 was also seen to improve mitochondrial function and rescue increased fragmentation in CRND8 transgenic mice, as well as improve cognitive deficits (W. Wang *et al.*, 2017). MDIVI1 treatment has also been studied in combination with SS-31, where it was found that mitochondrial dysfunction was more significantly improved when both treatments were administered (Reddy, Manczak, *et al.*, 2018). However, the action of MDIVI1 as an inhibitor of fission

has been questioned by Bordt *et al.* (2017), who proposed that it is instead an inhibitor of complex I. They observed respiratory impairment, but no mitochondrial elongation in primary neurons, and the effects were not mimicked by deletion of Drp1. While there is evidence of increased fragmentation and Drp1 activity in AD, this is far from consistent, as discussed in previous chapters of this thesis. Kleele *et al.* (2021) recently proposed two distinct types of fission, both reliant on Drp1. It may be that the alterations seen in AD are due to one of these types only. It may also be that there are cell type differences in the changes in Drp1 and mitochondrial fission in AD. As such, global inhibition of Drp1 may have a detrimental effect, and so it is still unclear as to whether Drp1 inhibition is a viable target for human AD.

Another mitochondrial process which has been targeted for treatment of AD is mitophagy. Mitophagy enhancers such as Urolithin A, actinonin, and tomatidine, have been shown to increase cell survival, increase mRNA and protein expression associated with mitochondrial fusion and mitophagy, and reduce mitochondrial fragmentation in HT22 cells transfected with either mutant APP (Kshirsagar *et al.*, 2022) or tau (Kshirsagar *et al.*, 2021). Urolithin A and actinonin have also been shown to reduce cognitive impairment, A β accumulation, and neuroinflammation in an APP/PSEN1 mouse model (Fang *et al.*, 2019; Gong *et al.*, 2019), and in a first in human trial, Urolithin A was shown to be safe, as well as improve mitochondrial health (Andreux *et al.*, 2019). Recently, Xie *et al.*, (2022) identified Kaempferol and Rhapontigenin in an AI-driven virtual screen as enhancers of mitophagy. Treatment with either in 3Tg mice was seen to improve memory, reduce A β and tau pathology, and increase the survival and functionality of glutamatergic and cholinergic neurons (Xie *et al.*, 2022).

We identified UDCA, a bile acid currently used to treat primary biliary cirrhosis, as improving mitochondrial function in both sAD and fAD patient derived fibroblasts (Bell *et al.*, 2018). UDCA conjugated to taurine (TUDCA) has been seen to reduce apoptosis in a mouse neuroblastoma cell line with an APP mutation, reducing caspase activity (Ramalho *et al.*, 2006), as well as improving memory deficits and reducing A β accumulation in an APP/PSEN1 mouse model (Lo *et al.*, 2013; Dionísio *et al.*, 2015). In our study, UDCA was seen to rescue MMP, as well as increase both total levels, and mitochondria located Drp1 (Bell *et al.*, 2018).

5.1.2 Phenotypic vs Target Driven Approaches to Drug Screening

There are several approaches which can be taken to identify new, potentially disease modifying compounds. These include both phenotypic and target-driven approaches. This screen will use a phenotypic approach, in which a cell-based assay is used to identify compounds which affect disease

associated pathologies, in this case mitochondrial function and morphology. Historically, drug discovery was mostly phenotypic but with developments in genetics, pharmacology, and biochemistry, there came a shift to more target driven approaches (Zheng, Thorne and McKew, 2013). In this approach, a specific molecular target is identified, and compounds are assessed for an effect specifically on that target. This approach is generally simpler, cheaper, and easier to run than a phenotypic screen, and has proved to be successful in the discovery of small molecule compounds as well as antibody treatments and gene therapy (Croston, 2017). Furthermore, having knowledge of the target enables a compound to be optimised to have the desired effect and as such, increases the chances of success (Croston, 2017).

However, a target driven screen is reliant on the identification of a suitable target. In the case of AD and other complex diseases, target identification is not always straightforward. It is unknown what the precise cause of AD is, and likely that more than one pathological mechanism contributes to the disease. A lack of a confirmed target makes this type of approach difficult and may lead to wasted resources if a target is not able to be validated, and proves to be unsuccessful in affecting disease progression or symptoms. Furthermore, targets identified in simple models will not necessarily act the same in a complex biological system, and this can also lead to failure in clinical trials (Zheng, Thorne and McKew, 2013; Croston, 2017). A single target and mechanism of action may also fail to fully encapsulate the effect of a compound; drugs can have off target effects which may not be identified in this type of focused screen (Croston, 2017).

On the other hand, phenotypic screens offer an unbiased approach, looking generally for an effect on disease associated mechanisms rather than focussing on a single target. This type of screen is more physiologically relevant and as such, success from this type of approach may be more translational and have more success in clinical trials (Zheng, Thorne and McKew, 2013). It also enables the identification of novel targets, which is key in AD where drugs targeting many known targets have failed in clinical trials (Zheng, Thorne and McKew, 2013; Croston, 2017).

As part of this project, a focus group was designed, organised, and carried out with people affected by dementia, family members, and healthcare professionals, to discuss their views on drug discovery in AD. One of the discussion points was whether they saw more value in a phenotypic or target-based approach. The consensus was that while a target driven approach may initially increase the likelihood of success, given the lack of success of AD treatments, the broader approach of a phenotypic screen was advantageous. It was also mentioned that if a treatment was proven to be safe and have a disease modifying effect, it was not necessarily important to them to understand the

precise mechanism of action. However, it was noted that not all patients and family members would necessarily share this view.

5.1.3 High Throughput Drug Screening using Patient Fibroblasts

This chapter will utilise high content imaging as a high throughput screening method. High content imaging uses automated microscopy-based assays to study various aspects of cellular function and morphology (Joshi and Lee, 2015), in this case of the mitochondria. Cells are treated with compounds, and the effects of these compounds on various functional and morphological parameters is assessed. Assays can be miniaturised through the use of multi-well plates, enabling large compound libraries to be assessed in a short space of time. This is a powerful drug discovery tool which has been employed to study mitochondrial parameters in various conditions (Sahdeo *et al.*, 2014; Hou *et al.*, 2017; Shlevkov *et al.*, 2019), including neurodegenerative diseases such as PD (Scott *et al.*, 2020).

Fibroblasts are a particularly useful model for high throughput drug screening; they recapitulate many of the pathological phenotypes seen in more relevant cell types, and are more time and cost efficient for large compound libraries, enabling only the most effective compounds to be carried forward into more costly models. Fibroblasts have been used to identify disease-modifying compounds in a range of different conditions, including mitochondrial diseases (Golubitzky *et al.*, 2011; Sahdeo *et al.*, 2014), and lysosomal diseases (Ribbens *et al.*, 2013; Xu *et al.*, 2013). In Leigh Syndrome, a paediatric mitochondrial disease, a vitamin E derivative Trolox was found to reduce oxidative stress in patient fibroblasts with a complex I deficiency (Koopman *et al.*, 2008). Trolox derivatives were then generated, and their efficacy in patient fibroblasts assessed via artificial intelligence and machine learning, where a lead compound was identified and further optimised (Blanchet *et al.*, 2015). From these further optimisations, KH176 (Sonlicromanol) was chosen based on its efficacy as well as other important considerations such as chemical stability and blood brain barrier permeability (De Haas *et al.*, 2017). KH176 has since undergone phase I and IIa clinical trials for the treatment of mitochondrial diseases, and has been shown to be safe and well tolerated (Koene *et al.*, 2017; Janssen *et al.*, 2019), and is currently undergoing a phase IIb clinical trial (NCT02544217; A Dose-escalating Clinical Trial With KH176). This success story highlights the meaningful use of fibroblasts in identifying disease-modifying compounds with the potential for clinical success.

Fibroblasts have also been used in screening for compounds which have an effect on neurodegenerative diseases, for example, Friedrich's Ataxia, a rare autosomal recessive disorder

caused by reduced levels of the mitochondrial protein frataxin (Y. Li *et al.*, 2016; Rufini *et al.*, 2022). Peroxisome proliferator-activated receptor gamma (PPAR γ) agonists were proposed as a therapeutic for Friedrich's Ataxia, and were found to increase frataxin mRNA and protein in patient fibroblasts, as well as increase the expression of antioxidant SOD2 (Marmolino *et al.*, 2009, 2010). PPAR γ agonist MIN-102 (Leriglitazone) is currently in clinical trials for the treatment of Friedrich's Ataxia (NCT03917225; A Clinical Study to Evaluate the Effect of MIN-102 on the Progression of Friedreich's Ataxia in Male and Female Patients), again highlighting the potential of compounds first identified in fibroblasts. In our lab, high content drug screening methods in a fibroblast model were key in identifying UDCA as a modulator of mitochondrial function in PD (Mortiboys, Aasly and Bandmann, 2013; Mortiboys *et al.*, 2015; Payne *et al.*, 2020), a compound which is now in clinical trials for PD (NCT03840005; Trial of Ursodeoxycholic Acid (UDCA) for Parkinson's Disease: The "UP" Study). We have since found that UDCA also rescues mitochondrial deficits in AD (Bell *et al.*, 2018).

In AD, patient fibroblasts were first proposed as a model for therapeutic screening many years ago (Malow, Baker and Blass, 1989), and were used to identify L-carnitine as having a beneficial effect in AD patient cells. L-carnitine is still the subject of much research within the field (Kepka *et al.*, 2020; Pennisi *et al.*, 2020).

5.1.4 Aims and Objectives

Previous work in AD fibroblasts has found a reduction in MMP in both sAD and PSEN1 fibroblasts, including cell lines used in this chapter, as well as morphological changes such as an increased number of mitochondria accumulated in the perinuclear region, an increase in the percentage of the cell area taken up by long mitochondria, and a more fused mitochondrial network (Bell *et al.*, 2018).

Therefore we hypothesize that small molecules can be found which can beneficially modulate the mitochondrial phenotype in sAD fibroblasts. The aim of this chapter is to screen a compound library from an industrial collaborator for compounds which have a beneficial effect on mitochondrial function and morphology in fibroblasts from AD patients. The objectives are:

1. To screen 21,000 compounds in one sAD line and identify those which have a significant effect on MMP, percentage of mitochondria in the perinuclear region, percentage of the cell taken up by long mitochondria, and mitochondrial count per cell
2. To assess the dose response of compounds identified as hits from objective 1 in one sAD line, and identify a final hit list of top performing compounds
3. To investigate whether these compounds have a similar effect in fibroblasts taken from a patient with a PSEN1 mutation

4. To assess the effect of the top performing compounds in a further three control and three sAD lines taken from a different patient cohort, to validate their positive effect on mitochondrial parameters

5.2 Drug Screening Methods

5.2.1 Compound Library

A compound library consisting of 21,000 compounds was provided by an industrial collaborator, Eli Lilly, in 384 well low dead volume (LDV) source plates. Compounds were provided in DMSO at a stock concentration of 1mM, and were stored in the MultiPod storage system (Roylean). This system removes oxygen and humidity, reducing damage to compounds and extending their lifespan. Structures were not provided, in order to prevent bias. Compounds were screened for an effect on mitochondrial function and morphology parameters, based on deficits previously seen in sAD fibroblasts.

A brief overview of the drug screen process carried out in this project is shown in figure 90.

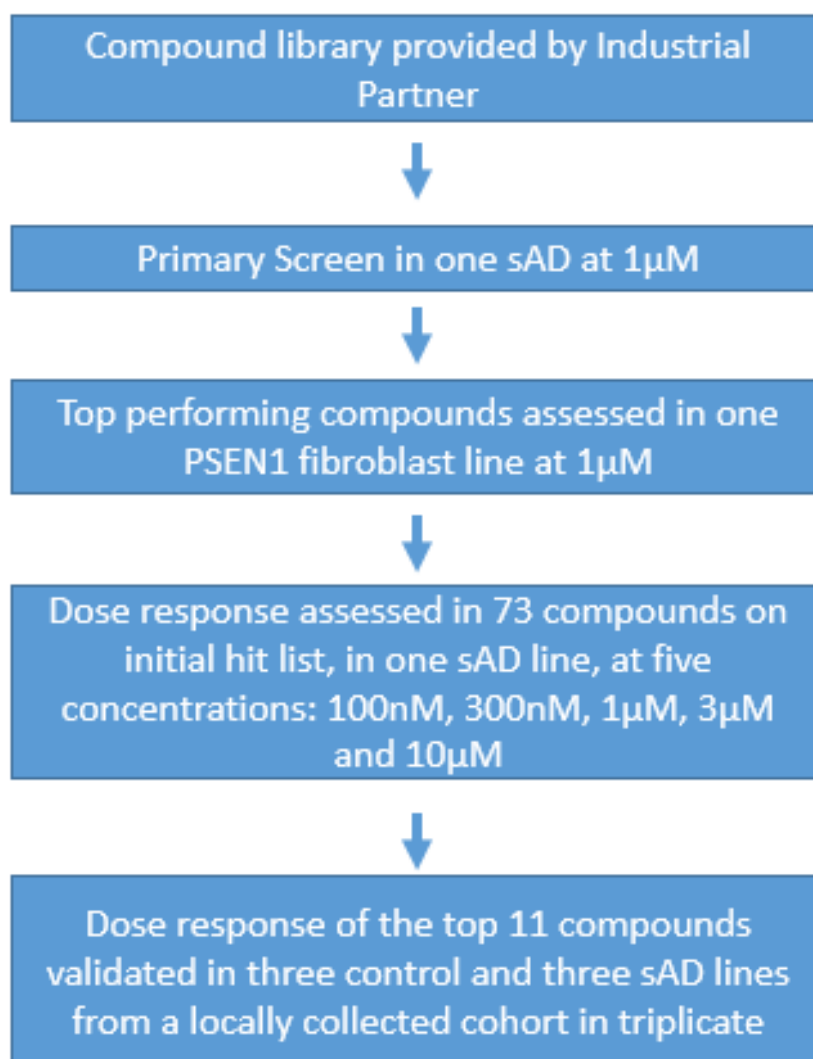


Figure 90: A brief overview of the drug screen process carried out in this project.

5.2.2 Primary Drug Screen

For the primary screen, sAD fibroblasts were cultured as described previously. Cell lines used were from the Coriell cell repository (AG08597; male, 50 years; AG08243; male, 72 years), and all show reductions in MMP, increased percentage of mitochondria in the perinuclear region, and a more fused mitochondrial network. When confluent, cells were plated into either 1536 well plates (Greiner), at a density of 150 cells per 5 μ l of media per well, or in 384 well plates (Greiner), at a density of 420 cells per 40 μ l of media per well. Cells were drugged 24 hours after plating, using the Echo 550 Liquid Handling System (Labcyte). This is an automated system, which uses acoustic droplet ejection, by which sound waves are used to move very small volumes of liquid without any physical contact. This increases precision and accuracy, whilst also decreasing the chance of contamination (Q. Guo *et al.*, 2021).

For the primary screen, a programme was designed on the Echo 550 by which 1536 well cell plates could be drugged by four separate 384 well LDV source plates, where each well of cells was treated by a different compound. Compounds were stored at a stock concentration of 1mM, and so 5nl of this stock solution was transferred to each well to give a final concentration of 1 μ M. Alongside the wells containing compounds of interest, four columns (128 wells) spread across the plate were treated with 5nl of a DMSO vehicle control. Another three columns (96 wells) were drugged with 5nl of a 1mM stock of UDCA to give a final concentration of 1 μ M. This was used as a positive control, as it has previously demonstrated a mitochondrial rescue effect in sAD fibroblasts (Bell *et al.*, 2018). A plate map is shown in figure 91.

A separate programme was designed for the drugging of 384 well plates. In this case, 40nl was transferred into each well from a single source plate, again to give a 1 μ M final concentration. Two columns (32 wells) at the start and end of the plate were treated with 40nl DMSO vehicle control, and two columns with 40nl of 1mM stock UDCA, giving a final concentration of 1 μ M. A plate map is shown in figure 92.



Figure 91: Plate map used for 1536 well plates in the primary screen. Columns 1, 23, 24, and 47 are treated with 5nI DMSO vehicle control, shown in pink. Columns 2, 24, 25, and 48 are treated with 1 μ M UDCA positive control, shown in orange. Columns 3-22 rows A-D are treated with 1 μ M compounds from source plate 1. Columns 27-46 rows A-D are treated with 1 μ M compounds from source plate 2. Columns 2-33 rows E-H are treated with 1 μ M compounds from source plate 3. Columns 27-46 rows E-H are treated with 1 μ M compounds from source plate 4. Each different shade of green represents a different source plate.

	1	2	3	4	5	6	7	8	9	10	11	12	13	14	15	16	17	18	19	20	21	22	23	24
A	DMSO	UDCA	Drug Plate																				DMSO	UDCA
B																								
C																								
D																								
E																								
F																								
G																								
H																								
I																								
J																								
K																								
L																								
M																								
N																								
O																								
P																								

Figure 92: Plate map used for 384 well plates in the primary screen. Columns 1 and 23 are drugged with a 40nl DMSO vehicle control, shown in pink. Columns 2 and 24 are drugged with 1 μ M UDCA positive control, shown in orange. Columns 3-22 are drugged with a 1 μ M compounds of interest from a single source plate, shown in green.

The mitochondrial membrane potential assay was used to measure mitochondrial membrane potential as a measure of function, as well as mitochondrial morphology.

To carry out the mitochondrial membrane potential assay, cells were incubated for one hour with a working solution of 80nM tetramethylrhodamine, methyl ester (TMRM; Invitrogen), and 10 μ M Hoechst (Sigma) in phenol red free minimum essential media (MEM; Gibco by ThermoFisher Scientific). As previously described (Chapter 4, section 4.3.5), TMRM is cationic, staining the most negative part of the cell, and so can be used as a measure of mitochondrial membrane potential. However, TMRM can be used in two modes; to determine that staining is in the correct mode, in previous work a validation assay was carried out using carbonyl cyanide m-chlorophenyl hydrazone (CCCP; Sigma), a mitochondrial uncoupler which dissipates the membrane potential. A reduction in fluorescent intensity was noted, indicating TMRM was being used correctly. Immediately before imaging, wells were washed with 5 μ l MEM for 1536 well plates, or 40 μ l for 384 well plates. Cells were imaged using InCell 2000 high content imager (GE Healthcare Life Sciences), or the Opera Phenix (Perkin Elmer). A total of 5 fields of view, approximately 20 cells per well, were imaged per well for 1536 well plates, and 10 fields of view, approximately 60 cells per well, for 384 well plates, using the Cy3 channel (excitation 645/30; emission 705/72) and the DAPI channel (excitation 350/50; emission 455/50). Exposure time was optimised for each plate.

5.2.3 Primary Drug Screen Analysis

Images were analysed using either InCell Developer Toolbox software (GE Healthcare Life Sciences) or Harmony software (Perkin Elmer), to obtain a range of mitochondrial parameters. Images were segmented to show the nuclei, cells, and individual mitochondria (figure 93). As a functional parameter, mitochondrial membrane potential, based on the intensity of TMRM staining and normalised to cell area, was assessed. Furthermore, several morphological parameters were studied including mitochondrial count per cell, mitochondria accumulated in the perinuclear region where the perinuclear region is defined as a 27% region around the nucleus, and percentage of long mitochondria, where a long mitochondrion is defined as having a form factor of less than 0.48. Form factor is a measure of mitochondrial interconnectivity calculated using the following equation: $(pm^2)/(4\pi am)$ where pm is the length of the mitochondrial perimeter and am is the area of the mitochondrion. An increase in form factor indicates a more fused network. The above parameters were chosen based on previous work, which showed alterations in these measures in sAD fibroblasts compared to controls (Bell et al., 2018).

An initial hit list of compounds was determined, with a hit defined as a compound which had a significant effect on one or more of the four parameters described above. The mean and standard deviation of the DMSO negative control was calculated, and a significant effect characterised as a value outside of the range of three standard deviations above and below the DMSO mean. Data was also represented as a z score for each compound for each parameter, calculated as follows: $Z = (x - \mu) / \sigma$ where μ =population mean and σ =population standard deviation.

Compounds were then further evaluated to establish a refined hit list. The refined hit list was determined using the following scoring system. A score of three was given to all compounds appearing on the initial hit list, with a potential extra score of two for positive effect on MMP, one for form factor, and one for mitochondrial count per cell. These parameters were chosen as a general indication of functional and morphological effects, with an equal weighting given to function and morphology. For each compound, the percentage increase in MMP and mitochondrial count and the percentage decrease in form factor from the DMSO mean was calculated. This percentage of the weighting score for each parameter was then added to the initial starting score of the compound. Final hits were identified as those with a total final score of four or above. This scoring system was chosen as it allows all the critical mitochondrial parameters to be taken into consideration in a single score, as opposed to ranking all compounds on each parameter separately, enabling better comparisons to be made of the compound effects on mitochondrial health as a whole.

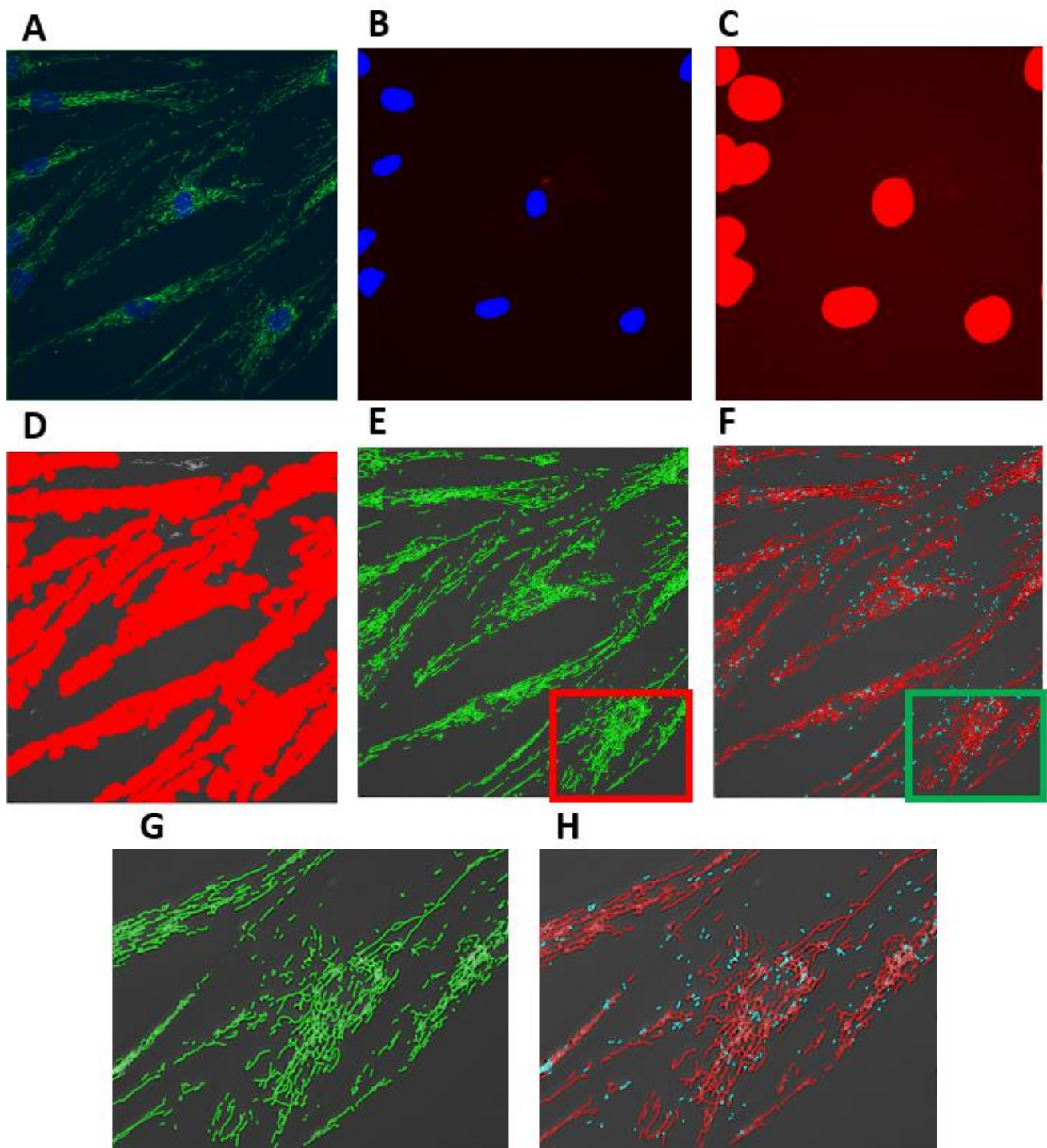


Figure 93: Analysis and segmentation of MMP assay in InCell Developer Toolbox in patient fibroblasts. A) Original input image, Hoechst staining to represent the nucleus shown in blue and TMRM staining shown in green. B) Segmentation of the nuclei. C) Identification of the perinuclear region. D) Segmentation of the cells. E) Segmentation of all mitochondria. F) Segmentation of long (red) and short (blue) mitochondria. G) Zoomed in image of the area in the red box in E, showing segmentation of all mitochondria. H) Zoomed in image of the area in the green box in F, showing segmentation of the short and long mitochondria.

5.2.4 Screening compounds in one PSEN1 line

PSEN1 fibroblasts were cultured as previously described. Cell line used was from the Coriell cell repository (ND34733; male, 60 years). Fibroblasts were plated, assayed, and analysed as described above. Compounds were not scored or ranked based on their effect on PSEN1 fibroblasts, the effect of compounds on the refined hit list was simply compared to the effect in sAD fibroblasts. This data was not taken into account going forward. Compounds did not have the same beneficial effect in PSEN1 fibroblasts as they did in sAD fibroblasts, and so it was decided to focus on sAD only.

5.2.5 Dose Response Screen

73 compounds from the final hit list were taken forward for dose response analysis in a sAD cell line from the Coriell repository (AG07872; male, 53 years). Fibroblasts were cultured and plated into 384 well plates as previously described. Cells were again drugged using the Echo 550 liquid handling system. A new programme was designed for the dose response, in which cells were drugged with five different concentrations. A new source plate was obtained from the industrial collaborators containing the 73 top compounds at a 10mM concentration in DMSO, and was again stored using the MultiPod storage system. This was diluted further in DMSO to give a 2mM stock concentration on the same source plate, and the Echo 550 was programmed to dispense 2.5nl, 6nl, 20nl, 60nl, and 200nl, to give final concentrations of 100nM, 300nM, 1µM, 3µM and 10µM respectively. UDCA and DMSO were again used as positive and negative controls, and were dispensed in the same manner. A plate map is shown in figure 94.

Three plates were imaged in total to assess each of the 73 compounds at the five selected concentrations in a single sAD cell line, two full plates according to the plate map below (figure 94) and one with the remaining compounds. The mitochondrial membrane potential assay was carried out as previously described, with assays being carried out on the Opera Phenix (Perkin Elmer).

	1	2	3	4	5	6	7	8	9	10	11	12	13	14	15	16	17	18	19	20	21	22	23	24	
a																									
b																									
c			DMSO	UDCA 100nM	2 100nM	4 100nM	6 100nM	8 100nM	10 100nM	12 100nM	14 100nM	16 100nM	18 100nM	20 100nM	22 100nM	24 100nM	26 100nM	28 100nM	30 100nM	32 100nM	34 100nM	DMSO			
d			DMSO	300nM	300nM	300nM	300nM	300nM	300nM	300nM	300nM	300nM	300nM	300nM	300nM	300nM	300nM	300nM	300nM	300nM	300nM	300nM	DMSO		
e			DMSO	1uM	1uM	1uM	1uM	1uM	1uM	1uM	1uM	1uM	1uM	1uM	1uM	1uM	1uM	1uM	1uM	1uM	1uM	1uM	DMSO		
f			DMSO	3uM	3uM	3uM	3uM	3uM	3uM	3uM	3uM	3uM	3uM	3uM	3uM	3uM	3uM	3uM	3uM	3uM	3uM	3uM	DMSO		
g			DMSO	10uM	10uM	10uM	10uM	10uM	10uM	10uM	10uM	10uM	10uM	10uM	10uM	10uM	10uM	10uM	10uM	10uM	10uM	10uM	DMSO		
h			UDCA 100nM	1 100nM	3 100nM	5 100nM	7 100nM	9 100nM	11 100nM	13 100nM	15 100nM	17 100nM	19 100nM	21 100nM	23 100nM	25 100nM	27 100nM	29 100nM	31 100nM	33 100nM	35 100nM	UDCA 100nM			
i			300nM	300nM	300nM	300nM	300nM	300nM	300nM	300nM	300nM	300nM	300nM	300nM	300nM	300nM	300nM	300nM	300nM	300nM	300nM	300nM	300nM	300nM	300nM
j			1uM	1uM	1uM	1uM	1uM	1uM	1uM	1uM	1uM	1uM	1uM	1uM	1uM	1uM	1uM	1uM	1uM	1uM	1uM	1uM	1uM	1uM	1uM
k			3uM	3uM	3uM	3uM	3uM	3uM	3uM	3uM	3uM	3uM	3uM	3uM	3uM	3uM	3uM	3uM	3uM	3uM	3uM	3uM	3uM	3uM	3uM
l			10uM	10uM	10uM	10uM	10uM	10uM	10uM	10uM	10uM	10uM	10uM	10uM	10uM	10uM	10uM	10uM	10uM	10uM	10uM	10uM	10uM	10uM	10uM
m																									
n																									
o																									
p																									

Figure 94: Plate map used for dose response screen. Columns 3 and 22 rows c-g are treated with DMSO vehicle control. Columns 3 and 22 rows h-l, and column 4 rows c-g are treated with UDCA positive control. All other wells are treated with compounds from the hit list. There are 35 compounds on the plate at five concentrations: 100nM, 300nM, 1µM, 3µM, and 10µM. Each compound is represented on the plate map by a different colour. The outer wells in red are left empty, while the white wells are untreated cells.

5.2.6 Dose Response Analysis

Harmony analysis was carried out as previously described (Chapter 2, section 2.8.2). Dose response was investigated in three parameters, MMP, form factor, and mitochondrial count per cell, again to give a general indication of functional and morphological response.

Statistical analysis of dose response data was carried out using GraphPad Prism 7. Concentrations were transformed to logarithms, and a nonlinear regression was applied to the data, using the 'log(agonist) vs response' equation to calculate information such as the EC50, and 95% confidence intervals. The 11 compounds which demonstrated the most promising dose response in the selected parameters were chosen to take forward for further screening. This was defined as compounds which had a consistently positive effect across all concentrations, and the best maximal effects.

5.2.7 Dose Response in a Locally Collected Cohort of Fibroblasts

The top 11 compounds identified by the dose response screen were taken forward and the dose response was assessed in a locally collected cohort of fibroblasts (Research and Ethics Committee number: 16/YH/0155), in two control lines (Control 1, male, 53 years; Control 7, male, 56 years) and three sAD lines (sAD 1, male, 53 years; sAD 2, male, 60 years; sAD 9, female, 79 years). A third control age and sex matched with sAD 9 was initially planned to be included, but issues with cell growth and time constraints meant this was impossible.

While previous screens had only been carried out on patient fibroblasts, top compounds were also tested on control fibroblasts to see whether they had the same effect as they did in the patient fibroblasts. Cells were cultured and plated as previously described in 384 well plates, with half the plate seeded with control fibroblasts and half with sAD fibroblasts. Cells were drugged with the Echo 550 in the same manner and at the same range of concentrations as previously used, 100nM, 300nM, 1 μ M, 3 μ M and 10 μ M, with two wells per concentration according to the plate map shown in figure 95. DMSO and UDCA were again used as a negative and positive control respectively (figure 95). The mitochondrial membrane potential assay with imaging on the InCell was carried out as previously described (Section 5.2.3).

5.2.8 Dose Response in a Locally Collected Cohort Analysis

InCell Developer Toolbox analysis was carried out as previously described. Dose response was investigated in three parameters: MMP, form factor, and mitochondrial count per cell. This was repeated in triplicate in each of the six cell lines used. Triplicate repeats for each line were combined, and statistical analysis was carried out using GraphPad Prism 7 as described above. Group effects were also assessed by combining all control lines, and all sAD lines, and statistical analysis carried out in the same way.

	1	2	3	4	5	6	7	8	9	10	11	12	13	14	15	16	17	18	19	20	21	22	23	24
a																								
b		Control											sAD											
c		Hit 1 10uM	Hit 1 10uM	Hit 3 10uM	Hit 3 10uM	Hit 5 10uM	Hit 5 10uM	Hit 7 10uM	Hit 7 10uM	Hit 9 10uM	Hit 9 10uM	Hit 1 10uM	Hit 1 10uM	Hit 3 10uM	Hit 3 10uM	Hit 5 10uM	Hit 5 10uM	Hit 7 10uM	Hit 7 10uM	Hit 9 10uM	Hit 9 10uM			
d		3uM	3uM	3uM	3uM	3uM	3uM	3uM	3uM	3uM	3uM	3uM	3uM	3uM	3uM	3uM	3uM	3uM	3uM	3uM	3uM	3uM	3uM	
e		1uM	1uM	1uM	1uM	1uM	1uM	1uM	1uM	1uM	1uM	1uM	1uM	1uM	1uM	1uM	1uM	1uM	1uM	1uM	1uM	1uM	1uM	
f		300nM	300nM	300nM	300nM	300nM	300nM	300nM	300nM	300nM	300nM	300nM	300nM	300nM	300nM	300nM	300nM	300nM	300nM	300nM	300nM	300nM	300nM	
g		100nM	100nM	100nM	100nM	100nM	100nM	100nM	100nM	100nM	100nM	100nM	100nM	100nM	100nM	100nM	100nM	100nM	100nM	100nM	100nM	100nM	100nM	
h		Hit 2 10uM	Hit 2 10uM	Hit 4 10uM	Hit 4 10uM	Hit 6 10uM	Hit 6 10uM	Hit 8 10uM	Hit 8 10uM	Hit 10 10uM	Hit 10 10uM	Hit 2 10uM	Hit 2 10uM	Hit 4 10uM	Hit 4 10uM	Hit 6 10uM	Hit 6 10uM	Hit 8 10uM	Hit 8 10uM	Hit 10 10uM	Hit 10 10uM			
i		3uM	3uM	3uM	3uM	3uM	3uM	3uM	3uM	3uM	3uM	3uM	3uM	3uM	3uM	3uM	3uM	3uM	3uM	3uM	3uM	3uM	3uM	
j		1uM	1uM	1uM	1uM	1uM	1uM	1uM	1uM	1uM	1uM	1uM	1uM	1uM	1uM	1uM	1uM	1uM	1uM	1uM	1uM	1uM	1uM	
k		300nM	300nM	300nM	300nM	300nM	300nM	300nM	300nM	300nM	300nM	300nM	300nM	300nM	300nM	300nM	300nM	300nM	300nM	300nM	300nM	300nM	300nM	
l		100nM	100nM	100nM	100nM	100nM	100nM	100nM	100nM	100nM	100nM	100nM	100nM	100nM	100nM	100nM	100nM	100nM	100nM	100nM	100nM	100nM	100nM	
m		UDCA 10uM	3uM	1uM	300nM	100nM	Hit 11 10uM	3uM	1uM	300nM	100nM	UDCA 10uM	3uM	1uM	300nM	100nM	Hit 11 10uM	3uM	1uM	300nM	100nM			
n		UDCA 10uM	3uM	1uM	300nM	100nM	Hit 11 10uM	3uM	1uM	300nM	100nM	UDCA 10uM	3uM	1uM	300nM	100nM	Hit 11 10uM	3uM	1uM	300nM	100nM			
o		DMSO 10uM	10uM	3uM	3uM	1uM	1uM	300nM	300nM	100nM	100nM	DMSO 10uM	10uM	3uM	3uM	1uM	1uM	300nM	300nM	100nM	100nM			
p																								

Figure 95: Plate map used to assess dose response in a locally collected cohort of patient and control fibroblasts. Columns 3-12 contain control fibroblasts and columns 13-22 contain sAD fibroblasts. Rows m-n columns 3-7 and 13-17 were treated with positive control UDCA, and row o was treated with vehicle control DMSO. Two wells were treated with each concentration of each hit compound in both the control line and the sAD line. Each compound is represented by a different colour. The outer wells in red were left empty.

5.3 Results

5.3.1 Primary Drug Screen in One sAD Fibroblast Line

This screen was set up in previous work by Professor Heather Mortiboys, in fibroblasts from AD patients using the same assay design and analysis. Using this experimental set up, Professor Mortiboys assessed the robustness and reproducibility of the assay using standard drug discovery methods of various plate maps with hi and low conditions, where hi is treated with an optimum concentration of a compound and low is vehicle treated. Using integrated weave plate maps, Professor Mortiboys was able to show that the calculated Z' score for this assay in AD fibroblasts was 0.6 for MMP and 0.65 for percentage long mitochondria in a 384 well plate format, and 0.5 for MMP and 0.65 for percentage long mitochondria in a 1536 well plate format. These Z' values give an indication of the robustness and reproducibility of the assay, and show that these are well within the tolerated range for a phenotypic assay. While Z' > 0.5 is used for a target driven assay, below 0.5 is often accepted for a phenotypic assay. Professor Mortiboys then provided training in this assay, and checked the robustness in my hands before the screen was undertaken.

Approximately 70% of the compound library provided was screened at 1 μ M in one sAD patient fibroblast line from the Coriell cell repository. Compounds were investigated for an effect in four parameters, mitochondrial membrane potential, perinuclear percentage, mitochondrial number per cell, and percentage of long mitochondria. Representative images are shown in figure 96 of vehicle and compound of interest treated fibroblasts. In figure 96c, it can be seen that the compound has increased the MMP, as shown by an increase in the intensity of the TMRM staining shown in green, and mitochondrial count per cell as shown by an increase in the amount of green staining, when compared to the DMSO treated cells in figure 96a-b. In figure 96d, the compound has decreased the number of mitochondria per cell, shown by the reduction in the amount of green TMRM staining when compared to DMSO treated cells in 114a-b.

For this project, a compound was defined as having a significant effect if it gave a measure that was outside of the range of the DMSO mean \pm 3SD, a method which has been used previously (Mortiboys, Aasly and Bandmann, 2013). At this stage, there was no distinction between compounds having a positive or negative effect. Approximately 3% of compounds were identified as having a significant effect on at least one parameter in sAD patient fibroblasts. This included 165 compounds having an effect on MMP, and 322 having an effect on at least one of the morphology parameters. Of these, 40 compounds had an effect on both function and morphology.

A large amount of data was produced by this screen, and the data has been represented in two ways. Firstly, the raw data is shown, in which each compound is represented as a black dot, and the DMSO mean, and DMSO mean \pm 3SD, is also shown. These graphs show how the hits were spread across the plate, and give an indication of the number of compounds per plate which were considered a hit. Secondly, data is represented as z scores and ranked according to the size and direction of the effect. A z score shows how far from the data set mean each value is; a positive z score indicates a value above the mean, and a negative z score indicates a value below the mean. In this more standardised format, it becomes more clear how data points were spread around the mean, and enables easier comparisons between multiple parameters and multiple plates, in particular for intensity values such as the MMP, as this can be easily affected by day to day variability.

Figure 97a-b shows representative graphs for MMP across one 1536 well plate. Figure 97a shows there are 25 compounds on this plate which are increasing MMP enough compared to the DMSO mean to be considered a hit. Figure 97b shows that on this plate, approximately 58% of compounds show reduced MMP in comparison to the plate mean. Z scores ranged from -3.74 to 20.7, and were distributed evenly around the mean, though with a slight bias towards a reduction in MMP. There are three compounds in particular which greatly increased MMP in comparison to the plate mean, with z scores of 8.4, 12.0, and 20.7.

Figure 97c-d shows representative graphs for mitochondrial count per cell across one 1536 well plate. Figure 97c shows that 21 compounds increased mitochondrial count per cell to a level great enough to be counted as a hit. There was 80 compounds which reduced mitochondrial count per cell to below the DMSO - 3SD threshold, indicating a negative effect on mitochondrial morphology. In figure 97d, approximately 60% of compounds showed a reduction in mitochondrial count per cell compared to the plate mean. Z scores ranged from -4.64 to 8.8, and were again distributed evenly around the plate mean with a slight bias towards reduced count. There were several compounds which increased mitochondrial count per cell to a great extent, two in particular showed very high z scores of 8.2 and 8.8 compared to other compounds; the next highest z score was 6.36.

Figure 97e-f shows representative graphs for the percentage of the area taken up by long mitochondria across one 1536 well plate. Figure 97e shows 9 compounds increased the percentage of the area taken up by long mitochondria to above the DMSO mean + 3SD, and 12 compounds reduced this percentage to below DMSO mean - 3SD. This is less hit compounds than were identified on this plate for the other parameters. Figure 97f shows that the compounds in the parameter are more concentrated around the mean, with a smaller range of z scores from -3.4 to

5.1. Approximately 42% of compounds reduce the area taken up by long mitochondria in comparison to the plate mean. No compounds stand out as having a particularly large effect in comparison to the other compounds.

Figure 97g-h shows the percentage of mitochondria accumulated in the perinuclear region across one 1536 well plate. Figure 97g shows 12 compounds which are increasing the parameter enough to be classed as a hit, and 88 compounds which reduced the percentage to below the threshold. Figure 97h shows that approximately 57% of compounds are reducing the percentage of perinuclear mitochondria in comparison to the plate. Z scores ranged from -3.9 to 7.8.

In order to refine the list of compounds to enable validation studies, the initial list of compounds affecting at least one parameter was refined to include only compounds which had a positive effect on multiple parameters, either function or morphology, or those which had a very large effect on MMP, using the scoring system previously described. This scoring system was used so that all parameters assessed could be incorporated into a single score, enabling easier comparisons between the different compounds. The top 73 compounds as ranked by the scoring system were taken forward for further analysis. Of these, 21 had a positive effect on MMP only, 33 had a positive effect on morphology only, and 19 had a positive effect on both.

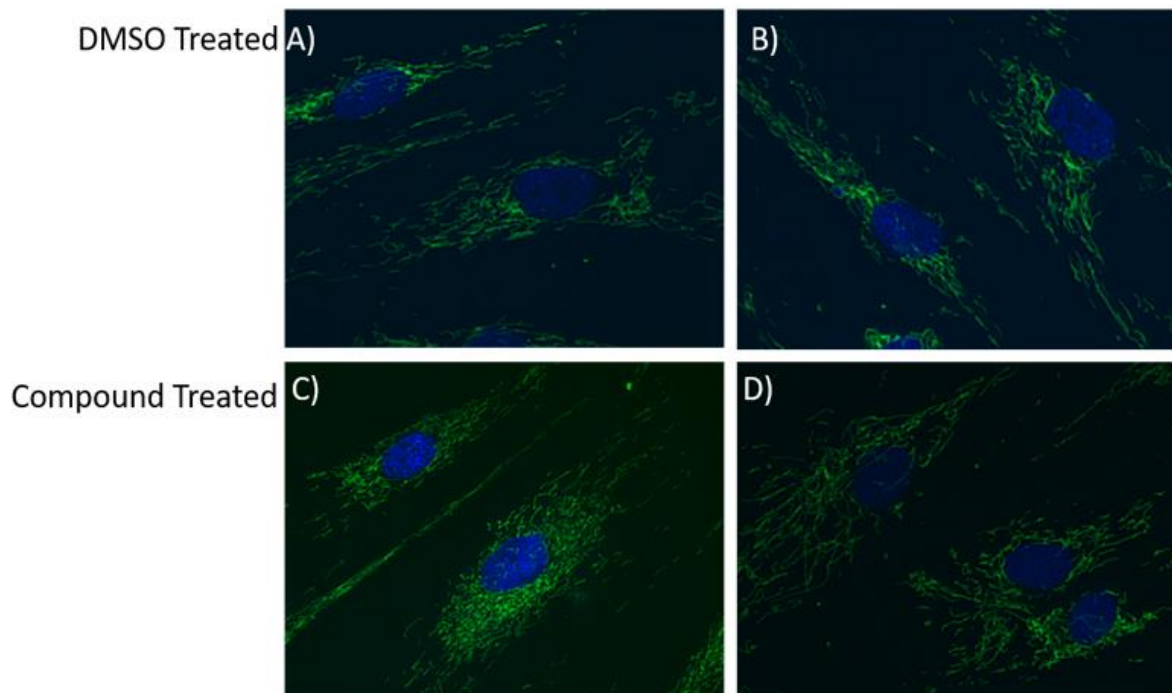


Figure 96: Representative images of treated fibroblasts. The Hoechst stain is shown in blue, representing the nuclei. Green staining shows the mitochondria labelled by TMRM. All contrast settings are the same, set to the DMSO images. A, B) Representative images of fibroblasts treated with a DMSO vehicle control. C) Representative image of fibroblasts treated with a compound which has significantly increased mitochondrial number and membrane potential. D) Representative image of fibroblasts treated with a compound which has decreased mitochondrial number.

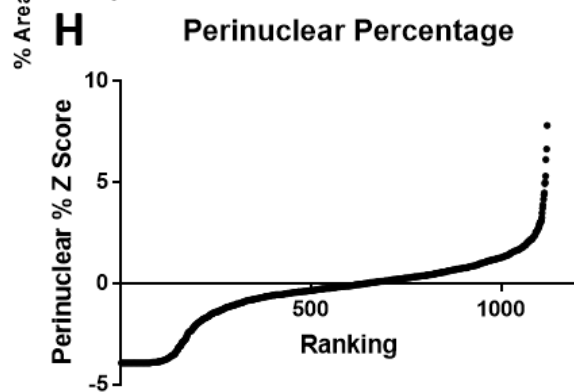
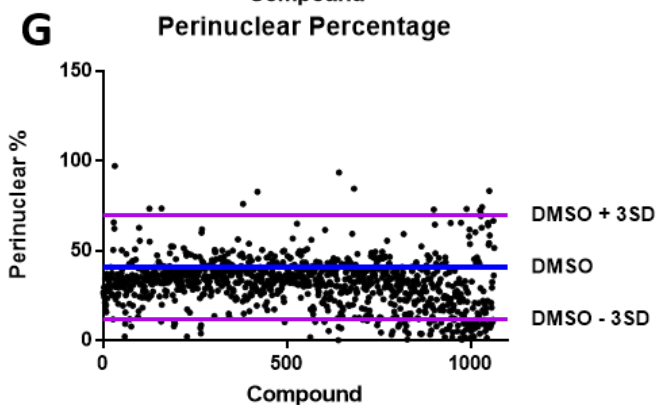
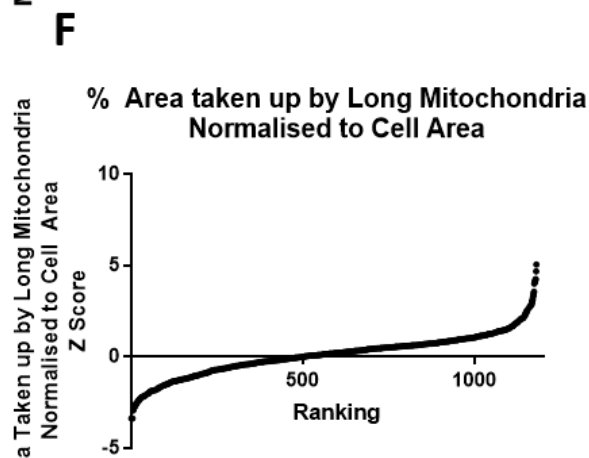
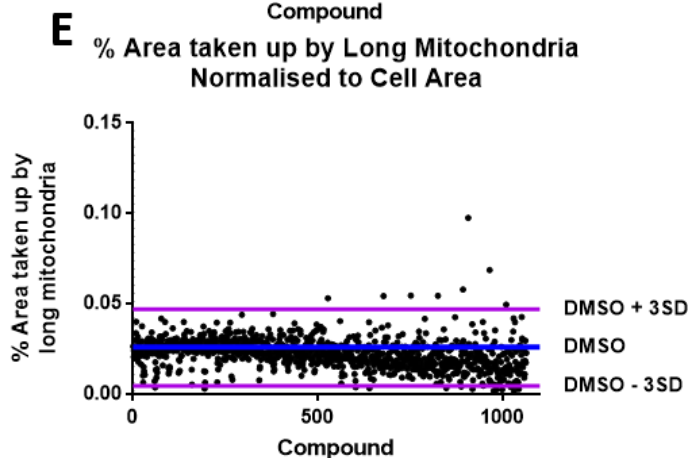
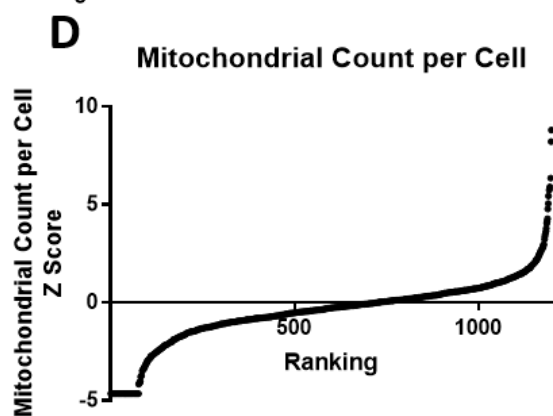
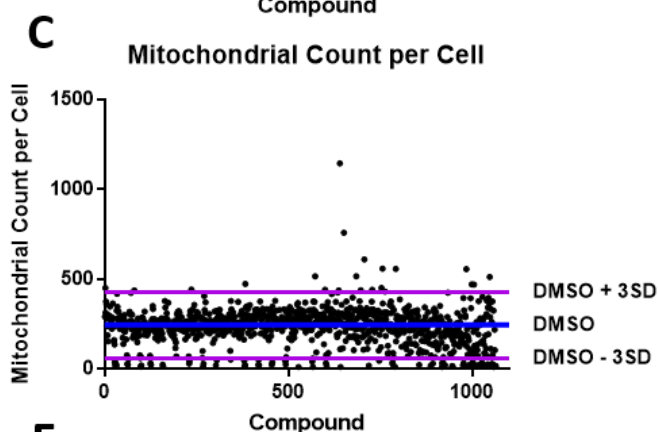
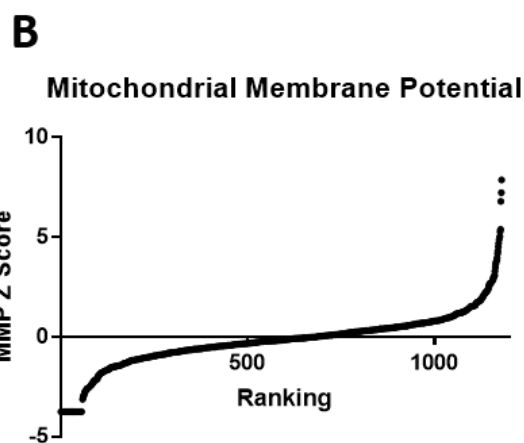
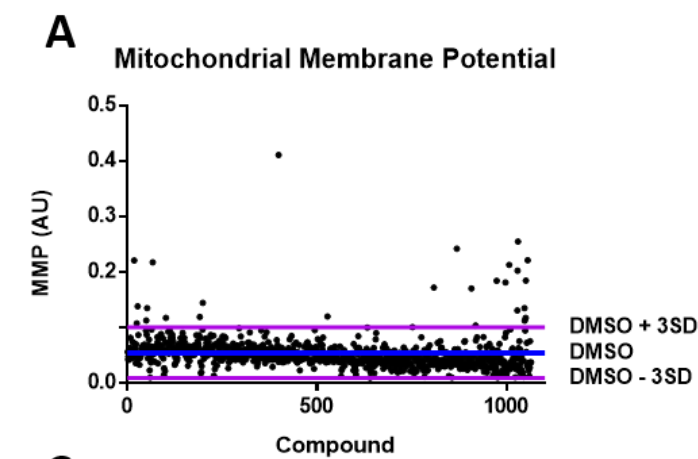


Figure 97: Representative graphs showing results for one 1536 well plate. For A, C, E, G, each point represents the raw value for each individual compound on the plate in each parameter. The blue line represents the DMSO mean, and the purple lines represent the DMSO mean \pm 3SD. Dots above or below the purple lines represent compounds which were initially counted as a hit. For B, D, F, H, each point represents a z score for a different compound, calculated as follows: $Z = (x-\mu)/\sigma$ where μ =population mean and σ =population standard deviation.

A) Representative graph showing mitochondrial membrane potential raw values across one 1536 well plate in comparison to DMSO mean and DMSO \pm 3SD. B) Representative graph showing z scores for mitochondrial membrane potential across one 1536 well plate. C) Representative graph showing mitochondrial count per cell raw values across one 1536 well plate in comparison to DMSO mean and DMSO \pm 3SD. D) Representative graph showing z scores for mitochondrial count per cell across one 1536 well plate. E) Representative graph showing percentage area taken up by long mitochondria raw values across one 1536 well plate in comparison to DMSO mean and DMSO \pm 3SD. F) Representative graph showing z scores for the percentage of mitochondria accumulated in the perinuclear region across one 1536 well plate. G) Representative graph showing perinuclear percentage as raw values across one 1536 well plate in comparison to DMSO mean and DMSO \pm 3SD. H) Representative graph showing z scores for the percentage of the cell taken up by long mitochondria across one 1536 well plate.

5.3.2 Compounds Having an Effect in a sAD Line Do Not Have the Same Effect in a PSEN1 Line

Approximately 60% of the library was also screened at 1 μ M in PSEN1 fibroblasts, but due to time constraints, a full analysis of this data was not possible. Instead, compounds which had been identified in the refined hit list were investigated and compared to the effect in sAD fibroblasts. This was a total of 65 compounds, as the remaining 8 compounds from the refined hit list were not assayed in the PSEN1 fibroblast line. The phenotype seen in the PSEN1 fibroblasts is similar to the sAD fibroblasts, a reduced MMP, reduced mitochondrial count per cell, increased mitochondria in the perinuclear region, and an increased percentage of the area taken up by long mitochondria. These deficits are greater in the PSEN1 fibroblasts, and on the whole, more consistent between PSEN1 lines than between sAD lines. It was found that in the 65 compounds compared, none of the same effects were seen in PSEN1 fibroblasts as were seen in sAD fibroblasts. Representative graphs can be seen in figure 98, showing the difference in response of an example compound in each parameter, between sAD and PSEN1 fibroblasts.

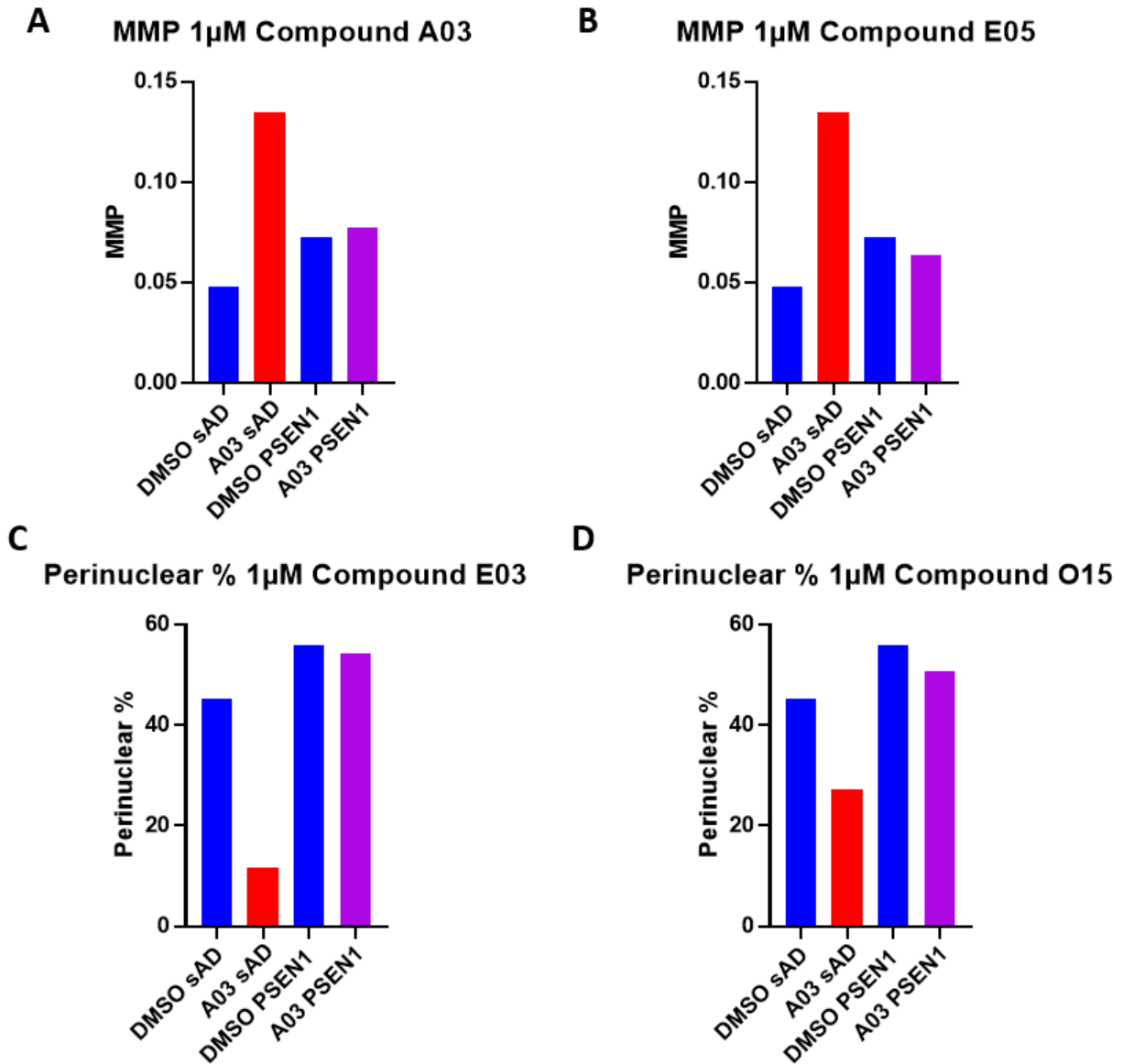


Figure 98: Representative graphs showing compounds which have a positive effect in a sAD fibroblast line do not have the same effect in a PSEN1 fibroblast line. Each bar represents data from one well of a 1536 or 384 well plate. A) 1 μ M treatment with Compound A03 increases MMP in a sAD fibroblast line but not in a PSEN1 line. B) 1 μ M treatment with Compound E05 increases MMP in a sAD fibroblast line but not in a PSEN1 line. C) 1 μ M treatment with Compound E03 decreases the accumulation of mitochondria in the perinuclear region in a sAD line but not in a PSEN1 line. D) 1 μ M treatment with Compound O15 decreases the accumulation of mitochondria in the perinuclear region in a sAD line but not in a PSEN1 line.

5.3.3 Dose Response of Hit Compounds in One sAD Fibroblast Line

The final hit list of 73 compounds was assessed for a dose response in one sAD line from the Coriell cell repository. Cells were treated at several doses: 100nM, 300nM, 1 μ M, 3 μ M and 10 μ M.

Representative graphs show dose response in MMP, form factor, and mitochondrial count in a range of compounds (figure 99). In this case, a positive effect would consist of increased MMP, decreased form factor (indicating a more fragmented network), and an increase in mitochondrial count.

Compound C17 shows a positive response in MMP, where the MMP increases with the dose, peaking at the 3 μ M dose, where a 45% increase in MMP is seen compared to DMSO. This drops slightly to a 38% increase at the 10 μ M dose (figure 99a). The form factor after treatment with compound C17 also shows a positive response, decreasing by 2.3% at 100nM compared to DMSO and peaking at a 5.6% decrease at 10 μ M (figure 99e). Compound K17 also shows a positive response in MMP, initially showing only a 5% increase at the lowest dose of 100nM, but dramatically increasing to a 60% increase at 300nM, and ultimately peaking at 10 μ M where a 74% increase is seen (figure 99b). Again, a positive effect is also seen in form factor, where a 3.5% decrease is seen compared to DMSO at 100nM, and a 4.4% decrease at the 300nM dose. Form factor then increases slightly, before ultimately being decreased by 4.6% at the highest dose. Compound E05 demonstrates a positive response in mitochondrial count. No increase from DMSO is seen at 100nM, but a 17% increase in mitochondria per cell is seen at 300nM. This takes a small dip at 1 μ M, to a 13% increase, before gradually increasing with the dose to a 35% increase at 10 μ M (figure 99i). Compound A03 also shows a positive response in mitochondrial count per cell, peaking at a 47% increase at 1 μ M.

Not all compounds showed a positive response at all doses. Compound K03 initially showed a positive response in all parameters at 100nM, increasing MMP by 105%, decreasing form factor by 0.9%, and increasing mitochondrial count per cell by 32%. This effect decreased as the concentration increased in all parameters, eventually dipping below DMSO levels at 3 μ M, by 11% in MMP, and 13% in mitochondrial count, and going above DMSO levels in form factor by 1% at the 300nM dose (figure 99c, g, k). This suggests this compound may be toxic at higher doses. Another example of a potentially toxic compound is G07. This showed an increase in MMP, peaking at a 102% increase at the 300nM dose, but this was decreased to almost zero at the 10 μ M dose, suggesting it is toxic at the higher dose (figure 99d). Some compounds also increased form factor and reduced mitochondrial count per cell, such as K11 in form factor which increased as the dose increased to a maximum increase of 3.2% at 10 μ M (figure 99h), and G13 in mitochondrial count per cell which also decreased as the dose increased to a maximum decrease of 14% at 10 μ M (figure 99l).

Of the 73 compounds tested, 26 compounds showed a consistent increase in MMP across the doses, while 18 showed either a consistent decrease, or a decrease as the dose increased, and 29 showed either no response or a variable response. In the form factor parameter, 21 compounds showed a consistent decrease, 18 showed a consistent or dose dependent increase, and 34 showed no response, or a variable response. For mitochondrial count per cell, only 9 compounds showed a consistently beneficial response across multiple doses, 16 showed a decrease, and 48 showed either a variable or no response. There were 7 compounds which had a consistently beneficial effect in mitochondrial function, and at least one of the morphology parameters. The values for the minimum and maximum dose, maximum percentage increase, and EC50 for each parameter is shown in appendix 1. While the majority of compounds increased in each parameter in at least one dose, this effect was often inconsistent and in many cases, this variability has led to an inability to calculate accurate EC50 values. For the MMP, the highest maximum increase was 215%, while the lowest increase was 13%, and three compounds did not increase MMP at any dose. The EC50s varied between 19.78nM and 133,550nM, though many fall between the 100nM and 1000nM range. For the form factor, the maximum percentage decrease was generally lower than that for MMP which is to be expected, as small changes in this value translate to significant alterations in mitochondrial morphology. The smallest maximum percentage decrease was 0.9%, while the largest was 67%, and two compounds did not decrease form factor at any dose. The EC50s varied between 6.8nM and 26,962nM, with many falling between 300nM and 3000nM. For the mitochondrial count per cell, again there was in general a smaller increase than in the MMP, from 0.09% to 76%, with 11 compounds which decreased the mitochondrial count per cell, more than the other parameters assessed. The EC50s varied from 40.05nM to 71,196nM, with most between 300nM and 2000nM. In general, higher EC50s were seen for the morphology parameters than the functional parameters, suggesting that a higher dose of these compounds is needed to affect morphology than to affect mitochondrial function. 11 compounds were chosen for further analysis, which were found to have the most promising dose response in one or more parameters.

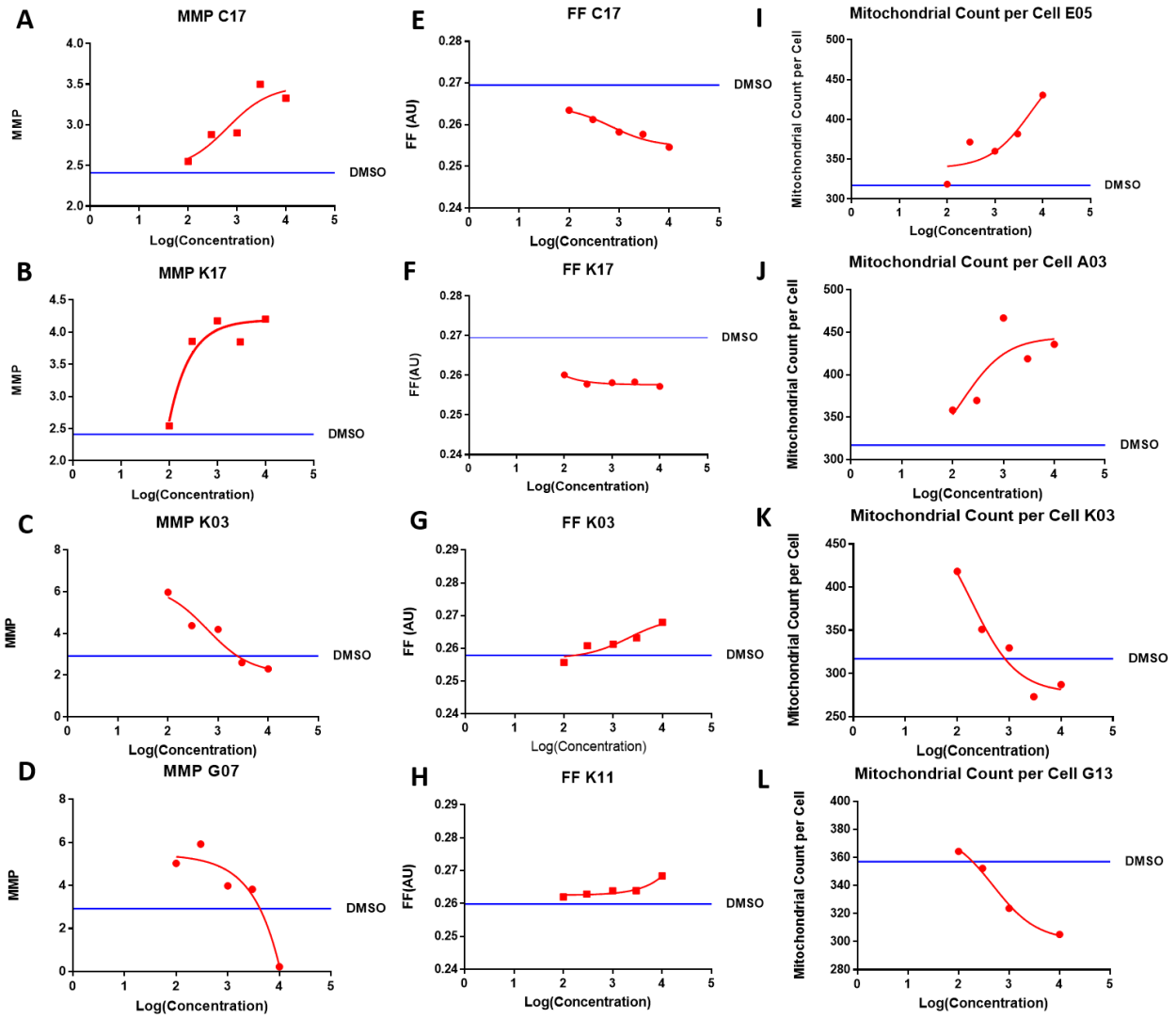


Figure 99: Representative graphs showing dose response in a range of compounds. Each point represents the average value per cell, from one well of a 384 well plate. The blue line represents the DMSO mean for the plate, and the red line represent the nonlinear regression between the dose and the effect. A) Dose response of compound C17 on MMP, compared to DMSO vehicle control, showing a positive response, peaking at 3 μ M. B) Dose response of compound K17 on MMP, compared to DMSO vehicle control, showing a positive response. C) Dose Response of compound K03 on MMP, compared to DMSO vehicle control, showing an initially positive response which decreases at higher doses. D) Dose Response of compound G07 on MMP, compared to DMSO vehicle control, which increases MMP peaking at the 300nM dose, before decreasing to almost zero at 10 μ M. E) Dose response of compound C17 on form factor, compared to DMSO vehicle control, which shows a positive response. F) Dose response of compound K17 on form factor, compared to DMSO vehicle control, showing a positive response. G) Dose response of compound K03 on form factor, compared to DMSO vehicle control, showing an initial decrease but increasing at higher concentrations. H) Dose response of compound K11 on form factor, compared to DMSO vehicle control. I) Dose response of compound E05 on mitochondrial count per cell, compared to DMSO vehicle control, which shows a positive response peaking at 300nM. J) Dose response of compound A03 on mitochondrial count per cell, compared to DMSO vehicle control, which shows a positive response peaking at 1 μ M. K) Dose response of compound K03 on mitochondrial count per cell, compared to DMSO vehicle control, which initially shows a positive response which decreases with higher concentrations. L) Dose response of compound G13 on mitochondrial count per cell, compared to DMSO vehicle control, which decreases mitochondrial count below DMSO levels at almost all concentrations.

5.3.4 Dose Response of the Top 11 Compounds in Three Control and Three sAD Fibroblast Lines from a Locally Collected Cohort

The 11 compounds which showed the most promising dose response were taken forward for further screening in three control and three sAD fibroblast lines in a locally collected cohort. Fibroblasts were treated at the concentrations previously used in analysis of the dose response: 100nM, 300nM, 1µM, 3µM and 10µM. In this case, a positive response is demonstrated by an increase in MMP, a decrease in form factor, and an increase in mitochondrial count per cell. All parameters for all lines were normalised to the DMSO control level for that line for each repeat, to decrease background noise from variation between repeats on different days, and to assess the compound effect in the cleanest way possible.

Of the 11 compounds tested, none showed a consistently positive effect across all control and sAD all lines assessed. In the control lines, three compounds showed a positive effect in both MMP and form factor in one control line, and another four showed a positive response in form factor only. No compounds showed a consistent increase in the mitochondrial count per cell in either control line. In the sAD lines, only three compounds showed a consistently beneficial effect in MMP. There were five compounds which were found to be beneficial on the form factor in at least one sAD line, of which four also increased mitochondrial count per cell. There were a further five compounds which improved mitochondrial count only. All of the ten compounds which improved mitochondrial count did so in at least two of the sAD lines, with two compounds having a positive effect in all three, making the mitochondrial count the parameter with the greatest effect across sAD lines. The values for the minimum and maximum dose, the maximum percentage increase for MMP and mitochondrial count and decrease for form factor, as well as the EC50, for each parameter in each compound for each individual line is shown in appendix 2. Many compounds did not have much effect on the parameters assessed in these lines, and in general, the maximum response was lower than in the Coriell line used in previous dose response experiments. Again, this and variability meant that EC50s could not always be calculated. For the MMP, the biggest maximum increase was 103%, while the lowest was 0.8%, and in some cases there was no increase at all. The EC50s vary between 13.46nM and 12,074nM, though most fall between the 100nM to 1000nM range. The EC50 also varies between different lines for the same compound, for example, compound G15 which has an EC50 of 13.46nM in sAD 1, but an EC50 of 697.7nM in sAD 9, and 1641nM in control 2. For the form factor, the size of the effect was generally much lower than in the previous dose response analysis, ranging from a 0.3% increase to an 8.1% decrease. This may be due to the differences in calculating this parameter. The EC50s were generally higher than for MMP but also show a larger range, from

8.019nM to 62,819nM. For the mitochondrial count per cell, the maximum increase in the sAD lines was typically higher than in the previous dose response analysis, ranging from 0.7% to 127%, but with most showing an increase of at least 30%. On the other hand, the controls range from a 1.6% to a 26% increase. The EC50s are quite variable, ranging from 1.73nM to 11,388nM. Data for two compounds, E21 and K17, will be outlined below.

Compound E21 showed a varied response in the different lines assessed, as well as in the repeats for each line. In control 1, MMP showed no response until the highest concentration of 10 μ M, when it showed an increase of 43% compared to DMSO levels (Figure 100a). Form factor was initially decreased by 5.3% but did increase back to DMSO levels at the higher doses, particularly 3 μ M, where it was 2.2% higher than the DMSO mean (figure 100b). Mitochondrial count per cell was decreased by 17% at 300nM, by 11% at 1 μ M, and 13% at the 3 μ M dose (figure 100c). In control 7, MMP demonstrated a gradual increase as the concentration increased, starting with a 7.6% increase at 100nM and increasing to a 28% increase at 10 μ M (figure 100d). Form factor also showed a positive response, while no effect was seen at the lowest dose, a 4.3% decrease was seen at 300nM, and a 4.6% decrease at the highest dose (figure 100e). Mitochondrial count was initially increased slightly at the 100nM and 300nM, by 11% and 6% respectively, but then returned to DMSO levels (figure 100f). In sAD 1, MMP did not change much from DMSO control levels (figure 100g), form factor was increased slightly at the lowest dose, by 5.3%, and slightly decreased by 4.2% at the highest dose (figure 100h). Mitochondrial count was increased by 92% at 100nM, but this gradually decreased as the dose decreased, only showing a 14% increase at 10 μ M (figure 100i). In sAD 2, MMP again did not change much from DMSO control levels, though was increased by 20% at the 3 μ M dose (figure 100j). Form factor was decreased at all concentrations, with a maximum decrease of 2.5% at 1 μ M, with the exception of 300nM which was at DMSO control levels (figure 100k). Mitochondrial count was increased at all doses, peaking at a 23% increase at 1 μ M (figure 100l). In sAD9, MMP was slightly increased at all concentrations except 3 μ M, with a maximum increase of 22% at 300nM (figure 100m). Form factor was slightly increased by 2.8% at the lowest dose, but decreased in all others, with the largest decrease of 4.8% at 300nM (figure 100n). Mitochondrial count increased as the concentration increased, from a 21% increase at 100nM to a 58% increase at 3 μ M, but at 10 μ M it remained at DMSO control levels (figure 100o). When control and sAD lines were combined, MMP was increased at 3 μ M (controls 15%, sAD 14%) and 10 μ M (controls 36%, sAD 10%), and this was stronger in the control lines (figure 102b). Form factor showed a positive response in the control lines, being decreased at all concentrations, with the maximum decrease of 4.3% at 300nM. sAD lines initially show an increase of 2.2% at 100nM before decreasing, with a maximum decrease compared to the DMSO mean of 3.4% at 10 μ M (figure 102d). Mitochondrial

count per cell shows no response in control lines, but is increased in sAD lines at all concentrations except 10 μ M, with a maximum increase of 44% at 3 μ M (figure 102f).

Compound K17 also showed a varied response. In control 1, MMP remained around DMSO control levels but was slightly increased by 19% at 3 μ M (figure 101a). Form factor showed no response at the lower doses, but gradually decreased from 1 μ M, with a maximum decrease of 6.6% at 3 μ M (figure 101b), and mitochondrial count per cell showed no response (figure 101c). In control 7, MMP was slightly increased in all concentrations except 300nM, with a maximum increase of 29% at 1 μ M (figure 101d). Form factor initially showed no response, but was decreased by 5.2% at 1 μ M, which remaining consistent at the two higher doses (figure 101e). Mitochondrial count (figure 101f) did not show any response, with the exception of a reduction of 10% in mitochondrial count at 100nM. In sAD 1, MMP showed no response (figure 101g), whilst form factor initially increased by 3.2% at 100nM, before gradually decreasing after 300nM, to a maximum decrease of 6.9% at 10 μ M (figure 101h). Mitochondrial count was increased by 49% at 100nM, 46% at 300nM, and 53% at 1 μ M, but this effect was decreased to only 36% and 20% above DMSO levels at 3 μ M and 10 μ M respectively (figure 101i). In sAD 2, there was no clear response in MMP (figure 101j). The form factor was slightly decreased by 2.7% at 1 μ M and 2.7% at 10 μ M (figure 101k), and the mitochondrial count was increased at all concentrations, peaking at a 25% increase at 1 μ M (figure 101l). In sAD 9, there was no response in MMP except at 3 μ M where there was a 24% decrease (figure 101m). Form factor was reduced by 33% at 100nM, and by 24% at 3 μ M (figure 101n). Mitochondrial count was increased in at all concentrations, peaking at a 42% increase at 300nM though this effect did start to decrease at higher doses, only showing a 24% increase at 10 μ M (figure 101o). When control and sAD lines were combined, MMP showed a slight increase of 10% at 1 μ M and 11% at 10 μ M in controls and by 10% and 25% at 3 μ M and 10 μ M respectively in sAD lines (figure 102a). Form factor was decreased at all concentrations in control lines, with a maximum decrease of 6.1% at 3 μ M but showed a more variable response in sAD lines, with a decrease of 10% at 3 μ M, but an increase of 2.6% at 10 μ M (figure 102c). Mitochondrial count, as with compound E21, shows no response in control lines but is increased in sAD lines, with a maximum increase of 36% at 1 μ M (figure 102e).

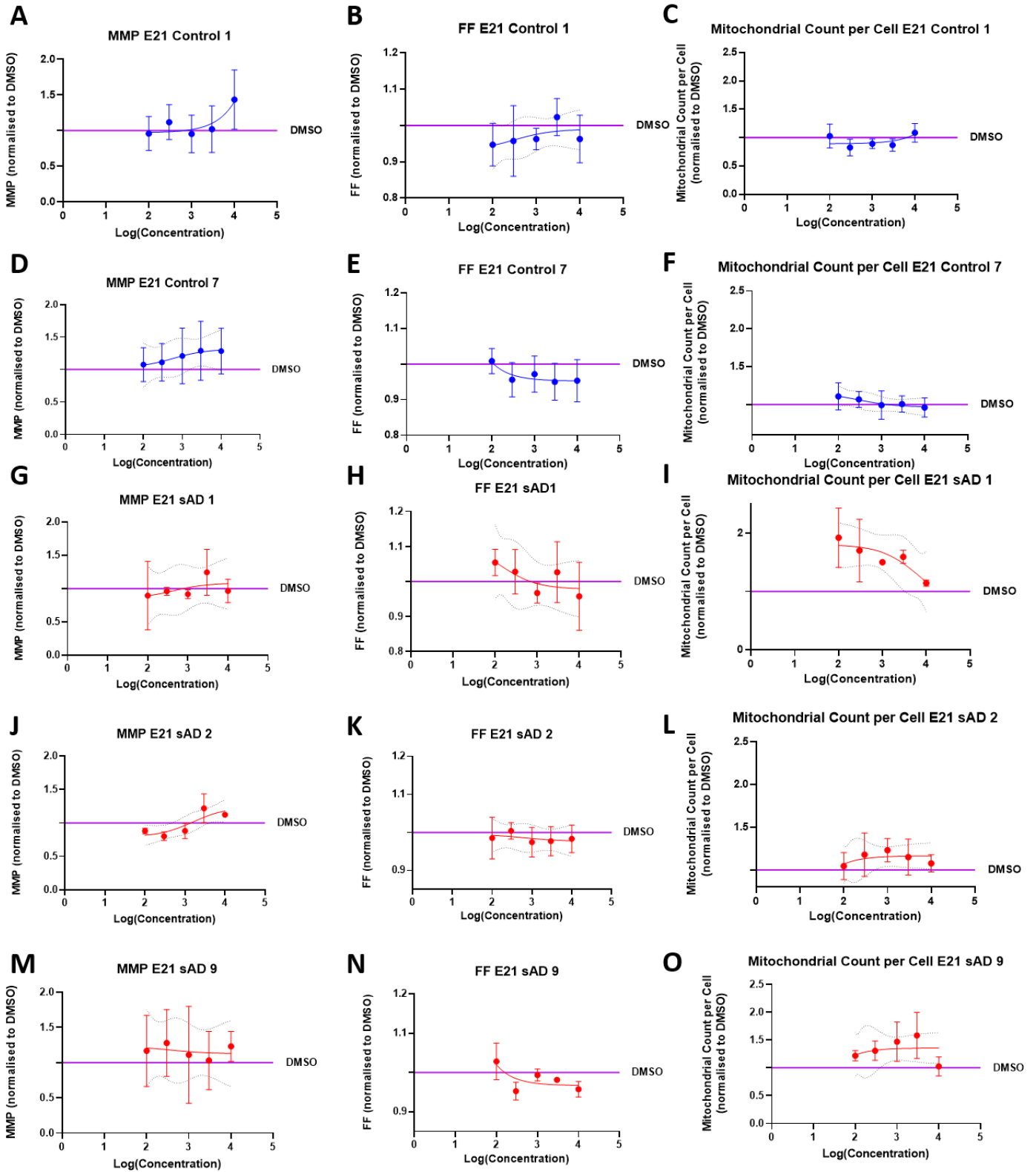


Figure 100: Dose response in MMP, Form Factor, and mitochondrial count per cell in two control and three sAD fibroblast lines, in compound E21. Each data point shows mean \pm SD (control 1 and control 7 n=4, sAD 1 n=2, sAD 2 and sAD 9 n=3), normalised to DMSO control mean which is shown with a purple line. 95% confidence limits are shown with a dotted line, and the nonlinear regression between concentration and response is shown by a solid line in blue for controls and red for sAD lines. A) Dose response of compound E21 on MMP, compared to DMSO vehicle control in control 1, which shows no response except at 10 μ M. B) Dose response of compound E21 on FF, compared to DMSO vehicle control in control 1, which shows an initial decrease but a return to DMSO control levels at the higher doses. C) Dose response of compound E21 on mitochondrial count per cell, compared to DMSO vehicle control in control 1, showing a decrease at 100nM, 1 μ M, and 3 μ M doses. D) Dose response of compound E21 on MMP, compared to DMSO vehicle control in control 7, which shows a gradual increase as the dose increases. E) Dose response of compound E21 on FF, compared to DMSO control in control 7, which decreases as the dose decreases. F) Dose response of compound E21 on mitochondrial count per cell, compared to DMSO vehicle control in control 7, which shows a positive response at 100nM and 300nM doses. G) Dose response of compound E21 on MMP, compared to DMSO control in sAD 1, showing no clear response. H) Dose response of compound E21 on FF, compared to DMSO control in sAD 1, showing no clear response. I) Dose response of compound E21 on mitochondrial count per cell, compared to DMSO control in sAD 1, showing an increase at 100nM which gradual decreases as the dose increases. J) Dose response of compound E21 on MMP, compared to DMSO control in sAD 2, showing no clear response. K) Dose response of compound E21 on FF, compared to DMSO control in sAD 2, which shows a positive response. L) Dose response of compound E21 on mitochondrial count per cell, compared to DMSO control in sAD 2, showing a positive response, peaking at 1 μ M. M) Dose response of compound E21 on MMP, compared to DMSO control in sAD 9, showing a slight increase. N) Dose response of compound E21 on FF, compared to DMSO control in sAD 9, showing a decrease at most concentrations, with the greatest decrease at 300nM. O) Dose response of compound E21 on mitochondrial count per cell, compared to DMSO control in sAD 9, which shows a positive response except at the highest concentration.

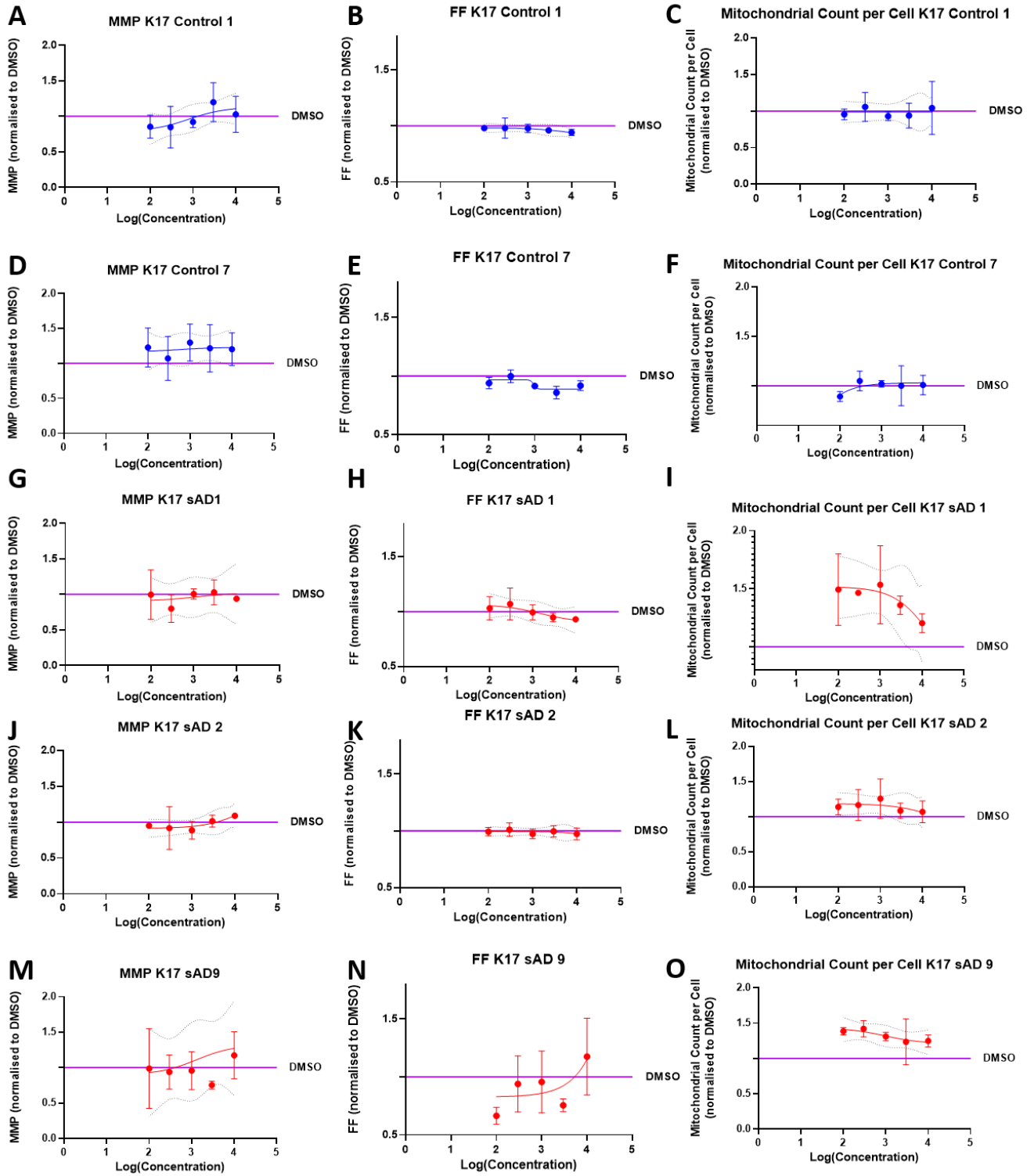


Figure 101: Dose response in MMP, Form Factor, and mitochondrial count per cell in two control and three sAD fibroblast lines, in compound K17. Each data point shows mean \pm SD (control 1 and control 7 n=4, sAD 1 n=2, sAD 2 and sAD 9 n=3), normalised to DMSO control mean which is shown with a purple line. 95% confidence limits are shown with the dotted line, and the nonlinear regression between the concentration and the response are shown by the solid lines in blue for the controls and red for the sAD lines. A) Dose response of compound K17 on MMP, compared to DMSO vehicle control in control 1, which shows no clear response. B) Dose response of compound K17 on FF, compared to DMSO vehicle control in control 1, which shows a gradual decrease from 1 μ M. C) Dose response of compound K17 on mitochondrial count per cell, compared to DMSO vehicle control in control 1, which shows no response. D) Dose response of compound K17 on MMP, compared to DMSO vehicle control in control 7, which shows a slight increase in all concentrations except 300nM. E) Dose response of compound K17 on FF, compared to DMSO control in control 7, which shows no response. F) Dose response of compound K17 on mitochondrial count per cell, compared to DMSO vehicle control in control 7, which shows no response, except a large decrease at 100nM. G) Dose response of compound K17 on MMP, compared to DMSO control in sAD 1, showing no response. H) Dose response of compound K17 on FF, compared to DMSO control in sAD 1, showing a gradual decrease from 300nM. I) Dose response of compound K17 on mitochondrial count per cell, compared to DMSO control in sAD 1, showing an increase at all concentrations but the greatest increase at 100nM, 300nM, and 1 μ M. J) Dose response of compound K17 on MMP, compared to DMSO control in sAD 2, showing no clear response. K) Dose response of compound K17 on FF, compared to DMSO control in sAD 2, which shows a slight decrease at 1 μ M and 10 μ M. L) Dose response of compound K17 on mitochondrial count per cell, compared to DMSO control in sAD 2, showing a positive response, peaking at 1 μ M. M) Dose response of compound K17 on MMP, compared to DMSO control in sAD 9, showing no clear response. N) Dose response of compound K17 on FF, compared to DMSO control in sAD 9, showing a decrease at 100nM and 3 μ M. O) Dose response of compound K17 on mitochondrial count per cell, compared to DMSO control in sAD 9, which shows an increase at all doses, though this did start to decrease at higher concentrations.

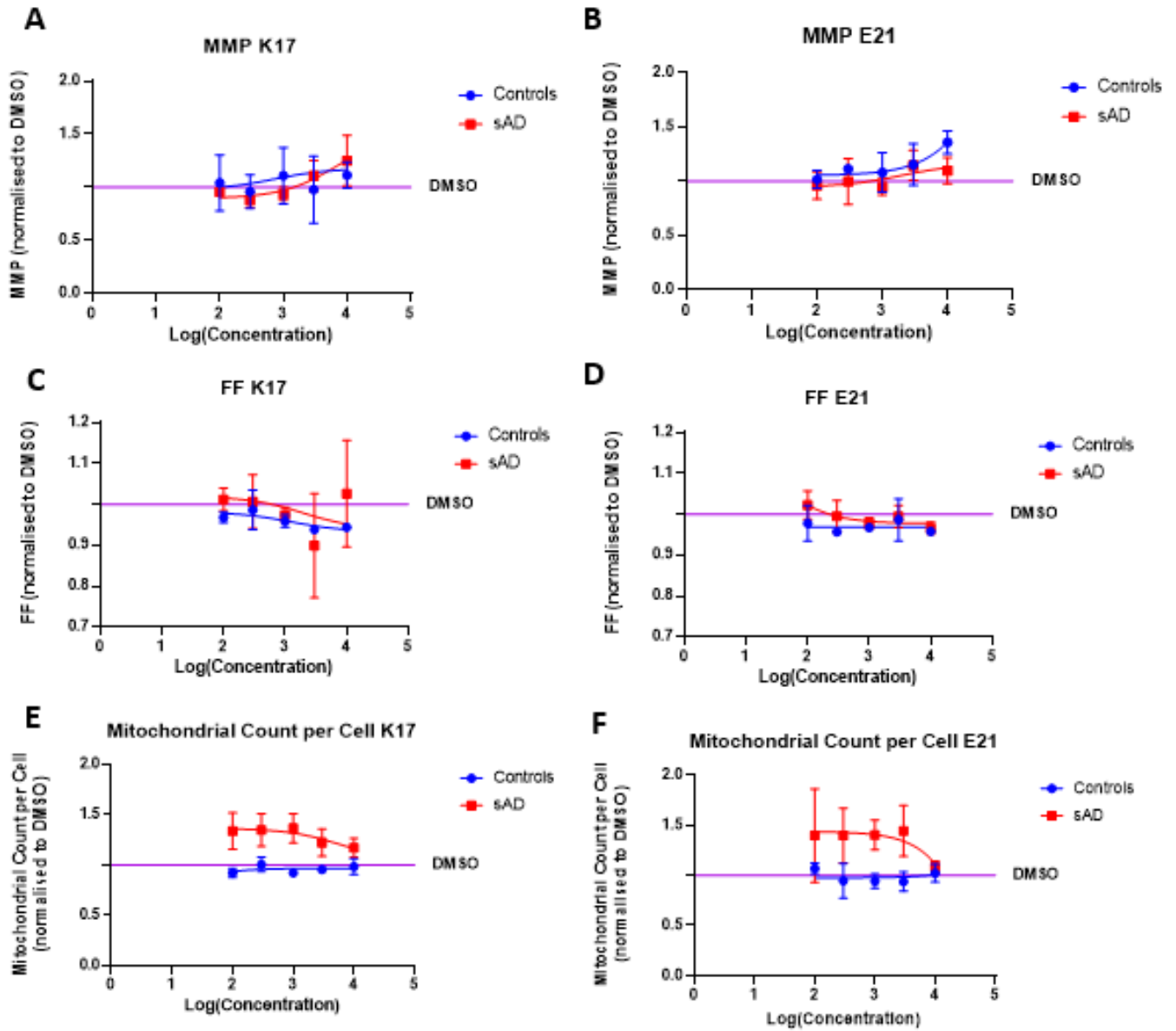


Figure 102: Dose response in combined controls and combined sAD lines, in MMP, FF, and mitochondrial count per cell, in compounds K17 and E21. Each data point represents the mean \pm SD for all lines combined for each concentration, normalised to the DMSO mean per day. Controls are shown in blue, and sAD lines in red, and the solid lines show the nonlinear regression between the concentration and the response. DMSO mean is represented by a purple line. A) Dose response of compound K17 on MMP in combined controls and SAD lines, compared to DMSO vehicle control, which shows a slight increase at 3 μ M and 10 μ M. B) Dose response of compound E21 on MMP in combined controls and SAD lines, compared to DMSO vehicle control, which shows a positive response at the higher doses in both control and sAD, though this is greater in the control. C) Dose response of compound K17 on FF in combined controls and SAD lines, compared to DMSO vehicle control. Controls show a positive response while sAD lines initially show an increase, but this decreases as the concentration decreases to below DMSO levels. D) Dose response of compound E21 on FF in combined controls and SAD lines, compared to DMSO vehicle control. Controls show a positive response while sAD lines initially show an increase, but this decreases as the concentration decreases to below DMSO levels. E) Dose response of compound K17 on mitochondrial count per cell in combined controls and SAD lines, compared to DMSO vehicle control. There is no response in control lines, but a positive response in sAD lines. F) Dose response of compound E21 on mitochondrial count per cell in combined controls and SAD lines, compared to DMSO vehicle control which shows no response in control lines but a positive response in sAD lines, with the exception of the 10 μ M dose.

5.3.5 Overall Performance of the Top 11 Compounds in all Stages of the Screen

The top 11 compounds did not perform consistently across all stages of the screen, including the primary screen, the initial dose response in one sAD line, and the second dose response analysis in three control and three sAD fibroblast lines. Table 23 shows whether the compounds had a positive, negative, or unclear/no effect at each stage.

The majority of compounds improved MMP in the primary screen, and this was validated in the initial dose response in all but one line. However, in the second dose response, only three of the 11 compounds were seen to have a positive response in the lines tested, with most having either an unclear effect or no effect at all. The opposite occurred in the morphology parameters tested; in the primary screen no compounds had a positive effect on form factor and only E21 increased the mitochondrial count per cell. However, in both dose response tests, the number of compounds improving mitochondrial morphology was increased (table 22).

Compound A05 was the highest scoring compound in the primary screen, greatly increasing the MMP in the sAD line, despite having no significant effect on the morphology parameters. This effect on MMP disappeared in the dose response screens, with the first dose response analysis actually showing a negative effect on MMP (table 22). On the other hand, compounds K17 and E21 did not

affect MMP in the primary screen, instead having a large effect on mitochondrial count. This effect remained for E21, and for K17 in the second dose response analysis despite a negative effect seen in the first dose response. Interestingly, these compounds also showed a positive effect on MMP in both dose response analyses when higher doses were applied (table 22).

Table 22: The performance of the top 11 compounds across all stages of the screen, in MMP, form factor, and mitochondrial count per cell. Green indicates a positive response, red indicates a negative response, and yellow indicates no response, or an unclear response. Columns labelled P show response in the primary screen, columns labelled DR1 show response in the first dose response analysis, and DR2 shows response in the second dose response analysis. The score column indicates the algorithm score given to the compound after the primary screen.

Compound	Score	MMP P	MMP DR1	MMP DR2	FF P	FF DR1	FF DR2	Count P	Count DR1	Count DR2
A03	4	Green	Green	Yellow	Green	Green	Green	Yellow	Green	Green
A05	6.8	Green	Red	Yellow	Green	Red	Green	Green	Red	Green
C07	4.3	Green	Green	Yellow	Green	Red	Green	Yellow	Red	Green
C17	4.6	Green	Green	Yellow	Green	Green	Yellow	Green	Yellow	Green
C21	5	Green	Green	Yellow	Green	Green	Yellow	Green	Green	Green
E05	4	Green	Green	Yellow	Green	Green	Yellow	Green	Green	Green
E21	5.7	Yellow	Green	Green	Red	Green	Green	Green	Green	Green
G15	6.2	Green	Green	Red	Yellow	Green	Yellow	Green	Green	Green
K15	5.9	Green	Green	Green	Yellow	Green	Yellow	Green	Green	Green
K17	4.2	Yellow	Green	Green	Yellow	Green	Green	Green	Red	Green
O05	6.6	Green	Green	Yellow	Red	Green	Green	Red	Green	Green

5.4 Discussion

A phenotypic screen was carried out on a library of 21,000 compounds provided by an industrial collaborator, looking for a significant effect on mitochondrial function and/or mitochondrial morphology in a patient derived fibroblast model. Due to time restraints caused by the COVID-19 pandemic, only 70% of this library was screened.

5.4.1 Primary Screen

In the first instance, sAD fibroblasts were treated with 1 μ M compounds and the effect on several mitochondrial parameters was assessed. Cell lines used throughout most of this chapter were obtained from the Coriell Cell Repository. This was due to ethical considerations as data from the initial screen was shared with the industrial collaborator. Data obtained from sAD lines collected locally was not shared with the collaborator. sAD was chosen initially instead of fAD as the majority of cases of AD are sporadic, with only a small percentage caused by familial mutations.

The parameters used in the primary screen were as follows: MMP, mitochondrial count per cell, percentage of mitochondria in the perinuclear region, and percentage of the cell taken up by long mitochondria. These parameters were chosen based on previous work in the lab which showed significantly decreased MMP, decreased mitochondrial count per cell, increased percentage of mitochondria in the perinuclear region and increased percentage of long mitochondria per cell in both sAD and PSEN1 patient fibroblasts. Furthermore, MMP and percentage of long mitochondria per cell were seen to be improved with 100nM UDCA treatment (Bell *et al.*, 2018).

The initial plan was to complete all of the primary screen in 1536 well plates. This is the most time efficient way to screen large compound libraries, enabling four 384 well source plates to be screened in one assay, and as such, quartering the time needed to screen the whole library. There are some practicalities of 1536 well plates which must be considered, including liquid handling. The use of very small volumes and very small wells increases the risk of human error. Furthermore, completing wash steps and adding dyes in the assay takes a longer amount of time for a 1536 well plate, and so cells are kept out of the incubator for a longer period of time. However, this would be kept consistent across the whole library.

Unfortunately, several obstacles were encountered in the setting up of this screen. The 1536 well plates initially caused some problems with equipment such as the design of the programme on the Echo 500, and the suitability of the plates for use with the high screen imaging equipment. Initially, the Opera Phenix was used to image plates, but difficulties were encountered when a new brand of

1536 well plates were used. The base of the new plates was too thin, and as such were not compatible with the Opera Phenix. Instead, the InCell 2000 had to be used; this has led to some variability in the analysis of some plates compared to others, including how the form factor was calculated. Furthermore, in order to maintain work-flow while these issues were dealt with, 384 well plates were used to assay some compounds. Whilst the assay was carried out in the same way, it is possible that there are differences between the two plate types which may have affected the results. These include differences in the growth of the cells, and differences in edge effects of the plate, as well as the practical issues mentioned earlier such as the amount of time cells were out of the incubator during the assay. Cells in 1536 well plates would have been out of the incubator longer, and as such, would be under more stressful conditions. This may have affected the efficacy of the compounds.

From the 70% of compounds assayed, approximately 3% of compounds were identified as being outside the range of the DMSO mean \pm 3SD in at least one parameter, and so having a significant effect. Interestingly, the majority of these compounds were having an effect on function, with many also having an effect on morphology, though some only affected one or the other. This initial list of compounds was refined further to identify compounds to be taken forward for further screening. The previously described scoring system was used to select compounds which had an effect on multiple parameters or had a large effect on MMP. MMP was considered the most important parameter as ultimately, the goal is to improve mitochondrial function in the hope of improving cell survival. This refined list included 73 compounds, which were taken forward for further analysis.

5.4.2 Screening in a PSEN1 Fibroblast Line

The majority of compounds from the refined list of hits in the sAD fibroblast line were tested in a PSEN1 fibroblast line, at a 1 μ M dose. Interestingly, none of the compounds were seen to have a significant effect in the PSEN1 line. Alterations in both mitochondrial function and morphology have been found in both sAD (Xinglong Wang *et al.*, 2008; Amit U. Joshi *et al.*, 2018; Bell *et al.*, 2018; Drabik, Piecyk, *et al.*, 2021) and fAD fibroblasts (Gray and Quinn, 2015; Bell *et al.*, 2018). However, there are differences in the precise pathologies present in the fibroblasts. For example, we found that whilst sAD fibroblasts showed a decrease in several parameters relating to mitochondrial respiration including oxygen consumption, and spare capacity, PSEN1 fibroblasts showed an increase. It was suggested that this may be due to uncoupling of the mitochondria in PSEN1 fibroblasts, or that PSEN1 fibroblasts are relying on other energy pathways (Bell *et al.*, 2018). This

suggests that there are different pathological mechanisms leading to mitochondrial dysfunction in fAD and sAD fibroblasts. Therefore, it is perhaps unsurprising that these compounds are having a different effect in PSEN1 fibroblasts than in sAD fibroblasts. It may be that the mechanism by which they are improving mitochondrial function and altering mitochondrial morphology is not present in PSEN1 fibroblasts.

PSEN1 mutations are not the only mutations which lead to fAD. Other genes which are implicated include PSEN2 and APP. The compounds tested here may have an effect on cells with mutations in these genes, and this would be an interesting area for further investigations of this library. The difference seen in the efficacy of these compounds in sAD and PSEN1 fibroblasts has wider implications in the treatment of AD. Current treatments do not differentiate between sAD and fAD, however they may be acting via different mechanisms and so may need to be treated in different ways. As shown here, a treatment which is effective in sAD will not necessarily be effective in PSEN1 or other forms of fAD, and vice versa. As such, future treatment strategies should take this into account and investigate the effects of treatments in both sAD and fAD. Future work in this library should focus on screening the rest of the library in a PSEN1 line to determine whether any of the compounds which do not have a significant effect in sAD fibroblasts improve mitochondrial function and morphology in PSEN1 fibroblasts.

5.4.3 Dose Response

73 compounds were taken forward and assessed for dose response, at the following concentrations: 100nM, 300nM, 1 μ M, 3 μ M and 10 μ M. These concentrations were chosen to include some lower and some higher than the original dose in the primary screen. Many, though not all, compounds replicated the positive response identified in the primary screen. The reason for these discrepancies may be due to the fact that only a single well was assessed per compound in the primary screen; it is possible that had more wells been tested in the original screen then the effect would have disappeared. Furthermore, multiple sAD lines were used in the primary screen, as a time saving method. The sAD fibroblast line used for dose response analysis was not necessarily the same as used for the compounds in the primary screen. Differences between the lines may mean that that some compounds will not have a significant effect across multiple cell lines.

Some compounds showed a positive effect at lower doses, which disappeared when higher doses were given. This suggests that that these compounds may actually be toxic at higher doses, for

example, compound G07 which severely reduced MMP at the 10 μ M dose. These compounds would not be suitable to take forward for further testing.

An inconsistent response was seen across the different doses in some compounds. This variability could be due to practical issues; again, only one well per concentration was assessed and assaying more wells per concentration may have made the response more clear. Alternatively, the compound may just have an unreliable and inconsistent effect, and as such, these compounds were not considered for further investigations.

The top 11 compounds were chosen based on the size and consistency of their effect on the MMP as a measure of mitochondrial function, and the form factor and mitochondrial count per cell as a measure of morphology. Interestingly, the majority of these compounds showed more of an effect on the morphology in the dose response analysis than in the primary screen. This may be due to differences in analysis between InCell Developer Toolbox and Harmony, as previously discussed, or could be due to cell line differences. It could also be because of the higher doses used; it may be that many compounds need to be administered in higher doses to have a significant impact on mitochondrial morphology whereas MMP can be improved at lower doses. This can be seen in compound E21, where the EC50 for the MMP is 158.6nM whereas the EC50 for mitochondrial count per cell is 8721nM, as well as in compound E05 where the EC50 for MMP is 737.4nM, the EC50 for form factor is 907.3nM and the EC50 for mitochondrial count per cell is even higher, at 5841nM (appendix 1). This raises interesting questions about the optimum dose for these compounds, and whether it is beneficial to increase the dose to improve mitochondrial morphology, when the effect on MMP is apparent at a lower dose. The goal of altering morphology is ultimately to increase mitochondrial function and so it would seem unnecessary to increase the dose when a lower dose is sufficient for the MMP to be increased.

5.4.4 Dose response in a Locally Collected Cohort

To validate the dose response seen in a single sAD line, further dose response analyses were carried out. Three control and three sAD lines were picked from a locally sourced cohort. The three sAD patients chosen all had alterations in the parameters assessed. The same concentrations were used as in the previous analysis. Much variability was seen in comparison to the first dose response analysis, as well as between the different lines assessed here.

The majority of the top compounds did not show an effect of the compounds on MMP, despite increases in MMP seen in both the primary and first dose response screen. This may be due to the lines used. As previously mentioned, both the primary and initial dose response screen were carried

out in sAD lines obtained from the Coriell Cell Repository. These lines are bought commercially and so are generally at a higher passage than cells which have been grown from the biopsy in Sheffield, which may have had an effect on the efficacy of the compound. The patients who donated these samples were also younger on average than the patients who donated locally. Further age-related changes may have occurred in the locally sourced cells which have an impact on the effectiveness of the compound in increasing MMP.

In terms of morphology, as with the previous dose response analysis, more of an effect was seen than in the primary screen. In general, less of an effect was seen on form factor than the previous dose response screen, but every compound showed an increase in mitochondrial count per cell. Again, the passage and age of the patient may have had an impact on the ability of the compounds to affect these parameters, as well as the higher sample size assessed. Furthermore, as previously discussed, differences in the imaging and analysis methods may also have impacted these parameters.

Differences were also seen between control and sAD patient fibroblasts, in particular in the mitochondrial count per cell. There was an increase in mitochondrial count per cell with all compounds, but no response in the control lines. This may be because there is no deficit in the mitochondrial count per cell in the first place. Mitochondrial count is a balance, and a deviation from this balance in either direction would be detrimental for the cell. As such, it is possible that compensatory mechanisms occur within the control cells in response to these compounds to prevent an unnecessary increase in the number of mitochondria per cell.

There was also differences seen between the different sAD lines at this stage. As demonstrated in previous chapters of this thesis, the pathology seen in sAD cells is not always consistent and occurs to different extents in different cell lines. Whilst all lines used did have a deficit in the parameters selected, the level of alteration differed and so it is not surprising that different lines respond to compounds differently. This highlights the benefits of a personalised medicine approach to the treatment of AD; some treatments may work well for some patients but not for others dependent on the specific pathology of each patient.

5.4.5 The Top 11 Compounds

REDACTED

REDACTED

REDACTED

Table 19: The name and structure of the top 11 compounds identified in this screen.

REDACTED

5.4.6 Advantages and Limitations of this Screen

This screen was carried out in patient derived fibroblasts. Many advantages of fibroblasts as a model of AD have been discussed in a previous chapter, including the fact that they maintain the genetic background of the patient, and changes which have accumulate within the cell with age. They are also able to model sporadic disease, which is important for the screening of new compounds as the majority of AD is sporadic, and so a compound which improves sporadic AD will benefit more patients in the long run. Though fibroblasts are not directly affected by neurodegenerative diseases such as AD, alterations in biological mechanisms, specifically in the mitochondria, have been seen (Gray and Quinn, 2015; Bell *et al.*, 2018; Trushina, 2019). As such, they provide a biological system in which compounds can be screened for engagement with certain biological processes, in this case mitochondrial function and morphology. One of the greatest advantages of using fibroblasts for high throughput screening, is that they are cost and time effective. More disease relevant models, such as patient derived neural cells and animal models, are more costly in both time and money and as such, a large screen in these models would not be feasible. In the focus group carried out as part of this project, the value of different models in the drug screening process was discussed. It was agreed that patient fibroblasts were a powerful tool, due to their ability to reflect aging processes in the cell, as we as being directly derived from people with AD.

As part of this screen, compounds were assessed for an effect in both mitochondrial function and morphology. Previous work by our lab and others have shown that there are significant alterations in morphology as well as in function (Wang *et al.*, 2009; Bell *et al.*, 2018; Joshi *et al.*, 2019). Since many processes are altered in the mitochondria in AD, it is beneficial to search for a treatment which will affect multiple mechanisms to give the greatest chance of having a disease modifying effect.

There are several limitations to this screen, many of which have already been identified.

Unfortunately, several practical issues were encountered in setting up the screen. 1536 well plates were not a technique which had regularly been used in the lab before, and as such, there were some issues with setting up the primary screen. This led to inconsistencies in the imaging equipment used to run the assays, and as a result, the software used in analysis. While efforts were taken to make the results as comparable as possible, these different methods of analysis may have impacted the results. Also, 384 well plates were used in place of 1536 well plates for some compounds. Again, this may have had practical implications on cell growth and time out of the incubator during assays.

There are other limitations in the design of the study, including the use of only one well per compound in the primary screen. This was done in order to screen the library as quickly as possible,

but may have led to false positive or false negative results, with no technical repeats to confirm the results. This also applies to the dose response assays, where only one well was assessed per concentration. Also, several wells had to be excluded as they failed quality control checks, for example having too few cells in the well or too few mitochondria per cell. Due to time constraints, these wells could not be repeated and so no data was obtained for these compounds. If more time was available, it would have been beneficial to repeat the primary screen in triplicate to confirm that the results seen were true, as well as repeat any wells which were excluded. Unfortunately, this was not feasible in the time available.

Furthermore, for the primary screen and initial dose response, only one sAD line was used for each compound. As discussed above, the pathology seen in sAD cells is not always consistent and so different lines are likely to respond differently to compounds. Whilst this was investigated in the top 11 compounds, it would have been beneficial to look at the response of multiple cell lines to all compounds, especially as varied results were seen in the top 11.

5.5 Conclusions and Future Work

The first steps for any future work should be to screen the rest of the compound library, and identify any further hits. The library should also be screened in a PSEN1 line, and this process repeated, to identify compounds which may be beneficial to fAD even if they are not to sAD.

Unfortunately, the top compounds identified in this screen do not show a robust and replicable effect across the multiple cell lines tested in this chapter. As previously discussed, it may be that these compounds are only beneficial in a subset of AD patients, dependent on the extent of the mitochondrial dysfunction in each individual. It would be interesting to carry out further screening on a more stratified group of patients. Unfortunately, further stratification of this cohort is not feasible due to the relatively small sample size.

It would however be of value to identify the effect of these compounds on other measures of mitochondrial function and morphology, to potentially identify one or two lead compounds. This should include further assays to measure mitochondrial function including the ATP assay to assess cellular ATP levels, as well as a more in depth look at the effect of the compounds on mitochondrial respiration using the seahorse assay. Further investigations into their effect on morphology should also be carried out including assessment of the expression of proteins involved in mitochondrial quality control which have been identified in this thesis as being reduced in sAD.

When asked about what next steps would be the most important to them, the attendees of the focus group carried out as part of this project suggested that it would be more valuable to them to

first identify whether the top compounds work in multiple models of AD before doing in depth work into the mechanism of action. Therefore, another key area for further screening would be to test the hit compounds on a more disease relevant model, such as patient derived iNeurons. This would determine whether these compounds have a similar effect on the central cells which are affected in the disease, as they do on the periphery.

Chapter Six: General Discussion

AD is progressive, incurable, and the most common cause of dementia worldwide. Treatments for AD are currently very limited, only providing symptomatic relief for some patients. While a small percentage of AD cases have known genetic causes, the majority of cases are sporadic. sAD has a complex aetiology, with many interacting pathologies including mitochondrial dysfunction. This project has built on previous findings of mitochondrial morphology abnormalities and deficits in Drp1 protein levels and localisation in sAD patient fibroblasts. The hypothesis was that the mitochondrial phenotype seen in Alzheimer's patient cells is driven by abnormalities in fission and fusion processes, and that small molecules can be found which beneficially modulate the mitochondrial phenotype in AD.

The first aim was to investigate mechanisms leading to and resulting from reduced levels of Drp1 in sAD and control fibroblasts. It was found that there is a decrease in several key mitochondrial fission proteins including Drp1 receptors Fis1, Mff, and MiD49, but there was no significant difference in the localisation and interactions of these proteins with Drp1. There was no change seen in BAP31-Fis1 mitochondria ER contact sites, which are involved in the pre-constriction of the mitochondria, or in fusion protein OPA1.

The second aim was to investigate the mitochondrial phenotype in a patient derived neuronal model. A general population of iNeurons generated from iNPCs were chosen as a model, and this population was seen to express neuronal markers TUJ, MAP2, and NeuN. When assessed for markers of more specific neuronal types, expression was seen to be variable, suggesting heterogeneity between populations from different differentiations. sAD iNeurons were seen to recapitulate a decrease in MMP seen in fibroblasts, but the morphology phenotypes were variable, with some lines showing a more fragmented morphology and some showing a more fused morphology.

The third aim was to determine whether the same mechanisms are seen leading to mitochondrial morphology changes in iNeurons as in fibroblasts. While alterations to the fission mechanism were seen in all sAD iNeuron lines, there was no consistent pattern in the direction or severity of these alterations.

The fourth aim was to screen a compound library for compounds which have a beneficial effect on mitochondrial function and morphology in sAD fibroblasts. While some compounds showed a rescue effect in some of the deficits assessed, this was not consistent across all lines tested. sAD is a complex disease with variable phenotypes, and when attempting to identify a treatment, better patient stratification may be beneficial.

6.1 Models of Alzheimer's disease

Modelling neurodegenerative diseases such as AD is complicated; no model is able to perfectly represent all aspects of the disease. Each model offers a unique perspective on AD pathogenic mechanisms. For example, post mortem tissue shows the end stage of the disease in a patient derived model, while animal models enable the study of pathogenic mechanisms, and importantly therapeutic interventions, in a whole organism context, and immortal cell lines offer a relatively simple model in which to study the effect of specific pathology such as A β or tau. Modelling sAD is especially difficult, due to the heterogeneity and unknown causes of the disease, and it is an advantage of patient derived cells that they are able to do this.

This project utilised two different patient derived cell models of sAD, fibroblasts and iNPC derived iNeurons. Several advantages and disadvantages of both these models have been highlighted (Chapter 3 section 3.3.11, Chapter 4 section 4.3.3), as well as the unique usefulness of fibroblasts in high throughput drug screening (Chapter 5, section 5.1.2). However, a disadvantage of both models is that they are a single cell type, grown in a 2D culture. This does not accurately represent the complexity of the brain, and does not take into account other neural cell types which may also be affected. Further work could focus on investigating iNeurons as part of a co-culture model. Co-cultures have previously been used to demonstrate that both astrocytes (Limbad *et al.*, 2020; Wasilewski *et al.*, 2022) and microglia (Lee and Choi, 2022) contribute to the neuronal phenotype seen in AD, and it would be interesting to see if other cell types impact the alterations seen in sAD iNeurons here.

Another more physiologically relevant model is a 3D organoid model. These are a relatively new technology, where either primary or iPSC derived cells are cultured on a 3D scaffold, to better represent the environment of the brain. The first cerebral organoids were shown to replicate cortical development, and consisted of stratified cortical layers (Lancaster and Knoblich, 2014). In AD, cerebral organoids developed from NPCs with fAD mutations (Choi *et al.*, 2014; Raja *et al.*, 2016; Gonzalez *et al.*, 2018), as well as those developed from sAD derived iPSCs (Chen *et al.*, 2021) show both A β and tau pathology. However, there are still several limitations with these models; often the cells do not mature fully, which is especially important in an age related disease such as AD. There is also to date very few studies which have incorporated other cell types into a 3D model, and a lack of vasculature which reduces the physiological relevance of the model (Kim, Li and Mahairaki, 2021; Bubnys and Tsai, 2022). Nevertheless, organoid models have a huge amount of potential in the future, to both investigate AD pathogenic mechanisms and screen potential treatments, in an environment which is more similar to the brain than a 2D cell culture model.

6.2 Mitochondrial Fission in sAD

Much of this project focussed on the process of mitochondrial fission, in both sAD fibroblasts and iNeurons. In fibroblasts, there was a shift towards decreased fission, with a more fused mitochondrial network, and reductions in key fission related proteins, whereas the phenotype in iNeurons was less consistent. However, in general, it is clear that the fission mechanism is imbalanced in both cell types, and this likely plays a role in the deficits in mitochondrial function seen in both cell types.

There are other ways to assess mitochondrial fission which were not carried out here. While protein levels, localisation, post translational modifications, and protein-protein interactions can give an indication about the process, they do not definitively assess whether fission itself is increased or decreased. It is a complicated process, with many factors involved which have not been investigated here, for example further post translational modifications such as SUMOylation. There is also a lack of understanding about the precise role of some of the proteins assessed here in the fission process, and more work is needed to understand the function of these proteins in healthy mitochondria. Live fission could be assessed to determine if the changes noted in the different steps of the process ultimately affect the level of fission. This can be carried out through the use of time lapse imaging and super-resolution microscopy, such as structured illumination microscopy, which can be used to visualise the dynamic processes within sub-cellular compartments.

The alterations in fission proteins were seen to be associated with mitochondrial morphology measures; in fibroblasts there is a significant linear regression between form factor and Drp1, form factor and Fis1, and a close to significant linear regression between form factor and Mff. In iNeurons, there is a close to significant linear regression between Drp1 and form factor, and Drp1 and mitochondrial count per cell, and a significant linear regression between form factor and MiD49. This provides evidence for an association between these proteins and mitochondrial morphology. There was also an association seen between some of these proteins and mitochondrial function. In fibroblasts, Drp1 and Fis1 both had a significant linear regression with MMP, while the linear regression between MiD49 and MMP was approaching significance. In iNeurons, this association was only seen between Drp1 and MMP. This provides evidence for these proteins impacting both mitochondrial morphology, and ultimately mitochondrial function. To provide further evidence for this connection, further overexpression experiments could be done in the fibroblasts. Attempts were made to assess the effect of Drp1 overexpression on mitochondrial morphology in the fibroblasts, but this was unsuccessful. Potential optimisation of this was previously discussed (Chapter 3, section 3.3.10), and success here would give some indication as to the importance of Drp1 in the sAD

morphology phenotype. The effect of overexpression of Drp1 on functional measures such as MMP could also be measured, as well as the protein levels of the Drp1 receptors. The receptors themselves, particularly Fis1 and Mff as these are the ones which show an association with morphology and function measures, could also be overexpressed, to see if this can rescue alterations in morphology and function. Whilst a transient overexpression may not last long enough to necessarily see this level of change, a stable overexpression method such as lentiviral transduction could be used in which the plasmid DNA is permanently integrated into the cell's genome. Alternatively, to determine whether decreased Drp1 is a driving factor in sAD, small molecule inhibitors of Drp1 could be used in control cells to determine whether this replicates the phenotype seen in sAD cells. The most commonly used inhibitor of Drp1 is MDIVI1, though as mentioned previously (Chapter 5, section 5.1.1) this has been questioned (Bordt *et al.*, 2017). P110 could also be used, though this specifically affects Drp1 interactions with Fis1 (Amit U. Joshi *et al.*, 2018) and would give evidence of the importance of these interactions in particular in the sAD phenotype. More recently, novel inhibitors of Drp1 GTPase activity were identified via in silico screening, Drpitor1 and related compound Drpitor1a, both of which had a greater potency than MDIVI1 (Wu *et al.*, 2020). In iNeurons, the picture is more complex, as not all sAD lines share the same alterations, and there are fewer associations seen between the receptors and morphology or function. However, increased Drp1 was associated with a decrease in MMP. To investigate this further, Drp1 could be knocked down in the iNeurons, or the Drp1 inhibitors discussed above could be used, to determine whether this has an effect on mitochondrial function. This would give a better indication as to the importance of these proteins in the pathogenic mechanisms seen in sAD, and whether modulation of these proteins is a viable therapeutic target.

Another process which could be further investigated is mitochondrial fusion. The balance between these processes is key in the regulation of mitochondrial morphology. Fusion protein OPA1 was looked at briefly in the fibroblast model, and Mfn1 and Mfn2 had also previously been investigated in a small number of the fibroblast lines (Bell *et al.*, 2018), and no differences were seen between patients and controls. These proteins were not assessed in the iNeuron model; this would be an area for further study. Previous work studying these proteins in AD models is contrasting, with some seeing increased levels in transgenic mouse (Xu *et al.*, 2017) and tau overexpression models (Li *et al.*, 2016), and others seeing a decrease in both fAD (Calkins *et al.*, 2011; Kandimalla *et al.*, 2018b; Djordjevic *et al.*, 2020) and sAD (Drabik, Piecyk, *et al.*, 2021) models, while in iPSC derived neurons, no difference was seen in either Mfn1 or Mfn2 (Birnbaum *et al.*, 2018). Given the differences seen between the fission phenotype in the two cell types studied here, it is possible that there is alterations in the fusion mechanism in the iNeurons which are not seen in the fibroblasts, and are

contributing to the morphological and functional differences seen, and this should be investigated further.

Another area for further study is the downstream effects of mitochondrial fission. Firstly, the downstream effects on the mitochondrial network itself. Mitochondrial fission usually leads to either mitochondrial biogenesis or degradation. Mitochondrial biogenesis could be assessed in both the fibroblast and the iNeuron model by looking into the expression of various genes and proteins involved in this process, for example peroxisome proliferator activated receptor γ coactivator (PGC1 α), the master regulator of mitochondrial biogenesis, nuclear respiratory factor 1/2 (NRF1/2) or transcription factor A (TFAM) (Popov, 2020). PGC1 α has been seen to be reduced in various models of AD including transgenic mice (Gong *et al.*, 2010; Wang *et al.*, 2021) and post mortem tissue (Qin *et al.*, 2009; Katsouri *et al.*, 2011). In fibroblasts, an increase in the percentage of mitochondria accumulated in the perinuclear region was seen, which may indicate an issue in mitophagy. Mitophagy could also be studied in these models, by investigating the co-localisation of lysosomes and mitochondria, or by investigating the levels of mitophagy proteins parkin or PINK1. Deficits in mitophagy have been previously seen in AD, including an accumulation of damaged mitochondria (Ye *et al.*, 2015; Martín-Maestro *et al.*, 2016; Martín-Maestro, Gargini, García, *et al.*, 2017), and alterations in PINK1 and parkin localisation (Manczak, Mao, Marcus J Calkins, *et al.*, 2010; Hu *et al.*, 2016; Martín-Maestro *et al.*, 2016; Manczak *et al.*, 2018; Cummins *et al.*, 2019). Furthermore, reducing mitophagy has been shown to improve A β and tau accumulation (Fang *et al.*, 2019; Xiong *et al.*, 2020; Xie *et al.*, 2022), cell survival (Xie *et al.*, 2022), and cognition in animals models (Fang *et al.*, 2019; Xie *et al.*, 2022), highlighting the importance of effective degradation of dysfunctional mitochondria.

Fission and fusion are key in the ability of the mitochondria to produce ATP, but they are also important in several other functions of the mitochondria, one of which is apoptosis, a programmed cell death used to remove damaged cells. During apoptosis, the mitochondria become depolarised, and cytochrome c is released from the mitochondrial membrane. Drp1 has been shown to be important in apoptosis, with Drp1 inhibition seen to prevent the loss of MMP and cytochrome c release, and ultimately preventing cell death (Frank *et al.*, 2001), though others found that downregulation of Drp1 simply delayed apoptosis rather than prevent it completely (Estaquier and Arnoult, 2007). In Cockayne syndrome group A, a rare disorder of premature aging, inhibition of Drp1 was seen to significantly reduce levels of apoptosis (Pascucci *et al.*, 2021). A β has been seen to induce neuronal apoptosis (Obulesu and Lakshmi, 2014), and it may be that changes in Drp1 expression also play a role in this process.

Mitochondrial quality control has also been shown to be involved in the innate immune response. The mitochondria are involved in antiviral signalling; viral RNA binds to retinoic acid-inducible gene 1-like receptors (RLRs), which then bind to mitochondrial antiviral signalling protein (MAVS) on the outer mitochondrial membrane, which then leads to the production of pro-inflammatory cytokines via nuclear factor κ B (NF κ B) activation (West, Shadel and Ghosh, 2011). Inducing mitochondrial elongation has been seen to enhance MAVS signalling, while fragmentation reduced it (Castanier *et al.*, 2010; Zemirli *et al.*, 2014). The immune system has been seen to play a key role in AD, with increased neuroinflammation and microglial activation commonly seen (reviewed by Lee, Cho and Ryu, 2021; Leng and Edison, 2021), and it is possible that Drp1 alterations are involved in this pathology.

This project studied mitochondrial fission in a cohort of sAD patient cells; another area for further study would be to investigate this process in fAD patient cells. sAD and fAD differ in terms of age of onset, aetiology, and disease progression. Previous work has also shown that they may differ in terms of mitochondrial phenotype, for example PSEN1 fibroblasts were found to have significantly increased mitochondrial respiration and spare capacity, while sAD fibroblasts showed a reduced spare capacity (Bell *et al.*, 2018). While previous work in the lab found that both total levels, and Drp1 localised to the mitochondria, was decreased in three PSEN1 fibroblast lines (Bell *et al.*, 2018), differences were seen between sAD fibroblasts and iNeurons, and so there will potentially be differences in PSEN1 iNeurons compared to the corresponding fibroblasts. Furthermore, it is possible that further work would uncover differences in the pathogenic mechanisms between the two types of AD. This is important from a therapeutic standpoint; treatments which are successful in sAD may not be successful in fAD and vice versa, as was shown in Chapter 5. This highlights the importance of fully characterising the mitochondrial phenotype in both fAD and sAD, including alterations in mitochondrial quality control.

6.3 Mitochondrial Involvement in Other sAD Mechanisms

There are several other pathogenic mechanisms which could be investigated in these cell models, in the context of mitochondrial dysfunction in sAD. The mitochondria are highly important and have a wide range of functions within the cell, and so dysfunction in this organelle will impact many cellular processes. One aspect which was briefly investigated in Chapter 3 is mitochondria-ER contact sites. The role of these contacts was discussed in the context of mitochondrial fission, but the involvement of these sites in cellular function is far more extensive. They are important in calcium homeostasis, lipid transfer, and autophagy (Xu, Wang and Tong, 2020). Importantly in AD, particularly fAD, they are also the predominant site for γ secretase activity (Area-Gomez and Schon, 2016). In both sAD

and fAD fibroblasts, it has been seen that communication between the mitochondria and the ER is increased (Area-Gomez *et al.*, 2012), and in an APP/PSEN1 mouse model, changes in proteins associated with these contacts was seen before the onset of cognitive symptoms (Völgyi *et al.*, 2018). In a *Drosophila* model, increasing mitochondria-ER contact through an engineered linker led to increased locomotor activity and lifespan, and in *Drosophila* expressing mutant A β peptides, increasing contact sites reduced climbing deficits, and increased lifespan (Garrido-Maraver, Loh and Martins, 2020). This highlights the importance, and therapeutic potential of mitochondria-ER contact sites in AD. Further types of mitochondria-ER contact site including VAPB-PTPIP51, and VDAC-GRP75-IP3R, could be investigated in the fibroblasts and in the iNeurons, to give a better indication of how this is affected as a whole in this sAD model.

Another pathogenic mechanism in which the mitochondria are involved is A β and tau pathology. The question of whether mitochondrial deficits precede this neuropathology remains unanswered, but it is clear that the two mechanisms interact (Rhein *et al.*, 2009; Santangelo *et al.*, 2021; Terada *et al.*, 2021; Wilkins *et al.*, 2022). The presence of A β and tau pathology was not confirmed in these cell models, though both A β (Joachim, Mori and Selkoe, 1989; Gray and Quinn, 2015; Bhattacharya *et al.*, 2020), and tau (Jong *et al.*, 2003; Ploia *et al.*, 2011) have previously been seen in patient fibroblasts. In iPSC derived neurons, A β 1-42 has been seen after 75 days of differentiation (Arber *et al.*, 2019), and tau pathology has also been noted (C. Wang *et al.*, 2017). There are several methods which could be used to assess both A β and total or phosphorylated tau levels in this model. One of the most commonly used methods is an ELISA, though some have suggested that this alone may be insufficient as it can often lead to an underestimate of the A β levels present, and suggest that western blotting or mass spectrometry may give more reliable results (Adlard *et al.*, 2014). Furthermore, the effect of A β or tau on the mitochondrial phenotypes shown here could be investigated by treating cells with A β or tau protein, and assessing any change in the mitochondrial phenotype. This may give some evidence as to whether A β and tau pathology has a direct impact on mitochondrial dysfunction.

6.4 Mitochondrial Quality Control as a Therapeutic Target in AD

As part of this project, a large compound library was screened for an effect on mitochondrial function and/or morphology in sAD patient fibroblasts. Unfortunately, none of the top compounds selected showed a robust and replicable effect across the multiple lines tested, on either mitochondrial function or morphology. Despite this, improving mitochondrial function remains an appealing target for further therapeutic studies. In animal models, improving mitochondrial function has been seen to improve cognitive performance (M. J. McManus, Murphy and Franklin, 2011; W.

Wang *et al.*, 2017; Fang *et al.*, 2019; Xie *et al.*, 2022), and mitochondrial dysfunction in fibroblasts has been seen to correlate with neuropsychological tests (Bell *et al.*, 2020). This demonstrates that there is a real chance that modulating the mitochondrial phenotype can improve the quality of patient's lives, and slow the disease progression.

Whether mitochondrial quality control specifically presents a good target requires further investigation. Previous studies have noted the therapeutic potential of Drp1, including work in our lab which found that UDCA improved mitochondrial function, and that this effect disappeared when Drp1 was knocked down (Bell *et al.*, 2018), and work by Reddy and colleagues, who propose Drp1 inhibition as a treatment mechanism (Reddy, Manczak and Yin, 2017; Reddy, Manczak, *et al.*, 2018). A treatment targeted towards mitochondrial quality control should aim to readdress the balance between mitochondrial fission and fusion. From evidence presented here, these processes are altered in different ways dependant on the patient, and on the cell type. A blanket increase or decrease in either process could potentially be detrimental to patient health, or cause various side effects. The work presented in chapter 5 showed that when sAD and control cells were treated with the top compounds, mitochondrial count was increased in the sAD lines but no effect was seen in the controls; this demonstrates that compounds can have differing effects on mitochondria dependent on the specific phenotypes which are present in the cell. Another aspect which should be taken into account when targeting mitochondrial fission specifically is the recent discovery of different types of fission (Kleele *et al.*, 2021). Increasing or decreasing all fission may disrupt the balance further, and so a more subtle approach may be needed, for example, specifically targeting proteins which are primarily involved in one type of fission.

Based on the evidence presented here, and in previously published work, not every patient with AD shows the same type and extent of mitochondrial pathology. Furthermore, in the work presented in Chapter 5, not every patient cell line shows the same response to the compounds tested. This variability in response is not necessarily unexpected. While the ideal would be to find a compound with a high efficacy in every AD patient, the complexity and differences in the pathologies observed, as well as individual differences in patient age, genetics, co-morbidities, and environmental factors, make this unlikely. Therefore, better patient stratification and a personalised medicine approach would seem to be the best approach towards future treatments of AD. It is clear that some sAD lines assessed here showed much greater alterations in the mitochondrial phenotype, and so it is logical that these patients would benefit more from a mitochondrial targeted therapy than others. In these cases, patient stratification is vital to determine which patients will benefit the most from specific therapies. This is also an important consideration for clinical trials; the ultimate goal is to develop a

new, disease modifying therapy for AD and stratifying participants in clinical trials based on those who are most likely to benefit from a treatment is key, and may lead to a greater chance of success.

6.5 Final Conclusions

The main question this project aimed to answer was whether the mitochondrial phenotype seen in Alzheimer's patient cells is driven by abnormalities in the fission and fusion processes. The fission process in particular was seen to be altered in both sAD fibroblasts and iNeurons, and changes to the some of the proteins involved in this process were seen to be associated with changes in morphology and function seen in sAD cells. This suggests that the fission process is an important factor in mitochondrial pathology, though whether it is a cause or consequence of other mechanisms requires further work to elucidate.

The severity of alterations was seen to differ between different patients; this suggests that mitochondrial fission abnormalities are not seen to the same extent in all cases of AD. This is especially important in the context of a mitochondria targeted treatment, and highlights the importance of patient stratification, and the potential benefits of a personalised medicine approach in improving patients' quality of life.

Appendices

Appendix 1: Cortical Neuron Differentiation Optimisation

Cortical neurons are the cell type most significantly affected in AD, and so are the most disease relevant model to study pathogenic mechanisms. There was no existing protocol for the differentiation of cortical neurons from iNPCs and so initially, differentiation was based on a published protocol of differentiation of cortical neurons from iPSCs from Shi, Kirwan and Livesey (2012), with advice from Professor Laura Ferraiuolo and Dr Cleide Souza. Differentiation was initially carried out in control lines from the Coriell Institute as these are the most well characterised iNPC lines currently available in the lab.

Due to significant differences in iPSC and iNPC methodology, several changes were made from the published protocol. The published protocol was followed from the neural induction step. It is stated in the protocol that after eight to 12 days, a neuroepithelial sheet should be seen. Given the significant differences between the iPSC and iNPC methods, it was expected that we would not see this, and so we continued when confluency was reached, which was after three days. The re-plating step also differed slightly from the established protocol but was used as it had previously been used for iNPC derived dopaminergic neurons (Carling *et al.*, 2020). Following re-plating, the Shi, Kirwan and Livesey (2012) protocol includes a neural stem cell expansion step. This was excluded, again based on differences in iNPC generation; iNPCs had already proliferated to full confluency. This protocol was further optimised over several rounds of differentiation. Supplementary Table 1 gives an overview of the different optimisation steps carried out.

Supplementary Table 1: Conditions used for cortical neuron differentiation optimisation. Conditions highlighted in red are those changed from the previous round of differentiation.

Round	Cell Line(s) Used	NPC plating density	NPC media	Induction Factors	Coating	Re-plating Density	Maintenance Factors	Length of Protocol
1	ND29510	100,000	Fibroblast Growth Factor Basic (FGFb)	1µM Dorsomorphin (Cayman Chemical Company)	Laminin	5000 OR 10,000 OR 20,000	None	5000 and 10,000 were lost at re-plating, and 20,000 fixed at day 9.

				1μM SB431542 (Cayman Chemical Company)				
2	ND29510	100,000	FGFb	1μM Dorsomorphin 1μM SB431542	Laminin	50,000 OR 70,000	None	Fixed at day 6, and day 9
3	ND29510	100,000	FGFb	1μM Dorsomorphin 1μM SB431542 (+ 2.5μM DAPT)	Laminin	70,000	15ng/ml OR 30ng/ml OR 50ng/ml Brain derived neurotrophic factor (BDNF; PeproTech)	Fixed at day 9
4	GM04188 and GM13335	100,000	FGFb	1μM Dorsomorphin 1μM SB431542 2.5μM DAPT	Laminin	70,000	30ng/ml BDNF OR 30ng/ml BDNF 1μM Forskolin (Cayman Chemical Company) OR 30ng/ml BDNF 10μM Forskolin OR 30ng/ml BDNF 1μM Forskolin 15ng/ml Ciliary neurotrophic factor (CNTF; PeproTech) OR 30ng/ml BDNF	Fixed at day 12

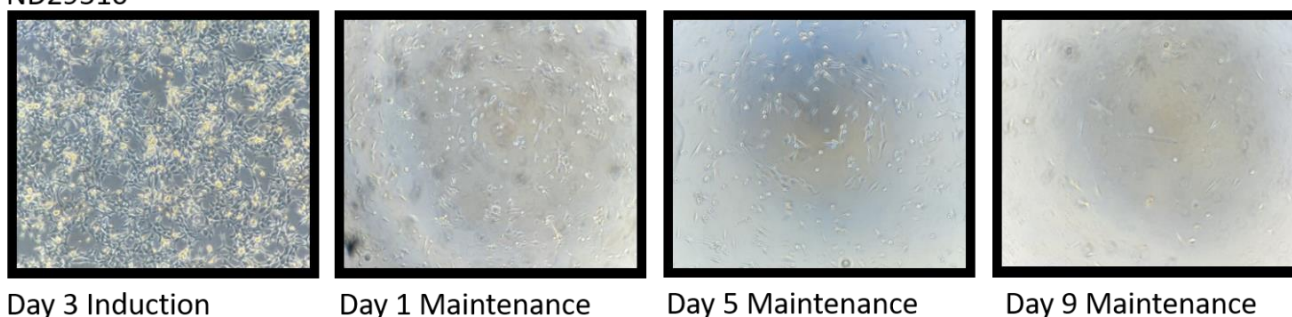
							10µM Forskolin 15ng/ml CNTF	
5	GM04188	100,000	FGFb	1µM Dorsomorphin 1µM SB431542 2.5µM DAPT	Laminin	70,000	30ng/ml BDNF 10µM forskolin	Fixed at day 23
6	GM13335	100,000	FGFb	1µM Dorsomorphin 1µM SB431542 2.5µM DAPT	Laminin	70,000	30ng/ml BDNF 10µM forskolin	Fixed at day 12
7	Control 7 and sAD 9	100,000	FGFb	1µM Dorsomorphin 1µM SB431542 2.5µM DAPT	Laminin	70,000	30ng/ml BDNF 10µM forskolin	Fixed at day 13
8	Control 7 and sAD 9	50,000 OR 100,000 OR 200,000	FGFb Free	1µM Dorsomorphin 1µM SB431542 2.5µM DAPT	Laminin	70,000	30ng/ml BDNF 10µM forskolin	Fixed at day
9	Control 7	100,000	FGFb Free	1µM Dorsomorphin 1µM SB431542 2.5µM DAPT	Laminin OR pLo OR fibronectin	70,000	30ng/ml BDNF 10µM forskolin	Fixed at day
10	Control 7	100,000	FGFb free	1µM Dorsomorphin	Laminin	70,000	30ng/ml BDNF 10µM forskolin	Fixed at day

				1 μ M SB431542 2.5 μ M DAPT			1 μ M Y-27632 dihydrochloride	
--	--	--	--	---	--	--	--------------------------------------	--

Differentiation Round 1 and 2: ND29510

In round 1, cells were plated at three different densities, based on the density used in the protocol for dopaminergic differentiation (Carling *et al.*, 2020). The two lower densities, 5000 and 10,000, were lost at the re-plating stage. The higher density, 20,000, survived re-plating but cell death occurred consistently throughout the protocol and cells were ultimately stopped at maintenance day 9 (see supplementary figure 1).

ND29510

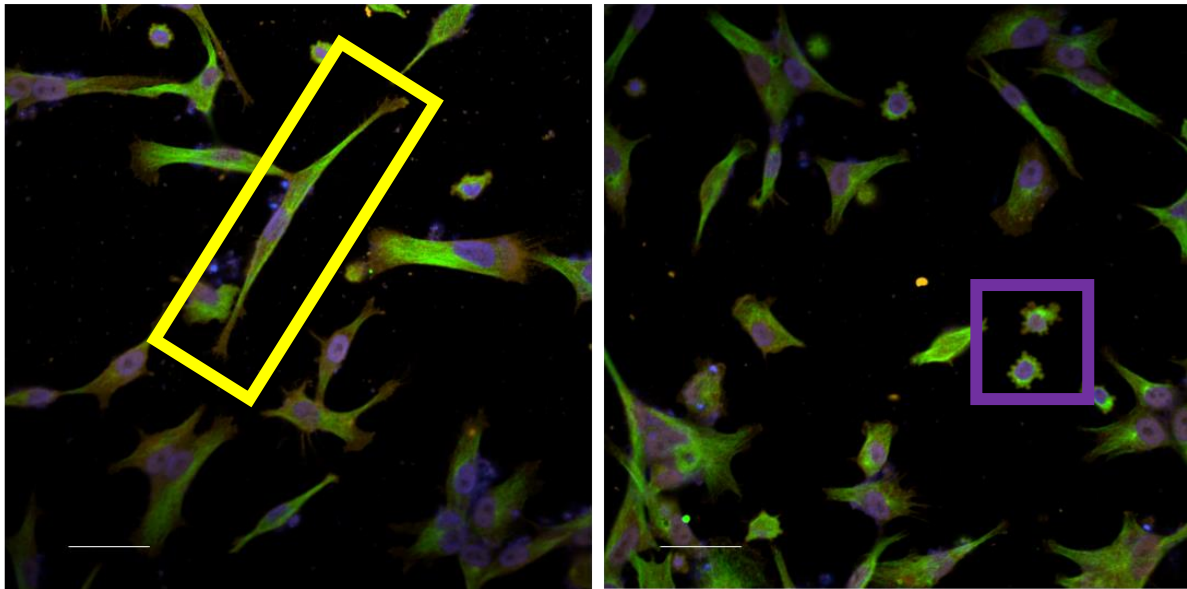


Supplementary Figure 1: Representative images of cells plated at 20,000 per well throughout the first round of differentiation. Cells were consistently lost throughout the protocol, and protocol was stopped at day 9. Images were taken manually using the standard brightfield microscope, so no scale bar can be included.

Cell death was thought to be due to a density issue and so during round 2, cells were plated at two higher densities, 50,000 and 70,000. Cell death was still seen throughout the protocol. Surviving cells were fixed at day 6, and stained for TUJ, a neuron specific class 3 tubulin, and TBR1, a transcription factor used as a marker of deep layer cortical neurons observed early in differentiation (Shi, Kirwan and Livesey, 2012) (see supplementary figure 2). 96% of cells were found to be TUJ positive though whilst some cells showed neuron-like morphology, many did not. Furthermore, TBR1 staining was

seen at low levels throughout the cell, and not localised to the nucleus. It is possible that this was due to autofluorescence of the cells, as the signal intensity was not much above background.

ND29510 Hoescht/TUJ/TBR1

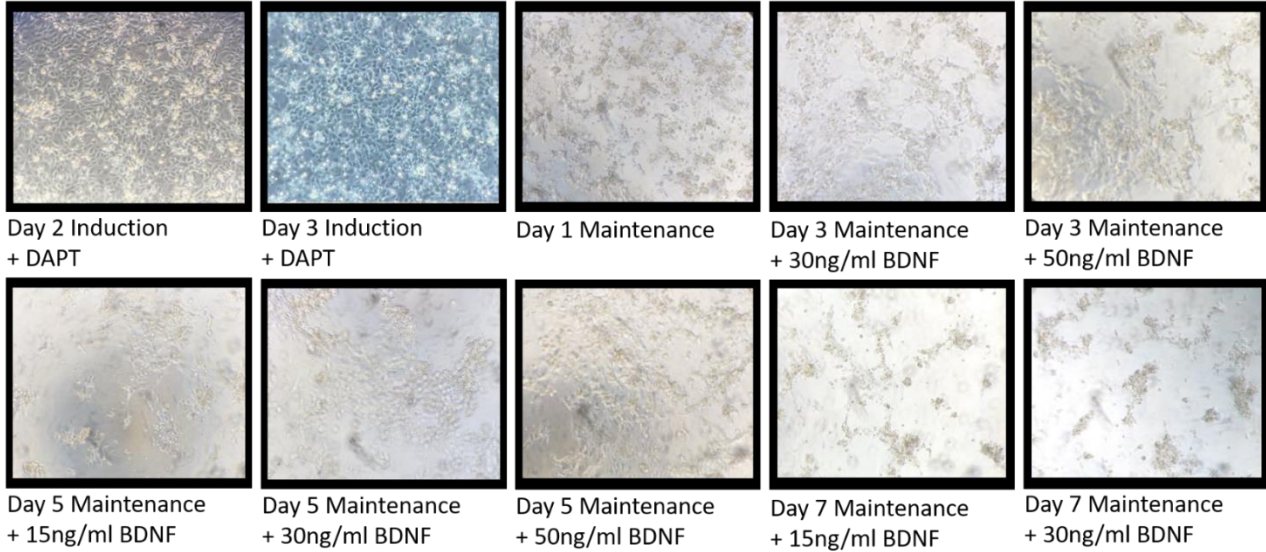


Supplementary Figure 2: Immunocytochemistry staining of cells on maintenance day 6 of the differentiation protocol, for neuronal marker TUJ and deep layer cortical neuron marker TBR1, scale bar = 50 μ m. Blue staining is Hoechst, for the nuclei, green staining in TUJ and red staining is TBR1. Yellow box outlines a cell which demonstrated elongated morphology as expected for neurons, whereas the purple box outlines cells which show smaller, more rounded morphology. TBR1 staining is mis-localised, and present at low levels throughout the cell.

Differentiation Round 3: ND29510

Due to problems with cell death early in the protocol, BDNF was added to the maintenance media to promote cell survival at three different concentrations. DAPT was also added to the induction media to prevent cells following an astrocyte lineage. Cells were replated at a density of 70,000. Cells maintained a more neuronal morphology throughout differentiation, however, cell death still occurred throughout the protocol (see supplementary figure 3) and cells were fixed at maintenance day 9.

ND29510

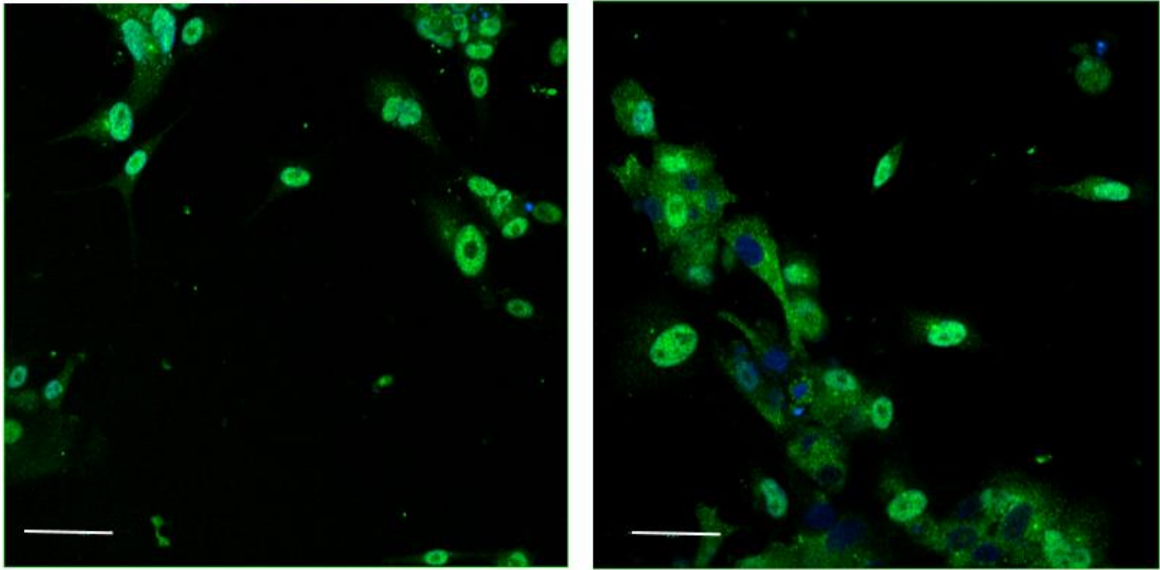


Supplementary Figure 3: Representative images of cells throughout the third round of differentiation.

Cells showed a more neuronal morphology compared to previous attempts at differentiation, but cell death occurred throughout the protocol and cells were fixed at day 9. Images were taken manually using the standard brightfield microscope, so no scale bar can be included.

Cells were stained at day 9 for TBR1, which demonstrated nuclear localisation in many cells, but other cells also had cytoplasmic location of TBR1 (see supplementary figure 4). On average, approximately 56% of cells were positive for TBR1 expression in the nucleus. The different BDNF concentrations did not differ significantly, therefore 30ng/ml was used for future rounds of differentiation.

ND29510 [Hoescht/TBR1](#)

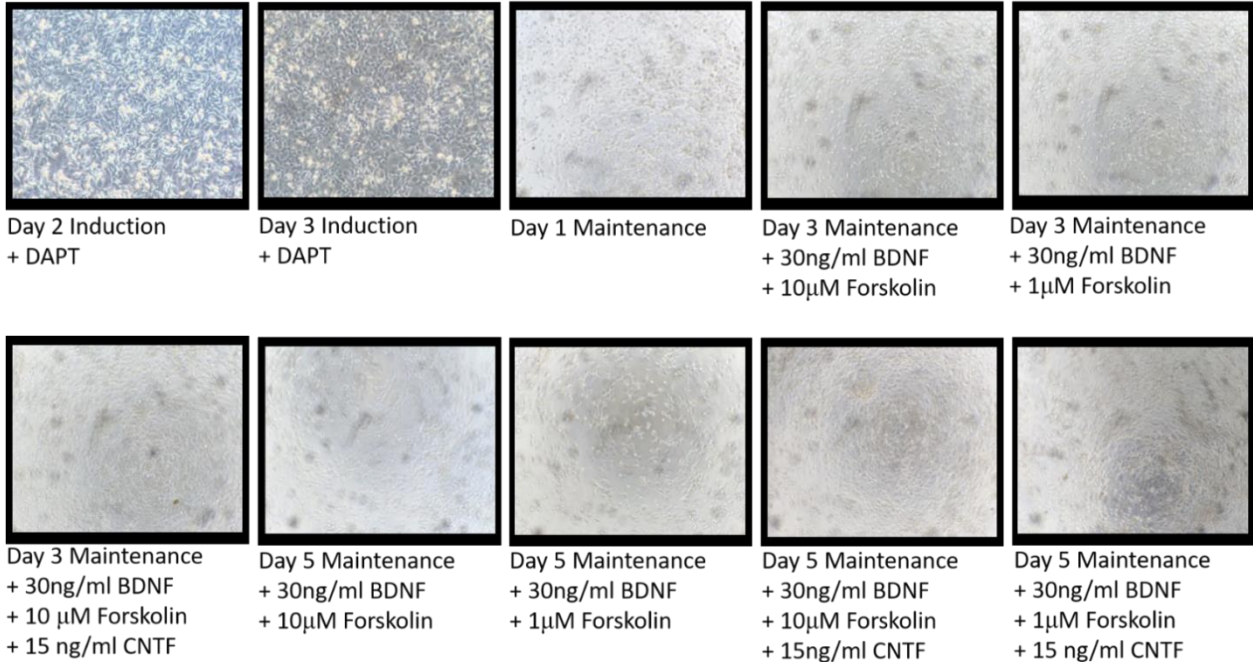


Supplementary Figure 4: Immunocytochemistry staining for deep layer cortical neuron marker TBR1 at maintenance day 9, scale bar = 50 μ m. Blue staining is Hoechst for the nuclei, green staining is TBR1. Some TBR1 staining is correctly localised to the nucleus, though there are is also cytoplasmic staining.

Differentiation Round 4: GM04188 and GM13335

Despite some cells staining positive for TBR1, in order to produce a higher yield and to increase chances of upper layer cortical neuron formation, cells require a longer time frame to differentiate. As such, further modifications were made to the protocol including the addition of forskolin, which increases cyclic AMP levels, and CNTF, a neurotrophic factor. For the fourth round of differentiation, two different lines were used, GM04188 and GM13335. Cell survival was improved in both lines, though GM04188 showed better survival and morphology than GM13335. The 10 μ M forskolin condition showed better cell survival than 1 μ M. Conditions with CNTF showed a better survival than those without, but also demonstrated a less neuronal morphology (see supplementary figures 5-6). Cells were fixed at day 15 (supplementary figures 7-8) and stained for TBR1 and TUJ at 15 days post re-plating (supplementary figure 9). The highest levels of TUJ positive staining were seen in the 10 μ M forskolin condition, with 78% positive cells in GM04188 and 94% positive cells in GM13335, though in some cells TUJ staining did not show clear neuronal processes. When CNTF was added, expression of TUJ was decreased, to 70% in GM04188 and 53% in GM13335. Relatively high levels of TBR1 nuclear staining were also seen in the 10 μ M condition, with 81% positive cells in GM04188 and 72% in GM13335. Again, this was decreased when CNTF was added, to 79% in GM04188 and 49% in GM13335.

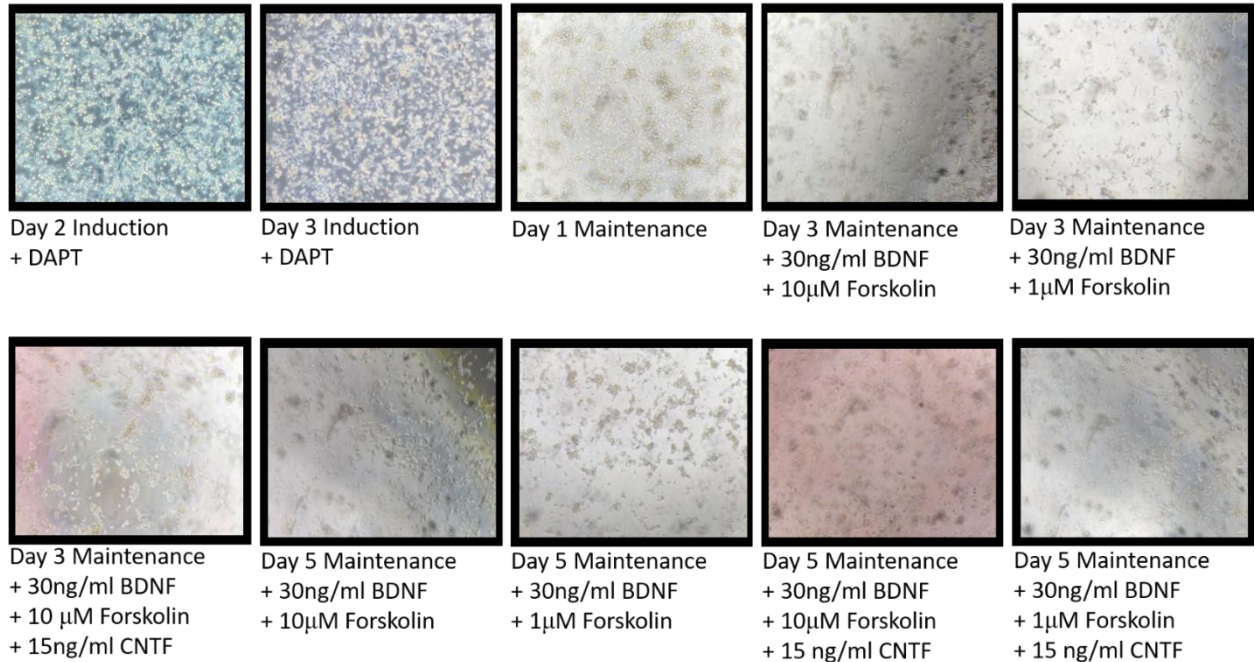
GM04188



Supplementary Figure 5: Representative images of GM04188 throughout the differentiation protocol.

Cell survival was improved compared to previous rounds of differentiation, more so in 10µM forskolin and CNTF conditions. Forskolin only conditions demonstrate the most neuronal morphology. Images were taken manually using the standard brightfield microscope, so no scale bar can be included.

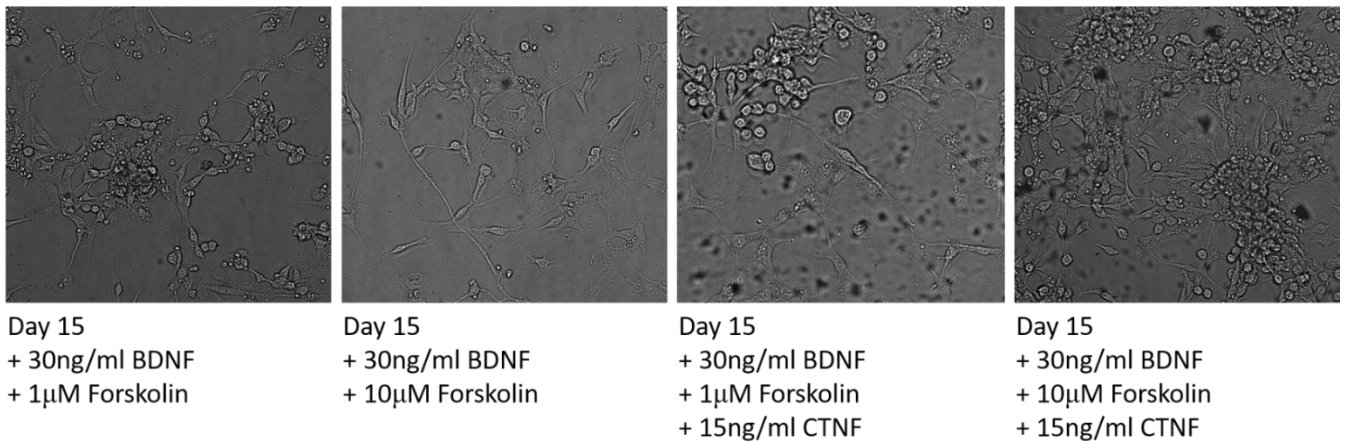
GM13335



Supplementary Figure 6: Representative images of GM13335 throughout the differentiation protocol.

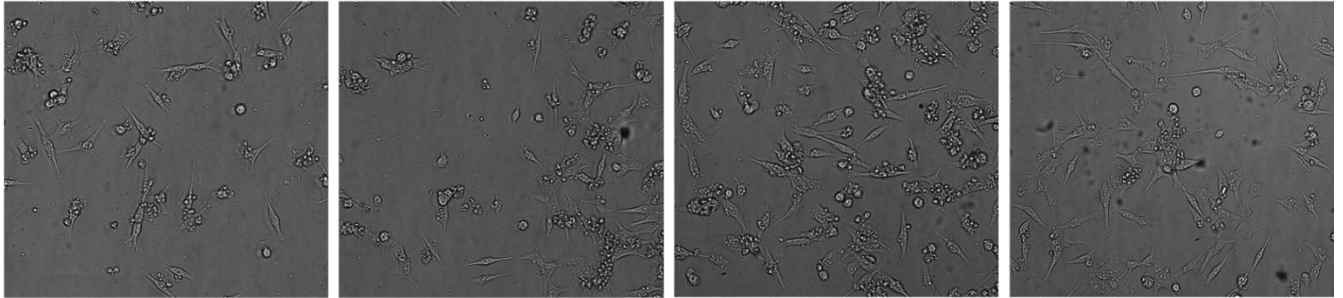
GM13335 showed a less neuron-like morphology, and more cell death than GM04188. As with GM04188, the 10µM forskolin condition showed the most neuronal morphology and better cell survival. Images were taken manually using the standard brightfield microscope, so no scale bar can be included.

GM04188



Supplementary Figure 7: Representative brightfield images of GM04188 at day 15 maintenance. Cells display neuron-like morphology, including projections and collecting of cell bodies.

GM13335



Day 15
+ 30ng/ml BDNF
+ 1 μ M Forskolin

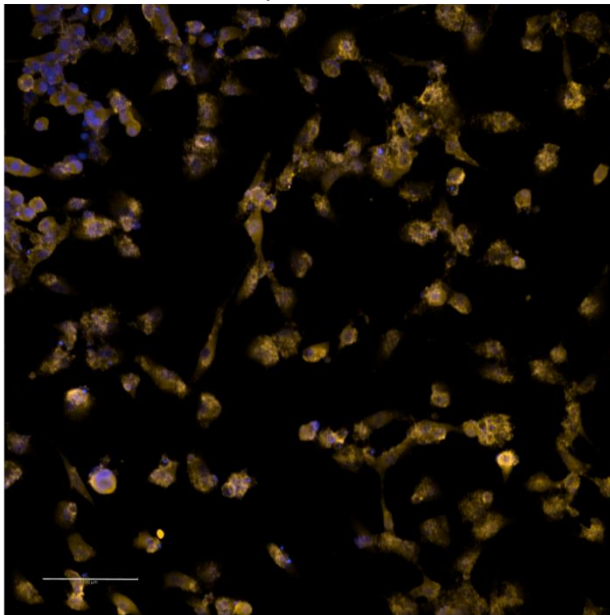
Day 15
+ 30ng/ml BDNF
+ 10 μ M Forskolin

Day 15
+ 30ng/ml BDNF
+ 1 μ M Forskolin
+ 15ng/ml CNTF

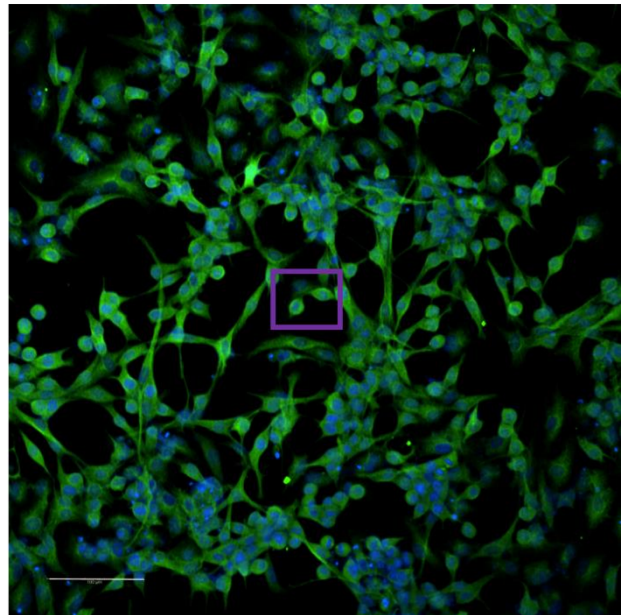
Day 15
+ 30ng/ml BDNF
+ 10 μ M Forskolin
+ 15ng/ml CNTF

Supplementary Figure 8: Representative brightfield images of GM13335 at day 15 maintenance. Cells are elongated, and display some neuron-like morphology.

GM04188 Hoescht/TBR1



Hoescht/TUJ

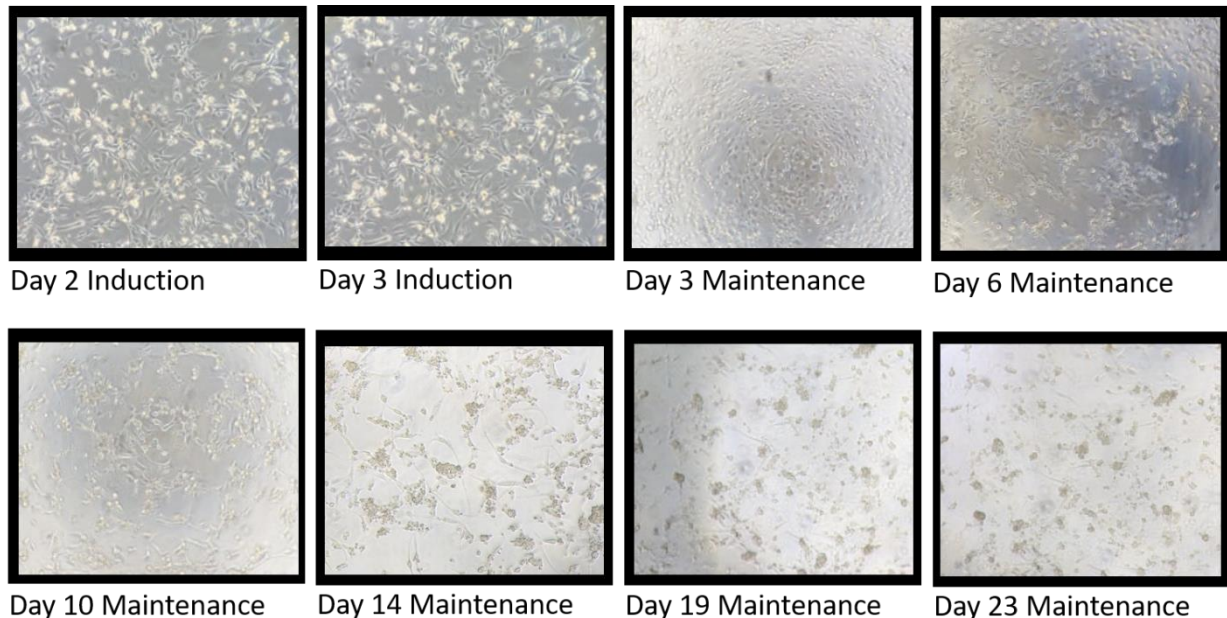


Supplementary Figure 9: Representative immunocytochemistry staining for TBR1 and TUJ at maintenance day 15 in the BDNF and 10 μ M forskolin condition, scale bar = 100 μ m. Blue staining is Hoechst for the nuclei, red is TBR1 and green is TUJ. TBR1 staining shows some localisation to the nuclear area, though this is not consistent in all cells. TUJ staining shows some processes, though not in all cells. Many cells show TUJ staining only around the nucleus, as highlighted by the purple box.

Differentiation Round 5 and 6: GM04188 and GM13335

Based on previous rounds of differentiation, 30ng/ml BDNF and 10 μ M forskolin were chosen as maintenance factors for following rounds. Cell survival was greatly improved compared to previous rounds, with cells surviving until day 23 of maintenance, though some cell death still occurred (supplementary figures 10-11). Cell morphology was the most neuronal between 14 and 19 days.

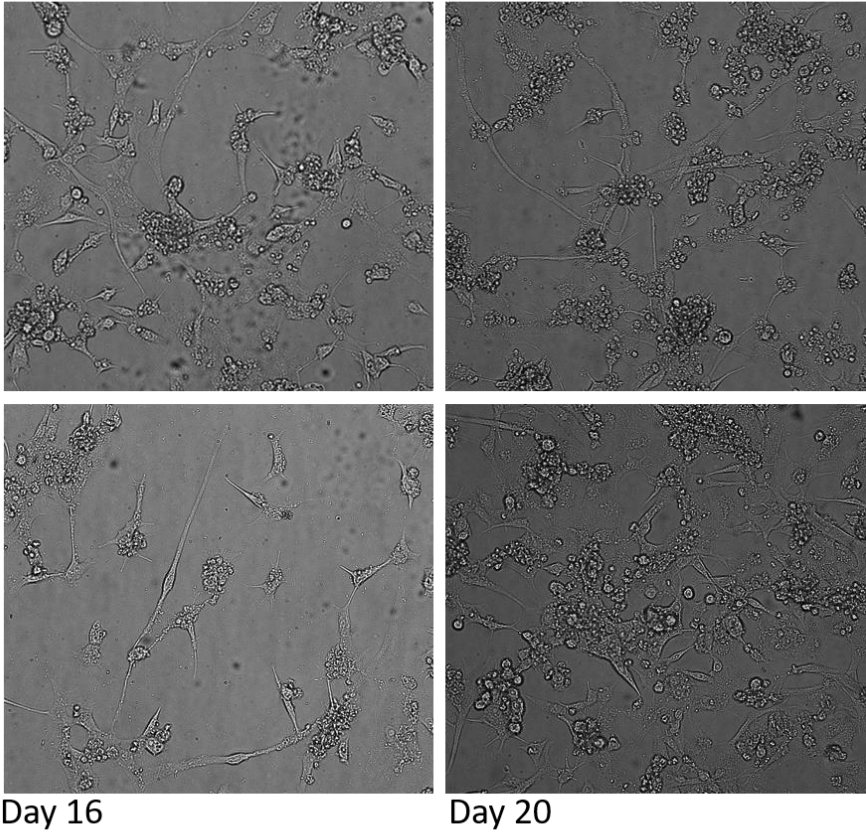
At day 23, cells were stained for neuronal marker TUJ, as well as MAP2, a neuron specific cytoskeletal protein, and neuronal nuclei (NeuN), a neuron specific nuclear protein (supplementary figures 12-13). They were also stained for SATB2 (supplementary figure 14), a nuclear located DNA binding protein used as a marker of upper layer cortical neurons, seen later in differentiation (Shi, Kirwan and Livesey, 2012). After 23 days of differentiation, 100% of cells were TUJ positive, though again, not all showed typical neuronal morphology. Furthermore, 100% of cells showed positive staining for MAP2, a more mature neuronal marker, and 95% showed positive nuclear staining of NeuN, though there was also some staining throughout the cell. Approximately 85% of cells showed positive nuclear staining for SATB2, though some SATB2 was mis-localised, showing staining in the cytoplasm.



Supplementary Figure 10: Representative images of cells throughout the fifth round of differentiation.

Cell survival was greatly improved compared to previous rounds, with cells surviving until day 23. Cells showed neuronal morphology and projections; this is best seen between days 14 and 19. Images were taken manually using the standard brightfield microscope, so no scale bar can be included.

GM04188

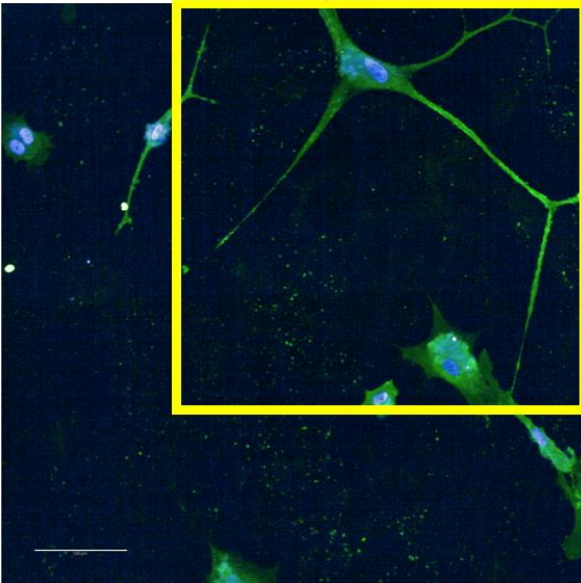


Day 16

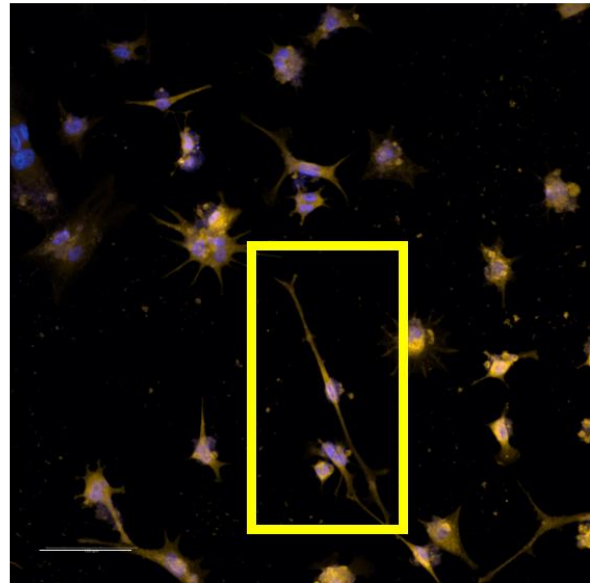
Day 20

Supplementary Figure 11: Representative brightfield images of GM04188 throughout the protocol at day 16 and day 20 maintenance. Cells are elongated, and display some neuron-like morphology.

GM04188 Hoescht/TUJ

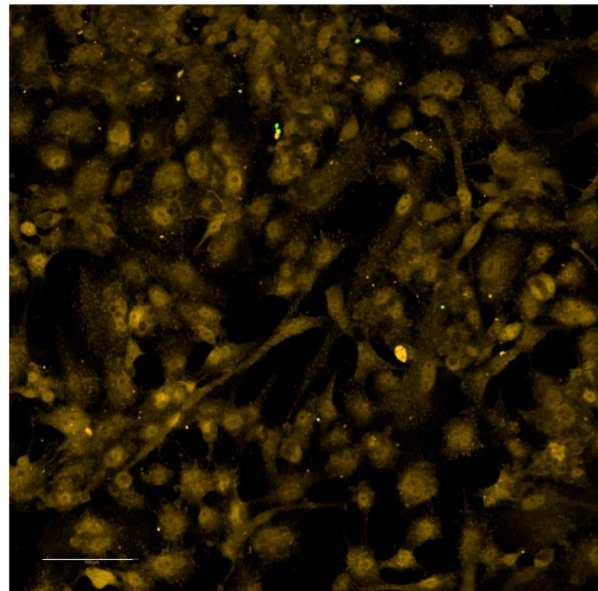
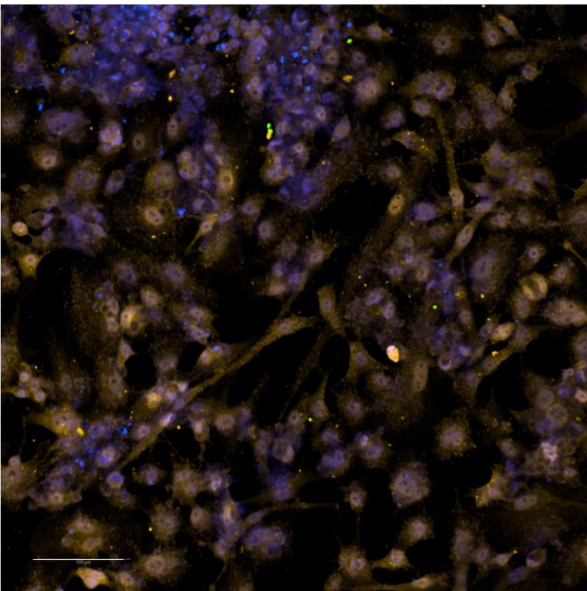


Hoescht/MAP2



Supplementary Figure 12: Immunocytochemistry staining for neuronal markers TUJ and MAP2 at day 23, scale bar = 100 μ m. Blue staining is Hoechst for the nuclei, green is TUJ and red is MAP2. TUJ and MAP2 staining shows staining of some processes, highlighted in yellow, showing neuronal morphology. However, this is not consistent in all cells.

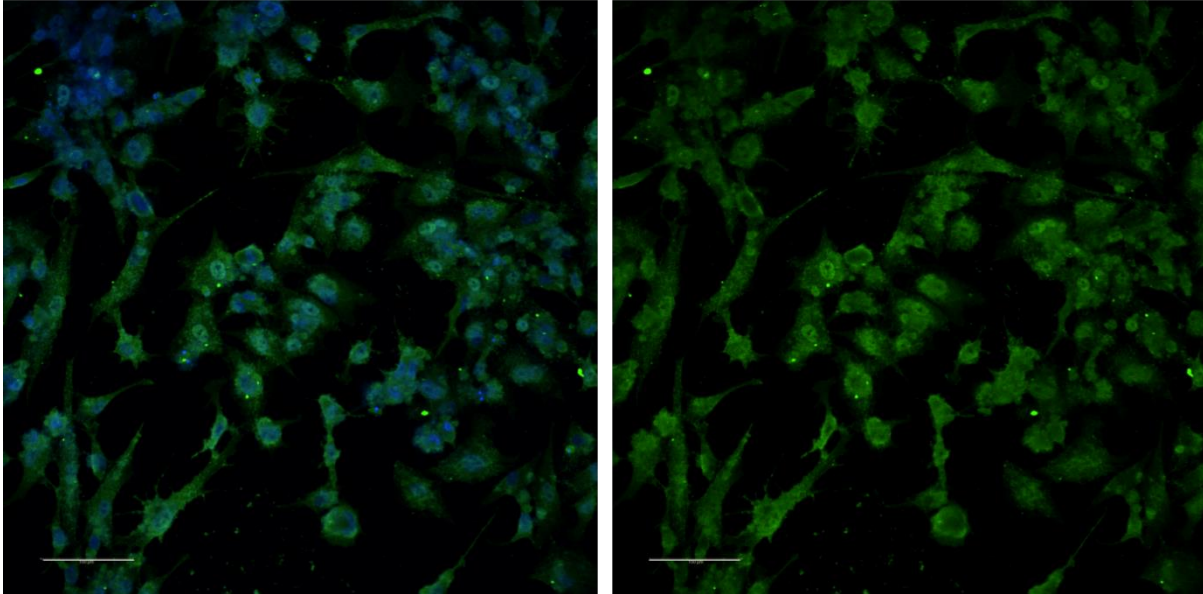
GM04188 Hoescht/NeuN



Supplementary Figure 13: Immunocytochemistry staining for neuronal marker NeuN at day 23, scale bar = 100 μ m. Blue staining is Hoechst for the nuclei, and red is NeuN. NeuN shows both nuclear and

cytoplasmic staining, though staining is of a higher intensity in the nucleus compared to the cytoplasm in many cells.

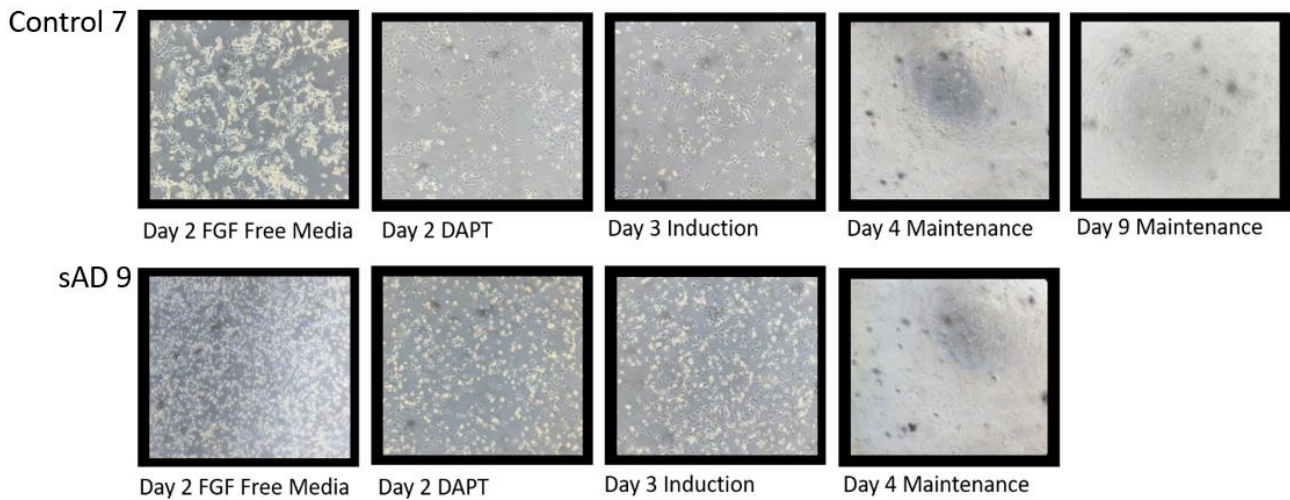
GM04188 Hoescht/SATB2



Supplementary Figure 14: Immunocytochemistry staining for upper layer cortical neuronal marker SATB2 at day 23, scale bar = 100 μ m. Blue staining is Hoechst for the nuclei, and green is SATB2. SATB2 shows both nuclear and cytoplasmic staining, though staining is of a higher intensity in the nucleus compared to the cytoplasm in many cells.

Differentiation Round 7: Control 7 and sAD 9

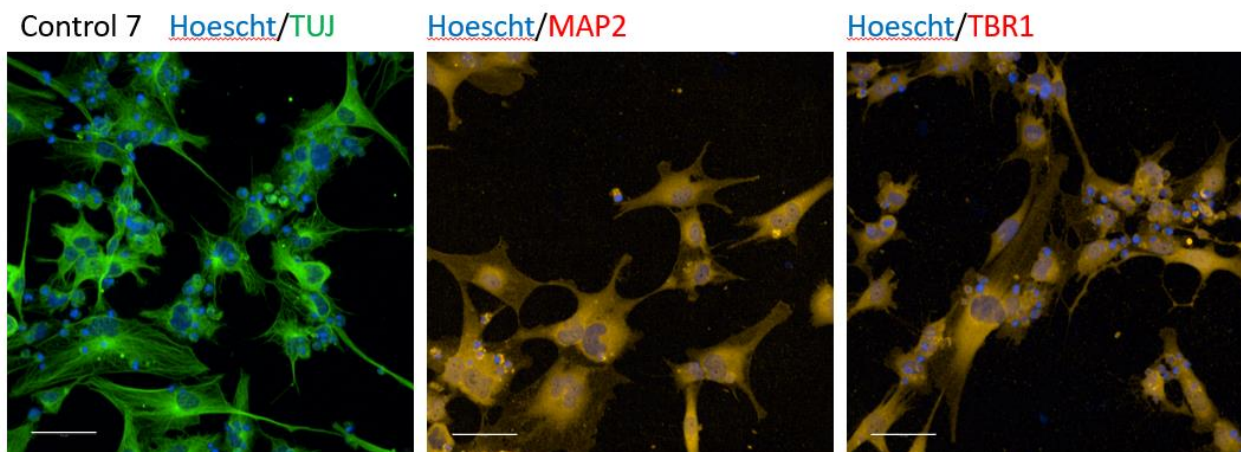
Following some success in cell survival and neuronal marker expression, the protocol was tested in iNPCs reprogrammed from fibroblasts taken from the locally collected cohort used in the majority of this project. Cells did not survive as well as the previously used lines, and were fixed at day 13 (supplementary figure 15).



Supplementary Figure 15: Representative images of control 7 and sAD 9 throughout the differentiation protocol. Cell survival was worse than the previous round using cells from the Coriell Cell Repository. Images were taken manually using the standard brightfield microscope and so no scale bars can be included.

Differentiation Round 8: Control 7 and sAD 9

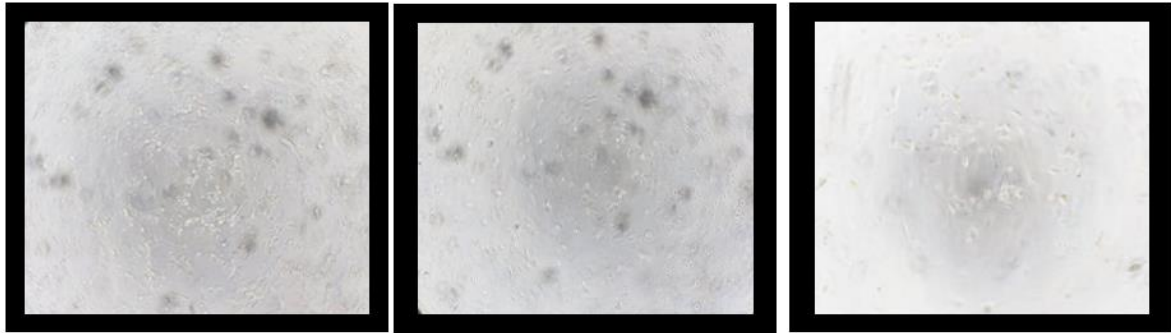
It was thought that cell death occurring early in the protocol may be due to issues at the start of the protocol, at the NPC stage. After consulting further with Professor Laura Ferraiuolo and Dr Cleide Souza, it was decided that plating at different iNPCs densities at the start of the protocol may help the cells to survive further through the protocol. Furthermore, a key issue identified by Shi, Kirwan and Livesey (2012) was the use of FGFb during differentiation, as high levels can caudalise the regional identity of NPCs (Muhr, Jessell and Edlund, 1997) and lead to them losing their cortical identity. The iNPCs from which the neurons were generated must be grown in FGFb, otherwise they will not proliferate. To minimise the effect of this FGFb on the cortical identity of the neurons produced, an FGF free media step was included in the differentiation protocol. NPCs were plated at densities of 50,000, 100,000, and 200,000 and then left in FGFb free media for four days. This improved cell survival near the start of the protocol, but many cells were still being lost after replating, during the maintenance stage. Cells were fixed at day 13 and stained for neuronal markers TUJ and MAP2, as well as cortical neuron marker TBR1. Whilst 96% of cells stained positively for TUJ, only 22% were positive for MAP2, and neuronal morphology was not consistently seen in all cells. Furthermore, 74% of cells were positive for nuclear TBR1, but much TBR1 staining was mis-localised (supplementary figure 16).



Supplementary Figure16: Representative images of immunocytochemistry staining for neuronal markers TUJ and MAP2, and cortical neuron marker TBR1 in control 7, at day 13 after maintenance, scale bar = 50 μ m. Whilst most cells are positive for TUJ and MAP2, not all cells show neuronal morphology. TBR1 staining is present but mis-localised.

Differentiation Round 9: Control 7

To try and improve cell survival after re-plating, different coatings were applied at the re-plating stage including laminin, as used by Shi, Kirwan and Livesey (2012), poly-ornithine (pLo) with laminin following a protocol provided by Dr Cleide Souza, and fibronectin, as used for plating both iNPCs and iNPC-derived dopaminergic neurons (Carling *et al.*, 2020). An increased amount of cell death was observed with a fibronectin coating, while a slight increase in cell death was also noted with a pLo and laminin coating (supplementary figure 17). It was decided that future differentiations would continue to use a laminin coating.



Day 7 Laminin

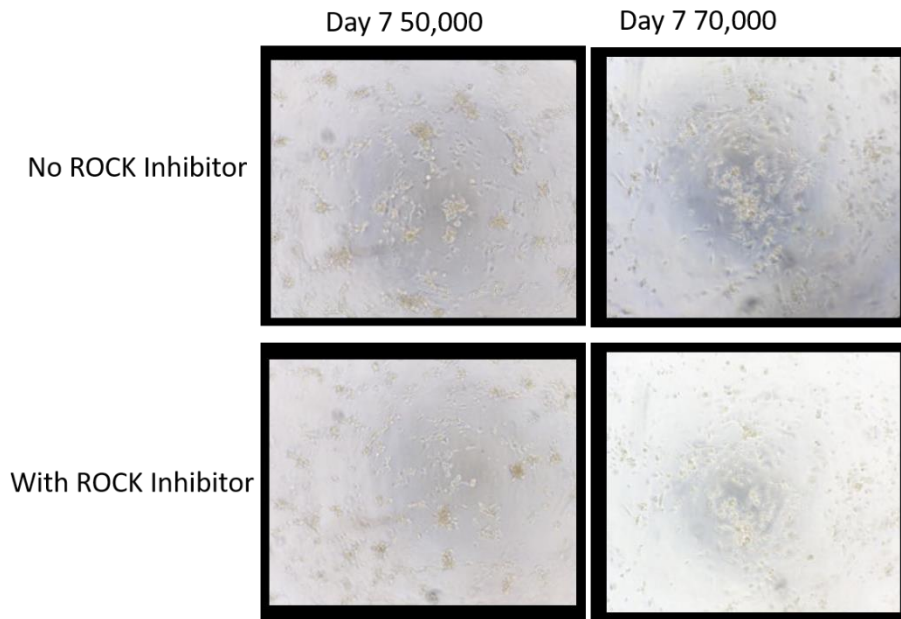
Day 7 pLo + Fibronectin

Day 4 Fibronectin

Supplementary Figure 17: Representative images of control 7 during differentiation when seeded onto different coatings. An increased amount of cell death was seen when a fibronectin coating was used, with few cells remaining at day 4 of maintenance. A slight increase in cell death was noted at day 7 when a pLo coating was used, when compared to a laminin coating. Images were taken manually using the standard brightfield microscope and so no scale bars can be included.

Differentiation Round 10: Control 7

In a further attempt to improve cell survival throughout the maintenance stage of the protocol, 1 μ M Y-27632 dihydrochloride, a Rho kinase (ROCK) inhibitor which has previously been seen to improve cell survival (Watanabe *et al.*, 2007), was added to the maintenance media. Very little difference was seen between the cells with and without the ROCK inhibitor (supplementary figure 18).



Supplementary Figure 18: Representative images of control 7 with and without the ROCK inhibitor. Very little difference was seen in cell survival between the two conditions. Images were taken manually using the standard brightfield microscope and so no scale bars can be included.

At this stage of optimisation, the labs shut down due to the COVID-19 pandemic. Once labs were reopened at reduced capacity, the decision was made to move forward with an already established protocol for producing generic neurons from iNPCs, in order to save time and maximise the amount of data which could be collected from a patient-derived neural model.

Appendix 1.2 Attempts to Optimise Cortical Neuron Differentiation from iNPCs Discussion

In AD, amyloid and tau pathology (Braak and Braak, 1991, 1995; Cho *et al.*, 2016), as well as mitochondrial deficits (Armand-Ugon *et al.* 2017), are more prominent in cortical neurons, and so a cortical neuron model was initially chosen for this project. iNPCs from many of the fibroblast lines assessed in Chapter 3 had been previously generated by Dr Simon Bell and Professor Laura Ferraiuolo, plus iNPCs have many advantages including the retention of many age related phenotypes, and the practicality of less time consuming differentiation protocols. It was therefore decided that cortical neurons would be generated from these iNPCs. Whilst there are well established protocols for differentiation of motor neurons (Meyer *et al.*, 2014), and dopaminergic neurons (Carling *et al.*, 2020), there is no established protocol for producing cortical neurons from iNPCs. Optimisation of a protocol was attempted, using a protocol for differentiating cortical

neurons from iPSCs (Shi, Kirwan and Livesey, 2012) as a base. Unfortunately, despite several attempts at optimisation this proved to be unsuccessful within the time available.

Initially success was seen in differentiating cortical neurons from control lines obtained from the Coriell cell repository, with the most successful differentiation protocol showing cells surviving to day 23. Some, though not all, showed neuronal morphology, and expression of neuronal markers was high, with 100% of cells expressing TUJ and MAP2, 95% expressing NeuN in the nucleus, and approximately 85% of cells expressing upper layer cortical neuron marker SATB2. Other protocols have generated similar levels of receptor expression, including Boissart *et al.*, (2013) who produced a population of upper layer glutamatergic cortical neurons from a stable population of late cortical progenitor cells obtained via patterning with epidermal growth factor (EGF), FGF2, and BDNF, of which 80% were TUJ positive, 80% were vGlut1 and vGlut2 positive, and 70% were positive for upper layer cortical neuron markers CUX1, CUX2, and BRN2 after 21 days of differentiation. Cao *et al.* (2017) also generated a glutamatergic neuron population, via the addition of sonic hedgehog inhibitor cyclopamine, of which 42% of cells were SATB2 positive after 90 days differentiation. Zhang *et al.* (2013) bypassed the usual neural induction and patterning stages by overexpressing NGN2 via lentivirus, and culturing with BDNF and neurotrophin 3, as well as a feeder layer of mouse glia, and were able to produce close to 100% of MAP2 and NeuN positive cells, with many also showing expression of cortical markers CUX1 and BRN2 by 21 days. This indicates that the protocol optimised here is highly efficient, producing a similar or higher percentage of neurons expressing both general neuronal markers and cortical specific markers than many of the published protocols, in a shorter timeframe than many iPSC derived differentiation protocols. However, this success did not translate into success in differentiating cortical neurons from locally collected control and sAD lines, with the main issue being cell death throughout the protocol.

Several steps were taken to improve cell survival, including trying different coatings, changes in the early NPC stages of differentiation, and the addition of a ROCK inhibitor. The ROCK inhibitor was only assessed at one concentration prior to labs being closed due to the COVID-19 pandemic, and it is possible that a higher concentration of this would improve cell survival. There are several other factors which have previously been used to promote cortical neuron maturation and survival, including ascorbic acid (Hyvärinen *et al.*, 2019; Autar *et al.*, 2022), which has been suggested to play an important role in the development of central nervous system (CNS) neurons (Lee *et al.*, 2003), and neurotrophin 3 (Espejo *et al.*, 2000; Lu *et al.*, 2008). Furthermore, whilst forskolin was added in this protocol to increase the activation cyclic AMP, others have added cyclic AMP directly (Autar *et al.*, 2022). With more time, addition of these factors into the protocol could have been tested and

optimised, and may have led to increased success in differentiating cortical neurons from the locally collected cohort.

Appendix 2: Dose response analyses

Appendix 2.1: Values for the minimum and maximum dose, maximum percentage increase, and EC50 of all compounds in the first dose response analysis. Compounds highlighted in green were chosen for further analysis.

Compound	MMP 100nM	MMP 10µM	MMP Max %	EC50 (nM)	FF 100nM	FF 10µM	FF Max %	FF EC50	Count 100nM	Count 10µM	Count % Max	Count EC50
A03	5.638093	5.530736	108.1420146	NA	8.159019	7.508159	28.11663	NA	358.3846	435.9556	76.47880824	154.3
C03	5.721974	5.75427	97.03489073	NA	8.220362	7.973102	29.07986	NA	440.2353	386.3333	38.72066444	NA
E03	3.850464	3.579528	164.5374041	NA	6.689217	6.549556	49.999	NA	452.4063	422.2143	42.55581625	NA
G03	4.205537	5.0294	72.21424776	NA	7.30076	7.369575	19.60012	898.7	356.2353	409.2821	38.64652007	1016
I03	2.980159	1.968726	13.05858174	NA	6.240944	5.701638	0.868032	NA	283.907	261.9744	10.39480227	NA
K03	5.977	2.305966	104.6615021	609.5	8.338701	5.791722	30.93808	227.2	418.2	287.0976	31.77721521	191.8
M03	3.667703	4.534948	145.7137163	NA	6.836665	7.488307	44.01456	6.758	453.24	496.4231	56.42576204	NA
O03	5.42834	4.028925	85.87455555	19.78	8.098749	6.686612	27.17024	42.76	383.2821	326.7679	26.50061225	1127
A05	1.795552	2.451009	-2.820747068	1879	5.54757	5.784496	-4.65637	1170	247.6667	290.5814	-4.0866692	3410
C05	4.29869	1.632418	47.19363437	NA	7.140634	5.511096	12.12548	NA	387.5	238.8421	22.10346938	NA
E05	3.498775	3.439078	81.32574222	737.4	6.757796	6.422843	23.03244	907.3	318.6389	430.5135	35.65726958	5841
G05	3.505676	2.803774	46.75407611	NA	6.823381	6.255456	8.388236	NA	379.0667	326.2	30.39944693	NA
I05	4.38443	0.286077	50.12950139	198.5	7.286473	4.966745	14.41551	NA	356.5385	131.1538	30.82947171	7244
K05	0.79882	3.812099	30.53202403	NA	5.235034	6.458877	1.420224	NA	156.25	329.6964	9.61973671	NA
M05	5.040611	3.009609	72.59812932	1022	7.762189	6.474596	21.88542	841.1	354.4	323.7059	15.91280772	955.4
O05	4.710844	5.703728	107.0420061	NA	7.820613	8.029896	33.9729	2530	362.2222	371.25	21.33275228	NA
A07	4.226863	1.462041	44.73416947	158.8	7.013024	5.515729	10.12169	NA	366.325	248.5517	15.4311056	2144
C07	3.623159	1.201059	24.06243323	NA	5.498637	5.286777	-12.3029	NA	160.8525	273.04	1.674125219	NA
E07	1.540567	1.215596	-45.42389619	NA	6.935385	5.596341	8.90257	NA	314.125	165.931	-1.017413373	70.75
G07	5.033057	0.223732	102.8026676	NA	6.732605	7.246102	18.3964	NA	360.3571	296.4054	17.1090436	322.3
I07	3.41117	3.971637	62.76680984	NA	7.530056	5.000307	33.40959	26244	376.175	339	25.08868651	NA
K07	4.535121	4.646921	59.60125077	543.7	7.094996	7.205859	15.99546	1243	411.2195	426.1463	34.28113985	NA
M07	3.593232	4.14994	64.06589847	NA	6.625708	7.179936	21.28808	NA	335.4186	332.8	8.703976445	996.9
O07	3.211801	2.832236	82.39671391	642.8	6.811114	6.491015	27.55332	739.4	451.0455	311.2903	42.12702038	NA
A09	3.287742	4.146581	41.9851926	NA	6.870233	7.221792	13.39986	NA	310.6552	311.7674	29.87082556	607.7
C09	4.828521	4.968392	97.7300961	323	7.574681	7.552486	26.65032	NA	380.8108	333.9245	19.99566415	NA
E09	5.249486	2.610972	97.89859856	NA	7.867668	6.373715	29.56628	NA	320.2453	332.75	26.31700014	4712
G09	4.304786	4.072901	50.67777644	NA	7.313752	7.113927	18.94759	NA	406.2813	299.3023	35.27488878	NA
I09	3.495934	3.998331	74.68607384	3322	7.060789	6.929108	21.65466	3071	322.9655	338.525	6.671166376	NA
K09	2.752411	4.689711	67.15095575	3317	6.418827	7.244026	15.11309	5145	288.9091	335.1731	5.614963489	NA
M09	6.345766	4.444001	117.2886066	227.5	8.893086	7.578749	39.64328	130.3	280.5472	174.2429	-1.285410794	624.9
O09	5.344186	4.767234	82.99299556	NA	7.917257	7.558239	24.32037	NA	323.4167	280.4074	11.90920039	NA
A11	3.481945	2.617074	33.84937571	133550	6.745431	6.169762	11.1366	NA	353.0256	202.06	11.24038849	16067
C11	3.648446	2.099942	32.74642245	NA	6.798637	6.867277	6.798637	NA	352.975	293.7188	5.1759897	NA
E11	2.659301	3.524586	20.68714492	7862	6.277376	6.701763	6.236654	6294	361.6452	317.587	-15.59962414	NA
G11	4.828422	4.421532	123.34496	NA	7.038597	6.930387	36.21313	NA	418.0238	392	72.65275518	356.7
I11	1.222806	1.211336	84.7884516	NA	4.92288	5.082325	24.82314	NA	400.7778	288.6667	12.8627737	NA
K11	5.264192	3.335162	118.2777749	395	7.180366	5.922365	31.10406	608.4	394.549	458.4167	28.3029889	NA
M11	5.597544	2.919594	132.1000923	NA	7.677143	5.968711	40.17455	NA	349.8462	325.5806	16.43763384	NA
O11	3.129826	4.045954	71.50641831	NA	6.215551	6.586964	22.17428	NA	351.6563	449.1818	25.71829844	NA
A13	3.016482	2.579237	115.6890965	8601	6.041422	5.846456	34.09956	11851	416.4828	352.7143	16.56640795	NA
C13	4.372213	4.508036	99.89360176	NA	6.696576	6.819648	27.66883	NA	382.4146	386.234	16.69117974	NA
E13	3.240688	3.602351	93.46082049	NA	6.011803	6.518825	32.39307	NA	353.25	321.6176	37.77870388	NA
G13	5.048197	3.42333	109.3216221	NA	7.195186	6.303611	31.37465	NA	364.3542	305.175	1.976504951	NA
I13	4.778403	2.604368	98.13471361	NA	7.089412	5.73874	29.44336	25.58	389.7333	280.9	10.29988612	NA
K13	4.774431	3.177067	97.9700161	NA	7.015375	6.185323	28.09154	NA	298.4407	415.871	16.3951756	NA
O13	2.881392	0.913047	65.43325978	107314	5.974001	4.9675	18.14097	NA	347.5588	109.7949	0.094964263	NA
A15	4.003885	3.301949	88.22736218	111.5	6.335564	6.154407	26.99237	223.9	404.5217	594.6538	66.4334216	NA
C15	2.305936	3.924654	103.8185193	NA	5.729157	6.543205	22.38216	NA	360.4167	372.3846	23.15499103	71196
E15	1.981381	2.686859	53.1302064	NA	5.348082	5.747548	15.1565	NA	370.3103	369.8286	19.83292111	1339
G15	3.62201	3.685551	65.83903265	NA	6.412681	6.478295	20.11165	NA	246.1228	437.9394	22.57174308	1425
I15	2.124893	3.285259	80.26536534	NA	5.559997	6.027926	21.62077	NA	299.8438	274.3729	7.876911985	NA
K15	3.037862	3.764395	76.28915609	NA	6.021397	6.3119	23.95518	NA	332.2632	351.6304	19.03018901	46.05
M15	2.768656	1.477586	63.42463016	NA	5.781708	5.218575	18.41133	NA	313.1463	381.7895	12.14823269	1227
O15	2.484719	1.852135	50.21180133	18972	5.811231	5.455169	13.77633	26962	318.5152	270.8182	-4.377144428	NA
A17	1.791682	3.356249	39.16562383	8560	5.414424	6.192406	13.0652	14567	286.6429	353.6585	7.231641992	NA
C17	2.550582	3.328083	45.00517064	637.4	5.68722	6.127549	14.3709	234.9	417.5313	420.2105	17.60972739	NA

E17	1.744455	1.754264	-0.48331173	NA	5.383405	5.364051	3.97519	445.7	379.0909	308.8929	6.687857533	NA
G17	4.167259	1.805337	82.69967085	NA	6.585177	5.302895	20.23669	NA	336.9057	319.1613	12.37544162	NA
I17	4.44626	4.458564	84.87270773	NA	6.58103	6.557692	20.16097	NA	338.6129	338.0806	-0.157602053	NA
K17	2.542979	4.203435	74.29387808	NA	5.7626	6.609935	20.68874	NA	326.6053	264.2027	-0.555063739	NA
M17	3.169401	3.162064	100.3873211	52888	5.918625	4.907777	22.03725	NA	331.24	297.9524	9.145285247	NA
O17	2.474585	2.193342	33.86847585	700.8	5.650337	5.575699	10.20843	NA	253.2667	331.5667	11.04353494	NA
A19	1.654064	0.590238	22.09720636	NA	5.286048	4.909824	8.609227	NA	296.7586207	126.875	19.82097322	NA
C19	4.250663	2.357318	76.25216964	15870	6.249855	4.956342	14.11415	NA	289.6977	120.4857	-17.61202243	NA
E19	1.868392	1.458046	175.5269947	NA	5.352426	5.31153	31.96189	NA	249.6667	245.4333	-7.429379251	NA
G19	7.613328	3.964569	215.6838305	7416	8.101253	6.402896	47.91824	10897	333.8077	324.0339	-2.33287983	147.5
I19	3.098674	3.552697	109.0450115	NA	5.979267	6.374572	27.0709	319.8	383.8537	294.5	7.434081283	313.1
K19	2.171171	3.764562	56.0961714	NA	5.539805	6.451205	17.79053	NA	297.2368	307.1064	-6.453819464	1369
M19	2.764853	2.224498	14.64360736	NA	5.839165	5.54646	6.615488	NA	337.8378	317.0789	10.72337691	1980
A21	9.200384	11.55416	96.73845063	4669	10.97455	12.60077	47.79102	6258	385.8286	334.1837	70.84564628	453.3
C21	14.4397	8.994046	145.8719808	NA	14.30611	10.90627	67.79249	1181	400.5192	372.0682	63.03246569	NA
E21	8.225616	5.599328	100.6869574	158.6	10.48015	8.507204	47.50918	NA	304.7368	405.5455	64.16852204	8721

Appendix 2.2: Values for the minimum and maximum dose, maximum percentage increase (for MMP and count per cell) or decrease (for form factor), and EC50 of all compounds in the second dose response analysis, for each individual line tested.

Compound	Cell Line	MMP 100nM	MMP 10µM	MMP Max %	EC50 (nM)	FF 100nM	FF 10µM	FF Max %	FF EC50	Count 100nM	Count 10µM	Count Max %	Count EC50
A03	Control 1	0.858452	1.0262	16.5737	NA	1.013783	0.962451	3.7549	NA	0.985514	0.904209	6.2282	NA
A03	Control 7	0.9766	1.3583	35.83	2620	0.980842	0.965591	4.0654	33.1	1.008864	0.939497	12.7654	9855
A03	sAD 1	0.999923	0.874907	21.7458	990	1.014924	1.013555	3.882	122.6	1.259353	1.416237	78.2576	1.728
A03	sAD 2	1.166037	1.032864	16.6037	391	0.95598	0.957433	4.2567	NA	1.140327	1.166078	30.6537	46
A03	sAD 9	1.00415	1.161039	78.6037	133.5	0.997173	0.960314	3.9686	702.2	1.324657	1.054943	32.4657	NA
A05	Control 1	0.886567	0.89258	-4.1148	21.31	1.000503	0.985642	1.4358	NA	1.127633	1.01841	17.2355	11226
A05	Control 7	0.9729	1.0093	4.3	3675	1.02795	1.009605	1.2274	252.5	1.036217	1.016008	18.176	1429
A05	sAD 1	1.261261	0.959744	103.5645	NA	0.994822	0.918393	8.1607	NA	1.195132	1.562693	56.2693	11388
A05	sAD 2	1.024161	1.027138	2.7138	407.7	0.965528	0.959655	4.0345	NA	1.177088	1.270304	27.0304	27.86
A05	sAD 9	0.835167	0.971624	-2.8376	NA	0.999286	0.98068	2.8351	1068	1.109246	1.496004	49.6004	310.3
E05	Control 1	0.993654	0.835667	16.512	NA	1.012752	1.022018	3.8085	1595	0.90745	0.955879	14.3949	887
E05	Control 7	0.8817	0.9368	18.9	NA	0.986414	0.991219	6.9818	NA	1.140687	1.134067	12.6302	3865
E05	sAD 1	0.876946	1.414362	24.5018	128.5	1.030439	1.02305	2.7543	458.5	1.229798	1.14447	39.0613	671.8
E05	sAD 2	0.772014	0.795259	17.4052	NA	0.959541	0.986955	4.8141	NA	1.203777	1.109304	24.4915	NA
E05	sAD 9	0.75481	1.020389	13.5799	NA	1.010814	0.955238	4.0042	9244	1.438931	1.518234	44.9359	43.11
O05	Control 1	0.895769	1.16512	9.595	NA	0.997593	0.961915	3.5562	62819	1.086528	1.143949	3.5649	NA
O05	Control 7	0.9439	1.159	-6.32	9676	0.970829	0.930182	1.609	58.28	0.999875	1.043205	14.0687	1824
O05	sAD 1	1.155711	0.926351	58.8771	NA	1.044806	0.972457	2.0352	578.1	1.302321	1.225702	63.2887	NA
O05	sAD 2	0.989122	1.142448	-3.2291	465.4	0.978127	0.964484	4.0459	69.2	1.111257	1.053291	20.3777	17.27
O05	sAD 9	1.007143	1.135799	2.0389	NA	0.991137	0.966739	4.4762	NA	1.408026	1.36088	77.1381	698.2
C07	Control 1	0.86966	0.89944	6.3118	NA	0.992273	0.986428	2.8763	882.3	0.896877	1.109377	10.9377	588.5
C07	Control 7	1.0397	1.1744	20.96	NA	0.958933	0.966454	7.531	8.019	1.044953	0.982757	14.5544	2144
C07	sAD 1	0.753989	1.078893	50.7018	288.4	1.01412	0.964763	7.5756	185	1.236578	1.238115	41.0029	8734
C07	sAD 2	0.826749	1.008932	0.8932	NA	0.980079	0.969161	4.1615	14.49	1.105623	1.318692	31.8692	276.1
C07	sAD 9	0.909666	1.201989	20.1989	698.2	0.987101	0.94288	5.712	11.53	1.241387	1.213862	46.5564	11.53
C17	Control 1	0.865723	0.955885	1.1247	NA	1.030569	0.995202	2.7419	731.9	0.8831	1.0275	26.05	2412
C17	Control 7	0.8969	1.1623	22.76	12482	0.993884	0.992911	2.315	39.77	1.101314	0.86452	10.1314	NA
C17	sAD 1	0.873302	0.865511	-1.1841	NA	1.024631	1.065968	2.145	18667	1.456109	1.294975	69.1144	487.4
C17	sAD 2	0.870949	0.911256	-6.9735	NA	1.001078	0.961469	3.8531	335.3	1.121048	1.073374	12.8948	NA
C17	sAD 9	0.721714	1.021819	2.1819	NA	0.995635	0.962159	3.7841	21937	1.457661	1.297054	45.7661	NA
E21	Control 1	0.957588	1.434986	43.4986	NA	0.946759	0.962428	4.2812	1107	1.0288	1.0861	8.61	NA
E21	Control 7	1.0763	1.2836	28.96	413.9	1.008357	0.953378	4.9988	92.08	1.107357	0.959629	10.7357	362.8
E21	sAD 1	0.892041	0.966467	24.825	1033	1.053769	0.957202	4.2798	NA	1.923712	1.145348	92.3712	NA
E21	sAD 2	0.88366	1.119547	20.016	2921	0.985159	0.983117	2.5672	447.3	1.04537	1.076636	23.0673	66.3
E21	sAD 9	1.108418	1.208226	22.6152	NA	1.028428	0.957552	4.7543	298	1.217425	1.026959	58.1255	41.53
C21	Control 1	0.937607	1.072121	7.2121	319.7	0.977659	0.983684	5.6984	69.19	0.868	0.8323	-13.2	46.01
C21	Control 7	0.983	1.1103	14.45	NA	0.986379	0.952749	4.7251	4043	1.074022	0.962141	7.4022	69.76
C21	sAD 1	1.099685	1.184725	42.778	12074	1.029239	1.013438	4.4537	962.8	1.201092	0.76334	74.8778	NA
C21	sAD 2	1.124928	0.854117	12.4928	316.4	0.986711	0.942178	7.2183	908.9	0.848298	0.866559	0.7107	NA
C21	sAD 9	1.045417	1.023031	4.5417	333	0.989169	1.006085	1.0831	122	1.432512	1.291461	44.1374	NA
K17	Control 1	0.854568	1.027648	19.9679	NA	0.976882	0.944278	6.6261	40.94	0.9555	1.0419	5.77	NA
K17	Control 7	1.227	1.2019	29.68	484.2	0.959417	0.943338	5.696	928.9	0.892806	0.930516	-2.4828	NA
K17	sAD 1	0.993079	1.525294	52.5294	NA	1.031701	0.930633	6.9367	3102	1.493392	1.20447	53.5669	NA
K17	sAD 2	0.951563	1.092752	9.2752	NA	0.992309	0.972725	2.7275	1583	1.139705	1.069559	25.8223	NA
K17	sAD 9	0.921577	1.135596	27.4946	1668	0.981559	0.957119	4.2881	3450	1.385046	1.248681	42.077	NA
K15	Control 1	1.019509	0.920917	2.2139	2271	1.006819	1.00703	1.3227	13819	0.9174	1.0274	7.14	5633
K15	Control 7	1.1197	0.9278	15.59	2387	0.977636	0.990326	3.9221	532.1	1.069015	0.966734	10.4828	2056
K15	sAD 1	0.811769	1.551137	55.1137	NA	1.015283	0.996608	0.3392	44.22	1.663774	1.354063	127.4014	NA
K15	sAD 2	0.965304	1.070194	7.0194	NA	0.992065	0.985043	2.0857	4901	1.105687	0.967767	28.8782	NA
K15	sAD 9	0.963333	0.890256	-3.6667	470.5	0.97577	0.97841	2.423	NA	1.094329	1.405237	42.9272	276.9
G15	Control 1	0.874452	0.860649	27.5698	673	1.026579	1.023193	1.3093	NA	0.9048	0.988	11.43	410.6
G15	Control 7	1.2806	0.981	28.06	1641	1.005897	1.00294	1.0233	NA	0.90345	0.832803	1.6698	2020
G15	sAD 1	0.916353	0.871616	8.226	13.46	1.038169	1.029553	-0.4206	NA	1.139598	1.576279	95.6939	40.46
G15	sAD 2	0.938853	0.97332	-2.668	27.11	1.00355	1.015147	-0.355	321.6	1.022319	1.024095	10.3703	NA
G15	sAD 9	1.407547	0.923705	40.7547	697.7	1.033582	0.973964	2.9729	368.8	1.447184	1.490953	49.0953	2159

Bibliography

- A A Saraiva, M M Borges, M D Madeira, M A Tavares, M. M. P.-B. (1985) 'Mitochondrial abnormalities in cortical dendrites from patients with Alzheimer's disease', *J Submicrosc Cytol*, 17(3), pp. 459–64.
- Adlard, P. A. *et al.* (2014) 'β-amyloid in biological samples: not all Aβ detection methods are created equal', *Frontiers in Aging Neuroscience*. Frontiers Media SA, 6(AUG). doi: 10.3389/FNAGI.2014.00203.
- Aguer, C. *et al.* (2011) 'Galactose Enhances Oxidative Metabolism and Reveals Mitochondrial Dysfunction in Human Primary Muscle Cells', *PLoS ONE*. Public Library of Science, 6(12). doi: 10.1371/JOURNAL.PONE.0028536.
- Ahmed, M. E. *et al.* (2019) 'Synergy in Disruption of Mitochondrial Dynamics by Aβ (1-42) and Glia Maturation Factor (GMF) in SH-SY5Y Cells Is Mediated Through Alterations in Fission and Fusion Proteins', *Molecular Neurobiology*. doi: 10.1007/s12035-019-1544-z.
- Alavi, M. V. (2021) 'Tau phosphorylation and OPA1 proteolysis are unrelated events: Implications for Alzheimer's Disease', *Biochimica et biophysica acta. Molecular cell research*. Biochim Biophys Acta Mol Cell Res, 1868(12). doi: 10.1016/J.BBAMCR.2021.119116.
- Aldana, B. I. *et al.* (2017) 'Characterization of energy and neurotransmitter metabolism in cortical glutamatergic neurons derived from human induced pluripotent stem cells: A novel approach to study metabolism in human neurons', *Neurochemistry international*. Neurochem Int, 106, pp. 48–61. doi: 10.1016/J.NEUINT.2017.02.010.
- Aldana, B. I. *et al.* (2020) 'Glutamate-glutamine homeostasis is perturbed in neurons and astrocytes derived from patient iPSC models of frontotemporal dementia', *Molecular Brain*. BioMed Central, 13(1). doi: 10.1186/S13041-020-00658-6.
- Alonso, A. D. C. *et al.* (2001) 'Hyperphosphorylation induces self-assembly of tau into tangles of paired helical filaments/straight filaments', *Proceedings of the National Academy of Sciences of the United States of America*. Proc Natl Acad Sci U S A, 98(12), pp. 6923–6928. doi: 10.1073/PNAS.121119298.
- Alston, C. L. *et al.* (2017) 'The genetics and pathology of mitochondrial disease', *The Journal of Pathology*. Wiley-Blackwell, 241(2), p. 236. doi: 10.1002/PATH.4809.
- Alward, W. L. M. (2003) 'The OPA1 gene and optic neuropathy', *The British Journal of Ophthalmology*. BMJ Publishing Group, 87(1), p. 2. doi: 10.1136/BJO.87.1.2.
- Alzheimer, A. (1907) 'Ueber eine eigenartige Erkrankung der hirnrinde', *Allgemeine Zeitschrift fur Psychiatrie und Psychisch-gerichtliche Medizin*. doi: 10.1002/ca.980080612.
- Ambasudhan, R. *et al.* (2011) 'Direct reprogramming of adult human fibroblasts to functional neurons under defined conditions', *Cell Stem Cell*. doi: 10.1016/j.stem.2011.07.002.
- Anand, R. *et al.* (2014) 'The i-AAA protease YME1L and OMA1 cleave OPA1 to balance mitochondrial fusion and fission', *Journal of Cell Biology*. doi: 10.1083/jcb.201308006.
- Andreux, P. A. *et al.* (2019) 'The mitophagy activator urolithin A is safe and induces a molecular signature of improved mitochondrial and cellular health in humans', *Nature metabolism*. Nat Metab, 1(6), pp. 595–603. doi: 10.1038/S42255-019-0073-4.
- Antczak, C. *et al.* (2014) 'A high content assay to assess cellular fitness', *Combinatorial chemistry & high throughput screening*. Comb Chem High Throughput Screen, 17(1), pp. 12–24. doi: 10.2174/13862073113169990056.
- Arber, C. *et al.* (2019) 'Familial Alzheimer's disease patient-derived neurons reveal distinct mutation-specific effects on amyloid beta', *Molecular Psychiatry* 2019 25:11. Nature Publishing Group, 25(11), pp. 2919–2931. doi: 10.1038/s41380-019-0410-8.
- Arber, C. *et al.* (2021) 'Familial Alzheimer's Disease Mutations in PSEN1 Lead to Premature Human Stem Cell Neurogenesis', *Cell reports*. Cell Rep, 34(2). doi: 10.1016/J.CELREP.2020.108615.
- Area-Gomez, E. *et al.* (2009) 'Presenilins are enriched in endoplasmic reticulum membranes associated with

mitochondria', *American Journal of Pathology*, 175(5), pp. 1810–1816. doi: 10.2353/ajpath.2009.090219.

Area-Gomez, E. *et al.* (2012) 'Upregulated function of mitochondria-associated ER membranes in Alzheimer disease', *EMBO Journal*. doi: 10.1038/emboj.2012.202.

Area-Gomez, E. and Schon, E. A. (2016) 'Mitochondria-associated ER membranes and Alzheimer Disease', *Current opinion in genetics & development*. NIH Public Access, 38, p. 90. doi: 10.1016/J.GDE.2016.04.006.

Armand-Ugon M, Ansoleaga B, Berjaoui S, F. I. (2017) 'Reduced Mitochondrial Activity is Early and Steady in the Entorhinal Cortex but it is Mainly Unmodified in the Frontal Cortex in Alzheimer's Disease.', *Curr Alzheimer Res*, 14(12), pp. 1327–1334.

Arriagada, P. V. *et al.* (1992) 'Neurofibrillary tangles but not senile plaques parallel duration and severity of Alzheimer's disease', *Neurology*. doi: 10.1212/wnl.42.3.631.

Ashrafi, G. *et al.* (2014) 'Mitophagy of damaged mitochondria occurs locally in distal neuronal axons and requires PINK1 and Parkin', *The Journal of Cell Biology*. The Rockefeller University Press, 206(5), p. 655. doi: 10.1083/JCB.201401070.

Aslan Karakelle, N., Dinçer, S. and Yar Sağlam, A. S. (2021) 'The effect of intracerebroventricular amyloid beta 1-42 application on cognitive functions in aged rats supplemented with taurine and the change of peroxisomal proteins in this process', *Brain research bulletin*. Brain Res Bull, 172, pp. 89–97. doi: 10.1016/J.BRAINRESBULL.2021.04.011.

Atkins, K. *et al.* (2016) 'The role of Drp1 adaptor proteins MiD49 and MiD51 in mitochondrial fission: implications for human disease', *Clinical Science*. doi: 10.1042/CS20160030.

Atri, A. (2019) 'The Alzheimer's Disease Clinical Spectrum: Diagnosis and Management', *Medical Clinics of North America*. Elsevier, 103(2), pp. 263–293. doi: 10.1016/J.MCNA.2018.10.009.

Auburger, G. *et al.* (2012) 'Primary skin fibroblasts as a model of Parkinson's disease', *Molecular Neurobiology*. doi: 10.1007/s12035-012-8245-1.

Autar, K. *et al.* (2022) 'Stem Cell Reports Article A functional hiPSC-cortical neuron differentiation and maturation model and its application to neurological disorders', *Stem Cell Reports*, 17, pp. 96–109. doi: 10.1016/j.stemcr.2021.11.009.

Baker, A. C., Ko, L. W. and Blass, J. P. (1988) 'Systemic manifestations of Alzheimer's disease', *AGE*. doi: 10.1007/BF02431774.

Balin, B. J. and Hudson, A. P. (2014) 'Etiology and pathogenesis of late-onset Alzheimer's disease.', *Current allergy and asthma reports*, p. 417. doi: 10.1007/s11882-013-0417-1.

Ballard, P. A., Tetrad, J. W. and Langston, J. W. (1985) 'Permanent human parkinsonism due to 1-methyl-4-phenyl-1,2,3,6-tetrahydropyridine (MPTP): seven cases', *Neurology*. Neurology, 35(7), pp. 949–956. doi: 10.1212/WNL.35.7.949.

Baxter, K. K., Uittenbogaard, M. and Chiaramello, A. (2012) 'The Neurogenic Basic Helix-Loop-Helix Transcription Factor NeuroD6 Enhances Mitochondrial Biogenesis and Bioenergetics to Confer Tolerance of Neuronal PC12-NeuroD6 Cells to the Mitochondrial Stressor Rotenone', *Experimental cell research*. NIH Public Access, 318(17), p. 2200. doi: 10.1016/J.YEXCR.2012.07.004.

Becerra Colorado, N. Y. *et al.* (2018) 'Polyplex System Versus Nucleofection for Human Skin Cell Transfection and Effect of Internal Ribosome Entry Site Sequence', *Tissue engineering. Part C, Methods*. Tissue Eng Part C Methods, 24(4), pp. 233–241. doi: 10.1089/TEN.TEC.2017.0435.

Begni, B. *et al.* (2004) 'Oxidative stress impairs glutamate uptake in fibroblasts from patients with Alzheimer's disease.', *Free radical biology & medicine*, 37(6), pp. 892–901. doi: 10.1016/j.freeradbiomed.2004.05.028.

Bell, S. M. *et al.* (2018) 'Ursodeoxycholic Acid Improves Mitochondrial Function and Redistributes Drp1 in Fibroblasts from Patients with Either Sporadic or Familial Alzheimer's Disease', *Journal of Molecular Biology*. doi: 10.1016/j.jmb.2018.08.019.

Bell, S. M. *et al.* (2020) 'Deficits in mitochondrial spare respiratory capacity contribute to the neuropsychological changes of Alzheimer's disease', *Journal of Personalized Medicine*. doi: 10.3390/jpm10020032.

- Bellenguez, C. *et al.* (2022) 'New insights into the genetic etiology of Alzheimer's disease and related dementias', *Nature Genetics*. Nature Publishing Group, 54(4), p. 412. doi: 10.1038/S41588-022-01024-Z.
- Bergström, P. *et al.* (2016) 'Amyloid precursor protein expression and processing are differentially regulated during cortical neuron differentiation', *Scientific Reports*. doi: 10.1038/srep29200.
- Bhattacharya, A. *et al.* (2020) 'Inhibition of 37/67kda laminin-1 receptor restores app maturation and reduces amyloid- β in human skin fibroblasts from familial alzheimer's disease', *Journal of Personalized Medicine*. doi: 10.3390/jpm10040232.
- Bierer, L. M. *et al.* (1995) 'Neocortical Neurofibrillary Tangles Correlate with Dementia Severity in Alzheimer's Disease', *Archives of Neurology*. doi: 10.1001/archneur.1995.00540250089017.
- Birnbaum, J. H. *et al.* (2018) 'Oxidative stress and altered mitochondrial protein expression in the absence of amyloid- β and tau pathology in iPSC-derived neurons from sporadic Alzheimer's disease patients', *Stem Cell Research*. doi: 10.1016/j.scr.2018.01.019.
- Bivona, T. G. *et al.* (2006) 'PKC regulates a farnesyl-electrostatic switch on K-Ras that promotes its association with Bcl-XL on mitochondria and induces apoptosis', *Molecular Cell*. doi: 10.1016/j.molcel.2006.01.012.
- Blanchet, L. *et al.* (2015) 'Quantifying small molecule phenotypic effects using mitochondrial morpho-functional fingerprinting and machine learning', *Scientific Reports 2015 5:1*. Nature Publishing Group, 5(1), pp. 1–7. doi: 10.1038/srep08035.
- Blass, J. P. and Zemcov, A. (1984) 'Alzheimer's disease - A metabolic systems degeneration?', *Neurochemical Pathology*. doi: 10.1007/BF02834249.
- van der Blik, A. M., Shen, Q. and Kawajiri, S. (2013) 'Mechanisms of mitochondrial fission and fusion', *Cold Spring Harbor Perspectives in Biology*. doi: 10.1101/cshperspect.a011072.
- Boissart, C. *et al.* (2013) 'Differentiation from human pluripotent stem cells of cortical neurons of the superficial layers amenable to psychiatric disease modeling and high-throughput drug screening', *Translational Psychiatry 2013 3:8*. Nature Publishing Group, 3(8), pp. e294–e294. doi: 10.1038/tp.2013.71.
- Bordt, E. A. *et al.* (2017) 'The Putative Drp1 Inhibitor mdivi-1 Is a Reversible Mitochondrial Complex I Inhibitor that Modulates Reactive Oxygen Species', *Developmental Cell*. doi: 10.1016/j.devcel.2017.02.020.
- Borghese, L. *et al.* (2010) 'Inhibition of notch signaling in human embryonic stem cell-derived neural stem cells delays G1/S phase transition and accelerates neuronal differentiation in vitro and in vivo', *Stem cells (Dayton, Ohio)*. *Stem Cells*, 28(5), pp. 955–964. doi: 10.1002/STEM.408.
- Bosetti, F. *et al.* (2002) 'Cytochrome c oxidase and mitochondrial F1F0-ATPase (ATP synthase) activities in platelets and brain from patients with Alzheimer's disease', *Neurobiology of aging*. *Neurobiol Aging*, 23(3), pp. 371–376. doi: 10.1016/S0197-4580(01)00314-1.
- Bossy, B. *et al.* (2010) 'S-nitrosylation of DRP1 does not affect enzymatic activity and is not specific to Alzheimer's disease', *Journal of Alzheimer's Disease*, 20(SUPPL.2). doi: 10.3233/JAD-2010-100552.
- Braak, H. and Braak, E. (1991) 'Neuropathological staging of Alzheimer-related changes', *Acta neuropathologica*. *Acta Neuropathol*, 82(4), pp. 239–259. doi: 10.1007/BF00308809.
- Braak, H. and Braak, E. (1995) 'Staging of alzheimer's disease-related neurofibrillary changes', *Neurobiology of Aging*, 16(3), pp. 271–278. doi: 10.1016/0197-4580(95)00021-6.
- Bragina, O. *et al.* (2010) 'Smoothed agonist augments proliferation and survival of neural cells', *Neuroscience letters*. *Neurosci Lett*, 482(2), pp. 81–85. doi: 10.1016/J.NEULET.2010.06.068.
- Brieger, K. *et al.* (2012) 'Reactive oxygen species: from health to disease', *Swiss Medical Weekly 2012 :33*. *EMH Media*, 142(33). doi: 10.4414/SMW.2012.13659.
- Bubnys, A. and Tsai, L. H. (2022) 'Harnessing cerebral organoids for Alzheimer's disease research', *Current Opinion in Neurobiology*. Elsevier Current Trends, 72, pp. 120–130. doi: 10.1016/J.CONB.2021.10.003.
- Buckley, R. F. *et al.* (2017) 'Region-specific association of subjective cognitive decline with tauopathy independent of global β -amyloid burden', *JAMA Neurology*. doi: 10.1001/jamaneurol.2017.2216.
- Butterfield, D. A. and Mattson, M. P. (2020) 'Apolipoprotein E and oxidative stress in brain with relevance to

- Alzheimer's disease', *Neurobiology of disease*. Neurobiol Dis, 138. doi: 10.1016/J.NBD.2020.104795.
- Caiazzo, M. *et al.* (2015) 'Direct conversion of fibroblasts into functional astrocytes by defined transcription factors', *Stem Cell Reports*. doi: 10.1016/j.stemcr.2014.12.002.
- Calkins, M. J. *et al.* (2011) 'Impaired mitochondrial biogenesis, defective axonal transport of mitochondria, abnormal mitochondrial dynamics and synaptic degeneration in a mouse model of Alzheimer's disease', *Human Molecular Genetics*, 20(23), pp. 4515–4529. doi: 10.1093/hmg/ddr381.
- Cao, S. Y. *et al.* (2017) 'Enhanced derivation of human pluripotent stem cell-derived cortical glutamatergic neurons by a small molecule', *Scientific Reports 2017 7:1*. Nature Publishing Group, 7(1), pp. 1–11. doi: 10.1038/s41598-017-03519-w.
- Carling, P. J. *et al.* (2020) 'Deep phenotyping of peripheral tissue facilitates mechanistic disease stratification in sporadic Parkinson's disease', *Progress in Neurobiology*. doi: 10.1016/j.pneurobio.2020.101772.
- Cascella, R. and Cecchi, C. (2021) 'Calcium dyshomeostasis in Alzheimer's disease pathogenesis', *International Journal of Molecular Sciences*. doi: 10.3390/ijms22094914.
- Castanier, C. *et al.* (2010) 'Mitochondrial dynamics regulate the RIG-I-like receptor antiviral pathway', *EMBO reports*. EMBO Rep, 11(2), pp. 133–138. doi: 10.1038/EMBOR.2009.258.
- Cereghetti, G. M. *et al.* (2008) 'Dephosphorylation by calcineurin regulates translocation of Drp1 to mitochondria', *Proceedings of the National Academy of Sciences of the United States of America*. Proc Natl Acad Sci U S A, 105(41), pp. 15803–15808. doi: 10.1073/PNAS.0808249105.
- Chakrabarti, R. *et al.* (2018) 'INF2-mediated actin polymerization at the ER stimulates mitochondrial calcium uptake, inner membrane constriction, and division', *Journal of Cell Biology*. doi: 10.1083/jcb.201709111.
- Chandra, D. *et al.* (2004) 'Association of active caspase 8 with the mitochondrial membrane during apoptosis: potential roles in cleaving BAP31 and caspase 3 and mediating mitochondrion-endoplasmic reticulum cross talk in etoposide-induced cell death', *Molecular and cellular biology*. Mol Cell Biol, 24(15), pp. 6592–6607. doi: 10.1128/MCB.24.15.6592-6607.2004.
- Chang, C. R. *et al.* (2010) 'A Lethal de Novo Mutation in the Middle Domain of the Dynamin-related GTPase Drp1 Impairs Higher Order Assembly and Mitochondrial Division', *The Journal of Biological Chemistry*. American Society for Biochemistry and Molecular Biology, 285(42), p. 32494. doi: 10.1074/JBC.M110.142430.
- Chasseigneaux, S. and Allinquant, B. (2012) 'Functions of A β , sAPP α and sAPP β : similarities and differences', *Journal of Neurochemistry*. John Wiley & Sons, Ltd, 120(SUPPL. 1), pp. 99–108. doi: 10.1111/J.1471-4159.2011.07584.X.
- Chen, D. *et al.* (2003) 'Adaptive and innate immune responses to gene transfer vectors: role of cytokines and chemokines in vector function', *Gene Therapy 2003 10:11*. Nature Publishing Group, 10(11), pp. 991–998. doi: 10.1038/sj.gt.3302031.
- Chen, G. F. *et al.* (2017) 'Amyloid beta: structure, biology and structure-based therapeutic development', *Acta Pharmacologica Sinica 2017 38:9*. Nature Publishing Group, 38(9), pp. 1205–1235. doi: 10.1038/aps.2017.28.
- Chen, X. *et al.* (2021) 'Modeling Sporadic Alzheimer's Disease in Human Brain Organoids under Serum Exposure', *Advanced science (Weinheim, Baden-Wuerttemberg, Germany)*. Adv Sci (Weinh), 8(18). doi: 10.1002/ADVS.202101462.
- Cheng, L. *et al.* (2014) 'Generation of neural progenitor cells by chemical cocktails and hypoxia', *Cell Research*. doi: 10.1038/cr.2014.32.
- Cho, D.-H. H. *et al.* (2009) 'S-nitrosylation of Drp1 mediates beta-amyloid-related mitochondrial fission and neuronal injury.', *Science*, 324(5923), pp. 102–105. doi: 10.1126/science.1171091.
- Cho, H. *et al.* (2016) 'In vivo cortical spreading pattern of tau and amyloid in the Alzheimer disease spectrum', *Annals of Neurology*. John Wiley & Sons, Ltd, 80(2), pp. 247–258. doi: 10.1002/ANA.24711.
- Choi, S. H. *et al.* (2014) 'A three-dimensional human neural cell culture model of Alzheimer's disease', *Nature*. doi: 10.1038/nature13800.
- Cimini, A. *et al.* (2009) 'Early Biochemical and Morphological Modifications in the Brain of a Transgenic Mouse

Model of Alzheimer's Disease: A Role for Peroxisomes', *Journal of Alzheimer's Disease*. IOS Press, 18, pp. 935–952. doi: 10.3233/JAD-2009-1199.

Cioffi, F., Adam, R. H. I. and Broersen, K. (2019) 'Molecular Mechanisms and Genetics of Oxidative Stress in Alzheimer's Disease', *Journal of Alzheimer's disease : JAD*. J Alzheimers Dis, 72(4), pp. 981–1017. doi: 10.3233/JAD-190863.

Citron, M. *et al.* (1994) 'Excessive production of amyloid β -protein by peripheral cells of symptomatic and presymptomatic patients carrying the Swedish familial Alzheimer disease mutation', *Proceedings of the National Academy of Sciences of the United States of America*. doi: 10.1073/pnas.91.25.11993.

Cline, E. N. *et al.* (2018) 'The Amyloid- β Oligomer Hypothesis: Beginning of the Third Decade', *Journal of Alzheimer's disease : JAD*. J Alzheimers Dis, 64(s1), pp. S567–S610. doi: 10.3233/JAD-179941.

Correia, S. C. *et al.* (2013) 'Mitochondrial abnormalities in a streptozotocin-induced rat model of sporadic Alzheimer's disease.', *Current Alzheimer research*, 10(4), pp. 406–19. doi: 10.2174/1567205011310040006.

Cribbs, J. T. and Strack, S. (2007) 'Reversible phosphorylation of Drp1 by cyclic AMP-dependent protein kinase and calcineurin regulates mitochondrial fission and cell death', *EMBO Reports*. European Molecular Biology Organization, 8(10), p. 939. doi: 10.1038/SJ.EMBOR.7401062.

Croston, G. E. (2017) 'The utility of target-based discovery', *Expert Opinion on Drug Discovery*. doi: 10.1080/17460441.2017.1308351.

Cuadrado-Tejedor, M. *et al.* (2021) 'Amyloid-Driven Tau Accumulation on Mitochondria Potentially Leads to Cognitive Deterioration in Alzheimer's Disease', *International journal of molecular sciences*. Int J Mol Sci, 22(21). doi: 10.3390/IJMS222111950.

Cummins, N. *et al.* (2019) 'Disease-associated tau impairs mitophagy by inhibiting Parkin translocation to mitochondria', *The EMBO journal*. EMBO J, 38(3). doi: 10.15252/EMBJ.201899360.

Curti, D. *et al.* (1997) 'Oxidative metabolism in cultured fibroblasts derived from sporadic Alzheimer's disease (AD) patients', *Neuroscience Letters*, 236(1), pp. 13–16. doi: 10.1016/S0304-3940(97)00741-6.

D, W. *et al.* (2022) 'Reactive Astrocytes Contribute to Alzheimer's Disease-Related Neurotoxicity and Synaptotoxicity in a Neuron-Astrocyte Co-culture Assay', *Frontiers in cellular neuroscience*. Front Cell Neurosci, 15. doi: 10.3389/FNCEL.2021.739411.

Dana, H. *et al.* (2019) 'High-performance calcium sensors for imaging activity in neuronal populations and microcompartments', *Nature Methods 2019 16:7*. Nature Publishing Group, 16(7), pp. 649–657. doi: 10.1038/s41592-019-0435-6.

Davies, P., Katzman, R. and Terry, R. D. (1980) 'Reduced somatostatin-like immunoreactivity in cerebral cortex from cases of alzheimer disease and alzheimer senile dementia', *Nature*. doi: 10.1038/288279a0.

Davis, C. H. O. *et al.* (2014) 'Transcellular degradation of axonal mitochondria', *Proceedings of the National Academy of Sciences of the United States of America*. National Academy of Sciences, 111(26), pp. 9633–9638. doi: 10.1073/PNAS.1404651111/-/DCSUPPLEMENTAL.

Delmotte, Q. *et al.* (2020) 'Sonic Hedgehog Signaling Agonist (SAG) Triggers BDNF Secretion and Promotes the Maturation of GABAergic Networks in the Postnatal Rat Hippocampus', *Frontiers in Cellular Neuroscience*. Frontiers Media S.A., 14, p. 98. doi: 10.3389/FNCEL.2020.00098/BIBTEX.

Desai, R. *et al.* (2020) 'Mitochondria form contact sites with the nucleus to couple prosurvival retrograde response', *Science advances*. Sci Adv, 6(51). doi: 10.1126/SCIADV.ABC9955.

Dionísio, P. A. *et al.* (2015) 'Amyloid- β pathology is attenuated by tauroursodeoxycholic acid treatment in APP/PS1 mice after disease onset', *Neurobiology of aging*. Neurobiol Aging, 36(1), pp. 228–240. doi: 10.1016/J.NEUROBIOLAGING.2014.08.034.

Dixit, S., Fessel, J. P. and Harrison, F. E. (2017) 'Mitochondrial dysfunction in the APP/PSEN1 mouse model of Alzheimer's disease and a novel protective role for ascorbate', *Free Radical Biology and Medicine*, 112, pp. 515–523. doi: 10.1016/j.freeradbiomed.2017.08.021.

Djordjevic, J. *et al.* (2020) 'Early Onset of Sex-Dependent Mitochondrial Deficits in the Cortex of 3xTg Alzheimer's Mice', *Cells*. Multidisciplinary Digital Publishing Institute (MDPI), 9(6). doi: 10.3390/CELLS9061541.

- Donner, L. *et al.* (2021) 'Impact of amyloid- β on platelet mitochondrial function and platelet-mediated amyloid aggregation in Alzheimer's disease', *International Journal of Molecular Sciences*. MDPI, 22(17). doi: 10.3390/IJMS22179633/S1.
- Doody, R. S. *et al.* (2013) 'A Phase 3 Trial of Semagacestat for Treatment of Alzheimer's Disease', *New England Journal of Medicine*, 369(4), pp. 341–350. doi: 10.1056/NEJMoa1210951.
- Doody, R. S. *et al.* (2014) 'Phase 3 Trials of Solanezumab for Mild-to-Moderate Alzheimer's Disease', *New England Journal of Medicine*, 370(4), pp. 311–321. doi: 10.1056/NEJMoa1312889.
- Drabik, K., Piecyk, K., *et al.* (2021) 'Adaptation of mitochondrial network dynamics and velocity of mitochondrial movement to chronic stress present in fibroblasts derived from patients with sporadic form of Alzheimer's disease', *FASEB Journal*. doi: 10.1096/fj.202001978RR.
- Drabik, K., Malińska, D., *et al.* (2021) 'Effect of chronic stress present in fibroblasts derived from patients with a sporadic form of ad on mitochondrial function and mitochondrial turnover', *Antioxidants*. doi: 10.3390/antiox10060938.
- Ehres, S. *et al.* (2009) 'Regulation of OPA1 processing and mitochondrial fusion by m-AAA protease isoenzymes and OMA1', *The Journal of cell biology*. *J Cell Biol*, 187(7), pp. 1023–1036. doi: 10.1083/JCB.200906084.
- Espejo, M. *et al.* (2000) 'Increased survival of dopaminergic neurons in striatal grafts of fetal ventral mesencephalic cells exposed to neurotrophin-3 or glial cell line-derived neurotrophic factor', *Cell transplantation*. *Cell Transplant*, 9(1), pp. 45–53. doi: 10.1177/096368970000900107.
- Estaquier, J. and Arnoult, D. (2007) 'Inhibiting Drp1-mediated mitochondrial fission selectively prevents the release of cytochrome c during apoptosis', *Cell Death & Differentiation* 2007 14:6. Nature Publishing Group, 14(6), pp. 1086–1094. doi: 10.1038/sj.cdd.4402107.
- Fang, E. F. *et al.* (2019) 'Mitophagy inhibits amyloid- β and tau pathology and reverses cognitive deficits in models of Alzheimer's disease', *Nature Neuroscience* 2019 22:3. Nature Publishing Group, 22(3), pp. 401–412. doi: 10.1038/s41593-018-0332-9.
- Fivenson, E. M. *et al.* (2017) 'Mitophagy in neurodegeneration and aging', *Neurochemistry International*. doi: 10.1016/j.neuint.2017.02.007.
- Fonseca, T. B. *et al.* (2019) 'Mitochondrial fission requires DRP1 but not dynamin', *Nature*. doi: 10.1038/s41586-019-1296-y.
- Frank, S. *et al.* (2001) 'The role of dynamin-related protein 1, a mediator of mitochondrial fission, in apoptosis', *Developmental cell*. *Dev Cell*, 1(4), pp. 515–525. doi: 10.1016/S1534-5807(01)00055-7.
- Fransen, M., Lismont, C. and Walton, P. (2017) 'The peroxisome-mitochondria connection: How and why?', *International Journal of Molecular Sciences*. doi: 10.3390/ijms18061126.
- Frédéric Cassé, Kevin Richetin, N. T. (2018) 'Astrocytes' Contribution to Adult Neurogenesis in Physiology and Alzheimer's Disease', *Frontiers in Cellular Neuroscience*, doi.org/10.
- Friedman, J. R. *et al.* (2011) 'ER tubules mark sites of mitochondrial division', *Science*. doi: 10.1126/science.1207385.
- Fu, J. *et al.* (2014) 'Disruption of SUMO-Specific Protease 2 Induces Mitochondria Mediated Neurodegeneration', *PLOS Genetics*. Public Library of Science, 10(10), p. e1004579. doi: 10.1371/JOURNAL.PGEN.1004579.
- Gandre-Babbe, S. and van der Blik, A. M. (2008) 'The Novel Tail-anchored Membrane Protein Mff Controls Mitochondrial and Peroxisomal Fission in Mammalian Cells', *Molecular Biology of the Cell*. doi: 10.1091/mbc.e07-12-1287.
- Garrido-Maraver, J., Loh, S. H. Y. and Martins, L. M. (2020) 'Forcing contacts between mitochondria and the endoplasmic reticulum extends lifespan in a Drosophila model of Alzheimer's disease', *Biology Open*. Company of Biologists, 9(1). doi: 10.1242/BIO.047530.
- Gatto, N. *et al.* (2021) 'Directly converted astrocytes retain the ageing features of the donor fibroblasts and elucidate the astrocytic contribution to human CNS health and disease', *Aging Cell*. Wiley-Blackwell, 20(1). doi: 10.1111/ACEL.13281.

- Ge, Y. *et al.* (2020) 'Two forms of opa1 cooperate to complete fusion of the mitochondrial inner-membrane', *eLife*. doi: 10.7554/eLife.50973.
- Ghiasi, P. *et al.* (2012) 'Mitochondrial complex I deficiency and ATP/ADP ratio in lymphocytes of amyotrophic lateral sclerosis patients', *Neurological research*. *Neurol Res*, 34(3), pp. 297–303. doi: 10.1179/1743132812Y.0000000012.
- Giannakopoulos, P. *et al.* (2003) 'Tangle and neuron numbers, but not amyloid load, predict cognitive status in Alzheimer's disease', *Neurology*. doi: 10.1212/01.WNL.0000063311.58879.01.
- Gilkerson, R., De La Torre, P. and St. Vallier, S. (2021) 'Mitochondrial OMA1 and OPA1 as Gatekeepers of Organellar Structure/Function and Cellular Stress Response', *Frontiers in Cell and Developmental Biology*. doi: 10.3389/fcell.2021.626117.
- Goldstein, J. C. *et al.* (2000) 'The coordinate release of cytochrome c during apoptosis is rapid, complete and kinetically invariant', *Nature Cell Biology*. doi: 10.1038/35004029.
- Golpich, M. *et al.* (2017) 'Mitochondrial Dysfunction and Biogenesis in Neurodegenerative diseases: Pathogenesis and Treatment', *CNS Neuroscience and Therapeutics*, pp. 5–22. doi: 10.1111/cns.12655.
- Golubitzky, A. *et al.* (2011) 'Screening for active small molecules in mitochondrial complex I deficient patient's fibroblasts, reveals AICAR as the most beneficial compound', *PLoS ONE*. doi: 10.1371/journal.pone.0026883.
- Gong, B. *et al.* (2010) 'SCFFbx2-E3-ligase-mediated degradation of BACE1 attenuates Alzheimer's disease amyloidosis and improves synaptic function', *Aging cell*. *Aging Cell*, 9(6), pp. 1018–1031. doi: 10.1111/J.1474-9726.2010.00632.X.
- Gong, Z. *et al.* (2019) 'Urolithin A attenuates memory impairment and neuroinflammation in APP/PS1 mice', *Journal of neuroinflammation*. *J Neuroinflammation*, 16(1). doi: 10.1186/S12974-019-1450-3.
- Gonzalez, C. *et al.* (2018) 'Modeling amyloid beta and tau pathology in human cerebral organoids', *Molecular psychiatry*. *Mol Psychiatry*, 23(12), pp. 2363–2374. doi: 10.1038/S41380-018-0229-8.
- Grant, W. B. *et al.* (2002) 'The significance of environmental factors in the etiology of Alzheimer's disease', *Journal of Alzheimer's Disease*. doi: 10.3233/JAD-2002-4308.
- Gray, N. E. and Quinn, J. F. (2015) 'Alterations in mitochondrial number and function in Alzheimer's disease fibroblasts', *Metabolic Brain Disease*, 30(5), pp. 1275–1278. doi: 10.1007/s11011-015-9667-z.
- Gu, L. and Guo, Z. (2013) 'Alzheimer's A β 42 and A β 40 peptides form interlaced amyloid fibrils', *Journal of neurochemistry*. *NIH Public Access*, 126(3), p. 305. doi: 10.1111/JNC.12202.
- Guo, C. *et al.* (2013) 'SEN3-mediated deSUMOylation of dynamin-related protein 1 promotes cell death following ischaemia', *The EMBO journal*. *EMBO J*, 32(11), pp. 1514–1528. doi: 10.1038/EMBOJ.2013.65.
- Guo, C. *et al.* (2021) 'SEN3 Promotes an Mff-Primed Bcl-x L -Drp1 Interaction Involved in Cell Death Following Ischemia', *Frontiers in cell and developmental biology*. *Front Cell Dev Biol*, 9. doi: 10.3389/FCELL.2021.752260.
- Guo, Q. *et al.* (2021) 'A review on acoustic droplet ejection technology and system', *Soft Matter*. The Royal Society of Chemistry, 17(11), pp. 3010–3021. doi: 10.1039/D0SM02193H.
- De Haas, R. *et al.* (2017) 'Therapeutic effects of the mitochondrial ROS-redox modulator KH176 in a mammalian model of Leigh Disease', *Scientific Reports 2017 7:1*. Nature Publishing Group, 7(1), pp. 1–11. doi: 10.1038/s41598-017-09417-5.
- Haileselassie, B. *et al.* (2019) 'Drp1/Fis1 interaction mediates mitochondrial dysfunction in septic cardiomyopathy', *Journal of Molecular and Cellular Cardiology*. doi: 10.1016/j.yjmcc.2019.04.006.
- Hamel, E. *et al.* (2008) 'Oxidative stress and cerebrovascular dysfunction in mouse models of Alzheimer's disease', *Experimental physiology*. *Exp Physiol*, 93(1), pp. 116–120. doi: 10.1113/EXPPHYSIOL.2007.038729.
- Han, H. *et al.* (2020) 'PINK1 phosphorylates Drp1S616 to regulate mitophagy-independent mitochondrial dynamics', *EMBO Reports*. European Molecular Biology Organization, 21(8). doi: 10.15252/EMBR.201948686.
- Hancock, M. K. *et al.* (2015) 'A Facile Method for Simultaneously Measuring Neuronal Cell Viability and Neurite Outgrowth', *Current Chemical Genomics and Translational Medicine*. Bentham Science Publishers, 9(1), p. 6. doi: 10.2174/2213988501509010006.

- Harder, Z., Zunino, R. and McBride, H. (2004) 'Sumo1 Conjugates Mitochondrial Substrates and Participates in Mitochondrial Fission', *Current Biology*. Cell Press, 14(4), pp. 340–345. doi: 10.1016/J.CUB.2004.02.004.
- Hardy, J. and Higgins, G. (1992) 'Alzheimer's disease: the amyloid cascade hypothesis', *Science*, 256(5054), pp. 184–185. doi: 10.1126/science.1566067.
- Hartl, D. *et al.* (2012) 'Presymptomatic alterations in energy metabolism and oxidative stress in the APP23 mouse model of Alzheimer disease', *Journal of proteome research*. J Proteome Res, 11(6), pp. 3295–3304. doi: 10.1021/PR300021E.
- Hauptmann, S. *et al.* (2009) 'Mitochondrial dysfunction: An early event in Alzheimer pathology accumulates with age in AD transgenic mice', *Neurobiology of Aging*, 30(10), pp. 1574–1586. doi: 10.1016/j.neurobiolaging.2007.12.005.
- Head, B. *et al.* (2009) 'Inducible proteolytic inactivation of OPA1 mediated by the OMA1 protease in mammalian cells', *The Journal of Cell Biology*. The Rockefeller University Press, 187(7), p. 959. doi: 10.1083/JCB.200906083.
- Hemachandra Reddy, P., Manczak, M. and Kandimalla, R. (2017) 'Mitochondria-targeted small molecule SS31: A potential candidate for the treatment of Alzheimer's disease', *Human Molecular Genetics*. doi: 10.1093/hmg/ddx052.
- Henley, J. M., Carmichael, R. E. and Wilkinson, K. A. (2018) 'Extranuclear SUMOylation in Neurons', *Trends in Neurosciences*. Elsevier Current Trends, 41(4), pp. 198–210. doi: 10.1016/J.TINS.2018.02.004.
- Hirsch, T. *et al.* (2006) 'Adenoviral gene delivery to primary human cutaneous cells and burn wounds', *Molecular Medicine*. BioMed Central, 12(9–10), pp. 199–207. doi: 10.2119/2006-00031.HIRSCH/FIGURES/6.
- HN, C. *et al.* (2017) 'Exome Sequencing of Extended Families with Alzheimer's Disease Identifies Novel Genes Implicated in Cell Immunity and Neuronal Function', *Journal of Alzheimer's Disease & Parkinsonism*. doi: 10.4172/2161-0460.1000355.
- Hou, S. *et al.* (2017) 'Drug Library Screening for the Identification of Ionophores That Correct the Mistrafficking Disorder Associated with Oxalosis Kidney Disease', *SLAS Discovery*. doi: 10.1177/2472555217689992.
- Hu, H. *et al.* (2017) 'A Mitocentric View of Alzheimer's Disease', *Molecular Neurobiology*, pp. 6046–6060. doi: 10.1007/s12035-016-0117-7.
- Hu, W. *et al.* (2015) 'Direct Conversion of Normal and Alzheimer's Disease Human Fibroblasts into Neuronal Cells by Small Molecules', *Cell Stem Cell*. doi: 10.1016/j.stem.2015.07.006.
- Hu, Y. *et al.* (2016) 'Tau accumulation impairs mitophagy via increasing mitochondrial membrane potential and reducing mitochondrial Parkin', *Oncotarget*. Oncotarget, 7(14), pp. 17356–17368. doi: 10.18632/ONCOTARGET.7861.
- Hutton, M. *et al.* (1998) 'Association of missense and 5'-splice-site mutations in tau with the inherited dementia FTDP-17', *Nature*. doi: 10.1038/31508.
- Hyvärinen, T. *et al.* (2019) 'Functional characterization of human pluripotent stem cell-derived cortical networks differentiated on laminin-521 substrate: comparison to rat cortical cultures', *Scientific Reports 2019 9:1*. Nature Publishing Group, 9(1), pp. 1–15. doi: 10.1038/s41598-019-53647-8.
- Ishihara, N. *et al.* (2009) 'Mitochondrial fission factor Drp1 is essential for embryonic development and synapse formation in mice', *Nature Cell Biology*, 11(8), pp. 958–966. doi: 10.1038/ncb1907.
- Islinger, M. *et al.* (2018) 'The peroxisome: an update on mysteries 2.0', *Histochemistry and Cell Biology*. Springer, 150(5), p. 443. doi: 10.1007/S00418-018-1722-5.
- Jalewa, J., Sharma, M. K. and Hölscher, C. (2016) 'Novel incretin analogues improve autophagy and protect from mitochondrial stress induced by rotenone in SH-SY5Y cells', *Journal of Neurochemistry*. John Wiley & Sons, Ltd, 139(1), pp. 55–67. doi: 10.1111/JNC.13736.
- James, D. I. *et al.* (2003) 'hFis1, a novel component of the mammalian mitochondrial fission machinery', *Journal of Biological Chemistry*. doi: 10.1074/jbc.M303758200.
- Jankowsky, J. L. *et al.* (2004) 'Mutant presenilins specifically elevate the levels of the 42 residue β -amyloid

peptide in vivo: Evidence for augmentation of a 42-specific γ secretase', *Human Molecular Genetics*. doi: 10.1093/hmg/ddh019.

Janssen, M. C. H. *et al.* (2019) 'The KHENERGY Study: Safety and Efficacy of KH176 in Mitochondrial m.3243A>G Spectrum Disorders', *Clinical pharmacology and therapeutics*. Clin Pharmacol Ther, 105(1), pp. 101–111. doi: 10.1002/CPT.1197.

Jeong, Y. Y. *et al.* (2022) 'Broad activation of the Parkin pathway induces synaptic mitochondrial deficits in early tauopathy', *Brain*. Oxford University Press (OUP). doi: 10.1093/BRAIN/AWAB243.

Jia, Y.-L. *et al.* (2015) 'SS31, a Small Molecule Antioxidant Peptide, Attenuates β -Amyloid Elevation, Mitochondrial/Synaptic Deterioration and Cognitive Deficit in SAMP8 Mice', *Current Alzheimer Research*. doi: 10.2174/1567205013666151218150004.

Joachim, C. L., Mori, H. and Selkoe, D. J. (1989) 'Amyloid β -protein deposition in tissues other than brain in Alzheimer's disease', *Nature*. doi: 10.1038/341226a0.

Johnston, J. A. *et al.* (1994) 'Increased β -amyloid release and levels of amyloid precursor protein (APP) in fibroblast cell lines from family members with the Swedish Alzheimer's disease APP670/671 mutation', *FEBS Letters*. doi: 10.1016/0014-5793(94)01137-0.

JONG, Y.-J. I. *et al.* (2003) 'Alzheimer's disease skin fibroblasts selectively express a bradykinin signaling pathway mediating tau protein Ser phosphorylation', *The FASEB Journal*. doi: 10.1096/fj.02-1147fje.

Joshi, A. *et al.* (2012) 'Comparison of clinical characteristics between familial and non-familial early onset Alzheimer's disease', *Journal of neurology*. NIH Public Access, 259(10), p. 2182. doi: 10.1007/S00415-012-6481-Y.

Joshi, Amit U. *et al.* (2018) 'Drp1/Fis1 interaction mediates mitochondrial dysfunction, bioenergetic failure and cognitive decline in Alzheimer's disease', *Oncotarget*. doi: 10.18632/oncotarget.23640.

Joshi, Amit U *et al.* (2018) 'Inhibition of Drp1/Fis1 interaction slows progression of amyotrophic lateral sclerosis', *EMBO Molecular Medicine*. doi: 10.15252/emmm.201708166.

Joshi, A. U. *et al.* (2019) 'Drp1/Fis1-mediated mitochondrial fragmentation leads to lysosomal dysfunction in cardiac models of Huntington's disease', *Journal of Molecular and Cellular Cardiology*. doi: 10.1016/j.yjmcc.2018.12.004.

Joshi, P. and Lee, M. Y. (2015) 'High content imaging (HCI) on miniaturized three-dimensional (3D) cell cultures', *Biosensors*. doi: 10.3390/bios5040768.

Kam, M. K. *et al.* (2020) 'Amyloid-beta oligomers induce Parkin-mediated mitophagy by reducing Miro1', *Biochemical Journal*. Portland Press, 477(23), pp. 4581–4597. doi: 10.1042/BCJ20200488.

Kandimalla, R. *et al.* (2016) 'Reduced dynamin-related protein 1 protects against phosphorylated Tau-induced mitochondrial dysfunction and synaptic damage in Alzheimer's disease', *Human Molecular Genetics*. doi: 10.1093/hmg/ddw312.

Kandimalla, R. *et al.* (2018a) 'Hippocampal phosphorylated tau induced cognitive decline, dendritic spine loss and mitochondrial abnormalities in a mouse model of Alzheimer's disease', *Human Molecular Genetics*. doi: 10.1093/hmg/ddx381.

Kandimalla, R. *et al.* (2018b) 'Hippocampal phosphorylated tau induced cognitive decline, dendritic spine loss and mitochondrial abnormalities in a mouse model of Alzheimer's disease', *Human Molecular Genetics*. Oxford University Press, 27(1), p. 30. doi: 10.1093/HMG/DDX381.

Kandimalla, R. *et al.* (2021) 'A partial reduction of Drp1 improves cognitive behavior and enhances mitophagy, autophagy and dendritic spines in a transgenic Tau mouse model of Alzheimer disease', *Human Molecular Genetics*. Oxford University Press (OUP), 00, pp. 1–18. doi: 10.1093/HMG/DDAB360.

Kashatus, J. A. *et al.* (2015) 'Erk2 phosphorylation of Drp1 promotes mitochondrial fission and MAPK-driven tumor growth', *Molecular cell*. Mol Cell, 57(3), pp. 537–551. doi: 10.1016/J.MOLCEL.2015.01.002.

Katsouri, L. *et al.* (2011) 'PPAR γ co-activator-1 α (PGC-1 α) reduces amyloid- β generation through a PPAR γ -dependent mechanism', *Journal of Alzheimer's disease : JAD*. J Alzheimers Dis, 25(1), pp. 151–162. doi: 10.3233/JAD-2011-101356.

- Kelso, G. F. *et al.* (2001) 'Selective targeting of a redox-active ubiquinone to mitochondria within cells: Antioxidant and antiapoptotic properties', *Journal of Biological Chemistry*. doi: 10.1074/jbc.M009093200.
- Kepka, A. *et al.* (2020) 'Preventive Role of L-Carnitine and Balanced Diet in Alzheimer's Disease', *Nutrients*. *Nutrients*, 12(7), pp. 1–21. doi: 10.3390/NU12071987.
- Khansarizadeh, M. *et al.* (2016) 'Identification of possible cytotoxicity mechanism of polyethylenimine by proteomics analysis', *Human & experimental toxicology*. *Hum Exp Toxicol*, 35(4), pp. 377–387. doi: 10.1177/0960327115591371.
- Kim, H. J. *et al.* (2021) 'Oncogenic KRAS: Signaling and drug resistance', *Cancers*. doi: 10.3390/cancers13225599.
- Kim, J. *et al.* (2011) 'Direct reprogramming of mouse fibroblasts to neural progenitors', *Proceedings of the National Academy of Sciences*. doi: 10.1073/pnas.1103113108.
- Kim, S. J., Li, J. and Mahairaki, V. (2021) 'Stem cell-derived three-dimensional (organoid) models of Alzheimer's disease: a precision medicine approach', *Neural Regeneration Research*. Wolters Kluwer -- Medknow Publications, 16(8), p. 1546. doi: 10.4103/1673-5374.303019.
- Kish, S. J. *et al.* (1992) 'Brain Cytochrome Oxidase in Alzheimer's Disease', *Journal of Neurochemistry*, 59(2), pp. 776–779. doi: 10.1111/j.1471-4159.1992.tb09439.x.
- Klann, I. P. *et al.* (2020) 'Ebselen reversed peripheral oxidative stress induced by a mouse model of sporadic Alzheimer's disease', *Molecular biology reports*. *Mol Biol Rep*, 47(3), pp. 2205–2215. doi: 10.1007/S11033-020-05326-5.
- Kleele, T. *et al.* (2021) 'Distinct fission signatures predict mitochondrial degradation or biogenesis', *Nature*. doi: 10.1038/s41586-021-03510-6.
- Knight, R, Khondoker, M, Magill, N, Stewart, R, Landau, S. (2018) 'A Systematic Review and Meta-Analysis of the Effectiveness of Acetylcholinesterase Inhibitors and Memantine in Treating the Cognitive Symptoms of Dementia', *Dementia and geriatric cognitive disorders*, 45, pp. 131–151.
- Koch, A, Yoon, Y, Bonekamp, NA, McNiven, MA, Schrader, M. (2005) 'A Role for Fis1 in Both Mitochondrial and Peroxisomal Fission in Mammalian Cells', *Molecular Biology of the Cell*, 16(11), pp. 5077–5086. doi: 10.1091/mbc.e05-02-0159.
- Koch, J. *et al.* (2016) 'Disturbed mitochondrial and peroxisomal dynamics due to loss of MFF causes Leigh-like encephalopathy, optic atrophy and peripheral neuropathy', *Journal of Medical Genetics*. doi: 10.1136/jmedgenet-2015-103500.
- Koene, S. *et al.* (2017) 'KH176 under development for rare mitochondrial disease: a first in man randomized controlled clinical trial in healthy male volunteers', *Orphanet Journal of Rare Diseases*. *BioMed Central*, 12(1). doi: 10.1186/S13023-017-0715-0.
- Koirala, S. *et al.* (2013) 'Interchangeable adaptors regulate mitochondrial dynamin assembly for membrane scission', *Proceedings of the National Academy of Sciences of the United States of America*. doi: 10.1073/pnas.1300855110.
- Koopman, W. J. H. *et al.* (2008) 'Mitigation of NADH: Ubiquinone oxidoreductase deficiency by chronic Trolox treatment', *Biochimica et Biophysica Acta (BBA) - Bioenergetics*. Elsevier, 1777(7–8), pp. 853–859. doi: 10.1016/J.BBABIO.2008.03.028.
- Korobova, F., Ramabhadran, V. and Higgs, H. N. (2013) 'An actin-dependent step in mitochondrial fission mediated by the ER-associated formin INF2', *Science*. doi: 10.1126/science.1228360.
- Koster, J. and Waterham, H. R. (2017) 'Transfection of Primary Human Skin Fibroblasts for Peroxisomal Studies', *Methods in Molecular Biology*. Humana Press, New York, NY, 1595, pp. 63–67. doi: 10.1007/978-1-4939-6937-1_7.
- Kou, J. *et al.* (2011) 'Peroxisomal alterations in Alzheimer's disease', *Acta neuropathologica*. *Acta Neuropathol*, 122(3), pp. 271–283. doi: 10.1007/S00401-011-0836-9.
- Kshirsagar, S. *et al.* (2021) 'Mitophagy enhancers against phosphorylated Tau-induced mitochondrial and synaptic toxicities in Alzheimer disease', *Pharmacological research*. *Pharmacol Res*, 174. doi:

10.1016/J.PHRS.2021.105973.

Kshirsagar, S. *et al.* (2022) 'Protective effects of mitophagy enhancers against amyloid beta-induced mitochondrial and synaptic toxicities in Alzheimer disease', *Human molecular genetics*. Hum Mol Genet, 31(3), pp. 423–439. doi: 10.1093/HMG/DDAB262.

Kucharski, M., Mrowiec, P. and Ocioń, E. (2021) 'Current standards and pitfalls associated with the transfection of primary fibroblast cells', *Biotechnology Progress*. American Chemical Society (ACS), 37(4), p. e3152. doi: 10.1002/BTPR.3152.

Kühlbrandt, W. (2015) 'Structure and function of mitochondrial membrane protein complexes', *BMC Biology*. BioMed Central Ltd., 13(1), pp. 1–11. doi: 10.1186/S12915-015-0201-X/FIGURES/9.

Kumar, P., Nagarajan, A. and Uchil, P. D. (2019) 'Electroporation', *Cold Spring Harbor Protocols*. Cold Spring Harbor Laboratory Press, 2019(7), p. pdb.top096271. doi: 10.1101/PDB.TOP096271.

Ladewig, J. *et al.* (2012) 'Small molecules enable highly efficient neuronal conversion of human fibroblasts', *Nature Methods*. doi: 10.1038/nmeth.1972.

Lancaster, M. A. and Knoblich, J. A. (2014) 'Generation of cerebral organoids from human pluripotent stem cells', *Nature Protocols* 2014 9:10. Nature Publishing Group, 9(10), pp. 2329–2340. doi: 10.1038/nprot.2014.158.

Lapasset, L. *et al.* (2011) 'Rejuvenating senescent and centenarian human cells by reprogramming through the pluripotent state', *Genes and Development*. doi: 10.1101/gad.173922.111.

LaRocca, T. J. *et al.* (2014) 'Mitochondrial Quality Control and Age-Associated Arterial Stiffening', *Experimental gerontology*. NIH Public Access, 0, p. 78. doi: 10.1016/J.EXGER.2014.07.008.

Lee, H. *et al.* (2020) 'The short variant of optic atrophy 1 (OPA1) improves cell survival under oxidative stress', *Journal of Biological Chemistry*. doi: 10.1074/jbc.RA119.010983.

Lee, H., Smith, S. B. and Yoon, Y. (2017) 'The short variant of the mitochondrial dynamin OPA1 maintains mitochondrial energetics and cristae structure', *Journal of Biological Chemistry*. doi: 10.1074/jbc.M116.762567.

Lee, J. E. *et al.* (2016) 'Multiple dynamin family members collaborate to drive mitochondrial division', *Nature*. doi: 10.1038/nature20555.

Lee, J. Y. *et al.* (2003) 'Ascorbate-induced differentiation of embryonic cortical precursors into neurons and astrocytes', *Journal of neuroscience research*. J Neurosci Res, 73(2), pp. 156–165. doi: 10.1002/JNR.10647.

Lee, S. and Choi, W.-S. (2022) 'Protective Role of Microglia on Neuronal Survival after Exposure to Amyloid Beta', *Chonnam medical journal*. Chonnam Med J, 58(1), p. 13. doi: 10.4068/CMJ.2022.58.1.13.

Lee, S. J., Cho, H. J. and Ryu, J. H. (2021) 'Innate Immunity and Cell Death in Alzheimer's Disease', *ASN NEURO*. SAGE Publications, 13. doi: 10.1177/17590914211051908.

Leng, F. and Edison, P. (2021) 'Neuroinflammation and microglial activation in Alzheimer disease: where do we go from here?', *Nature reviews. Neurology*. Nat Rev Neurol, 17(3), pp. 157–172. doi: 10.1038/S41582-020-00435-Y.

Lepski, G. *et al.* (2013) 'cAMP promotes the differentiation of neural progenitor cells in vitro via modulation of voltage-gated calcium channels', *Frontiers in Cellular Neuroscience*. Frontiers Media SA, 7(SEP). doi: 10.3389/FNCEL.2013.00155.

Leuner, K. *et al.* (2012) 'Mitochondrion-Derived Reactive Oxygen Species Lead to Enhanced Amyloid Beta Formation', *Antioxidants & Redox Signaling*, 16(12), pp. 1421–1433. doi: 10.1089/ars.2011.4173.

Li, H. *et al.* (2008) 'Bcl-xL induces Drp1-dependent synapse formation in cultured hippocampal neurons', *Proceedings of the National Academy of Sciences of the United States of America*. Proc Natl Acad Sci U S A, 105(6), pp. 2169–2174. doi: 10.1073/PNAS.0711647105.

Li, J. *et al.* (2015) 'Pharmacological activation of AMPK prevents Drp1-mediated mitochondrial fission and alleviates endoplasmic reticulum stress-associated endothelial dysfunction', *Journal of Molecular and Cellular Cardiology*. doi: 10.1016/j.yjmcc.2015.07.010.

- Li, X. C. *et al.* (2016) 'Human wild-type full-length tau accumulation disrupts mitochondrial dynamics and the functions via increasing mitofusins', *Scientific Reports*, 6. doi: 10.1038/srep24756.
- Li, Y. *et al.* (2016) 'Establishment and Maintenance of Primary Fibroblast Repositories for Rare Diseases-Friedreich's Ataxia Example', *Biopreservation and biobanking*. Biopreserv Biobank, 14(4), pp. 324–329. doi: 10.1089/BIO.2015.0117.
- Li, Z. *et al.* (2004) 'The Importance of Dendritic Mitochondria in the Morphogenesis and Plasticity of Spines and Synapses', *Cell*. Cell Press, 119(6), pp. 873–887. doi: 10.1016/J.CELL.2004.11.003.
- Limbad, C. *et al.* (2020) 'Astrocyte senescence promotes glutamate toxicity in cortical neurons', *PLoS one*. PLoS One, 15(1). doi: 10.1371/JOURNAL.PONE.0227887.
- Lin, M. Y. *et al.* (2017) 'Releasing Syntaphilin Removes Stressed Mitochondria from Axons Independent of Mitophagy under Pathophysiological Conditions', *Neuron*. Neuron, 94(3), pp. 595-610.e6. doi: 10.1016/J.NEURON.2017.04.004.
- Lin, Y. T. *et al.* (2018) 'APOE4 causes widespread molecular and cellular alterations associated with Alzheimer's disease phenotypes in human iPSC-derived brain cell types', *Neuron*. NIH Public Access, 98(6), p. 1141. doi: 10.1016/J.NEURON.2018.05.008.
- Liu, J. L. *et al.* (2018) 'Iron and Alzheimer's disease: From pathogenesis to therapeutic implications', *Frontiers in Neuroscience*. doi: 10.3389/fnins.2018.00632.
- Liu, M. L. *et al.* (2013) 'Small molecules enable neurogenin 2 to efficiently convert human fibroblasts into cholinergic neurons', *Nature Communications*. doi: 10.1038/ncomms3183.
- Liu, R. and Chan, D. C. (2015) 'The mitochondrial fission receptor Mff selectively recruits oligomerized Drp1', *Molecular Biology of the Cell*. doi: 10.1091/mbc.E15-08-0591.
- Liu, T. *et al.* (2013) 'The mitochondrial elongation factors MIEF1 and MIEF2 exert partially distinct functions in mitochondrial dynamics', *Experimental Cell Research*. doi: 10.1016/j.yexcr.2013.07.010.
- Liu, W. *et al.* (2013) 'Mitochondrial fusion and fission proteins expression dynamically change in a murine model of amyotrophic lateral sclerosis', *Current neurovascular research*. Curr Neurovasc Res, 10(3), pp. 222–230. doi: 10.2174/15672026113109990060.
- Livingston, Gill *et al.* (2020) 'The Lancet Commissions Dementia prevention, intervention, and care: 2020 report of the Lancet Commission The Lancet Commissions', *thelancet.com*, 396, pp. 413–459. doi: 10.1016/S0140-6736(20)30367-6.
- Lo, A. C. *et al.* (2013) 'Tauroursodeoxycholic acid (TUDCA) supplementation prevents cognitive impairment and amyloid deposition in APP/PS1 mice', *Neurobiology of Disease*. doi: 10.1016/j.nbd.2012.09.003.
- Loson, O. C. *et al.* (2013) 'Fis1, Mff, MiD49, and MiD51 mediate Drp1 recruitment in mitochondrial fission', *Molecular Biology of the Cell*. doi: 10.1091/mbc.E12-10-0721.
- Losón, O. C. *et al.* (2014) 'The mitochondrial fission receptor MiD51 requires ADP as a cofactor', *Structure*. doi: 10.1016/j.str.2014.01.001.
- Lu, H. *et al.* (2008) 'Retrovirus delivered neurotrophin-3 promotes survival, proliferation and neuronal differentiation of human fetal neural stem cells in vitro', *Brain research bulletin*. Brain Res Bull, 77(4), pp. 158–164. doi: 10.1016/J.BRAINRESBULL.2008.02.037.
- Lunnon, K. *et al.* (2017) 'Mitochondrial genes are altered in blood early in Alzheimer's disease', *Neurobiology of Aging*, 53, pp. 36–47. doi: 10.1016/j.neurobiolaging.2016.12.029.
- Lythgoe, M. P., Jenei, K. and Prasad, V. (2022) 'Regulatory decisions diverge over aducanumab for Alzheimer's disease', *BMJ*. British Medical Journal Publishing Group, 376, p. e069780. doi: 10.1136/BMJ-2021-069780.
- Macdonald, R. *et al.* (2018) 'Mitochondrial abnormalities in Parkinson's disease and Alzheimer's disease: can mitochondria be targeted therapeutically?', *Biochemical Society Transactions*. doi: 10.1042/BST20170501.
- Maiti, P. *et al.* (2021) 'Preservation of dendritic spine morphology and postsynaptic signaling markers after treatment with solid lipid curcumin particles in the 5x^{FAD} mouse model of Alzheimer's amyloidosis', *Alzheimer's research & therapy*. Alzheimers Res Ther, 13(1). doi: 10.1186/S13195-021-00769-9.

- Malow, B. A., Baker, A. C. and Blass, J. P. (1989) 'Cultured Cells as a Screen for Novel Treatments of Alzheimer's Disease', *Archives of Neurology*. American Medical Association, 46(11), pp. 1201–1203. doi: 10.1001/ARCHNEUR.1989.00520470057027.
- Manczak, M., Mao, P., Calkins, Marcus J, *et al.* (2010) 'Mitochondria-targeted antioxidants protect against amyloid-beta toxicity in Alzheimer's disease neurons.', *Journal of Alzheimer's disease : JAD*. NIH Public Access, 20 Suppl 2(Suppl 2), pp. S609-31. doi: 10.3233/JAD-2010-100564.
- Manczak, M., Mao, P., Calkins, Markus J., *et al.* (2010) 'Mitochondria-targeted antioxidants protect against amyloid- β toxicity in Alzheimer's disease neurons', *Journal of Alzheimer's Disease*. doi: 10.3233/JAD-2010-100564.
- Manczak, M. *et al.* (2016) 'Protective effects of reduced dynamin-related protein 1 against amyloid beta-induced mitochondrial dysfunction and synaptic damage in Alzheimer's disease', *Human Molecular Genetics*. doi: 10.1093/hmg/ddw330.
- Manczak, M. *et al.* (2018) 'Hippocampal mutant APP and amyloid beta-induced cognitive decline, dendritic spine loss, defective autophagy, mitophagy and mitochondrial abnormalities in a mouse model of Alzheimer's disease', *Human Molecular Genetics*. doi: 10.1093/hmg/ddy042.
- Manczak, M., Calkins, M. J. and Reddy, P. H. (2011) 'Impaired mitochondrial dynamics and abnormal interaction of amyloid beta with mitochondrial protein Drp1 in neurons from patients with Alzheimer's disease: Implications for neuronal damage', *Human Molecular Genetics*, 20(13), pp. 2495–2509. doi: 10.1093/hmg/ddr139.
- María José Pérez, Daniela P. Ponce, Alejandra Aranguiz, Maria I. Behrens, and R. A. Q. (2018) 'Mitochondrial permeability transition pore contributes to mitochondrial dysfunction in fibroblasts of patients with sporadic Alzheimer's disease', *Redox Biology*, 15(37).
- Marmolino, D. *et al.* (2009) 'PPAR-gamma agonist Azelaoyl PAF increases frataxin protein and mRNA expression: new implications for the Friedreich's ataxia therapy', *Cerebellum (London, England)*. Cerebellum, 8(2), pp. 98–103. doi: 10.1007/S12311-008-0087-Z.
- Marmolino, D. *et al.* (2010) 'PGC-1alpha down-regulation affects the antioxidant response in Friedreich's ataxia', *PloS one*. PLoS One, 5(4). doi: 10.1371/JOURNAL.PONE.0010025.
- Martín-Maestro, P. *et al.* (2016) 'PARK2 enhancement is able to compensate mitophagy alterations found in sporadic Alzheimer's disease', *Human molecular genetics*. Hum Mol Genet, 25(4), pp. 792–806. doi: 10.1093/HMG/DDV616.
- Martín-Maestro, P., Gargini, R., A. Sproul, A., *et al.* (2017) 'Mitophagy Failure in Fibroblasts and iPSC-Derived Neurons of Alzheimer's Disease-Associated Presenilin 1 Mutation', *Frontiers in Molecular Neuroscience*, 10. doi: 10.3389/fnmol.2017.00291.
- Martín-Maestro, P., Gargini, R., García, E., *et al.* (2017) 'Slower Dynamics and Aged Mitochondria in Sporadic Alzheimer's Disease', *Oxidative Medicine and Cellular Longevity*, 2017, pp. 1–14. doi: 10.1155/2017/9302761.
- Van Marum, R. J. (2009) 'Update on the use of memantine in Alzheimer's disease', *Neuropsychiatric Disease and Treatment*.
- Matsuyama, S. S. and Bondareff, W. (1994) 'Tau-like immunoreactivity in Alzheimer and control skin fibroblasts', *Journal of Neuroscience Research*. doi: 10.1002/jnr.490390503.
- Maurer, I., Zierz, S. and Möller, H. J. (2000) 'A selective defect of cytochrome c oxidase is present in brain of Alzheimer disease patients', *Neurobiology of Aging*, 21(3), pp. 455–462. doi: 10.1016/S0197-4580(00)00112-3.
- McKhann, G. M. *et al.* (2011) 'The diagnosis of dementia due to Alzheimer's disease: Recommendations from the National Institute on Aging-Alzheimer's Association workgroups on diagnostic guidelines for Alzheimer's disease', *Alzheimer's and Dementia*. doi: 10.1016/j.jalz.2011.03.005.
- McManus, Meagan J, Murphy, M. P. and Franklin, J. L. (2011) 'The mitochondria-targeted antioxidant MitoQ prevents loss of spatial memory retention and early neuropathology in a transgenic mouse model of Alzheimer's disease.', *The Journal of neuroscience : the official journal of the Society for Neuroscience*. NIH Public Access, 31(44), pp. 15703–15. doi: 10.1523/JNEUROSCI.0552-11.2011.

- McManus, M. J., Murphy, M. P. and Franklin, J. L. (2011) 'The Mitochondria-Targeted Antioxidant MitoQ Prevents Loss of Spatial Memory Retention and Early Neuropathology in a Transgenic Mouse Model of Alzheimer's Disease', *Journal of Neuroscience*. doi: 10.1523/jneurosci.0552-11.2011.
- Melak, M., Plessner, M. and Grosse, R. (2017) 'Actin visualization at a glance', *Journal of Cell Science*. doi: 10.1242/jcs.189068.
- Melentijevic, I. *et al.* (2017) 'C. elegans neurons jettison protein aggregates and mitochondria under neurotoxic stress', *Nature* 2017 542:7641. Nature Publishing Group, 542(7641), pp. 367–371. doi: 10.1038/nature21362.
- Merino-Serrais, P. *et al.* (2013) 'The influence of phospho-tau on dendritic spines of cortical pyramidal neurons in patients with Alzheimer's disease', *Brain*. Oxford University Press, 136(6), p. 1913. doi: 10.1093/BRAIN/AWT088.
- Mertens, J. *et al.* (2015) 'Directly Reprogrammed Human Neurons Retain Aging-Associated Transcriptomic Signatures and Reveal Age-Related Nucleocytoplasmic Defects', *Cell Stem Cell*. doi: 10.1016/j.stem.2015.09.001.
- Mertens, J. *et al.* (2021) 'Age-dependent instability of mature neuronal fate in induced neurons from Alzheimer's patients', *Cell stem cell*. Cell Stem Cell, 28(9). doi: 10.1016/J.STEM.2021.04.004.
- Meyer, K. *et al.* (2014) 'Direct conversion of patient fibroblasts demonstrates non-cell autonomous toxicity of astrocytes to motor neurons in familial and sporadic ALS', *Proceedings of the National Academy of Sciences*, 111(2), pp. 829–832. doi: 10.1073/pnas.1314085111.
- Mikael Marttinen, Mari Takalo, Teemu Natunen, Rebekka Wittrahm, Sami Gabbouj, Susanna Kempainen, Ville Leinonen, Heikki Tanila, A. H. and M. H. (2018) 'Molecular Mechanisms of Synaptotoxicity and Neuroinflammation in Alzheimer's Disease', *Frontiers in Neuroscience*. doi: doi.org/10.3389/fnins.2018.00963.
- Miller, K. E. and Sheetz, M. P. (2004) 'Axonal mitochondrial transport and potential are correlated', *Journal of Cell Science*. The Company of Biologists, 117(13), pp. 2791–2804. doi: 10.1242/JCS.01130.
- Ming Hsu, C. Y. and Uluda Ğ, H. (2012) 'A simple and rapid nonviral approach to efficiently transfect primary tissue-derived cells using polyethylenimine', *Nature Protocols* 2012 7:5. Nature Publishing Group, 7(5), pp. 935–945. doi: 10.1038/nprot.2012.038.
- Misgeld, T. and Schwarz, T. L. (2017) 'Mitostasis in neurons: Maintaining mitochondria in an extended cellular architecture', *Neuron*. NIH Public Access, 96(3), p. 651. doi: 10.1016/J.NEURON.2017.09.055.
- Miskinyte, G. *et al.* (2017) 'Direct conversion of human fibroblasts to functional excitatory cortical neurons integrating into human neural networks', *Stem cell research & therapy*. Stem Cell Res Ther, 8(1). doi: 10.1186/S13287-017-0658-3.
- Misra, A., Chakrabarti, S. S. and Gambhir, I. S. (2018) 'New genetic players in late-onset Alzheimer's disease: Findings of genome-wide association studies', *The Indian journal of medical research*. Indian J Med Res, 148(2), pp. 135–144. doi: 10.4103/IJMR.IJMR_473_17.
- Montes de Oca Balderas, P. (2021) 'Mitochondria–plasma membrane interactions and communication', *Journal of Biological Chemistry*. Elsevier, 297(4), p. 101164. doi: 10.1016/J.JBC.2021.101164.
- Morena, J., Gupta, A. and Hoyle, J. C. (2019) 'Charcot-Marie-Tooth: From Molecules to Therapy', *International Journal of Molecular Sciences*. Multidisciplinary Digital Publishing Institute (MDPI), 20(14). doi: 10.3390/IJMS20143419.
- Mortiboys, H. *et al.* (2015) 'UDCA exerts beneficial effect on mitochondrial dysfunction in LRRK2 G2019S carriers and in vivo', *Neurology*, 85(10), pp. 846–852. doi: 10.1212/WNL.0000000000001905.
- Mortiboys, H., Aasly, J. and Bandmann, O. (2013) 'Ursocholic acid rescues mitochondrial function in common forms of familial Parkinson's disease', *Brain*, 136(10), pp. 3038–3050. doi: 10.1093/brain/awt224.
- Mozdy, A. D., McCaffery, J. M. and Shaw, J. M. (2000) 'Dnm1p GTPase-mediated mitochondrial fission is a multi-step process requiring the novel integral membrane component Fis1p', *Journal of Cell Biology*. doi: 10.1083/jcb.151.2.367.
- Muhr, J., Jessell, T. M. and Edlund, T. (1997) 'Assignment of early caudal identity to neural plate cells by a

- signal from caudal paraxial mesoderm', *Neuron*. doi: 10.1016/S0896-6273(00)80366-9.
- Mutisya, E. M., Bowling, A. C. and Beal, M. F. (1994) 'Cortical cytochrome oxidase activity is reduced in Alzheimer's disease.', *Journal of Neurochemistry*, 63(6), pp. 2179–84. doi: 10.1046/j.1471-4159.1994.63062179.x.
- Naseri, N. N. *et al.* (2019) 'The complexity of tau in Alzheimer's disease', *Neuroscience Letters*. doi: 10.1016/j.neulet.2019.04.022.
- Nasrabad, S. E. *et al.* (2018) 'White matter changes in Alzheimer's disease: a focus on myelin and oligodendrocytes', *Acta neuropathologica communications*. doi: 10.1186/s40478-018-0515-3.
- Ng, Y. S. and Turnbull, D. M. (2016) 'Mitochondrial disease: genetics and management', *Journal of Neurology*. Springer, 263(1), p. 179. doi: 10.1007/S00415-015-7884-3.
- Niemann, A. *et al.* (2005) 'Ganglioside-induced differentiation associated protein 1 is a regulator of the mitochondrial network: new implications for Charcot-Marie-Tooth disease', *The Journal of Cell Biology*. The Rockefeller University Press, 170(7), p. 1067. doi: 10.1083/JCB.200507087.
- Obulesu, M. and Lakshmi, M. J. (2014) 'Apoptosis in Alzheimer's Disease: An Understanding of the Physiology, Pathology and Therapeutic Avenues', *Neurochemical Research*. Springer Science and Business Media, LLC, 39(12), pp. 2301–2312. doi: 10.1007/S11064-014-1454-4/FIGURES/2.
- Ohgidani, M. *et al.* (2014) 'Direct induction of ramified microglia-like cells from human monocytes: Dynamic microglial dysfunction in Nasu-Hakola disease', *Scientific Reports*. doi: 10.1038/srep04957.
- Oksanen, M. *et al.* (2017) 'PSEN1 Mutant iPSC-Derived Model Reveals Severe Astrocyte Pathology in Alzheimer's Disease', *Stem Cell Reports*. doi: 10.1016/j.stemcr.2017.10.016.
- Olgun, A. and Akman, S. (2007) 'Mitochondrial DNA-Deficient Models and Aging', *Annals of the New York Academy of Sciences*. John Wiley & Sons, Ltd, 1100(1), pp. 241–245. doi: 10.1196/ANNALS.1395.025.
- Osellame, L. D. *et al.* (2016) 'Cooperative and independent roles of the Drp1 adaptors Mff, MiD49 and MiD51 in mitochondrial fission', *Journal of Cell Science*. doi: 10.1242/jcs.185165.
- Otera, H. *et al.* (2010) 'Mff is an essential factor for mitochondrial recruitment of Drp1 during mitochondrial fission in mammalian cells', *Journal of Cell Biology*. doi: 10.1083/jcb.201007152.
- Otera, H., Ishihara, N. and Mihara, K. (2013) 'New insights into the function and regulation of mitochondrial fission', *Biochimica et Biophysica Acta (BBA) - Molecular Cell Research*, 1833(5), pp. 1256–1268. doi: 10.1016/j.bbamcr.2013.02.002.
- Padmanabhan, P., Kneynsberg, A. and Götz, J. (2021) 'Super-resolution microscopy: a closer look at synaptic dysfunction in Alzheimer disease', *Nature reviews. Neuroscience*. Nat Rev Neurosci, 22(12), pp. 723–740. doi: 10.1038/S41583-021-00531-Y.
- Paidi, R. K. *et al.* (2015) 'Mitochondrial Deficits Accompany Cognitive Decline Following Single Bilateral Intracerebroventricular Streptozotocin.', *Current Alzheimer research*, 12(8), pp. 785–795. doi: 10.2174/1567205012666150710112618.
- Palmer, C. S. *et al.* (2011) 'MiD49 and MiD51, new components of the mitochondrial fission machinery', *EMBO Reports*. doi: 10.1038/embor.2011.54.
- Palmer, C. S. *et al.* (2013) 'Adaptor proteins MiD49 and MiD51 can act independently of Mff and Fis1 in Drp1 recruitment and are specific for mitochondrial fission', *Journal of Biological Chemistry*. doi: 10.1074/jbc.M113.479873.
- Paredes, R. M. *et al.* (2008) 'Chemical Calcium Indicators', *Methods (San Diego, Calif.)*. NIH Public Access, 46(3), p. 143. doi: 10.1016/J.YMETH.2008.09.025.
- Parker, W. D. (1991) 'Cytochrome oxidase deficiency in Alzheimer's disease', *Annals of the New York Academy of Sciences*. Ann N Y Acad Sci, 640, pp. 59–64. doi: 10.1111/J.1749-6632.1991.TB00191.X.
- Parker, W. D. *et al.* (1994) 'Reduced platelet cytochrome c oxidase activity in Alzheimer's disease.', *Neurology*, 44(6), pp. 1086–90. doi: 10.1212/WNL.44.6.1086.
- Parker, W. D., Filley, C. M. and Parks, J. K. (1990) 'Cytochrome oxidase deficiency in Alzheimer's disease.',

Neurology, 40(8), pp. 1302–3. doi: 10.1212/WNL.40.8.1302.

Pascucci, B. *et al.* (2021) 'DRP1 Inhibition Rescues Mitochondrial Integrity and Excessive Apoptosis in CS-A Disease Cell Models', *International journal of molecular sciences*. *Int J Mol Sci*, 22(13). doi: 10.3390/IJMS22137123.

Payne, T. *et al.* (2020) 'Ursodeoxycholic acid as a novel disease-modifying treatment for Parkinson's disease: Protocol for a two-centre, randomised, double-blind, placebo-controlled trial, the "UP" study', *BMJ Open*. BMJ Publishing Group, 10(8). doi: 10.1136/BMJOPEN-2020-038911.

Pedrola, L. *et al.* (2005) 'GDAP1, the protein causing Charcot-Marie-Tooth disease type 4A, is expressed in neurons and is associated with mitochondria', *Human molecular genetics*. *Hum Mol Genet*, 14(8), pp. 1087–1094. doi: 10.1093/HMG/DDI121.

Pedrola, L. *et al.* (2008) 'Cell expression of GDAP1 in the nervous system and pathogenesis of Charcot-Marie-Tooth type 4A disease', *Journal of cellular and molecular medicine*. *J Cell Mol Med*, 12(2), pp. 679–689. doi: 10.1111/J.1582-4934.2007.00158.X.

Pelucchi, S. *et al.* (2022) 'Synaptic dysfunction in early phases of Alzheimer's Disease', *Handbook of clinical neurology*. *Handb Clin Neurol*, 184, pp. 417–438. doi: 10.1016/B978-0-12-819410-2.00022-9.

Pennisi, M. *et al.* (2020) 'Acetyl-L-Carnitine in Dementia and Other Cognitive Disorders: A Critical Update', *Nutrients 2020, Vol. 12, Page 1389*. Multidisciplinary Digital Publishing Institute, 12(5), p. 1389. doi: 10.3390/NU12051389.

Pérez, M. J. *et al.* (2017) 'Mitochondrial bioenergetics is altered in fibroblasts from patients with sporadic Alzheimer's disease', *Frontiers in Neuroscience*, 11(OCT). doi: 10.3389/fnins.2017.00553.

Perry, S. W. *et al.* (2011) 'Mitochondrial membrane potential probes and the proton gradient: A practical usage guide', *BioTechniques*. Future Science Ltd London, UK, 50(2), pp. 98–115. doi: 10.2144/000113610/ASSET/IMAGES/LARGE/TABLE1.JPEG.

Peterson, C. and Goldman, J. E. (1986) 'Alterations in calcium content and biochemical processes in cultured skin fibroblasts from aged and Alzheimer donors.', *Proceedings of the National Academy of Sciences of the United States of America*. doi: 10.1073/pnas.83.8.2758.

Pijuan, J. *et al.* (2022) 'Mitochondrial Dynamics and Mitochondria-Lysosome Contacts in Neurogenetic Diseases', *Frontiers in Neuroscience*. Frontiers Media SA, 16, p. 784880. doi: 10.3389/FNINS.2022.784880.

Piyooosh Sharma, Pavan Srivastava, Ankit Seth, Prabhash Nath, Tripathi Anupam, Banerjee Sushant, S. (2018) 'Comprehensive review of mechanisms of pathogenesis involved in Alzheimer's disease and potential therapeutic strategies', *Progress in Neurobiology*.

Ploia, C. *et al.* (2011) 'JNK plays a key role in tau hyperphosphorylation in alzheimer's disease models', *Journal of Alzheimer's Disease*. doi: 10.3233/JAD-2011-110320.

Plucińska, G. and Misgeld, T. (2016) 'Imaging of neuronal mitochondria in situ', *Current opinion in neurobiology*. *Curr Opin Neurobiol*, 39, pp. 152–163. doi: 10.1016/J.CONB.2016.06.006.

Popov, L. D. (2020) 'Mitochondrial biogenesis: An update', *Journal of Cellular and Molecular Medicine*. Wiley-Blackwell, 24(9), p. 4892. doi: 10.1111/JCMM.15194.

Del Prete, D. *et al.* (2017) 'Localization and Processing of the Amyloid- β Protein Precursor in Mitochondria-Associated Membranes', *Journal of Alzheimer's Disease*. doi: 10.3233/JAD-160953.

Prieto, J. *et al.* (2016) 'Dysfunctional mitochondrial fission impairs cell reprogramming', *Cell Cycle*. doi: 10.1080/15384101.2016.1241930.

Qi, X. *et al.* (2011) 'Aberrant mitochondrial fission in neurons induced by protein kinase C δ under oxidative stress conditions in vivo', *Molecular Biology of the Cell*. doi: 10.1091/mbc.E10-06-0551.

Qi, X. *et al.* (2013) 'A novel Drp1 inhibitor diminishes aberrant mitochondrial fission and neurotoxicity', *Journal of Cell Science*. doi: 10.1242/jcs.114439.

Qi, Y. *et al.* (2017) 'Combined small-molecule inhibition accelerates the derivation of functional cortical neurons from human pluripotent stem cells', *Nature Biotechnology 2016 35:2*. Nature Publishing Group, 35(2),

pp. 154–163. doi: 10.1038/nbt.3777.

Qin, W. *et al.* (2009) 'PGC-1 α Expression Decreases in the Alzheimer Disease Brain as a Function of Dementia', *Archives of neurology*. NIH Public Access, 66(3), p. 352. doi: 10.1001/ARCHNEUROL.2008.588.

Qu, L. *et al.* (2019) 'The ras superfamily of small gtpases in non-neoplastic cerebral diseases', *Frontiers in Molecular Neuroscience*. doi: 10.3389/fnmol.2019.00121.

Raja, W. K. *et al.* (2016) 'Self-organizing 3D human neural tissue derived from induced pluripotent stem cells recapitulate Alzheimer's disease phenotypes', *PLoS ONE*. doi: 10.1371/journal.pone.0161969.

Ramalho, R. M. *et al.* (2006) 'Tauroursodeoxycholic acid modulates p53-mediated apoptosis in Alzheimer's disease mutant neuroblastoma cells', *Journal of Neurochemistry*, 98(5), pp. 1610–1618. doi: 10.1111/j.1471-4159.2006.04007.x.

Ramamoorthy, M. *et al.* (2012) 'Sporadic Alzheimer disease fibroblasts display an oxidative stress phenotype', *Free Radical Biology and Medicine*, 53(6), pp. 1371–1380. doi: 10.1016/j.freeradbiomed.2012.07.018.

Rambold, A. S. *et al.* (2011) 'Tubular network formation protects mitochondria from autophagosomal degradation during nutrient starvation', *Proceedings of the National Academy of Sciences*. doi: 10.1073/pnas.1107402108.

Raphael Wittenberg, Bo Hu, Luis Barraza-Araiza, A. R. (2019) *Projections of older people with dementia and costs of dementia care in the United Kingdom, 2019–2040*.

Reddy, P. H., Yin, X. L., *et al.* (2018) 'Mutant APP and amyloid beta-induced defective autophagy, mitophagy, mitochondrial structural and functional changes and synaptic damage in hippocampal neurons from Alzheimer's disease', *Human Molecular Genetics*. doi: 10.1093/hmg/ddy154.

Reddy, P. H., Manczak, M., *et al.* (2018) 'Synergistic Protective Effects of Mitochondrial Division Inhibitor 1 and Mitochondria-Targeted Small Peptide SS31 in Alzheimer's Disease', *Journal of Alzheimer's Disease*. doi: 10.3233/JAD-170988.

Reddy, P. H., Manczak, M. and Yin, X. (2017) 'Mitochondria-Division Inhibitor 1 Protects Against Amyloid- β induced Mitochondrial Fragmentation and Synaptic Damage in Alzheimer's Disease.', *Journal of Alzheimer's disease : JAD*. NIH Public Access, 58(1), pp. 147–162. doi: 10.3233/JAD-170051.

Rhein, V. *et al.* (2009) 'Amyloid-beta and tau synergistically impair the oxidative phosphorylation system in triple transgenic Alzheimer's disease mice', *Proceedings of the National Academy of Sciences of the United States of America*. Proc Natl Acad Sci U S A, 106(47), pp. 20057–20062. doi: 10.1073/PNAS.0905529106.

Ribbens, J. *et al.* (2013) 'A High-throughput Screening Assay using Krabbe Disease Patient Cells', *Analytical biochemistry*. NIH Public Access, 434(1), p. 15. doi: 10.1016/J.AB.2012.10.034.

Ring, K. L. *et al.* (2012) 'Direct reprogramming of mouse and human fibroblasts into multipotent neural stem cells with a single factor', *Cell Stem Cell*. doi: 10.1016/j.stem.2012.05.018.

Roger, A. J., Muñoz-Gómez, S. A. and Kamikawa, R. (2017) 'The Origin and Diversification of Mitochondria', *Current biology : CB*. Curr Biol, 27(21), pp. R1177–R1192. doi: 10.1016/J.CUB.2017.09.015.

Rönnbäck, A. *et al.* (2016) 'Mitochondrial dysfunction in a transgenic mouse model expressing human amyloid precursor protein (APP) with the Arctic mutation', *Journal of Neurochemistry*, 136(3), pp. 497–502. doi: 10.1111/jnc.13410.

Rosdah, A. A. *et al.* (2020) 'New perspectives on the role of Drp1 isoforms in regulating mitochondrial pathophysiology', *Pharmacology & therapeutics*. Pharmacol Ther, 213. doi: 10.1016/J.PHARMTHERA.2020.107594.

Rose, J. *et al.* (2017) 'Mitochondrial dysfunction in glial cells: Implications for neuronal homeostasis and survival', *Toxicology*. doi: 10.1016/j.tox.2017.06.011.

Roy-Choudhury, G. and Daadi, M. M. (2019) 'Assay for Assessing Mitochondrial Function in iPSC-Derived Neural Stem Cells and Dopaminergic Neurons', *Methods in molecular biology (Clifton, N.J.)*. Methods Mol Biol, 1919, pp. 161–173. doi: 10.1007/978-1-4939-9007-8_12.

Rufini, A. *et al.* (2022) 'Drug Repositioning in Friedreich Ataxia', *Frontiers in Neuroscience*. Frontiers Media SA,

16. doi: 10.3389/FNINS.2022.814445.

Sahdeo, S. *et al.* (2014) 'High-throughput screening of FDA-approved drugs using oxygen biosensor plates reveals secondary mitofunctional effects', *Mitochondrion*. doi: 10.1016/j.mito.2014.07.002.

Saint-Aubert, L. *et al.* (2016) 'Regional tau deposition measured by [18F]THK5317 positron emission tomography is associated to cognition via glucose metabolism in Alzheimer's disease', *Alzheimer's Research & Therapy*. BioMed Central, 8(1). doi: 10.1186/S13195-016-0204-Z.

Saito T, Iwata N, Tsubuki S, Takaki Y, Takano J, Huang SM, Suemoto T, Higuchi M, S. T. (2005) 'Somatostatin regulates brain amyloid beta peptide Abeta42 through modulation of proteolytic degradation', *Nat Med*, 11, pp. 434–439.

Santangelo, R. *et al.* (2021) 'β-amyloid monomers drive up neuronal aerobic glycolysis in response to energy stressors', *Aging (Albany NY)*. Impact Journals, LLC, 13(14), p. 18033. doi: 10.18632/AGING.203330.

Savva, G. M. *et al.* (2009) 'Age, Neuropathology, and Dementia', *New England Journal of Medicine*, 360(22), pp. 2302–2309. doi: 10.1056/NEJMoa0806142.

Schapira, A. H. V. *et al.* (1989) 'Mitochondrial complex I deficiency in Parkinson's disease', *Lancet (London, England)*. Lancet, 1(8649), p. 1269. doi: 10.1016/S0140-6736(89)92366-0.

Schapira, A. H. V. *et al.* (1990) 'Mitochondrial complex I deficiency in Parkinson's disease', *Journal of neurochemistry*. J Neurochem, 54(3), pp. 823–827. doi: 10.1111/J.1471-4159.1990.TB02325.X.

Schwartzentruber, A. *et al.* (2020) 'Oxidative switch drives mitophagy defects in dopaminergic parkin mutant patient neurons', *Scientific reports*. Sci Rep, 10(1). doi: 10.1038/S41598-020-72345-4.

Scott, H. L. *et al.* (2020) 'A dual druggable genome-wide siRNA and compound library screening approach identifies modulators of parkin recruitment to mitochondria', *Journal of Biological Chemistry*. doi: 10.1074/jbc.RA119.009699.

Shen, Q. *et al.* (2014) 'Mutations in Fis1 disrupt orderly disposal of defective mitochondria', *Molecular Biology of the Cell*. doi: 10.1091/mbc.e13-09-0525.

Shi, P. *et al.* (2021) 'HDAC6 Signaling at Primary Cilia Promotes Proliferation and Restricts Differentiation of Glioma Cells', *Cancers*. Cancers (Basel), 13(7). doi: 10.3390/CANCERS13071644.

Shi, Y., Kirwan, P. and Livesey, F. J. (2012) 'Directed differentiation of human pluripotent stem cells to cerebral cortex neurons and neural networks', *Nature Protocols*. doi: 10.1038/nprot.2012.116.

Shlevkov, E. *et al.* (2019) 'A High-Content Screen Identifies TPP1 and Aurora B as Regulators of Axonal Mitochondrial Transport', *Cell Reports*. doi: 10.1016/j.celrep.2019.08.035.

Simmen, T. *et al.* (2005) 'PACS-2 controls endoplasmic reticulum-mitochondria communication and Bid-mediated apoptosis', *The EMBO journal*. EMBO J, 24(4), pp. 717–729. doi: 10.1038/SJ.EMBOJ.7600559.

Simpson, J. C. *et al.* (2000) 'Systematic subcellular localization of novel proteins identified by large-scale cDNA sequencing', *EMBO Reports*. doi: 10.1093/embo-reports/kvd058.

Singh, A., Zhi, L. and Zhang, H. (2019) 'LRRK2 and mitochondria: Recent advances and current views', *Brain research*. NIH Public Access, 1702, p. 96. doi: 10.1016/J.BRAINRES.2018.06.010.

Slager, R. E. *et al.* (2003) 'Mutations in RAI1 associated with Smith-Magenis syndrome', *Nature Genetics*. doi: 10.1038/ng1126.

Smith, E. F., Shaw, P. J. and De Vos, K. J. (2019) 'The role of mitochondria in amyotrophic lateral sclerosis', *Neuroscience letters*. Neurosci Lett, 710. doi: 10.1016/J.NEULET.2017.06.052.

Soininen H, Syrjänen S, Heinonen O, Neittaanmäki H, Miettinen R, Paljärvi L, Syrjänen K, Beyreuther K, R. P. (1992) 'Amyloid beta-protein deposition in skin of patients with dementia', *The Lancet*, 25, p. 245.

Son, E. Y. *et al.* (2011) 'Conversion of mouse and human fibroblasts into functional spinal motor neurons', *Cell Stem Cell*. doi: 10.1016/j.stem.2011.07.014.

Song, Y. H., Yoon, J. and Lee, S. H. (2021) 'The role of neuropeptide somatostatin in the brain and its application in treating neurological disorders', *Experimental and Molecular Medicine*. doi: 10.1038/s12276-

021-00580-4.

Song, Z. *et al.* (2007) 'OPA1 processing controls mitochondrial fusion and is regulated by mRNA splicing, membrane potential, and Yme1L', *Journal of Cell Biology*. doi: 10.1083/jcb.200704110.

Stelzmann, R. A., Norman Schnitzlein, H. and Reed Murtagh, F. (1995) 'An english translation of alzheimer's 1907 paper, ??ber eine eigenartige erkankung der hirnrinde??', *Clinical Anatomy*. doi: 10.1002/ca.980080612.

Sung, P. J. *et al.* (2013) 'Phosphorylated K-Ras limits cell survival by blocking Bcl-xL sensitization of inositol trisphosphate receptors', *Proceedings of the National Academy of Sciences of the United States of America*. doi: 10.1073/pnas.1306431110.

Swerdlow, R. H., Burns, J. M. and Khan, S. M. (2010) 'The Alzheimer's Disease Mitochondrial Cascade Hypothesis', *Journal of Alzheimer's disease : JAD*. NIH Public Access, 20(Suppl 2), p. 265. doi: 10.3233/JAD-2010-100339.

Swerdlow, R. H., Burns, J. M. and Khan, S. M. (2014) 'The Alzheimer's disease mitochondrial cascade hypothesis: Progress and perspectives', *Biochimica et Biophysica Acta - Molecular Basis of Disease*, pp. 1219–1231. doi: 10.1016/j.bbadis.2013.09.010.

Swerdlow, R. H. and Khan, S. M. (2004) 'A "mitochondrial cascade hypothesis" for sporadic Alzheimer's disease', *Medical hypotheses*. Med Hypotheses, 63(1), pp. 8–20. doi: 10.1016/J.MEHY.2003.12.045.

Tadato, B. *et al.* (2010) 'OPA1 disease alleles causing dominant optic atrophy have defects in cardiolipin-stimulated GTP hydrolysis and membrane tubulation', *Human Molecular Genetics*. Oxford University Press, 19(11), p. 2113. doi: 10.1093/HMG/DDQ088.

Takahashi, K. and Yamanaka, S. (2006) 'Induction of Pluripotent Stem Cells from Mouse Embryonic and Adult Fibroblast Cultures by Defined Factors', *Cell*. doi: 10.1016/j.cell.2006.07.024.

Tay, S. H. *et al.* (2021) 'Generation of Cortical, Dopaminergic, Motor, and Sensory Neurons from Human Pluripotent Stem Cells', *Methods in Molecular Biology*. Springer, New York, NY, pp. 1–19. doi: 10.1007/7651_2021_399.

Terada, T. *et al.* (2021) 'Mitochondrial complex I abnormalities is associated with tau and clinical symptoms in mild Alzheimer's disease', *Molecular neurodegeneration*. Mol Neurodegener, 16(1). doi: 10.1186/S13024-021-00448-1.

Terada, T. *et al.* (2022) 'Mitochondrial complex I abnormalities underlie neurodegeneration and cognitive decline in Alzheimer's disease', *European journal of neurology*. Eur J Neurol. doi: 10.1111/ENE.15246.

Tian, E. *et al.* (2016) 'Small-Molecule-Based Lineage Reprogramming Creates Functional Astrocytes', *Cell Reports*. doi: 10.1016/j.celrep.2016.06.042.

Tilokani, L. *et al.* (2018) 'Mitochondrial dynamics: Overview of molecular mechanisms', *Essays in Biochemistry*. doi: 10.1042/EBC20170104.

Tonge, P. D. and Andrews, P. W. (2010) 'Retinoic acid directs neuronal differentiation of human pluripotent stem cell lines in a non-cell-autonomous manner', *Differentiation; research in biological diversity*. Differentiation, 80(1), pp. 20–30. doi: 10.1016/J.DIFF.2010.04.001.

Toyama, E. Q. *et al.* (2016) 'AMP-activated protein kinase mediates mitochondrial fission in response to energy stress', *Science*. doi: 10.1126/science.aab4138.

Trushina, E. *et al.* (2012) 'Defects in mitochondrial dynamics and metabolomic signatures of evolving energetic stress in mouse models of familial alzheimer's disease', *PLoS ONE*, 7(2). doi: 10.1371/journal.pone.0032737.

Trushina, E. (2019) 'Alzheimer's disease mechanisms in peripheral cells: Promises and challenges', *Alzheimer's and Dementia: Translational Research and Clinical Interventions*. doi: 10.1016/j.trci.2019.06.008.

Uddin, M. S. *et al.* (2018) 'Autophagy and Alzheimer's disease: From molecular mechanisms to therapeutic implications', *Frontiers in Aging Neuroscience*. doi: 10.3389/fnagi.2018.00004.

Vantaggiato, C. *et al.* (2019) 'The fine tuning of drp1-dependent mitochondrial remodeling and autophagy controls neuronal differentiation', *Frontiers in Cellular Neuroscience*. doi: 10.3389/fncel.2019.00120.

- Vazquez-Martin, A. *et al.* (2012) 'Mitochondrial fusion by pharmacological manipulation impedes somatic cell reprogramming to pluripotency: new insight into the role of mitophagy in cell stemness', *Aging*. Aging (Albany NY), 4(6), pp. 393–401. doi: 10.18632/AGING.100465.
- Verburg, J. and Hollenbeck, P. J. (2008) 'Mitochondrial Membrane Potential in Axons Increases with Local Nerve Growth Factor or Semaphorin Signaling', *Journal of Neuroscience*. Society for Neuroscience, 28(33), pp. 8306–8315. doi: 10.1523/JNEUROSCI.2614-08.2008.
- Vierbuchen, T. *et al.* (2010) 'Direct conversion of fibroblasts to functional neurons by defined factors', *Nature*. doi: 10.1038/nature08797.
- Völgyi, K. *et al.* (2018) 'Early Presymptomatic Changes in the Proteome of Mitochondria-Associated Membrane in the APP/PS1 Mouse Model of Alzheimer's Disease', *Molecular neurobiology*. Mol Neurobiol, 55(10), pp. 7839–7857. doi: 10.1007/S12035-018-0955-6.
- Wakabayashi, J. *et al.* (2009) 'The dynamin-related GTPase Drp1 is required for embryonic and brain development in mice', *The Journal of cell biology*. J Cell Biol, 186(6), pp. 805–816. doi: 10.1083/JCB.200903065.
- Wang, C. *et al.* (2017) 'Scalable Production of iPSC-Derived Human Neurons to Identify Tau-Lowering Compounds by High-Content Screening', *Stem Cell Reports*. Elsevier, 9(4), p. 1221. doi: 10.1016/J.STEMCR.2017.08.019.
- Wang, D. B. *et al.* (2019) 'Neuronal susceptibility to beta-amyloid toxicity and ischemic injury involves histone deacetylase-2 regulation of endophilin-B1', *Brain Pathology*. doi: 10.1111/bpa.12647.
- Wang, J. *et al.* (2021) 'PGC-1 α reduces Amyloid- β deposition in Alzheimer's disease: Effect of increased VDR expression', *Neuroscience letters*. Neurosci Lett, 744. doi: 10.1016/J.NEULET.2020.135598.
- Wang, J. Z., Grundke-Iqbal, I. and Iqbal, K. (2007) 'Kinases and phosphatases and tau sites involved in Alzheimer neurofibrillary degeneration', *European Journal of Neuroscience*. doi: 10.1111/j.1460-9568.2006.05226.x.
- Wang, L. *et al.* (2014) 'Drp1 is dispensable for mitochondria biogenesis in induction to pluripotency but required for differentiation of embryonic stem cells', *Stem cells and development*. Stem Cells Dev, 23(20), pp. 2422–2434. doi: 10.1089/SCD.2014.0059.
- Wang, S. *et al.* (2012) 'Mitochondrial fission proteins in peripheral blood lymphocytes are potential biomarkers for Alzheimer's disease', *European Journal of Neurology*. doi: 10.1111/j.1468-1331.2012.03670.x.
- Wang, W. *et al.* (2017) 'Inhibition of mitochondrial fragmentation protects against Alzheimer's disease in rodent model', *Human Molecular Genetics*. Oxford University Press, 26(21), pp. 4118–4131. doi: 10.1093/hmg/ddx299.
- Wang, X. *et al.* (2008) 'Amyloid- overproduction causes abnormal mitochondrial dynamics via differential modulation of mitochondrial fission/fusion proteins', *Proceedings of the National Academy of Sciences*, 105(49), pp. 19318–19323. doi: 10.1073/pnas.0804871105.
- Wang, Xinglong *et al.* (2008) 'Dynamin-like protein 1 reduction underlies mitochondrial morphology and distribution abnormalities in fibroblasts from sporadic Alzheimer's disease patients', *American Journal of Pathology*, 173(2), pp. 470–482. doi: 10.2353/ajpath.2008.071208.
- Wang, X. *et al.* (2009) 'Impaired Balance of Mitochondrial Fission and Fusion in Alzheimer's Disease', *Journal of Neuroscience*, 29(28), pp. 9090–9103. doi: 10.1523/JNEUROSCI.1357-09.2009.
- Wang, X. and Davis, R. L. (2021) 'Early mitochondrial fragmentation and dysfunction in a Drosophila model for Alzheimer's Disease', *Molecular neurobiology*. NIH Public Access, 58(1), p. 143. doi: 10.1007/S12035-020-02107-W.
- Wang, Z. T. *et al.* (2020) 'Selective neuronal vulnerability in Alzheimer's disease', *Ageing Research Reviews*. Elsevier, 62, p. 101114. doi: 10.1016/J.ARR.2020.101114.
- Watanabe, K. *et al.* (2007) 'A ROCK inhibitor permits survival of dissociated human embryonic stem cells', *Nature Biotechnology* 2007 25:6. Nature Publishing Group, 25(6), pp. 681–686. doi: 10.1038/nbt1310.
- Waterham, H. R. *et al.* (2009) 'A Lethal Defect of Mitochondrial and Peroxisomal Fission', <http://dx.doi.org/10.1056/NEJMoa064436>. Massachusetts Medical Society, 356(17), pp. 1736–1741. doi:

10.1056/NEJMOA064436.

Webster, C. P. *et al.* (2016) 'The C9orf72 protein interacts with Rab1a and the ULK 1 complex to regulate initiation of autophagy', *The EMBO Journal*. doi: 10.15252/embj.201694401.

Weingarten, M. D. *et al.* (1975) 'A protein factor essential for microtubule assembly', *Proceedings of the National Academy of Sciences of the United States of America*. doi: 10.1073/pnas.72.5.1858.

West, A. P., Shadel, G. S. and Ghosh, S. (2011) 'Mitochondria in innate immune responses', *Nature reviews. Immunology*. *Nat Rev Immunol*, 11(6), pp. 389–402. doi: 10.1038/NRI2975.

Wiedemann, F. R. *et al.* (2002) 'Mitochondrial DNA and respiratory chain function in spinal cords of ALS patients', *Journal of neurochemistry*. *J Neurochem*, 80(4), pp. 616–625. doi: 10.1046/J.0022-3042.2001.00731.X.

Wilkins, H. M. *et al.* (2022) 'Mitochondrial Membrane Potential Influences Amyloid- β Protein Precursor Localization and Amyloid- β Secretion', *Journal of Alzheimer's disease : JAD*. *J Alzheimers Dis*, 85(1), pp. 381–394. doi: 10.3233/JAD-215280.

Wilson, E. L. and Metzakopian, E. (2021) 'ER-mitochondria contact sites in neurodegeneration: genetic screening approaches to investigate novel disease mechanisms', *Cell Death and Differentiation*. doi: 10.1038/s41418-020-00705-8.

Wong, Y. C., Ysselstein, D. and Krainc, D. (2018) 'Mitochondria–lysosome contacts regulate mitochondrial fission via RAB7 GTP hydrolysis', *Nature* 2018 554:7692. *Nature Publishing Group*, 554(7692), pp. 382–386. doi: 10.1038/nature25486.

Wu, D. *et al.* (2020) 'Identification of novel dynamin-related protein 1 (Drp1) GTPase inhibitors: Therapeutic potential of Drpitor1 and Drpitor1a in cancer and cardiac ischemia-reperfusion injury', *FASEB journal : official publication of the Federation of American Societies for Experimental Biology*. *FASEB J*, 34(1), pp. 1447–1464. doi: 10.1096/FJ.201901467R.

Wu, M. *et al.* (2021) 'The role of pathological tau in synaptic dysfunction in Alzheimer's diseases', *Translational neurodegeneration*. *Transl Neurodegener*, 10(1). doi: 10.1186/S40035-021-00270-1.

Xian, H. and Liou, Y. C. (2019) 'Loss of MIEF1/MiD51 confers susceptibility to BAX-mediated cell death and PINK1-PRKN-dependent mitophagy', *Autophagy*. doi: 10.1080/15548627.2019.1596494.

Xiao, Y. *et al.* (2021) 'Tetrahydrocurcumin ameliorates Alzheimer's pathological phenotypes by inhibition of microglial cell cycle arrest and apoptosis via Ras/ERK signaling', *Biomedicine and Pharmacotherapy*. doi: 10.1016/j.biopha.2021.111651.

Xie, C. *et al.* (2022) 'Amelioration of Alzheimer's disease pathology by mitophagy inducers identified via machine learning and a cross-species workflow', *Nature Biomedical Engineering* 2022 6:1. *Nature Publishing Group*, 6(1), pp. 76–93. doi: 10.1038/s41551-021-00819-5.

Xiong, X. *et al.* (2020) 'Study of mitophagy and ATP-related metabolomics based on β -amyloid levels in Alzheimer's disease', *Experimental cell research*. *Exp Cell Res*, 396(1). doi: 10.1016/J.YEXCR.2020.112266.

XU, D. *et al.* (2021) 'Blockage of Drp1 phosphorylation at Ser579 protects neurons against A β 1-42-induced degeneration', *Molecular Medicine Reports*. doi: 10.3892/mmr.2021.12296.

Xu, L. *et al.* (2022) 'Abnormal mitochondria in Down syndrome iPSC-derived GABAergic interneurons and organoids', *Biochimica et biophysica acta. Molecular basis of disease*. *Biochim Biophys Acta Mol Basis Dis*, p. 166388. doi: 10.1016/J.BBADIS.2022.166388.

Xu, L. L. *et al.* (2017) 'Mitochondrial dynamics changes with age in an APPsw/PS1dE9 mouse model of Alzheimer's disease', *NeuroReport*. doi: 10.1097/WNR.0000000000000739.

Xu, L., Wang, X. and Tong, C. (2020) 'Endoplasmic Reticulum–Mitochondria Contact Sites and Neurodegeneration', *Frontiers in Cell and Developmental Biology*. doi: 10.3389/fcell.2020.00428.

Xu, M. *et al.* (2013) 'A phenotypic compound screening assay for lysosomal storage diseases.', *Journal of Biomolecular Screening*, 19(1), pp. 168–175. doi: 10.1177/1087057113501197.

Yamano, K. *et al.* (2014) 'Mitochondrial Rab GAPs govern autophagosome biogenesis during mitophagy', *eLife*.

doi: 10.7554/elife.01612.

Yan, C. *et al.* (2019) 'Mitochondrial DNA: Distribution, Mutations, and Elimination', *Cells*. Multidisciplinary Digital Publishing Institute (MDPI), 8(4), p. 379. doi: 10.3390/CELLS8040379.

Yan, Q. W. *et al.* (2019) 'Effects of treadmill exercise on mitochondrial fusion and fission in the hippocampus of APP/PS1 mice', *Neuroscience Letters*. doi: 10.1016/j.neulet.2019.02.030.

Yang, D. *et al.* (1985) 'Mitochondrial origins.', *Proceedings of the National Academy of Sciences of the United States of America*. National Academy of Sciences, 82(13), p. 4443. doi: 10.1073/PNAS.82.13.4443.

Yang, N. *et al.* (2013) 'Generation of oligodendroglial cells by direct lineage conversion', *Nature Biotechnology*. doi: 10.1038/nbt.2564.

Yang, Y. *et al.* (2016) 'Mitochondria and Mitochondrial ROS in Cancer: Novel Targets for Anticancer Therapy', *Journal of cellular physiology*. *J Cell Physiol*, 231(12), pp. 2570–2581. doi: 10.1002/JCP.25349.

Yao, J. *et al.* (2009) 'Mitochondrial bioenergetic deficit precedes Alzheimer's pathology in female mouse model of Alzheimer's disease', *Proceedings of the National Academy of Sciences of the United States of America*. *Proc Natl Acad Sci U S A*, 106(34), pp. 14670–14675. doi: 10.1073/PNAS.0903563106.

Yao, P. J. *et al.* (2021) 'Mitochondrial Electron Transport Chain Protein Abnormalities Detected in Plasma Extracellular Vesicles in Alzheimer's Disease', *Biomedicines*. *Biomedicines*, 9(11). doi: 10.3390/BIOMEDICINES9111587.

Ye, X. *et al.* (2015) 'Parkin-mediated mitophagy in mutant hAPP neurons and Alzheimer's disease patient brains', *Human Molecular Genetics*. Oxford University Press, 24(10), p. 2938. doi: 10.1093/HMG/DDV056.

Yoon, Y. *et al.* (2003) 'The mitochondrial protein hFis1 regulates mitochondrial fission in mammalian cells through an interaction with the dynamin-like protein DLP1.', *Molecular and cellular biology*.

Young, M. L. and Franklin, J. L. (2019) 'The mitochondria-targeted antioxidant MitoQ inhibits memory loss, neuropathology, and extends lifespan in aged 3xTg-AD mice', *Molecular and cellular neurosciences*. *Mol Cell Neurosci*, 101. doi: 10.1016/J.MCN.2019.103409.

Yu, T., Fox, R.J., Burwell, L.S., Yoon, Y. (2005) 'Regulation of mitochondrial fission and apoptosis by the mitochondrial outer membrane protein hFis1', *Journal of Cell Science*, 118(18), pp. 4141–4151. doi: 10.1242/jcs.02537.

Yu, R., Jin, S., *et al.* (2019) 'Human Fis1 regulates mitochondrial dynamics through inhibition of the fusion machinery', *The EMBO Journal*. doi: 10.15252/embj.201899748.

Yu, R., Liu, T., *et al.* (2019) 'The phosphorylation status of Ser-637 in dynamin-related protein 1 (Drp1) does not determine Drp1 recruitment to mitochondria', *The Journal of biological chemistry*. *J Biol Chem*, 294(46), pp. 17262–17277. doi: 10.1074/JBC.RA119.008202.

Yu, R. *et al.* (2021) 'MIEF1/2 orchestrate mitochondrial dynamics through direct engagement with both the fission and fusion machineries', *BMC Biology*. doi: 10.1186/s12915-021-01161-7.

Zarrouk, A. *et al.* (2015) 'Fatty acid profiles in demented patients: identification of hexacosanoic acid (C26:0) as a blood lipid biomarker of dementia', *Journal of Alzheimer's disease : JAD*. *J Alzheimers Dis*, 44(4), pp. 1349–1359. doi: 10.3233/JAD-142046.

Zarrouk, A. *et al.* (2018) 'Lipid Biomarkers in Alzheimer's Disease', *Current Alzheimer Research*, 15(4), pp. 303–312. doi: 10.2174/1567205014666170505101426.

Zemirli, N. *et al.* (2014) 'Mitochondrial hyperfusion promotes NF- κ B activation via the mitochondrial E3 ligase MULAN', *The FEBS journal*. *FEBS J*, 281(14), pp. 3095–3112. doi: 10.1111/FEBS.12846.

Zhang, C., Rissman, R. A. and Feng, J. (2015) 'Characterization of ATP alternations in an Alzheimer's disease transgenic mouse model', *Journal of Alzheimer's Disease*, 44(2), pp. 375–378. doi: 10.3233/JAD-141890.

Zhang, Y. *et al.* (2013) 'Rapid Single-Step Induction of Functional Neurons from Human Pluripotent Stem Cells', *Neuron*. NIH Public Access, 78(5), p. 785. doi: 10.1016/J.NEURON.2013.05.029.

Zhang, Y. *et al.* (2017) 'Patient iPSC-Derived Neurons for Disease Modeling of Frontotemporal Dementia with Mutation in CHMP2B', *Stem Cell Reports*. Elsevier, 8(3), p. 648. doi: 10.1016/J.STEMCR.2017.01.012.

Zhang, Y. H. *et al.* (2018) ' α -Lipoic acid improves abnormal behavior by mitigation of oxidative stress, inflammation, ferroptosis, and tauopathy in P301S Tau transgenic mice', *Redox biology*. Redox Biol, 14, pp. 535–548. doi: 10.1016/J.REDOX.2017.11.001.

Zhang, Z. *et al.* (2016) 'Drp1, Mff, Fis1, and MiD51 are coordinated to mediate mitochondrial fission during UV irradiation-induced apoptosis', *FASEB Journal*. doi: 10.1096/fj.15-274258.

Zhao, J. *et al.* (2011) 'Human MIEF1 recruits Drp1 to mitochondrial outer membranes and promotes mitochondrial fusion rather than fission', *EMBO Journal*. doi: 10.1038/emboj.2011.198.

Zheng, W., Thorne, N. and McKew, J. C. (2013) 'Phenotypic screens as a renewed approach for drug discovery', *Drug Discovery Today*. doi: 10.1016/j.drudis.2013.07.001.

Zheng, X. *et al.* (2016) 'Metabolic reprogramming during neuronal differentiation from aerobic glycolysis to neuronal oxidative phosphorylation', *eLife*. Elife, 5(JUN2016). doi: 10.7554/ELIFE.13374.